Ninth International Conference on Permafrost

Proceedings of the Ninth International Conference on Permafrost
University of Alaska Fairbanks
June 29–July 3, 2008

Ninth International Conference on Permafrost

Edited by Douglas L. Kane and Kenneth M. Hinkel

Volume 2

Institute of Northern Engineering
University of Alaska Fairbanks
2008

Ninth International Conference on Permafrost
Edited by Douglas L. Kane and Kenneth M. Hinkel

Printed in the United States of America

Elmer E. Rasmuson Library Cataloging in Publication Data
International Conference on Permafrost (9th : 2008 : Fairbanks, Alaska)
Ninth International Conference on Permafrost /
edited by Douglas L. Kane and Kenneth M. Hinkel.
— Fairbanks, Alaska : Institute of Northern Engineering,
University of Alaska Fairbanks, 2008.
2 v., : ill., maps ; cm.
Includes bibliographical references and index.
June 29–July 3, 2008
1. Permafrost–Congresses. 2. Frozen ground–Congresses.
I. Title. II. Kane, Douglas L. II. Hinkel, Kenneth M.

GB641.I6 2008

ISBN 978-0-9800179-2-2 (v.1)
ISBN 978-0-9800179-3-9 (v.2)

Cover Photo: Low-Centered Polygons, North Slope, Alaska
© 2007 Steven Kazlowski / AlaskaStock.com

Production Editors: Thomas Alton and Fran Pedersen

UAF is an Affirmative Action / Equal Opportunity employer and educational institution.

Kane, D.L. & Hinkel, K.M. (eds). 2008. *Ninth International Conference on Permafrost.* Institute of Northern Engineering, University of Alaska Fairbanks (2 Vols.), 2140 pp.

Contents

Volume 1

Volume 2

Preface

Since the first International Permafrost Conference convened in 1963, we have sustained an international scientific and engineering collaborative effort until we now are immersed in this, the Ninth International Conference on Permafrost (NICOP). Considerable change has occurred over the past 45 years, resulting in heightened interest in the permafrost environment and understanding of its many aspects. Participation by engineers and scientists in advancing our knowledge of permafrost as a thermally impacted medium has continued to grow in the wake of both resource development and climate change.

The University of Alaska Fairbanks (America's Arctic University) is an excellent choice for the location of this conference. Permafrost is ubiquitous in Interior Alaska, and it influences many aspects of our society. Our local field trips are arranged around some of the most interesting phenomena here in the zone of discontinuous permafrost, including the world famous Permafrost Tunnel, the Trans Alaska Oil Pipeline, evidence of anthropogenic impacts on permafrost, and thermokarsting of warm permafrost. Fairbanks is also a good starting point for trips to other parts of Alaska, including the North Slope, Seward Peninsula, Denali National Park (Mount McKinley), and many other adventures. We have also taken this opportunity to offer courses related to the permafrost environment for high school and elementary teachers, advanced graduate students, and working professionals.

The University of Alaska Fairbanks hosted the Fourth International Conference on Permafrost in 1983. It was at this meeting that the International Permafrost Association (IPA) was formally established. IPA members are truly pleased with the strong international flavor of this year's conference, with approximately 30 countries participating. IPA's uninterrupted activities over the past 25 years are partially responsible for this concerted effort to expand our understanding of the permafrost environment, both spatially and temporally. It is also, however, abundantly clear that much of our current interest in this environment is driven by climate change.

Currently, many aspects of permafrost research are receiving considerable attention. These include carbon release into the atmosphere, discharge from catchments dominated with permafrost, the role of gas hydrates in cold environments, degrading permafrost and thermokarsting, infrastructure design in a changing environment, and the overarching issue of climate change on this thermally sensitive environment. It is essential that our scientific and engineering communities help our societies adapt to living and working on warming permafrost. Permafrost degradation will affect all aspects of life in the high latitudes and high elevations. We must anticipate the changes in ecology, hydrology, and infrastructure construction that will accompany degradation of permafrost with a warming climate. That is the challenge facing permafrost scientists and engineers. It is our hope that by sharing our knowledge and understanding, we may better serve our nations and people.

Enjoy the conference. We hope you will go home with increased knowledge and an invigorated appetite for expanding our understanding of the environment we call "permafrost."

—Douglas L. Kane
Water and Environmental Research Center, Institute of Northern Engineering
—Larry D. Hinzman
International Arctic Research Center

Acknowledgments

We, the organizers of the Ninth International Conference on Permafrost (NICOP), cannot sufficiently express our gratitude to those who have made NICOP both possible and successful. There are those who contributed financially by keeping the cost of the registration low, supporting young investigators, helping defer the cost of the proceedings, and sustaining many other behind-the-scenes activities. There are those who served on the numerous committees associated with this conference at the local, national, and international levels; we hope they found this exercise to be professionally rewarding. Finally, there are those who served as associate editors and reviewers of the more than 400 papers submitted. This conference is advertised as an International Conference; to be truly successful, much work must be done to overcome language barriers. While not always finding success in bringing a paper to publication, the associate editors and reviewers performed in a very commendable manner. Thank you all for your help.

—Douglas Kane, Larry Hinzman, and the Local Organizing Committee

NICOP Organizing Team Members

General Chair	Douglas Kane
Co-Chair	Larry Hinzman
Publications	Douglas Kane, Kenneth Hinkel, Thomas Alton, Fran Pedersen
Conference Facilitator	Elizabeth Lilly
Technical Program	Larry Hinzman
Short Courses	Larry Hinzman, Michael Lilly, Yuri Shur
Exhibits - Trade Show	Michael Lilly
Public Affairs	Marmian Grimes, Jenn Wagaman, Cherie Solie
Fundraising	Dave Norton, Jerry Brown, Larry Hinzman, Michael Lilly, James Rooney, Douglas Kane
Finance	Michael Lilly
Website	Gary Whitton
Special Events/Social	Elizabeth Lilly, Deborah Bennett, Melanie Jackson, Chris Lace
Young Researchers	Guido Grosse, Katey Walter, Andrew Balsar, Oliver Frauenfeld
ICOP-IPA-IPY Celebration	Jerry Brown, Jess Walker, John Zarling
Field Trip Guides	Deanne Stevens

U.S. Permafrost Association Board of Directors

Kenneth Hinkel, President
Yuri Shur, President-Elect
Oliver Frauenfeld, Secretary
Michael Lilly, Treasurer
Anna Klene, Member
Jennifer Harden, Member
Larry Hinzman, IPA Representative
Jon Zufelt, Past President

NICOP Program Committee

Larry Hinzman, Chair
Jerry Brown
Doug Goering
Jennifer Harden
Kenneth Hinkel
Douglas Kane
Frederick Nelson
Vladimir Romanovsky
Katey Walter
Jon Zufelt

Local Field Trip Organizers

James Begét
Deb Bennett
Nancy Bigelow
Patty Burns
Ed Clarke
Billy Connor
Charles Collins
Tom Douglas
Doug Goering
Jack Hébert
Melanie Jackson
Elden Johnson
Torre Jorgenson
Elizabeth Lilly
Michael Lilly
O.D. Odsather
Vladimir Romanovsky
Yuri Shur
Diana Solie
Katey Walter
Kenji Yoshikawa

Extended Field Trip Organizers

Donald “Skip” Walker
Tom Hamilton
Bill Streever
Chien-Lu Ping
Robert Gieck
Gary Michaelson
Torre Jorgensen
Jesse Walker
Caryn Rae
Kenneth Hinkel
Jerry Brown
Deanne Stevens
Jim Beget
Chris Burn
Antoni Lewkowicz
Tom Krzewinski
Phil Brease
Nel Caine
Koren Nydick
Elden Johnson
John Zarling
Ed Clarke
O.D. Odsather
Lee Schoen

Additional people who have assisted in NICOP Organization

Danielle Jamieson
Dan White
Michelle Bartlett
Wendy Warnick
Helga Wilm

U.S. National Committee

Jerry Brown, Chair
Roger Barry
Julie Brigham-Grette
Jody Deming
Craig Dorman
Kenneth Hinkel
Larry Hinzman
Douglas Kane
Frederick Nelson
Vladimir Romanovsky
Bill Streever
Rupert "Bucky" Tart
Patrick Webber
Jon Zufelt

International Organizing Committee

Antoni Lewkowicz, Chair
David Gilichinsky
Huijun Jin
Truls Mølmann
Marcia Phillips

NICOP Sponsors

Universities

University of Alaska International Polar Year (Gold plus)
University of Alaska President's Fund (Gold)
Alaska University Transportation Center (Gold)
University of Alaska Fairbanks Institute of Northern Engineering (Silver)
University of Alaska Fairbanks International Arctic Research Center (Silver)
University of Alaska Fairbanks Experimental Program to Stimulate Competitive Research (EPSCoR) (Bronze)
University of Colorado-National Snow and Ice Data Center (Contributor)

Government Agencies

Alaska Division of Geological & Geophysical Surveys, Fairbanks (Gold)
U.S. National Science Foundation (Silver)
U.S. Geological Survey (Silver)
U.S. Army Cold Regions Research and Engineering Laboratory (Bronze)
U.S. Department of Energy (Bronze)
U.S. Arctic Research Commission (Brass)
U.S. Bureau of Land Management (Brass)
Denali Commission (Brass)
North Slope Science Initiative (Brass)
U.S. Minerals Management Service (Contributor plus)
U.S. Fish & Wildlife Service, Fairbanks Field Office (Brass)

Corporate and Non-Governmental Organizations

Arctic Foundations, Inc., Anchorage (Gold)
Alyeska Pipeline Company, Anchorage (Silver)
BP Foundation (Bronze)
International Permafrost Association (Bronze plus)
GW Scientific, Fairbanks (Bronze)
Duane Miller & Associates, Anchorage (Bronze)
CH2MHILL Energy & Power, Anchorage (Brass)
ConocoPhillips Alaska (Brass)
EBA Engineering Consultants Ltd., Canada (Brass)
Golder Associates, Anchorage (Brass)
Shannon & Wilson, Inc. Seattle (Brass)
BeadedStream, LLC, Anchorage (Contributor)
Hawk Consultants, LLC, Anchorage (Contributor)
Houston Advanced Research Center (HARC) (Contributor)
Northern Engineering & Scientific (Contributor)
Northern Geotechnical Engineering, Inc., Anchorage (Contributor)
R&M Consultants, Inc., Anchorage (Contributor)
Tryck Nyman Hayes, Inc., Anchorage (Contributor)
Resource Data, Inc., Anchorage (Sustaining)
URS Corporation, Anchorage (Sustaining)
Usibelli Foundation (Sustaining)
Harley H. Hightower, FAIA, Anchorage (Sustaining)

ICOP Donor Circle (Contributor)

Jerry and Celia Brown
Edwin Clarke
Hugh M. French
Don W. Hayley
C.W. "Bill" Lovell
J. Ross Mackay (Honorary Member)
Michael C. Metz
Frederick E. Nelson
Jim and Florence Rooney
Rupert "Bucky" Tart
Ted B. Trueblood
H. Jess Walker
John Zarling

Individuals

Joe Malen

In-Kind Sponsors

ABR, Inc., Environmental Research and Services
Mountain Studies Institute
Pogo Mine, Teck Cominco Limited
University of Alaska Toolik Field Station
University of Cincinnati
University of Colorado, Institute of Arctic and Alpine Research
U.S. Army CRREL Permafrost Tunnel
U.S. Geological Survey
U.S. National Park Service

Associate Editors

Lukas Arenson, BGC Engineering, Canada
James Bockheim, University of Wisconsin, US
Julie Brigham-Grette, University of Massachusetts, US
Sherry Cady, Portland State University, US
Billy Connor, University of Alaska Fairbanks, US
Scott Dallimore, Geological Survey of Canada, CA
Claude Duguay, University of Waterloo, CA
Oliver Frauenfeld, University of Colorado, US
Hugh French, University of Ottawa, CA
Guido Grosse, University of Alaska Fairbanks, US
Stephan Gruber, University of Zurich, CH
Jennifer Harden, U.S. Geological Survey, US
Charles Harris, Cardiff University, UK
Christian Hauck, University of Karlsruhe, DE
Don Hayley, EBA Engineering Consultants, Ltd., CA
David Hik, University of Alberta, CA
Kenneth Hinkel, University of Cincinnati, USA
Hans-Wolfgang Hubberten, Alfred Wegener Institute, DE
Ole Humlum, University of Oslo, NO
Elden Johnson, Alyeska Pipeline Service Company, US
Torre Jorgenson, ABR Inc., US
John Kimble, Consulting Soil Scientist, US
Peter Kuhry, Stockholm University, SE
Philip Marsh, Environment Canada, CA
Chris McKay, NASA, US
James McNamara, Boise State University, US
Julian Murton, University of Sussex, UK
Frederick Nelson, University of Delaware, US
Mark Parsons, University of Colorado, US
Marcia Phillips, Swiss Federal Institute for Snow and Avalanche, CH
Volker Rachold, International Arctic Science Committee, SE
Vladimir Romanovsky, University of Alaska Fairbanks, US
Sharon Smith, Geological Survey of Canada, CA
Steve Solomon, Geological Survey of Canada, CA
Ted Vinson, Oregon State University, US
Daniel Vonder Mühll, ETH Zurich, CH
Patrick Webber, Michigan State University, US
John Zarling, Zarling Aero and Engineering, US

Reviewers

Clint Adler, Alaska DOT&PF, US
Thomas A. Ager, US Geological Survey, US
H. Jonas Akerman, Lund University, SE
Michel Allard, Université Laval, CA
Dale T. Andersen, NASA Ames, US
Lesleigh Anderson, US Geological Survey, US
Pat Anderson, University of Washington, US
Oleg A. Anisimov, State Hydrological Institute, RU
Lukas U. Arenson, BGC Engineering, CA
Arnold Arnoldusson, Norwegian Inst. of Land Inventory, NO
Valery Astakhov, National Research Inst. of Remote Sensing, RU
Tezera F. Azmatch, University of Alberta, CA
Megan Balks, University of Waikato, NZ
Andrew W. Balser, University of Alaska Fairbanks, US
Rene Barendregt, University of Lethbridge, CA
Brian Barnes, University of Alaska Fairbanks, US
David L. Barnes, University of Alaska Fairbanks, US
William Barr, University of Calgary, CA
Roger G. Barry, National Snow and Ice Data Center, US
Doug Benn, University Centre in Svalbard, NO
Bruce Bennett, Yukon Department of Environment, CA
Ivar Berthling, Norwegian University of Sci.and Tech., NO
Peter Blanken, University of Colorado, US
James Bockheim, University of Wisconsin, US
Xavier Bodin, University Paris/Joseph Fourier University, FR
Jan Boelhouwers, Uppsala University Uppsala, SE
Julia Boike, Alfred Wegener Institute, DE
W. Robert Bolton, Alfred Wegener Institute, DE
Christian Bommer, Swiss Fed. Inst. for Snow …, CH
Philip Bonnaventure, University of Ottawa, CA
Matthew T. Bray, University of Alaska Fairbanks, US
Alexander Brenning, University of Waterloo, CA
Gabriele Broll, University of Vechta, DE
Troy Brosten, Boise State University, US
Jerry Brown, International Permafrost Association, US
Bruce Brunette, Alaska DOT&PF, US
Margo M. Burgess, Geological Survey of Canada, CA
Christopher R. Burn, Carleton University, CA
Fabrice Calmels, University of Alberta, CA
Philip Camill, Carlton College, US
Iain B. Campbell, Land & Soil Consultancy Services, NZ
Sean K. Carey, Carleton University, CA
James W. Cassie, BGC Engineering Inc., CA
Beata Casto, University of Buffalo, US
Jessica E. Cherry, University of Alaska Fairbanks, US
Jens H. Christensen, Danish Meteorological Institute, DK
Hanne H. Christiansen, University Centre in Svalbard, NO
Evgenii Chuvilin, Moscow State University, RU
Graeme G.C. Claridge, Land & Soil Consultancy Services, NZ
Edwin S. Clark, Soils Alaska, US
Ian D. Clark, University of Ottawa, CA
Mark Clark, Natural Resources Conservation Service, US
Peter Cleall, University of Cardiff, UK
Gary D. Clow, US Geological Survey, US
Michael Cole, ABR Inc., US
Charles Collins, US Army, ERDC/CRREL, US

Jean Côté, Université Laval Québec, CA
Michelle Côté, Geological Survey of Canada, CA
Nicole Couture, McGill University, CA
Patrick Crill, Stockholm University, SE
Ronald P. Daanen, University of Alaska Fairbanks, US
Scott Dallimore, Geological Survey of Canada, CA
Debendra K. Das, University of Alaska Fairbanks, US
Simon Davies, Colorado School of Mines, US
Gregory P. De Pascale, William Lettis & Assoc. Inc., US
Reynald Delaloye, University of Fribourg, CH
Philip Deline, Université de Savoie, FR
Jack Dennett, EBA Engineering Consultants Ltd., CA
Alexander Derevyagin, Moscow State University, RU
Bernhard Diekmann, Alfred Wegener Institute, DE
Wojciech Dobinski, University of Silesia, PL
Yongtao Dong, University of Alaska Fairbanks, US
Guy Dore, Universite Laval, CA
D.S. Drozdov, Earth Cryosphere Institute, RU
Caroline Duchesne, Geological Survey of Canada, CA
Alejandra Duk-Rodkin, Geological Survey of, CA
Larry Dyke, Geological Survey of Canada, CA
Mark Ednie, Geological Survey of Canada, CA
Markus Egli, University of Zurich, CH
Olaf Eisen, Alfred Wegener Institute, DE
Wendy Eisner, University of Cincinnati, US
David Esch, Alaska DOT&PF (retired), US
Bernd Etzelmüller, University of Oslo, NO
Eugenie Euskirchen, University of Alaska Fairbanks, US
Zhaosheng Fan, University of Colorado, US
Herman Farbrot, University of Oslo, NO
Alexander N. Fedorov, Melnikov Permafrost Institute, RU
Michael G. Ferrick, US Army, ERDC/CRREL, US
Javier Fochesatto, International Arctic Research Center, US
Steven L. Forman, University of Illinois-Chicago, US
Daniel Fortier, University of Alaska Fairbanks, US
Richard Fortier, Université Laval, CA
Walter J. Fourie, University of Alaska Fairbanks, US
Pierre Francus, Inst. National de la Recherche Scientifique, CA
Oliver W. Frauenfeld, University of Colorado, US
Regula Frauenfelder, University of Oslo, NO
Barry M. Freifeld, Lawrence Berkeley National Laboratory, US
Hugh M. French, University of Ottawa, CA
Duane Froese, University of Alberta, CA
Rina Garcia, Stockholm University, SE
Gunther Ghysels, Ghent University, BE
I. Gidley, University of Calgary, CA
Robert E. Gieck, University of Alaska Fairbanks, US
Ted Goebel, Texas A&M University, US
Douglas J. Goering, University of Alaska Fairbanks, US
Jules M. Goldspiel, Cornell University, US
Michael Gooseff, Pennsylvania State University, US
Jacob Gorelik, Earth Cryosphere Inst. SB RAS, RU
Sergey Goryachkin, Geography Institute, Moscow, RU
Raoul Granger, National Hydrology Research Centre, CA
Mikhail N. Grigoriev, Permafrost Institute Yakutsk, RU
Guido Grosse, University of Alaska Fairbanks, US
Ed Grozic, EBA Engineering Consultants Ltd., CA
Jocelyn Grozic, University of Calgary, CA
Hansueli Gubler, AlpuG Davos, CH
Mauro Guglielmin, Insubria University Varese, IT
Steve D. Gurney, University of Reading, UK
Örjan Gustafsson, Stockholm University, SE
Spencer Guthrie, Brigham Young University, US
Wilfried Haeberli, University of Zurich, CH
Birgit Hagedorn, University of Alaska Anchorage, US
Tristram C. Hales, Cardiff University, UK
Svein-Erik Hamran, University of Oslo, NO
Chris Hanks, Alexco Resource Corp., US
Jennifer Harden, US Geological Survey, US
Charles Harris, University of Cardiff, UK
Robert N. Harris, Oregon State University, US
Stuart A. Harris, Calgary Alberta, CA
Bent Hasholt, University of Copenhagen, DK
Andreas Hasler, University of Zurich, CH
Steven Hastings, San Diego State University, US
C. Haththatowa, University of Calgary, CA
Christian Hauck, Karlsruhe Institute of Technology, DE
Helmut Hausmann, Technical University of Vienna, AT
Jennifer Heldmann, NASA Ames, US
Karen S. Henry, ERDC/CRREL, US
Rita Hermanns, Friedlipartner AG, CH
Thomas Herz, University of Giessen, DE
Ulrike Herzschuh, Alfred Wegener Institute, DE
Gloria Hicks, National Snow and Ice Data Center, US
Christin Hilbich, Friedrich-Schiller-Universität Jena, DE
Kenneth M. Hinkel, University of Cincinnati, US
Larry Hinzman, University of Alaska Fairbanks, US
Richard Hodgkins, Loughborough University, UK
Martin Hoelzle, University of Zurich, CH
Ed T. Hoeve, EBA Engineering Consultants Ltd., CA
Igor Holubec, I. Holubec Consulting Inc., CA
Anne Hormes, University Centre in Svalbard, NO
William T. Horne, EBA Engineering Consultants Ltd., CA
Hans-Wolfgang Hubberten, Alfred Wegener Institute, DE
Leroy Hulsey, University of Alaska Fairbanks, US
Ole Humlun, University of Oslo, NO
James Hunter, Geological Survey of Canada, CA
Atsushi Ikeda, University of Tsukuba, JP
Thomas Ingeman-Nielsen, Tech. University of Denmark, DK
Arne Instanes, Opticonsult Bergen, NO
Kenneth C. Irving, University of Alaska Fairbanks, US
Ketil Isaksen, Norwegian Meteorological Institute, NO
Mamoru Ishikawa, Hokkaido University, JP
Michel Jaboyedoff, University of Lausnne, CH
Matthias Jakob, BGC Engineering, CA
Richard Janowicz, Yukon Dept. of Environment, CA
Alexander Jarosch, University of British Columbia, CA
A. Jayasinghe, University of Calgary, CA
Margareta Johansson, Lund University, SE
Elden R. Johnson, Alyeska Pipeline Service Co., US
Ken Johnston, Earth Tech, CA
H. Jonas Akerman, Lund University, SE
Ben Jones, US Geological Survey, US
Kevin W. Jones, EBA Engineering Consultants Ltd., CA
Torre Jorgenson, ABR Inc., US
Håvard Juliussen, University Centre in Svalbard, NO
Andreas Kääb, University of Oslo, NO
Mikhail Kanevskiy, University of Alaska Fairbanks, US
Julian Kanigan, Indian and Northern Affairs, CA
Kumari Karunaratne, Carleton University, CA
Andreas Kellerer-Pirklbauer, University of Graz, AT
Martina Kern-Luetschg, Cardiff University, UK
Maureen Ketzler, US Forest Service, US
Alexander Kholodov, University of Alaska Fairbanks, US
John Kimble, Consulting Soil Scientist, US
Lorenz King, University of Giessen, DE

Kurt Kjær, University of Iceland, IS
Anna E. Klene, University of Montana, US
Michael Knapp, Alaska DOT&PF, US
Christof Kneisel Universität Würzburg, DE
Steven V. Kokelj, Indian and Northern Affairs, CA
Else Kolstrup, University of Uppsala, SE
Vladimir S. Kolunin, Earth Cryosphere Institute, RU
P.Y. Konstantinov, Melnikov Permafrost Institute, RU
Demitri Konyushkev, Docuchaev Soils Institute, RU
Michael Krautblatter, University of Bonn, DE
Thomas Krzewinski, Golder & Associates, US
Bernd Kulessa, Swansea University, UK
Anna N. Kurchatova, Tyumen State Oil and Gas University, RU
Denis Lacelle, Canadian Space Agency, CA
Branko Ladanyi, Polytechnique Montréal, CA
Christophe Lambiel, University of Lausanne, CH
Hugues Lantuit, Alfred Wegener Institute Potsdam, DE
David M. Lawrence, NCAR, US
Daniel Lawson, US Army, ERDC/CRREL, US
Marc Lebeau, Université Laval Québec QC, CA
Anne-Marie LeBlanc, Université Laval, CA
Jonah Lee, University of Alaska Fairbanks, US
Marina Leibman, Earth Cryosphere Institute, RU
Mathias Leopold, University of Jena, DE
David W. Leverington, Texas Tech University, US
Antoni Lewkowicz, University of Ottawa, CA
Xin Li, World Data Center for Glaciology Lanzhou, CN
Jenny Liu, University of Alaska Fairbanks, US
Shuhuang Liu, US Geological Survey, US
Jerónimo López-Martínez, University of Madrid, ES
Lorene A. Lynn, University of Alaska Fairbanks, US
Jacek Majorowicz, Northern Geothermal Consultants, CA
Galina Malkova, Russian Academy of Sciences, RU
Michael Manga, University of California Berkeley, US
Jan Mangerud, University of Bergen, NO
William F. Manley, University of Colorado, US
Gavin K. Manson, Natural Resources, CA
Sergei Marchenko, University of Alaska Fairbanks, US
Laurent Marescot, ETH Zuerich, CH
Margarita Marinonva, California Inst. of Technology, US
Philip Marsh, Nat. Hydrology Res. Centre Environment, CA
Irene Marzloff, Johann Wolfgang Goethe Univ., DE
Norikazu Matsuoka, University of Tsukuba, JP
Hansruedi Maurer, ETH Zurich, CH
Galina G. Mazhitova, Komi Science Centre, RU
William D. McCoy, Univ. of Massachusetts, US
Les McFadden, University of New Mexico, US
A. David McGuire, University of Alaska Fairbanks, US
Robert McHattie, Alaska DOT&PF (retired), US
Christopher McKay, NASA Ames Research Center, US
Fiona McLaughlin, Dept. of Fisheries and Oceans, CA
Malcolm McLeod, Landcare Research Hamilton, NZ
Nicola McLoughlin, University of Bergen, NO
Michael C. Metz, M.C. Metz Associates, US
Franz Meyer, Alaska Satellite Facility Fairbanks, US
Hanno Meyer, Alfred Wegener Institute, DE
Keith Meyer, Michael Baker Jr. Corp., US
Gary J. Michaelson, University of Alaska Fairbanks, US
Fred A. Michel, Carlton University Ottawa, CA
Nicole Mölders, University of Alaska Fairbanks, US
Jack D. Mollard, J.D. Mollard and Associates, CA
Dan Moore, University of British Columbia, CA
George Moridis, Lawrence Berkeley Laboratories, US
Thomas Moses, Alaska DOT&PF (retired), US
Michael Mungoven, USDA-NRCS, US
Julian B. Murton, University of Sussex, UK
Mark Musial, Golder Associates, US
Philippe Nater, GeoNum GmbH, CH
Frederick E. Nelson, University of Delaware, US
William G. Nelson, University of Alaska Anchorage, US
Heng Joo Ng, Schlumberger, CA
Derick Nixon, Nixon Geotech Ltd., CA
F. Mark Nixon, Geological Survey of Canada, CA
Jeannette Noetzli, University of Zurich, CH
Rune S. Ødegård, University of Gjovik, NO
Jonathan O'Donnell, University of Alaska Fairbanks, US
Stanislav Ogorodov, Moscow State University, RU
C. Ordonez, University of Calgary, CA
Kirk Osadetz, Geological Survey of Canada, CA
Thomas Osterkamp, University of Alaska Fairbanks, US
Jim M. Oswell, Naviq Consulting Inc., CA
Sam Outcalt, University of Michigan (retired), US
P. Paul Overduin, Alfred Wegener Institute, DE
Ron Paetzold, Geo-Watersheds Scientific, US
Michael Palmer, Indian and Northern Affairs, CA
Charles Paull, Monterey Bay Aquarium Research Inst., US
David Payer, US Fish and Wildlife Service, US
Rorik Peterson, University of Alaska Fairbanks, US
Richard Petrone, Wilfred Laurier University, CA
Eva-Maria Pfeiffer, University of Hamburg, DE
Marcia Phillips, Swiss Fed. Inst. for Snow …, CH
Ryan D. Phillips, C-CORE St John's Newfoundland, CA
Chien-Lu Ping, University of Alaska Fairbanks, US
Albert Pissart, Université de Liege, BE
Vladimir V. Pitulko, Inst. for History of Mat. Culture, RU
Lawrence J. Plug, Dalhousie University, CA
Stefan Pohl, Nat. Hydrology Res. Centre Environment, CA
Wayne Pollard, McGill University, CA
Olga Ponomareva, Earth Cryosphere Institute, RU
Anupma Prakash, University of Alaska Fairbanks, US
Jon Price, University of Waterloo, CA
William Quinton, Wilfred Laurier University, CA
Charles Racine, US Army, ERDC/CRREL (retired), US
Miguel Ramos, University of Alcala, ES
Gareth Rees, Scott Polar Research Institute, UK
J. Repelewska-Pękala, University of Maria Curie, PL
Anette Rinke, Alfred Wegener Institute, DE
Dan Riseborough, Geological Survey of Canada, CA
Armin Rist, Swiss Fed. Inst. for Snow …, CH
Stephen D. Robinson, St. Lawrence University, US
Isabelle Roer, University of Zurich, CH
Vladimir Romanovsky, University of Alaska Fairbanks, US
Bård Romstad, University of Oslo, NO
Vladislav Roujanski, EBA Engineering Consultants Ltd., CA
Stephan Saboundjain, Alaska DOT&PF, US
Torsten Sachs, Alfred Wagener Institute, DE
Kazuyuki Saito, University of Alaska Fairbanks, US
Michael Schirmer, Swiss Fed. Inst. for Snow …, CH
Lutz Schirrmeister, Alfred Wegener Institute, DE
Michael Schlegel, GeoEngineers Inc., US
Martin Schnebelli, Swiss Fed. Inst. for Snow …, CH
Edward A.G. Schuur, University of Florida, US
Georg Schwamborn, Alfred Wegner Institute, DE
Charles A. Schweger, University of Alberta, CA
Dmitry Sergeev, Institute of Environmental Geoscience, RU
Enrique Serrano, University of Valladolid, ES

Jack Seto, BGC Engineering Inc., CA
Natsagdorj Sharkhuu, Mongolian Academy of Sciences, MN
Nicolai I. Shiklomanov, University of Delaware, US
Yuri Shur, University of Alaska Fairbanks, US
Andrew G. Slater, University of Colorado, US
Lee Slater, Rutgers University, US
Chuck Slaughter, University of Idaho, US
Bruce Smith, Worley Parsons, CA
Orson P. Smith, University of Alaska Anchorage, US
Scott Smith, Research Branch Agriculture and Agri-Food, CA
Sharon Smith, Geological Survey of Canada, CA
Chris Spence, National Hydrology Research Centre, CA
Sarah M. Springman, ETH Zurich, CH
Blaire Steven, University of Wyoming, US
Christopher W. Stevens, University of Calgary, CA
De Anne Stevens, Alaska Dept. of Natural Resources, US
Marc Stiglitz, Georgia Institute of Technology, US
Vladimir Stolbovoy, Joint Research Centre of European …, IT
Dmity Streletskiy, University of Delaware, US
Robert Striegle, US Geological Survey, US
Tetsuo Sueyoshi, Hokkaido University, JP
Brad Sutter, NASA Ames Research Center, US
John Inge Svendssen, University of Bergen, NO
David Swanson, US Forest Service, US
Eors Szathmary, Eötvös Loránd University , HU
Pavel A. Tarasov, Free University of Berlin, DE
Charles Tarnocai, Agriculture and Agri-Food, CA
Rupert G. Tart, Golder Associates Ltd., US
Alan E. Taylor, ASL Environmental Sciences Inc., CA
Robert O. Taylor, Natural Resources, CA
Randi Thompson, BGC Engineering Inc., CA
Gennady S. Tipenko, Russian Academy of Sciences, RU
Horacio Toniolo, University of Alaska Fairbanks, US
J. Kenneth Torrance, University of Carleton, CA
Thomas P. Trainor, Univeristy of Alaska Fairbanks, US
Richard Trimble, EBA Engineering Consultants Ltd., CA
Dario Trombotto, Ianigla-Cricyt-Conicet, AR
Merritt R. Turetsky, Michigan State University, US
Craig Tweedie, University of Texas El Paso, US
William Ussler, Monterey Bay Aquarium Res. Inst., US
Jef Vandenberghe, Vrije Universiteit, NL
B. Van Vliet-Lanoë, Univ. Sciences et Tech. de Lille, FR
Yurij K. Vasilchuk, Moscow State University, RU
Alexander Vasiliev, Earth Cryosphere Institute, RU
Gonçalo Vieira, University of Lisbon, PT
Ted Vinson, Oregon State University, US
Jason G. Vogel, University of Florida, US
Daniel Vonder Mühll, ETH Zurich, CH
William Waite, US Geological Survey, US
Mark Waldrop, US Geological Survey, US
Donald Walker, University of Alaska Fairbanks, US
Katey Walter, University of Alaska Fairbanks, US
James Walters, University of Northern Iowa, US
B. Wang, Geological Survey of Canada, CA
KaiCun Wang, University of Maryland, US
Jeff Warburton, University of Durham, UK
Patrick J. Webber, Michigan State University, US
Matthias Wegmann, Institute of Safety and Security, CH
Malte Westerhaus, University of Karlsruhe, DE
Kimberly Wickland, US Geological Survey, US
Jacek Wierzchos, University of Lleida, ES
Cort J. Willmott, University of Delaware, US
William Winters, US Geological Survey, US
Stephen A. Wolfe, Geological Survey of Canada, CA
Ute Wollschlaeger, University of Heidelberg, DE
Ming-ko Woo, McMaster University, CA
Fred Wright, Geological Survey of Canada, CA
Yladimir Yakushev, VNIIGAZ, RU
Daqing Yang, University of Alaska Fairbanks, US
Edward Yarmak, Arctic Foundations, Inc., US
Shiqiang Ye, BC Hydro, CA
Kenji Yoshikawa, University of Alaska Fairbanks, US
Kathy Young, York University, CA
Dmitry Zamolodchikov, Ctr. for Ecol. and Prod. of Forests, RU
John P. Zarling, Zarling Aero and Engineering, US
Jay Zarnetske, Oregon State University, US
Aining Zhang, Natural Resources, CA
Gordon Zhang, EBA Engineering Consultants Ltd., CA
Tingjun Zhang, University of Colorado Boulder, US
Xiong Zhang, University of Alaska Fairbanks, US
Yu Zhang, Natural Resources, CA
Shu-ping, Zhao, CAREERI CAS, CN
Sergei Zimov, Northeast Science Station, RU
Jon E. Zufelt, US Army ERDC/CRREL, US

Experimental Research on Frost and Salt Heaving of Highway Foundation Soils in Seasonally Frozen Ground Regions in Gansu Province, Northwestern China

Guoyu Li
State Key Laboratory of Frozen Soil Engineering, CAREERI, Chinese Academy of Science, Lanzhou, Gansu 730000, China
Wenbing Yu
State Key Laboratory of Frozen Soil Engineering, CAREERI, Chinese Academy of Science, Lanzhou, Gansu 730000, China
Huijun Jin
State Key Laboratory of Frozen Soil Engineering, CAREERI, Chinese Academy of Science, Lanzhou, Gansu 730000, China
Yu Sheng
State Key Laboratory of Frozen Soil Engineering, CAREERI, Chinese Academy of Science, Lanzhou, Gansu 730000, China
Jilin Qi
State Key Laboratory of Frozen Soil Engineering, CAREERI, Chinese Academy of Science, Lanzhou, Gansu 730000, China
Lanzhi Lü
State Key Laboratory of Frozen Soil Engineering, CAREERI, Chinese Academy of Science, Lanzhou, Gansu 730000, China

Abstract

In the seasonally frozen ground regions in Gansu Province, Northwestern China, highway embankment and pavement have frequently been damaged due to the impacts of frost and salt heaving and thaw settlement, generally in the forms of pavement cracks and break-ups. Mechanisms and mitigative measures for these hazards have been puzzling geocryologists and road engineers. In this research repeated freeze-thaw experiments of saline soils sampled from the subgrade at highway segments with frequent and repeated damages, at periodically fluctuating temperatures, were conducted in order to investigate the relationship of freeze-thaw processes in saline foundation soils with the strengths and impacts of soil salinity on the stability of foundation soils. The experimental results showed that salinity and frost susceptibility had great impact on the deformation process in saline soils. The deformation of saline soil is accumulative within limited freeze-thaw cycles with sufficient water supply. Elevation of the embankment height, drainage, and salinity controls in subgrade and embankment fills were proposed to cost-effectively mitigate frost and salt heaving and subsequent thaw-weakening during highway design, construction, and maintenance periods in regions affected by seasonally frozen saline soils.

Keywords: frost action; frost heaving; highway foundations; saline soil; seasonally frozen ground; thaw-weakening.

Introduction

The area of salinized soils is 1.91 x 10^5 km^2, accounting for about 2.0% of the total land territory in China. It is distributed mainly in the arid, semi-arid, and cold regions. Gansu Province has a saline soil area of 1.16 x 10^4 km^2, one of the largest in China. The major centers for the distribution of saline soils, such as Dunhuang, Yumen, Jiuquan, Linze, Yongchang and Minqing, are located in the Hexi Corridor in Central and Western Gansu Province (Fig. 1) (Qiu et al. 1996, Xu et al. 1999). In addition, salts in the soil-water system can be partially crystallized and excluded, and migrate along the thermal, pressure, and moisture gradients.

Foundation soils can be significantly and differentially expanded from salt heaving, resulting in serious damages to roads and other buildings (Wu & Zhu, 2002). Studies on frost and salt heaving of saline soils have been intensively conducted both in laboratory tests and *in situ* observations in the field for many years. Xu et al. (1992) studied water and ion migration and its resultant deformation of soils in an experiment using the frozen Kaolin soil supplied with the NaCl solution. The result indicated that the deformation in the frozen Kaolin was mainly in the form of frost heaving. Qiu (1986) studied the processes of ion and water migration. He proposed that some ion types of salt for restraining frost heave. Fei et al. (1994) studied salt-heave characteristics of Xi'an Loess, and proposed that the salt-heave ratio was minimum for soils with 3% Na_2SO_4 and 1.8 g/cm^3 initial dry density. He further concluded that the salt heave of saline soil with Na_2SO_4 varied in a form of two parabolas with initial dry density and water content. Chen et al. (1988) suggested that the salt-heave ratio of silt with Na_2SO_4 changed exponentially with the cooling rate and the increasing overburden pressures. Xu et al. (1995, 1999) systemically studied frost and salt heave of soils, including changes of unfrozen water content, migration of moisture and ions, deformation due to salt heaving and its influencing factors, and coupled models for the prediction of frost and salt heaving. Wu & Zhu (2002) performed salt heave experiments of coarse-grained soil with Na_2SO_4 to analyze the processes of salt heave that affect the stability of building foundations. Results showed that the coarse-grained soil with a salt concentration layer could result in abrupt salt heaving that damaged engineering infrastructures. Liu et al. (2005)

Figure 1. Map of Gansu Province with main areas mentioned in paper.

carried out some experiments using soils with sulphates to measure the salt heave force and rate under a single factor and to study heave mechanisms. Other researchers mainly studied properties such as strength and deformation of saline soils, (Ogata et al. 1982, Sego et al. 1982), frost heave of saline soils (Chamberlian, 1983), the effect of salt enrichment on unfrozen water (Banin & Anderson, 1974), and water and ion migration in an open system (Ershov et al. 1989, 1991). In this paper, freeze-thaw experiments of typical soils, taken from the subgrade of highways where damages frequently occurred, have been conducted to study the characteristics of deformation processes due to the salt and frost heave and subsequent thaw weakening and settlement in Gansu Province. On the basis of this experimental study, some mitigative measures had been proposed to improve the stability of embankment and pavement soils in saline soil regions.

Experimental Process

Specimens for laboratory testing

Four soil specimens were studied in repeated freeze-thaw experiments in order to study deformation characteristics and processes caused by frost heave, salt expansion, and subsequent thaw settlement and weakening.

After careful field investigations on the damages of highway foundation soils in Gansu Province, northwestern China, three specimens of saline soils were sampled from road sections with severe damage in the embankment and pavement due to salt and frost heave. Sample No. 1 of silt was taken in Gaotai County along National Highway No. 109 (Fig. 1). Its field water content was 23.10% and salinity was very high. Salt crystals could be observed clearly. Numerous longitudinal and transverse cracks were found on the pavement where the specimen was taken. Sample No. 2 of silty clay was taken between Jiuquan to Jinta along National Highway No. 214. The climate is more arid in the area of Sample No. 2. The field water content was 5.18%. Sample No. 3 of fine silty sand was taken from the toe of the right side protection slope of National Highway No. 214 in the proximity of Jinta County, where visible white salt crystals occur on the adjacent ground surface. Field water content was 9.53%. In addition, another soil specimen, Sample No. 4 of clay, was obtained in the middle of the Maqü to Luqü section along National Highway No. 213, at an elevation of about 3500 m and with a cold climate. It was tested as a reference specimen because of very low salinity (Table 1).

The basic parameters, such as liquid and plastic limits, plastic index, and salinity, of the four specimens were measured in the State Key Laboratory of Frozen Soil Engineering, CAREERI, Chinese Academy of Science (Table 1). The ions in the tested saline soils mainly include Cl^-, NO^{3-}, SO_4^{2-}, Na^+, Ca^{2+}, Mg^{2+}, K^+.

Table 1. Liquid and plastic limits, plastic index, and salinity of three saline soil specimens and the reference sample.

Sample	Liquid limit (%)	Plastic limit (%)	Plastic index	Salinity (%)
No. 1	21.1	13.8	7.3	9.1
No. 2	27.9	17.9	10	2.79
No. 3	19.9	10.3	6.6	6.14
No. 4	28.2	19.1	15	0.15

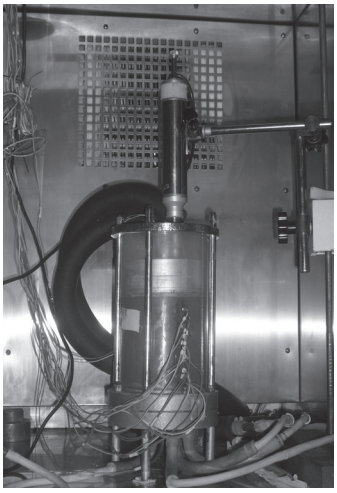

(a)

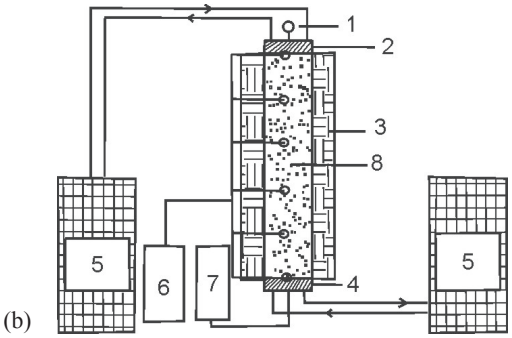

(b)

Figure 2. Diagram of experimental system for freeze-thaw testing of saline and reference soil specimens. Notes: (a) Photo of freeze-thaw experiment system; and (b) Simplified model of components in the experiment system. 1-Deformation sensor, 2-Top plate, 3-Insulation layer, 4-Bottom plate, 5-Cooling bath, 6-Temperature sensors, 7-Water supply, and 8-Testing sample.

Sample preparation

Soil samples taken and sealed in the field were placed in polymethyl methacrylate tubes, layer by layer, and compacted to a certain density. Soils were converted to testing specimens. Cylinder specimens were 100 mm high with a diameter of 101 mm. They were consolidated for 24 hours at room temperature for uniform moisture distribution. Then the repeated freeze-thaw tests were carried out.

Laboratory equipment

Laboratory equipment for performing repeated freeze-thaw tests on the four soil specimens was developed by the State Key Laboratory of Frozen Soils Engineering (Fig. 2).

The polymethyl methacrylate tube was filled with a soil specimen. The temperatures at the top and bottom plates were controlled by cooling baths. The temperature at the bottom plate remained at +1°C. The exterior of the tube was insulated. The experiment system was put into an insulated box with a constant temperature at +1°C.

Every 30 minutes, the temperature at each vertical interval of 10 cm in the tested soil columns was measured by thermal-susceptible resistance sensors with a precision of ±0.2°C. The deformation in the soil columns was measured by a deformation sensor with a precision of ±0.01mm at the top of the soil columns. The temperature at the top plate varied according to a sinusoidal function as follows:

$$T = -2.5 + 7.5\sin(\frac{2\pi}{72}t) \quad (1)$$

Water was sucked up into the soil columns through the bottom plate due to the temperature difference. A freeze-thaw cycle is 72 hours. Saline soil Sample Nos. 1, 2, and 3 experienced three freeze-thaw cycles. Sample 4 was subject to only one freeze-thaw cycle because it had low salinity, and the frost susceptibility was measured and used as a reference. The temperatures at different depths, and deformation of soil samples were measured and recorded automatically when the freeze-thaw experiments were carried out.

Results and Discussions

The test results for Sample No. 1 indicate that the deformation at the top plate increased at a sinusoidal variation of the top plate temperatures with the elapse of time (Fig. 3). The temperature at the top plate was negative, and the upper part of the soil sample was frozen at the beginning of the experiment. The relevant deformation had a quickly increasing trend during the first several hours. Then the deformation increased slowly until about 30 hours had elapsed, when the temperature at top plate was positive. Subsequently, the heave rate of the soil sample increased more pronouncedly when the temperature at the top plate became negative again. In addition, when the temperature at the top plate was in the range of 0°C to 2°C, the heave rate of the soil sample was still reasonably high, due to the salt heaving. No thaw settlement was observed during the entire deformation process, due to the high salinity of the soil sample. From the above analyses and discussions, it can be concluded that the deformation of Sample No. 1 mainly included frost and salt heaving.

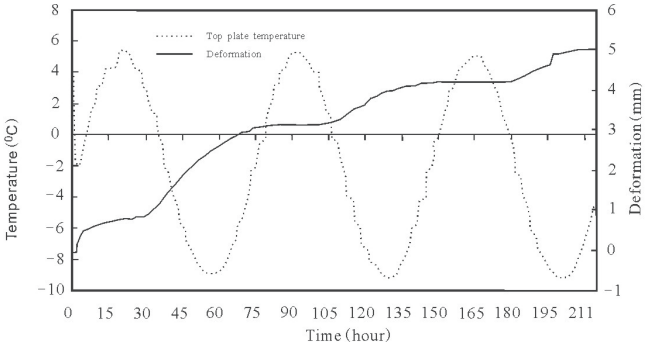

Figure 3. Temperature and the deformation processes of Sample 1

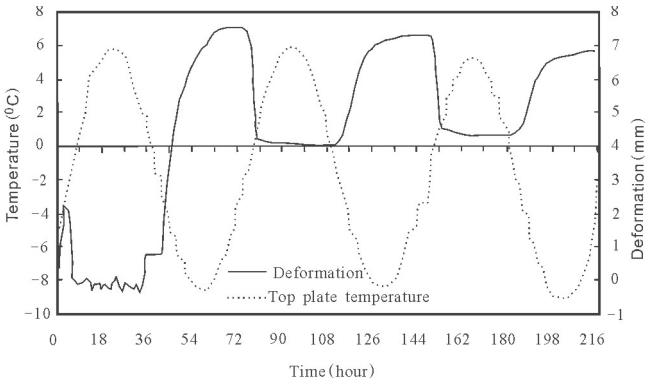

Figure 4. Temperature and the deformation processes of Sample 2.

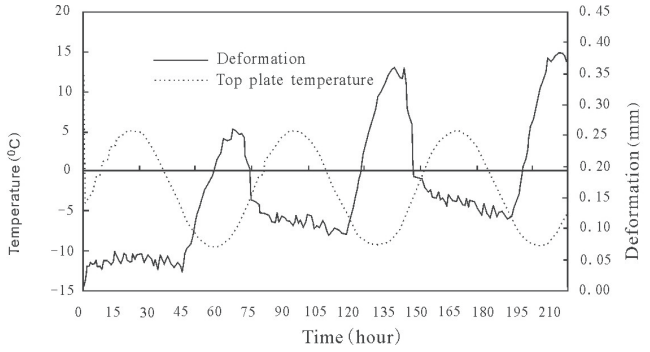

Figure 5. Temperature and the deformation processes of Sample 3

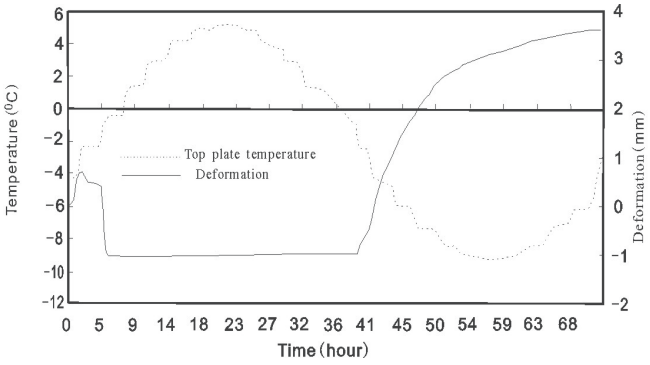

Figure 6. Temperature and the deformation processes of Sample 4.

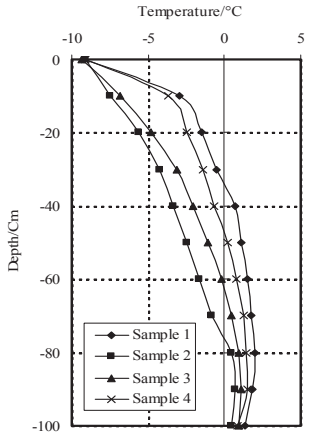

Figure 7. Temperature distribution curves in the tested soil columns when the top plate temperature reached -10°C, the minimum in the experiment.

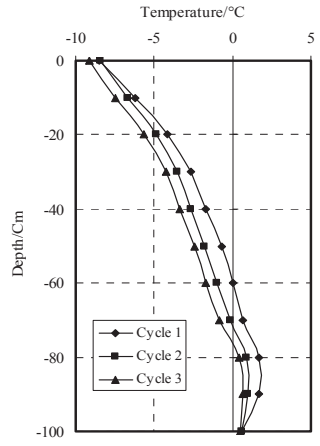

Figure 8. Temperature distribution curves of Sample No. 2 when the top plate temperature reached the minimum in different cycles.

Figure 4 is a diagram of the variation processes of the temperature and deformation at the top plate of Sample 2. The deformation of the soil sample gradually increased at the beginning when the temperature at the top plate was negative. A sudden decline of deformation of the soil sample occurred when the temperature at the top plate became positive, which mainly resulted from thaw settlement of the upper thawed soil. Slowly, the deformation kept almost steady, with only a slight decrease during the above-zero-temperature period. Subsequently, the deformation began to increase sharply when the temperature at the top plate was 2°C. It showed that salt heaving probably occurred. The deformation continued to rise sharply with the temperature becoming subzero and dropping continually. Meanwhile, it can be noted that the deformation was almost constant in the first few hours when temperatures dropped from 0°C to -2°C. That happened at each cycle. This indicates that there is a lag of deformation before cooling, due to insufficient time for deformation to occur. In the second cycle, the characteristics of the deformation process are similar to that of the first cycle. But the minimum amount of deformation of the soil sample corresponding to the positive temperature at the top plate was greater than that in the first cycle. It demonstrated

Table 2. Experimental results of four tested soil specimens.

Sample	Soil type	Salinity (%)	Deform-ation(mm)	Frozen depth(cm)	Water Uptake (ml)
No. 1	Silt	9.1	5	34	118
No. 2	Silty clay	2.79	7	76	89
No. 3	Silty sand	6.14	0.38	60	64
No. 4	Clay	0.15	3.6	47	45

that the deformation does not return to the initial position. There was a surplus heave deformation in Sample 2. The salt heave was not clear in the 2nd and 3rd cycles, probably because of a lack of salt after precipitation in the 1st cycle. From the above analyses and discussions, it can be seen that the deformation of Sample 2 was caused by frost heaving and thaw settlement, with possible salt heaving.

Figure 5 shows the variation processes of the temperature and the deformation at the top plate of Sample 3. The deformation of the soil sample began to increase when the temperature at the top plate was negative at the beginning. It was not clearer compared to that of Sample 2 (Fig. 4). When the top plate temperature became positive, the deformation was almost constant, with slight see-sawing decreases due to soil consolidation. When the temperature at the top plate decreased from a positive temperature to about -4.3°C, the deformation began to rise immediately and sharply. This showed that there was a longer lag of deformation compared to the temperature at the top plate, probably due to a high salinity (6.14%) and the soil type (silty sand), which are not favorable to soil freezing. Later, sudden settlement occurred in Sample 3 when the temperature increased to about -4.0°C. But it was still larger than that in the first cycle. This showed that the entire deformation was accumulative but smaller than Sample Nos. 1 and 2. It was difficult to determine the salt heave during the period of soil heave in Sample No. 3. So its deformation was mainly caused by frost heaving and thaw settlement, with possible salt heave, but the heave amount was smaller..

Sample No. 4, with low salinity, was tested for its frost-susceptibility. The deformation of the soil sample increased when the temperature at the top plate became negative at the beginning (Fig. 6). When the temperature reached the proximity of 0°C, sudden settlement of the soil sample occurred due to the thaw settlement of the upper part of the soil column. During the positive-temperature period at the top plate, the deformation kept stable. When the temperature decreased to about -0.6°C, the soil began to heave rapidly, until the temperature reached almost the minimum value of -9°C; then the increase of deformation slowed. However, even when the temperature rose within the subzero period, the frost heaving was still growing. This well confirmed that Sample No. 4 is a typical frost-susceptible soil.

Figure 7 shows the temperature distribution curves of the tested soil columns when the top plate temperature reached the minimum of -10°C during the 3rd cycle, except for Sample No. 4 in the 1st cycle. The frozen depth in Sample No. 2 was

the maximum, while that of Sample No. 1 was the minimum. Sample No. 4, though subject to one freeze-thaw cycle, was frozen more deeply than Sample No. 1. Generally, the frozen depth in silty sand is greater than that in silty clay because of its greater thermal conductivity (Xu et al. 2001), but that in Sample No. 3 of silty sand was less than that in Sample No. 2. This indicates that salinity can effectively retard cold wave propagation.

Figure 8 shows the temperature distribution curves of Sample No. 2, as an example, when the top plate temperature reached the minimum of -10°C in different cycles. Note that the frozen depth rises with the increasing number of freeze-thaw cycles. The variation process of the frozen depth in Sample Nos. 1 and 3 is similar to that in Sample No. 2.

According to the above analyses and discussions based on the experimental results for four tested specimens, heave deformation is mainly influenced by soil type, salinity, freeze-thaw cycle numbers, and others. The heave deformation in Sample No. 2 of silty clay, with moderate salinity, is the maximum (Table 2). However, the heave deformation in Sample No. 3 of silty sand, with the greater salinity, is the minimum. Sample No. 4 expands to a higher level even after one cycle. The heave deformation in Sample No. 1, with the highest salinity, reached a higher level, and without thaw settlement. It can also be found that there are the different threshold values in salinity and freeze-thaw cycle for the different saline soils to lead to salt heave and salt hazards. To determine the threshold values need further investigations in detail.

Conclusions and Recommendations

According to the experiment results, analyses, and discussions mentioned above the following preliminary conclusions can be made:

(1) The deformation of saline soil is accumulative within limited freeze-thaw cycles with sufficient water supply, i.e., the minimum deformation increases gradually with the increasing number of freeze-thaw cycles.

(2) Salinity has great impact on the deformation process of saline soil. The deformation of soil with very high salinity was mainly caused by frost and salt heaving, without thaw settlement.

(3) Frost susceptibility strongly influences the deformation processes of saline soil. The heave deformation of non-frost susceptible saline soil, even with the higher salinity, is small.

(4) To determine the occurrence of salt heave is difficult for ordinal soils with moderate salinity because it happens together with frost heave.

(5) The heave deformation in saline soils is mainly influenced by soil type, salinity, freeze-thaw cycle number, water supply, and others. It is a complicated process with water, heat, and salt transfer subject to the repeated freeze-thaw cycles.

(6) Therefore, elevation of the embankment height from ground water table or surface standing water levels, subgrade and local drainage control, and stricter control of salinity of fills could be used to effectively mitigate frost and salt heaving, and subsequent thaw settlement and weakening for the design, construction, and maintenance of highway foundations in areas affected by saline soil.

Acknowledgments

This work was supported by the Chinese Academy of Sciences Knowledge Innovation Key Directional Project "Mechanisms and mitigation of frost heaving and thaw settlement of pipeline foundation soils in permafrost regions" (Grant No. KZCX2-YW-311), National Science Foundation of China Projects (Nos. 40401010, 40471023, and 40640420072), the Chinese Academy of Sciences 100 Talents Programs "Stability of linear engineering foundation in warm permafrost regions under a change climate" and "Deformation and stability of roadbed in permafrost regions", and the Open Fund of the State Key Laboratory of Frozen Soils Engineering (Grant No. SKLFSE200702). Generous assistance from the NICOP editors and reviewers is greatly appreciated and thus acknowledged.

References

Banin, A. & Anderson, D.M. 1974. Effects of salt concentration during freezing on the unfrozen content of porous materials. *Water Resources Research* 10(1): 124-128.

Chamberlaine, E.J. 1983. Frost heave of saline soils. *Proceedings of 4th International Conference on Permafrost*, 121-126.

Chen, X., Qiu, G. & Wang, Y. 1988. On salt heave of saline soil. *Proceedings of 5th International Symposium on Ground Freezing*, 35-39 (in Chinese).

Ershov, E.D., et al. 1989. Deformation of frozen soil under the action of solution. In: *Collections of Geocryological Study*. Moscow: Moscow University Publishing House, 202-210.

Ershov, E.D., Lebedenko, Yu.P. & Xu, X. 1991. Water and ion migration of frozen soil in open system. *Proceedings of 6th International Symposium on Ground Freezing*, 17-24.

Fei, X., Li, B. & Wang, J. 1994. Salt expansion law of different dried unit weight for sulphate salty soil. *Journal of Glaciology and Geocryology* 16(3): 245-251 (in Chinese).

Liu, P., Wang, J., Jiang, J. & Wang, C. 2005. Experimental researches and analysis of expansion characteristics of sulphate salty soil. *Journal of Jilin University (Earth Science Edition)* 35(1): 74-78.

Ogata, N., Yasuta, M. & Kataoka, T. 1982. Salt concentration effects on strength of frozen soils. *Proceedings of 3rd International Symposium on Ground Freezing*, 3-10.

Qiu, G. 1986. Ion and water migration and frost heave of Morin clay during freezing. *Journal of Glaciology and Geocryology* 8(1): 1-14 (in Chinese).

Qiu, G., Zhao, L., Wang, S., Zhang, X., Sheng, W., Yue, H. & Jin, H. 1996. *The Seasonally Freezing Halic Soils and Their Improvement-utilization in the Hexi Corridor, Gansu, China*. Laznhou, China: Lanzhou University Press, 1-115 (in Chinese with an extended English abstract).

Sego, D.C., Schultz, T. & Banasch, R. 1982. Strength and deformation behavior of frozen sand with a saline pore fluid. *Proceedings of 3rd International Symposium on Ground Freezing*, 11-18.

Wu, Q. & Zhu, Y. 2002. Experimental studies on salt expansion for coarse grain soil under constant temperature. *Cold Regions Science and Technology* 34(2): 59-65.

Xu, X., Lebedenko, Yu.P., Chuvilin, E.M., Kliuchikov & K. Yu. 1992. Experimental study on processes of heat-mass transfer and deformation in system of frozen Kaolin and salt solution. *Journal of Glaciology and Geocryology* 14(4): 289-295 (in Chinese).

Xu, X., Wang, J., Zhang, L., Deng, Y. & Tao, Z. 1995. *Mechanisms of Frost Heaving and Salt Expansion of Soils*. Beijing: Science Press, 1-126 (in Chinese).

Xu, X., Wang, J., Zhang, L. & Deng, Y. 1999. *Mechanisms of Frost Heave and Salt Expansion of Soils*. Beijing & New York: Science Press.

Xu, X., Wang, J. & Zhang, L. 2001. *Frozen Soil Physics*. Beijing: Science Press, 77-91.

The Effect of the Global Radiation Budget on Seasonal Frozen Depth in the Tibetan Plateau

Ren Li
Cold and Arid Regions Environmental and Engineering Research Institute, Chinese Academy of Sciences, 320 Donggang West Road, LanZhou 730000, China

Lin Zhao
Cold and Arid Regions Environmental and Engineering Research Institute, Chinese Academy of Sciences, 320 Donggang West Road, LanZhou 730000, China

Yongjian Ding
Cold and Arid Regions Environmental and Engineering Research Institute, Chinese Academy of Sciences, 320 Donggang West Road, LanZhou 730000, China

Abstract

In this study, monthly average daily global radiation of 22 radiometric stations across the Tibetan Plateau were utilized to determine the coefficients of the monthly Angström–Prescott model for estimating global solar radiation from sunshine duration. Using the model, global solar radiation of another 116 meteorological stations across the Tibetan Plateau were estimated. Combined with frozen ground data measurement at 75 stations, global radiation effects on the maximum frozen depth of the active layer were discussed. The result showed that global radiation in the cold season (from October to February the next year) had much influence on maximum frozen depth of the active layer. The relationship between them in three typical stations showed a marked negative correlation. As a whole, the maximum frozen depth of the active layer in nearly 80% of investigation stations had the same relationship with the global solar radiation, while the others showed a positive correlation. This indicated that the maximum frozen depth of the active layer was the result of combined effects of several factors other than global radiation. Of these influencing factors, such as global solar radiation, local latitude, longitude, altitude, air temperature in cold season, relative humidity, accumulation of precipitation in cold season, etc., only local latitude, altitude, global solar radiation, and air temperature showed high correlation with frozen depth. Essentially, the influences of local latitude and altitude can be regarded as the effects of global radiation indirectly. As the local latitude and altitude influenced the distribution of global radiation, so the global radiation was an important affecting factor on the maximum frozen depth of the active layer.

Keywords: active layer depth; global radiation; relative sunshine duration; Tibetan Plateau.

Introduction

Solar radiation is a main source of the Earth's energy and the basic driving force of the physical and biological processes on the earth surface. The processes respond to the seasonal variations in solar radiation fluxes in a complex manner. The distribution of solar radiation around the world determines the planet's mean climate variation resulting from the thermal balance of the Earth–atmosphere system, and establishes atmospheric and oceanic circulation patterns (Souza, et al. 2005). Topographic conditions effect the distribution of solar radiation.

As for China, its regional topography is complex and its surface condition is varied. This is especially conspicuous in the Qinghai-Tibetan Plateau (TP) with higher altitude and complex terrain. The TP is one of the most complex geographical features in the world, with an average elevation about 4 km or more. Such land surface features make much difference in solar radiation among different regions across the TP and result in unequal surface heating by solar radiation (Ye & Gao 1979). Non-uniform distribution of solar energy on the land surface has much effect on climate over the TP and its surrounding area, and even on the global climate. In addition, the TP, which is a huge land mass standing in the mid-altitude troposphere with high altitude and complex terrain, lies in the transition zone between the tropical and sub-tropical and also in the heart zone of the famous monsoon region in the Northern Hemisphere; its dramatic heating and its strong continental strongly impact the Asian monsoon, global atmospheric circulation and global climate change (Ye & Gao 1979, Tao et al. 1999).

Moreover, the distribution of solar radiation across the TP has a decisive effect on a decision on the characteristics of plateau glaciers, permafrost, and vegetation distribution.

Furthermore, due to its unique geographic environment, the TP developed a large area of permafrost, which is the result of the climate change, and it also has feedback effect on climate. As an important component of cryosphere, which is an important driving force of global change and a connection for interaction of other layers in the climatic system, the presence and changes of the permafrost can affect the energy and water exchanges of the land-atmosphere system and further affect the formation and development

of regional climate (Yao et al. 2002, Zhang 2002). The active layer at the upper part of the permafrost is thawed in summer and frozen in winter. Permafrost changes, leading to changes in water and heat exchange characteristics between land and atmosphere, first by changing the water-heat states of the active layer, thereby causing changes and anomaly of the atmospheric circulation system (Wang et al. 2003), then affecting the weather system. Changes of the maximum frozen depth of the active layer are key indicators of climatic warming (Pavolv 1994). Thus, the maximum frozen depth of the active layer has a close relation with the climate.

As a product of climate change, features of permafrost are by the impacts of climate change, and global radiation in the TP is an important influencing factor on Plateau climate. Global radiation is the major source of ground heat in the TP. Fluctuations in global radiation will cause a corresponding impact to permafrost and its active layer (Kou et al. 1981). Study of the relationship between global radiation and frozen/thawed depth of the active layer do much to help us better understand the impact mechanism of the permafrost and its active layer. Relevant research work has been launched in the TP region and has achieved some results. In the early 1980s, Kou et al. (1981) studied the relationship between global radiation and the thawed depth of the active layer using the data measured at Fenghoushan at the TP. In their view, thawed depth of the active layer in the permafrost region was caused by solar radiant heat arriving at the surface and down into the ground, and the statistical relationship between them was established. The studies of Cheng et al. (1983, 1984, 1992) showed that the characteristics of the surface solar radiation latitudinal variation were important reasons for the permafrost zone. The variation of global radiation determined the annual mean temperature at the bottom of the freezing and thawing depth of the active layer (Zhou et al. 2000). Ding et al. (2000) discussed the relationship between the accumulative soil temperature at 4 cm depth below the surface and the freezing/thawing depth of the active layer of the TP. Research showed that the formation of permafrost and seasonal permafrost had a relationship with surface radiation-heat exchange. The structure of the radiation-heat balance had a decisive role in the formation and dynamics of frozen ground. The surface energy budget and the changing of the surface-air temperature were decided by the net radiation, which depends mostly on global radiation, surface condition, and net long-wave radiation (Zhou et al. 2000).

Those works mentioned above provided a basis for the mechanism research of permafrost in the TP; however, restricted by natural condition and outlay, those studies were only based on a single site and with a short-term dataset (Zhou et al. 2000). The work was small considering the large-scale and long-term dataset of the TP. For the whole TP, further works need to be done.

In this work, global radiation was estimated across the TP; its influence on the maximum frozen depth of the active layer was discussed. By multiple regression analysis method, several effect factors for the maximum frozen depth of the active layer were analyzed too.

Material and Method

Data used in this paper include frozen depth, global solar radiation, monthly accumulative precipitation, monthly average and extreme air temperatures, relative humidity, and relative sunshine duration. Frozen depth data in the cold season were collected in 75 meteorological stations from 1961–1998. Datasets of precipitation, monthly average air temperature and extreme temperatures, relative humidity, and relative sunshine duration were collected in 138 stations in the TP and its adjacent regions. These data were measured by corresponding observation criteria.

As for radiant data, there were only 22 radiometric stations in the TP and its adjacent regions; other meteorological stations are without radiation measurements, so global radiations in those stations was estimated. The AngstrÖm–Prescott model (APM) is the most convenient and widely used correlation for estimating global solar radiation (Liu & Ji 1985, Chegaar & Chibani 2001, Almorox & Hontoria 2004, Almorox et al. 2005), which is expressed by

$$Q / I_0 = a + bS_1 \tag{1}$$

where Q and I_0 are, respectively, the monthly mean daily global radiation (MJ.m-2.d-1) and daily extraterrestrial radiation on a horizontal surface (MJ.m-2.d-1); S_1 is relative duration of sunshine (the ratio between the number of hours of sunshine duration to the total number of daylight hours); a and b are empirically coefficients. Using the measured data of monthly average daily global solar radiation on horizontal surfaces and sunshine hours from 22 radiometric stations across the TP, as given in Table 1, coefficients a and b can be determined by the method of least squares. As a result, the APM over the TP can be written as (Li, et al. 2007):

$$Q / I_0 = 0.213 + 0.5691 S_1 \tag{2}$$

The performance of APM was evaluated by calculating the following statistical error test such as mean bias error (MBE), mean absolute error (MAE), root mean square error (RMSE), and mean relative error (MRE). These tests are fundamental measures of accuracy (Driesse & Thevenard 2002, Almorox & Hontoria 2004, El-Metwally 2004, Almorox et al. 2005, Tymvios & Jacovides 2005, Menges et al. 2006, Bulut & Büyükalaca 2007). They are defined as below:

$$MBE = \frac{1}{n}\sum_{i=1}^{n}\left(Q_{i,obs} - Q_{i,est}\right) \tag{3}$$

$$MAE = \frac{1}{n}\sum_{i=1}^{n}\left|Q_{i,obs} - Q_{i,est}\right| \tag{4}$$

$$RMSE = \sqrt{\frac{1}{n}\sum_{i=1}^{n}\left(Q_{i,obs} - Q_{i,est}\right)^2} \tag{5}$$

$$MRE = \frac{1}{n}\sum_{i=1}^{n}\left|\frac{Q_{i,obs} - Q_{i,est}}{Q_{i,obs}}\right| \quad (6)$$

The indexes (obs) and (est) identify observed and estimated values, respectively. Results of the APM, applied to the whole dataset available with 7400 samples from 22 radiometric stations across the TP, are illustrated in Figure 1. It can be seen from Figure 1 that the scattering of the data points was small. And the values of MBE, MAE, RMSE for the whole dataset result in -0.06, 1.22, 1.64 MJ.m-2.d-1, respectively. The value of MRE is 7.6%. Such results indicate that the agreement between the measured and estimated values is marked. It demonstrates that APM was acceptable for estimating monthly global solar radiation from relative sunshine duration over the TP. With Equation 2, the monthly average daily global radiation on a horizontal surface (Q) in MJ.m-2.d-1 from January 1961 to December 2000 at 116 meteorological stations can be estimated. Finally, its monthly total can be obtained too.

For convenience of analysis, the statistical variable, accumulative anomaly for Q and FD is introduced. It is defined as

$$x_j = \sum_{i=1}^{j}\left(x_i - \bar{x}\right) \qquad (j \le n) \quad (7)$$

where x_j is the accumulative anomaly value of Q or FD from first year to the j year, $\bar{x}$ is the average value of the whole dataset, and n is the length of the dataset.

Results and Discussion

EOF (Empirical Orthogonal Function) analysis results showed that Yushu (33°01′N, 97°01′E, 3682.2 m), Lenghu (38°45′N, 93°20′E, 2770.0 m) and Delingha (37°22′N, 97°22′E, 2982.4 m) were typical sites (Xu, et al. 1990, Wang et al. 2003), so the influence of global radiation on the maximum frozen depth of the active layer in these three typical sites is discussed at first.

Figure 2 shows the influences of the accumulative anomalies of global radiation on the maximum frozen depth of the active layer in three typical stations at the TP. It can

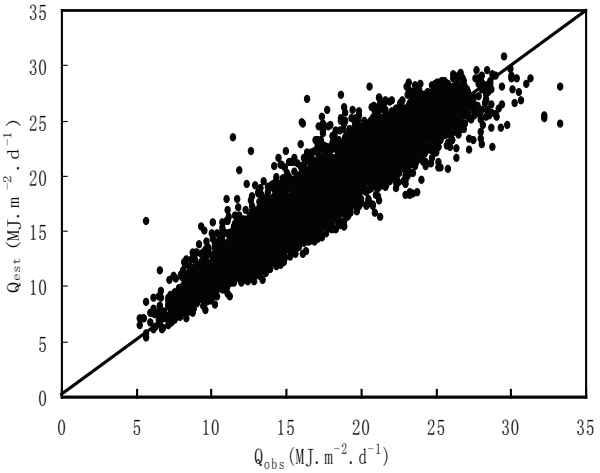

Figure 1. Results comparison between Q_{est} and Q_{obs} on the TP.

Table 1. Geographical location, annual mean air temperature (Ta) and period of the radiometric station used in regression analysis.

station	Latitude (N)	Longitude (E)	Altitude(m) (above sea level)	Ta(°C)	period
Kuche	41° 43′	83° 04′	1072.5	11.3	Jul 1957-2000
Ruojiang	39° 02′	88° 10′	888.3	11.6	Jun 1957-2000
Hetian	37° 08′	79° 56′	1374.5	12.4	Jun 1957-2000
Kashi	39° 28′	75° 59′	1288.7	11.8	Jul. 1957-2000
Erjina	41° 57′	101° 04′	940.5	8.7	1992-2000
Gangcha	37° 20′	100° 08′	3301.5	-0.4	1993-2000
Gerlmod	36° 25′	94° 54′	2807.6	4.9	Jul 1957-2000
Xining	36° 43′	101° 45′	2295.2	5.9	1959-2000
Yushu	33° 01′	97° 01′	3681.2	3.0	Apr1960-2000*
Guole	34° 28′	100° 15′	3719.0	-0.4	1993-2000
Dunhuang	40° 09′	94° 41′	1139.0	9.3	Jul 1957-2000
Jiuquan	39° 46′	98°29′	1477.2	7.2	1993-2000
Minqin	38° 38′	103° 05′	1367.0	7.3	1961-2000
Garze	31° 37′	100° 00′	4414.9	5.6	1994-2000
Hongyuan	32° 48′	102° 33′	3492.7	1.3	1994-2000
Panzhihua	26° 35′	101° 44′	1190.1	20.8	1992-2000
Changdu	31° 09′	97° 10′	3306.0	7.5	1961-2000*
Naqu	31° 29′	92° 04′	4507.0	-1.4	1961-2000*
Lahsa	29° 40′	91° 08′	3648.7	7.9	1961-2000*
Lijiang	26° 52′	100° 13′	2392.4	12.6	1961-2000*
Kunming	25° 01′	102°41′	1891.4	14.8	1961-2000
Tengchong	25° 01′	98° 30′	1654.6	14.9	1961-2000

* some missing in dataset.

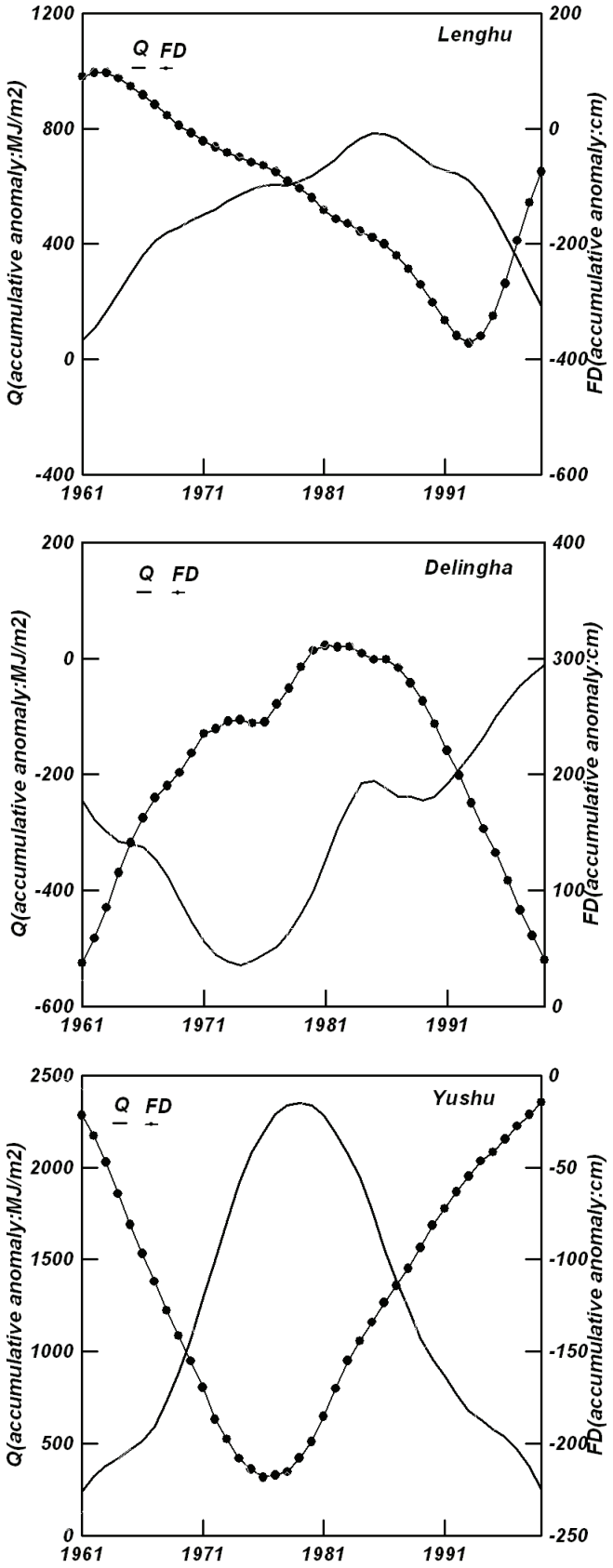

Figure 2. The influences of global radiation in three typical stations on the maximum frozen depth of the active layer.

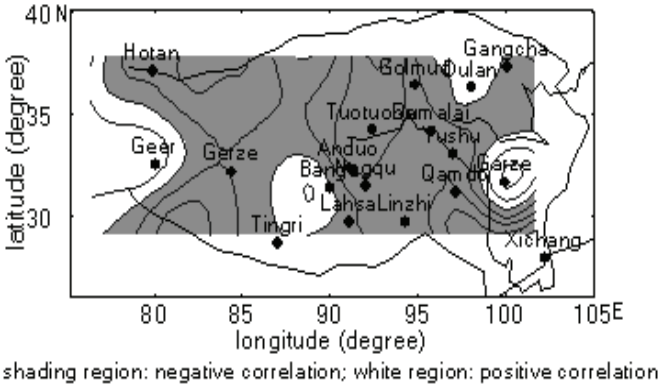

Figure 3. Distribution of the correlativity between global radiation and the maximum frozen depth of the active layer.

be seen from Figure 2 that the accumulative global radiation (Q) in cold season (from October to February of the next year) had much influence on FD. The relationship between them in three typical stations showed a marked negative correlation. How about the other stations across the TP? The relationships between global radiation and maximum frozen depth of the active layer in cold season across the TP for another 72 stations were also analyzed too. The results are illustrated in Figure 3.

Figure 3 shows the distribution of the correlativity between global radiation and maximum frozen depth of the active layer. In Figure 3, the shaded part stands for the negative correlation region, while the white part stands for the positive correlation region. As a whole, the maximum frozen depth of the active layer in nearly 80% of the investigation stations had the same relationship with global solar radiation as those typical stations, whereas the other 20% showed a positive correlation. It indicates that the maximum frozen depth of the active layer was influenced by other factors at the same time. In addition to global radiation, the maximum frozen depth of the active layer was the result of combined effects of other factors, such as soil water content, soil property, altitude and latitude, snowpack, vegetation, etc. But what is the importance among those factors mentioned above? Multiple regression analysis method was used here to answer the question. Factors such as global solar radiation, local latitude, longitude, altitude, average air temperature, relative humidity, and accumulation of precipitation in cold season were selected in the multiple regression analysis; among these factors only local latitude, altitude, global solar radiation and air temperature showed high correlation with frozen depth. The multiple regression equation could be written as

$$FD = -434.6 + 12.24\phi + 0.043H - 0.02Q - 6.74T_a \quad (8)$$

where Φ, H, Q, and Ta were the local latitude, altitude, global radiation, and air temperature at the station. The units of these variables were the same as those mentioned above.

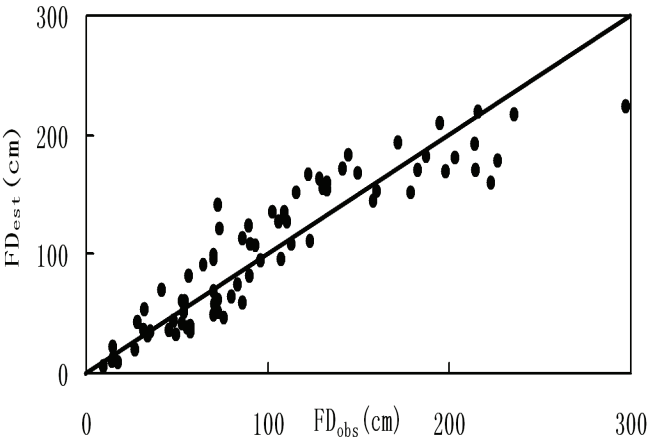

Figure 4. Comparison between the maximum frozen depth of the active layer values observed (FD_{obs}) and estimated (FD_{est}).

Global radiation was the amount from October to February of the next year. The air temperature, *Ta,* was the average value during the time range from October to February of the next year. The multiple correlation coefficient of Equation 8 was 0.90, the partial correlation coefficients for Φ, *H*, *Q* and *Ta* were 0.99, 0.98, 0.81, and 0.81, respectively. It indicated that the correlation between maximum frozen depth of the active layer and the four effective factors was good. The result between the observed and estimated frozen depth with Equation 8 is illustrated in Figure 4. It can be seen from Figure 4 that when the maximum frozen depth of the active layer is less than 300 cm, the agreement between the measured and computed values is good, and the scattering of the data points is small. It demonstrates that Equation 8 was acceptable for estimating the average of the maximum frozen depth of the active layer over the TP.

It can also be seen from Equation 8 that for the whole TP, the global ration showed a negative correlation with the maximum frozen depth of the active layer. The local latitude and altitude show positive correlation with the maximum frozen depth of the active layer. Essentially, the influences of local latitude and altitude can be regarded as the effects of global radiation indirectly. As the local latitude and altitude influence the distribution of global radiation, so the global radiation is an important affecting factor on the maximum frozen depth of the active layer.

Conclusions

From the above discussion, the following conclusions could be drawn:

(1) The APM was acceptable for the estimation of global solar radiation.

(2) Global radiation in the cold season greatly influenced the maximum frozen depth of the active layer. The relationship between them in three typical stations (Yushu, Lenghu, and Delingha) showed a marked negative correlation.

(3) For the whole TP, maximum frozen depth of the active layer in nearly 80% of all investigation stations had the same relationship with global solar radiation as the three typical stations; the others showed a positive correlation.

(4) The maximum frozen depth of the active layer was the result of combined effects of several factors except for global radiation. Among these influencing factors, local latitude, altitude, global solar radiation, and air temperature showed high correlation with the maximum frozen depth of the active layer.

(5) Global radiation was an important affecting factor on the maximum frozen depth of the active layer.

Due to a lack of data on soil properties of the TP, such as aspect was not considered in this work. Thus, further work needs to be done.

Acknowledgments

The authors thank the reviewers for their cogent suggestions. This work is supported by National Basic Research Project (973 Project), No.2007CB411504, National Natural Sciences Foundation of China, No. 40471026, 973 Project No. 2005CB422003, and the innovation project of CAREERI,CAS KZ2003111, KZ2003106.

References

Almorox, J. & Hontoria, C. 2004. Global solar radiation estimation using sunshine duration in Spain. *Energy Convers. Manage.* 45:1529–35.

Almorox, J. et al. 2005. Estimation of monthly Angstro¨m–Prescott equation coefficients from measured daily data in Toledo, Spain. *Renewable Energy* 30: 931–936.

Bulut, H. & Büyükalaca, O. 2007. Simple model for the generation of daily global solar-radiation data in Turkey. *Applied Energy* 84:477–491.

Chegaar, M. & Chibani, A., 2001. Global solar radiation estimation in Algeria. *Energy Conversion and Management* 42: 967-973.

Cheng, G.D. & Wu, B.J. 1983. Approach to the mathematical model of zonality of high-altitude permafrost. *Journal of Glaciology Cryopedology* 5(4):1-7.

Cheng, G.D. 1984. Problems on zonation of high-altitude permafrost. *ACT Geographica Sinica* 39(2):185-193.

Cheng, G.D. & Dramis, F. 1992. Distribution of mountain permafrost and climate. *Permafrost and Periglacial Process* 3(2):83-91.

Ding, Y.J. et al. 2000. The observational study on permafrost hydrology on large scale in the Qinghai-Tibetan Plateau. *Chinese Sciences Bulletin* 45(2): 208-214.

Driesse, A. & Thevenard, D. 2002. A test of Suehrcke's sunshine radiation relationship using a global data set. *Solar Energy* 72: 167–75.

El-Metwally, M. 2004. Simple new methods to estimate global solar radiation based on meteorological data in Egypt. *Atmos Res* 69: 217–39.

Kou, Y.G. et al. 1981. Investigation of solar radiation on Qinghai-Xizang Plateau and its neighboring districts and the relation between the radiation and permafrost on it. *Journal of Glaciology Cryopedology* 3(4): 25-32.

Li, R. et al. 2007. Global solar radiation estimation using sunshine duration over Tibetan Plateau. *Energy Conversion and Management* (under review).

Liu, Z.X. & Ji, G.L. 1985. The relation between global radiation and percentage of sunshine over the Qinghai Xizang Plateau and its contiguous zone. *Arid Land Geography* 8(4):51-58.

Menges, H.O. et al. 2006. Evaluation of global solar radiation models for Konya, Turkey. *Energy Conversion and Management* 47: 3149–3173.

Pavolv, A.V. 1994. Current change of climate and permafrost in the Arctic and Subarctic of Russian. *Permafrost and Periglacial Processes* 5: 101-110.

Souza, J.L., et al. 2005. Global solar radiation measurements in Maceió, Brazil. *Renewable Energy* 30: 1203–1220.

Tao, S. et al. 1999. *The Theory Research Advancement of TIPEX (part one)*. Beijing, China: Meteorological Press of China, in preface page.

Tymvios, F.S., et al. 2005. Comparative study of Angstro¨m and artificial neural networks methodologies in estimating global solar radiation. *Solar Energy* 78: 752–62.

Wang, C. et al. 2003. Study on relationship between frozen –thaw processes in Qinghai-Xizang Plateau and circulation in east Asia. *Chinese Journal of Geophysics* 46(3): 309-316 (in Chinese).

Xu, Guochang et al. 1990. The climatic characteristics of surface heating fields over the Qinghai-Xizang Plateau. *Plateau Meteorology* 9(1):32-43 (in Chinese).

Yao, T.D. et al. 2002. *The Dynamic Characteristics of Cryosphere in the Middle Part on the Qinghai-Tibetan Plateau.* Beijing China: Geological Press, in preface (in Chinese).

Ye, D. & Gao, Y. 1979. *Tibetan Plateau Meteorology.* Beijing: Science Press, 89-101 (in Chinese).

Zhang, T.J. 2002. A important landmark of representation on the Chinese permafrost study. *Journal of Glaciology Cryopedology* 24(3): 331-334 (in Chinese).

Tundra Soil-Water Content and Temperature Data in Support of Winter Tundra Travel

Michael R. Lilly
Geo-Watersheds Scientific, Fairbanks, Alaska
Ron F. Paetzold
Geo-Watersheds Scientific, College Station, Texas
Douglas L. Kane
University of Alaska Fairbanks, Fairbanks, Alaska

Abstract

Unfrozen soil-water content was monitored in the active layer of tundra soil, using TDR sensors at several locations on the North Slope of Alaska and in the Brooks Range foothills. In addition, soil temperature was monitored to a depth of 1.5 m at these locations using thermistors. Particular attention was paid to soil water and temperature behavior during freezing and thawing conditions. The upper organic layer of soil often exhibited very wet conditions and showed much greater temporal variability of soil moisture than the lower mineral soil layers. Permafrost acts as a barrier to water flow, so soils usually are wet as they thaw in the spring. Soil surface roughness and vegetation under tundra conditions make accurate placement of sensors almost impossible. Minor discrepancies between soil water freezing and thawing behavior must be tolerated. However, an overall picture of the processes still emerges. Results of this study may be useful in improving tundra travel guidelines. Currently, tundra travel is allowed if the soil temperature in the upper foot of soil is colder than -5°C. Soil-water content is not considered in the current management approach, though it can be used to help better describe the temperatures at which soil freezing is complete. The measured soil-moisture data indicates most of the soil-water freezing occurs above -2°C. This information indicates the -5°C temperature condition is very conservative and a warmer temperature management point should be considered.

Keywords: measurements; permafrost; soil moisture; soil temperature; tundra travel.

Introduction

A project was established in 2006 to gather data for use in addressing various surface transportation issues in northern Alaska. This report examines some of the results obtained thus far with respect to winter tundra travel. Current guidelines limit tundra travel to periods when the soil temperature at a depth of 30 cm is less than -5°C with snow cover depth minimums depending upon the type of tundra (Bader 2005). This criterion is based on the results of a three-year study (Bader & Guimond, 2004) and may be conservative.

Soil-temperature and water-content data are used in this paper to examine the possibility of using a slightly relaxed criterion that could result in longer periods of allowed tundra travel. This is based strictly on the freeze-thaw behavior of soil water. No measurements of soil strength were obtained. The objective is to examine the behavior of soil temperature and water content in tundra soils during the processes of freezing and thawing.

Materials and Methods

Twelve stations were installed in the fall of 2006. Eight of the stations are located on the coastal plain; the remaining four are in the northern foothills of the Brooks Range. The stations used in this report are located east of the Sagavanirktok River (Fig. 1).

Soil-water content was monitored at each station with Campbell Scientific, Inc. CS616 TDR-type sensors at depths of 10, 20, and 40 cm. The depths at some sites varied slightly due to soil conditions. The soil-water content sensors were installed horizontally with minimal soil disturbance. Factory calibration was used to convert raw readings to volume fraction soil-water content. TDR-type sensors respond to the soil dielectric constant, and since ice has a dielectric constant similar to dry soil, the sensor effectively responds to changes in unfrozen soil-water content. Hourly readings of unfrozen soil-water content were recorded.

Soil temperature was monitored at each station with YSI thermistors mounted in a string, at intervals to provide temperatures at 0, 5, 10, 15, 20, 40, 60, 80, 100, 120, 135, and 150 cm below the soil surface. The soil temperature string was placed into a hole drilled into the soil, and the evacuated soil was used to back-fill the hole. Hourly readings of soil temperature were recorded.

Other measurements include air temperature, relative humidity, net radiation, wind speed and direction, snow depth, and summer rain. Sensor readings at each station were measured and recorded with a Campbell Scientific, Inc CR1000 datalogger. Data were transmitted hourly to a central processing facility with FreeWave radios. Solar panels and a battery bank were used to provide power for each station throughout the year.

Results and Discussion

Ice formation within soil pores increases the bearing strength of freezing soils. Extremely dry soils, such as found

in the Dry Valleys of Antarctica, or dry gravel or organic soils exhibit no increase in bearing strength when frozen.

As soil water freezes, it acts as an impediment to the movement of soil particles, thus increasing the bearing strength of the soil. Water freezing in soil pores acts as if solid particles were growing in the pores. A graph of frozen soil-water content versus soil bearing strength in water- saturated soil would be a typical S-shaped curve. As soil water starts to freeze, little strength is added. At some point, the increase in strength with water content is dramatic. As the freezing process goes to completion, the curve levels off, and little strength is added during the last stages of freezing. The bearing strength of frozen soil is greater than the maximum of the strength of ice or of unfrozen soil.

Similarly, for unsaturated soils, higher water content up to some maximum, will result in higher strength when the soil freezes. Very low soil-water content does little to increase soil strength when the soil is frozen. As soil-water content increases, soil strength increases upon freezing.

Soil water does not completely freeze at temperatures below 0°C. As heat is removed from water, the temperature lowers until the freezing point is reached. At this point, the temperature remains constant until the liquid water solidifies, or changes to ice, at which time the temperature will once again start to drop. In soils, however, water does not all freeze at the same temperature. Some freezes at or near 0°C, while some freezes at much lower temperatures. No unique freezing point exists for soil water (Koopmans & Miller 1966). There are two reasons for this. One, soil water contains solutes or salts which lower the freezing point. As the soil water freezes, the salts become more concentrated due to exclusion from the ice. And two, the "structure" of soil water becomes increasingly ordered closer to soil particles. This changes the free energy of the soil water and lowers the freezing point. A similar phenomenon can be observed in capillary tubes (Edlefsen & Anderson 1943).

Increasing the solute concentration of soil water produces a minor effect compared to the "structuring" of the soil water near soil particles.

The water next to soil particles is the last to freeze, and will do so only at extremely low temperatures, due to its molecular interaction with the soil particles (Anderson et. al. 1973). Water is a polar molecule, and soil particles, especially clay and organic matter, have associated negative charges. Water molecules tend to align in an ordered fashion or "structure" next to soil particles. The effect decreases with distance from the soil particle. The ordered molecules are more difficult to freeze than those in bulk solution or free water. The amount of unfrozen water present depends principally upon temperature for a given soil material. Except for very low water contents, it is virtually independent of the total soil-water volume. The unfrozen-water content at a given temperature is mainly dependent on specific surface area of the soil. The amount of unfrozen water at a given temperature increases as the specific surface area of a soil increases.

Data are presented from station DBM4 Sag Ivishak Met, which was chosen as representative for this project. The

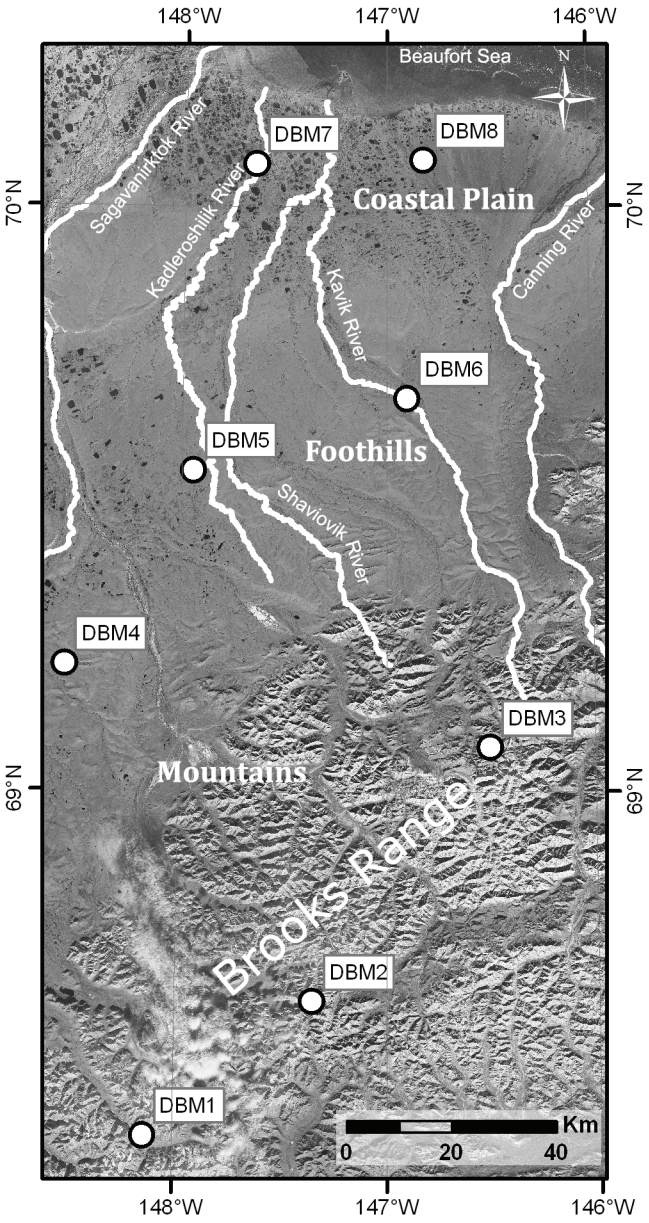

Figure 1. Study sites locations on the central North Slope, Alaska.

active layer thickness (Fig. 2) for this station, as determined by the point at which the maximum soil temperature line crosses the 0°C line, is approximately 60 cm for the period of measurement (October 1, 2006, to September 30, 2007). This is a fairly typical active layer thickness for the soils of this area. Active layer thickness varies from year to year depending on summer weather. The average soil temperature in the upper 150 cm was -4.15°C during the measurement period.

Other methods of active-layer strength determination may yield different results. Rod penetration is the most common method of determining active layer thickness. Problems with the rod penetration method include timing, presence of hard spots in the soil (ice lenses, rocks, compact areas, etc.), and operator consistency. It is also a labor-intensive method. An advantage of the penetration method is that it is usually

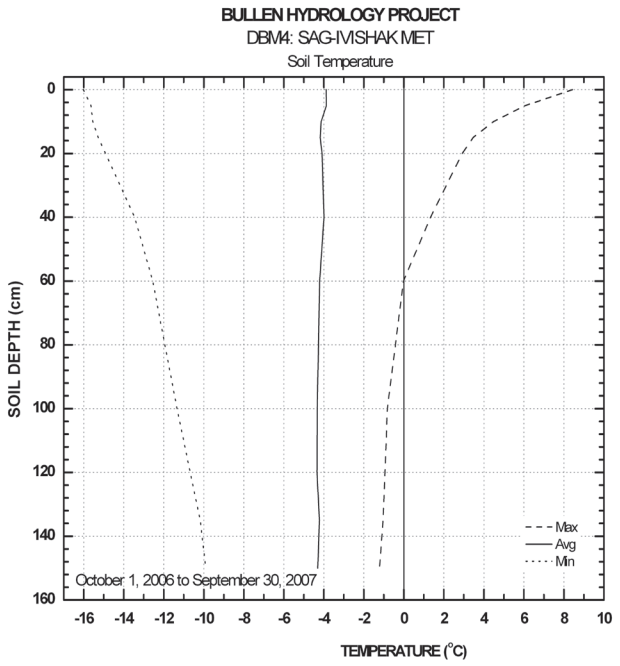

Figure 2. Average, maximum, and minimum soil temperature profiles for the DBM4 Sag Ivishak Met site.

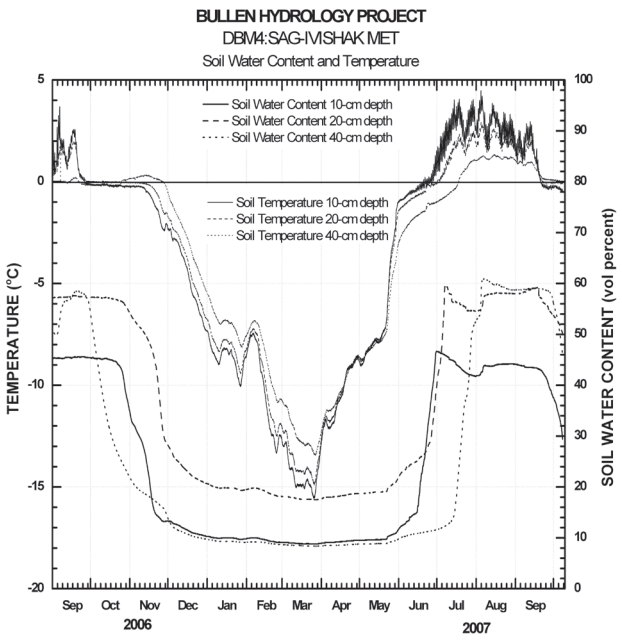

Figure 3. Soil-water content and temperature for the Sag-Ivishak (DBM4) meteorological station.

repeated over a relatively large area, resulting in an average, maximum, and minimum value for the area. One problem common to all methods is the location of the soil surface as a reference point for depth. This can be a very serious problem in tussock tundra.

Active layer thickness was generally a few centimeters less for the foothills stations than for those on the coastal plain. In addition, the soil at these sites remained frozen longer. Although soil temperatures vary among the stations, the relationship between soil temperature and soil water is consistent.

The soil-water content at the Sag Ivishak Met site was near saturation during the monitoring period from September 2006 to October 2007 (Fig. 2). This is typical of soils in this area. Often soils in northern Alaska are wetter in the spring and early summer, then dry out in the fall. During the summer, down-gradient drainage and evapotranspiration dry out the soils. The soil-water content at saturation in this soil is around 60% by volume. Normal mineral soils have a saturated-water content of around 40% to 45% by volume. The high-saturated water contents in the soils studied are attributed to high soil organic-matter content.

For greatest accuracy, the soil-water content sensors should be calibrated specifically to each soil, especially under conditions that depart from normal (Campbell Scientific, Inc. 2004). Although the absolute soil-water content may differ from that given by the factory calibration, the relative water contents and the behavior of phase change in relation to temperature should be accurate.

Freezing increases the complexity of the soil-water system. Water moves in response to various gradients, including thermal gradients. Water in soil moves from warm areas to cold areas. As water moves, in response to thermal gradients, it carries thermal energy or heat with it, thus modifying the thermal and hydraulic gradients.

Freezing of soil water changes its ionic concentration and thus its electrical properties, setting up new gradients and complicating water-content measurement based on electrical properties. The increase of solute concentration in soil water, due to solute expulsion from ice during freezing, can cause a minor decrease in the freezing point. This decrease is on the order of a few tenths of 1°C.

In spite of the complexity of determining soil-water content absolutely, much information may be extracted from the relative soil-water contents and the water-content curve shapes and positions.

Soil on Alaska's North Slope typically thaws from the top down, but freezes from both the top and bottom as shown in Fig. 3. These phenomena have been noted by others (Osterkamp & Romanovsky 1997, Romanovsky & Osterkamp 1997).

The unfrozen soil-water content curves indicate that water at the 40-cm depth began to freeze first, followed by that at the 10-cm depth. The water at the 20-cm depth was the last to freeze. As air temperature decreases and the days grow shorter in the fall, there is less heat transfer to the soil and it begins to freeze at the bottom of the active layer, just above the permafrost, depending on how cold the permafrost is. When the air temperature falls below freezing, water at the soil surface begins to freeze.

As the soil water freezes in the fall, the temperature remains near 0°C during the period of water-to-ice phase change. This phenomenon is often referred to as the zero curtain and is the result of the release of thermal energy during the phase change from water to ice.

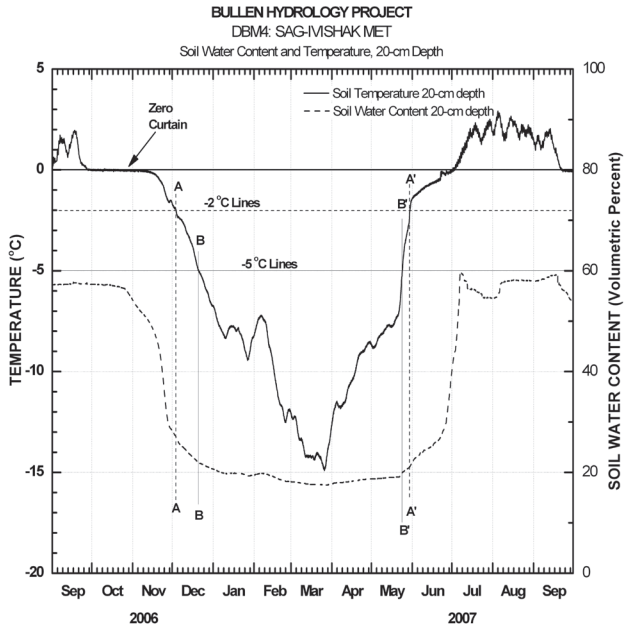

Figure 4. Soil temperature and water content for the 20-cm depth at Sag-Ivishak (DBM4) meteorological station.

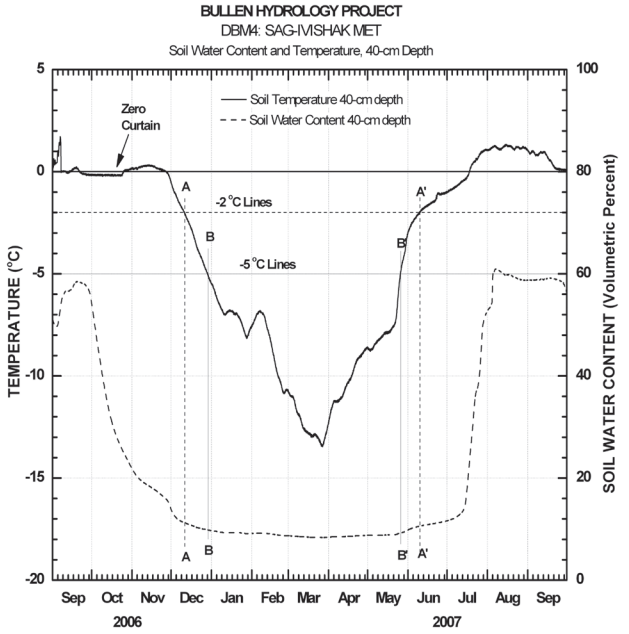

Figure 5. Soil temperature and water content for the 40-cm depth at Sag-Ivishak (DBM4) meteorological station.

The unfrozen-water content curve remains nearly constant during the initial period of the zero curtain. At some point, the soil water has lost most of its latent heat and rapid freezing occurs, as shown by the steep slopes of the curves in Figure 3. The unfrozen soil-water content curves then transition to a fairly constant unfrozen-water content, where very little further freezing occurs, even as the temperature markedly decreases. Sometimes this transition is rather abrupt, and sometimes it is more gradual.

Soil water at all sites studied thawed from the top down in the spring. In the spring, the days grow longer, air temperature increases, the snow begins to melt, and the soil thaws from the top down. Snowmelt water moves downward in response to gravity, warming the soil below.

Ice has a higher thermal conductivity than water, air, or soil. Thus ice is more efficient in transmitting thermal energy than water. This is another reason why soils thaw more quickly than they freeze.

In the spring, during thawing conditions, the soil temperature changes rapidly in response to liquid water moving into and through the soil. The temperature curve generally shows a slower rate of increase during the melting of the water at a particular depth. This is attributed to the latent heat required to thaw the ice. After the ice is thawed, the temperature resumes a rapid increase. The soil water generally thaws faster than it freezes. This may be attributed to the influence of liquid water moving through the soil, carrying thermal energy with it.

The phase-change period is shorter during the spring as the soil thaws and ice turns to liquid water. In addition, the temperature during this time usually is not constant at 0°C for any lengthy period of time. This may be attributed to meltwater carrying heat with it to underlying layers. During winter months, soils can desiccate and form thermal cracks. This increases the effective permeability of the soils, allowing more infiltration of water during snowmelt (Kane et. al. 2001).

Since no sensors were located at the 30-cm depth, data from 20 and 40 cm were used to approximate conditions there. Figures 4 and 5 show soil temperature and unfrozen-water content for the 20- and 40-cm depths, respectively.

Figures 4 and 5 show that soil water does not immediately begin to freeze at the onset of the zero curtain. Some time passes as the water is releasing latent heat while it starts to freeze. However, once started, the freezing process is relatively rapid.

Figure 5 shows a slight increase in soil temperature during the zero curtain during November. There is a corresponding decrease in the slope of the unfrozen-water content curve during this time. These features may be attributed to water moving into the soil layer at this point due to thermal gradients from the soil freezing above and below this depth. As the liquid water moves into this region, it carries heat or thermal energy with it, resulting in a slight increase in soil temperature.

Lines B and B' in Figures 4 and 5 indicate the time when the soil temperature drops below and rises above -5°C, respectively. During the time that the soil temperature is below -5°C, little additional unfrozen soil water will freeze even at soil temperatures well below -5°C. At these depths, the soil water is frozen to near its maximum level.

Lines A and A' show the conditions when the soil temperature is colder than -2°C. There is little difference in the frozen state of the soil water at these depths between -5°C and -2°C, particularly at the 40-cm depth. However, time that the soil is colder than -2°C is on the order of a month (Table 1), which is significant for tundra travel.

If we approximate the conditions at the 30-cm soil depth by the average of the 20- and 40-cm soil depths, Table 1

Table 1. Days soil temperature below certain levels for DBM4.

Soil temperature colder than	20-cm depth	40-cm depth	Avg of 20- and 40-cm depths
-1°C	195	209	202
-2°C	177	181	179
-3°C	169	165	167
-4°C	158	157	157
-5°C	154	148	151

shows that the soil was colder than 5°C during the winter of 2006–07 for approximately 151 days. During this time, the soil at the same depth was colder than -2°C for 179 days, four weeks longer. It was colder than -3°C for 167 days, 16 days longer. And the soil was colder than -4°C almost a week longer. Figures 3, 4, and 5 show steep curves for soil water freezing and thawing. When the soil reaches -2°C, the soil-liquid-water curve is near its minimum, and only minor freezing occurs at temperatures colder than this. Similar results were obtained for the foothills sites.

Again, no soil strength tests were performed, and the results indicate only the length of time that the soil was frozen at temperatures colder than indicated levels. However, it is known that the compressive (bearing) strength of the soils increases as the ice content increases.

Summary

Soil-water content and temperatures were monitored at twelve sites in northern Alaska from September 2006 through October 2007. Soil temperature and water behavior were observed during this time with particular attention paid to periods of freezing and thawing. Freezing started at the bottom of the active layer and proceeded from both the bottom and top of the active layer. During freezing, soil temperatures remained near zero while the soil water released its latent heat. This period is known as the zero curtain. At a point in the zero curtain, the soil water begins to freeze rapidly. When most of the water that was going to freeze had done so, a transition occurred to a nearly constant level of unfrozen soil-water content. Due to interaction with soil particles, soil water does not completely freeze. Soil temperatures colder than -2°C did not cause an appreciable increase in the amount of frozen soil water.

In the spring, the soils studied thawed from the top down. The thawing process was faster than freezing due to meltwater percolation. Also because of snowmelt, the soil-water content in the spring was at saturation. The difference in frozen soil-water content between -2°C and -5°C during the spring thaw was even less than it was in the fall during freezing.

A relaxation of the tundra travel guideline from a temperature of -5°C at a soil depth of 30 cm to a value between -2°C and -4°C could significantly increase the amount of time available for tundra travel. Further study needs to be undertaken to examine soil strength in the region between -2°C and -5°C before any changes in the guidelines are considered.

References

Anderson, D.M., Tice, A.R. & McKim, H.L. 1973. The unfrozen water and the apparent specific heat capacity of frozen soils. *Proceedings of the Second International Conference on Permafrost, Yakutsk, U.S.S.R.*, *North American Contribution.* Washington, D.C.: National Academy of Sciences, 289-295.

Bader, H.R. & Guimond, J. 2004. *Tundra Travel Modeling Project.* Alaska Department of Natural Resources, 65 pp. http://www.dnr.state.ak.us/mlw/tundra/TundraModelReport.pdf

Campbell Scientific, Inc. 2004. *CS616 and CS65 Water Content Reflectometers.* Campbell Scientific, Inc.

Bader, H.R. 2005 *Tundra Travel Research Project: Validation Study and Management Recommendations.* Alaska Department of Natural Resources, 20 pp. http:www.dnr.state.ak.us/mlw/tundra/validation2005final_with_figures.pdf.

Edlefsen, N.E. & Anderson, A.B.C. 1943. Thermodynamics of soil moisture. *Hilgardia* 15: 31-298.

Kane, D.L., Hinkel, K.M., Goering, D.J., Hinzman, L.D. & Outcalt, S.I. 2001. Non-conductive heat transfer associated with frozen soils. *Global and Planetary Change* 29: 275-292.

Koopmans, R.W.R. & Miller, R.D. 1966. Soil freezing and soil water characteristic curves. *Soil Sci. Soc. Am. Proc*. 66: 680-685.

Osterkamp, T.E. & Romanovsky, V.E. 1997. Freezing of the active layer on the coastal plain of the Alaskan Arctic. *Permafrost and Periglacial Processes* 8: 23-44.

Romanovsky, V.E. & Osterkamp, T.E.. 1997. Thawing of the active layer on the coastal plain of the Alaskan Arctic. *Permafrost and Periglacial Processes* 8: 1-22.

The Effect of Snow Cover on Permafrost Thermal Stability

Erwin L. Long
Arctic Foundations, Inc.
Edward Yarmak, Jr.
Arctic Foundations, Inc.

Abstract

The investigation to determine a cause for differential settlement of a tower foundation at Glennallen that had been stable for over 40 years led to the derivation of formulae that reflected Osterkamp's measurements for depth to base of permafrost in the area and included snow depths, temperatures, and quantity of thermosyphon cooling.

Keywords: Alaska; foundation; permafrost; snow depth; thermosyphon; warming.

Background

Two towers were constructed in 1960 on permafrost, using thermosyphon technology for passive subgrade cooling for the first time. The two Alaska Communications Systems (ACS) towers are both located in the vicinity of the Gulkana Airport. The Glennallen Tower is located approximately 4½ mi (7.2 km) southwest of the Gulkana Airport along the Glenn Highway, and the Aurora Tower is located approximately 21 mi (34 km) northeast of the Gulkana Airport and ½ mi (0.8 km) off the Tok Cutoff Highway. The locations of the tower sites are shown on Figure 1. Both sites are underlain by lakebed colodial clay silts which include coarser soils with cobbles and boulders dropped from glacial icebergs. The weather station at the Gulkana Airport has operated continuously since 1949. The construction of the Glennallen tower was begun one year after the construction of the Alaska Road Commission (ARC) complex on the west side of the ACS site. The ARC complex was constructed as if on a non-permafrost site, and the ARC recognized the existence of permafrost only after their water well froze up and considerable differential settlement of the structures in the complex occurred. The Aurora tower was constructed on virgin stunted black spruce terrain underlain with permafrost.

The Gulkana Airport is at an elevation of 1580 ft (482 m). The Aurora tower site is at 1890 ft (576 m), and the Glennallen tower site is at 1455 ft (443 m). Both towers are four-legged with post and pad type foundations. The individual tower leg foundations are composed of three 12-in (300 mm) XH pipe thermosyphons 24 ft (7.3 m) in length with the base plates 18 ft (5.5 m) below finished grade and are described in detail by Long (1963).

The Glennallen site was evaluated in 1981, and a new transmitter and equipment building was constructed on thermosyphon piling to the east of the tower. The new structure replaced the original building that was originally constructed on-grade and later refrigerated to minimize thaw settlement.

Both tower foundations were evaluated and soil temperatures measured in 1988. Soil temperatures were found to be warmer than anticipated in the original design. As a result, 170 ft^2 (15.8 m^2) finned condensers were added to two of the waveguide thermosyphon piles at the turf-covered Glennallen tower facility in 1989. Temperature measurements at the Aurora facility indicated a depth of thaw of over 20 ft (6.1 m) in the area surrounding the most southern tower leg foundation. To reverse the thawing found at Aurora, 510 ft^2 (47.4 m^2) finned condensers were added to the NW, SW, and SE foundations and 170 ft^2 (15.8 m^2) finned condensers were added to each of the waveguide foundations in 1989. Foundation temperatures seemed to be affected more by summer surface conditions than by the winter snow cover or the winter air temperature.

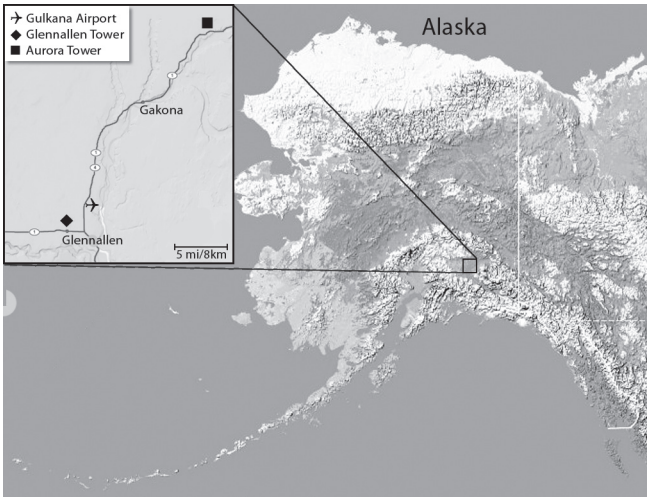

Figure 1. Location map.

In summer 2007, the foundations systems for each tower were inspected. Excessive settlement was found on two of the tower leg foundations at Glennallen. No settlement was found at Aurora. In order to prepare recommendations to stop the settlement at the Glennallen site, an in-depth evaluation was performed to determine the cause of the settlement. It was a goal to develop a method for better evaluation of permafrost stability with changing climate and to provide a means of pre-site evaluation.

Analysis

Osterkamp (2003) reported the depth to the base of permafrost at Gulkana for the period from 1985 to 2001. The depth to the base of permafrost is an excellent measure of the

long-term thermal stability of permafrost. This measurement includes all the effects of climate change at a particular site.

Measured thermal conductivity of snow varies primarily with density and ranges from 0.02 btu/hr•ft•°F (0.034 W/M°K) to 0.29 btu/hr•ft•°F (0.503 W/M°K) for densities from 14.7 lb/ft^3 (0.236 g/cm^3) to 32.2 lb/ft^3 (0.515 g/cm^3) (Sturm et al. 2002). In comparison, a typical extruded polystyrene insulation used in civil construction has a thermal conductivity of approximately 0.02 btw/hr•ft•°F (0.03 W/M°K) (ASHRAE Fundamentals 2001). By the numbers, the insulating value of snow is very apparent. Of course, this is nothing new to the people who live in the Arctic and Subarctic, where a snow pile may be the difference between comfortable survival and freezing to death.

The authors have seen instances where snow drifting caused by man-made structures has insulated the ground to such a degree that the depth to the top of permafrost at the end of the thawing season increased from 5 ft (1.5 m) to 14 ft (4.3 m) in two years. An increase in the natural snow depth will have similar albeit more subtle consequences. In the region where the Glennallen and Aurora towers are located, a small change in the surface heat balance equals a large change in the foundation soil properties.

An empirical equation (Equation 1), which included snow depth, was developed to approximate the degree of surface freezing affecting the local permafrost. Weather data from the Gulkana Airport show an average accumulated snow depth of 26.6 in (676 mm) with an average Freezing Index of 4621 °F-days (2567 °C-days) and an average Thawing Index of 2970 °F-days (1650 °C-days) from 1960 through 2007. The end of December accumulated snow depth (DAS) was selected to approximate available seasonal surface snow conditions. Twenty inches (508 mm) was selected as an approximate mean snow depth at the end of December.

Accumulated degree days =

$$-\left(n_f \circ d_f / \sqrt{\frac{DAS}{20}}\right) + \left(n_t \circ d_t\right) \qquad (1)$$

$^\circ d_f$ = Degree days freezing (°F)
$^\circ d_t$ = Degree days thawing (°F)
n_f = Winter air to surface temperature reference
n_t = Thawing air to surface reference
DAS = December accumulated snow depth (inches)
20 = Arbitrary snow depth reference (inches)

The results are shown as Figure 2 alongside a plot of the depth to the bottom surface of the permafrost presented by Osterkamp for Gulkana. Note that each plot fits the other well with a time offset to account for the depth to the base of the permafrost.

Equation 1 was then modified to represent the effect of the themosyphon cooling in a 70 ft (21 m) radius of the tower and building area. The work was done by trial and error so that the modified empirical equation would mimic the variation in the depth of the permafrost base over time.

The ground surface area being evaluated was selected as having a diameter approximately equal to the depth to the base of the permafrost. The magnitude of the supplemental cooling is a function of the thermosyphon radiator and is represented by its area (SF).

Accumulated degree days =

$$-\left(n_f \circ d_f / \sqrt{\frac{DAS}{20}}\right) - \left(\circ d_f * \frac{SF}{A}\right) + \left(n_t \circ d_t\right) \qquad (2)$$

SF = Square feet of radiation surface
A = Square feet of 70-foot radius area

The plots of Equation 2 for each of the tower sites are shown in Figure 3. It is very apparent that 1976 was a pivotal year for the cooling of permafrost at Gulkana.

The permafrost cooling period from 1960 to 1976 reflects the greater Freezing Index (4935 °F-days (2742 °C-days)) and lesser Thawing Index (2906 °F-days (1614 °C-days)) with an average snow cover of 19.4 in (493 mm) at the end of December while the period from 1978 to 2007 reflects the lower Freezing Index (4416 °F-days (2453 °C-days)) and greater Thawing Index (3012 °F-days (1,673 °C-days)) combined with a heavier snow cover of 34.1 in (866 mm).

Figure 4 compares the Glennallen tower area accumulated degree-days with thermosyphon conditions with the conditions south and west of the tower. Figure 5 shows the Aurora tower area accumulated degree-days with thermosyphon conditions, compared with surrounding area conditions. The Glennallen tower area had a good surface turf cover, while Aurora had an exposed gravel surface which increased its summer thaw. Aurora had a greater thermosyphon heat removal capacity, which improved its frost conditions over Glennallen during years of heavy snow cover.

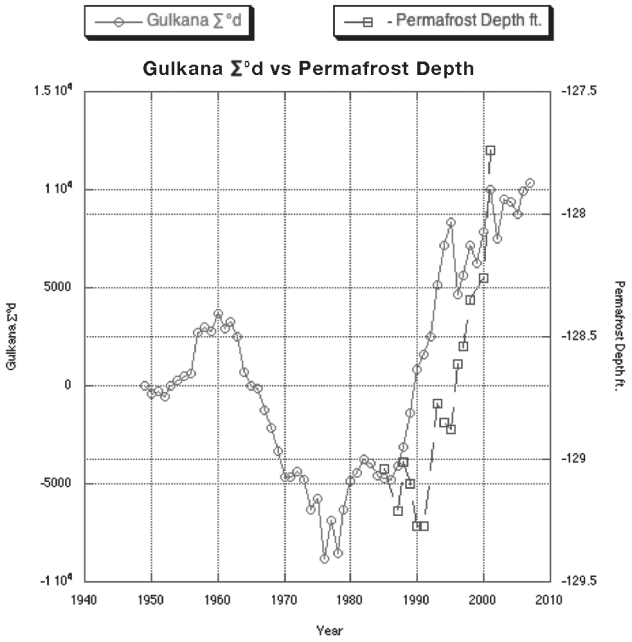

Figure 2. Equation 1 for Gakona airport

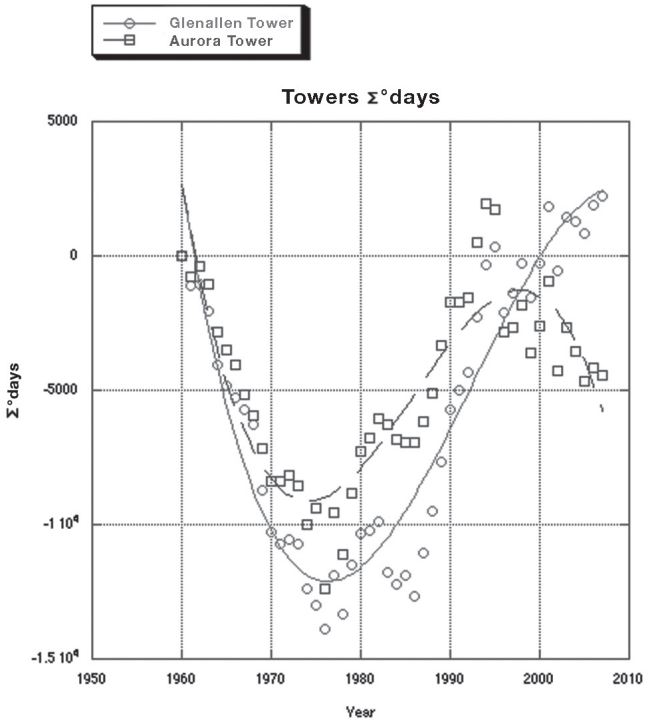

Figure 3. Equation 2 for Glennallen and Aurora towers.

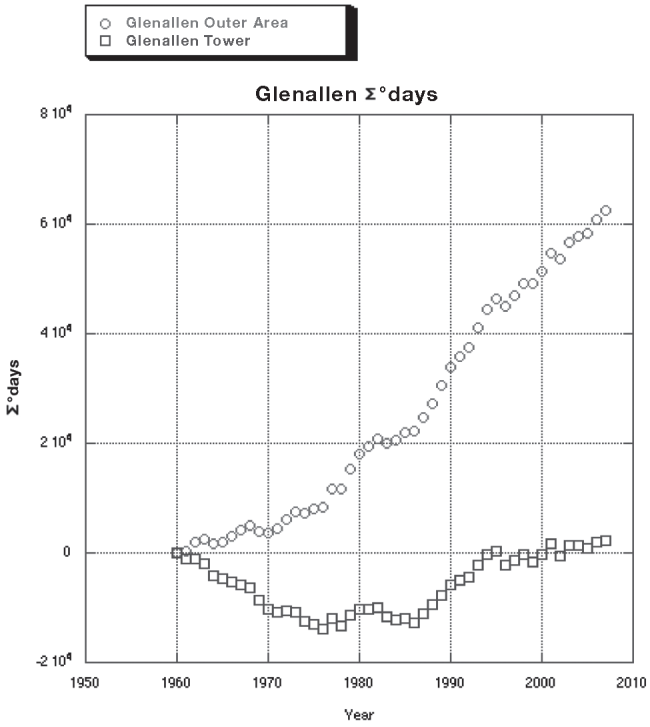

Figure 5. Aurora tower thermosyphon effects.

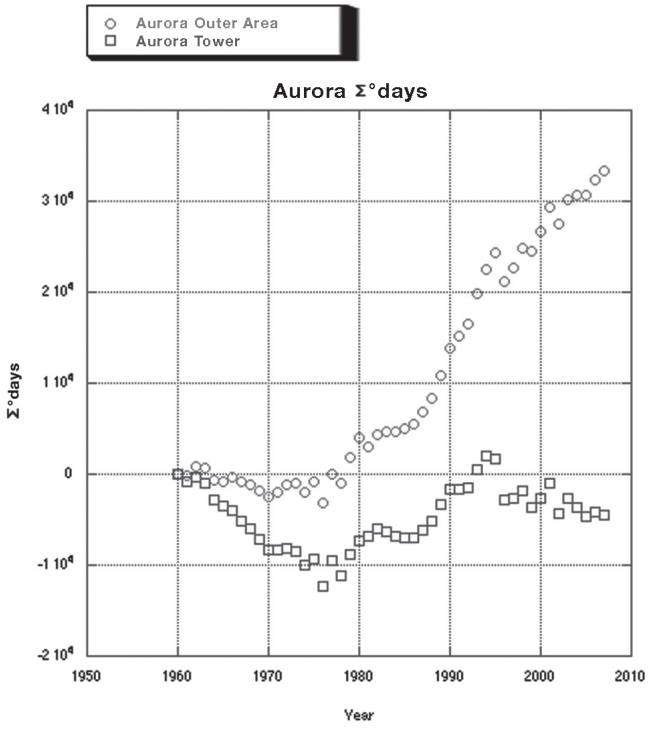

Figure 4. Glennallen tower thermosyphon effects.

With the prevalent colodial soil throughout the area, reduced temperatures will enhance ice lens formation as envisioned by Radd and Oevtle (1973), while warming will cause thawing and settlement (Nelson et al. 1983). By increasing the cooling capacity of the south and west foundations at Glennallen, ice lens formation and permafrost expansion below the foundation pads is expected to occur and help counteract the existing differential settlement and lateral thawing from the adjacent uncooled areas.

Conclusion

The data show that the greatest settlement occurred under the foundations with the least thermosyphon cooling capacity during periods of higher than normal snow cover. When analyzing the thermal conditions for a structure, the design should be area-wide and include snow conditions.

Recommendations

Increase the thermosyphon cooling of the foundations with the largest settlement at the Glennallen tower site.

References

ASHRAE Fundamentals. 2001. *Typical Thermal Properties of Common Building Insulating Materials.* American Society of Heating, Refrigeration and Air Conditioning Engineers, 25.5.

Long, E.L. 1963. The long thermopile. *Proceedings of the First International Conference on Permafrost, Lafayete, Indiana,USA:* 487-491.

Osterkamp, T.E. 2003. A thermal history of permafrost in Alaska. *Proceedings of the Eighth International Conference on Permafrost, Zurich, Switzerland*: 863-868.

Nelson, R.A.. Luscher, U., Rooney, J.W. & Stramler, A.A. 1983. Thaw strain data and thaw settlement predictions for Alaskan soils. *Proceedings of the Fourth International Conference on Permafrost, University of Alaska, National Academy Press*: 912-917.

Radd, F.J. & Oertle, D.H. 1973. Experimental pressure studies of frost heave mechanisms and the growth-fusion behavior of ice. North American Contribution, *Proceedings of the Second Second International Conference on Permafrost, Yakutsk, USSR*: 377-384.

Sturm, M., Perovich, D.K. & Holmgren, J. 2002. Thermal conductivity and heat transfer through the snow on the ice of the Beaufort Sea. *Journal of Geophysical Research* 107, American Geophysical Union.

Bibliography

Esch, David C. (ed.) 2004. *Thermal Analysis, Construction, and Monitoring Methods for Frozen Ground.* ASCE Technical Council on Cold Regions Engineering Monograph.

Kinney, Thomas C., Santana, Barry W., Hawkins, D. Michael, Long, Erwin L. & Yarmak Jr., Edward. *Foundation Stabilization of Gas Injection Facilities, Prudhoe Bay, Alaska*, 618-622.

Luscher, Ulrich & Afifi, Sherif S. *Thaw Consolidation of Alaskan Silts and Granular Soils*, 325-334.

North American Contribution. Second International Conference on Permafrost, Yakutsk, USSR, 1973.

Osterkamp, T.E. *Response of Alaskan Permafrost to Climate*, 145-152.

Proceedings of the Fourth International Conference on Permafrost. University of Alaska, National Academy Press, 1983.

Proceedings of the Sixth International Conference on Permafrost, South China University of Technology Press,1993.

Zhang, T. & Osterkamp, T.E. *Changing Climate and Permafrost Temperatures in the Alaskan Arctic*, 783-788.

Chronosequence of Forest Fire Effects on the Active Layer, Central Yakutia, Eastern Siberia

L. Lopez
The United Graduate School of Agricultural Sciences, Iwate University, Morioka 020-8550, Japan
G. Guggenberger
Martin Luther University, Halle-Wittenberg Institute of Agricultural and Nutritional Sciences, Soil Biology and Ecology Group Weidenplan 14 06108 Halle, Germany
E. Gerasimov
Permafrost Institute Siberian Branch, Ras, Yakutsk, Russia
R. Hatano
Graduate School of Agriculture, Hokkaido University, Sapporo, Hokkaido, 060-8589, Japan
A.N. Fedorov
Permafrost Institute Siberian Branch, Ras, Yakutsk, Russia

Abstract

Despite the large area that fire covers, its recurrent nature, and its ecological role in this boreal region, it has been poorly studied. This research was conducted in naturally burnt sites (five) with different post-fire periods; 4, 5, 15, 25, and 50 years and intact (*Larix cajanderi*) forest sites (three) that were considered as control sites. Sampled soil profiles included the active layer and the upper permafrost (0–1.7 m). The effect of fire on the aboveground can be clearly observed, but what happens in the belowground is not well understood in fire-prone eastern Siberia. Irreversible landscape changes occurred when the ice-rich and salty permafrost reached a degradation threshold. The results of this study show that the active layer of burnt sites older than 25 years does not differ significantly with the active layer of intact forests. On the other hand, the "younger" burnt sites showed a deepening of the active layer. The degrading and aggrading processes of the permafrost are apparently followed by hydro-geochemical processes supported by the poorly drained soil conditions of the active layer. In the intact forest sites, the soil ion profile shows increasing concentration downwards, especially in the permafrost layer. During the years of permafrost thawing, ions moved upward into the upper soil layers. Once the water balance of the site is balanced by the appearance of birch (*Betula platyphilla*), soil moisture in the lower layers starts accumulating, and this movement downward brings the ions back to the lower layers where, due to high water content and lower soil temperatures, they become trapped again in permafrost (aggrading). This process takes approximately 20 years. In conclusion, fires in central Yakutia are at present assimilated by the forest ecosystem and the drastic changes it experiences initially are temporal. The conditions necessary for a permanent change in this boreal forest ecosystem is the increase in fire frequency which would not allow forest regeneration.

Keywords: active layer; forest fires; global warming; permafrost regions; salinization.

Introduction

Forest fires in central Yakutia are recurrent phenomena that determine regeneration, carbon storage and temporal changes in land cover. The trigger for fire can be natural (lightning) or human caused (human activity), but the condition necessary for severe fire expansion is dry weather (long rainless periods), high temperatures and low relative humidity. Forest fires are a large source of both carbon dioxide and methane emissions. However, they are both a temporary source of carbon dioxide and usually a biogenic one (Radionow et.al. 2006). Under special circumstances, which are a combination of factors such as fire intensity and climatic cycles (Shender et al. 1999), its occurrence in ice-rich and shallow permafrost burnt sites can develop into thermokarst depressions (Czudek & Demek 1970, Brouchkov et al. 2004, Agafonov et al. 2004) or as is more general, forest can return to its former state (as before the disturbance occurs).

Forest fires in eastern Siberia are not crown fires which are more devastating in their effect (Harden et al. 2000), but surface fires (Mouillot & Field 2005) because of low tree density and because of the pyrophytic properties of larch trees (Nikolov & Helmisaari 1993, Tvsetkov 2004). Changes above ground can alter the movement of water and salts present in the lower part of the active layer and upper permafrost (Lopez et al. 2007a). The organic matter in the top layer cools the active layer, and its disappearance after severe fires results in active layer deepening. Forest fires in Siberia have been cited as large scale disturbances that can contribute to permafrost degradation if the soil thermal regime is altered by climatic change (Kasischke et al. 1995, Zimov et al. 1996). However, to our knowledge no study has focused on the long-term effect on the belowground after forest fires in eastern Siberia (several years after the fire

occurrence). If climatic warming increases fire frequency or intensity, the increase in annual thaw depths could result in active layer salinization within areas of salt-rich permafrost (Kokelj & Lewkowicz 1999, Lopez et al. 2007a). Thus, the objective of this study is to assess the process by which the forest ecosystem, especially belowground, recovers after a forest fire,

Materials and Methods

Site description

Neleger Experimental Station is located 30 km north-northwest from the city of Yakutsk (62º05′N, 129°45′) and belongs to the Yakutsk Permafrost Institute. Mean annual air temperature is -10 to -11°C; amplitude of monthly temperatures is about 62°C. Snow cover is 30–40 cm, but it has recently reached 60 cm. Icy deposits are located at depths from 1.5 m to about 3 m; they occur over more than half of the territory, have thicknesses of up to 20–25 m and are distributed in 18% or 76,000 km^2 of the territory of central Yakutia (Fedorov et al. 1991). The area consists of a group of Lena River terraces with elevations of 200–220 m a.s.l.; it is a region of continuous permafrost up to 400–500 m thick. Quaternary deposits are from a few meters to 200 m thick. The bedrock predominantly consists of limestones and argillites. Disturbances that occurred around 10,000 years ago, and still continue, have changed the landscape of this area to grassland (thermokarst depressions). Precipitation during the snow-free growing season is on average 110 mm, which is about half the annual precipitation, whereas the corresponding potential evaporation rate is 370 mm (Muller 1982). Soils in this region are classified as Gelisols; they are predominantly silty-clay-loam (SiCL) to silty-clay (SiC) in 70% of the territory and sandy-loam (SaL) in the remaining part.

Sampling

The sites selected were three intact forests (F1, F2 and F3) and five chronologically burnt forests (B1, 4 years; B2, 5 years; B3, 15 years; B4, 25 years; and B5, 50 years). The soil texture at all sites was silty-loam. Three 1.7 m-long soil profiles were sampled at each location in May 2006. The sampling took place when the soil profile was still frozen and required a boring machine. The frozen layer (permafrost) was measured in late September when the thawing front reached its maximum. The core samples were sectioned in 10-cm intervals, logged, double-bagged, and returned to a laboratory. Soil texture was determined by observation and feel.

Soil moisture and chemical analysis

Soil moisture was determined gravimetrically by drying to a constant weight at 105ºC for 24 hours. A different set of soil samples taken next to the samples used for soil moisture measurements, in each of the profiles, was air dried and then analyzed for pH in a supernatant suspension of 1:5 soil:deionized water mixture (pH meter HORIBA) and electric conductivity in a supernatant suspension of 1:5 soil:deionized water mixture (Page et al. 1982) (EC meter TOA CM-30V) for each sampling site. Electric conductivity of saturated paste (EC_e), used to evaluate saline and alkaline soils, was estimated using soil water 1:5 suspension measurements and following the relation obtained by Slavich & Petterson (1993) for each soil texture. One soil profile at each of the sites was subjected to ion content analysis: cations were measured by atomic absorption spectrophotometer (Hitachi Z5010) and anions by ion chromatograph (Dionex).

Results

Soil texture in the profile was predominantly silty-loam at all locations down to 1.5 to 1.6 m. At site F1, pure ice was found from 1.5 m. The ice found in that particular sampling is part of ice wedges that can be 8 m long. It is this ice that if melted could form pools and cause ground subsidence. Pure ice was not found in burnt sites during sampling, but layers with high ice content were found below the active layer. By principle ice wedges are distributed in areas were the soil is predominantly silty loam and they are absent in sandy loam soils.

Soil moisture

Soil moisture in the active layer sampled at the forest sites revealed different moisture conditions depending on the time elapsed after the fire occurrence. For the period when the sampling was conducted, a common pattern is observed for the forest sites: higher soil moisture in the upper part of the active layer (0 to 60 cm) with high soil moisture content (40 to 60%). This same pattern was observed in the B1, B2 and B3 site. In these three sites and in the forest sites, there exists a layer of lower soil moisture at the bottom of the active layer. In contrast, in sites B4 and B5 (25 and 50 years after fire occurrence), there is a built up of an ice-rich layer in the upper permafrost where soil moisture ranged from 0.4 to 0.6 cm^3.cm^{-3}). Soil moisture in the active layer at the "younger" burnt sites ranged from .2 to .4 cm^3.cm^{-3} at the surface of the mineral soil layer (below 10 cm). At approximately 120 cm depth at all burnt as well as intact forest sites, soil moisture increased, signaling the boundary zone or "shielding layer" between the active layer and area where ice-rich permafrost concentrates (Shur 1988). In the burnt sites the active layer depth ranged from approximately 130 to 160 cm depending on the time elapsed after the fire event (Fig.1). In each site, vegetation differs in biomass with grasses and fireweed

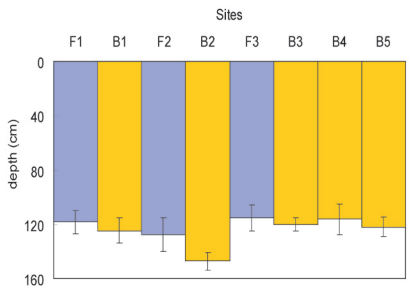

Figure 1. Soil thawing depth at the intact forest (F) and burnt (B) sites.

covering the recently burnt sites (B1 and B2) while birch dominates the sites burnt 15, 25 and 50 years ago (B3, B4 and B5). The size and age of trees differs accordingly but the most important characteristic is the vegetation succession. In B3, for instance, fireweed is non-existent and in B4 birch becomes dominant and its canopy covers the burnt site, while in the B5 site, larch trees are already present, although not still dominant.

Soil pH, EC_e and chemistry

Soil surface (0 to 15 cm) pH varies at the forest sites from 5.5 to 6.2 and then increases rapidly downwards. In the more recently burnt sites B1, B3 and B4, low pH values in the surface layer were observed, whereas pH in B2 and B5 were around 7. Regardless of the site, intact or burnt forest, pH shows a similar value of 8 from 50 cm downward. Despite significant differences observed in the total ion composition of the soil profile, no change was observed in the pH between the active layer and permafrost.

Electrical conductivity of the soil profile showed low values in the active layer (0.81±0.24) and high in the permafrost layer (1.0 to 3.0 $mS.cm^{-1}$) of the intact forest sites. In the burnt sites, EC_e is over 1.0 $mS.cm^{-1}$ and shows an increase in salt concentration in the active layer as compared to the intact forest site (Fig.2). Nevertheless, it is important to point out that EC_e in the B4 and B5 sites are similar to those in the intact forest. In general, the increase in salinity (using EC_e as a proxy) for the burnt sites in the active layer (1.03±0.19) is low in comparison to grasslands soil, for example. The most abundant ions in the active layer and upper permafrost are Cl^-, SO_4^{2-} and Na^+ (Lopez et al. 2007a). Of all these ions, it is the Na^+ that appears more mobile than the other two. As it was observed in the EC_e profile, ion concentration increases in the active layer as a result of fire disturbance. Na^+ moved upward in the B1, B2 and B3 sites, whereas in the B4 and B5 sites this was not observed and the concentration of Na^+ is similar to that in the active layer of the intact forest site. Cl^- appears to have decreased from the upper permafrost except for site B4, where the concentration in the permafrost was remarkably high. It was in the B2 and B3 sites that the increase of SO_4^{2-} was observed, while a decrease in the upper permafrost indicates that it was the source of this ion. Again, a remarkable concentration of SO_4^{2-} was observed in the upper permafrost layer of the B4 site as it was the case with Na^+.

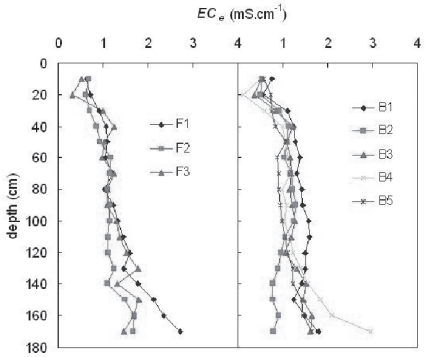

Figure 2. Electric conductivity in the intact forest (F) and burnt (B) sites. Each values are the mean of three samplings.

Discussion

Contrary to what has been suggested in previous studies, forest fires do not cause physical or chemical changes in the long-term that might bring changes in the landscape or specifically hinder the re-establishment of trees. These results, of course, do not suggest that thermokarst formations in the past were not triggered by forest fires. The conditions under which fires occurred at present differ from those during the early Holocene in which the landscape looks much different today than it did approximately 10,000 years ago. The thermokarst depressions intermingled within the forest and called "alas" are actually a drainage zone for the melting snow in early spring and the extreme precipitation events in summer (when the thawing layer is shallow and the storage capacity is low) that are characteristic in central Yakutia (Lopez et al. 2007b). Alas sites, where trees are not able to grow because of high salt content in the root zone (Desyatkin 1993, Lopez et al. 2007a) were caused by global climate changes that most probably triggered forest fires among several other climatic responses (Payette & Delwaide 2000). The results of this study suggest that at present, forests assimilate fires provided they keep the same frequency of occurrence to which they have been exposed during the Holocene. Unfortunately, fire frequency studies have been limited in Siberia, and other causes (political, social or economical) for fire have not been correctly addressed,

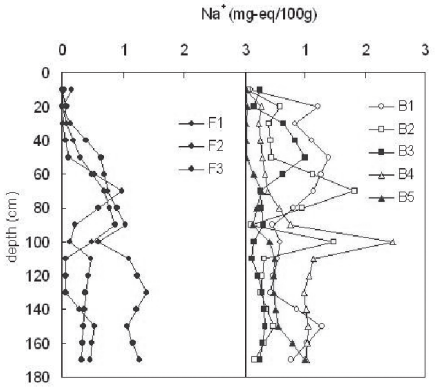

Figure 3. Na^+ profile in the soil profile (0-1.7 m) in the intact forest (F) and burnt (B) sites.

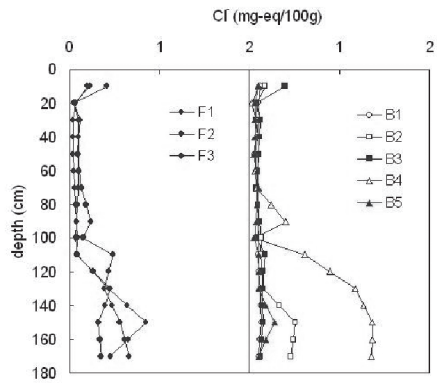

Figure 4. Cl^- profile in the soil profile (0-1.7 m) in the intact forest (F) and burnt (B) sites.

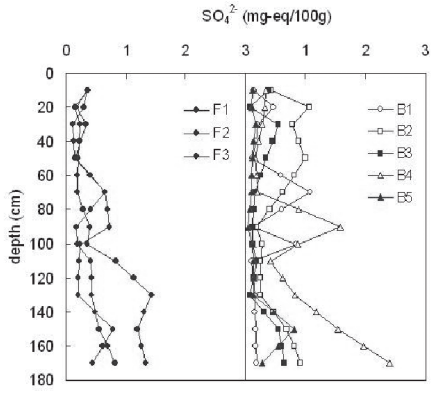

Figure 5. SO_4^{2-} profile in the soil profile (0-1.7 m) in the intact forest (F) and burnt (B) sites.

while global warming has been the most reasonable "pundit" to blame.

Soil moisture increased immediately in the active layer after clear-cut (Iwahana et al. 2005) sites in the same area whereas the cause for immediate increase of soil moisture in the active layer. In this experiment the same was not observed in the site more recently burnt (4 years) or in the other sites, suggesting that vegetation that appeared after severe forest fires (*Chamerion angustifolium*) transpired (2.6 mm d^{-1}, unpublished data) more than the vegetation that appears after clear-cuts. This transpiration rate is similar to the larch forest average transpiration of ~ 3 mm d^{-1} (Dolman et al. 2004, Ohta et al. 2001) in central Yakutia. After fires, the active layer is known to deepen in the first years and later recover to its former depth (Mackay 1995) following re-vegetation of the forest soil and thickening of the organic matter layer, factors that play an important role in keeping a thin active layer. Despite the spatiality of the sampling sites, recovery of the active layer has been also observed in this study. The difference of the above vegetation at each of the sites is thought to exert a strong influence on the water balance of the active layer, and thus cause movement of water that carries ions within its stream. The denser cover of birch trees 15 years after the fire occurrence is probably responsible for cooling of the active layer, as it can be observed from the active layer depth at each of the sites for the year when the experiment was conducted. The role of understory vegetation and the re-building of the organic mat cannot be set aside since they play an important role in keeping soil temperatures low in the soil (Harden et al. 2006). In the older burnt sites (25 years and 50 years) the depth of the active layer was found at around 110 cm depth which is similar to intact forest (Sawamoto et al. 2000). The B2 site had the deepest active layer (160 cm) in 2006. One of the explanation why B1 did not deepened as well could be that the fire in this latter site was light (not stand- replacing fire), and for that reason temperatures in this site were kept lower than in B2. As it has been observed in this study, deepening of the active layer has the potential to make soluble salts available for transport into the upper soil layers of the active layer. Elevated amounts of soluble salts in the root zone especially can affect negatively larch forest establishment because salinity affects plant growth and species diversity.

Between forest and thermokarst depressions in central Yakutia there is usually a belt of birch that marks a buffer zone where soil salt concentration is slightly higher than in the forest but lower than in the grassland soils (Lopez et al. 2007a). This spatial gradient of vegetation adaptability to soil conditions could be the explanation for chronological vegetation succession in fire-prone forest of eastern Siberia. According to information provided by local people, larch forest takes approximately 100 years to fully regenerate in this region.

The results of this study suggest that climate change, already observed in the form of increasing temperatures and increased precipitation in central Yakutia, have the potential to affect the boreal forest through forest fires but this will only happen if, prompted by higher summer temperatures, fire frequency increases prompted by higher summer temperatures, increases. Forest fires play a regeneration role that has been part of this boreal forest for centuries (Ivanova 1996) and has scarcely triggered thermokarst formations (Brouchkov et al. 2004). There should also be strong consideration of winter temperature and precipitation trends, since growing season hydrology and permafrost stability which is affected by winter conditions are strongly linked to the size and frequency of forest fires during the growing season (Ivanova. 1996, Harden et al. 2000) during the growing season.

Conclusions

The effects of forest fires in the boreal forest of central Yakutia are not permanent but are part of a regeneration cycle for the forest in this region. The steps leading to forest degradation (active layer continuous deepening, thawing of ice deposits, formation of pools on the forest soil, etc.) were not observed in the burnt sites in this study. On the contrary, forest fires appear as a temporal phenomenon that revitalizes the forest without affecting its stability.

Acknowledgments

The authors would like to thank the Ministry of Science, Culture and Education through Project RR2002. Our gratitude also goes to A. Cronin for making the English of this paper look "native."

References

Agafonov, L., Strunk, H. & Thomas, N. 2004. Thermokarst dynamics in Western Siberia: insights from dendrochronological research. *Palaeogeography, Palaeoclimatology, Palaeoecology* 209: 183-196.

Brouchkov, A., Fukuda, M., Fedorov, A.N., Konstantinov, P. & Iwahana, G. 2004. Thermokarst as a short-term permafrost disturbance, Central Yakutia. *Permafrost and Periglacial Processes* 15: 81-87.

Czudek, T. & Demek, J. 1970. Thermokarst in Siberia and its influence on the development of lowland relief. *Quaternary Research* 1: 103-120.

Desyatkin R.V. 1993. Syngenetic soil salinization during thermokarst alas formation. *Eurasian Soil Science* 25: 38-46.

Dolman, A.J., Maximov, T.C., Moors, E.J., Maximov, A.P., Elbers, J.A., Kononov, A.V., Waterloo, M.J. & Van der Molen, M.K. 2004. Net ecosystem exchange of carbon dioxide and water of far eastern Siberian larch (*Larix cajanderi*) on permafrost. *Biogeosciences* 1: 133-146.

Fedorov, A.N., Botulu, T.A. & Varlamov, C.P. 1991. Merzlotnie landshafti Yakutii (Poyacnitelnaya zapiska k "Merzlotna-Landshftnoi karte Yakutskoi ACCP masshataba 1:2,500,000. P.I. Melnikov (ed.), Moskow : GUGK, 2 pp.(in Russian).

Hamada, S., Ohta, T., Hiyama, T., Kuwada, T., Takahashi, A. & Maximov, T.C. 2004. *Hydrometeorological* behaviour of pine and larch forests in eastern Siberia. *Hydrological Processes* 18: 23-39.

Harden J.W., Trumbore, S.E., Stocks, B.J., Hirsch, A., Gower, S.T., O'Neill, K.P. & Kasischke, E.S. 2000. The role of fire in the boreal carbon budget. *Global Change Biology* 6: 174-184.

Harden J.W., Manies, K.L., Turetsky, M.R. & Neff, J.C. 2006. Effects of wildfire and permafrost on soil organic matter and soil climate in interior Alaska. *Global Change Biology* 12: 2391-2403.

Ivanova G.A. 1996. The extreme fire season in the central Taiga forest of Yakutia. In: J.G. Goldammer & V.V. Furyaev (eds.), *Fire in Ecosystems of Boreal Eurasia.* Dordrecht, the Netherlands: Kluwer Academic Publishers, 260-270.

Iwahana G.T., Machimura T., Kobayashi Y., Fedorov A.N., Konstantinov P.Y. & Fukuda M. 2005. Influence of forest clear-cutting on the thermal and hydrological regime of the active layer near Yakutsk, eastern Siberia. *J. Geophys. Research* 110: G02004, doi:10.1029/2005JG00039.

Kasischke E.S., Christensen N.L., Jr. & Stocks, B.J. 1995. Fire, global warming, and the carbon balance of boreal forests. *Ecological Applications* 5: 437-451.

Kokelj, S.V. & Lewkowicz, A.G. 1999. Salinization of Permafrost Terrain Due to Natural Geomorphic Disturbance, Fosheim Peninsula, Ellesmere Island. *Arctic* 52(4): 372-385.

Lopez, C.M.L., Brouchkov, A., Nakayama, H., Takakai, F., Fedorov, A.N. & Fukuda, M. 2007a. Epigenetic salinization and water movement in the active layer of Central Yakutia, Eastern Siberia. *Hydrological Processes* 21: 103-109.

Lopez, C.M.L., Saito, H., Kobayashi, Y., Shirota, T., Iwahana, G., Maximov, T.C. & Fukuda, M. 2007b. Inter-annual environmental-soil thawing rate variation and its control on transpiration from Larix cajanderi, Central Yakutia, Eastern Siberia. *Journal of Hydrology* 338: 251-260.

Mackay, J.R. 1995. Active layer changes (1968 to 1993) following the forest-tundra fire near Inuvik, N.W.T., Canada. *Arctic, Antarctic and Alpine Research* 27: 323-336.

Mouillot, F. & Field, C.B. 2005. Fire history and the global carbon budget carbon budget: a 1ºx1º fire history reconstruction for the 20th century. *Global Change Biology* 11: 398-430.

Nikolov, N. & Helmisaari, H. 1993. Silvics of the circumpolar boreal forest tree species. In: H.H. Shugart, R. Leemans & G. Bonan (eds.), *A Systems Analysis of the Global Boreal Forest.* Cambridge, England: Cambridge University Press, 111-132.

Ohta, T., Hiyama, T., Tanaka, H., Kuwada, T., Maximov, T.C., Ohata, T. & Fukushima., Y. 2001. Seasonal variation in the energy and water exchanges above and below a larch forest in eastern Siberia. *Hydrological Processes* 15: 1459-1476.

Page, A.L., Miller, R.H. & Keeney, D.R. 1982. *Methods of Soil Analysis, Second Edition.* Part 2-Chemical and *Microbiological Properties*, Second Edition. Madison, Wisconsin, 169 pp.

Payette, S. & Delwaide, A. 2000. Recent Permafrost Dynamics in a Subarctic Floodplain Associated with Changing Water Levels, Quebec, Canada. *Arctic, Antarctic and Alpine Research* 32: 316-323.

Radionow, A., Flessa, H., Kazansky, O. & Guggenberger, G., 2006. Organic matter composition and potential trace gas production of permafrost soils in the forest tundra in Northern Siberia. *Geoderma* 135: 49-62.

Sawamoto, T., Hatano, R., Yajima, T., Takahashi, K. & Isaev, AP. 2000. Soil respiration in Siberian Taiga Ecosystems with different Histories of Forest Fire. *Soil Science and Plant Nutrition* 46 (1): 31-42.

Shender, N.I., Romanovsky B.E. & Tetelbaum A.C. 1999. Prognoz estestbennoistoricheskih kolebanii klimata gorodov Yakutska i Ferbenska. *Nauka y Obrazobanie* 2: 24-29. (in Russian)

Shur, Y.L. 1998. *The Upper Horizon of Frozen Strata and Thermokarst.* Novosibirsk: Nauka, 212 pp.

Slavich, P.G. & Petterson, G.H. 1993. Estimating the Electrical Conductivity of Saturated Paste Extracts from 1:5 Soil:Water Suspensions and Texture. *Australian Journal of Soil Research* 31: 73-81.

Smith, M.W. 1975. Microclimatic Influences on Ground Temperatures and Permafrost Distribution, Mackenzie Delta, Northwest Territories. *Canadian Journal of Earth Science* 12: 1421-1438.

Tsvetkov, P.A. 2004. Pyrophytic properties of the Larch Larix gmelinii in Terms of Life Strategies. *Russian Journal of Ecology* 35: 224-229.

Zimov, S.A., Davidov, S.P., Voropaev, Y.V. & Prosiannikov, S.F. 1996. Siberian CO_2 efflux in winter as a CO_2 source and cause of seasonality in atmospheric CO_2. *Climatic Change* 33: 111-120.

Pedogenesis and Its Influence on the Structure of the Upper Layer of Permafrost

A.V. Lupachev
Institute of Physicochemical and Biological Problems in Soil Science of RAS
142290, Russia, Moscow Region, Pushchino, Institutskaya, 2
S.V. Gubin
Institute of Physicochemical and Biological Problems in Soil Science of RAS
142290, Russia, Moscow Region, Pushchino, Institutskaya, 2

Abstract

The structure of the upper layers of permafrost and their interaction with cryosols was studied. Cryogenic processes are widely distributed on loamy watersheds of North Jakutia's lowlands, where the active layer is relatively shallow. The upper layer of permafrost here is very complicated and its genesis is connected with the Holocene environmental conditions and pedogenic processes of that time. The authors propose the term "soil-cryogenic complex" that includes the soil profile, transient layer, and intermediate layer of permafrost. The role of the above-permafrost horizon of cryosols in forming structure, properties, and spatial differences of the transient layer was analyzed. Widely distributed lateral transition and accumulation of coarse organic matter between the elements of tundra microrelief were obtained.

Keywords: above-permafrost horizon; active layer; intermediate layer; lateral redistribution; soil organics; transition layer.

Introduction

In case of shallow thickness of the active layer (AL) (1 m and less), permafrost plays a great role in pedogenesis and determines the wide complex of signs and properties of cryosols. It is a significant physical and geochemical barrier that prevents vertical matter migration and determines its lateral redistribution (Shur 1988, Gubin 1994, Alekseev et al. 2003). The relatively high dynamics of AL thickness cause the formation of the complex structure of permafrost upper layers that reflect spatio-temporal interactions with pedogenesis.

Depending on climatic fluctuations, weather conditions, soil cover, and vegetation genesis, this zone of contact can appear as a component of the AL or as a component of permafrost (Shur & Jorgenson 1998, Shur et al. 2005).

The transient layer (TL) (the layer which thaws in the warmest conditions) and the intermediate layer (IL) (the layer of maximal Holocene thaw) are the upper layers of permafrost within this zone (Shur 1975, Shur 1988). The main properties and diagnostic signs of the TL, such as its thickness and the seasonal and long-term dynamics of being in a frozen or thawed state, are the significant factors that influence pedogenesis. It is well-known that the majority of pedogenic fieldwork in high-latitude areas is conducted in the summer, when the AL has not reached its maximum yet and the real above-permafrost soil horizon is still frozen. True thickness of the AL and the morphological structure of soils can be obtained only at the end of September–beginning of October, when surface freezing begins and snow cover becomes stable.

Methods

The moundy soil complex and TL were analyzed on loamy watershed sites of the Khomus-Yuriakh River (Indigirka lowland; 70°00′N, 153°36′E) and Sukharnaya River (Kolyma lowland; 69°30′N, 152°00′E). The basic deposits here are Late Pleistocene silty loams with the features of synlithogenic pedogenesis and with ice complex (yedoma formation). The IL thickness here is about 1–1.5 m. The vegetation cover is represented with moss-sedge-cotton-grass on the Indigirka site and with moss-sage-dryas on the Kolyma site. The mean gradients of the watershed slopes are about 2–3°. The Kolyma site has the features of steppe because of low thickness of snow cover and better drainage.

The structure of soils and the TL were analyzed at the beginning of autumn, when the AL had reached its relative maximum. On the Kolyma site, two trenches were dug through all microrelief elements (2 and 5 m long, 40 cm wide). The structure of soils, their horizon thickness, the AL thickness, and the TL structure (upper 20 cm) were studied. Near the trenches numerous additional soil pits (n = 15) were dug to obtain the variety of morphological properties of soils under the mounds of different height and types of vegetation and under the cracks of different depth.

On the Indigirka site, it was necessary to find two experimental, square sites because of more complete soil structure. The first (basic) site is on watershed (250 x 250 cm), and the second (additional) is on the top of a gentle slope (200 x 80 cm; 150 m from the first site; slope gradient, 3°). All of the microrelief elements were within these sites: low, middle, and high mounds with different vegetation, sedge-cotton-grass tussocks. Choosing the proper site, the maximal difference between mounds and crack surface was

a concern. The majority of elements within the sites was similar; surface structure, size of mounds and cracks, soil and vegetation cover, and quantity of patchy mounds. The main difference was in relatively more ponding of the second (slope) site which was reflected in a greater distribution of tussocks.

On the first site (watershed), soil and permafrost surfaces were graded. The highest point of a site was taken as "zero," with the precision of 1 cm and an interval of measure of 5 cm; 2500 measurements of each parameter were made. Measurements of soil horizon thickness (organogenic and above-permafrost) and the TL structure were made with an interval of 10 cm in 10 trenches, 25 cm wide.

After clearance of the site bottom, the lateral structure of the TL was analyzed. There are three main components of it: ice, ice-ground, and frozen coarse organics. Its ice saturation was estimated, and the cryogenic texture was obtained. Morphological analysis of soil profiles was made on the example of the most representative side of the trench, where samples were also taken. According to this data, schemes of soil and permafrost surface, TL structure, and vegetation-cover structure were made.

Additional soil pits (n = 15) were dug near the experimental sites and the TL structure was also studied to a depth of about 20 cm. The AL thickness was measured under the different types of mounds and cracks (n = 130).

The same measurements were made on the second site (slope), but the interval of measurements was 10 cm.

Results and Discussion

Comparison of the soil and permafrost surface schemes of the first Indigirka site (watershed) showed that the microelevations of the TL surface are under mounds and are represented by ice. The authors suggest that such structure of the TL surface can be determined by the previous history of soil-surface genesis, and propose the following model of ice formation.

At the earlier stages of nanorelief genesis (patchy mound with sparse vegetation), the AL thickness was more than under cracks. While thawed, water has accumulated here, and then with seasonal freezing, has turned to ice. This accumulation had a progressive tendency caused by ice forming on the one hand and by vegetation and organogenic horizon forming that has decreased the heat flux on the other hand. Heat absorption differences between ice, ice-ground, and frozen coarse organics determined different speeds of thaw, TL surface genesis, and structure formation (Mackay 1983).

The results of comparing soil surface and TL microrelief schemes of the second Indigirka site are a little bit different. Their topography is well expressed too, but the micro-depression zones of the TL surface are mainly distributed under the centers of mounds, and are presented by ice-grounds or coarse organics. The micro-elevations are under cracks filled with peat. Ice distribution in the TL is related to circumferential parts of mounds, and ice underlies 5–10 cm deeper than the TL surface. The same situation in the soil and the TL structure was obtained in numerous additional pits (n = 8) in microrelief and appears to be authentic for this region of the Indigirka lowland.

Another component of the above-permafrost horizon (AH) and TL formation was obtained in numerous soil pits and trenches. When the AL thickness reaches its relative maximum, the lower parts of soil profiles are over-saturated with water. The microdepressions of the TL surface microrelief become the channels, where the inrush of water is obtained. The scheme of possible fluxes, which was created by a method of relief plastic (Stepanov 2006) on data basis, coincided with the situation obtained in the field. Such water redistribution determines the coarse organic matter redistribution and discharge (Shuster et al, 2003, Mergelov 2006). The material is denuded from the microelevations of the TL surface and accumulates in the microdepressions. The obtained data show that the mean slope gradient is about 2–5°, and the maximal is 12–15° or even 20°. Such an active migration of small portions of wet peat along the microslopes can be forwarded by thaw of ice-ground with the reticulated cryotexture, which is distributed in negative microrelief forms.

The authors suppose that the difference in spatial structure of the TL and the AH is determined by the processes which occur in the lower parts of the soil profile and by the interaction of microrelief elements.

On the Indigirka site, in the majority of cryosols under mounds, the organogenic AH is forming. It consists of peat mixed with mineral material. Organic carbon content here is 4.7% (n = 6). These indexes are a little bit higher in the TL, but then they decrease with depth. Both horizons are spatially different. Zones which are extremely rich with organics are obtained here (23.4%). There are also flux-like zones in which the organic material is mixed with the mineral one (3.2%). As for the mean samples of coarse organic material, total organic carbon content is 10.1% for the first experimental site (n = 10) and 8.9% for the second (n = 6). The mean thickness of the AH is 7–12 cm, and the total thickness of this horizon with the TL is 25–32 cm. This data coincide with that of another author (Hinkel 2005).

The mean thickness of the peat (or duff) horizon is not more than 7–13 cm, and the quantity of organic carbon here is about 9%. So in some cases, the store of organic carbon in the system here (AH + TL) is even more than in the upper parts of soil profiles (except of peat soils in nanopolygonal cracks).

The given data allow us to single out the organogenic AH of Indigirka tundra soils that differs from similar horizons with cryoturbated organic material of the Kolyma lowland (Karavaeva 1969, Gubin 1994), other regions of North Jakutia (Elovskaya et al. 1979), and East European tundra (Ignatenko 1979). Soils with such an unusual lower horizon and TL were obtained earlier (in the 1980s–1990s) on watersheds of typical tundra in the Alazeya-Kolyma region. Distribution of such soils is limited, and the main requisition is the existence of cracks filled with peat that reach the surface

of permafrost. So the possibility of such a system forming is determined by contemporary and previous (Holocene) conditions (AL thickness, processes of frost heaving and peat forming, etc.).

Conclusions

An analysis of loamy watershed deposits and cryosols of North Jakutia lowlands shows the existence of a complex system of layers with different properties on the border between the AL and permafrost. Its genesis and structure are determined by the bioclimatic situation of the Holocene. The authors propose to single out this system as a "soil-cryogenic complex." Its structure is the following: soil profile: TL (a layer which thaws in the warmest conditions) and IL (a layer of maximal Holocene thaw). The border between the AH and TL is the arena of active pedogenesis, where its most specific features are reflected. The spatio-temporal differences of this system show the mechanisms of soil-cover genesis and the interactions between its elements. Such well-expressed permafrost microrelief determines the wide lateral redistribution, migration, and accumulation of coarse organic matter within this complex.

Acknowledgments

The authors thank Yuri Shur for the inspiration for this work and for genuine interest in it.

References

Alekseev, A., Alekseeva, T., Ostroumov, V., Siegert C. & Gradusov B. 2003. Mineral transformations in permafrost-affected soils, North Kolyma lowland, Russia. *Soil Science Society of America Journal* 67: 596-605.

Elovskaya, L.G., Petrova, E.I. & Teterina, L.V. 1979. Soils of North Jakutia. Nauka, Novosibirsk (in Russian).

Gubin, S.V. 1994. Late Pleistocene soil formation on sea-lowlands of North Jakutia. *Pochvovedenie* 8: 5-14 (in Russian).

Hinkel, K.M. 2005. Characteristics and significance of the transition zone in drained thaw-lake basins of the Arctic Coastal Plain, Alaska. Published 01.12.2005 online in *Goliath*.

Ignatenko, I.V. 1979. Soils of East-European tundra and forest-tundra. Nauka, Moscow (in Russian).

Karavaeva, N.A. 1969. Tundra soils of North Jakutia. Nauka, Moscow (in Russian).

Mackay, J.R. 1983. Downward water movement into frozen ground, western arctic coast, Canada. *Canadian Journal of Earth Sciences* 20(1): 120-134.

Mergelov, N.S. 2006. Origin of organic carbon pools in Kolyma cryosols: Phenomenon of organic carbon impregnation in mineral horizons. In *Proceedings of 18th World Congress of Soil Science July 9-15, 2006, Philadelphia, Pennsylvania, USA*.

Shur, Y.L. 1975. On the transient layer. In: P.F. Shvetsov & L.V. Chistotinov (Eds.), *Methods of Geocryological Studies*, Shvetsov, USSR Institute of Hydrogeology and Engineering Ecology, Moscow: 82-85 (in Russian).

Shur, Y.L. 1988. Upper horizon of permafrost and thermokarst. Nauka, Moscow (in Russian).

Shur, Y.L. & Jorgenson, M.T. 1998. Cryostructure development on the floodplain of Colville River Delta, northern Alaska. *Proceedings of Seventh International Conference on Permafrost*. Centre d'Etudes Nordiques, Universite Laval: Quebec: 993-1000.

Shur, Y.L., Hinkel, K.M. & Nelson, F.E. 2005. The transient layer: implications for geocryology and climate-change science. Published online in *Wiley Interscience*. DOI: 10.1002/ppp.518.

Shuster, P.F., Reddy, M.M., Aiken J.R. & Shanley, J.B. 2003. What effect does permafrost have on dissolved organic carbon transport to streams during snowmelt? *U.S. Geological Survey, Water Resources Discipline.*

Stepanov, I.N. 2006. Relief plastics theory and new thematic maps. Nauka, Moscow (in Russian).

Soil Properties of the Eroding Coastline at Barter Island, Alaska

Lorene A. Lynn, Chien-Lu Ping, Gary J. Michaelson
Palmer Research Center, Agricultural & Forestry Experiment Station, University of Alaska Fairbanks, Palmer, AK, USA
M. Torre Jorgenson
Alaska Biological Research, Inc., Fairbanks, AK, USA

Abstract

Erosion along Alaska's Beaufort Sea Coast introduces substantial quantities of largely undecomposed organic matter into the Arctic Ocean annually. Three bluff exposures along the northern coastline of Barter Island revealed organic materials extending 1.5 meters below the surface. Peat deposits (12–80 cm thick) are in sediments that extend to 1.8 meters and overlay sands and gravels, under which are alluvial-marine sediments. The bluff exposures are composed of 10–20% ice wedges and moisture content of the soil ranged 2–80%. Total carbon content in the active layer averaged 10% and 14% in the frozen soil. Total nitrogen was less than 2% throughout the soil profiles. Soil pH and electrical conductivity show a relationship between mineral soils at depth and increased values.

Keywords: Arctic Alaska; coastal erosion; cryogenesis; cryoturbation; gelisols, patterned ground soils.

Introduction

Coastal erosion is a growing concern in northern Alaska. The apparent accelerated rate of erosion along the Beaufort Sea coast of Alaska (Brown et al. 2003) may have major implications for life and development along the coast. Several coastal Native Alaska villages are battling against increasing storm intensity and frequency (McCabe et al. 2001), a continuing loss in duration of the protective sea ice (Fetterer 2002, IPCC 2007), and increasing summer temperatures (Jorgenson et al. 2006). All of these are causing increased erosion and permafrost degradation. In Kaktovik, located on Barter Island, the current airport and an old landfill site are rapidly eroding into the sea (Robinson 2004). Erosion along the arctic coastline of northern Alaska has also been hypothesized to be a significant influence on global climate change due to the input of carbon-rich peat soils into the ocean and carbon dioxide to the atmosphere (Jorgenson et al. 2005). The result may be a positive feedback to an Arctic warming cycle.

On polygonal terrain along the coast, soil physical structure and chemical properties are strongly related to ice wedge polygon development (Shur and Jorgenson 2007). This interactive-formative process may span a period of five to eight thousand years. Soil stratifications and physical structures are mixed and warped, by cryoturbation, at the boundary of ice wedges due to freeze-thaw cycles and ice wedge formation and reformation (Bockheim 2007). This situation complicates the examination of soil morphology and characterization of the active layer and renders the systematic interpretation of permafrost soils a challenge.

In the past, tundra soils have been a significant carbon sink because primary production has been greater than the slow decomposition rate of organic matter in cold and frozen permafrost soils (Hobbie et al. 2000, Ovenden 1990). As a consequence, it is estimated that tundra soils have accumulated an estimated 25–33% of the world's soil carbon (Oechel and Vourlitis 1995). Soils along the Arctic coastline contain large quantities of mostly poorly decomposed organic materials (Ovenden 1990, Ping et al. 1997). As the coast erodes, there is a change in the thermal regime of the soil and the ice wedges degrade. Moisture content decreases while temperatures increase, and as a result the active layer thickens.

Likewise, warming temperatures can cause large scale permafrost and ice wedge degradation (Jorgenson et al. 2006) which can in turn cause substantial changes in surface hydrology (Hinzman 2005). In the last several decades, temperatures have been on the rise in the Northern Hemisphere, most notably in the Arctic and Sub-Arctic (IPCC 2007), and there is evidence that this warming trend will continue unabated (Chapman and Walsh 1993, Serreze et al. 2001). The current warming trend in the arctic is evidenced by increased erosion of the northern coast of Alaska (Semiletov 1999, Brown et al. 2003), permafrost degradation (Jorgenson and Kreig 1988, Jorgenson et al. 2001), and decreased extent and duration of sea ice and hydrological changes (Morrison et al. 2000).

The ability to make predictions about changes in the soil depends on an understanding of what alterations are taking place and what interactions may occur between various soil properties. To understand the complex changes that may occur due to erosion of coastal soils, a detailed study of soil morphology, as well as chemical and physical soil processes is required. In this study we examine properties of the soils that are eroding along the coastine exposures near Kaktovic Alaska in order to better understand the processes occurring and materials being transferred to nearshore waters.

Methods

Sites for intensive investigation were selected on the northern shore of Barter Island, west of the village of Kaktovik. Three bluffs sites were selected for excavation and sampling (GPS: 70.13393N, -143.65578W, 70.13393N, -143.65245W, and 70.1345N, -143.66083W). Polygons

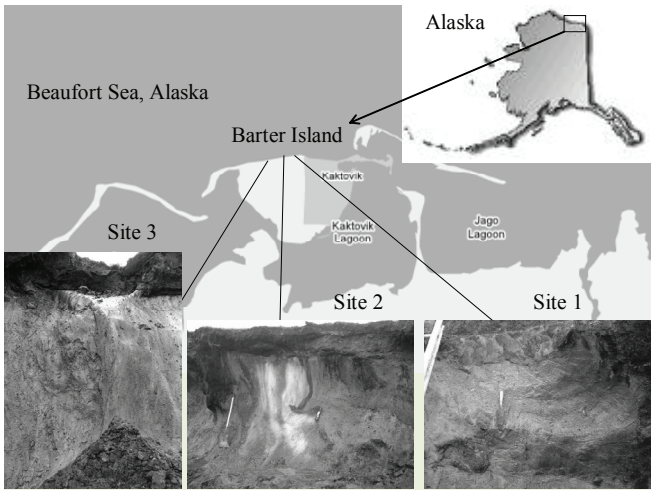

Figure 1. Site location and profile photos.

west of Kaktovik are very large and flat, measuring 12–20 m in diameter, indicating large ice wedge formation. Exposed ice wedges at the eroding bluff are indeed large, reaching 3–3.5 m in width. The large ice wedges and dense surface polygonal net in this area are consistent with high bluff alluvial-marine sediment landforms. Most of the vegetation cover along the northern Barter Island coastal bluff is sedge with some willow and small amounts of Dryas found on frost boils. Bluff exposures at three points located approximately 100 m apart (Fig. 1) were cleaned from the surface to a depth of 1.5 meters. Following removal of slumped and refrozen material, the soil layers were identified (Schoeneberger et al., 1998), dimensional samples were cut from the active layer, and dimensional core drilled with a SIPRE corer to a maximum depth of 1.5 m. All samples were kept frozen until time of analysis at the UAF-AFES Plant and Soils Laboratory at the Palmer Research Center. Soil bulk density and water contents were determined by weight difference of dimensional samples upon drying at 100°C. Total organic C (TOC) and N were determined using a LECO CHN analyzer and organic matter (%OM) by loss on ignition at 450°C. Exposure sediment, water, TOC, and N stocks were determined using the exposure description and analysis by the method of Kimble et al. (1993) to account for cryoturbation. Temperatures from near the surface soil and right above the permafrost table were measured with a thermometer.

Results and Discussion

Temperature

Soil temperatures in the first week of August, 2006, at the ground surface, measured from 5–7°C, and just above the permafrost 2–5°C. Surface temperatures are likely to vary based on weather conditions present.

Cryogenic features

Active layers along the northern coast of Barter Island averaged lower volumetric water at 38% compared to the permafrost which averaged 53% volumetric ice (Table 1).

Table 1. Soil properties for eroding shoreline at Barter Island, Alaska.

	Bluff Exposure		
Property	1	2	3
Bank height above water (m)	18	18	18
Mean thaw depth (cm)	45	36	54
Cumulative organic thickness (cm)	77	63	87
Maximum organic depth (cm)	133	78	127
Total amount of wedge ice volume (%)	21	20	18
Total organic carbon store in top 1m, excluding ice wedges, volumetric extrapolation from sample, (kg C/m²)	32	41	34

The high water content in active layers is positively related to organic matter which has high water holding capacity.

The high water (ice) content in permafrost is due to segregation of ice. The upper active layer is dryer than the permafrost due to exposure to warmer temperatures, drainage at the bluff face, and lateral movement to lower-lying thermo-erosion troughs nearby. In addition to buried organic layers holding water, ice lenses ranging in thickness from 1mm to 20mm were present in the permafrost cores. Vertically aligned ice bubbles in these ice lenses indicate that each lens is a former freezing front. In early winter, the thawed portion of the soil refreezes at two fronts: from the surface and from the underlying permafrost. Water in the active layer migrates toward these freezing fronts and low-lying water will migrate toward the lower freezing front. This vertical movement is evidenced in the bubble alignment. All three cores showed evidence of refreezing in the first 3 cm from a deeper thaw in a previous summer.

Ice wedge volume on Barter Island is higher compared to other portions of the Beaufort Sea coast. The high bluffs provide protection from direct ocean wave impact and erosion. Because of the volume of the large ice wedges, extensive cryoturbation is evident. As the ice wedges develop and expand, they squeeze the inter-laying soils, bending and distorting soil horizons, and altering bulk density and thus, moisture-holding capacity. This evidence of cryoturbation is strongest near the ice wedges and less in the center areas of polygons. Barter Island experiences short, cool summers and very cold winter temperatures. The severe cold can cause the surface soil layers to crack vertically. The combination of material falling or washing into these cracks, and the distortion imposed on soil layers by expanding ice wedges creates the cryoturbated features (Fig. 1).

Morphological properties

Depending on where the permafrost core is drilled in relation to the location of the ice wedges, great differences in soil stratigraphy are observed. For example, in the core at Site 1, a peat-filled crack extended from 125 to 133 cm below the surface, and vertically oriented layers of peat and sediments were found at a depth of 80–125 cm. The vertical

Table 2. Soil properties by horizon.

Exposure #	Horizon	Depth range (cm)	pH	EC ds cm²	Texture	Thermal State	Total OC (%)	Total N (%)	Total OM (%)
1	Oi/Oe	0-12	5.64	1.08	MK	AL	22.5	1.61	44.5
70.13393N	Bw	15-30	5.4	0.49	SIL	AL	2.47	0.148	3.99
-143.65578W	Oajj	30-45	4.98	0.58	MK	AL	14.7	0.810	30.2
	Oaf/Bgfjj	38-70	6.82	5.20	MK/SIL	Pf	7.21	0.498	14.4
	Bgf/Oafjj	70-99	6.79	11.25	SIL/MK	Pf	4.13	0.332	8.27
	Af/Oafjj	99-146	6.96	12.75	SI/MK	Pf	5.04	0.272	10.1
2	Oa	0-17	5.18	0.95	MK	AL	20.5	0.198	40.9
70.13393N	Bg	17-38	4.79	0.53	SIL (10% GR)	AL	19.9	1.15	39.8
-143.65245W	Oi/Bgjj	38-50	4.9	0.73	PTMK/SIL	AL	19.4	1.26	31.5
	Oaf/Bgfjj	50-75	4.93	2.35	MK/SIL	Pf	22.1	1.38	24.2
	Cf	79-94	7.04	2.37	S	Pf	0.770	1.52	1.54
3	Oa	0-19	6.58	0.86	MK	AL	14.4	0.00	28.9
70.1345N	Bw/Oajj	19-40	5.98	5.16	SIL	AL	19.7	1.34	20.0
-143.66083W	Oa	40-52	5.86	0.90	MK	AL	13.5	1.00	26.9
	Oa1/Bgf1	60-75	5.97	0.86	MK/SIL	Pf	14.7	0.953	35.4
	Oa2/Bgf2	80-85	6.53	1.15	MK/SIL	Pf	14.2	1.08	28.4
	Oa3/Bgf3	100-105	6.87	1.08	MK/SIL	Pf	6.50	1.05	13.0
	Oa4/Bgf4	117-127	6.78	1.65	MK/SIL	Pf	11.2	0.706	22.4
	Cf	140-155	7.36	2.52	S	Pf	1.13	0.0730	2.26

*AL=active layer; Pf=permafrost.

stratigraphy and high ice volume (50–70%) indicates that this core resides in close proximity to an ice wedge. Similar conditions existed at Site 3. The first attempt to drill a core at Site 2 resulted in a high ice volume sample with vertically oriented peat horizons, appearing as if cracks in the soil surface had filled with water, distorting the soil stratigraphy. At 97cm, gravel was encountered, drilling stopped, and a second, successful drilling, just 0.5m from the original site, resulted in the core used for analysis. The core at Site 2 had nearly horizontal soil layers with abrupt wavy boundaries. Layers of muck (sapric) alternated with mineral sediments, most likely deposited by eolian or alluvial processes. Organic-rich materials with lower ice volume (pore ice at 30%) were found from 50–70cm and below that marine-alluvial sand deposits were encountered.

All three sites followed similar general horizonation in the active layer. A thick organic layer (12–19cm) lay over silt, which lay over a more decomposed organic layer. Mixing of these layers due to cryoturbation was present in some cases, but the origin of the horizons could still be distinguished by texture (muck for organic materials and silt loam for Bg or Bw horizons). Organic matter was found cryoturbated deep into the permafrost to a depth of 133 cm. None of the bluff cores exhibited clear horizontal layering as the result of strong cryoturbation.

Redoximorphic features were observed in the root channels of the Bg and Bw horizons in the active layer (Fe-concentration 7.5 YR 5/8, matrix 2.5 Y 4/1). The saturated conditions created a reducing environment in which root channels become the source of oxygen in the redox process. Organic acids produced in the surface organic layers lower the pH and iron is reduced from Fe(III) to Fe(II). The reduced iron is water soluble and carried with water movement to the lower mineral layers. Roots extending into the mineral horizons exude oxygen where microbial activity facilitates oxidation and precipitation of the iron Fe(III) oxides resulting in the presence of reddish-brown soil mottling.

Soil physical properties

Thaw depth varied slightly among the 3 sites (45, 36, and 54 cm) most likely due to micro-topographical differences. Thaw depths are smallest in polygon troughs and deeper at the center of the polygon, and deeper again on the rim. Polygon troughs were generally avoided for pit excavation and coring, as they tend to have ice wedges (pure massive ice) below the surface. Thaw depths were not measured according to micro-topographical features, but in relationship to bluff excavations. Thaw depths of 25–50 cm are typical at bluff exposures along the Beaufort Sea coast, but varies somewhat based on annual climate at a particular site.

Soil textures at these locations were found to be fairly consistent. Muck layers (Oa) were found in the top 10–20 cm at all sites, followed by a silt loam horizon (Bg or Bw, 10–40 cm) and then a muck or muck/silt loam horizon (Oa/Bgjj) starting at 38 cm and extending to 100 cm in one site. Cores 2 and 3 had a Cf horizon of alluvial-marine sand at 79 and 140 cm respectively. This pattern of vertically stratified organics, mineral, organics, mixed organic/mineral, and sand

gives a glimpse into the formation of the soils at the coast. The surface organic layer has likely been developing for many hundreds of years. The underlying thick silt layer is an indicator of a long-term event of eolian or alluvial deposit, which was preceded by a period of plant growth similar to current conditions. Cryoturbation has largely erased similar historical pattern in the permafrost layers, but the underlying sand layers are remnants from the end of the last ice age.

Chemical properties

Surface organic horizons and buried organic layers contained the highest quantity of organic carbon (OC) averaging 19.1% and 12.0%, respectively, and the silt dominant layers contained 7.6% OC on average. The total nitrogen (N) averaged 1% with no clear correlation between the values and the soil type, mineral or organic. This may be due in part to the difficulty in separating the mineral and organic components in cryoturbated layers. The pH at each site tended to increase with depth, as did the EC, especially in the mineral horizons. Additionally, there is an inverse relationship between the TOC%, pH and EC, which reflects the strong influence of the organic matter on soil properties. Organic acids produced by the OM decrease the pH values, but also act as a buffer, neutralizing the salt effects. Thus, the EC was lower in organic-rich layers, but higher in the mineral soil. The higher pH values found in deeper, mineral soils are due to the calcareous nature of the parent materials (Ca-rich deposits from the Brooks Range). At bluff Site 1, the EC values are significantly higher between 38–146 cm. This may be due to one of two reasons. One theory is that these soils represent an old surface, a thaw lake that had at one time been flooded with seawater. Another possibility is that the neighboring area, which was treated with bio-solids for 13 years, affected surrounding soils. The high salt content of the waste may have migrated and moved deep under the surface through frost cracks and cryoturbation.

Conclusions

Soils along the high bluffs of Barter Island are characterized by high ice volume, both in size of ice wedges and segregated ice within the depth measured. Cold temperature and the wet tundra on the coastal plain contribute to such ice formation. Cryoturbation was found in all exposed bluff faces and permafrost cores drilled inland. All active layers exhibited a similar pattern of horizonation: thick surface organic layer over a mineral B horizon, with a cryoturbated O horizon underneath. Redoximorphic features exhibited in pore linings and masses were common in the mineral B horizons. All profiles contained high organic carbon and increasing pH with depth.

Additional research is currently underway on the soil properties of similar soils inland from the bluff, those not impacted by erosion, in an effort to add to the understanding of the impacts of coastal erosion on soil properties.

Acknowledgments

This project is funded by a grant from the National Science Foundation #0436179. Fugen Dou, Daniel Fortier, B.J. Haggard, Mikhail Kanevskiy, and David Weindorf helped with field collection.

References

Bockheim, J.G. 2007. Importance of cryoturbation in redistributing organic carbon in permafrost-affected soils. *Soil Science Society of America Journal* 71:1335-1342.

Brown, J., Jorgenson, M.T., Smith, O.P. & Lee, W. 2003. Long-term rates of erosion and carbon input, Elson Lagoon, Barrow, Alaska. In Phillips, M., Springman, S.M. & Arenson, L.U. (Eds.), *ICOP 2003 Permafrost: Proceedings of the 8th International Conference on Permafrost.* Netherlands: A. A. Balkema Publishers, 101-106.

Chapman, W. L. & Walsh, J.E. 1993. Recent variations of sea ice and air temperature in high latitudes. *Bull. Amer. Meterol. Society* 74:33-47.

Fetterer, F., Knowles, K., Meier, W., and Savoie, M. 2002, updated 2007. Sea ice index. Digital media. National Snow and Ice Data Center. Boulder, CO.

Hinzman, L.D., Kane, D.L. & Woo, M. 2005. Permafrost Hydrology. *Encyclopedia of Hydrological Sciences*. Indianapolis, IN: John Wiley & Sons, Ltd.

Hobbie, S.E, Schimel, J.P., Trumbore, S.E., & Randerson, J.R. 2000. Controls over carbon storage and turnover in high-latitude soils. *Global Change Biology* 6(s1):196-210.

IPCC. 2007. Summary for Policymakers. In: *Climate Change 2007: Impacts, Adaptation and Vulnerability.* Contribution of Working Group II to the Fourth Assessment Report of the Intergovernmental Panel on Climate Change, Parry, M.L., Canziani, O.F., Palutikof, J.P., van der Linden, P.J. & Hanson, C.E., Eds. Cambridge, UK: Cambridge University Press 7-22.

Kimble, J.M., Tarnocai, C., Ping, C.L., Ahrens, R., Smith, C.A.S., Moore, J. & Lynn, W. 1993. Determination of the amount of carbon in highly cryoturbated soils. In Gilichinsky, D.A. Ed. *Post-Seminar Proceedings of the Joint Russian-American Seminar on Cryopedology and Global Change.* Pushchino, Russia, 15-16 Nov. 1992. Pushchino, Russia: Russian Academy of Science.

Jorgenson, M.T., & Kreig, R.A. 1988. A model for mapping permafrost distribution based on landscape component maps and climatic variables. *Proc. Fifth Int. Conf. on Permafrost.* Trondheim, Norway: TAPIR Publishers, 176-183.

Jorgenson, M.T., Racine, C.H., Walters, J.C. & Osterkamp, T.E. 2001. Permafrost degradation and ecological changes associated with a warming climate in central Alaska. *Climate Change* 48:551-579.

Jorgenson, M. T., Ping, C.L. Guo, L. Shur Y., and. Brown, J. 2005. A multi-scale approach to assessing the flux and transformation of organic carbon across the eroding coastline of northern Alaska. Berichte Zur Polarund Meeresforschung 506:65-68.

Jorgenson, M.T., Shur, Y.L., and Pullman, E.R. 2006. Abrupt increase in permafrost degradation in Arctic Alaska. *Geophysical Research Letters* 33, L02503, doi:10.1029/2005GL024960.

McCabe, G.J., Clark, M.P., Serreze, M.C. 2001. Trends in northern hemisphere surface cyclone frequency and intensity. *Journal of Climate* 14:2763-2768.

Morison, J., Aagaard, K. & Steele, M. 2000. Recent environmental changes in the Arctic: a review. *Arctic* 53:359-371.

Oechel, W.C, Vourlitis, G.L., Hastings, S.J. & Bochkarev, S.A. 1995. Change in arctic CO2 flux over two decades: effects of climate change at Barrow, Alaska, *Ecological Applications* 5(3):846-855.

Ovenden, L. 1990 Peat accumulation in northern wetlands. *Quaternary Research* 33:377-386.

Ping, C.L., Michaelson, G.J., & Kimble, J.M. 1997. Carbon storage along a latitudinal transect in Alaska. *Nutrient Cycling Agroecosystems* 49:235-242.

Robinson, R.A. 2004. Villages affected by flooding and erosion have difficulty qualifying for federal assistance. Highlights of GAO-04-895T, a testimony before the Committee on Appropriations, United States Senate.

Schoeneberger, P.J., Wysocki, D.A., Benham, E.C. & Broderson, W.D. 1998. Field book for describing and sampling soils. Natural Resource Conservation Service, USDA, National Soil Survey Center. Lincoln, Nebraska.

Semiletov, I.P. 1999. Destruction of the coastal permafrost ground as an important factor in biogeochemistry of the Arctic Shelf waters. Transactions (Doklady) of the Russian Academy of Sciences, 368(6):679-682.

Serreze. M.C., Clark, M.P., Etringer A.J., & D.H. Bromwich. 2001. Variability and trends in the hydro-climatology of the major Eurasian Arctic drainages. In *Second Wadati Conference on Global Change and the Polar Climate,* March 7-9, 2001. Tsukuba, Japan 83-86

Shur, Y.L., Jorgenson, M.T. 2007. Patterns of permafrost formation and degradation in relation to climate and ecosystems. *Permafrost and Periglacial Processes* 18:7-19.

Global Land Use Change and Its Specificity in Permafrost-Affected Regions: Consequences for Cryosols

Dmitry I. Lyuri
Institute of Geography, Russian Academy of Science, Moscow, Russia
Sergey V. Goryachkin
Institute of Geography, Russian Academy of Science, Moscow, Russia

Abstract

The most specific land use change in high latitudes is the dynamics of agricultural lands. Contrary to the global zonal trend (northward increase of agricultural land abandoning), there was the growth of agricultural areas in cold and permafrost-affected regions both of Eurasia and North America. But since the 1990s the dynamics of agricultural land became divergent in different parts of the North. Due to the system economic crisis in Russia, the area of agricultural lands in permafrost-affected regions shrank greatly; however, in Alaska and Norway, farmlands continued to grow. It proves that increasing of agricultural lands of the North is mostly related to social and economic reasons, but not to climate change. Consequences for cryosols induced by both socio-economic and climate changes are mostly similar. They provoke the deepening of the active layer, development of thermokarst, and change of organic matter quality (degradation of peat and increase of soil humus content).

Keywords: agricultural lands; cryosols; global change; land use; permafrost; socio-economic change.

Introduction

Global climate change and the following landscape and ecosystem transformations are the most popular topics in geosciences including geocryology and soil science. However, global change overwhelms not only climate, but also socio-economic processes as well. The shift of oil and gas mining to the north is a very well-known trend in the world. Socio-economic processes in the North usually have their specificity (Forbes 1999), but their influence on the trends of land use change in high latitudes is not the focus of recent studies. Less is known about the main trends of permafrost-affected landscapes and ecosystems change due to alteration of land use in the North, and only last year, the scientific community began to pay attention (Gutman 2007). As for permafrost and soils, something is known about how they are changed under such transformations of vegetation as clear-cutting (Iwahana et al. 2005) and forest fires (Yoshikawa et al. 2003, Lopez et al. 2006). Much less is known on the agricultural transformation of northern soils. However, the last decades were very crucial to agricultural lands of the world as the intensification of relevant technologies and the rise of productivity resulted in a drastic decrease of arable lands in many countries. Almost nothing is known about what the situation with the dynamics of agricultural areas is in northern (perma)frost-affected regions of the world.

The goal of this paper is to assess the main processes of land use change (primarily agricultural) in northern regions in comparison with the global trend and the consequences for (perma)frost-affected soils—cryosols. Analyses of national and world statistics, literature, and field observations are the main methods in the study.

Change of Agricultural Land Use

Global trends of agricultural land use

Contrary to the slow growth of total agricultural areas in the world, more than 80 countries demonstrate the stable decrease of them. From 1961 to 2002, about 2.3 mln km^2 were abandoned from agricultural use, mostly in Russia, Australia, the USA, and West Europe. Six types of abandonment of agricultural lands were distinguished (Lyuri et al. 2006). The first four types are associated with countries, where decreasing of agricultural lands is a result of agricultural intensification. *US-type*: the decrease of agricultural area as a result of agricultural intensification with the increase of agricultural production. Twenty-one countries (US, UK, West Europe, Australia, India, Thailand, etc.) have this type of agricultural lands dynamic, and they abandon about 1.0 mln km^2 of agricultural area (43.5% of the world value) (Fig. 1).

Japan-type: the decrease of agricultural area as a result of agricultural intensification with the decrease of agricultural production (the course for food import). Two countries, Japan

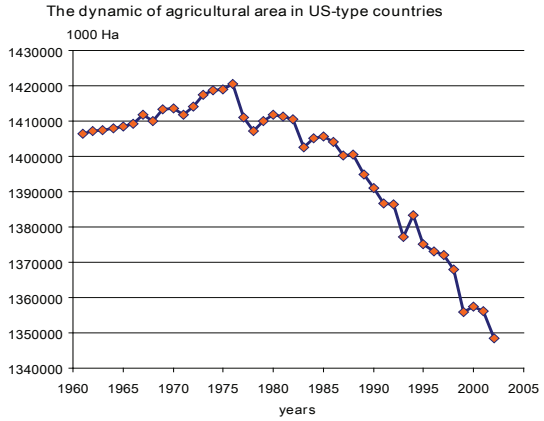

Figure 1. Data – http://faostat.fao.org/site/497/default.aspx.

and South Korea, abandoned 0.02 mln km² of agricultural area (<1% of the world value). *France-type*: the decrease of agricultural area as a result of agricultural intensification, then its increasing during last years with increasing of agricultural production (the course for food export). Six countries abandoned 0.1 mln km² of agricultural area (4%). *Hungary-type (transitional)*: the decrease of agricultural area as a result of agricultural intensification, then its decline as a result of deep economical crises. Nine countries (Poland, Hungary, and other countries of East Europe) abandoned 0.07 mln km² of agricultural area (3%).

Two other types of agricultural land abandonment are associated with countries where agricultural lands decrease as the result of crises, wars, revolutions, and other non-agricultural processes.

Russian-type: the enlargement of agricultural area, then its falling as a result of deep economical crises with the rise and then decrease of agricultural production. Seventeen countries (Russia, other countries of the former USSR, Bulgaria, and Romania) abandoned 0.85 mln km² of agricultural area (37.0% of the world value). *Miscellaneous-type*: the decrease of agricultural area with no relation to agricultural productivity and production. Twenty-one countries (Bangladesh, Cameroon, Lesotho, Nigeria, Swaziland, etc.) abandoned 0.25 mln km² of agricultural area (10.9%).

Abandoned agricultural area is substituted by two kinds of lands: (1) by settlements, infrastructure, industry, etc., and (2) by fallows. In the last case, fallows are usually a process of replacement by natural ecosystems.

Land use change in Russia and its northern regions

The dynamics of the areas of agricultural lands both in Russia as a whole and in its northern (perma)frost-affected regions is very specific. We have analyzed it separately for two essentially different periods: (1) for non-crisis 1960-1980, and (2) for the 1990s – system economic crisis in the country and afterwards. Figure 2 shows that the growth of the cropland areas has practically finished from the beginning of the 1960s for the whole territory of Russia. Cropland area expansion occurred only in the most southern regions; however, in boreal and temperate zones, it was stable or even diminishing.

The reverse situation took place in northern permafrost-affected areas. The intensive increase of the cropland area began from 1960-1970 and continued until the beginning of the crisis of 1990 (Fig. 3).

Similar patterns, but more complicated and controversial for northern territories, are characteristic for dynamics of arable lands and agricultural areas (Figs. 4, 5). Thus, the dynamics of the cultivated areas in permafrost-affected regions of Russia in the favorable 1960s-1980s was more similar to that of the most southern parts of the country, but not to adjoining boreal and temperate regions.

In the 1990s the system crisis had embraced all of the country, and in all regions of Russia there was a significant reduction of agricultural areas, including arable lands and crops (Figs. 6, 7).

Figure 2. Data – State Committee 1985-1998.

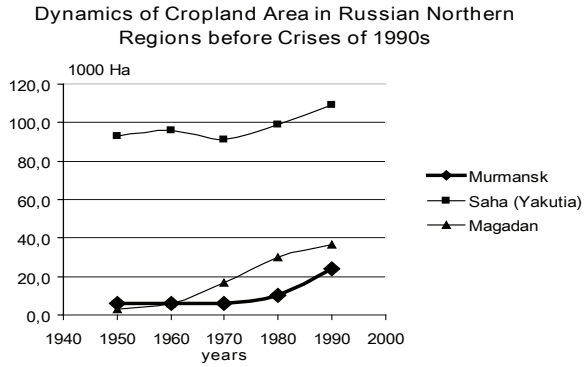

Figure 3. Data – State Committee 1985-1998.

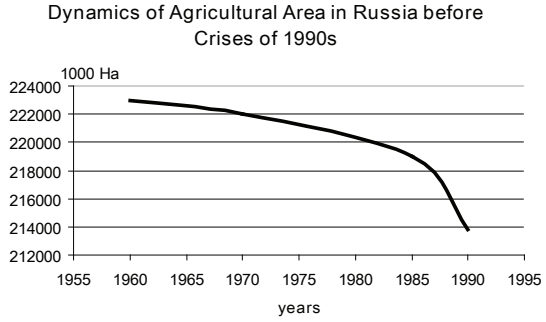

Figure 4. Data – State Committee 1985-1998.

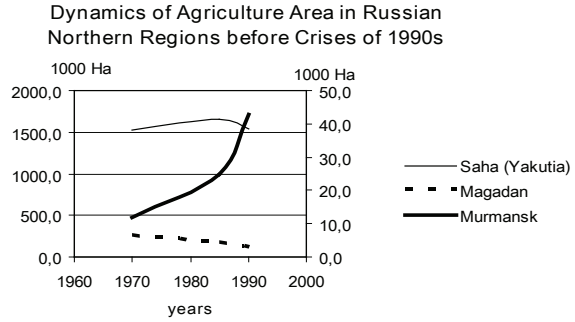

Figure 5. Left Y-axis is for Saha; right one, for others.. Data – State Committee 1985-1998.

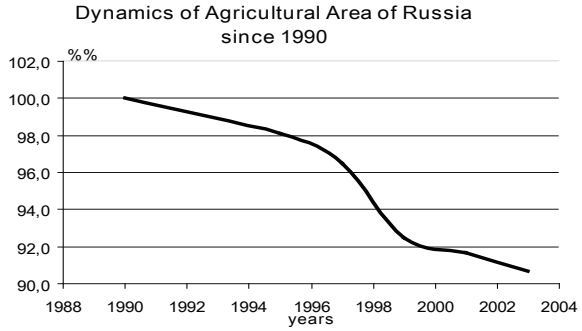

Figure 6. Data – State Committee 1985-1998, 2006.

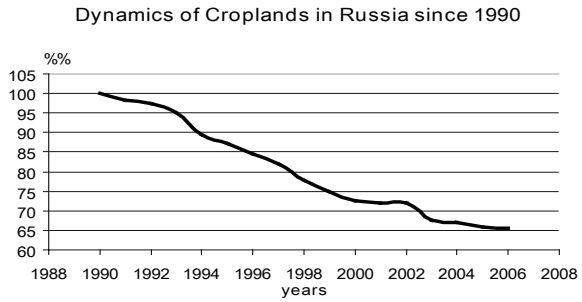

Figure 7. Data –State Committee 1985-1998, 2006.

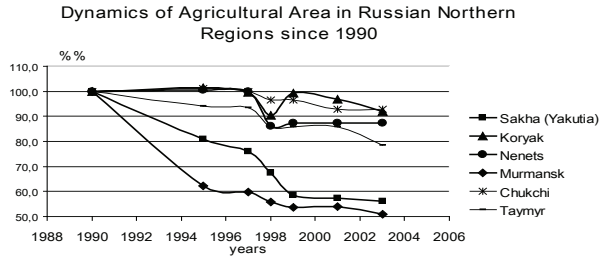

Figure 8. Data – State Committee 1985-1998, 2006.

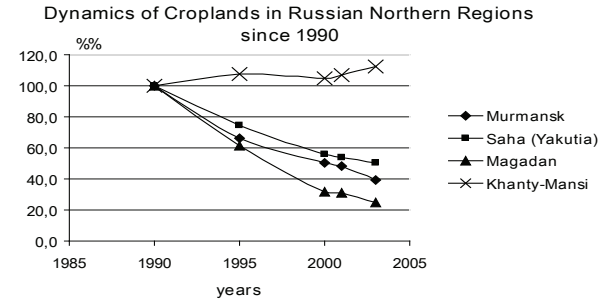

Figure 9. Data – State Committee 1985-1998, 2006.

Analogous processes took place in permafrost-affected regions of the country, though the unique subject of Russian Federation (Khanty-Mansi autonomous district), with some increase in the areas of croplands in crisis time, occurred namely in this zone. In all other northern regions, the agricultural areas were reduced, though this process had various rates. However, by the end of the 1990s in the majority of permafrost-affected regions the shrinkage of agricultural areas has practically stopped, and they were approximately stabilized. It is observed in the Murmansk area, Saha (Yakutia) (which has the greatest area of the agricultural lands in the permafrost-affected zone), in Nenets and Chukchi autonomous districts (Figs. 8, 9).

Such agricultural land stabilization has occurred more than in half of analyzed permafrost-affected regions. It is remarkable, but a similar effect of the termination of the shrinkage of agricultural areas takes place only in the most southern regions of the country, and in the boreal and temperate areas the process of croplands decrease proceeds with former intensity. Thus, the agricultural lands of permafrost-affected regions have reacted to the system crisis of the 1990s in a very specific form: Their dynamics even in these crisis years was more similar to dynamics in the most southern agriculturally productive areas of the country.

The effect of stabilization in cold regions, which in the south is related to the optimum for conducting agriculture by natural and demographic conditions, should be explained by other reasons. First, it is caused by the remoteness of these areas from the basic agricultural regions of the country; it makes the transportation of the foodstuffs here very expensive and focuses local producers and consumers on home resources. Secondly, it can be explained by the significant percentage in the population of local indigenous people for which the traditional agriculture is the core and even the only source of existence that forces them to stabilize the situation at a certain acceptable level as soon as possible. Besides that, a traditional economy is "economically isolated" and much more independent to financial cataclysms, legal problems, and other aspects of a system crisis than the modern economy.

Land use change in the north of Russia, US, and Europe

However, in spite of all specificity of the agriculture of permafrost-affected regions the general decrease of the agricultural areas in the north of Russia was very significant. So, arable lands of Russian northern regions in the period from 1990 until 2003 have decreased by 1.5 times (from 230,000 to 150,000 Ha) and reached practically the value of 1970 (Fig. 9).

However, the dynamics of Russian arable lands has a very severe pressure of economic crises. In this case it is very interesting what type of dynamics of agricultural lands was in other non-crisis permafrost-affected regions of the Northern Hemisphere. It was found out that in Alaska, the constant increase of the area of arable lands took place in the 1974-2004 period. It has extended practically in 5 times (Fig. 11). This Alaskan agricultural situation is principally contrary to the rest of the US, as the stable reduction of agricultural lands took place in the country at that time.

In another northern region—Norway—the other type of arable land dynamics takes place (Fig. 12). The expansion of arable lands from the middle of the 1990s was replaced by stabilization, and the last years, by insignificant reduction (approximately 3%). It essentially distinguishes Norway from all other countries of Western Europe, where from 1960-1980, there is a reduction of arable areas.

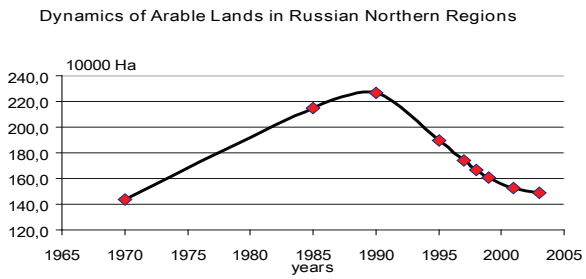

Figure 10. Data – State Committee 1985-1998, 2006.

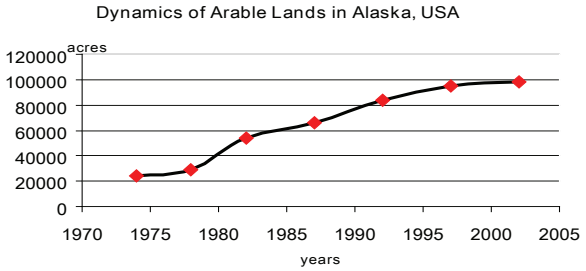

Figure 11. Data – USDA 2003.

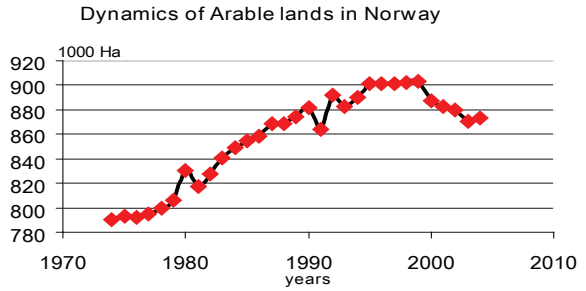

Figure 12. Data – http://faostat.fao.org/site/497/default.aspx.

Thus, the dynamics of arable lands in different cold regions of the Northern Hemisphere is essentially diverse. We see "growth-fall" in Russia, "growth" in Alaska and "growth-stabilization" in Norway. That allows the assumption that it is mainly defined by social and economic, but not by natural (changes of a climate) factors. Besides that, the dynamics of agricultural lands in permafrost-affected areas in different parts of the Northern Hemisphere are absolutely not similar to the mainland and neighbors: Alaska is different from the USA, and Norway, to all other countries of Western Europe. The Russian north is more likely similar to the Russian agriculturally productive south, than to the adjacent boreal and temperate regions.

Consequences of Land Use Change for Cryosols

Previous materials elucidated in the paper showed that agricultural use of soils in permafrost-affected regions of the world is growing or, at least, a stable factor of soil change. So, the influence of this type of land use on polar soils should be known as well as the other ones.

Figure 13. Total destruction of agricultural field after use of permafrost-affected soils for a cropland. Central Saha (Yakutia). Remnants of ploughed horizon proved the former tillage of these soils.

Our field studies in Central Saha (Yakutia) showed that the tillage of loamy soils resulted in occurrence of a humus horizon with a sharp lower boundary, as it is characteristic for all arable soils of the world. However, a specific tillage-induced feature is the lowering of the permafrost table often beneath 2 m (so after agricultural development, these permafrost-affected soils do not fit the criteria of Cryosols (WRB) and Gelisols (Soil Taxonomy) anymore).

But the most dangerous phenomena taking place after involvement of some permafrost-affected soils in agriculture is the total destruction of soil surface because of catastrophic development of thermokarst and thawing of underground ice wedges (Fig. 13).

Our data are in full correspondence with materials of Gavriliev (2004) who experimentally showed that after 12 years of agricultural use in Central Saha (Yakutia), ice wedges can thaw from a depth of 1.8 m to 3.2 m, and thermokarst holes can develop depths from 0 to 0.95 m.

The other data on tundra soils involved in agriculture from another part of the Eurasian cryosol area—northeast European Russia—also showed that they are characterized by development of sod and humus horizon instead of peaty litter and by occurrence of more contrast temperature regime with deep thawing of mineral horizons (Archegova et al. 2004).

Agriculture-induced soil change in permafrost areas has both similarity and difference with other types of land use and anthropogenic influence. As well as reindeer overgrazing, clear-cutting, and forest fires, it leads to active layer deepening (Broll 2000, Iwahana et al. 2005, Lopez et al. 2006). However, manure amendments for agriculture lead to an increase of carbon store in cryosols contrary to other

types of land use. Anthropogenic change of cryosols has mostly the same trend as induced by global climate change, at least in some regions of the cryopedosphere—active layer increase (Mazhitova et al. 2004).

Conclusions

Agricultural land use change in permafrost-affected regions is very specific and has other trends than boreal and temperate regions of the world. Cold regions have different types of dynamic: (1) growth in Alaska, US, (2) growth and stabilization in Norway, and (3) growth and fall in Russia due to economic crises of the 1990s. Land use change is caused by socio-economic but not by climatic reasons. The local agricultural economy of remote northern areas is much smaller and more independent than that of central productive regions; that is why it will be saved by local communities, especially by indigenous people.

The consequences for cryosols induced by both socio-economic and climate changes are mostly similar. They provoke the deepening of the active layer, development of thermokarst, and change of organic matter quality (degradation of peat and increase of soil humus content).

Acknowledgments

This study was conducted within the framework of the IPY Cluster Project #262 "Response of Arctic and Subarctic soils in a changing Earth: dynamic and frontier studies." Financial support was provided by the Presidium of Russian Academy of Sciences and its Department of Geosciences. The authors also acknowledge the Russian Foundation for Basic Research for the financial support of field investigation in Saha (Yakutia) and personally M. Zheleznyak, M. Grigoriev, R. Desyatkin, T. Maksimov, and P. Fedorov from Yakutsk for help in the organization of the expedition.

References

Archegova, I., Kotelina, N. & Mazhitova, G. 2004. Agricultural use of tundra soils in the Vorkuta area, Northeast European Russia. In: J. Kimble (ed.), *Cryosols. Permafrost-affected soils.* Springer: 661-676.

Broll, G. 2000. Influence of overgrazing by reindeer on soil organic matter and soil microclimate of well-drained soils in the Finnish Subarctic. In: R. Lal, J.M. Kimble & B.A. Stewart, *Global Climate and Cold Regions Ecosystems.* Boca Raton: CRC/Lewis Publ.: 163-176.

Forbes, B.C. 1999. Land use and climate change on the Yamal Peninsula of north-west Siberia: some ecological and socio-economic implications. *Polar Research* 18(2): 367-373.

Gavriliev, P.P. 2004. Classification of geocryological and soil processes on their danger for agricultural development. Permafrost-affected soil: diversity, ecology and conservation. *Proceedings of Russian scientific conference, June 28-30, 2004, Yakutsk.* Yakutsk: 149-154 (in Russian).

Gutman, G. 2007. Contribution of the NASA Land-Cover/ Land-Use Change Program to the Northern Eurasia Earth Science Partnership Initiative: An overview. *Global and Planetary Change* 56(3-4): 235-247. http://faostat.fao.org/site/497/default.aspx

Iwahana, G., Machimura, T., Kobayashi, Y., Fedorov, A.N., Konstantinov, P.Y., & Fukuda, M. 2005. Influence of forest clear-cutting on the thermal and hydrological regime of the active layer near Yakutsk, eastern Siberia, *J. Geophys. Res.* 110::G02004, doi:10.1029/2005JG000039.

Lopez, M.L., Nakayama, H., Takakai, F., Argunov, R., Fedorov, A.N. & Fukuda, M. 2006. Forest fires, a permanent or a temporal disturbance in Permafrost Regions: Central Yakutia, Eastern Siberia? *Forest Ecology and Management* 234(1): S178.

Lyuri, D., Karavaeva, N., Nefedova, T., Konyushkov, B. & Goryachkin, S. 2006. Self-Restoration of Post-Agrogenic Soils: Recent Process of Late Antropocene. *Abstracts. 18th World Congress of Soil Science July 9-15 Philadelphia, Pennsylvania, USA.* CD-ROM, 27-2.

Mazhitova, G., Malkova, G., Chestnykh, O. & Zamolodchikov, D. 2004. Active-layer spatial and temporal variability at European Russian circumpolar-active-layer-monitoring (CALM) sites. *Permafrost and Periglacial Processes* 15(2): 123-139.

State Committee for Statistics. 1985-1998. Agriculture. Moscow, Goskomstat (in Russian).

State Committee for Statistics. 2006. Agriculture, Hunt and Forestry. Moscow, Goskomstat (in Russian).

USDA 2003. 2002 Census of Agriculture - State Data. National Agricultural Statistics.

Yoshikawa, K., Bolton, W.R., Romanovsky, V.E., Fukuda, M. & Hinzman, L.D. 2002. Impacts of wildfire on the permafrost in the boreal forests of Interior Alaska, *J. Geophys. Res.* 107, 8148, doi:10.1029/2001JD000438.

Control of Asymmetrical Subgrade Temperature with Crushed-Rock Embankments Along the Permafrost Region of the Qinghai-Tibet Railway

Wei Ma, Luxin Zhang, Qingbai Wu
State Key Laboratory of Frozen Soil Engineering, Cold and Arid Regions Environmental and Engineering Research Institute, 320 Donggang West Road, Lanzhou, 730000, China

Abstract

On the basis of in situ tests of embankments with different crushed rock structures, this paper studied methods for controlling asymmetrical subgrade temperature. It is found that these methods can slowly change the ground temperature regime, but cannot completely adjust the asymmetrical subgrade temperature. Small changes in thickness and grain size of crushed rock had only a limited effect on controlling asymmetrical temperature regime. Compared with the ground temperature regime under different structures of crushed rock slope protection of the same height, it is found that the ground temperature under the south shoulder of an embankment with full crushed rock coverage is lower than that under an embankment with partial coverage, and that the ground temperature under the north shoulder of an embankment with partial coverage is lower than that of a slope with full coverage. It is suggested, therefore, that the south-facing slope be fully covered with crushed rock with thicker structures, while the north-facing slope be partially covered with crushed rock and thinner structures.

Keywords: crushed rock structure embankment; permafrost region; Qinghai-Tibet Railway; south- and north-facing slope of the embankment; temperature regime.

Introduction

Using an active cooling embankment to protect the underlying permafrost, a lot of engineering measures were successfully applied in permafrost engineering construction, especially in the Qinghai-Tibet Railway (QTR) (Rooney 1997, Georing et al. 1996, 2000, 2001, 2003, Ma et al. 2002, Cheng 2003). For instance, they include crushed rock embankments, embankments with crushed rock slope protection, embankments with thermo-siphons and permafrost bridges etc. Their cooling effects have been studied (Georing et al, 1996, 2000, 2001, 2003, Wu et al. 2006, Sun et al. 2004). These measures have ensured that the QTR successfully passes through the warm permafrost regions with high ice contents. Long-term monitoring data along the QTR showed that these measures have different cooling effects in permafrost regions with different ground temperatures (Wu et al. 2005, Ma et al. 2006). In particular, no matter what embankment structure was used, there was a thermal difference between the south- and north-facing slopes of the embankment, an asymmetrical temperature regime was formed under the embankment -- the ground temperature under the south side shoulder is higher than that under the north side shoulder (Sun et al. 2004, Wu et al. 2005). This kind of temperature distribution can cause the potential instability of the embankment. It is therefore necessary to adjust the asymmetrical temperature distribution under embankments by using special measures.

Along QTR, on the basis of in situ tests and temperature monitoring of embankments with different crushed rock structures (3 embankments with the slopes fully covered by crushed rock, 3 embankments with the slopes partially covered with crushed rock with different grain sizes and 1 embankment with the slope partially covered with the filling soil of the embankment), this paper analyzed and compared the changes in the ground temperature regime under the embankment with different structures. Observations should provide fundamental data for preventing and fixing of the potential damage to embankments.

Test Sections and Schemes

The test site is in the Wudaoliang area along the QTR, which is a plateau with lacustrine deposits and thick ground ice area covered by 5%–6% vegetation, altitude of 4500–4700 m. The mean annual air temperature is -5.6°C and the mean annual range of air temperature is 22.3°C. The mean annual precipitation is 264.8 mm and the maximum snow depth is 14 cm.

DK1082+350–DK1082+500 was the test section of embankments with the slopes fully covered with crushed rock with different thicknesses; DK1082+650–DK1082+850 was the test section of embankments with the slopes partially covered by crushed rock with different grain size and an embankment with the slope partially covered with soil. Their details are shown in Table 1.

The original embankment in the test section is a common soil embankment built in 2002. The width of the track surface is 7.1 m, the height of embankment is 2.0–2.8 m and the gradient of embankment is 1:1.5. The widths of the south- and north-facing partial slope protection using soil are 3 m and 2 m.

For the requirements of the tests, we changed the original design. In the section DK1082+350–DK1082+500, we only fully covered crushed rock with different thickness on the slope of the original embankment (shown in Fig. 1). In the sections of DK1082+650–DK1082+750 and DK1082+800–DK1082+850, we use a partial coverage of crushed rock with

Table 1. Test schemes.

QTR kilometer post	T_{cp} * / °C	Mean height of embankment/m	Structure size of Slope protection of embankment	Structure type of embankment
DK1082+350-DK1082+400	-2.35	2.51	Thickness of the south/north-faced slope: 1.0 m/0.6 m ; Crushed rock size: 10 cm	Embankments with the slopes fully covered by crushed rock
DK1082+400-DK1082+450	-2.35	2.65	Thickness of the south/north-faced slope: 1.3 m/0.8 m; Crushed rock size: 10 cm	
DK1082+450-DK1082+500	-2.35	2.79	Thickness of the south/north-faced slope: 1.6 m/1.0 m ; Crushed rock size: 10cm	
DK1082+650-DK1082+700	-2.35	2.35	Width of the south/north-faced slope: 6.0/4.0 m Crushed rock size: 20 cm; Thickness: 1.5 m	Embankments with the slopes partially covered by crushed rock
DK1082+700-DK1082+750	-2.35	2.25	Width of the south/north-faced slope: 6.0/4.0 m; Crushed rock size: 30 cm Thickness: 1.5 m	
DK1082+800-DK1082+850	-2.35	2.76	Width of the south/north-faced slope: 5.0/3.0 m; Crushed rock size: 10 cm Thickness: 1.5 m	
DK1082+750-DK1082+800	-2.35	2.11	Width of the south/north-faced slope: 5.0/3.0 m; Thickness: 1.5 m	Embankment with the slope partially covered by soil

* T_{cp} is mean annual ground temperature at depth of 15 m from the original ground level down (shown in Fig. 4).

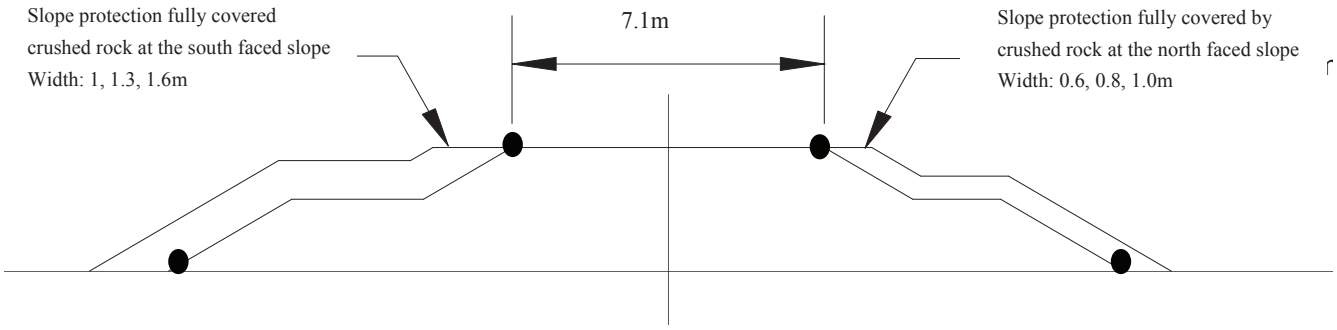

Figure 1. The cross section sketch map of embankment with the slope protection fully covered by crushed rock in DK1082+350–DK1082+500.

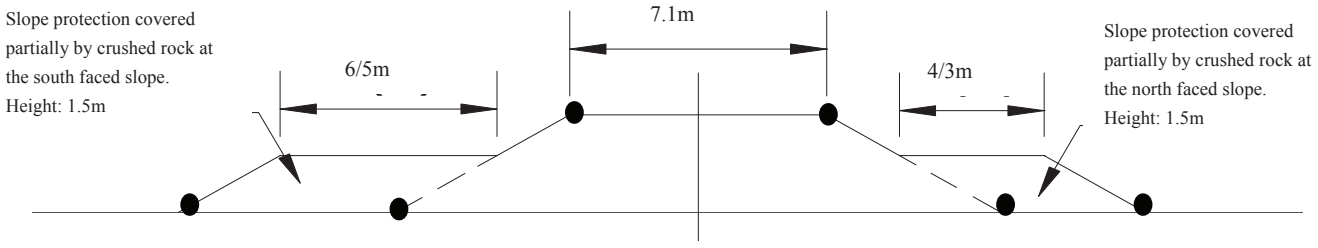

Figure 2. The cross section sketch map of embankment with the slope protection partially covered by crushed rock in DK1082+650–DK1082+850.

different widths and grain sizes to replace the original slope protection partially covered by soil (shown in Fig. 2). In the section of DK1082+750–DK1082+800, we only widened the original soil slope protection to 5.0/3.0m (shown in Table 1). Per test section, the length is 50 m, a lot of tests indicated that they are long enough to eliminate the thermal boundary effects from adjacent embankment sections (Wu et al. 2006, Sun et al. 2004, Ma et al. 2006).

DK1082+375, DK1082+425, DK1082+475, DK1082+675, DK1082+725, DK1082+775, and DK1082+825 respectively were chosen as monitoring profiles of ground temperature. In DK1082+375, DK1082+425, and DK1082+475, four boreholes were installed in each profile–on the south and north shoulder of the embankments and at the

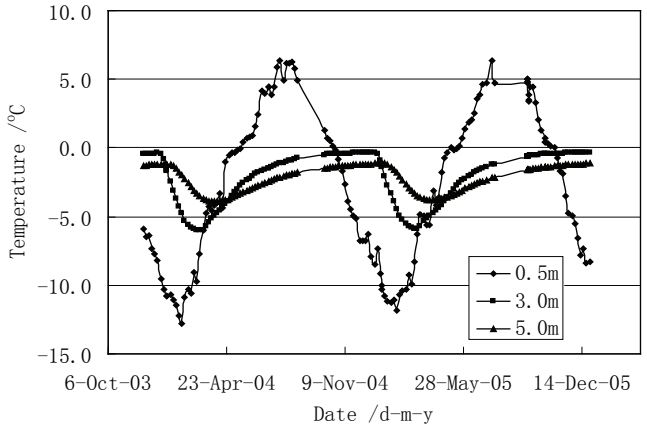

Figure 3. Ground temperature changes vs. time at different depths in the natural borehole (DK1082+600).

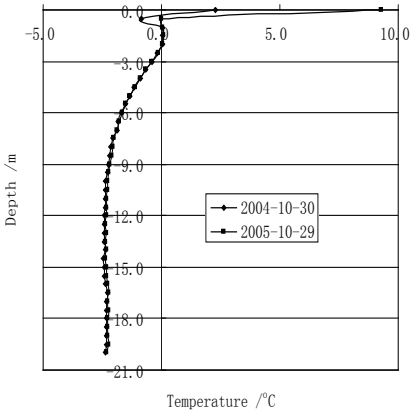

Figure 4. Ground temperature changes with depth when the thawing depth reached the maximum in the natural borehole (DK1082+600).

south and north toe for embankments with partial slope protection using soil (shown in Fig. 2 marked by "●"). In DK1082+675, DK1082+725, DK1082+775, DK1082+825, six boreholes were installed in each profile–the south and north shoulder and toe of embankment, the south and north toe of slopes partially covered by crushed rock, respectively (shown in Fig. 3 marked by "•"). Also a reference borehole 20 m deep was installed 20m away from the north slope toe of embankment at DK1082+600 to measure the natural ground temperatures.

A galvanized iron pipe was placed in each borehole. A thermometric string (the thermocouples placed at 0.5 m intervals) was installed in each pipe to record the temperatures at different depths.

The thermocouples were manufactured by the State Key Laboratory of Frozen Soil Engineering, Cold and Arid Regions Environmental and Engineering Research Institute, CAS, and the precision is ±0.05ºC. All data were collected using a Datataker 500 from Oct. 2003 to Dec. 2005.

Results and Analysis

Natural ground temperature changes

Figures 3 and 4 show the ground temperature changes with time at different depths and with depth when the thawing depth reached a maximum in the natural borehole. It is found that the permafrost table was at 2.0 m and the mean annual ground temperature was -2.35°C. It was also found there were little or no changes in the permafrost table or in the mean annual ground temperature. The air temperature therefore had very little effect on ground temperatures during the experimental years at the test site. So, we will not consider the effect of air temperature on temperature regime of embankment in following discussion.

Ground temperature changes under embankment with the slope protection partially covered by soil

Figure 5 shows the ground temperature changes with time at different depths and locations beneath the embankments. Compared with the slope shoulders and toes of embankment, it is found that the ground temperatures at the south shoulder and toe of the embankment were above -2°C and clearly higher than these under the north shoulder and toe. With increasing time, the minimum ground temperature at 0.4 m keeps slight increase, and under 0.4 m, they decrease slightly, and the decreasing range of ground temperature was about 0.2°C–0.3°C. Under the north shoulder of the embankment, the ground temperatures were about 1°C to -5.3°C. In the course of time, they decreased considerably, and the decreasing range of ground temperature is about 0.5°C to 1.1°C. Such developments would cause larger and larger ground temperature difference between the south and north slopes of the embankment and increase the potential instability of the embankment. So, this method can be put away first.

Ground temperature changes under the embankment with the slope protection fully covered by crushed rock

Figure 6 shows the typical ground temperature changes with time at different depths and positions under the embankments at DK1082+375. It can be seen that with the slope fully covered with crushed rock, the ground temperatures under embankment decrease noticeably, but the rate of decrease of ground temperature under the south side shoulder was less than that under the north side shoulder ground temperature difference, particularly under the toe of embankment. With increasing thickness of the crushed rock layer, the ground temperature difference decreases gradually under the south and north shoulders. Compared with embankments DK1082+425 and DK1082+475, the embankment structure with the thicknesses on the south/north-faced slopes of 1.6 m/1.0 m (DK1082+475) is better than the others. The difference exists mainly in the change of minimum ground temperature. The maximum ground temperature has no obvious relationship with thickness of the crushed rock layer. For the embankments with the thicknesses of crushed rock layer of 0.6 m and 1.0 m (DK1082+375), 0.8 m and 1.3 m (DK1082+425), 1.0 m and 1.6 m (DK1082+475), respectively, the differences in the minimum ground temperature at different depths under the south and north side shoulders were 1.29°C to 2.68°C, 0.98°C to 1.98°C, 0.90°C to 1.89°C, respectively. In addition,

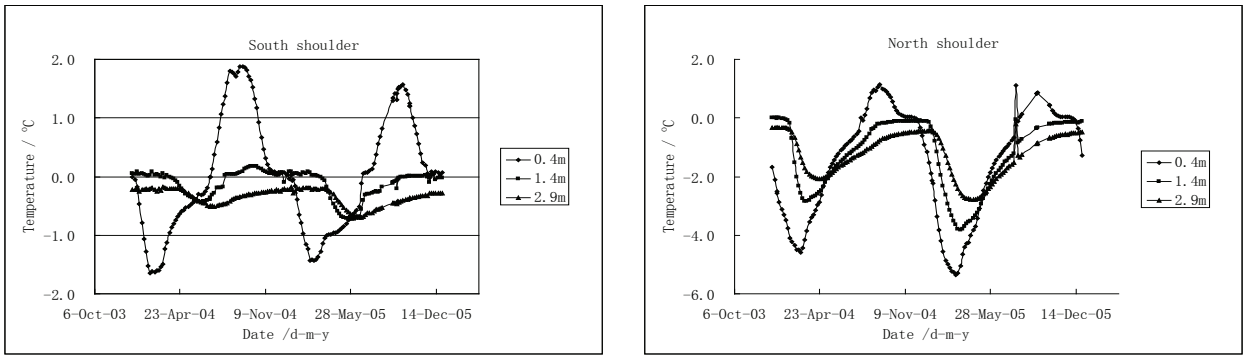

Figure 5 Ground temperature changes vs. time at different depths under embankment with the slope protection partially covered by soil (DK1082+775).

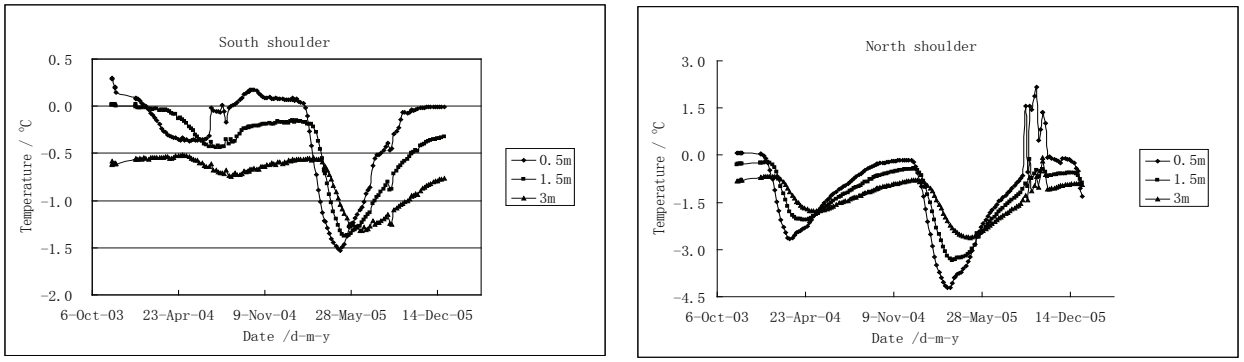

Figure 6. Ground temperature changes vs. time at different depths under the embankment with the slope protection fully covered by crushed rock (DK1082+375).

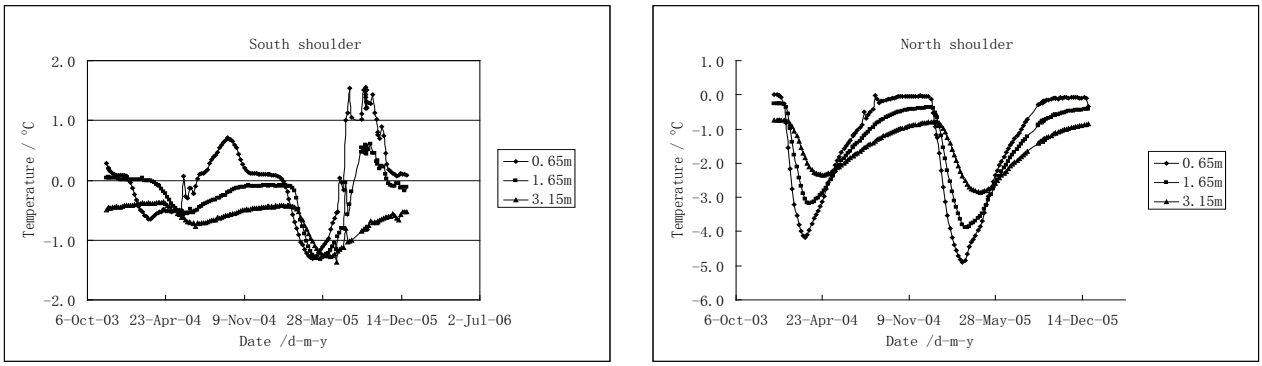

Figure 7. Ground temperature changes vs. time at different depths under the embankment with the slope protection partially covered by crushed rock (DK1082+675).

it is found that the minimum ground temperature in shallow layers under embankment had larger ground temperature differences than that in deeper layers.

Ground temperature changes under embankments with the slope protections partially covered by crushed rock

Figure 7 shows typical ground temperature changes with time at different depths and positions under the embankments at DK1082+675. It can be seen that with the slope partially covered by crushed rock, the ground temperature under the embankment decreased noticeably. Compared with minimum ground temperature, it was found that the rate of decrease of ground temperature under the south shoulder was larger than that under the north shoulder. The same was true for the south and north toes. However, a ground temperature difference still exists between the south-and north-facing slope of the embankment, particularly under the shoulders of the embankment. The ground temperature difference under the south and north shoulder and toe decreased gradually with time. Comparing with the ground temperature change under the shoulders and toes at DK1082+675, +725, +825, found that adjustment of the asymmetrical thermal regime under the embankment structure is best with the widths of the south/north-faced slopes of 4.0 m/6.0 m, using the crushed rock size of 30 cm (DK1082+725). Second best is the embankment with the widths of the south/north-faced slopes of 4.0m/6.0m and the crushed rock size of 20 cm (DK1082+675). The embankment with the widths

Table 2. Maximum thaw depth at the south and north shoulders of embankments.

Monitoring profile	Location	Height of embankment /m	Maximum thawing depth in 2003 /m	Maximum thawing depth in 2004 /m	Maximum thawing depth in 2005 /m	Structure type of embankment
DK1082+375	South shoulder	2.49	4.0	3.51	2.93	Embankments with the slopes fully covered by crushed rock
	North shoulder	2.53	3.25	2.48	2.46	
DK1082+425	South shoulder	2.59	4.0	3.41	3.82	
	North shoulder	2.71	3.6	3.33	3.29	
DK1082+475	South shoulder	2.76	4.0	3.66	3.36	
	North shoulder	2.81	3.5	2.62	3.00	
DK1082+675	South shoulder	2.28	4.1	3.62	3.43	Embankments with the slopes partially covered by crushed rock
	North shoulder	2.42	3.2	2.89	2.87	
DK1082+725	South shoulder	2.13	3.6	3.47	3.18	
	North shoulder	2.36	3.5	3.32	2.90	
DK1082+825	South shoulder	2.80	5.1	4.77	4.42	
	North shoulder	2.72	3.8	3.5	3.35	
DK1082+775	South shoulder	2.04	4.1	3.85	3.54	Embankment with the slope partially covered by soil
	North shoulder	2.17	3.8	3.54	2.96	

of the south/north-faced slopes of 3.0 m/5.0 m and the crushed rock size of 10 cm is the worst (DK1082+825). The difference of the minimum ground temperature at different depths under the south and north toe was 1.11°C to 1.27°C, 1.6°C to 2.26°C, 1.94°C to 3.2°C, respectively. In addition, the minimum ground temperature in shallow layers under embankment has larger ground temperature differences than that at deep layers.

Discussion and Suggestions

In general, choice of good embankment structure must consider both the ground temperature difference and the maximum thawing depth (permafrost table) between the south- and north-facing slopes of the embankments.

On the basis of observations, it is seen that except for the embankments with slope protection partially covered with soil, the other embankment structures achieved a certain adjustment of the asymmetrical thermal regime.

Compared with the thickness and size change of crushed rock, it is found that with full coverage using crushed rock, the ground temperature difference decreased gradually with increasing thickness of the crushed rock layer. For the slopes partially covered with crushed rock, the adjusting effect of the asymmetrical temperature distribution using larger grain sizes is better than the others. But, a small change in the thickness or grain size cannot completely adjust the asymmetrical temperature distribution in this test. Based on ground temperatures under the south and north shoulders, the ground temperature with full coverage with crushed rock under the south shoulder was lower than that using partial coverage with crushed rock, and the ground temperature of the partial coverage with crushed rock under the north shoulder is lower than that using coverage with crushed rock. For integrated effect of ground temperature regime, the asymmetrical temperature distribution adjustment using full coverage with crushed rock was better than partial coverage with crushed rock.

Table 2 shows the changes in the maximum thawing depth under the south and north shoulders for different monitoring profiles. Except for the monitoring profiles of DK1082+425 (south shoulder), DK1082+475 (north shoulder), and DK1082+825 (north shoulder) where the maximum thawing depth decreased from 2003 to 2004 and increased from 2004 to 2005, the others decreased from 2003 to 2005. Through in-situ investigation, we found that abnormal change of the maximum thawing depth in DK1082+425 (south shoulder), DK1082+475 (north shoulder), and DK1082+825 (north shoulder) were caused by rainwater massed at the slope toe of the embankment. The maximum thawing depth for full coverage with crushed rock under the south shoulder is less than that of using partial coverage with crushed rock, and the maximum thawing depth for partial coverage with crushed rock under the north shoulder is less than that of using full coverage. Compared with the difference of the maximum

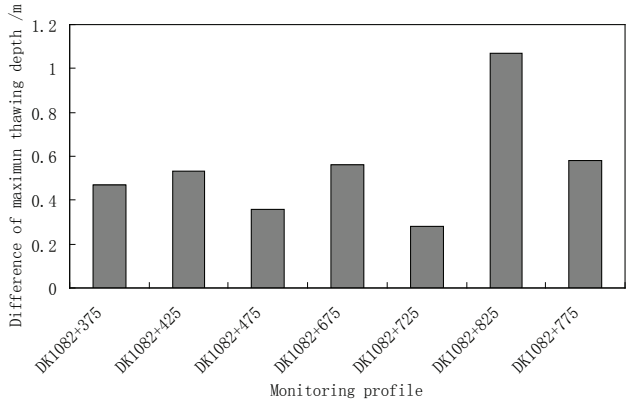

Figure 8. Difference of the maximum thawing depth between the south and north shoulder for different monitoring profiles in 2005.

thawing depth between the south and north shoulders in 2005, the differences at DK1082+475 and DK1082+725 are still less than the others, they are 0.36 m and 0.28 m, respectively (shown in Fig.8).

In other words, the better embankment structures for adjusting asymmetrical permafrost table were the embankments with slope protection using partial coverage with crushed rock with widths of the south/north-faced slope of 4.0 m/6.0 m and a crushed rock size of 30 cm (DK1082+725), as well as embankments with slope protection using full coverage with crushed rock and thickness of the south/north-facing slopes of 1.0 m/1.6m and the crushed rock size of 10 cm (DK1082+475).

Based on the above discussions, we can say that under the conditions of our test sections, these methods can slowly change the ground temperature regime but cannot absolutely adjust the asymmetrical temperature distribution under the embankments. In these testing programs the small change in thickness and grain size of the crushed rock had only a limited effect on adjusting and controlling the asymmetrical temperature regime. After integrated considering of the difference of ground temperature and the maximum thawing depth under the north shoulders and toes of the embankment, as well as economical cost, we suggest that the south-faced slope is better fully covered by crushed rock with wider and thicker structure. For the north-facing slope partial coverage with crushed rock that is narrower and thinner is better.

The above conclusions were drawn only based on three years of data and the lower temperature permafrost region; the effect of the warming climate was not considered. At present, we want to re-monitor these test sections and set up some new monitoring profiles in the higher temperature permafrost regions along the QTR and the Qinghai-Tibet Highway, and hope some new results can be found.

Acknowledgments

This work was supported in part by the grant of the Western Project Program of the Chinese Academy of Sciences (KZCX2-XB2-10) and the Natural Science Foundation of China (Grant No. 40401013 and 50534040).

References

Cheng, G.D. 2003. Impact of local factors to the permafrost distribution and its enlightenment to design of the Qinghai-Tibet Railway [J]. *Sciences in China* (Series D) 33(6): 602-607 (in Chinese with English abstract).

Georing, D.J. & Kumar P. 1996. Winter-time convection in open-graded embankments [J]. *Cold Regions Science and Technology* 24(1): 57-74.

Goering, D.J. 2001. Parks/Chena Ridge air convection embankment experimental feature. *Phase II Final Report*: *Oct. 1999 to Sept. 2000*. Report N. FHWA-AK-RD-01-02 (INE/TRC 02.21), Washington, DC: Federal Highway Administration.

Georing, D.J. & Kumar P. 2000. Convection heat transfer in railway embankment ballast[A]. *Ground Freezing 2000*[C], Rotterdam: Balkema: 31-36.

Georing, D.J. 2003. Passively cooled railway embankments for use in permafrost areas [J]. *Journal Cold Regions Engineering* 17(3): 119-133.

Ma, W., Cheng, G.D. & Wu, Q.B. 2002. Preliminary study on technology of cooling foundation in permafrost regions [J]. *Journal of Glaciology and Geocryology* 24(5): 579-587 (in Chinese with English abstract).

Ma, W., Wu, Q.B. & Cheng, G.D. 2006. Analyses of temperature fields under the embankment with crushed-rock structures along the Qinghai-Tibet Railway [J]. *Journal of Glaciology and Geocryology* 28(4): 586-595 (in Chinese with English abstract).

Rooney, J.W. 1997. Rock fill embankment applications for convective foundation cooling on BAM railway system [A]. *Proceedings of the 5th International Symposium on Cold Regions Development* [C], Anchorage, ASCE, 399-402.

Sun, Z.H., Ma, W. & Li, D.Q. 2004. Experimental study on cooling effect of air convection embankment with crushed rock slope protection in permafrost regions. [J]. *Journal of Glaciology and Geocryology* 26(4): 435-439 (in Chinese with English abstract).

Wu, Q.B., Cheng, G.D., Ma, W., et al. 2006. Technical approaches on ensuring permafrost thermal stability for Qinghai-Xizang Railroad construction [J]. *Geomechanics and Geoengineering* 1(2):119-128.

Wu, Q.B., Zhao, S.Y., Ma, W. et al. 2005. Monitoring and analysis of cooling effect of block-stone embankment for Qinghai-Tibet Railway. *Chinese Journal of Geotechnical Engineering* 27(12): 1386—1390.

Estimation of Frost Heave and the Stress-Strain State of the Buried Chilled Gas Pipeline

M.A. Magomedgadzhieva
State Engineering Designing Research Institute "Fundamentproject," Moscow, Russia
N.B. Kutvitskaya
State Engineering Designing Research Institute "Fundamentproject," Moscow, Russia
S.E. Grechishchev
State Engineering Designing Research Institute "Fundamentproject," Moscow, Russia

Abstract

It is well known that frost heave occurs in zones of thawed and non-anchored frost-susceptible soils under the effect of buried chilled gas pipelines. This phenomenon is due (related) to the specific stress-strained state of freezing soils. Simulation results revealed the following special features of the process: peak linear heave load increases with a decrease in permeability and with an increase in soil freezing rate; peak linear heave load increases in the following succession: sand–sandy loam–loam–clay; and peak linear heave load varies with time and achieves maximum values during the first year of operation of a gas pipeline. Appropriate thermal insulation can eliminate frost heave entirely. The technical decisions providing engineering protection are developed on the basis of soil thermal behavior simulations and strain calculations. These decisions will ensure the stability of the planned pipeline embedding during the whole operation period.

Keywords: buried pipeline; discontinuous permafrost; freezing rate; frost heave; heave load; stress-strained state; permeability.

Introduction

It is well known that frost heave occurs in zones of thawed (under ponds, lakes, bogs) non-anchored frozen soils under the effect of chilled gas pipelines. This phenomenon is related to the specific stress-strained state of freezing soils. Estimation of the displacement of a buried pipeline as a result of frost heave has been a problem because of the lack of appropriate theoretical analysis.

The phenomenon of the frost heave of chilled pipelines in unfrozen soils has been studied since the 1980s. The first approximate theoretical analysis of this phenomenon was undertaken by Grechishchev (1994). Experimental studies of the frost heave of chilled buried pipelines under natural conditions were carried out in France (Williams, 1986, 1989) and Alaska (Akagawa et al. 2004, Kanie et al. 2004).

The calculation of the theoretical peak heave force has remained the pri chilled pipeline on the surrounding soils, the theoretical peak frost heave force applied to a chilled pipeline, and the stress-strain state of the pipeline were evaluated.

Computation procedure was as follows. First, the anticipated thermal behavior of soil was estimated. Based on the obtained thermal behavior parameters (soil freezing above the pipe, soil freezing under the pipe, peak annual freezing rate under the pipe), maximum possible frost heave force applied to the chilled pipeline was estimated. Finally, the obtained linear pull-out force values were applied to the pipeline to estimate its stress-strained state.

Anticipated changes in the thermal conditions of soils underlying the pipeline during construction and operation periods were estimated using the specially developed PROGNOZ software (RSN 67-87), providing a possibility to make allowances for geological and geocryological section heterogeneity, soil physical and thermal properties, and the anthropogenic thermal effects. Mathematical simulation in this software is achieved by enthalpy finite-difference method on an explicit two-layer grid. Simulation was two-dimensional.

The applied calculation method (10) provided a possibility to estimate the values of normal heave forces applied to gas pipe or the confining force to be applied to the pipe to ensure its stability.

Software package Mathcad 2001 was developed for the numerical solution of model equations.

The stress-strained state of the gas pipeline was estimated using the Cosmos Works software based on the finite-element method. Normal frost heave force value was assumed to be equal to estimated heave load (shut-off pressure). Also, gas pipeline actual operating pressure and the subsoil and transmitted gas temperatures were assigned.

Initial Data

By way of a case study, given below are computation results for Olekmisk conditions. The pipeline diameter is 1400 mm, the pipe center depth is 1.5 m, and the operating pressure is assumed to be 10 MPa.

The frost heave of a buried chilled gas pipeline was estimated for the case of discontinuous permafrost with a roof foundering of 10 m and average annual soil temperature of minus 0.1°C at the annual zero amplitude depth. Calculations

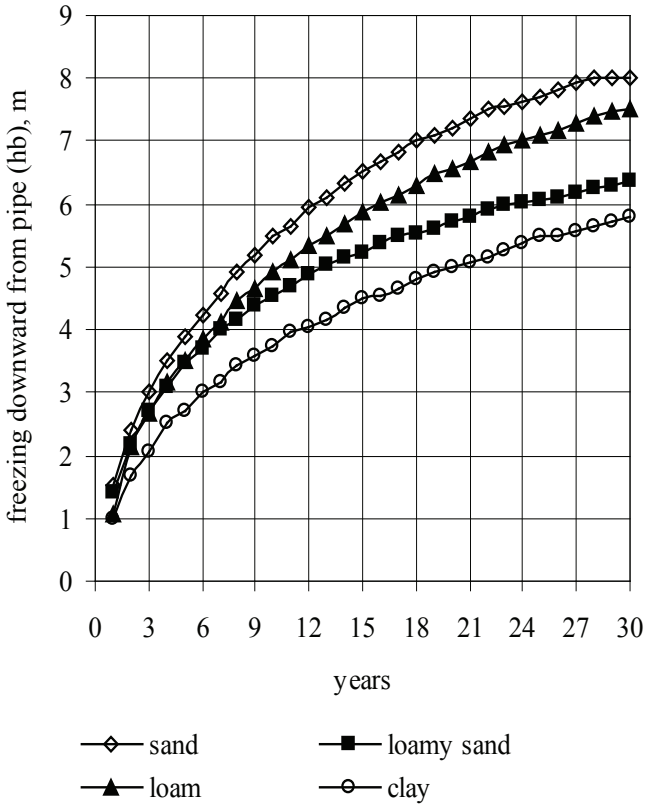

Figure 1. Change of depth freezing downwards from a chilled gas pipeline with time.

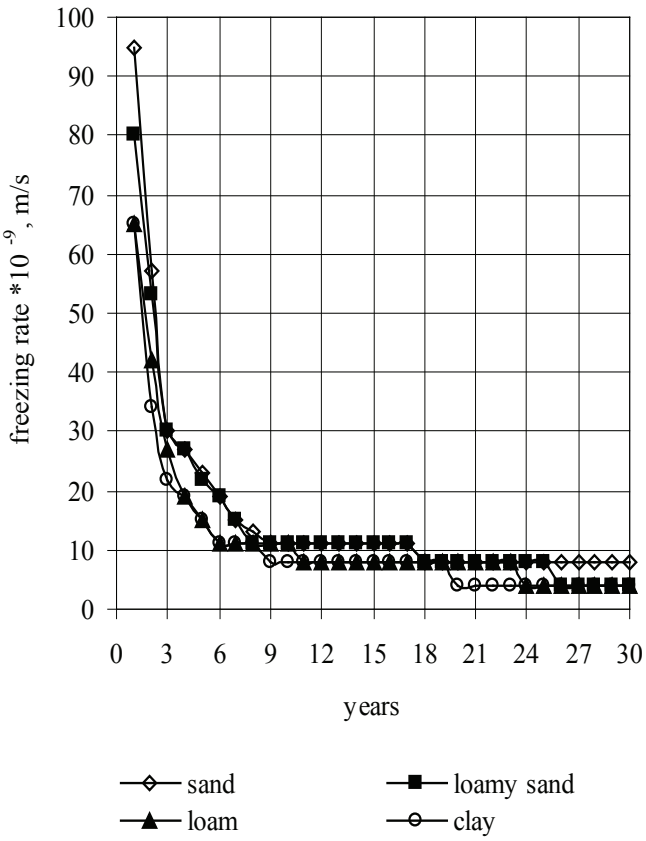

Figure 2. Change of freezing rate with time.

were performed for sand, loamy sand, loam and clay soils.

Calculations for the pipe-soil boundary were made for transmitted gas temperature varying in time from minus 7.5°C in winter to minus 2°C in summer. The following cases were studied: pipe without thermal covering and pipe with a thermal covering with a thermal resistance to heat transfer of 3.6 W/m²×°C (with reference to clay soil).

Results

Thermal behavior calculation results are illustrated by Figure 1 and 2. The obtained data suggest that freezing depth (Fig. 1) and rate (Fig. 2) increase in the following succession: clay–loam–sandy loam–sand.

Peak linear heave load as a function of freezing rate is shown in Figure 3. As obvious from the figure, peak linear load value varies with time and is the highest during the first year of the gas pipeline operation period.

Data shown in Figure 3 also demonstrate the increase in peak linear heave load with an increasing soil freezing rate.

Peak heaving load as a function of soil permeability is shown in Figure 4. Analysis of data shown in Figure 4 suggests that the effect of soil permeability on linear heave load value is significant. Linear load value increases with a decrease in permeability.

Analysis of calculation results (Figs. 3 and 4) suggests that peak linear heave load increases in the following succession: sand–sandy loam–loam–clay.

The stress-strained state of pipeline under the estimated peak heaving load was estimated. Pipeline heave buckling (displacement), in this case, may be as large as 0.5 m.

Heat isolation restricts subsoil freezing. Heat isolation with a thermal resistance to heat transfer of 3.6 W/m²×°C eliminates soil freezing under the pipeline completely. It follows that it is possible to select isolation thickness sufficient for the complete elimination of pipeline heave buckling.

Based on calculation results, engineering solutions can be worked out for stabilizing the planned chilled buried pipeline position: application of a heat insulation cover with a thickness determined by special calculations; application of ice-and-soil supports or chemically stabilized soils with screw-in anchors, to which pipeline is fastened by special heavy-duty belts. The calculated linear heave load values shall be borne by these anchors.

Conclusions

1. Simulation data analysis has revealed the following tendencies of the process: Peak linear heave load grows with a decrease in permeability and with an increase in soil freezing rate; peak linear heave load increases in the following succession: sand–sandy loam–loam–clay; and peak linear heave load varies with time and achieves maximum values during the first year of a gas pipeline operation period.

2. Integrated predictive estimation of the thermal and

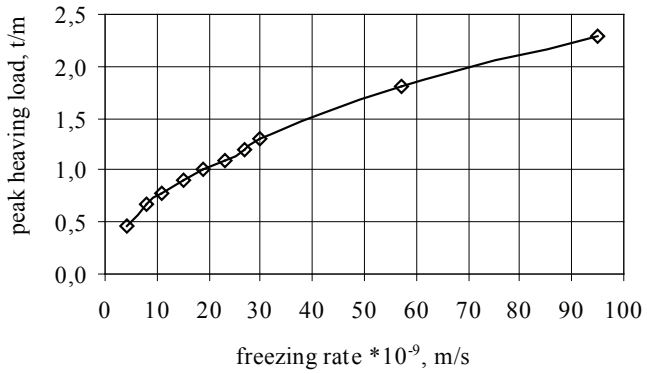

Figure 3. Variation of peak heaving load and freezing rate.

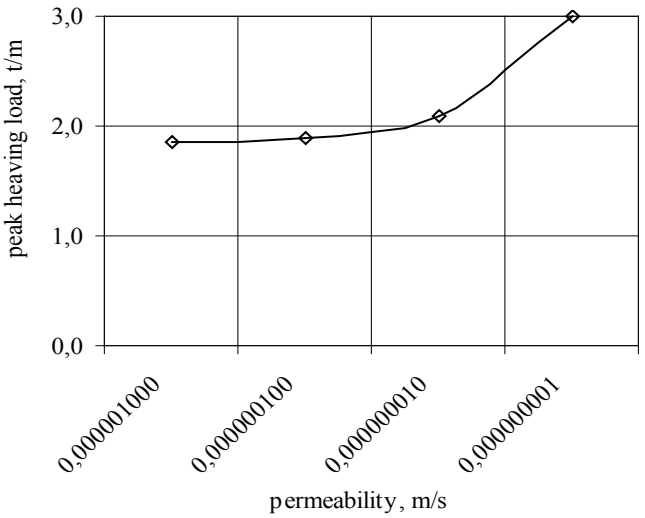

Figure 4. Variation of peak heaving load and permeability.

strain behavior of soils at the early stage of project designing provides the opportunity to identify and recommend the optimum temperatures of the piped product to minimize the thermal effect on the subsoil. At later stages of project designing (project design, detailed engineering), engineering protection solutions are developed on the basis of thermal behavior modeling and strain computation to ensure the stabilization of the planned pipeline position during the whole operation period.

References

Williams, P.J. 1986, 1989. Pipelines and Permafrost.

Grechishchev, S.E. 1994. Evaluation of Interaction of Buried Chilled Pipeline with Soils in Taliks Using thermodynamic model. *Proceeding of 7th International Cold Regions Engineering specialty conference*, *Canadian Society for civil Engineering, Edmonton*: 805-814.

Akagawa, S., Kim, K., Huang, S., Kanie, S. & Fukuda, M. 2004. Frost heave prediction of chilled gas pipeline in non-permafrost section of discontinuous permafrost. *Proceeding International Conference Cryosphere of Oil and Gas Bearing Provinces*, *Tyumen*: 43.

Kanie, S., Akagawa, S., Sato, M. & Mikami, T. 2004. Evaluation of interactive behavior between chilled gas pipeline and frost soil for structural design. *Proceeding International Conference Cryosphere of Oiland Gas Bearing Provinces*, *Tyumen*: 53.

Grechishchev, S.E., Magomedgadzhieva M.A. & Dmitrieva, S.P. 2005. Special features of frost heave of a buried chilled gas pipeline. *Proceedings of the Fifteenth International Offshore and Polar Engineering Conference, II, Seoul, Korea, June 19–24:* 57-62.

RSN 67-87. Engineering researches for construction. Drawing up of the forecast of changes of a temperature regime of soils by numerical methods.

Analysis of Discharge Characteristics in a Region of Continuous Permafrost: Yana Basin in Siberia

Ipshita Majhi
WERC, University of Alaska Fairbanks
Daqing Yang
WERC, University of Alaska Fairbanks

Abstract

Yana basin was analyzed to understand the hydrology of the catchment, since it is situated in a continuous permafrost region with minimal human impact. The discharge analysis revealed the typical permafrost laid hydrograph with peak summer flood in June and minimum flow from November to April. Temperature and precipitation did not show any significant trend over 70 years. Statistical analysis showed a mixed trend for the stations examined, but there is no significant trend observed for winter months. There is a relationship between snow water equivalent and discharge, but further examination is needed to document the relation. Overall, a better understanding of hydrology was gained through this analysis.

Keywords: hydrology; permafrost; snow water equivalent; Yana.

Introduction

Rivers provide a vital link by integrating, spatially as well as temporally, atmospheric and land surface processes at catchment level, thereby providing a mechanism to detect climate change (Déry et al. 2005).

Significant changes have been observed in the large arctic river basins. For instance, Ye et al. (2003) and Yang et al. (2004) found Lena and Yenisei River discharges increase during the winter months and shift in peak discharge timing in Siberia mostly due to reservoir regulation. Small coastal rivers with no regulation and scarce population density provide an ideal medium to understand the effect of climatic variation on streamflow.

The emphasis of this research is to gain a better understanding of various parameters which affect the unregulated Yana River basin in Eastern Siberia. The basin was chosen for this analysis, since it is a non-regulated mid sized watershed, and streamflow response to snowmelt is direct without reservoir interference or other anthropogenic activities. This analysis will enhance our knowledge of discharge response to changes in precipitation, temperature and snow cover.

Study area, data, and method

The Yana basin is one of the large rivers in northeast Asia with a basin area of 238,000 km^2. The river flows north for 879 km, passing through subarctic and arctic region, and finally discharges into the Laptev Sea at 72°N .The Yana River lies between the East Siberian lowland and the Verkhoyano range. In the lowlands the elevation does not exceed 150 m. The climate in this region is continental. Precipitation ranges from 200–400 mm/year in the lowlands to 400–500 mm/year on the ridges. Continuous permafrost with infrequent taliks as well as widely developed taliks occurs everywhere.

Hydrological observations in the Siberian regions, such as discharge, stream water temperature, river-ice thickness, and dates of river freeze-up and break-up, have been carried out since the mid 1930s by the Russian Hydro Meteorological Services (Shiklomanov et al. 2000). The discharge data are now available from the R-Arctic Net (v.3.)-(www.r-arcticnet.sr.unh.edu/main.html) online.

In addition, subbasin mean monthly temperature and precipitation were obtained from University of New Hampshire (http://rims.unh.edu) along with the Special Sensor Microwave/Imager (SSM/I), remote sensing snow water equivalent data (SWE). As part of our preliminary analysis we defined the natural climatic variation through temperature and precipitation interannual variability, mean, standard deviation, and linear trend. Second, we analyzed monthly and annual discharge records along the main stream to quantify discharge change. Third, we compared snow water equivalent, precipitation, temperature, and discharge as a function of time to assess their relationship.

Result and Discussion

Climate-hydrology

Annual temperature during 1930–2000 ranged from -16°C to -12°C; the cold temperature is characteristic of a region with continuous permafrost (Fig. 1). The basin is characterized by a long cold season of eight months, with temperatures ranging from -10°C in September to around -2.5°C in May. The brief warm season has a temperature range of 9°C in June to 3°C in August, with July being the warmest month (mean temperature of 13°C). The coldest month is January with a mean monthly temperature of -40°C.

Mean annual precipitation over the basin ranges from 145 mm to 300 mm, with an average value of 220 mm (Fig. 1). There is minimal precipitation ranging around 5 mm in January, February, and March. Peak precipitation is in the months of July and August with an average rain depth of 45 mm. Monthly mean value of precipitation for September,

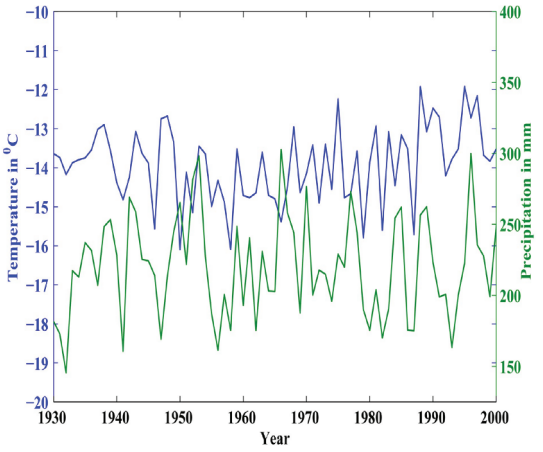

Figure 1. Interannual variability for temperature and precipitation at Yana basin from 1930–2004.

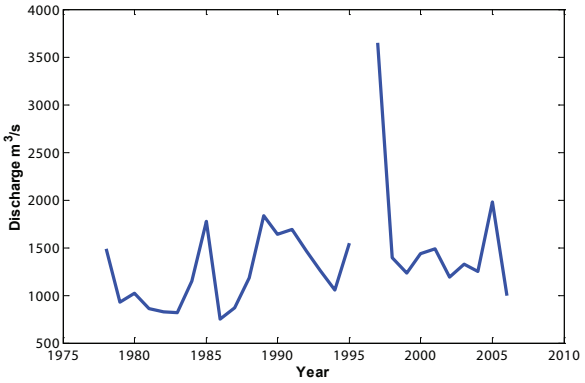

Figure 2. Interannual variability for discharge at Yana basin from 1976–2006.

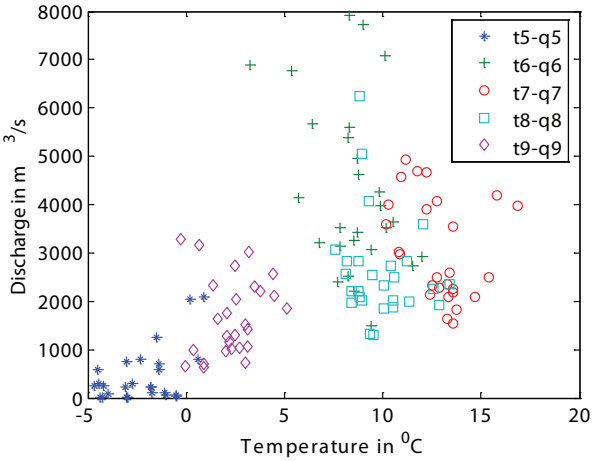

Figure 3. Discharge (q) and temperature (t) comparison from May to September with no lag.

October, November, and December are 25 mm, 15 mm, 10 mm, and 7 mm.

Temperature and precipitation interannual variability (standard deviation) did not show any significant upward trend from 1930–2000. The highs and lows of precipitation and temperature show consistency, indicating with higher annual temperature there is higher annual precipitation. To understand the basin hydrology, annual flow, monthly flow and variation (standard deviation) and trend are analyzed

It was found that basin discharge is typical of continuous permafrost region (Kane 1997) with peak flow in June and low flow dominating from October to April. Trend analysis shows mixed results for all the stations, but negligible or no change is observed during the cold season from October to April.

Discharge, temperature, precipitation, and Special Sensor Microwave/Imager (SSMI) SWE analysis

The discharge regime at the outlet shows interannual variation from 1600 m^3/s to 800 m^3/s with a tendency towards decreasing trend from 1988–2000 (Fig. 2). The variation in monthly streamflow is generally small for the cold season (October to April) and large in summer months, mainly due to floods associated with snowmelt and storm activities.

Correlation between temperature and discharge was examined to understand the effect of higher or lower temperature fluctuation on mean discharge. Statistical analysis of annual mean discharge at the basin outlet and temperature annual mean showed a positive correlation (R = 0.30). There is no consistent relationship for warm and cold season for zero time lag, which could be due to no flow for most of the cold season in the Yana basin (Fig. 3). The only statistically significant month was May with a strong positive correlation (R = 0.48). Yang et al. (2002), observed a similar relationship for Lena basin, emphasizing that higher temperature in May will lead to larger snowmelt floods. This relationship shows that during transition period, as the watershed warms up, snow cover disappears and evaporation starts to dominate (Yang et al. 2002). Since this is a smaller basin compared to other large Siberian rivers, even one month lag does not show any significant relationship except a high positive correlation between November to December (R = 0.47); that is, higher temperature in November leads to more discharge in December.

Statistical analysis for correlation between precipitation and discharge showed a positive relationship for interannual comparison (R = 0.24), indicating that some years with higher precipitation showed higher average discharge. The winter months of January (R = 0.43) and March (R = -0.32) showed a negative relationship for zero lag, and other months from October to April showed no significant relationship. This could be because cold months are characterized by snow cover accumulation, and discharge is mostly base flow or no flow (Yang et al. 2002).

Discharge and SWE follow an inverse relationship, with the advent of snowmelt at about day 86 (last week of March), and it finally disappears at day 150 day around the last week of May on average (Fig. 5). The discharge subsequently peaks on day 160. This is typical of arctic regions underlain with continuous permafrost. The time series of discharge and snow water equivalent emphasizes the inverse relationship. High value of snow water equivalent does not always lead to high peak discharge; this could be due to different ablation

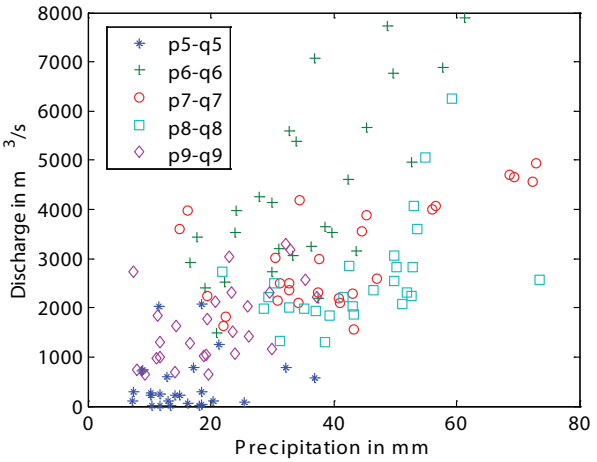

Figure 4. Discharge(q) and precipitation (p) comparison from May to September with no lag.

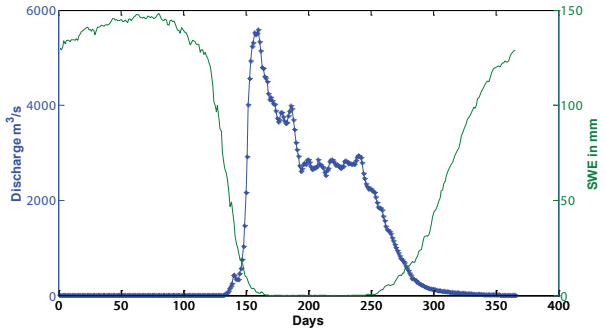

Figure 5. Daily mean discharge and SWE relationship.

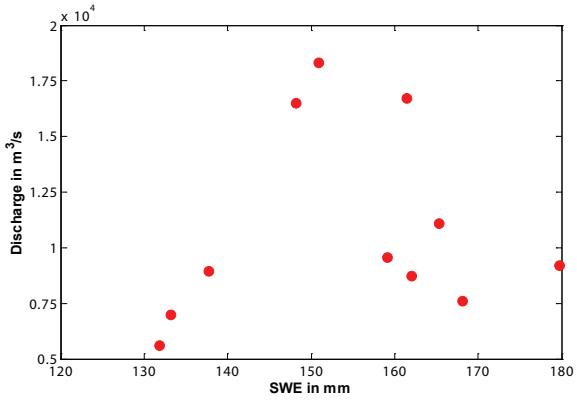

Figure 6. Daily maximum discharge and SWE relationship.

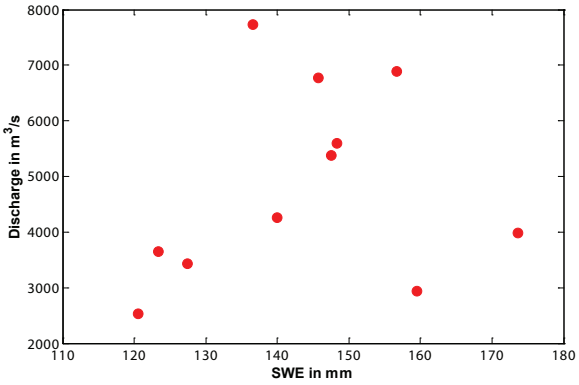

Figure 7 Monthly maximum discharge and SWE relationship.

rates, which are variable from year to year. We calculated the ablation rate around mid May to the first week of June and it varies from as low as 2 mm/day to as high as 16 mm/day at the start of snowmelt; the rates change with increase in temperature.

Highest daily value of SWE and discharge are compared, and their relationship (Fig. 6) follows a Gaussian curve. Increase in discharge is associated with increase in snow water equivalent (SWE), but there are some discrepancies for some years.

There is a lot of missing data for some years, and the mean value could be shifted to the month of August resulting in a lower peak. On looking at mean monthly maximum discharge in June and mean maximum SWE in March, the relationship is more linear with two outliers at the high end of SWE, which is similar to the daily maximum SWE and discharge relationship. The result indicates that on average, a year of higher precipitation in winter will lead to higher peak discharge.

The dates for maximum snow and discharge for each year are analyzed (Fig. 7), and no major change or shift is found in the timing of peak discharge and maximum snow water equivalent.

Conclusion

Significant changes have been observed in the large arctic river basins. For instance, Ye et al. (2003) and Yang et al. (2004) found Lena and Yenisei River discharges increase during the winter months and shift in peak discharge timing in Siberia mostly due to reservoir regulation. In our study of the Kolyma basin, we also found significant increase in winter discharge by as much as 522%-3157% downstream of the dam from December to April (Majhi et al. in press). Our results indicate that the Yana basin does not show any significant change in discharge.

Temperature and precipitation interannual variability (standard deviation) did not show any significant upward trend from 1930–2000. The peaks and lows of precipitation and temperature show consistency, indicating with higher annual temperature there is higher annual precipitation. Most of the precipitation falls in the summer months from June to September. Temperature shows a basin high of around 15°C in summer and a low of -40°C in January. Basin discharge is typical of continuous permafrost region with peak flow in June and low flow dominating from October to April. Trend analysis shows mixed results for all the stations, but negligible or no change is observed during the cold season from October to April.

The only statistically significant month for temperature and discharge was May with a strong positive correlation . Yang et al (2002), observed a similar relationship for the Lena basin, emphasizing that higher temperature in May will lead to larger snowmelt floods. Correlation between precipitation and discharge showed a positive relationship for interannual comparison, indicating that some years with

higher precipitation showed higher average discharge. The winter months of January and March showed a negative relationship for zero lag, and other months from October to April showed no significant relationship, while there was significant relationship from June to September for no lag. This could be due to quick response of discharge to rain events, since the Yana is comparatively a medium-sized basin.

Overall there is a need to better understand discharge dynamics to further the hydrological cycle and its implications. Monitoring snow pack variability for the arctic region has implications in the context of global change, since it is fundamental to estimate the change in freshwater flux. Moreover, changes in snow depth and timing alter the surface albedo, resulting in feedbacks at both regional and global scale. The analysis reported may be very useful in improving the snow and discharge relationship in hydrological models.

References

Déry, S.J. & Wood, E.F. 2005. Decreasing river discharge in northern Canada. *Geophys. Res. Lett.* 32: L10401, doi:10.1029/2005GL022845.

Déry, S.J., Stieglitz, M., McKenna, E.C. & Wood, E.F. 2005. Characteristics and trends of river discharge into Hudson, James and Ungava Bays, 1964–2000. *Journal of Climate* 18: 2540-2557.

Kane, D.L. 1997. The impact of arctic hydrologic perturbations on arctic ecosystems induced by climate change. *Ecological Studies* 124: 63-81.

Shiklomanov, I.A. & Shiklomanov, A.I. 2003. Climatic change and the dynamics of river runoff into the Arctic Ocean. *Water Resources* 30: 593-601.

Yang, D., Kane, D.L., Hinzman, L., Zhang, X., Zhang, T. & Ye, H. 2002. Lena River hydrologic regime and recent change. *Journal of Geophysical Research Atmosphere* 107(D23): 4694, doi.

Yang, D., Ye, B. & Shiklomanov, A. 2004a. Streamflow characteristics and changes over the Ob River watershed in Siberia. *Journal of Hydrometeorology* 5: 69-84.

Ye, B., Yang, D. & Kane, D.L. 2003: Changes in Lena River streamflow hydrology: Human impacts versus natural variations. *Water Resour. Res.* 39: 1200, doi:10.1029/2003WR001991.

Modeling Temperature Profiles Considering the Latent Heat of Physical-Chemical Reactions in Permafrost and Gas Hydrates: The Mackenzie Delta Terrestrial Case

Jacek A. Majorowicz
NGC EDMONTON, 105 Carlson Close, Edmonton, Canada, T6R 2J8
Kirk Osadetz
Geological Survey of Canada, 3303 - 33rd St. NW, Calgary, Canada, T2L2A7
Jan Safanda
Geophysical Institute, Czech Academy of Sciences, 141-31 Praha 4, Czech Republic

Abstract

To understand better the formation and history of petroleum gas hydrates in terrestrial permafrost regions, we have performed numerical temperature profile modeling in response to surface forcing due to both the glacial-interglacial history and future climate change, where atmospheric CO_2 has doubled due to climate change. The models are constrained by heat flow from deep wells, thermal conductivity, latent heat, and the observed permafrost and gas hydrate thicknesses. The models consider the pressure–depth dependence of ice and gas hydrate thawing points over the entire gas hydrate and permafrost intervals, in contrast to previous models that considered only a thin layer using a constant dissociation temperature. In areas of thick permafrost, results show that a thinned gas hydrate layer persisted through previous interglacials, and that future warming before the "natural" end of the current interglacial will not destabilize the gas hydrate layer significantly. Therefore, present changes in temperature gradient reflect transient conditions, and they should not be used to derive thermal conductivity in permafrost regions using a constant heat flow assumption. We also find that the ratio of temperature gradients within and below the permafrost has very little to do with the thermal conductivity ratio of the permafrost, although this is less appropriate in the sub-permafrost layers due to the buffering effects of overlying ice-bearing permafrost. Models with unfrozen-frozen thermal conductivities of 2.4–3.6 W/(m.K), and with an unfrozen-frozen conductivity ratio of 2.1–3.4 W/(m.K), (that is, very similar conductivity ratios 1:1.5 and 1:1.6) give dramatically different thermal gradient ratios 1:5.4 and 1:2.9, respectively.

Keywords: climate change; gas hydrate; latent heat; permafrost.

Introduction

To understand better the formation and history of petroleum gas hydrates (GHs) in terrestrial permafrost regions, we have performed numerical modeling of the surface forcing due to both glacial-interglacial history and future climate change. Persistent GH layers in a terrestrial environment of thick permafrost in cold regions sequester methane and impede its migration into the atmosphere. The Mallik site in the Mackenzie Delta (MD) is an excellent example of such GH deposits (Dallimore & Collett 2005, Smith & Judge 1995, Judge et al. 1994, Judge & Majorowicz 1992). We examine this hypothesis by modeling terrestrial MD GH thickness variations below an ice-bearing permafrost (IBP) layer in response to past and future surface temperature changes, using a 1D thermal model that assumes no water or gas flow. Past surface forcing uses a detailed Holocene glacial-interglacial history compiled from other sources (Taylor et al. 2005). We also consider the implications of a warmer future based on a doubling of atmospheric CO_2 resulting in a local mean surface temperature increase of 2°C /100 yrs.

Method

Solving the transient heat conduction equation gives the temporally dependent subsurface temperature change in response to surface forcing:

$$C_v\, \partial T/\partial t = \partial[K(\partial T/\partial z)]/\partial z + A \qquad (1)$$

where T is the temperature, K is the thermal conductivity, C_v is the volumetric heat capacity, A is the rate of heat generation per unit volume, z is the depth, and t is the time in a one-dimensional layered geothermal model. We employed a computer code to simulated temporal subsurface temperature changes in response to surface forcing (Safanda et al. 2004). Within the model, Equation 1 is solved numerically by an implicit finite-difference method similar to that described by Galushkin (1997). The upper boundary condition is the temporally varying surface temperature, and the lower boundary condition is a constant heat flow density at 15 km depth. The depth grid steps are: 2, 5, 10, 50, 100, 250, and 500 m deep; model layers are defined between: 0–100, 100–1500, 1500–2000, 2000–2500, 2500–5000, 5000–10,000, and 10,000–15,000 m deep. Time steps vary between 0.5 yr to 50 yr, depending on the amplitude of surface temperature changes.

The finite-difference scheme of Equation 1 on the depth and time grids, together with the upper and lower boundary conditions, leads to a system of difference equations for unknown values T_{k-1}^{n+1}, T_k^{n+1}, T_{k+1}^{n+1} (where the subscript k and the superscript n denote a value at the k-depth step and the n-th time step) within a tri-diagonal matrix, which was solved by the forward method (Peaceman & Rachford 1955).

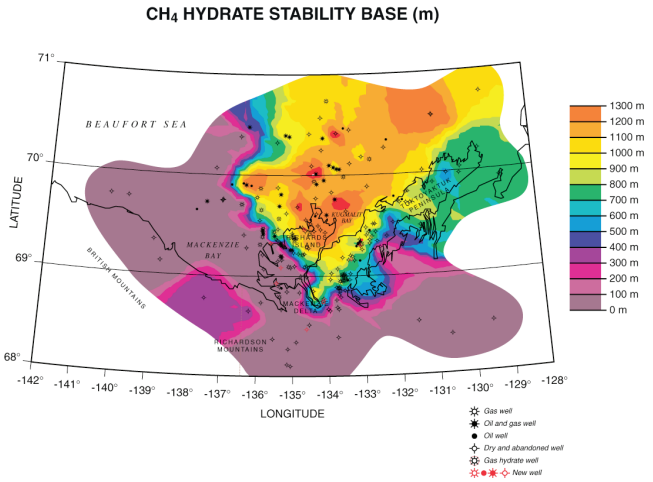

Figure 1. Depth to GH base of Type I stability in the BMB based on the interpretation of measured temperature logs, bottom hole temperature data (Fig. 2) and T-z calculations (modified from Majorowicz and Hannigan 2000) that are constrained additionally by both deep heat flow and base of the IBP. Modelling undertaken here is for northern Richards Island (near centre of figure).

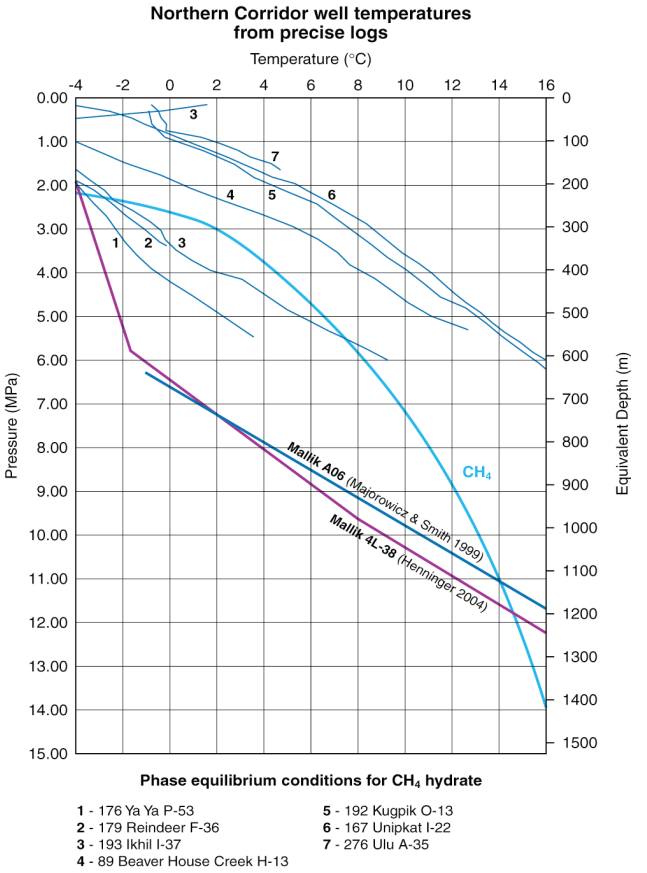

Figure 2. Example of temperature-depth profiles vs. the equilibrium GH stability curve. Examples of precise logs observed in wells years after the end of the drilling disturbance are from Taylor et al. (1982).

To estimate effective thermal conductivity values and volumetric heat capacity, it was necessary to consider the respective geometric and arithmetic averages of the constituent values for the rock matrix, water, ice, and GH in proportion to their volumetric fractions (Galushkin 1997, Nixon 1986). A consumption or release of the latent heat, L, in water/ice (334 kJ.kg^{-1}) and GH (430 kJ.kg^{-1}) accompanying either thawing or freezing was included. The effects of interstitial ice and GH were accounted for using apparent heat capacity (Carslaw & Jaeger 1959), when the volumetric heat capacity is increased in the depth sections of the model where the thawing and freezing occurs; that is, where the temperature is within the thawing range between the temperature of solidus T_S, and liquidus, T_L, at the actual simulation time step.

The liquidus and solidus temperatures of water/ice and GH are depth and hydrostatic pressure dependent (Galushkin 1997) and solidus temperatures were 0.2°C lower than liquidus temperatures. A contribution to the heat capacity from the latent heat = $\rho\Phi L/(T_L\text{-}T_S)$ was considered, where ρ is the density of either ice or GH, and Φ is a fraction of the total volume occupied by these phases. In the IBP zone, we infer the 30% rock matrix porosity to be fully occupied by water at temperatures above T_L, and by ice at temperatures below T_S. Within the GH stability zone, the GH saturation in matrix porosity was inferred to be 60%. For the model to be tractable, the model IBP and GH stability zones are assumed not to overlap, which follows common observation in the study area that GHs are not generally found within the IBP (Dallimore & Collett 2005). The salt concentration 9 g/L was considered constant with depth, and the p-T phase curves were adjusted to this value.

Numerical code performance was tested by comparing model results against the analytical solidification problem solution (Carslaw & Jaeger 1959), where the molten half-space at liquidus temperature, 1300°C, is in contact with a solid half-space at zero temperature and releases the latent heat of 477 kJkg^{-1} in the temperature range 1100°C–1300°C. Comparison of the differences between the numerical and analytical temperature profiles found them to be within about 20°C. If we assume that the magnitude of the difference is proportional to the temperature range, that is, to the contrast at the contact of the molten and solid half-spaces, the error expected for the IBP and GH numerical simulations should be about 100 times smaller (i.e., tenths of a °C) because of the scale of both the temperature range and surface temperature variations that are used in our simulations. A similar error range was estimated by halving the time and/or depth steps.

Our model uses deep heat flow, thermal conductivity, present IBP and Type I GH thicknesses, and a surface melting temperature (-0.576°C) that considers groundwater salinities (9 g/L). It employs latent heat effects throughout the IBP and GH layers, which improves upon previous models (e.g., Taylor et al. 2005). The models are constrained by deep heat flow from bottom hole temperatures in deep wells (Majorowicz et al. 1990) and thermal conductivity, latent heat, present IBP thickness, and present Type I GH thicknesses (Henniges et al. 2005). The models consider the pressure–depth dependence of ice assuming hydrostatic (e.g., Lachenbruch et al. 1982) and GH thawing points over

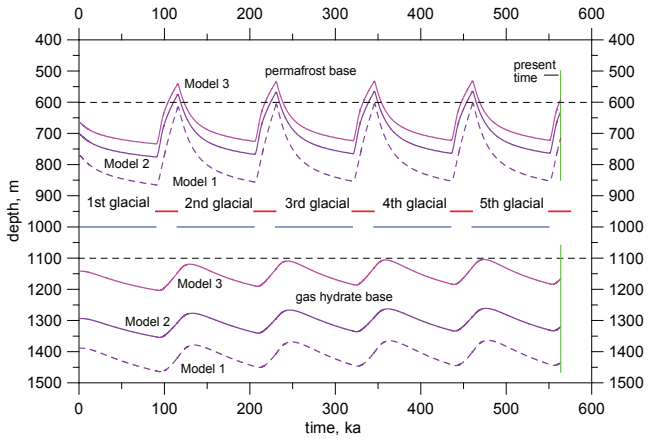

Figure 3. Simple test results of glacial-interglacial surface forcing upon permafrost and GH (Models 1–3 are described in the text). (Time scale shown is 600 ka. Dotted lines show the present base of permafrost and GH. Glacial-interglacial timing and temperature magnitudes are based on Muller & MacDonald (2000) and Taylor et al. (2005).

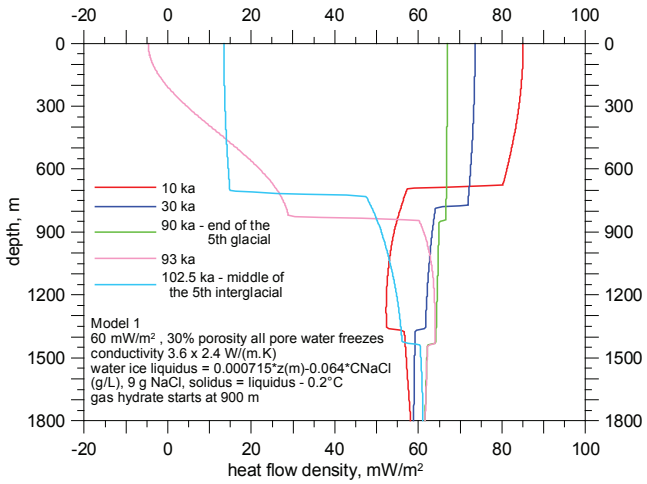

Figure 4. The heat flow and depth profiles for different phases of the glacial cycle for Model 1.

the entire expected extent of the IBP and GH layers (Sloan 1998). Previously published models have considered only a thin layer using a constant dissociation temperature (Taylor et al. 2005).

Current Gas Hydrate Stability Zone

The GH stability zone is currently widespread both in the onshore and offshore BMB, especially to the east of Mackenzie Bay (Fig. 1). There the GH stability zone base reaches 1.5 km deep, where the IBP is thick and the heat flow is low (Figs. 1, 2).

Modeling Results

We have simulated the downward propagation of the surface warming and cooling attending the cyclical glacial and interglacial models for a Richards Island location (Fig. 1). The dependence of the thermal conductivity on water/ice content and the specific heat of the rock section on the porosity and the proportion of interstitial water and ice are important. Accounting for the effect of the latent heat necessary to thaw the interstitial ice in the IBP layer is crucial for matching observations at realistic time rates. In the absence of this heat sink provided by thawing ice in the IBP, the subsurface warming would proceed much faster.

Models of the past history of permafrost and GH layers

Individual computational models use the characteristics of IBP and GH formation and dissipation as functions of temperature history, constrained by present temperature observations and current IBP and GH layer thicknesses. The surface climate history for the end of the Wisconsinan and Holocene is after Fig. 3b in Taylor et al. (2005); Pleistocene surface history of glacials and interglacials is after Muller and MacDonald (2000). Forward modeling of the past history for the IBP and GH layers on Richard's Island in the vicinity of the Mallik well (Dallimore et al. 1999, Dallimore & Collett 2005) can be calibrated against present-day observed IBP and GH zones, which have bases at about 600 m and about 1100 m, respectively.

The numerical solution of the transient heat conduction equation (eq. 1) was applied to model time vs. temperature, depth, IBP characteristics using latent heat effects (Galushkin 1997). This new model employs the pressure–depth dependence of ice and GH thawing points and considers latent heat effects in subsurface heat transport modeling and their impact on paleo-temperature reconstructions across the entire GH layer and not just its boundaries. All models account for latent heat by means of the apparent specific heat, which is a standard treatment. The model also considers diffusive heat flow related to surface-subsurface coupling.

Figure 3 shows three models of the surface temperature forcing effect on IBP and GHs, which currently have observed bases at about 600 m and about 1160–1170 m, respectively:

Model 1 is a simple test of glacial-interglacial forcing upon IBP and GH layers, where the GH zone is constrained to be 900 m deep or deeper. Results show that the model base of IBP and GH is much deeper than the currently observed values, despite a high heat flow value of 60 mW/m^2 (Majorowicz et al. 1990, Henniges et al. 2005). We infer that the frozen IBP conductivity, 3.6 W/(m.K), is lower than that used in this model, which is based on a measured GH layer conductivity of 2.4 W/(m.K), where the pore space of 30% is filled with water and adjusted using the geometric mean to the pore space filled with water ice. We considered glacial-interglacial cycle lengths of 115 ka, of which 90 ka are glacial and 25 ka are interglacial. The present day is 13.5 ka after the last glacial interval. In Model 1, the mean temperature during glacial intervals was -17°C (Allen et al. 1988) and the mean temperature during interglacials was -4°C, which is slightly higher than the present -6.5°C at the Mallik site.

Model 2, like Model 1, considers the climatic history proposed by Taylor et al. (2005, Fig. 3b). We note that in

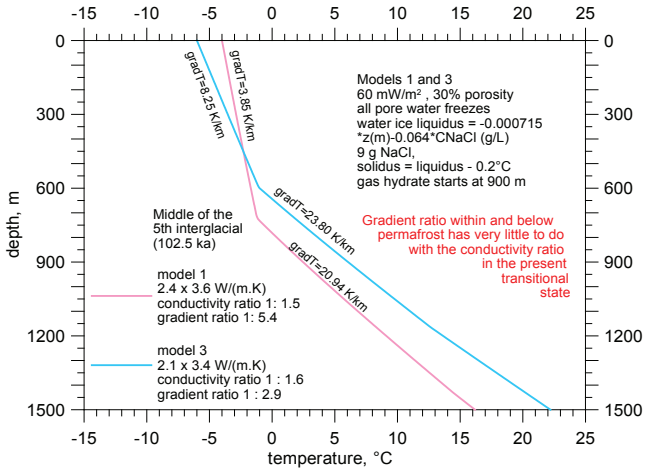

Figure 5. Thermal gradient for the frozen-unfrozen system vs. thermal conductivity ratio (Models 1 vs. 3).

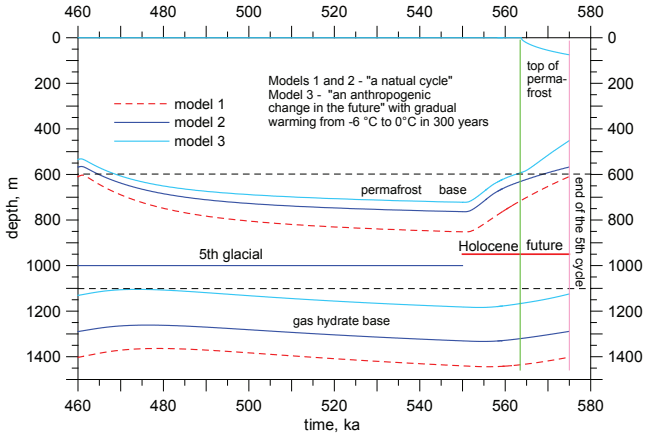

Figure 6. Consequences of the global climate change model that considers 6°C gradual warming projected 300 years into the future. Present time is marked by a green line.

Model 2 the base of both the IBP and the GH layers occurs ~100 m shallower than that calculated by Model 1, mainly due to higher average temperatures during glacial intervals (-15°C, rather than -17°C). In Model 2 the predicted current base of IBP, 13.5 ka after the onset of Holocene warming, is 657 m (-1.04°C) while the base of the GH layer is 1262 m (13.45°C), both of which are slightly too deep for observed values (Fig. 3).

Model 3 is a model that employs a surface warming like that of Model 2. However, Model 3 employs a frozen-thawed conductivity varying from 3.4 (frozen) to 2.1 (unfrozen) W/(m·K) compared with 3.6 (frozen) to 2.4 (unfrozen) W/(m·K) used in Models 1 and 2. This results in an appreciable improvement of the fit to observations. Figure 7 illustrates the position of the current base of the IBP. The calculated present base of IBP is very close to the observed depth of 600 m and the GH layer base is at ~1.17 km (Fig. 3).

All the models indicate generally similar thickness variations of the IBP and GH layers during glacial-interglacial cycles. Both the IBP and GH layers increase in thickness during glacial intervals and decrease in thickness during interglacial intervals. For Model 3 these variations are about 190 m for the IBP and about 80–90 m for the GH layer.

Model 2 predicts that the base of both IBP and GH layers are 100 m higher than those predicted in Model 1, mainly due to a higher average temperature mainly due to assumed warmer glacial, -15°C instead of -17°C. Yet, the predicted current IBP and GH layer bases were still slightly deeper than observed values. Model 3 improves the fit between the observed and predicted current IBP and GH layer characteristics as a result of changes to the frozen-thawed conductivities resulting in an appreciably improved fit to observed values. Today, 13.5 ka after the end of the last glacial interval, Model 3 predictions are very close to the observed IBP base (600 m) while the predicted current base of the GH layer is just slightly deeper (1160–1170 m) than the observed depth (1100 m).

Models of IBP and GH layer characteristics that are based on historical surface temperature forcing are both robust and informative. The predicted heat flow-depth profiles for Model 1 (Fig. 4) illustrate the different phases of the glacial cycle (Fig. 3, Model 1). For example, at 10 ka after the onset of the glacial interval, the base of the IBP, at 700 m, is moving downward, with an attendant heat release, while simultaneously the base of the GH, at 1350 m, is moving upward and consuming heat. The thermal inertia impact on sub-permafrost GH layer thinning is delayed and responsive to surface forcing, rather than leading and causative, due to the buffering effect of the overlying permafrost layer.

Models indicate that heat flow at depths above 1.5 km is in a transient state. Heat flow below that depth is stable, within the measurement error. The simple glacial-interglacial model also indicates that the ratio of temperature gradients within and below the IBP has very little to do with the conductivity ratio of the permafrost and sub-permafrost layers, such that even current temperature profiles are transient. Models with an unfrozen-frozen conductivity ratio = 2.4/3.6 W/(m.K), and models with an unfrozen-frozen conductivity ratio = 2.1/3.4 W/(m.K) give very similar conductivity ratios 1:1.5 and 1:1.6, but are characterized by dramatically different thermal gradient ratios: 1:5.4 and 1:2.9 (Fig. 5).

Below the buffering effects of the IBP the estimated conductivity, K, in the GH zone (Wright et al. 2005; Henninges et al. 2005) is based on both temperature gradients from a precise temperature profile (Henninges et al. 2005) and the deep heat flow, Q = 60 mW/m² (Majorowicz & Smith 1999). The estimates employ the equation:

$$Q/GradT=K \qquad (2)$$

This is a correct assumption for steady state situations only, such as non-ice bearing permafrost areas with constant surface *T*. The resulting conductivity estimates are correct below the IBP, within the heat flow measurement error of 10%–15%, (Fig. 4).

The impact of future warming

Surface temperature will change dramatically accompanying the projected doubling of atmospheric CO_2

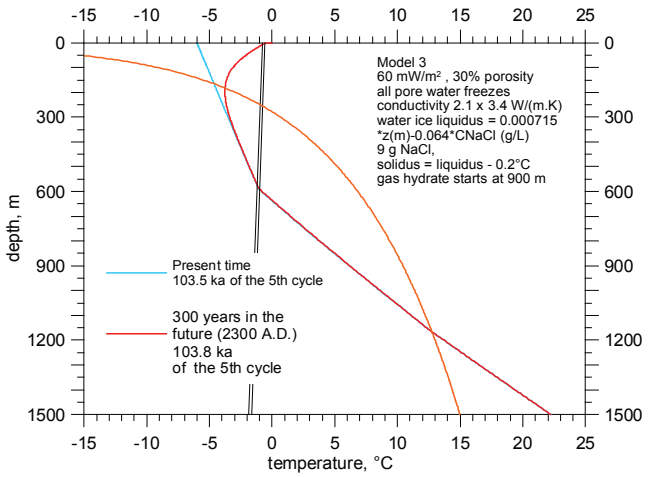

Figure 7. T-z profile corresponding to the expected future warming since present warming by a rate of 2°C/century from -6°C to 0°C.

resulting in future climate warming during the next 300 years. We predict the consequences of such a mean surface temperature change, from -6°C to 0°C, considering past history followed by gradual warming, at a rate of 2°C per century. The future predictions are shown in Figures 6 and 7. Hypothesizing a time corresponding to the "natural" end of this interglacial about 11.5 ka in the future, the model predicts that the IBP will have thawed by ~150 m from below and 70–80 m from the surface. The predicted accompanying GH layer thinning is very small and within the range of previous natural cycle variations (Fig. 3), in spite of the accelerated surface warming accompanying climate change.

Conclusions

Model results that consider latent heat effects of water/ice and GH formation and dissipation show that:

1. Historical and future surface temperature forcing implications for both IBP and GHs can be modeled successfully using available Pleistocene glacial-interglacial and Holocene surface temperature histories. Model GH layer thickness generally increases during colder intervals (i.e., glacial) and decreases during warmer intervals (i.e., interglacial). For Model 3, which most closely resembles observed values, these variations are ~190 m for the IBP and about 80–90 m for the GH layer. Where the IBP layer is thick it is unlikely that sub-permafrost GHs disappeared entirely during previous interglacial intervals, nor are they expected to disappear prior to the "natural" end of the current interglacial. In regions of thick terrestrial permafrost like the Mackenzie Delta, GH layers can act as a persistent sink for and barrier to the migration of methane.

2. Models that consider the consequences of current climate warming trends indicate that, when the current interglacial interval ends "naturally" ~11.5 ka from now, the study area IBP will have thawed ~150 m from below and 70–80 m from the top. The attending GH disassociation inferred is very small and comparable to that of model natural variations accompanying preceding glacial-interglacial cycles.

3. Temperature gradient ratios within the IBP are not strongly dependent on the conductivity ratio between permafrost and sub-permafrost layers, as the current temperature profile is a transient one. A model with an unfrozen-frozen conductivity of 2.4–3.6 W/(m.K) and a model with an unfrozen-frozen conductivity ratio 2.1–3.4 W/(m.K) result in very similar conductivity ratios, 1:1.5 and 1:1.6, but these two alternatives have dramatically different thermal gradient ratios of 1:5.4 and 1:2.9, respectively.

4. The hypothesis that links sudden glacial terminations to major methane emissions from large, rapid GH destabilization events (Nisbet 1990, 2002, Kennett et al. 2003) presumes that GHs destabilize rapidly in response to environmental change late in glacial intervals, and that they serve at other times as a sink for and barrier to the migration of methane into the atmosphere. This hypothesis applies mainly to marine GHs, which may be more easily destabilized than are the terrestrial sub-permafrost GHs we modeled.

Our study shows that terrestrial GHs below thick IBP vary in thickness in response to surface temperature history changes, but that terrestrial thermal inertia conserves both IBP and sub-permafrost GHs delaying and reducing methane release. Terrestrial thermal inertia also imposes a phase-delay between surface temperature warming and the subsequent onset of GH dissociation, making it unlikely that terrestrial GHs below thick permafrost could rapidly reinforce climate warming events, consistent with the hypothesis. The implications of latent heat effects and thermal inertia for submarine gas hydrates remain to be determined; however, our model results appear consistent with recent observations of methane isotopic compositions from ice cores (Sowers et al. 2006).

References

Allen, D., Michel, F. & Judge, A. 1988. The permafrost regime in the Mackenzie Delta-Beaufort Sea Region, N.W.T. and its significance to the reconstruction of the paleoclimatic history. *Journal of Quaternary Science*, INQUA Volume, June 1988: 3-13.

Carslaw, H.S. & Jaeger, J.C. 1959. *Conduction of Heat in Solids*, 2nd ed. Oxford University Press.

Dallimore, S.R., Uchida, T. & Collett, T.S. (eds.) 1999. *Scientific Results from JAPEX/INOC/GSC Mallik 2L-38 GH Research Well, Mackenzie Delta, Northwest Territories.* Canada. Geol. Surv. Canada, Bull. 544: 403 pp.

Dallimore, S.R. & Collett, T.S. (eds.) 2005. *Scientific Results from the Mallik 2002 Gas Hydrate production Research Well Program, Mackenzie Delta, Northwest Territories, Canada.* Geol. Surv. Canada Bull. 585: 140p. CD and Charts.

Galushkin, Yu. 1997. Numerical simulation of permafrost evolution as a part of sedimentary basin modeling: permafrost in the Pliocene-Holocene climate history of the Urengoy field in the West Siberian basin, *Can. J. Earth Sci*. 34: 935-948.

Henniges, J., Huenges, E. & Burkhard, H. 2005. In situ thermal conductivity of gas hydrate bearing sediments of the Mallik 5L-38 well. *J. Geophys. Res*. 110: B11206

Judge, A.S. &. Majorowicz, J.A. 1992. Geothermal conditions for gas hydrate stability in the Beaufort-Mackenzie area-the global change aspect. *Paleogeography Paleoclimatology and Paleoecology, Global & Planetary Change Section*, 98: 251-263.

Judge, A.S., Smith, L.S. & Majorowicz, J.A. 1994. The current distribution and thermal stability of natural gas hydrates in the Canadian Polar margin. *Proceedings of the IVth International Offshore and Polar Engineering Conference, Osaka.* The International Society of Offshore Polar Engineering, v. V I: 307-314.

Majorowicz, J.A. & Hannigan, P.K. 2000. Stability zone of natural gas hydrates in a permafrost – bearing region of the Beaufort–Mackenzie basin: Study of a feasible energy source. *Nat. Res. Res.* 9: 3-25.

Majorowicz, J.A. & Osadetz, K.G. 2001. Basic geological and geophysical controls bearing on gas hydrate distribution and volume in Canada. *AAPG Bulletin*, 85(7): 1211-1230.

Majorowicz, J.A., Judge, A. & Jones, F.W. 1990. Deep subpermafrost thermal regime in the Mackenzie Delta basin, northern Canada-analysis from petroleum bottom-hole temperature data. *Geophysics* 55: 362-371.

Majorowicz, J.A. & Smith, S.L. 1999. Review of ground temperatures in the Mallik field area: a constraint to the methane hydrate stability. In: S.R. Dallimore, T. Uchida & T.S. Collett (eds.), *Scientific Results from JAPEX/JNOC/GSC Mallik 2L-38 Gas Hydrate Research Well, Mackenzie Delta, Northwest Territories, Canada.* Geological Survey of Canada Bulletin 544: 45-56.

Muller, R.A. & MacDonald, G.J. 2000. *Ice Ages and Astronomical Causes: Data, Spectral Analysis, and Mechanisms.* Berlin: Springer Praxis, 318 pp.

Nisbet, E.G. 1990. The end of the ice age. *Can. J. Earth Sci*. 27: 148-157.

Nisbet, E.G. 2002. Have sudden large releases of methane from geological reservoirs occurred since the Last Glacial Maximum, and could such releases occur again? *Phil. Trans. R. Soc. Lond*. A 360: 581-607.

Nixon, J.F. 1986. Thermal simulation of subsea saline permafrost, *Can.J.Earth Sci.* 23: 2039-2046.

Peaceman, D.W & Rachford, H.H 1955. The numerical solution of parabolic and elliptic differential equations. *Journal of the Society for Industrial and Applied Mathematics* 3: 28-41.

Safanda, J., Szewczyk, J. & Majorowicz, J.A. 2004. Geothermal evidence of very low glacial temperatures on the rim of the Fennoscandian ice sheet. *Geophys. Res. Lett.* 31: L07211.

Sloan, E.D. 1998. *Clathrate Hydrates of Natural Gases*, 2nd ed., New York: Marcel Dekker Inc., 705 pp.

Smith, S.L. & Judge, A.S. 1995. *Estimate of Methane Hydrate Volumes in the Beaufort Mackenzie Region, Northwest Territories.* Geological Survey of Canada Current Research 1995, Part B: 81-88.

Sowers, T. 2006. Late Quaternary atmospheric CH_4 isotope record suggests marine clathrates are stable. *Science* v. 311: 838-840.

Taylor, A.E., Burgess, M., Judge A. &. Allen, V.S. 1982. Canadian Geothermal Data Collection Ä Northern Wells 1981, *Geothermal Series, Earth Physics Branch, E.M.R., Canada* 13: 153 pp.

Taylor, A.E., Dallimore,S.R., Hyndman, R. & Wright, J.F. 2005. Comparing the sensitivity of permafrost and marine gas hydrate to climate warming. In: S.R. Dallimore & T.S. Collett (eds.), *Scientific Results from the Mallik 2002 Gas Hydrate Production Research Well Program, Mackenzie Delta, Northwest Territories, Canada.* Geological Survey of Canada, Bulletin. 585: p. 130 and paper 52.

Wright J.F., Nixon, F.M., Dallimore, S.R., Henninges, J. & Cote, M.M. 2005. Thermal conductivity of sediments within the gas hydrate bearing interval at the Mallik 5L-38 gas hydrate production well. In: S.R. Dallimore & T.S. Collett (eds.), *Scientific Results from the Mallik 2002 Gas Hydrate Production Research Well Program, Mackenzie Delta, Northwest Territories, Canada.* Geological Survey of Canada, Bulletin. 585: 129-130.

The Last Twenty-Five Years of Changes in Permafrost Temperature in the European Russian Arctic

G.V. Malkova
Earth Cryosphere Institute, Russian Academy of Sciences, Moscow, Russia

Abstract

The 24-year-long permafrost temperature records from the long-term permafrost monitoring station Bolvansky are presented in this paper and analyzed in relation to climatic changes. The results of this analysis show that changes in mean annual ground temperatures generally follow the mean annual air temperatures. The warming trend in the air temperatures for the entire period of measurement at this site is 0.04°C/yr. Observed trends in mean annual permafrost temperatures vary from 0.003°C/yr to 0.02°C/yr in different natural landscapes. The warming trend in permafrost temperature for the entire period of measurement in anthropogenic landscapes is 0.04°C/year. A weak negative trend is observed in thawed boreholes (-0.012°C/year). For the last 10 years, an increase in climatic variability and an interchange of extremely cold and extremely warm years were observed, that led at first to a considerable increase in permafrost temperature. In 2007, a weak decrease in temperature was observed in most of the monitored boreholes.

Keywords: air temperature; climate change; permafrost temperature; thermal monitoring; trend.

Introduction

The geocryological observations show a general increase in permafrost temperatures during the last several decades in Alaska (Clow & Urban 2003, Osterkamp & Romanovsky 1999, Osterkamp 2003, Romanovsky 2006, Romanovsky et al. 2002) and northwest Canada (Smith et al. 2005, Burgess & Smith 2003). At some locations near the southern boundary of permafrost in Alaska, this warming has already resulted in permafrost thawing from the top down (Jorgenson et al. 2001, Osterkamp et al. 2000).

The cryolithozone of the European part of Russia extends predominantly just north of the Arctic Circle. Permafrost in this region is well studied. During the 1970s and 1980s, due to oil and gas field exploration and development, many drilling and geophysical surveys were carried out in the European North. State engineering-geological mapping (1:200,000 scale) was also accomplished. These activities provided important information on permafrost extent, thickness, and temperature regime. In order to investigate in detail the geocryological conditions of this region, several long-term permafrost-monitoring stations were established, in both natural settings and in settings disturbed by human activities. During the 1980s, there were 14 geocryological long-term monitoring stations where the ground temperature was measured in several dozens of boreholes. During the last ten years, the development of oil and gas fields in the European North has progressed rapidly. The building of oil-shipping terminals was accomplished in the coastal zone of the Barents Sea and Pechora Bay (Varandey et al.). With all these developments, current data on changes in geocryological conditions have turned out to be insufficient. Today, regular temperature measurements in boreholes are carried out only at Vorkutinsky and Bolvansky long-term monitoring stations. In 2006 and 2007, after an 11-year time gap, permafrost temperature measurements were conducted successfully in several reference boreholes at two more former long-term monitoring stations, Rogovoy and Korotaikha. Results of these geocryological studies are cited in the scientific literature (Kakunov & Sulimova 2005, Kakunov et al. 2006, Oberman 1998, 2001, 2006, 2007, Malkova 2005, 2006, 2007, Mazhitova et al. 2004, Oberman & Mazhitova 2001). The locations of the active stations are shown in Figure 1.

According to the mentioned publications by Kakunov and Oberman, the considerable increase in mean annual permafrost temperatures during the last two to three decades is typical for southern regions of the permafrost in the Russian European North (Vorkutinsky, Rogovoy and Korotaikha stations). This increase resulted in partial permafrost thawing, from the top down, and in a reduction in size of permafrost islands in the sporadic permafrost zone. New closed taliks appeared in the areas of high-temperature permafrost; the thickness of the existing closed taliks has increased. In areas directly affected by the human activity, the increase of permafrost temperature at the depth of zero annual amplitude varied from 0.2°C to 1.6°C during the period of observation. Fewer changes in permafrost were observed at the Arctic coast of the Barents Sea where the Bolvansky long-term observation station is situated on undisturbed landscape. In this paper the changes in permafrost that have occurred at the Bolvansky monitoring station during the last 25 years and their relation to observed climatic changes will be examined.

Methods of Measurements

The long-term permafrost monitoring station, Bolvansky, was established in 1983 at the location of the Bolvansky Cape weather station which has existed since 1935 (Fig. 1). Within the region (total area of 10 km²) twenty-five 12–15 m deep and 65–87 mm diameter boreholes were drilled in various landscape conditions. Each borehole was equipped

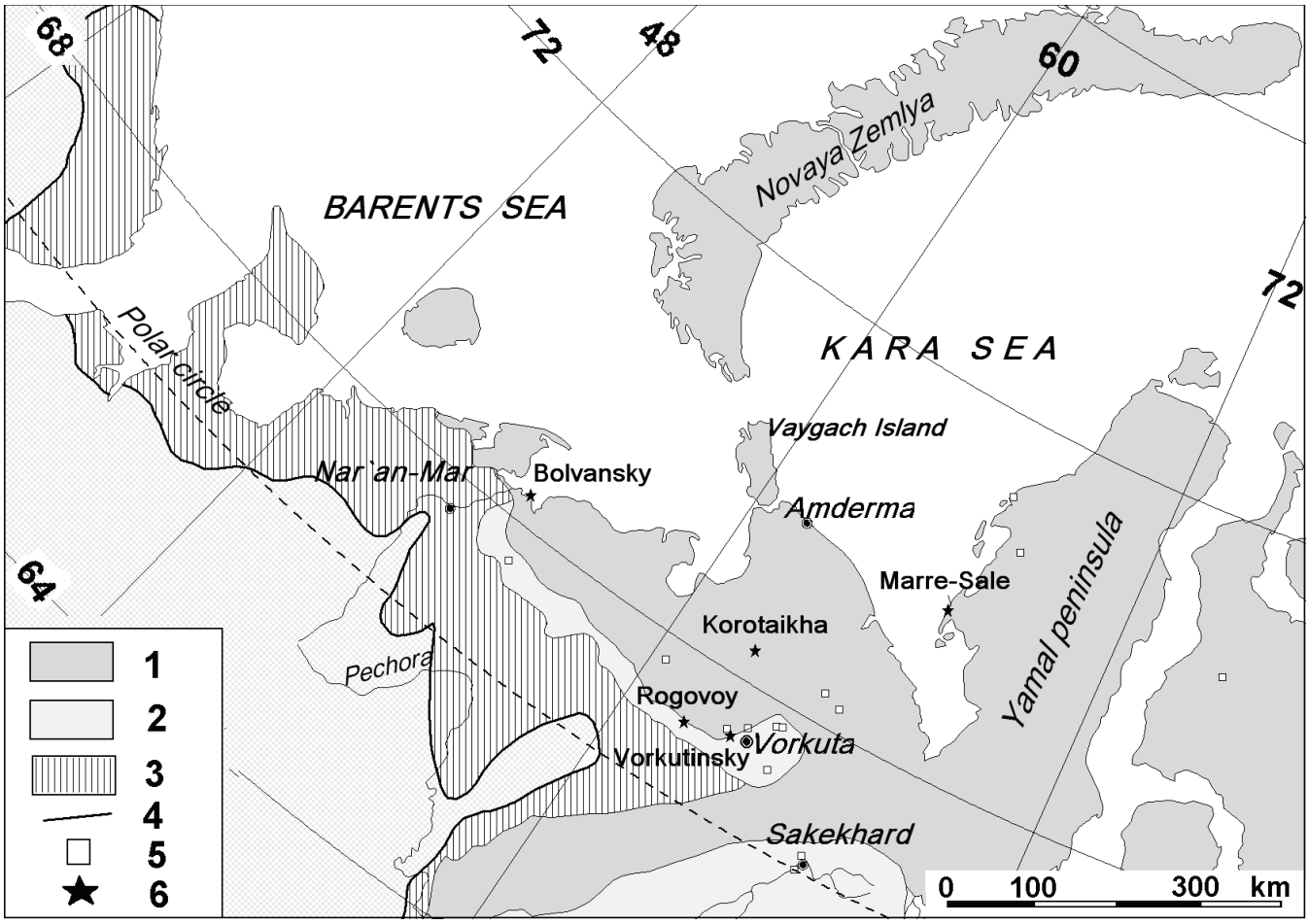

Figure 1. Location of long-term permafrost monitoring stations and permafrost spatial continuity in the European Russian Arctic: 1 – continuous permafrost, 2 – discontinuous permafrost, 3 – sporadic permafrost, 4 - southern boundary of permafrost distribution, 5 – closed permafrost monitoring stations, 6 – stations still in operation.

with steel casing to the depth of 3–5 meters, and was closed with a metal cap. A wooden box filled with sawdust was built around the aboveground portion of the casing to provide thermal insulation. Temperature measurements were taken three times a month using a string of mercury thermometers. The thermometers were located at depths of 1–6, 8, 10, 12, and 15 m. From 1983 until 1993, year-round studies were performed at this station. After 1993, observation sites and boreholes were abandoned for technical and organizational reasons. The results of the first ten years of geocryological study were archived as survey reports at the Russian Geological Data Center and have never been published in scientific literature.

In 1999, after a six-year break in measurements, 10 boreholes again were prepared for temperature measurements. Until 2005, ground temperature measurements were conducted there once a year at the end of the summer. LPC data loggers and strings of sensors in rubber cable were used in these measurements. The sensors were positioned at the same depths as in the previous period of measurements. Besides temperature measurements in boreholes, annual observations of temperature in the active layer have been carried out at the Circumpolar Active Layer Monitoring (CALM) project site. Soil temperatures are obtained with thermistor sensors inserted in the ground at various depths in the active layer and near-surface permafrost. The active layer depth at this site varies from 1–1.2 m. Therefore, the sensors in the active layer are installed at depths of 0.05, 0.25, 0.5, 0.75, 1, and 1.25 m. Readings are recorded at a regular time interval by battery-operated multi-channel data loggers (Brown et al. 2000).

In 2006, with technical support from the international project TSP, 4-channel automated HOBO U12 sets were installed in four key boreholes situated in various landscape conditions. Temperature is recorded automatically 4 times year-round. The first collection of data from the equipped boreholes was carried out at the end of summer 2007. At the same time four more HOBO U12 sets were installed in additional boreholes. Since 2007, all measurements are carried out every 6 hours; that is, four times a day. The sensors in the boreholes are installed at depths of 1 (or 3 m), 5, 7, and 10 m. This has permitted monitoring of permafrost temperature dynamics both in time and depth at each borehole. Through the entire time of measurements, we used three different types of thermometers. However, the error associated with the instrumentation was insignificant (<0.1°C) and corrections to the data were made accordingly.

The obtained information was processed in accordance with

Table 1. Mean annual permafrost temperature at the Bolvansky long-term monitoring station.

Borehole #	Landscape characteristics	Range of interannual fluctuations of the mean annual permafrost temperature, °C	Fluctuation amplitude, °C	Standard deviation	Long-term trend, °C /year (see Figure 2)
51	Edge of a drained lake, tundra	-1.0…-1.4	0.4	0.13	0.013
53	Gentle ridge, tundra	-1.7…-2.1	0.4	0.12	0.003
54	Gentle ridge, tundra	-1.8…-2.4	0.6	0.17	0.009
55	Edge of a ravine, tundra	-1.3…-1.9	0.6	0.21	0.015
56	Upper reaches of a ravine, peatland	-0.5…-0.8	0.3	0.10	0.011
59	Apex of a gentle ridge, tundra	-1.6…-2.3	0.7	0.21	0.023
60	Apex of a gentle ridge, disturbed tundra	-1.4…-2.4	1.0	0.36	0.040
61	Bottom of a drained lake, bog	+0.3…+0.8	0.5	0.17	-0.012
65	Gentle hillslope, tundra	-1.2…-1.7	0.5	0.15	0.011
83	Apex of a gentle ridge, tundra	-2.1…-2.5	0.4	0.17	0.007

prescribed protocol. Daily mean, monthly mean and mean annual ground temperatures were calculated. Calculation of trends and the regression equations were performed using the Microsoft Excel program. Climate data from the main weather stations (Nar'an-Mar, Vorkuta, Amderma, Fig. 1) of the European North were collected from the meteorological Internet site (http://meteo.infospace.ru/wcarch/html/r_index.sht) and processed similarly.

General Characteristics of the Research Region

The long-term permafrost monitoring station, Bolvansky, (68°17.3′N, 54°30.0′E) is located at the Pechora River Delta, on the northernmost extremity of Bolvansky Cape, which juts out into Pechora Bay (Barents Sea basin). The Bolvansky Cape weather station operated from 1935 to 1998. Long-term mean annual air temperature is -4.4°C, and precipitation is 404 mm. The area is represented by undulating marine plain with numerous lake depressions and large flat-bottomed valleys, some with permanent creeks. Elevations range from 20 to 35 m a.s.l. Quaternary deposit, a boulder sandy loam, is more than 100 m thick. Polygonal peatlands and fens with peat thickness ranging from 0.5–5 m occupy the inter-hill areas and depressions. The area is geocryologically unstable due to its location at the western extremity of the continuous permafrost zone in Europe and the near proximity of the discontinuous and sporadic permafrost zones. Permafrost exists just below the active layer under elevated and flat surfaces, whereas a deep position of the permafrost table is typical for valley bottoms, both dry and with flowing water. Open taliks occur under the Pechora valley, under Pechorskaya and Bolvanskaya Bays, and under many lakes (Mazhitova et al. 2004). The thickness of permafrost in this area is 100 to 200 m (Oberman & Mazhitova 2001).

The mean annual permafrost temperature at 10–12 m depth depends on landscape conditions and varies from -0.5°C to -2.5°C (according to measurements in 25 boreholes). In elevated areas and on hilltops the permafrost temperature varies between -2.0°C and -2.5°C. Within polygonal peatlands, on the slopes, and in the cols of hills with tundra vegetation the permafrost temperature varies from -1.5°C to -2.0°C. For the edges of lakes and terraces and also for the headstreams of small creeks, typical permafrost temperatures are in the range of -0.6°C to -1.4°C. On the bottoms of ravines and lakes, the permafrost surface is lowered in the depth from several meters to dozens of meters, and temperature of the thawed ground at the depth of 10 m is from +0.3°C to +1.0°C. The range of permafrost temperatures observed during the research period from 1983 to 2007 in presently operational boreholes are shown in Table 1 and Figure 2.

The mean annual air temperature in Bolvansky Cape according to the data from the weather station (until 1998) and from our data loggers (1999–2007) is shown in Figure 3. During the last decades, the two coldest periods, from 1985–1987 and from 1997–1999, are easily noticeable. Since the mid-1980s, two periods of warming were observed. The first one was from the mid-1980s to the mid-1990s and the second one in 2000–2005. According to the data from the Institute of Global Climate and Ecology (Rosgidromet and RAS), a general gradual increase of precipitation (5%–10% per 10 years) was observed. The years with maximum amount of precipitation (including snow) were 1990–1991, 1995–1996, and 2001–2002. The maximum snowfall occurred in 1981–1982 (snow accumulation was about 380 mm). The winters of 1985–1986, 1994–1995, and 2000–2001 had little snow accumulation (about 150 mm).

Results and Discussion

During the period between 1984 and 2007, a weak positive trend in the mean annual permafrost temperatures

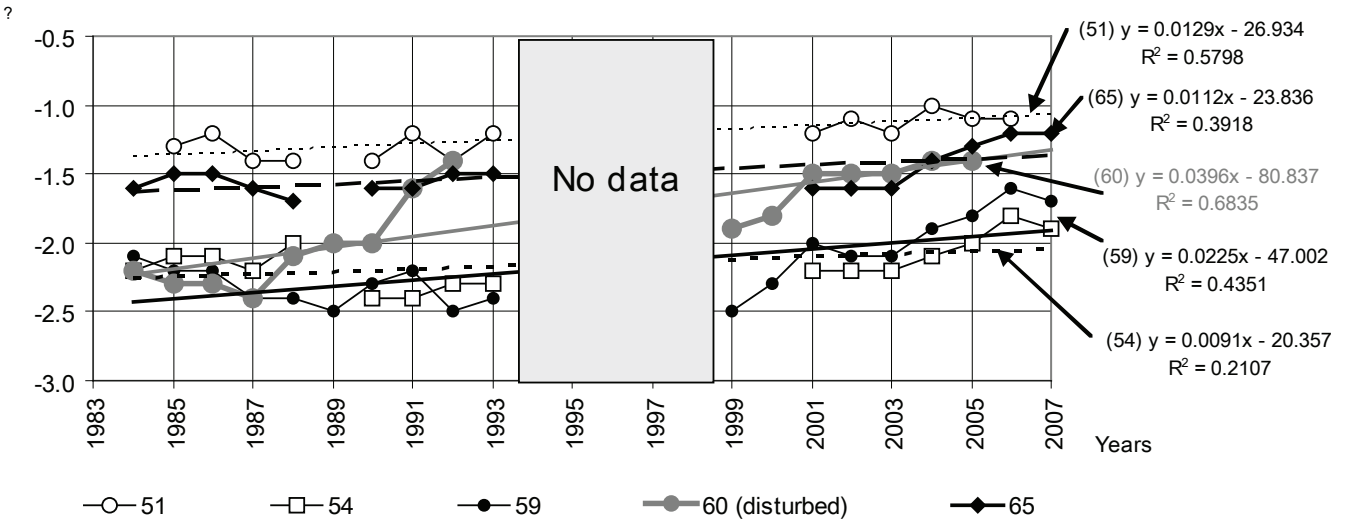

Figure 2. Mean annual permafrost temperatures and the long-term trends (from 1983 to 2007) in their variations measured in boreholes 51, 54, 59, 60, and 65 at the depth of 10 m.

(from 0.003°C/year to 0.02°C/year in the various landscape conditions) has been observed. During the same period, the trend of air temperature change of 0.04°C/year was much more pronounced (Fig. 3). An undoubted synchronism in soil and air temperature changes has been typical for all boreholes. During this period, the standard deviation of permafrost temperature interannual variability in the undisturbed landscapes has varied in rather narrow limits from 0.10 to 0.21. The standard deviation for disturbed conditions was 0.36.

During the last 8 years, the permafrost temperature has undergone especially considerable changes due to the greater interannual variations in the mean annual air temperature. Subsequent to anomalously severe 1998, we observed a noticeable decrease of the permafrost temperature in 1999. On the contrary, a warm 2000 as well as 2005 caused the increase in mean annual ground temperature in 2001 and its substantial increase in 2006. After relatively cold 2006 (the mean annual air temperature decreased by 2°C) some decrease (by 0.1°C to 0.2°C) of the permafrost temperature was observed in the boreholes at the end of the warm season.

Borehole #59 is the key for this long-term monitoring station. It is situated on the top of a gentle ridge in landscape conditions typical for this region. A CALM site where active layer monitoring is also performed is co-located with this borehole. The most complete set of observations of natural parameters is available for this borehole location. Besides the permafrost temperature measurements in the borehole (down to 10 m to 15 m in different years), the year-round active layer temperature data (with some gaps) and the maximum thawing depth are available for this location.

Figure 3 shows the mean annual air temperature variations at the Bolvansky station and the active layer and permafrost temperatures during the period of instrument measurements in the boreholes. During the last 10 years, the mean annual air temperature has undergone the greatest changes. The absolute minimum of the mean annual air temperature (-9.1°C) during the entire period of measurements started in 1935 was observed in 1998. Only 3 months in 1998 posted monthly mean temperatures above 0°C. At the same time, 2005 was the warmest on record with the mean annual temperature at -0.8°C. The duration of the period with positive monthly air temperatures was 6 months during that year.

The mean annual active layer temperature at a depth of 1.2 m ranged from -3.5°C to -0.5°C or 1°C to 2°C higher than the air temperature (due to the combination of a warming effect of snow and a negative thermal offset in the active layer). In general, the active layer temperature changes followed the changes in the air temperature, though within a smaller range. Especially significant decrease in the active layer temperatures was observed in the years with the low-snow winters. More frequently, the active layer temperatures ranged between -2°C and -3°C. As evident from Figure 3, the mean annual active layer temperature recently has a tendency towards increase. Since 2005, the active layer temperature has been increasing, staying in the range between -1°C and -2°C. In order to switch from seasonal thawing to seasonal freezing, the mean annual temperature at the bottom of the active layer is required to rise above 0°C. However, our data show that, up to the present day, the state of permafrost in the research region within each landscape type has been rather stable.

During the period of observations, the variations in the mean annual permafrost temperature in the Borehole 59 at the depth of zero amplitude have been relatively small. A decrease in ground temperature by 0.1°C or 0.2°C usually happens one or two years after a decrease in mean annual air temperature. The lowest permafrost temperature (-2.4°C) was observed in 1999 after a period of climatic cooling. Then, the permafrost temperature began to increase persistently following an increase in air temperature. However, the warming trend in the permafrost temperature was considerably smaller than the trend in the air temperature.

Borehole #60 was drilled on the same gentle ridge where the CALM site is situated, 100 m away from Borehole #59.

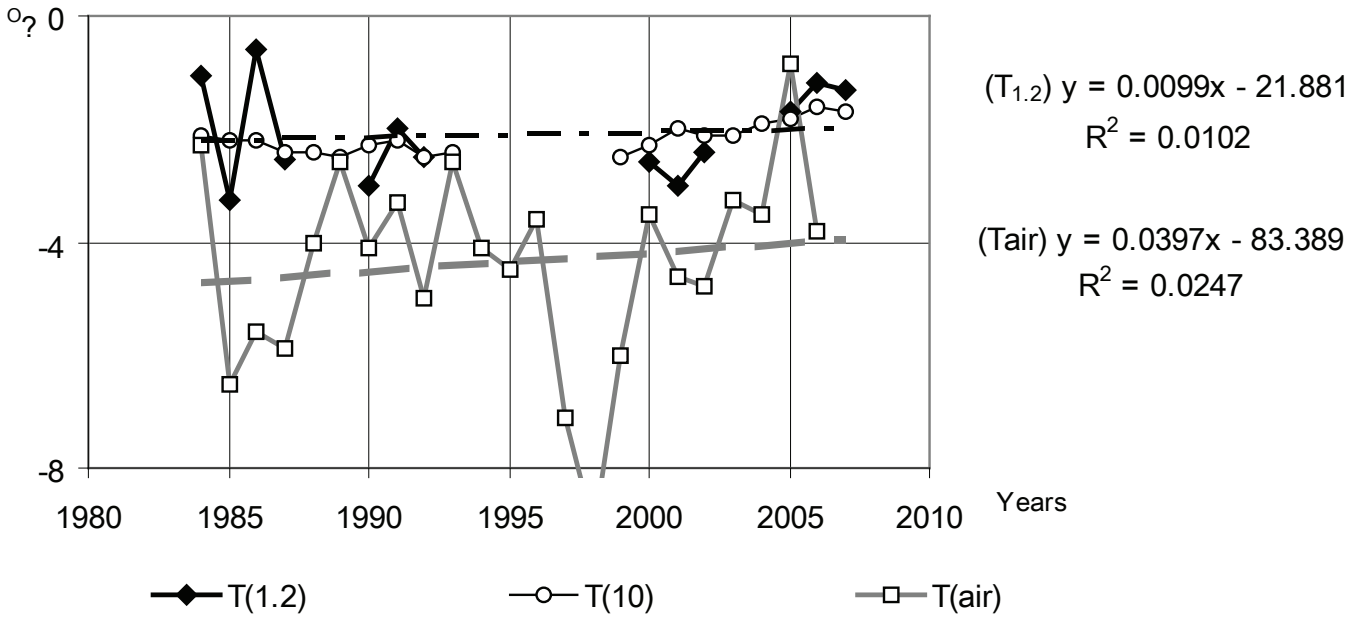

Figure 3. Mean annual temperatures of air, active layer (at the depth 1.2 m) and permafrost (at the depth 10 m) at the Bolvansky geocryological station, Borehole # 59. Grey dashed line is a linear trend of average annual air temperature.

This site was intentionally disturbed by removal of vegetation and organic soil layer. Figure 2 shows that during the first several years after the disturbance, after a small delay, a sharp increase in the mean annual ground temperature by 1°C occurred. During the first 15 years, a partial re-vegetation occurred at this site and, as a result, a decrease of permafrost temperature took place, by 1999–2000, but not to the initial values. The thickness of the snow cover did not change significantly at this disturbed site as compared with the undisturbed sites. In summer time, the amount of absorbed radiation was enlarged due to the stripping of the heat-insulating layers (vegetation and organic soil horizon). It resulted in the warming of the permafrost upper horizons. As the disturbed site gradually, naturally re-vegetated, a progressive decrease in mean annual permafrost temperature began (during 1992–1999 permafrost temperature at the depth of 10 m decreased from -1.4°C to -1.9°C) despite the observed increase in mean annual air temperature during this period (Pavlov & Malkova 2005, Malkova-Ananieva 2005). Further increase of the mean annual air temperature in 2000, 2003, and especially in 2005 again resulted in further ground warming by 0.3°C. According to our observations, the average long-term positive trend in permafrost temperature in the disturbed conditions was the largest for this long-term monitoring station and was equal to 0.04°C/year (Table 1).

Unfortunately, during the anomalously warm season of 2005, the thawing depth increased significantly within the limits of the disturbed site and Borehole #60 was filled with water and froze through the entire depth. Further temperature measurements are impossible.

Perennial observations of ground temperature in the thawed borehole situated in a drained lake basin (Borehole #61) have demonstrated a rather high long-term variability of ground temperature at the depth of 10–12 m (0.5°C) and a slightly negative temperature trend (-0.012°C/year). So, even under conditions of contemporary increase in mean annual air temperature, conditions for some decrease of ground temperature can be created at the bottom of drained lakes. Most likely, this is the result of changes in hydrological regime of the bog situated within the drying/drained lake bottoms. Namely, the lowering of the water level, due to the development of the erosion network, may explain these observations.

Conclusions

Conducted studies have demonstrated that the state of continuous permafrost of the coastal areas of the European North is still stable under the conditions of the recent increase in mean annual air temperature.

The permafrost temperature is a sensitive indicator of climatic changes, but the amplitudes of its variations were in a range between 0.3°C and 0.6°C, whereas the mean annual air temperature varied within 5°C during the same time period. Temperature changes at a depth of 10 m were observed in one or two years after the air temperature change.

The trends in the mean annual permafrost temperature increase are 2 to 10 times smaller than the trends of the increase in mean annual air temperature in various landscape conditions. For a significant change in the permafrost temperature regime, a combination of climate warming and surface disturbances is required.

The active layer temperature is determined both by the air temperature and by the snow cover thickness affecting the winter cooling rate under tundra conditions. The occurred climatic changes are not yet enough for the long-term thawing of the permafrost and for the transformation of the seasonally thawing layer into seasonally freezing layer in the studied area, which is located within the continuous permafrost zone.

Acknowledgments

This research was funded by the Polar Earth Science Program, Office of Polar Programs, National Science Foundation (ARC-0632400 and ARC-0520578) and CALM II project. Help in the fieldwork and in preparation and equipment of the boreholes was provided by D.S. Drozdov and A.B. Malkov.

References

Brown J., Hinkel, K.M. & Nelson, E.F. 2000. The Circumpolar Active Layer Monitoring (CALM) program: Research designs and initial results. *Polar Geography* 24(3): 165-258.

Burgess, M.M. & Smith, S.L. 2003. 17 years of thaw penetration and surface settlement observations in permafrost terrain along the Norman Wells pipeline, Northwest Territories, Canada. In: M. Phillips, S. Springman & L.U. Anderson, (eds.), *Permafrost, Eighth International Conference, Proceedings* Lisse, Netherlands: Balkema, Vol. 1: 107-112.

Clow, G.D. & Urban, F.E. 2003. GTN-P Monitoring network: detection of a 3 K permafrost warming in northern Alaska during the 1990's, *First Study of Environmental Arctic Change (SEARCH) Open Science Meeting, 27-30 October 2003, Seattle, WA*.

Jorgenson, M.T., Racine, C.H., Walters J.C. & Osterkamp, T.E. 2001. Permafrost degradation and ecological changes associated with a warming climate in central Alaska. *Climatic Change* 48(4): 551-571.

Kakunov, N.B. & Sulimova, E.I. 2005. Results of the observations of the ground temperature on the European North-East in the period of climatic warming 1970–2003 *Materials of the Third Conference of Russian Geocryologists* (2): 84-90. (in Russian).

Kakunov, N.B. & Sulimova, E.I. 2006. Methods of reconstructing the dynamics of southern boundary of permafrost and their temperature conditions in the European north-east of Russia for the last 230 years. *Earth Cryosphere Assessment: Theory, Applications and Prognosis of Alterations* (1): 76-78.

Malkova-Ananjeva, G.V. 2005. Frozen ground response to recent climate changes in the European North *2nd European Conference on Permafrost, Potsdam, Programme and Abstracts*: 137.

Malkova, G.V. 2006. Estimation of changes of geocryological characteristics in top horizons of permafrost in conditions of a varying climate and technogenesis. *Earth Cryosphere Assessment: Theory, Applications and Prognosis of Alterations* 1: 82-86.

Malkova, G.V. 2007. Generalization of the temperature measurement results at the Bolvansky geocryological steady-state-station. Cryogenic recourses of the Polar regions. *Materials of the International Conference. Salekhard, V.1*: 140-143 (in Russian).

Mazhitova, G.G, Malkova-Ananjeva, G.V, Chestnykh, O.L. & Zamolodchikov, D.D. 2004. Active layer spatial and temporal variability at European Russian Circumpolar-Active Layer-Monitoring (CALM) sites. *Permafrost and Periglacial Processes* 15: 123-139.

Oberman, N. G. 1998. Permafrost and cryogenic processes in the East-European Subarctic. *Eurasian Soil Science* 5: 540-550.

Oberman, N. G. 2001. Interdecadal dynamics of permafrost on the European North-East of Russia. *Materials of the Second Conference of Russian Geocryologists* (2): 212-217. (in Russian).

Oberman, N.G. & Mazhitova, G.G. 2001. Permafrost dynamics in the northeast of European Russia at the end of the 20th century. *Norsk Geografisk Tidsskrift–Norwegian Journal of Geography* 55(4): 241–244.

Oberman, N.G. 2006. Long-term tendencies of natural cryolithozone evolytion the north-east *Earth Cryosphere Assessment: Theory, Applications and Prognosis of Alterations* 1: 93-96.

Oberman, N.G. 2007. Some peculiarities of current degradation of permafrost in the Pechora-Ural region. *Cryogenic Resources of Polar Regions*: 95-99.

Osterkamp, T.E. 2003. A thermal history of permafrost in Alaska. In: M. Phillips, S. Springman and L.U. Anderson, (eds.), *Permafrost, Eighth International Conference, Proceedings* Lisse, Netherlands: Balkema, vol. 2: 863-868.

Osterkamp, T.E. & Romanovsky, V.E. 1999. Evidence for warming and thawing of discontinuous permafrost in Alaska. *Permafrost and Periglacial Processes* 10(1): 17-37.

Osterkamp, T.E., Viereck, L., Shur, Y., Jorgenson, M.T., Racine, C., Doyle, A. & Boone, R.D. 2000. Observations of thermokarst and its impact on boreal forests in Alaska, U.S.A. *Arctic, Antarctic and Alpine Research* 32; 303-315.

Pavlov, A.V. & Malkova, G.V., 2005. *Contemporary changes of climate in northern Russia*.: Album of small-scale maps: 54. (in Russian).

Romanovsky, V.E. 2006. Thermal state of permafrost in Alaska during the last 20 years. *Earth Cryosphere Assessment: Theory, Applications and Prognosis of Alterations* (1): 96-101.

Romanovsky, V.E., Burgess, M., Smith, S., Yoshikawa, K. & Brown, J. 2002. Permafrost temperature records: indicator of climate change. *EOS* 83(50): 589, 593-594.

Smith, S.L., Burgess, M.M., Riseborough, D. & Nixon, F.M. 2005. Recent trends from Canadian permafrost thermal monitoring network sites. *Permafrost and Periglacial Processes* 16: 19-30.

Numerical Modeling of Spatial Permafrost Dynamics in Alaska

Sergei Marchenko
Geophysical Institute, University of Alaska Fairbanks, USA
Vladimir Romanovsky
Geophysical Institute, University of Alaska Fairbanks, USA
Gennady Tipenko
Institute of Geoecology, Russian Academy of Science, Russia

Abstract

The Geophysical Institute Permafrost Laboratory model (GIPL) simulates soil temperature dynamics and the depth of seasonal freezing and thawing by solving 1D non-linear heat equations with phase change numerically. In this model the process of soil freezing/thawing is occurring in accordance with the unfrozen water content curve and soil thermal properties, which are specific for each soil layer and for each geographical location. At the present stage of development, the GIPL 2.0 model is combined with ArcGIS to facilitate preparation of input parameters and visualization of simulated results in the form of digital maps. The future climate scenario was derived from the Massachusetts Institute of Technology MIT-2D climate model output for the 21st century. This climate scenario was used as a driving force in the GIPL model. Initial results of calculations show that by the end of the current century widespread permafrost degradation could begin everywhere in Alaska southward from the Brooks Range.

Keywords: active layer thickness; ground temperature; numerical modeling; thawing permafrost.

Introduction

Many components of the cryosphere, particularly sea ice, glaciers, and permafrost, react sensitively to climate change. Climatic changes and changes in permafrost were reported recently from many regions of the Northern Hemisphere (Jin et al. 2000, Oberman & Mazhitova 2001, Harris & Haeberli 2003, Sharkhuu 2003, Romanovsky et al. 2002, Marchenko et al. 2007). Significant changes in permafrost temperatures were observed in Alaska. Ground temperature data from Alaska available for the last 30 years demonstrate an increase in permafrost temperatures by 0.5°C–3°C (Osterkamp & Romanovsky 1999, Osterkamp 2005). Recent observations show that the warming of permafrost has continued into the 21st century in Alaska (Clow & Urban 2002, Romanovsky et al. 2002, Romanovsky et al. 2003). While the increase in permafrost temperature may change many of its physical properties, the major threshold occurs when permafrost starts to thaw from its top down. The thawing and freezing of soils in arctic and sub-arctic regions is affected by many factors, with air temperature, vegetation, snow accumulation, and soil moisture among the most significant. To investigate how observed and projected changes in these factors influence permafrost dynamics in Alaska, we developed a numerical Geophysical Institute Permafrost Laboratory (GIPL) model. In this paper we will first describe this model. Then we will show how this model should be calibrated and validated before being used for projections of future changes in permafrost as a result of changes in climatic and other environmental conditions. After validation, the model was used to develop one possible scenario of the permafrost dynamics in Alaska during the current century.

Previous spatial modeling of permafrost

Recently, there have been a number of experiments to simulate soil temperature and permafrost dynamics on regional and global scales (Anisimov & Nelson 1997, Stendel & Christensen 2002, Sazonova & Romanovsky 2003, Oelke & Zhang 2004, Lawrence & Slater 2005, Zhang et al. 2006, Saito et al. 2007). There are two major approaches to spatial modeling of permafrost. One of them is to include a permafrost module directly into GCM. The second one employs the use of stand-alone equilibrium or transient permafrost models. These models are forced by the climatic outputs produced by GCMs. There were a few examples of simulations and forecasts of permafrost dynamics using coupled global climate models (Stendel & Christensen 2002, Lawrence & Slater 2005, Nicolsky et al. 2007, Saito et al. 2007), but some of the modeled results generated a significant controversy (Burn & Nelson 2006, Delisle 2007). The simplified treatment of subsurface thermal processes and problematic settings of the soil properties and lower boundary conditions precluded proper representation of the future permafrost dynamics in these GCMs (Burn & Nelson 2006).

In this research we used the GIPL-2.0 model, which is a numerical simulator of the temporal and spatial transient response of permafrost to projected changes in climate.

Methods

GIPL-2.0 model

A previous version of this model (GIPL-1.0) is an equilibrium, spatially distributed, analytical model for computation of the active layer thickness and mean annual ground temperatures (Sazonova & Romanovsky 2003). The GIPL-2.0 model simulates soil temperature dynamics and the depth of seasonal freezing and thawing by solving 1D non-linear heat equations with phase change numerically. In this model the process of soil freezing/thawing is occurring

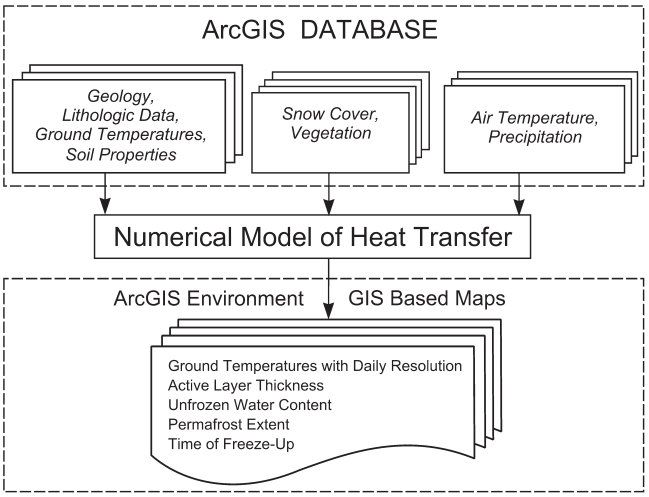

Figure 1. The GIPL-2.0 model schematic diagram.

in accordance with the unfrozen water content curve and soil thermal properties, which are specific for each soil layer and for each geographical location. The Special Enthalpy formulation of the energy conservation law makes it possible to use a coarse vertical resolution without loss of latent heat effects in the phase transition zone even in case of fast temporally and spatially varying temperature fields. At the present stage of development, the GIPL model is combined with ArcGIS to facilitate preparation of input parameters (climate forcing from observations or from Global or Regional Climate Models) and visualization of simulated results in the form of digital maps. The input data are incorporated into GIS and contain the information on geology, soils properties, vegetation, air temperature, and snow distribution (Fig. 1).

The soil characterization used in the GIPL-2.0 model is based on extensive empirical observations conducted in representative locations that are characteristic for the major physiographic units in Alaska.

The numerical solution of heat transfer is implemented in the extended program module, which can be called from the GIS environment. GIS allows visualization of input and output parameters and their representation in the form of digital maps. The new version of GIPL 2.0 simulates soil temperature and liquid water content fields for the entire spatial domain with daily, monthly, and yearly resolution. The merge of the new GIPL and the GIS technique provides a unique opportunity to analyze spatial features of permafrost dynamics with high temporal resolution.

Mathematical model

The basic mathematical model in our approach is the Enthalpy formulation of the one-dimensional Stefan problem (Alexiades & Solomon 1993, Verdi 1994). We used the quasi-linear heat conduction equation, which expresses the energy conservation law:

$$\frac{\partial H(y,t)}{\partial \tau} = div(\lambda(y,t)\nabla t(y,\tau)),\ y \in \Omega,\ \tau \in \Psi \qquad (1)$$

where $H(y, t)$ is the enthalpy

$$H(y,t) = \int_0^t C(y,s)ds + L\Theta(y,t) \qquad (2)$$

where $C(y, t)$ is the heat capacity, L is the latent heat, $\lambda(y, \tau)$ is thermal conductivity and $\Theta(y, t)$ is the volumetric unfrozen water content. The Equation (1) is complemented with boundary and initial conditions. The computational domain $0 \le \Omega \le 1000$ is extended to 1000 m in depth, and the time interval Ψ is 200 years with an initial temporal step of 24 hours.

Dirichlet's conditions $t(\tau)$ were set at the upper boundary. An empirical method of geothermal heat flux estimating (Pollack et al. 1993) in each grid point was applied for the lower boundary conditions.

$$\left.\frac{\partial t}{\partial \tau}\right|_{y=0} = t(\tau), \qquad \left.\frac{\partial t(\tau)}{\partial y}\right|_{y=1000} = g \qquad (3)$$

where g is a geothermal gradient at the lower boundary.

A fractional step approach (Godunov splitting) was used to obtain a finite difference scheme (Marchuk 1975). The idea is to divide each time step into two steps. At each step, the spatial dimension (in the depth) is treated implicitly:

$$\frac{H(t_i^{n+1}) - H(t_i^{n+1/2})}{\Delta\tau_n} = \frac{2}{(\Delta h_{i+1} + \Delta h_i)} \times \left(\lambda_{i+1/2}^{n+1} \frac{\left(t_{i+1}^{n+1} - t_i^{n+1}\right)}{\Delta h_{i+1,y}} - \lambda_{i-1/2}^{n+1} \frac{\left(t_i^{n+1} - t_{i-1}^{n+1}\right)}{\Delta h_{i,y}} \right) \qquad (4)$$

where $\Delta h_{i,y}$ is the spatial steps on the non-uniform grid.

The resulting system of finite difference equations is non-linear, and to solve it Newton's method was employed at each time step. On the first half step (4) in a case when a non-zero gradient of temperature exists, we use the difference derivative of enthalpy:

$$\frac{\partial H(t_i)}{\partial t} = 0.5\left[\frac{H(t_i) - H(t_{i-1})}{(t_i - t_{i-1})} + \frac{H(t_{i+1}) - H(t_i)}{(t_{i+1} - t_i)} \right] \qquad (5)$$

The analytical derivative of representation (2) has to be used in the case of zero-gradient temperature fields. The second half step (4) is treated similarly. Thereby, we can employ any size spatial steps without any risk of losing any latent heat effects within the phase transition zone for fast temporally and spatially varying temperature fields.

Model validation and calibration

Ground temperature measurements of a very high quality (precision generally at 0.01°C) in shallow boreholes were used for initial model validation. More than 15 shallow boreholes (1–1.2 m in depth) across Alaska from north to south were available for validation (Romanovsky & Osterkamp 1997). The temperature measurements in the shallow holes were

performed with vertical spacing of 0.08–0.15 m. At most of these sites, soil water content and snow depth also were recorded. In addition, more than 25 relatively deep boreholes from 29 m to 89 m in depth (Osterkamp & Romanovsky 1999, Osterkamp 2003) along the same transect were available for model validation in terms of permafrost temperature profiles and permafrost thickness.

Different earth's materials have varying thermal properties. The soil thermal conductivity and heat capacity vary within the different soil layers, as well as during the thawing/freezing cycles, and depend on the unfrozen water content that is a certain function of temperature. The method of obtaining these properties is based on the numerical solution for a coefficient inverse problem, and on minimization locally on the misfit between measured and modeled temperatures by changing thermal properties along the direction of the steepest descent. The method used and its limitations are described in more detail elsewhere (Nicolsky et al., in review).

There are two basic approaches to the calibration of modeled permafrost temperatures against the observed data, which can be distinguished by their use of temporal or spatial relationships. With the temporal approach, the quality of the modeling series is assessed by time series regression against measured data. The quantitative relationship between simulated and measured data is then determined for a ''calibration'' period with some instrumental data withheld to assess the veracity of the relationship with independent data. Figure 2 illustrates the results of the model calibration for the specific site, West Dock (70°22'28.08"N, 148°33'7.8"W).

In the spatial approach, assemblages of the observed data from a number of different geographic locations with different landscape settings determine the quality of the modeling results. To achieve geographic correspondence between the scale of observation and modeling, we utilized a regional-scale permafrost characterization based on observations obtained from representative locations. Additional comparison of model-produced ground temperatures, active layer thickness, and spatial permafrost distribution with measured ground temperatures at the Alaskan sites shows a good agreement.

Input data set

In order to assess possible changes in the permafrost thermal state and the active layer depth, the GIPL-2.0 model was implemented for the entire Alaskan permafrost domain for the 1900–2100 time interval. For this study we used an input data set with grid boxes size 0.5° × 0.5°. Input parameters to the model are spatial datasets of mean monthly air temperature and snow water equivalent (SWE), prescribed soil thermal properties and water content, which are specific for each soil layer and for each geographical location. Initial distribution of temperature with depth was derived from the borehole temperature measurements obtained in Alaska by different researchers during the last several decades (Brewer 1958, Lachenbruch & Marshall ti

For climate forcing we used two data sets. For the period of

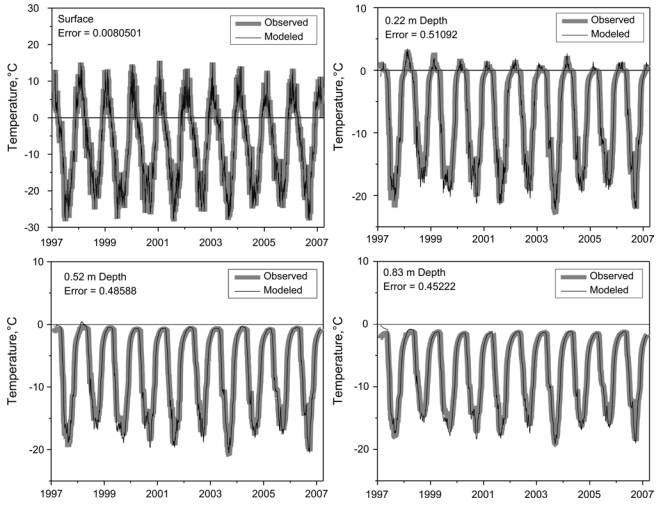

Figure 2. Example of the temporal model calibration for specific site.

1900–2000 climatic conditions, the CRU2 data set with 0.5° × 0.5° latitude/longitude resolution (Mitchell & Jones 2005) was used. The future climate scenario was derived from the MIT-2D integrated global system model (IGSM) developed at the Massachusetts Institute of Technology (MIT), which is a two dimensional (zonally averaged) atmospheric model coupled with a diffusive ocean model that simulates the surface climate over the land and ocean for 23 latitudinal bands globally (Sokolov & Stone, 1998). Snow data for the entire simulated period 1900–2100 were derived from the terrestrial ecosystem model (TEM) (Euskirchen et al. 2006). We used the MIT-2D output for the 21st century with a doubling, gradual increase of atmospheric CO_2 concentration by the end of the current century that corresponds to the IPCC SRES emission scenario A1B.

Results and Discussion

We compared ground temperatures at the depths of 2 m, 5 m, and 20 m for three snapshots of 2000, 2050, and 2100 (Fig. 3). If compared with present-day conditions, the greatest changes in temperatures for the 2050 and 2100 snapshots will occur at 2 m depth (Figs. 3 A, B, C). Results of calculation show that by the end of the current century, the mean annual ground temperatures (MAGT) at 2 m depth could be above 0°C everywhere southward of the sixty-sixth latitude, except for the small patches at the high altitudes of the Alaska Range and the Wrangell Mountains (Fig. 3C). The area of about 850,000 km^2 (about 57% of the total area of Alaska) will be involved in the widespread permafrost degradation and could contain both areas with completely disappeared permafrost and areas where thawing of permafrost is ongoing. It should be noted that by the term "thawing permafrost" we understand a situation when the permafrost table is lowered and a residual thawed layer (talik) between the seasonally frozen layer and the permafrost table continuously exists throughout the year.

According to calculations, the modern extent of the area with MAGT at 5 m depth above 0°C is about 125,000 km^2.

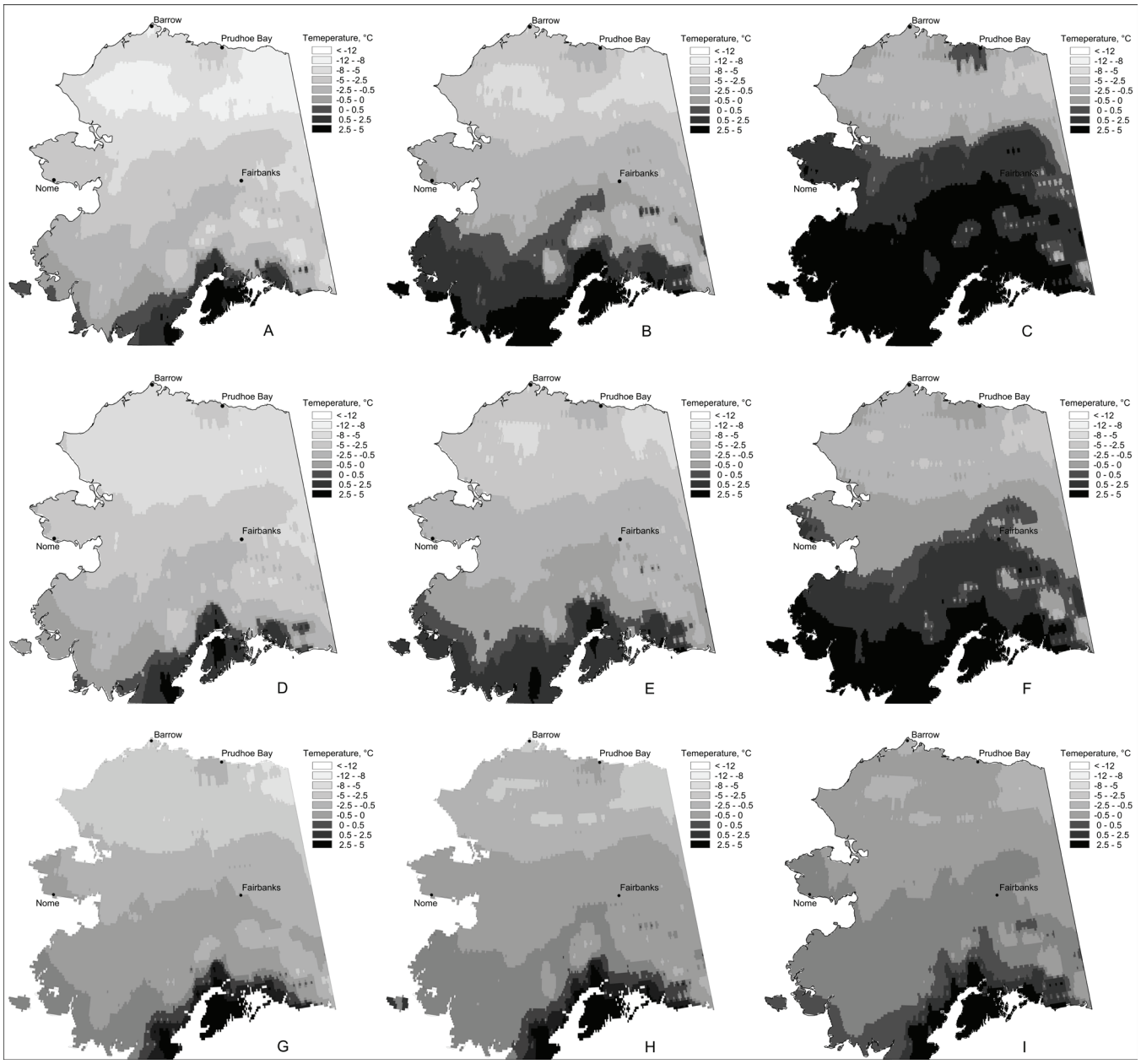

Figure 3. Projected mean annual ground temperatures at 2 m (A, B, C), 5 m (D, E, F), and 20 m (G, H, I) depths on 2000 (A, D, G), 2050 (B, E, H), and 2100 (C, F, I) using climate forcing from MIT-2D output for the 21st century.

The model-produced ground temperatures with positive MAGT at 5 m depth could occupy approximately 659,000 km^2 (about 45% of the total area of Alaska) by the end of the current century and could extend into the Interior of Alaska (Fig. 3F).

While the permafrost temperatures at 20 m depth could change significantly within a range of negative temperatures, the area with MAGT above 0°C at 20 m depth would not expand too much, even by 2100 (Figs. 3 G, H, I). The difference between these areas in 2000 and in 2100 does not exceed 100,000 km^2 (Figs. 3 G, I). Changes in permafrost temperatures will be much more pronounced within the areas with colder permafrost in comparison with areas where the permafrost temperature is presently close to 0°C. Also, it will not increase significantly in the areas of peat lands with a sufficiently deep organic layer. Projected changes in areas of MAGT above 0°C at the different depths and for the different times according to the MIT-2D climate change scenario are presented in Table 1.

Table 2 presents the statistics of modeled MAGT variables for the three snapshots obtained from 34,434 grid cells within the entire Alaskan domain. While the mean value and sums of MAGT at the depths of 2 m and 5 m turned to above 0°C by the end of the current century, the same characteristics for 20 m depth remain below 0°C (Table 2).

Statistics on active layer thickness (ALT) also have shown significant response to the scenario of climate change. The simulated mean values of ALT for the whole Alaskan permafrost domain are 0.78 m, 1.33 m, and 2.4 m for 2000, 2050, and 2100 respectively.

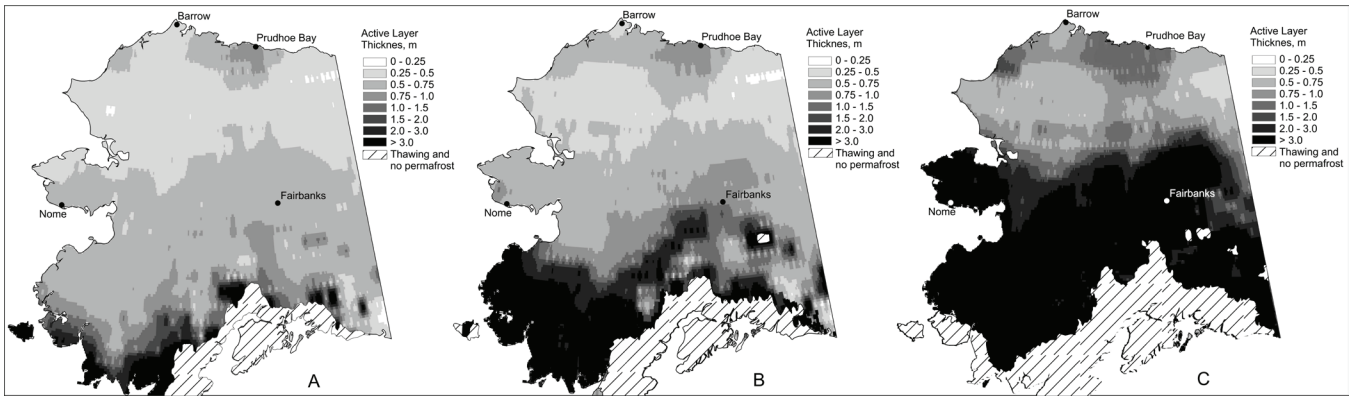

Figure 4. Projected active layer thickness and extent of thawing permafrost area in 2000 (A), 2050 (B), and 2100 (C) using climate forcing from MIT-2D output for the 21st century.

The area of thawing permafrost (permafrost table located deeper than 3 m) also increased according to our model from 65,000 km^2 in 2000, to 240,000 km^2 by 2050, and to 720,000 km^2 by 2100 (Fig. 4).

Conclusions

According to the future climate scenario derived from the MIT-2D climate model and the TEM output for the 21st century, widespread permafrost degradation could be observed everywhere in Alaska southward from the Brooks Range by the end of the current century. It means that the permafrost table in this region will be lowered down to 3–10 m in depth, and some small and thin patches of permafrost at the southernmost regions of Alaska could disappear completely. Nevertheless, permafrost thicker than 15–20 m in depth could still survive deeper than 10–15 m, even in the regions with widespread long-term thawing of permafrost. In the regions with ice-rich permafrost, the thawing processes will extended for a long time, especially in the regions with undisturbed surfaces. Modeling results show the Alaskan North Slope will not be experiencing a substantial widespread permafrost thawing and degradation during the present century.

Table 1. Areas of simulated MAGT above 0°C at the different depths and for the different times (thousands km^2/percent of the total area of Alaska).

Depth	2000	2050	2100
2 m	138.8/9.4	410.3/27.8	850.5/57.6
5 m	126.7/8.6	280.2/18.9	658.9/44.6
20 m	103.2/6.7	133.5/9.03	196.4/13.3

Table 2. Statistics of modeled MAGT variables within the entire calculated Alaskan spatial domain (34,434 grid cells).

Statistics	2000	2050	2100
2 m Depth			
Min	-12.52	-8.74	-5.44
Max	4.72	7.30	11.62
Mean	-4.32	-1.47	1.58
5 m Depth			
Min	-8.45	-6.62	-5.43
Max	3.71	5.00	10.46
Mean	-3.69	-1.68	0.54
20 m Depth			
Min	-9.86	-7.74	-5.38
Max	4.85	6.46	8.53
Mean	-3.32	-1.86	-0.62

Acknowledgments

This research was funded by the ARCSS Program and by the Polar Earth Science Program, Office of Polar Programs, National Science Foundation (OPP-0120736, OPP-0352957, OPP-0352958, ARC-0632400, ARC-0520578, ARC-0612533, IARC-NSF CA: Project 3.1 Permafrost Research), by a NASA Water and Energy Cycle grant, and by the State of Alaska. We would like to thank Dr. N. Shiklomanov from the University of Delaware for helpful discussions. We would also like to thank two anonymous reviewers for very helpful suggestions that were used to improve the manuscript.

References

Anisimov, O.A. & Nelson, F.E. 1997. Permafrost zonation and climate change in the northern hemisphere: results from transient general circulation models. *Climatic Change* 35: 241–258.

Alexiades, V. & Solomon, A.D. 1993. *Mathematical Modeling of Melting and Freezing Processes*. Washington: Hemisphere, 325 pp.

Brewer, M.C. 1958. Some results of geothermal investigations of permafrost in northern Alaska. *Transaction, AGU* 39: 19-26.

Burn, C.R. & Nelson, F.E. 2006. Comment on "A projection of severe near-surface permafrost degradation during the 21st century" by David M. Lawrence & Andrew G. Slater. *Geophysical Research Letters* 33, L21503, DOI:10.1029/2006GL027077.

Clow, G.D. & Urban, F.E. 2002. Largest permafrost warming in northern Alaska during the 1990s determined from GTN-P borehole temperature measurements. *EOS, Transactions of the AGU* 83(47), F258.

Delisle, G. 2007. Near-surface permafrost degradation: How severe during the 21st century? *Geophysical Research Letters* 34, L09503, DOI:10.1029/2007GL029323

Euskirchen, E.S., McGuire, A.D., Kicklighter, D.W., Zhuang, Q., Clein, J.S., Dargaville, R.J., Dye, D.G., Kimball, J.S., McDonald, K.C., Melillo, J.M., Romanovsky, V.E. & Smith, N.V. 2006. Importance of recent shifts in soil thermal dynamics on growing season length, productivity, and carbon sequestration in terrestrial high-latitude ecosystems. *Global Change Biology* 12: 731-750.

Harris, C. & Haeberli, W. 2003. Warming permafrost in European mountains. *World Meteorol. Org. Bull.* 52(3): 6 (See also *Global and Planetary Change* 39: 215–225).

Jin, H., Li, S., Cheng, G., Shaoling, W. & Li, X. 2000. Permafrost and climatic change in China. *Global and Planetary Change* 26(4): 387-404.

Lachenbruch, A.H. & Marshall, B.V. 1986. Changing climate: Geothermal evidence from permafrost in the Alaskan Arctic. *Science.* 234: 689–696.

Lawrence, D.M.& Slater, A.G. 2005. A projection of severe near surface permafrost degradation during the 21st century. *Geophys. Res. Lett*. 32, L24401, doi:10.1029/2005GL025080.

Marchenko, S., Gorbunov, A. & Romanovsky, V. 2007. Permafrost warming in the Tien Shan Mountains, central Asia. *Global and Planetary Change* 56: 311-327.

Marchuk, G.I. 1975. *Methods of Numerical Mathematics (Applications of Mathematics)*. New York: Springer-Verlag, 316 pp.

Mitchell, T.D. & Jones, P.D. 2005. An improved method of constructing a database of monthly climate observations and associated high-resolution grids. *International Journal of Climatology* 25(6): 693-712.

Nicolsky, D.J., Romanovsky, V.E. & Tipenko, G.S. 2007. Estimation of thermal properties of saturated soils using in-situ temperature measurements. *The Cryosphere* 1: 41–58.

Nicolsky, D.J., Romanovsky, V.E., Alexeev, V.A. & Lawrence, D.M. 2007. Improved modeling of permafrost dynamics in a GCM land-surface scheme, *Geophys. Res. Lett.* 34, L08501, doi:10.1029/2007GL029525.

Oberman, N.G. & Mazhitova, G.G. 2001. Permafrost dynamics in the northeast of European Russia at the end of the 20th century. *Norwegian Journal of Geography* 55: 241-244.

Oelke, C. & Zhang, T. 2004. A model study of circum-arctic soil temperatures. *Permafrost Periglacial Processes* 15: 103–121.

Osterkamp, T.E. & Romanovsky, V.E. 1999. Evidence for warming and thawing of discontinuous permafrost in Alaska. *Permafrost and Periglacial Processes* 10: 17-37.

Osterkamp, T.E. 2003. Establishing long-term permafrost observatories for active-layer and permafrost investigations in Alaska: 1977–2002. *Permafrost and Periglacial Processes* 14: 331–342.

Osterkamp, T.E. 2005. The recent warming of permafrost in Alaska. *Global and Planetary Change* 49: 187–202.

Pollack, H.N., Hurter, S.J. & Johnson, J.R. 1993. Heat flow from the earth's interior: analysis of the global data set. *Reviews of Geophysics* 31(3): 267-280.

Romanovsky, V.E. and Osterkamp, T.E. 1997. Thawing of the active layer on the coastal plain of the Alaskan Arctic. *Permafrost and Periglacial Processes* 8(1): 1-22.

Romanovsky, V., Burgess, M., Smith, S., Yoshikawa, K. & Brown, J. 2002. Permafrost temperature records: indicators of climate change, *EOS, AGU Trans.* 83(50): 589-594.

Romanovsky, V.E., Sazonova, T.S., Balobaev, V.T., Shender, N.I. & Sergueev, D.O. 2007. Past and recent changes in permafrost and air temperatures in Eastern Siberia. *Global and Planetary Change* 56: 399-413.

Saito, K., Kimoto, M., Zhang, T., Takata, K. & Emori, S. 2007. Evaluating a high-resolution climate model: Simulated hydrothermal regimes in frozen ground regions and their change under the global warming scenario. *J. Geophys. Res*. 112: F02S11.

Sazonova, T.S. & Romanovsky, V.E. 2003. A model for regional-scale estimation of temporal and spatial variability of the active layer thickness and mean annual ground temperatures. *Permafrost and Periglacial Processes* 14(2): 125-139.

Sharkhuu, N. 2003. Resent Changes in permafrost of Mongolia. *Proceedings of the 8th International Conference on Permafrost, Zurich, Switzerland, July 2*: 1029-1034.

Sokolov, A.P. & Stone, P.H. 1998. A flexible climate model for use in integrated assessments. *Climate Dynamics* 14: 291-303.

Stendel, M. & Christensen, J.H. 2002. Impact of global warming on permafrost conditions in a coupled GCM. *Geophysical Research Letters* 29(13): 1632, 10.1029/2001GL014345.

Verdi, C. 1994. *Numerical aspects of parabolic free boundary and hysteresis problems. Lecture Notes in Mathematics*. New York: Springer-Verlag, 213-284.

Zhang, Y., Chen, W. & Riseborough, D.W. 2006. Temporal and spatial changes of permafrost in Canada since the end of the Little Ice Age. *J. Geophys. Res.* 111: D22103, doi:10.1029/2006JD007284.

Development of Frost-Crack Polygonal Relief in the Central Part of Tazovskiy Peninsula

Sergey Marchenko
Moscow State University, Geographical Faculty, Moscow, Russia
Dinara Abliazina
Moscow State University, Geographical Faculty, Moscow, Russia
Frederick Arnold
University of Hamburg, Soil Studies Institute, Hamburg, Germany

Abstract

On the Tazovskiy Peninsula (north of West Siberia) patterned ground is spread on considerable territory. In July 2007 different aspects of the process in the central part of the peninsula were explored. Descriptions and measurements of contemporary and ancient polygonal structures and certain parts of them were done near the Yubileinoe gas field and the town of Yamburg. On this basis we retraced the development of polygonal relief from ice wedges of first generation to ice-wedge casts. In contemporary climate conditions in the central part of Tazovskiy Peninsula, the process of frost wedging and development of polygonal relief takes place on peat grounds. The most typical dimensions of blocks are 10–15 m, and very often they are poorly expressed in relief. Ancient ice wedging of the Pleistocene period had much greater scales and was spread on mineral grounds as well. The thickness of ice wedges evidently reached 1–2 m.

Keywords: frost cracking; ice wedges; polygonal relief.

Introduction

One of the distinctive features of the cryolithosphere is patterned ground. North of western Siberia the phenomena is well spread on considerable territories, where severe climate in combination with ground conditions leads to frost cracking and formation of polygons. In July 2007 different aspects of the process in the central part of Tazovskiy Peninsula were explored. The exploration took place near the Yubileinoe gas field and the town of Yamburg. On the basis of certain examples, we retraced development of polygonal relief: from ice wedges of the first generation to the ice wedge casts.

Study Area

Exploration was carried out in the eastern and southern parts of Tazovskiy Peninsula (West Siberia, Russia). The territory is tectonic plate with Palaeogenic basement covered with a thick layer of sediments (Popov 1989). In the upper part, the sediments have marine, alluvial, and lacustrine genesis of different epochs of Pleistocene and are made up with loam, clay sand, and sand. The territory in general has poor vertical disarticulation caused mainly by cryogenic and fluvial processes. The vegetation is mainly tundra and forest tundra: *carex*, shrubs and bushes *betula nano, salix, ledum, eriophorum*; moss and lichens are widely spread: *cetraria islandica, sphagnum balticum*; very often they form polygonal peatlands. The main climate features are big yearly and weekly amplitudes of temperature with very cold winters. Mean January temperatures are -28°C; mean July temperatures are -12°C. Descriptions and measurements were done in two spots: forest-tundra territories near the Yubileinoe Gas Facility (65°57′N, 75°42′E) and tundra territories near the town of Yamburgh (68°00′N, 74°50′E).

Methods

To study the processes of frost-cracking and polygonal-relief formation, we made descriptions and measurements on spots that were selected to provide grounds, vegetation, and landscape diversity. Ice wedges and ice wedge casts were described in an exposure and in pits. Measurements were done with tape, ruler, and compass. To estimate the climatic parameters from the point of frost cracking (and

Table 1. Meteorological data for Noviy Urengoi and Noviy Port, 2005–2007.

	Period	Novii Urengoi	Period	Novii Port
Mean Yearly temperatures, dgr C	2005 after 23.06	2.291	2005 after 05.03	-1.285
	2006	-9.407	2006	-8.74
	2007	-8.738	2007	-4.91
Mean January temperatures, dgr C	2006	-30.493	2006	-36.19
	2007	-14.418	2007	-13.719
Mean July temperatures, dgr C	2005	13.085	2005	16.719
	2006	13.688	2006	16.651
	2007	16.5	2007	19.666
Annual precipitation, mm	2005 after 23.06	636.6	2005 after 05.03	392
	2006	912.9	2006	548
	2007	548	2007	499
Dates of stable temperature transition over/below 0 dgr C	2005 after 23.06	nd/15.10	2005 after 05.03	13.05/15.10
	2006	31.05/28.09	2006	30.05/29.09
	2007	15.06/14.10	2007	02.06/14.10
Quantity of negative degree*days after stable temperature transition below 0 dgr C	2005 after 23.06	nd	2005 after 05.03	nd
	2006	-4391.247	2006	-4514.08
	2007	-3136.67	2007	-4915.312
Quantity of positive degree*days after stable temperature transition above 0 dgr C	2005 after 23.06	nd	2005 after 05.03	1578.034
	2006	990.831	2006	1364.45
	2007	1132.924	2007	1399.004

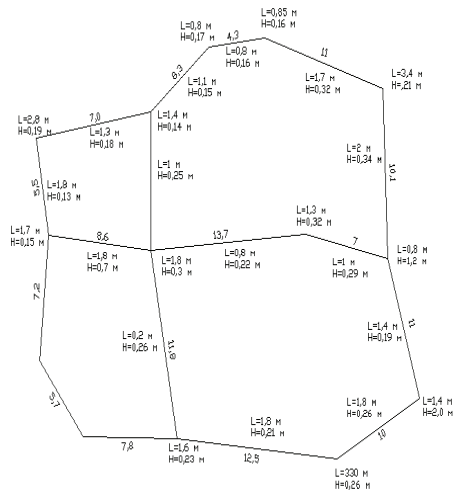

Figure 1. Results of measuring of a typical group of polygons near Ngarka-Poilovo-Yakha River (all values are in m).

Figure 2. A growing gully on the bank of Ngarka-Poilovo-Yakha River.

consequently polygonal system formation), we collected and analyzed meteorological data from Internet archives. We used meteorological data from the weather stations of Noviy Urengoi town and the village Noviy Port. The first town lies 40 km to the east of Yubileinoe and has nearly the same geographical conditions. Noviy Port and Yamburg are situated on the different banks of Obskaya Guba Bay, but have approximately the same latitude; the distance is 88 km. Thus a high correlation between meteorological conditions on the named weather stations and corresponding research sites is expected.

Site 1

The first place of exploration was situated in the valley of the Ngarka-Poilovo-Yakha River (67°53′40″N, 75°45′25″E). It is a wet territory with hummocks. During the Sartan time (22,000–18,000 years ago), strong cryogenesis led to formation of huge ice wedges in the lagoon sediments of Kargin time (40,000–22,000 years ago). During the Holocene the wedges partially degraded and formed ice wedge casts, overlain by

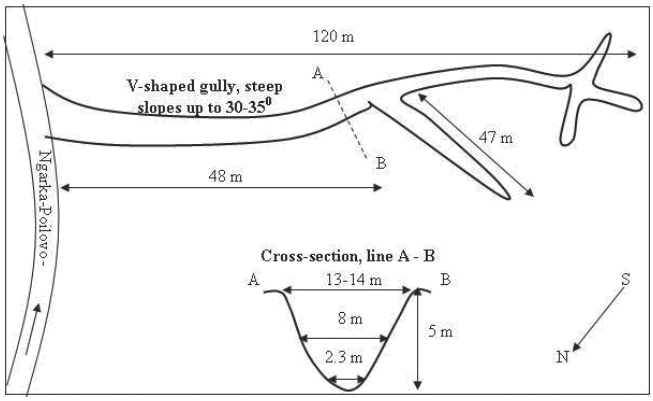

Figure 3. Gully scheme (67°53′40″N, 75°45′25″E).

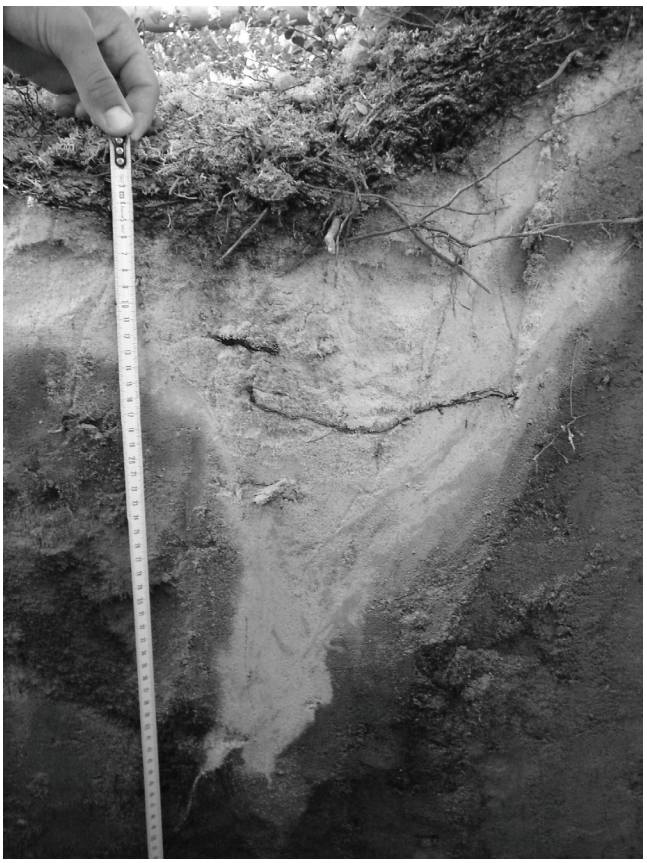

Figure 4. Sandy ice-wedge cast near the source of one of minor watercourses in the southern part of the Tazovskiy Peninsula.

peat up to 50 cm thick. On the surface of a small polygonal peat plateau, we sighted ice veins of the first generation. They are vein-like vertical ice inclusions up to 3 cm thick in the body of peat in different phases of decomposition. The peat plateau is a formed polygonal structure; typical dimensions of the blocks are 8–10 m in diameter. Judging by the considerable spreading of values, the polygons seem to be old enough as they reveal several generations of frost-cracking. In places where tensions in winter due to some reasons were higher, the peat is divided into polygons of smaller dimensions. Polygons are divided by depressions up to 0.4 m deep, in the depressions V-shaped ice wedges are detected. We have measured a group of polygons; the

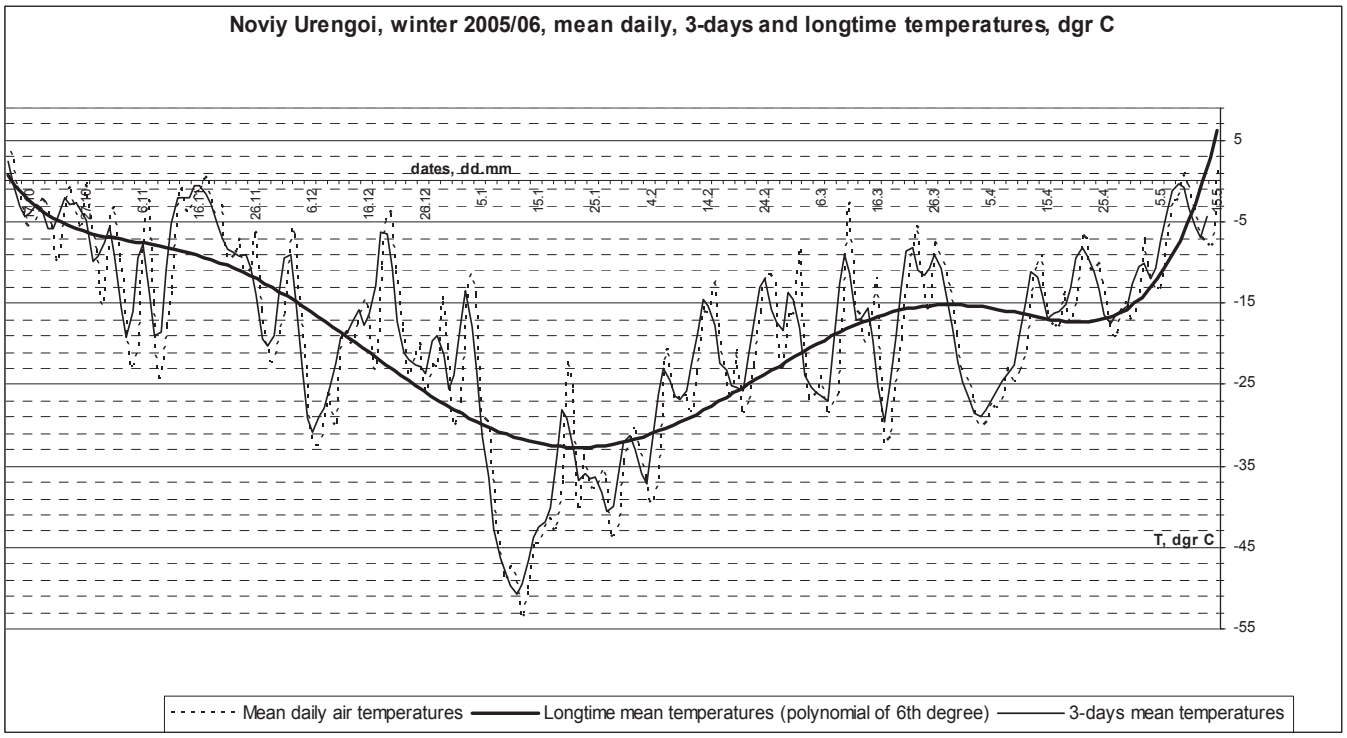

Figure 5.

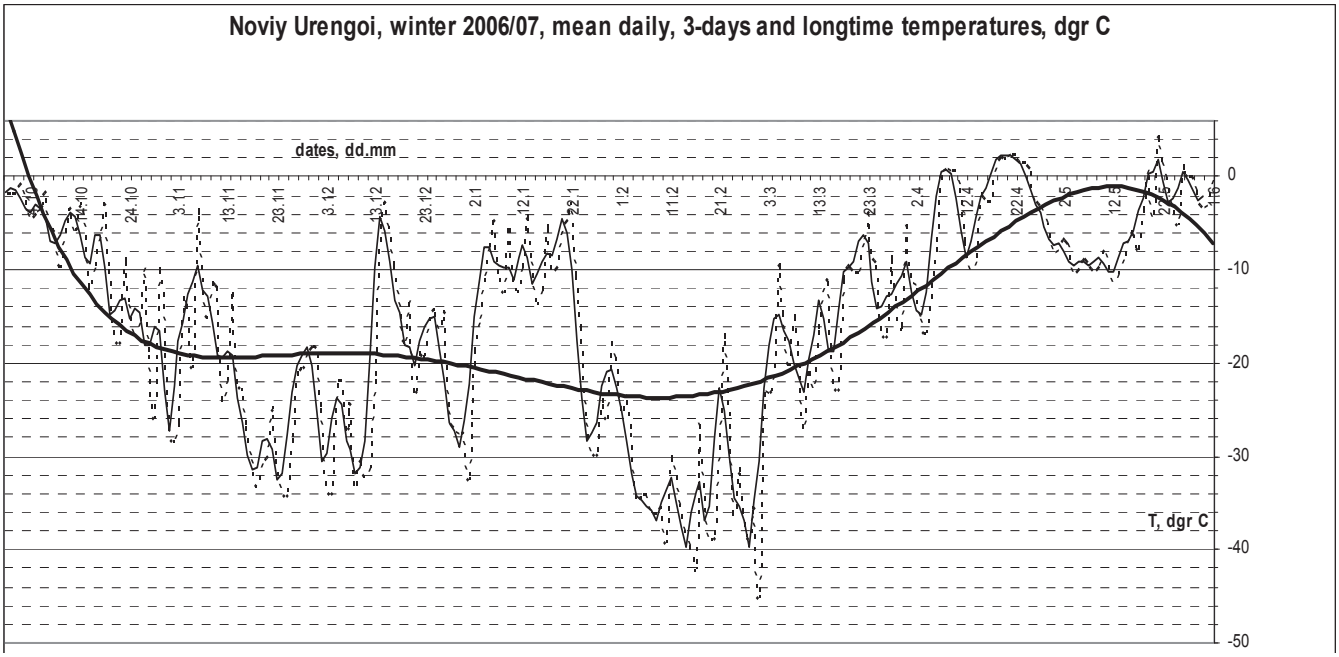

Figure 6.

results are shown on the Figure 1. The wedges separating the blocks open in the exposure on precipitous bank of the river Ngarka-Poilovo-Yakha; they can be retraced up to the depth of 2–2.5 m. Their complicated genesis is seen in the form: the bottom of a wedge is usually in the mineral sandy sediments where it developed as an epigenetic ice wedge, the part of wedge is almost strictly V-shaped; but in peat horizon which overcovers the mineral sediments from the depth of 1.5 it loses the strictness of form and is a syngenetic ice wedge. It is obvious that with the development of the peat plateau the conditions of heat exchange process changed, resulting in frost cracking and development of polygonal structures.

What is important about the ice wedges when they are revealed on banks of rivers, seas, and even minor

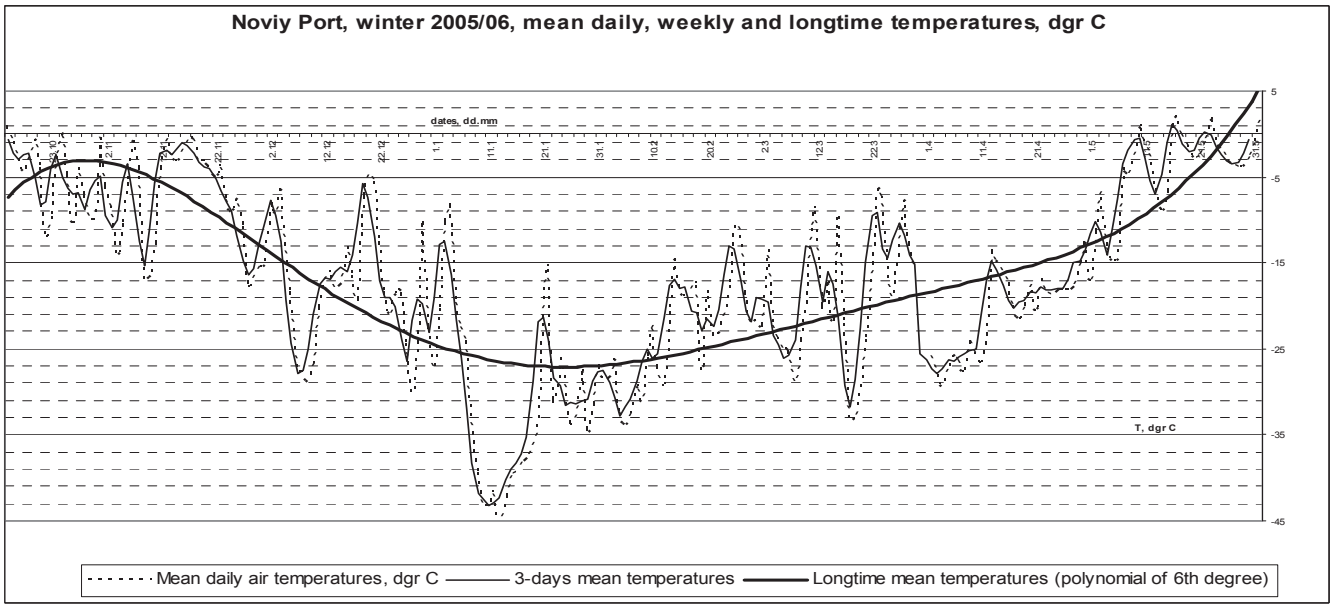

Figure 7.

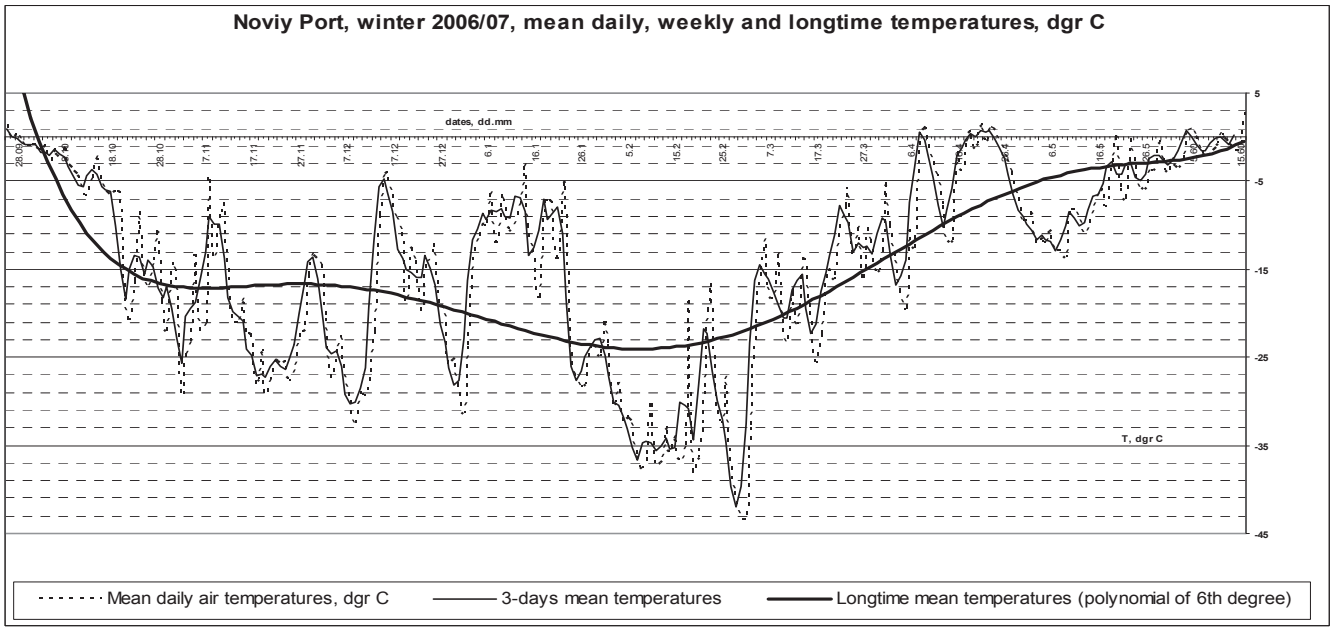

Figure 8.

watercourses is that while degrading they can advantage development of thermal erosion. Very often the forming gullies endanger different buildings, roads, plants, etc. And near the river Ngarka-Poilovo-Yakha vivid examples of the process can be detected (Figs. 2, 3).

The gullies form thermo-erosional outlets up to 8 m deep. One of them cuts through the right steep slope of the river and grows every year in the southwestern direction with speeds up to 4 m/year, thus endangering a gas cleaning and piping facility. The gully has a sophisticated formation with a number of tributaries; the tributaries inherit the polygonal form of wedges. Degrading, the wedges form linear depressions and during the spring seasons melting waters form watercourses in the depressions which hastens the gully growth. There was an attempt to stop the process - a unique construction of concrete and steel designed to help the melting waters in spring to flow faster and to prevent the banks from thermo-erosion was erected. But unfortunately the process of gully growing was not stopped completely. Another gully situated in 100 m to the south was detected (Fig. 3). Equal processes takes place on the bold shore of the Obskaya Guba Bay (Kara sea).

Site 2

On the bank of a thermokarst lake near the Yubileinoe gas field, northward of the previous spot, another small polygonal peat plateau is detected (67°57′01″N 75°52′13.3″E). It is

Table 2.

Decrease of T, °C	Number of fast (<10 days) decreases of air temperatures, mean daily temperatures in comparison with 3-days mean temperatures	
	Winter 2005/06	Winter 2006/07
5 to 10	14	10
11 to 15	4	11
16 to 20	4	2
21 to 25	2	1
25 to …	1	0
5 to …	25	24

Number of long decreases (>10 days) of air temperatures, mean daily temperatures in comparison with 20-days mean temperatures

Winter 2005/06	Winter 2006/07
3	4

Table 3.

Decrease of T, °C	Number of fast (<10 days) decreases of air temperatures, mean daily temperatures in comparison with 3-days mean temperatures	
	Winter 2005/06	Winter 2006/07
5 to 10	12	13
11 to 15	5	6
16 to 20	1	3
21 to 25	1	0
25 to …	1	0
5 to …	20	22

Number of long decreases (>10 days) of air temperatures, mean daily temperatures in comparison with 20-days mean temperatures

Winter 2005/06	Winter 2006/07
3	4

on the next stage of development, the polygons are uneven blocks usually pentahedral. The ice-wedges are on the stage of degradation – they do not reveal clearly in the upper 40 cm, while the wedges in the previous spot could easily be opened in the upper 30 cm. The depressions in between polygons are also poorly expressed. Measurements of a group of polygons were done. It was found out that apart from rather old polygons formed in the Sartan time, there were also new ones of smaller dimensions. The wedges and depressions dividing the old polygons are much more vividly expressed in the relief. Typical values for the first are 16–20 m in diameter. The latter are 8–12 m. and seem to have appeared after a fire that took place on the spot in 2005. The fire was quenched soon after it started, thus it did not spread on the nearby territories. Nevertheless it annihilated all the vegetation on the territory of about 30 by 30 m and now its spread is marked by poor vegetation and rests of ash. In winter 2005/06, that turned out to be extremely cold, frost polygons of a new generation developed on the territory limited by the edges of the fire spread.

Site 3

On the watershed near the source of one of the minor watercourses on the south of Tazovskiy Peninsula (66°0′35.6″N, 75°46′33.6″E), ancient polygonal structures were detected. They form characterful "avenues" up to 3–4 m wide, crossing with almost regular angles of 90 degrees. The "avenues" are also marked by vegetation: it varies from larch shaws on top of the polygons to lichens in the depressions. Typical dimensions of polygons are 17–20 in diameter. In about 500 m to the west the remains of a polygonal plateau were found. Ancient blocks are marked by relief features and vegetation. Differences are similar to those on the previous spot. In a dug prospect hole a sandy ice-wedge cast reveals itself in the loamy bearing strata (Fig. 4) Under the whitish sandy horizons there is a fine brownish horizon width, where the contents of organic material is increased. Below there are clear spots of ferritization on the contact with containing ground. The cast has the width of 30 cm in its upper part and 17 cm in the middle, while the depth is 50 cm.

Site 4

Near the valley of Halmer-Yakha River (65°58′45.8″N, 75°46′11.6″E) ancient polygonal structures on mineral grounds are detected, the surface is covered with larch shaws. Measurement of typical dimensions of polygons were made: the values for a typical group of polygons is 12.5 m by 12.5 m; 18.5 m by 11.5 m; 6.5 m by 9 m; 11 m by 9.5 m. The blocks are separated by depressions of considerable size: typical values of width are: 6.6 m; 5 m; 4.5 m; 5.7 m; they are up to 1 m deep.

Analysis of Meteorological Data

Frost cracking strongly depends on climatic conditions. Cracks appear when thermal tensions in the ground exceed the ground's tenacity. The tensions depend on thermal gradients and in general temperature increases with depth and temperature amplitudes decrease with depth. Thus thermal tensions that cause frost cracking depend on decreases of air temperature, especially when they reach considerable values in a short time. (Kudriavtsev 1978). According to the field research carried out by Mackay. (1974) north of Canada and by Podborniy (1976) in the lower reach of Yenisei River, frost cracking takes place when air temperatures lower below the average meaning for winter months. According to the research results near Ust'-Port (Yenisei delta, 69°39′45″N, 84°24′36″E) frost cracks can open both in the beginning and in the end of a rather long (1–2 months) cold period. The research also showed that even short (1–2 days) cold periods can lead to frost cracking. (Podborniy 1978). We tried to analyze meteorological data from the point of frost crack and consequently polygonal blocks formation. The results are given in the Figures 5, 6, 7, and 8 and in Tables 2 and 3.

Conclusions

According to the recent research done by Pavlov and Malkova (2005), the increase of annual air temperature relative to the norm in the region (calculated as mean in 1951–1990) of Tazovskiy Peninsula is 1.2°C, and in relation to the cold 1950s the value is about 1.6°C and the amplitude contraction owing to climate warming is 2°C. (Pavlov & Malkova 2005). On the basis of the data and of the descriptions and measurements done the following conclusions can be made. In contemporary climate conditions in the central part of Tazovskiy Peninsula, the process of frost wedging and development of patterned grounds takes place mainly on peat grounds with considerable humidification. In other cases degradation of frost-crack relief prevails. The factor of vegetation has a significant influence on the process, removing of destruction of vegetation can facilitate the development of polygonal structures. The most typical dimensions of blocks are 10–15 m, very often they are poorly expressed in relief. Development of polygons starts with formation of narrow ice wedges of the first generation, which slowly year after year grow and cross. While crossing they separate the polygonal blocks usually pentahedral or hexahedral. Ancient ice wedging of the Pleistocene period had much greater scales and spread on mineral grounds as well. The thickness of ice wedges evidently reached 1–2 m. Nowadays we can estimate the scale of cracking and development of polygons by investigating numerous ice wedge casts, forms of relief, vegetation, soils and other components of landscape.

Acknowledgments

The authors are grateful to the following persons for help and support in the project, both in the field works and in the process of article preparation: V.I. Grebenets (Moscow State University, Geographical faculty, Department of Cryolithology and Glaciology, Russia); Professor Eva-Maria Pfeiffer (University of Hamburg, Soil Studies Institute, Hamburg, Germany); V.V. Rogov (Moscow State University, Geographical Faculty, Department of Cryolithology and Glaciology, Russia); and A.N. Kurchatova (T'umen State Oil and Gas University, Russia).

References

Kudriavtsev, V.A. 1978. *General Geocryology.* Moscow: publishing house of Moscow State University, 456 p.

Pavlov, A.V. & Malkova, G.V. 2005. *Contemporary Changes of Climate in Northern Russia: Album of Small-scale Maps*. Novosibirsk: publishing house "Geo", 54 pp. (in Russian).

Podbornii, E.E. 1978. Time and intensity of frost crack formation. *Problems of Cryolithology VII*. Moscow: publishing house Science, 239 pp.

Popov, A.I. 1989. *Regional Cryolithology*. Moscow: publishing house of Moscow State University, 256 pp. (in Russian).

Popov, A I., Rozenbaum G.E. & Tumel' N.V. 1985 *Cryolithology*. Moscow: publishing house of Moscow State University, 239 pp.

New Insights into Spatial Uncertainty in Predictive Periglacial Modeling

Mathieu Marmion
Department of Geography, University of Oulu, P.O. Box 3000, 90014 Oulu, Finland
Thule Institute, University of Oulu, P.O. Box 7300, 90014 Oulu, Finland
Miska Luoto
Department of Geography, University of Oulu, P.O. Box 3000, 90014 Oulu, Finland
Jan Hjort
Department of Geography University of Helsinki, P.O. Box 64, 00014 Helsinki, Finland
Miia Parviainen
Department of Geography, University of Oulu, P.O. Box 3000, 90014 Oulu, Finland

Abstract

In this study, we produced maps of the uncertainty of predictions, provided by eight state-of-the-art modeling techniques for sorted (SP) and non-sorted (NSP) patterned ground, in subarctic Finland, at a 1.0 ha resolution. Five uncertainty classes (UC) represent the agreement between the different modeling techniques. The resulting uncertainty maps reflect the reliability of the estimates for the studied periglacial landforms in the modeled area. Our results showed a significant negative correlation between the uncertainty classes and the accuracy of the modeling techniques. On average, when all models agreed, the mean AUC values were 0.891 (NSP) and 0.886 (SP), and 0.494 (NSP) and 0.510 (SP) when only four models agreed. Mapping of the uncertainty of predictions in geomorphology can help scientists to improve the reliability of their data and modeling results.

Keywords: predictive accuracy; uncertainty classes; uncertainty mapping.

Introduction

Various modeling techniques are increasingly used in geomorphology in order to predict the spatial distribution of earth surface processes and landforms (Guzzetti et al. 1999). The development of spatial modeling in geomorphology is based on three trends: growth in the availability of remote sensed (RS) data and development of GIS techniques integrated with novel statistical methods (Walsh et al. 1998). Among several other applications, spatial modeling is used to assess the stability of terrain (Ermini et al. 2005) and to map glaciated landscapes (Brown et al. 1998) and periglacial processes (Hjort & Luoto 2006). In geomorphology, numerous areas have a lack of data, particularly in remote areas where field investigations are difficult to acquire. The predictions are used to fill these shortcomings in order to create more complete geomorphological maps (Vitek et al. 1996).

The used modeling techniques do not always provide robust predictions (Luoto & Hjort 2005). The reliability of the predictions can be improved by reducing the uncertainty of the models by using consensus methods (Thuiller 2004) or choosing a method which predicts most robustly a certain landform type (Luoto & Hjort 2005). However, these two approaches deal with the modeling uncertainty at a global scale (e.g., the whole modeled area). In this study, we propose a new approach, which does not aim to reduce the modeling uncertainty at a global scale, but to map it at a local scale.

Eight explanatory variables of 6998 grid squares were used as input into eight state-of-the-art modeling techniques to model the spatial distribution of sorted (SP) and non-sorted (NSP) patterned ground in subarctic Finland, at a 1.0 ha resolution. The eight modeling techniques are based on regression, machine learning, and classification algorithms. The accuracy of the models was evaluated using an independent test dataset (2999 grid squares) by the area under the curve (AUC) of a receiver operating characteristic (ROC) plot.

Material and Methods

Material

A dataset of 9997 grid squares at a 1.0 ha resolution was randomly divided into two subsets. The first subset (70%, 6998 grid squares) was used to calibrate the models, and the second subset (30%, 2999 grid squares) was used to evaluate the predictive performance of the models. In the whole study area, the prevalence of NSP and SP was 0.228 and 0.167, respectively. The prevalence was 0.227 (NSP) and 0.167 (SP) for the calibration dataset, 0.229 (NSP) and 0.167 (SP) for the evaluation dataset. Patterned ground was mapped *in situ* and it was located with a GPS-device in the whole study area of 100 km^2 during the field investigation in summer 2002. In total, eight explanatory variables were calculated for all of the grid squares to reflect the studied environmental conditions. The mean altitude (m), the mean slope angle (°), the wetness index, and the proportion of concave topography (%) were derived directly from a digital elevation model (DEM) at 20 m resolution. The proportions of four soil types, namely peat, glacigenic deposit, sand (and gravel), and rock terrain were derived from the digital soil map. More information about the record presences of the patterned grounds and the explanatory variables can be found in the study by Luoto & Hjort (2005).

Methods

The eight modeling techniques belong to three main categories of methods: three regression methods: Generalized Linear Model (GLM), Generalized Additive Model (GAM), and Multivariate Adaptive Regression Splines (MARS); two classification methods: Classification Tree Analysis (CTA) and Mixture Discriminant Analysis (MDA); and three machine learning methods: Artificial Neural Network (ANN), Random Forest (RF), and Generalized Boosting Methods (GBM).

GLMs are mathematical extensions of linear models (McCullagh & Nelder 1989) and have the ability to handle non-linear relationships and different types of statistical distributions characterizing spatial data. In this study, GLMs were built based on third order polynomial functions. GAMs are non-parametric extensions of GLM, using a smoothing spline with four degrees of freedom. GAM combines linear and additive response shapes within the same models (Hastie & Tibshirani 1990). MARS combines classical linear regression, mathematical construction of splines and binary recursive portioning producing linear or non linear models (Friedman 1991). These three regression methods are frequently used, and one example of utilization can be found in Luoto & Hjort (2005).

CTA is a binary based classification method and is an alternative to regression techniques (Breiman et al. 1984). At each node of the tree, a true/false decision is taken considering only one environmental parameter. Then the node separates a class into two different sub-classes whose purity level increases. CTA has been frequently used in geomorphology (Luoto & Hjort 2005). MDA is an extension of linear discriminant analysis (Venables & Ripley 2002). The environmental parameters form classes, for which density distribution is a mixture of Gaussian distributions. A set of environmental parameters is classified into the class with the maximum probability to belong to this class. MDA was used in geomorphology by Meritt & Wohl (2003).

ANNs, machine learning methods, are rule-based methods which have the ability to build accurate models when the functional form of the underlying equations is unknown (Lek & Guegan 1999). A network contains three different kinds of layers: the input layer, the intermediate layer, and the output layer. Each layer contains "neurons." The output of the previous layer of neurons is added, using weighted factors. This process is done until processing of the output layer. Examples of utilization of ANN can be found in Ermini et al. (2005). RF is based on multiple trees methods, generating several hundreds of random trees (Breiman 2001). Each tree is grown by selecting randomly a training dataset as many times as there are observations among the whole set of observation, with replacement from the original dataset. To be classified, vectors of environmental variables are input into each tree. Each tree gives a classification. The classification which appears the most often is attributed. GBM is the third implemented machine learning method and is also based on binary trees (Ridgeway 1999). To classify a vector, it is possible to use a CTA. A prior single tree classification can be improved as long as there is an estimate residual. This residual can be used as input into a second CTA, used to improve the prior classification. The sequence is repeated as long as necessary, decreasing step by step the estimate residual. To our knowledge, RF and GBM have not been used in geomorphological research.

All implemented modeling techniques except ANN were run in R environment (R Development Core Team 2004) under the BIOMOD framework (Thuiller 2003). ANN was run using the nnet library in S-plus.

The probability values of presence for SP and NSP provided by the modeling techniques were combined using a mean function as suggested by Johnson & Omland (2004). The outputs of the eight modeling techniques were then binarized using the prevalence of both landforms as a classification threshold (Liu et al. 2005). Each grid square of the modeled area was classified into five uncertainty classes (UC), reflecting the modeling agreement between the different modeling techniques (UC0 when all models agreed, UC4 when only four models agreed).

The predictive accuracy of the modeling techniques was assessed measuring the area under the curve (AUC) of a receiver operating characteristic (ROC) plot. This is a graphical method assessing the agreement between the observed presence/absence records and the model predictions, by representing the relationship between the false positive fraction and the true positive fraction of the related confusion matrix of the evaluated model (Fielding & Bell, 1997). The range of AUC is from 0.0 to 1.0, and a model providing excellent prediction has an AUC higher than 0.9; a fair model has an AUC in between 0.7 and 0.9, and a model is considered poor when the AUC is below 0.7 (Swets 1988).

Results

The performance of all eight modeling techniques is presented in Table 1. ANN was the most robust modeling technique, with mean AUC values of 0.861 and 0.859 for SP and NSP, respectively. On the contrary, MDA and RF had the lowest modeling performances with mean AUC values of 0.806 and 0.819, respectively. The AUC values of the mean projections were 0.898 for SP and 0.893 for NSP.

The mean AUC values were 0.891 and 0.886 for NSP and SP when all eight modeling techniques agreed, whilst 0.494 and 0.510 when only four models agreed. Furthermore, for all the models, there was a significant negative correlation between the uncertainty classes and the accuracy of the modeling technique (Table 1). The decrease of mean AUC values is the highest from the UC0 to the UC1, with a mean difference of 0.252 (NSP) and 0.219 (SP). ANN disagreed the most with the other modeling techniques, with 669 cases out of 1622 (amount of UC1 grid squares) for NSP and with 955 out of 1687 for SP (UC1).

Spatial distributions based on mean predictions of the eight modeling techniques and uncertainty maps of SP and NSP are presented in Figure 1. The majority of grid squares had a null

Table 1. AUC values based on of the eight different modelling techniques for non-sorted (NSP) and sorted (SP) patterned ground. Additionally, the correlation between uncertainty classes and AUC values are presented, as well as the false positive (FP; proportion of negative observations that were erroneously predicted as positive) and the false negative (FN: proportion of positive observations that were erroneously predicted as negative) fractions for each model and both landform types.

	ANN	**CTA**	**GAM**	**GBM**
	NSP – SP	NSP - SP	NSP - SP	NSP - SP
Calibration	0.844 – 0.860	0.833 – 0.824	0.834 – 0.839	0.839 – 0.852
Evaluation	0.859 – 0.861	0.826 – 0.825	0.837 – 0.840	0.834 – 0.849
Uncertainty class				
0	0.923 – 0.906	0.888 – 0.877	0.886 - 0.885	0.886 – 0.885
1	0.600 – 0.695	0.659 – 0.650	0.668 – 0.682	0.664 – 0.705
2	0.515 – 0.637	0.584 – 0.689	0.596 – 0.653	0.531 – 0.724
3	0.540 – 0.510	0.499 – 0.569	0.481 – 0.437	0.528 – 0.487
4	0.405 – 0.489	0.519 – 0.403	0.478 – 0.647	0.432 – 0.487
Correlation coef.	-0.886 ;-0.958	-0.903 ; -0.940	-0.943 ; -0.717	-0.939 ; -0.939
1-specificity (FP)	0.266 ; 0.338	0.144 ; 0.119	0.166 ; 0.191	0.155 ; 0.135
1-sensitivity (FN)	0.225 ; 0.146	0.283 ; 0.300	0.269 ; 0.219	0.279 ; 0.267

Table 1 continues.

	GLM	**MARS MDA**	**RF**	***Mean***	
	NSP - SP	NSP - SP	NSP - SP	NSP – SP	*NSP - SP*
Calibration	0.833 – 0.835	0.836 – 0.845	0.810 – 0.819	0.976 – 0.988	*0.851 – 0.858*
Evaluation	0.833 – 0.839	0.838 – 0.849	0.820 – 0.806	0.819 – 0.813	*0.833 – 0.835*
Uncertainty class					
0	0.884 – 0.885	0.882 – 0.885	0.893 – 0.876	0.885 – 0.885	*0.891 – 0.886*
1	0.657 – 0.681	0.665 – 0.658	0.566 – 0.589	0.635 – 0.676	*0.639 – 0.667*
2	0.556 – 0.678	0.551 – 0.730	0.542 – 0.573	0.581 – 0.489	*0.557 – 0.647*
3	0.512 – 0.383	0.699 – 0.644	0.614 – 0.535	0.578 – 0.486	*0.556 – 0.506*
4	0.499 – 0.589	0.537 – 0.627	0.569 – 0.317	0.515 – 0.519	*0.494 – 0.510*
Correlation coef.	-0.908 ; -0.775	-0.727 ; -0.790	-0.642 ; -0,930	-0.875 ; -0.848	*-0.853 ; -0.862*
1-specificity (FP)	0.163 ; 0.201	0.211 ; 0.199	0.126 ; 0.154	0.040 ; 0.086	*0.159 ; 0.178*
1-sensitivity (FN)	0.276 ; 0.221	0.211 ; 0.197	0.351 ; 0.291	0.271 ; 0.086	*0.271 ; 0.216*

uncertainty for SP and NSP, representing 68.5% and 67.8% of the whole area, respectively. For the different uncertainty classes these indices were for SP and NSP 16.9% and 16.2% (UC1), 6.7% and 8.1% (UC2), 5.0% and 5.4% (UC3), and 3.0% and 2.6% (UC4). In addition, the prediction of NSP seemed to be underestimated by most of the models. On average, the false negative fraction (FN = 0.271; proportion of positive observations that were erroneously predicted as negative) is higher than the false positive faction (FP = 0.159; proportion of negative observations that were erroneously predicted as positive).

Discussion

Statistical modeling techniques are increasingly used to map earth surface processes and landforms (Gruber & Hoelzle 2001, Hjort 2006, Brenning et al. 2007). In general, geomorphological data are sparse, and the utilization of modeling techniques can help to gather new spatial information (Vitek et al. 1996). Nevertheless, predictive modeling is only relevant if the accuracy of the predictions is known. Several studies have focused on the predictive accuracy of the models (Gruber & Hoelzle 2001, Luoto & Hjort 2005, Hjort & Luoto 2006). The spatial uncertainty of the models has commonly been reduced by combining the output of several models (e.g., consensus methods) or by selecting the most robust modeling techniques for a given landform. However, both these strategies reduce the predictive uncertainty of the models in the modeled area as a whole, whereas the mapping of the spatial uncertainty at a local scale would improve our understanding of the behavior of the models in individual grid squares.

The strong negative correlation between the uncertainty classes and the predictive accuracy of the models underlines the relevance of the multi-model approach. Grid squares in which all models agreed had high modeling accuracy. However, when the predictions disagreed, the predictive accuracy of the models decreased significantly. These results are confirmed by Nilsson et al. (2000), who used a multi-model approach in cell biology.

In this study, the mean probability values of the predictions based on all eight modeling techniques were more robust than the probability values based on single modeling techniques (see Johnson & Omland 2004). This improvement of accuracy is global. The uncertainty maps presented in Figure 1 delineate that the uncertainty is the highest on the edges of the clumped presences. These areas are transitional zones between suitable and non-suitable environments for both SP

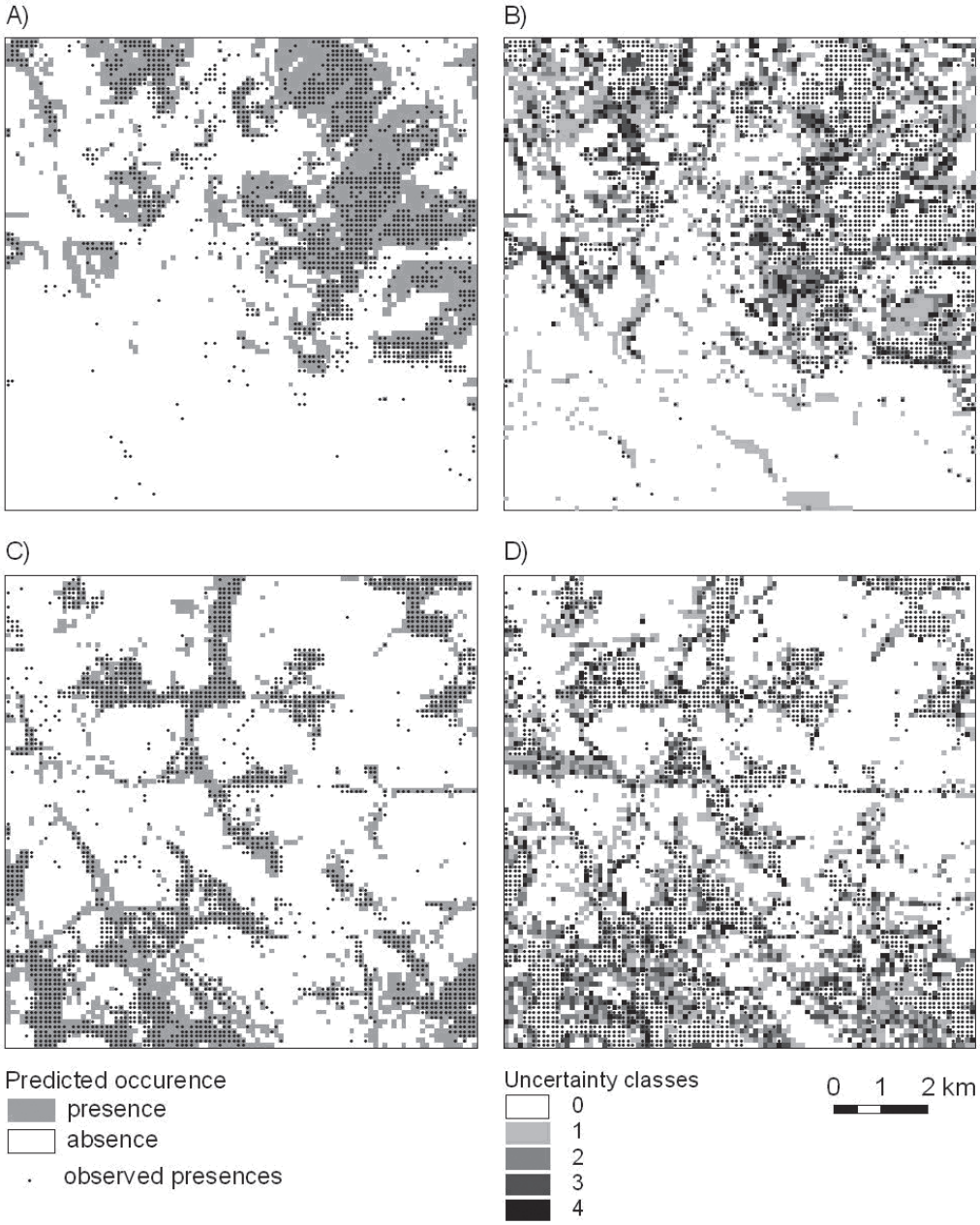

Figure 1. Spatial distribution based on mean predictions of the eight modeling techniques of sorted (A) and non-sorted (C) patterned ground and their uncertainty maps (B and D, respectively).

and NSP. As a consequence, the models have difficulty in differentiating the occurrence of the studied landform types in those areas. The fact that only few spots are predicted with a low accuracy is an asset for scientists who desire to improve the reliability of their data. In this case, the uncertainty analysis indicated that ca. 70% of the study area was accurately modeled for both landforms, thus the field investigations should be focused on the remaining 30% of the study area. It also confirms the assumption that models based on different mathematical algorithms provide rather similar predictions for most of the study area. Moreover, the fact that the NSP are underestimated by the models is partly due to the prevalence used as threshold to convert the output of the models to presences/absences.

Conclusion

Mapping of the uncertainty of predictions is a novel approach to representing the spatial reliability of predictions. It does not improve predictive accuracy of the models, but it provides a consistency map of the predictions. As a consequence, predictive maps can be interpreted simultaneously with uncertainty information, improving the understanding of potential pitfalls of the modeling exercise. We conclude that uncertainty mapping should be taken into account to deepen the understanding of the modeling procedure and to optimize field investigations to gather new field data.

Acknowledgments

MM and MP were funded by the Academy of Finland (project grant 116544). JH was funded by the Finnish Cultural Foundation. The comments of two unknown referees helped greatly in improving this paper.

References

Breiman, L., Friedman, F., Olshen, F. & Stone, C. 1984. *Classification and regression trees.* Pacific Grove, USA: Wadsworth.

Breiman, L. 2001. Random Forests. *Machine Learning* 45: 5-32.

Brenning, A., Grasser, M. & Friend, D.A. 2007. Statistical estimation and generalized additive modeling of rock glacier distribution in the San Juan Mountains, Colorado, United States. *Journal of Geophysical Research* 112.

Brown, D., Lusch, D. & Duda, K. 1998. Supervised classification of types of glaciated landscapes using digital elevation data. *Geomorphology* 21: 233-250.

Ermini, L., Catani, F. & Casagli, N. 2005. Artificial natural networks applied to landslide susceptibility assessment. *Geomorphology* 66: 327-343.

Fielding, A. & Bell, J. 1997. A review of methods for the assessment of prediction errors in conservation presence/absence models. *Environmental Conservation* 24: 38-49.

Friedman, J. 1991. Multivariate adaptive regression splines. *Annals of Statistics* 19: 1-141.

Gruber, S. & Hoelzle, M. 2001. Statistical modelling of mountain permafrost distribution: local calibration and incorporation of remotely sensed data. *Permafrost and Periglacial Processes* 12: 69-77.

Guzzetti, F., Carrara, A., Cardinali, M. & Reichenbach, P. 1999. Landslide hazard evaluation: a review of current techniques and their application in a multi-scale study, Central Italia. *Geomorphology* 31: 181-216.

Hastie, T. & Tibshirani, R. 1990. *Generalized additive models.* London: Chapman and Hall, 335 pp.

Hjort, J. 2006. *Environmental factors affecting the occurrence of periglacial landforms in Finnish Lapland: a numerical approach*. Shaker Verlag, Aachen, 162 pp.

Hjort, J. & Luoto, M. 2006. Modelling patterned ground distribution in Finnish Lapland: an integration of topographical, ground and remote sensing information. *Geografiska Annaler* 88A: 19-29.

Johnson, J.B. & Omland, K.S. 2004. Model selection in ecology and evolution. *Trends in Ecology & Evolution* 19: 101-108.

Lek, S. & Guegan, J. 1999. Artificial neural networks as a tool in ecological modelling, an introduction. *Ecological Modelling* 120: 65-73.

Liu, C., Berry, P.M., Dawson, T.P. & Pearson, R.G. 2005. Selecting thresholds of occurrence in the prediction of species distributions. *Ecography* 28: 385-393.

Luoto, M. & Hjort, J. 2005. Evaluation of current statistical approaches for predictive geomorphological mapping. *Geomorphology* 67: 299-315.

McCullagh, P. & Nelder, J.A. 1989. *Generalized linear models.* New York: Chapman & Hall.

Merritt, D.M. & Wohl, E.E. 2003. Downstream hydraulic geometry and channel adjustment during a flood along an ephemeral, arid-region drainage. *Geomorphology* 52: 165-180.

Nilsson, J., Persson, B. & von Heijne, G. 2000. Consensus prediction of membrane protein topology. *FEBS Letters* 486: 267-269.

Ridgeway, G. 1999. The state of boosting. *Computing Sciences and Statistics* 31: 172-181.

Swets, K. 1988. Measuring the accuracy of diagnostic systems. *Science* 240: 1285-1293.

Team, R.D.C. 2004. *R: A language and environment for statistical computing.* Vienna, Austria. R Foundation for Statistical Computing. http://www.R-project.org.

Thuiller, W. 2003. BIOMOD – Optimizing predictions of species distributions and projecting potential future shifts under global change. *Global Change Biology* 9: 1353-1362.

Thuiller, W. 2004. Patterns and uncertainties of species' range shifts under climate change. *Global Change Biology* 10: 2020-2027.

Venables, W.N. & Ripley, B.D. 2002. *Modern applied statistics with S.* Berlin: Springer-Verlag, 495 pp.

Vitek, J.D., Giardino, T.R. & Fitzgerald, J.W. 1996. Mapping geomorphology: a journey from paper maps, through computer mapping to GIS and virtual reality. *Geomorphology* 16: 233-249.

Walsh, S.J., Butler, D.R. & Malanson, G.P. 1998. An overview of scale, pattern, process relationships in geomorphology: a remote sensing and GIS perspective. *Geomorphology* 21: 183-205.

Modeling Discharge During the Rapid Drainage of Thaw Lakes in the Western Canadian Arctic

Philip Marsh
Environment Canada, National Water Research Institute, Saskatoon, Canada
Mark Russell
Environment Canada, National Water Research Institute, Saskatoon, Canada
Cuyler Onclin
Environment Canada, National Water Research Institute, Saskatoon, Canada
Heather Haywood
Environment Canada, National Water Research Institute, Saskatoon, Canada

Abstract

A large number of thaw lakes in the Western Canadian Arctic are prone to rapid or catastrophic drainage, with 41 lakes draining over a 57-year period in the study area. These lakes range in size up to 560 ha in area and up to 5 m in depth. Evidence suggests that such lakes may drain in less than 24 hours and the resulting drainage from even small lakes may have a peak discharge that is much larger than that experienced during normal spring snowmelt from small headwater basins. As a result, these drainage events play an important role in landscape evolution and may pose a significant threat to proposed pipelines in the study area. This paper will present information on the size and volume of lakes that have drained in the past, and provide order-of-magnitude estimates of discharge during lake drainage.

Keywords: discharge; lakes; rapid drainage; permafrost.

Introduction

The Arctic Coastal plain of northwest Canada is extremely lake rich. At the scale of approximately 10 km x 10 km, lake coverage varies from 15% to 50% of the total surface area. These lakes developed in an ice-rich permafrost environment during a postglacial warm period between 13,000 BP and 8,000 BP (Mackay 1992). Many of these lakes formed due to thawing of ice-rich permafrost that resulted in the settlement of the ground surface (Mackay 1992). Since that time, lake drainage, and disappearance of lakes from this landscape, has occurred at a rate of 1 to 2/year for Richards Is. and the Tuktoyaktuk Peninsula (Mackay 1992, Marsh & Neumann 2001). Such drainage occurs due to the melting or erosion of drainage channels through the ice-rich permafrost (Marsh & Neumann 2001). Similar thaw lake formation and drainage processes occur in the Alaskan Coastal Plain (Brewer et al. 1993) and Banks Island (Harry & French 1983), as well as the Yukon Coastal Plain, the Hudson Bay Lowland, and Siberia.

Mackay (1988, 1992) suggested that lake drainage occurs as underground tunnel flow through interconnecting ice wedge cracks, or by sustained flow through ice wedge troughs. Although drainage is often initiated as tunnel flow, the roof of the tunnel typically collapses during drainage, resulting in an open channel. Observations after drainage (Mackay 1988, 1992, Brewer et al. 1993), and through modeling of outflow (Marsh & Neumann 2001) suggest that lake drainage is often rapid or catastrophic, with partial or complete lake drainage occurring in less than 24 hours.

Through the application of an ice-dammed lake model, Marsh & Neumann (2001) demonstrated that the rate of drainage of permafrost-dammed lakes was at least partially explained by rapid melting of ground ice due to warm water flowing through the channel. They also demonstrated that the maximum discharge during drainage from a small lake (8.1 ha) was similar in magnitude to the spring peak discharge from a drainage basin of 6000 ha in area.

The rapid drainage of lakes modifies the landscape by decreasing lake area and deepening of lake outlet channels. Such events, with drainage channels up to 5 to 10 m in width and 5 m in depth and hundreds of m in length, may pose a significant hazard to pipelines proposed in the area north of Inuvik, NWT. In addition, the high discharge from these events may pose a danger to downsteam infrastructure related to pipeline development.

Marsh & Neumann (2001) estimated the discharge from two drained lakes north of Inuvik, NWT. However, there is no information on the size or volume of a wider range of drained lakes in the study area or of the possible discharge from these lakes. Since there are a large number of lakes in the area north of Inuvik where rapid lake drainage occurs, and since no approach has yet been described to predict which lakes are more prone to drainage, there are no observations of discharge from rapidly draining lakes. In addition, there is only a very small chance of obtaining such discharge measurements in the near future. As a result, the only method available to provide order-of-magnitude estimate of discharge for a lake drainage event is to apply a model such as tested by Marsh & Neumann (2001).

In order to provide order-of-magnitude estimates of discharge during lake drainage events, this paper will (1) evaluate the range of lake size and volume found in the study area and characterize the drainage channel dimensions for

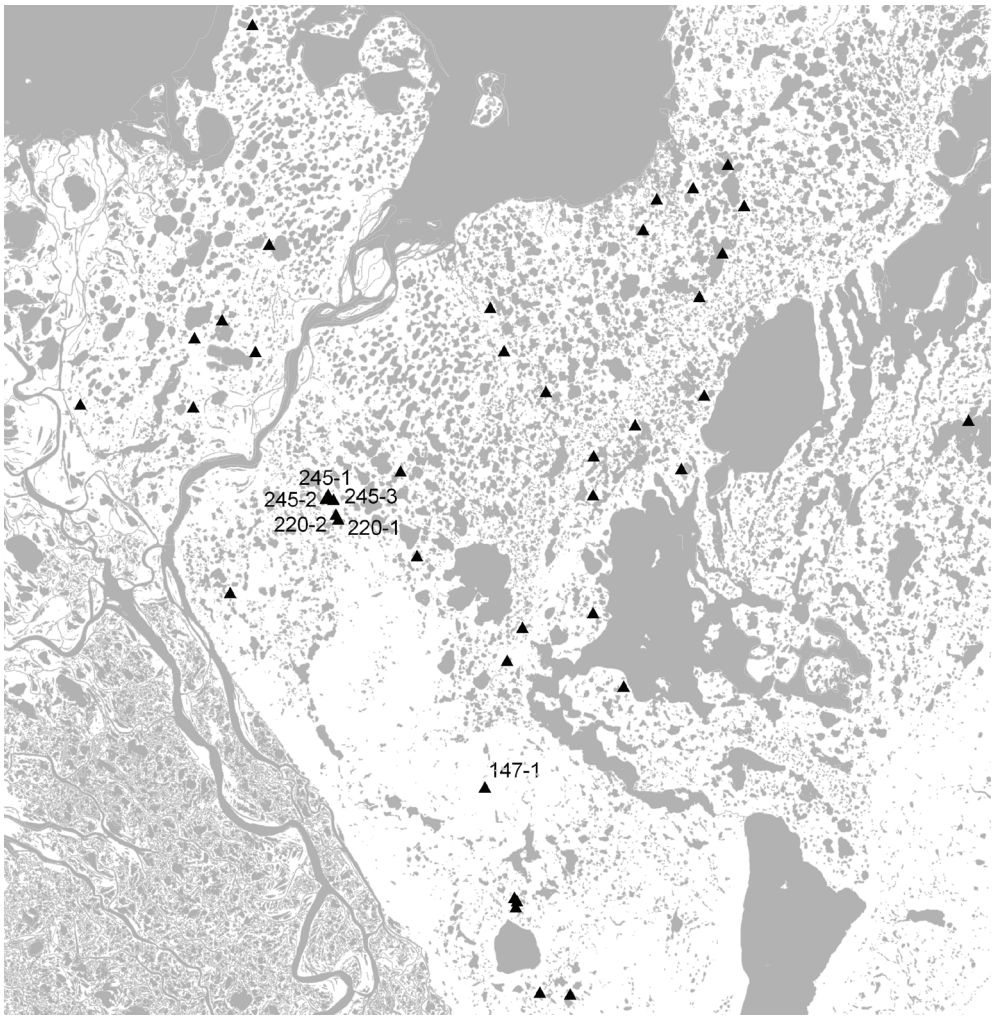

Figure 1. Study area north of Inuvik, NWT, and to the immediate west of the Mackenzie Delta. The 41 lakes that drained between 1950 and 2004 are shown by black triangles. Lakes studied in detail are numbered on the map. Lake number 147-1 is also called TVC Lake.

drained lakes in an area north of Inuvik, NWT, and (2) utilize a simple model to consider the range of possible discharge from these lakes.

Study Area and Methods

The study area includes the area north of Inuvik to the Beaufort Sea, and east from the Mackenzie Delta to near Tuktoyaktuk, NWT. There are 14,457 lakes, covering 19% of the 11,000 km^2 study area. Marsh et al. (2005) mapped drained lakes in this area (Fig. 1), using a combination of aerial photographs from 2000, topographic maps based on 1950 aerial photographs, and field observations. The present paper extends the size of the study area. For this expanded area, there are 41 lakes that drained between 1950 and 2000. The area of these lakes prior to lake drainage was determined from topographic maps and aerial photographs.

The area, volume, and average depth for 6 lakes (numbered in Fig. 1) in the study area was estimated from a high resolution digital elevation model (DEM) obtained from airborne LiDAR flown in August 2004. This DEM has 2 m pixels, with a vertical accuracy of 0.3 m and a horizontal accuracy of 0.6 m. Discharge from these 6 drained lakes was estimated using the methodology of Marsh & Neumann (2001), who applied an ice-dammed lake model from Clarke (1982).

Marsh & Neumann (2001), using discharge data estimated for Illisarvik Lake as derived from Mackay (1981), showed that modeled discharge for Illisarvik Lake was similar to observed for the first 3.5 hr of the modeled 5 hr discharge period. After this time, actual discharge was lower than modeled, with the observed peak being approximately 45% of observed. Marsh & Neumann (2001) suggested that this was due to the fact that channel enlargement by ice melt dominated the first portion of the melt period, while sediment erosion dominated the last portions of the lake drainage event. Following these results, modeled discharge estimates provided in this paper should be considered maximum possible discharge, with actual discharge likely being less.

Lake temperature, as required by the Marsh & Neumann (2001) model, was measured along a vertical profile from the lake surface to lake bed at a typical lake in the study area. Temperatures were measured from late June to early September, a period when many drainage events occur.

Results

Observations of a recent lake drainage channel

During the summer of 2006, a small lake in the study area drained. Although the lake was not observed during the drainage event, observations of the drainage channel soon after lake drainage, demonstrated two features typical of lake drainage as suggested by Mackay (1992) and Marsh & Neumann (2001). First, significant amounts of ground ice were observed along the walls of the drainage channel. Secondly, a surface vegetation mat extended across one portion of the channel, clearly suggesting that at least during the early portion of the event, drainage occurred by subsurface flow through a tunnel. At some point during the event, much of the tunnel collapsed, creating an open channel. Both of these observations further support the hypothesis that lake drainage occurs as tunnel flow through areas of high ground ice concentration, and provide further justification to use an ice-dammed lake model to estimate discharge from rapidly draining lakes (Marsh & Neumann, 2001).

Modeled discharge during lake drainage

Marsh & Neumann (2001) showed the sensitivity of lake discharge during rapid draining events to variations in lake water temperature, channel roughness, and ground ice content. However, due to a lack of data, they did not consider other factors affecting discharge, including lake volume, the length of the drainage channel, and the vertical drop along the drainage channel.

Lake area, volume, channel length, and vertical drop along the channel was obtained from LiDAR data for a series of 5 lakes within the study area and for TVC Lake discussed by Marsh & Neumann (2001). These data show a wide range of lake volumes, with average depth varying from 1.7 to 5.7 m. In addition, channel lengths varied from 8 m to over 500 m, and vertical drop varied between near zero and 14 m (Table 1).

In order to estimate discharge from these lakes during a period of rapid drainage, we used standard values for channel roughness and ground ice content from Marsh & Neumann (2001). Marsh & Neumann (2001) also showed that lake discharge is very sensitive to water temperature, with discharge increasing in magnitude with rising water temperature. The measured average water temperature for one year, from late June to early September, was 13°C at a typical lake in the study area. This temperature was used for all model runs. As noted by Marsh & Neumann (2001), modeled lake discharge increases with water temperature.

Figure 2. shows the discharge vs. time since start of discharge for each of the lakes in Table 1. Note the gradually rising discharge as the channel tunnel increases in cross-sectional area due to ice melting. Discharge continues to increase until the peak value is reached, after which the discharge rapidly drops to zero as the lake volume goes to zero, with maximum discharge ranging from 60 to 370 m^3/s.

As Marsh & Neumann (2001) suggested, however, it is likely that the peak value is less than shown in Figure 2, with the only example from Marsh & Neumann (2001) being 45% of modeled. In that example, discharge peaked, and then gradually decreased instead of rapidly dropping as shown in Figure 2. Even if discharge peaked at a value of 45% of that shown in Figure 2, it would be extremely high for such small headwater lake basins. For the larger lakes, it is likely that peak discharge would be orders of magnitude higher than the spring peak runoff.

Table 1. Lake area, volume, channel length, and vertical drop along the lake outlet channel for 6 study lakes as derived from LiDAR.

Lake #	Area ha	Volume m^3	Channel Length m	Vertical drop along lake outlet channel m
245-1	39.5	790,340	540	1
245-2	21.8	435,668	111	1
245-3	50.0	999,904	240	2
220-2	36.0	770,502	318	5
220-1	82.5	1,650,594	8	0.1
147-1 (TVC)	8.5	112,500	450	14
220-2 + 220-1	118.6	2,421,096	318	5

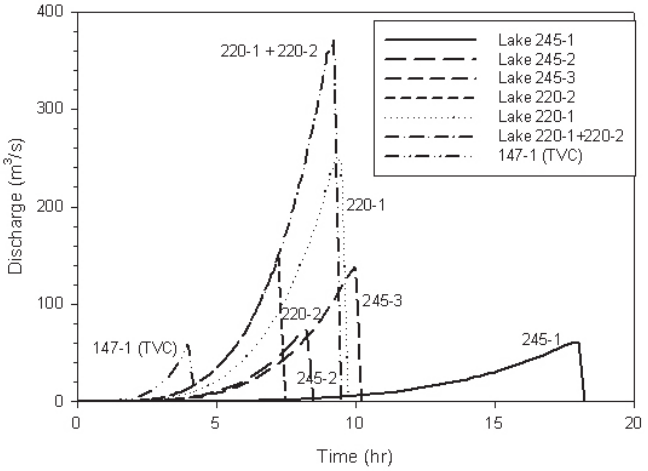

Figure 2. Modeled discharge during rapid lake drainage events. Time is in hours since the start of drainage. Note that Marsh & Neumann (2001) suggested that actual maximum discharge may be less than modeled as the regime changes from melt dominated to erosion dominated.

Lake discharge compared to lake area

A total of 41 lakes drained in the study area during the period 1950 to 2007. These lakes varied in area from a minimum of 0.36 ha, to a maximum of 561 ha, with the majority of lakes less than 100 ha in area (Fig. 3). Since the 6 detailed study lakes described above, are within the size range typical of the study area, they allow us to consider the range of discharges that may occur from the majority of rapidly draining lakes.

Using measured lake volume, channel length, and vertical drop along the channel, the modeled discharge increases linearly with area (Fig. 4). The lack of scatter is surprising

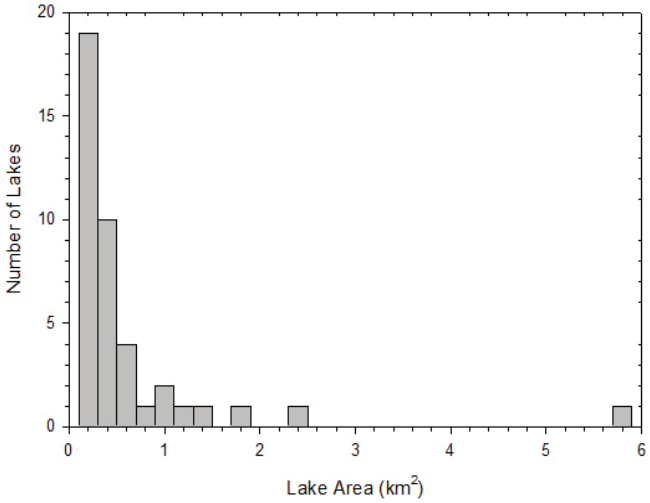

Figure 3. Histogram showing number of lakes within each area group. Note that of the 41 lakes in total, most lakes are in the range from 0 to 100 ha (0 to 1 km^2), a similar range to the 6 lakes in the detailed study area with LiDAR data.

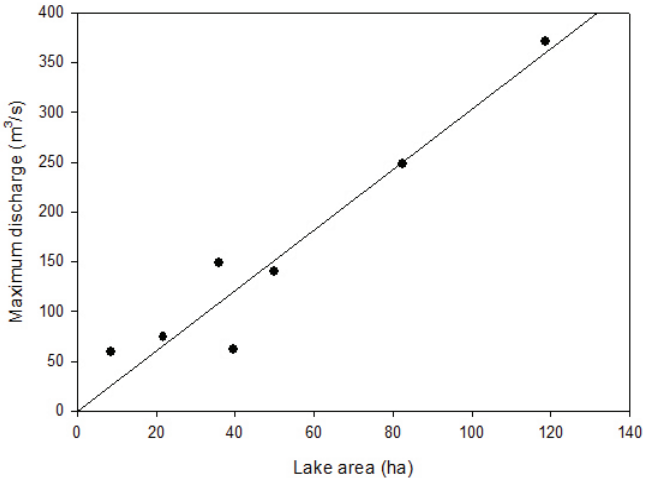

Figure 4. Relationship between lake area and modeled maximum discharge, showing a good linear relationship between the two. However, Marsh & Neumann (2001) suggested that actual maximum discharge is often less than modeled as the regime changes from melt dominated to erosion dominated.

given the range of lake depths (and therefore volume for lakes of any given size) and the variations in channel parameters (Table 1). However, it does suggest that lake size alone, may be used to provide order-of-magnitude estimates of lake discharge.

Although Figure 4 suggests a reasonable relationship between lake area and discharge for a small number of lakes, it would be expected that variations in average depth and channel length and vertical drop along the channel would result in a large variation in discharge for any lake of a given size. Given the data in Table 1, it is possible to estimate the range of possible discharges from rapidly draining lakes, of any given size.

Figure 5 shows possible discharge for increasing lake area, each with a range of lake conditions found in the study area (Table 1). As expected, there is a wide range of possible

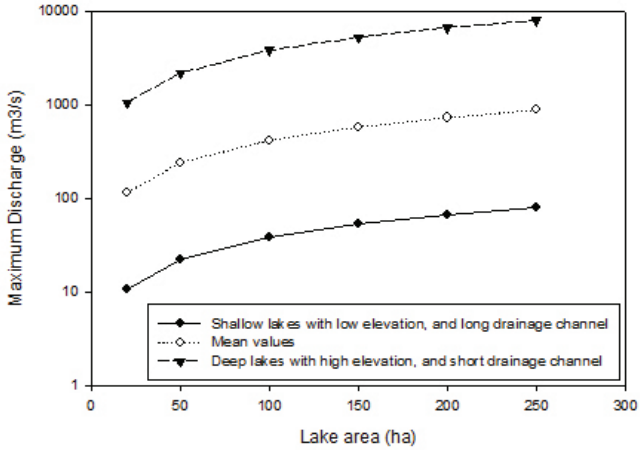

Figure 5. Discharge for lakes with average depth, channel length, and channel slope. Also shown, are maximum expected discharge for deep lakes, with short, steep drainage channels, and for shallow lakes with long, gentle drainage channels.

discharges, with higher discharge for deep lakes with short, steep drainage channels, and lower discharge for shallow lakes, with long, gradual drainage channels.

Grouping of drained lakes

Many drained lakes appear in groups, extending downstream along a drainage path. This is the case with lakes 245-1 to 220-1 shown in Figure 1. It is unknown if such groupings occur due to larger amounts of ground ice and ice wedge occurrence at these sites, or whether drainage occurred in an upstream lake with resulting higher downstream lake levels resulting in drainage of subsequent downstream lakes.

However, for the groupings of lakes 245-1 to 220-1, if drainage first occurred in the furthest upstream lake, we can estimate the maximum rise in water level for each downstream lake from our knowledge of lake areas and volumes.

In this case, drainage of the uppermost two lakes, followed by drainage of each subsequent lake would result in an increase in lake level by approximately 5 m, 14 m, and 34 m in the downstream 3 lakes. The increase in lake level is obviously an over-estimate, as it is assumed that all lake water would be added instantaneously to each downstream lake with no additional outflow from each lake. A complete and more accurate analysis of such a combined drainage event is not possible without additional information. However, it clearly indicates that if an upstream lake drained first, it would result in a very rapid rise in water levels in the downstream lakes. As Mackay (1991) noted, lake drainage can occur in ice-rich terrain under a number of conditions, including high water levels over topping ice wedges, with subsequent melting of ice wedges. Another possibility is that downstream drainage was initiated by mechanical erosion of the existing lake outlet channels and subsequent exposure of ground ice in the channel walls. Once ground ice was exposed, it would likely be prone to rapid melting of ice, channel enlargement, and increased discharge.

Conclusions

Previously drained lakes in the study area north of Inuvik, NWT, range in size up to 560 ha in area, with depths between 1.7 and 5.7 m. Previously published studies and observations in a recently drained lake suggest that lake drainage occurs over a short time, due to melting of ice-rich permafrost, and that flow often occurs within a subsurface tunnel. Detailed information on lake volume, channel length, and vertical drop along the drainage channel from LiDAR, are available for 6 lakes in the study area. Based on these data, as well as measured lake water temperature, and standard values for other parameters from Marsh & Neumann (2001), discharge from these 6 lakes would vary from 60 to 370 m^3/s. Using data for these lakes to estimate a range of possible lake discharge suggests that for shallow lakes with a long, low-slope outlet channel, discharge could range from 10 to 80 m^3/s, while for deep lakes with short, steep outlet channel, the discharge could vary from 1,000 to nearly 10,000 m^3/s. However, as noted by Marsh & Neumann (2001), it is likely that ice melting dominates only the initial rise to a peak, with actual peak discharge being roughly half of that suggested by the ice-dammed lake model. Even with this, model results suggest that discharge from a large, deep, rapidly draining lake could be orders of magnitude higher than that which would occur during spring snowmelt from such small headwater basins.

Acknowledgments

We would like to acknowledge funding from the Program for Energy R&D – Pipelines, from the Environment Canada Northern Energy Project, and from Environment Canada, National Water Research Institute. In addition, fieldwork in such northern locations would not be possible without support from the Aurora Research Institute and Polar Continental Shelf Project.

References

Brewer, M.C., Carter, L.D. & Glenn, R. 1993. Sudden drainage of a thaw lake on the Alaskan Arctic coastal plain. *Proceedings of the Sixth International Conference on Permafrost, Beijing, China.* , Guangzhou, China: University of Technology Press: 48-53.

Clarke, G.K.C. 1982. Glacier outburst floods from "Hazard Lake," Yukon Territory, and the problem of flood magnitude prediction. *Journal of Glaciology* 28(98): 3-21.

Harry, D.G. & French, H.M. 1983. The orientation and evolution of thaw lakes, Southwest Banks Island, Canadian Arctic. *Proceedings of the Fourth International Conference on Permafrost.* Washington, DC: National Academy Press: 456-461.

Mackay, J.R. 1981. *An Experiment in Lake Drainage, Richards Island, Northwest Territories: A Progress Report.* Current Research, Part A, Geol. Surv. Canada, Paper 81-1A, 63-68.

Mackay, J.R. 1988. *Catastrophic Lake Drainage, Tuktoyaktuk Peninsula Area, District of Mackenzie*. Current Research, Part D, Geol. Surv. Canada, Paper 88-1D, 83-90.

Mackay, J.R. 1992. Lake stability in an ice-rich permafrost environment: Examples from the western Arctic coast. In: R.D. Robarts & M.L. Bothwell (eds.), *Aquatic Ecosystems in Semi-Arid Regions: Implications for Resource Management*. NHRI Symposium Series 7. Environment Canada: Saskatoon, Saskatchewan. 1-26.

Marsh, P. & Neumann, N.N. 2001. Processes controlling the rapid drainage of two ice-rich permafrost-dammed lakes in NW Canada. *Hydrological Processes* 15: 3433-3446.

Marsh, P., Russell, M. & Onclin, C. 2005. The hydrology of lakes in the Western Canadian Arctic – implications to proposed natural gas development. *15th International Northern Research Basins Symposium and Workshop Luleå to Kvikkjokk, Sweden, 29 Aug.–2 Sept. 2005,* 131-140.

Ice Wedge Polygon Dynamics in Svalbard: High-Resolution Monitoring by Multiple Techniques

Norikazu Matsuoka
Geoenvironmental Sciences, University of Tsukuba, Tsukuba, Japan
Hanne H. Christiansen
The University Centre in Svalbard, UNIS, Longyearbyen, Norway

Abstract

Techniques were combined to detect the timing and magnitude of thermal contraction cracking and to associate cracking with seasonal soil deformation in low-centered polygonal ground. An ice wedge trough rimmed by ramparts was instrumented with extensometers, breaking cables, shock loggers, thermistors, moisture sensors and an automatic camera. Three years (2004–2007) of monitoring highlighted, in general, symmetrical horizontal movements between the trough and ramparts. The ramparts extended in winter and shrank in summer mainly associated with frost heave and thermal deformation within the active layer. The trough showed the opposite movements, with winter shrinkage and summer extension, except for extension during mid to late winter. The frozen active layer cracked significantly in a very cold period in the late winter of 2006. Following the generation of superficial cracking, the trough began extending when the surface temperature rapidly lowered below -20°C. A major cracking event occurred when the permafrost top temperature reached -10°C, although the crack did not reach the permafrost.

Keywords: field monitoring; ice wedge; periglacial; permafrost; Svalbard; thermal contraction cracking.

Introduction

Thermal contraction cracking and associated ice wedge formation in frozen ground have been studied by theoretical considerations (e.g., Lachenbruch 1962, Plug & Werner 2001) and by field observations (e.g., Mackay & Burn 2002, Fortier & Allard 2005, Kokelj et al. 2007). In particular, long-term monitoring in the Canadian Arctic has provided data on cracking frequency, spatiotemporal variability of cracking activity and seasonal deformation of ice wedge polygons (Mackay 1992, 2000; Mackay & Burn 2002). A notable result is that not only thermal contraction in winter, but also seasonal soil expansion and contraction contribute to the development of the surface morphology and subsurface structure around the polygons. However, the detailed processes of soil deformation and cracking, as well as thermal conditions at which the ground cracks, are still uncertain, because of the lack of continuous recording of soil movement, cracking and contributing parameters.

This paper proposes a synthetic automatic monitoring system allowing year-round, concurrent monitoring of soil dilatation and cracking across a polygon trough, soil temperature, moisture, and snow conditions. Data for the first three years (2004–2007) are combined with data from manual observations of new-crack distribution and soil movement to discuss the timing and detailed processes of soil deformation and cracking.

The Study Site

The monitoring site is located on a fluvial, loess-covered terrace in the Adventdalen valley, Svalbard, Norway (Fig.

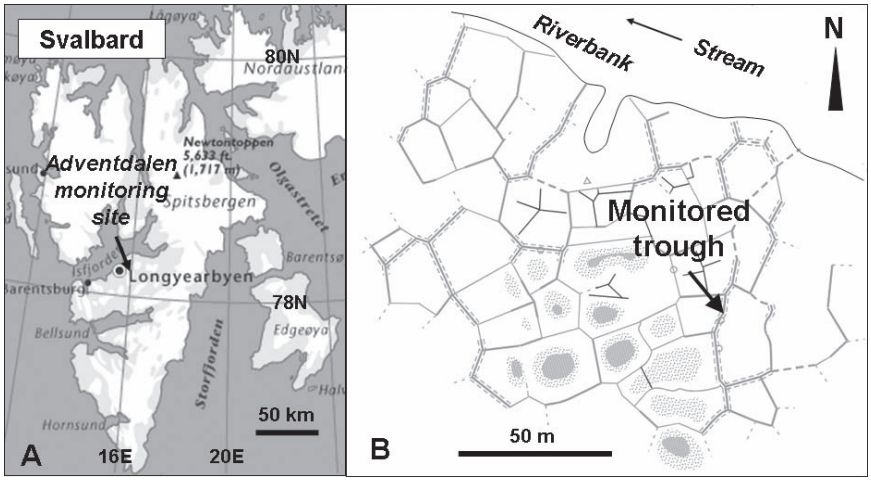

Figure 1. (A) Location map. (B) Polygonal patterns at the monitoring site. Thick solid line: major crack (trough). Thin solid line: secondary crack. Single broken line: tertiary crack. Solid line surrounded by broken lines: trough with well-defined ramparts. Dotted area: bog. Dark area: pond in July 2006.

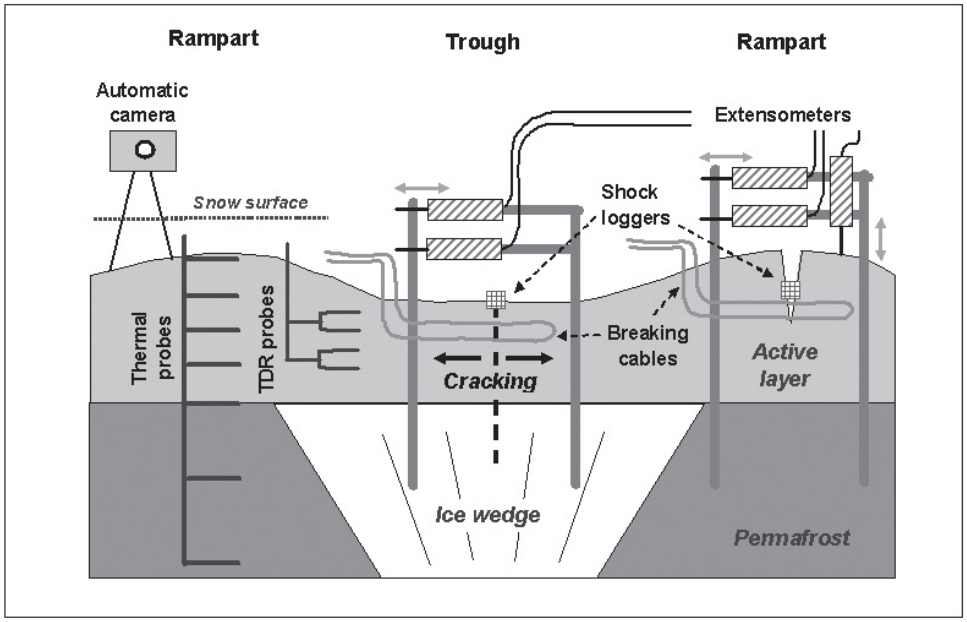

Figure 2. The schema of the automated monitoring system in a section (ca. 5 m wide and 2 m high) across an ice wedge trough with associated ramparts.

1A), where previous investigations report active ice wedge cracking (Christiansen 2005), and field measurements are carried out regularly throughout the year. Low-centered polygons (quadrangles to hexagons) 10–30 m in diameter dominate the ground (Fig. 1B). They are subdivided in places by secondary or tertiary cracks (troughs). The top 1.0 m of the soil consists of fine-grained loess, with the upper 0.5 m rich in organic material. The monitored ice wedge trough is 2.5 m wide and 0.3 m deep, with a rampart on each side. Open cracks develop at the top of the ramparts. Boreholes drilled across the trough showed that the maximum active layer depth (given by the top of the ice wedge) is about 0.95 m, and the ice wedge is about 2.5 m wide at the top.

The mean annual air temperature is -5.3°C and annual precipitation is 192 mm (1986–2006) at the Longyearbyen Airport meteorological station 10 km west of the monitoring site (www.met.no). Large fluctuations in air temperature between 0°C and -20°C to -30°C are common in winter due to the maritime setting with alternations in air masses between low-pressure system coming from the south and polar high-pressure conditions, contrasting with rather stable temperatures (5°C–8°C) in summer.

Instrumentation

Figure 2 illustrates the automatic monitoring system installed in the ice wedge trough and associated ramparts. Soil movements and cracking are monitored with three kinds of instruments. Kyowa extensometers attached to two vertical stakes anchored in permafrost measure horizontal movements across the trough and one of the ramparts at a resolution of 0.04 mm (cf. Matsuoka 1999). The base of the stakes is located at 20–40 cm below the permafrost table. Two extensometers at different heights (0.2 and 0.4 m above the ground) document tilting of the stakes. A vertical extensometer measures frost heave and thaw settlement on the rampart surface. The timing of cracking is monitored hourly by subsurface breaking cables made of very thin copper wires (cf. Mackay 1992) installed at 0.2 and 0.5 cm depth across the trough and in one rampart. Miniature 1-D accelerometers (Tinytag shock loggers, TGP-0605) placed in the top of thermal contraction cracks in the trough (3 loggers), and in the bottom of cracks in the ramparts (4 loggers), provide continuous hourly registration of impacts (e.g., cracking) given by the magnitude of acceleration up to 49 m/s2 at a resolution of 0.2 m/s2. Thermistors measure soil temperatures at 0.02, 0.2, 0.6, 1.0, 1.5 and 2.0 m depths below the top of a rampart every hour. The two deeper thermistors provide temperatures in permafrost and the one at 1.0 m nearly represents the TTOP (temperature at the top of permafrost). Campbell time domain reflectometry (TDR) probes measure the volumetric liquid moisture of the soil at 0.2 and 0.4 m depths below the rampart every six hours. An automatic camera photographs the monitoring site daily to display the snow depth, ground and snow surface conditions.

Following the monitoring of active layer temperatures and snow depth from 2002 (Christiansen 2005), the multi-technique monitoring started in the summer of 2004 (monitoring of the horizontal movement on the rampart started in the 2005 summer). Three years of data have been obtained by the summer of 2007. Most of the sensor-logger systems provided continuous data for the three years. However, problems with data loggers or sensors interrupted data acquisition of permafrost temperatures and vertical soil movement on the rampart in the first year (2004–05), cable breaking on the rampart in the second year (2005–06) and shock events from spring to summer of 2007. A year period is defined here as 365 days from 1 August.

Manual distance measurements have also been carried out since the 2003 summer. Distances between benchmark rods lined across the polygons were periodically measured. The occurrence of new cracks (or recurrence of old cracks) and snow depths are visually inspected all year round.

Results and Interpretations

Soil temperature and moisture

Ground surface temperatures showed significant fluctuations in winter, following air temperatures with minimum time lag (Fig. 3A, B). Such a correlation results from the shallow snow cover, the maximum depth being 5 cm over the ramparts and 30 cm in the troughs. The mean annual TTOP was coldest (-5.2°C) in the first year, followed by the third (-4.2°C) and second (-3.7°C) years.

The first year (2004–05) experienced cold periods in late November with a minimum surface temperature of -25°C and in early March with surface cooling to -33°C. TTOP fell below -10°C only during these two periods, which were separated by a long, relatively warm period.

Figure 3 summarizes results for the later two years (2005–2007), when nearly all datasets were available. The 2005-06 winter on the whole experienced mild climate. However, following a rise to nearly 0°C in mid-January 2006, the ground surface was cooled below -20°C (minimum -23°C) several times in February and March, during which TTOP fell below -10°C (Fig. 3B). The 2006–07 winter was also mild: the surface temperature fell below -20°C only briefly in late January (minimum -23°C) and in early April, and TTOP reached -10°C only in late February.

Water content in the active layer varied seasonally. The unfrozen soil in summer had high and variable contents, whereas the frozen soil in winter had low and stable values (Fig. 3C). The thawed soil at 0.2 m depth showed more varying water contents than at 0.4 m depth. In the 2006 summer, for example, the former experienced a period with relatively low volumetric water contents of 32%–35% from late July to early August, which was preceded and followed by periods with higher water contents of 38–45%, while the water content at 0.4 m depth was nearly stable at 33%–37%. The water content at 0.2 m depth temporarily rose to 62% in the early summer of 2007, reflecting rapid thawing of the soil (cf. Fig. 3B).

Soil deformation and cracking

In the first winter, the horizontal extensometers showed minor seasonal movement (<5 mm) with trough extension in early winter and shrinkage in early summer. Shock loggers located in the trough recorded frequent acceleration events from late February to middle March, when rapid ground cooling resulted in TTOP below -10°C. However, no breaking cables were cut, indicating the absence of cracking in the active layer below the monitored trough. Thus, the shock loggers probably sensed only superficial cracking.

The vertical extensometer recorded frost heave activity within the active layer for the later two years (Fig. 3D). The seasonal frost heave apparently amounted to about 20 mm, but this value probably underestimated the actual amount by about 40 mm, because the lowered level after the annual freeze-thaw cycle in 2005–06 implies upfreezing of the anchored stakes in winter. The lowering was possibly enhanced by deep thaw into the top of ice-rich permafrost during summer. Seasonal thawing was accompanied by two-step settlements in May and August, which presumably originated from thawing of ice-rich layers near the top and bottom of the active layer, respectively (cf. Matsuoka and Hirakawa 2000).

The horizontal extensometers showed, on the whole, opposite movement directions between the trough and rampart (Fig. 3E, F). The trough shrank in early winter and extended in early summer, while the rampart did the opposite at the same time. The symmetrical movements were also confirmed by the manual distance survey of the inter-benchmark distances across several parts of the ice wedge trough and ramparts. The repetition of seasonal movements resulted in interannual expansion of the rampart and contraction of the trough, and the former was about 50% greater than the latter (Fig. 3E, F).

A comparison between horizontal and vertical movements suggests that the crack in the rampart opened during frost heaving in winter and closed during thaw consolidation in summer (Fig. 3D, F). The correspondence was disturbed in early August 2006, during which the rampart crack extended by about 20 mm, while the ground gradually settled. Continuous records of cable breaking were missing, but a manual check of the cable continuity revealed that the two cables in the rampart were cut between 8 July and 16 August, probably due to the crack extension. The crack extension synchronized with the trough shrinkage by about 10 mm. The horizontal movements at both the rampart and trough were nearly stabilized in late August, while the ground significantly settled until seasonal frost heave began.

The horizontal extensometers also indicated temporary tilting of the stakes, as the upper extensometers (0.4 m in height) at both the rampart and trough showed wider annual ranges of horizontal movements than the lower ones (0.2 m) (Fig. 3E, F). The rampart experienced a maximum outward tilting of 1.8° during the third winter, and the trough had a maximum inward tilting of 0.2° during the second winter. Although the direction of tilting changed seasonally, the net outward tilting across the rampart and net inward tilting across the trough cumulated interannually. The former was greater than the latter, which corresponded to the difference in the net rampart extension and trough shrinkage.

The symmetrical movements between the trough and rampart were, however, disturbed in both late winters, during which only the trough extended in response to intensive cooling (Fig. 3E). This movement probably reflected thermal contraction in the frozen soil. The breaking cables in the trough detected cracking only in the second winter (Fig. 3I), although the shock loggers in the trough indicated increasing acceleration when the ground surface cooled rapidly below -15°C in all winters (Fig. 3G). The rampart shock loggers showed significant events which started when the ground

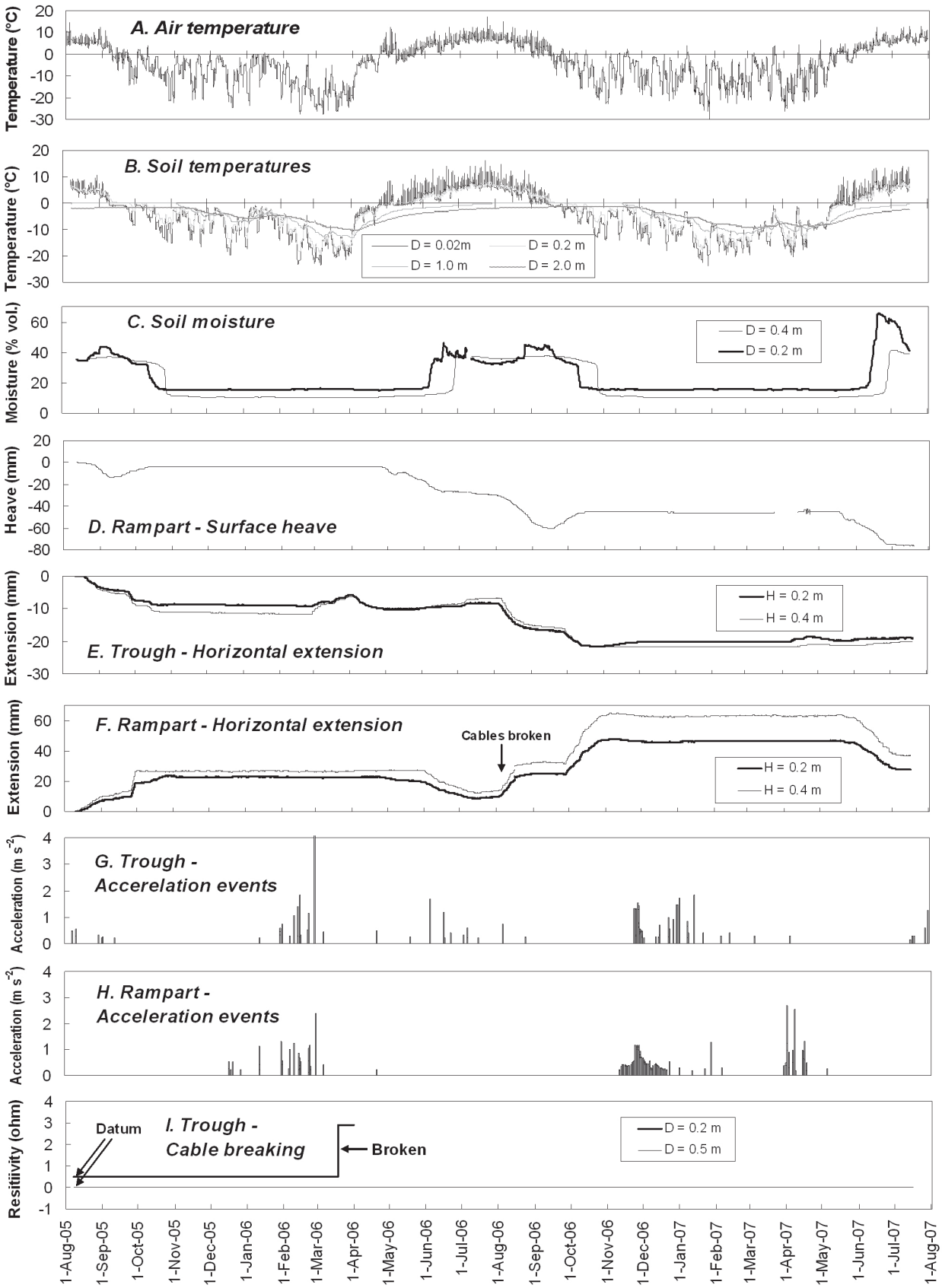

Figure 3. Summary of data from August 2005 to July 2007. The acceleration values in G represent averages of three loggers installed along the monitored trough and those in H averages of four loggers along the rampart. Acceleration values below 0.2 m s^{-2} are removed.

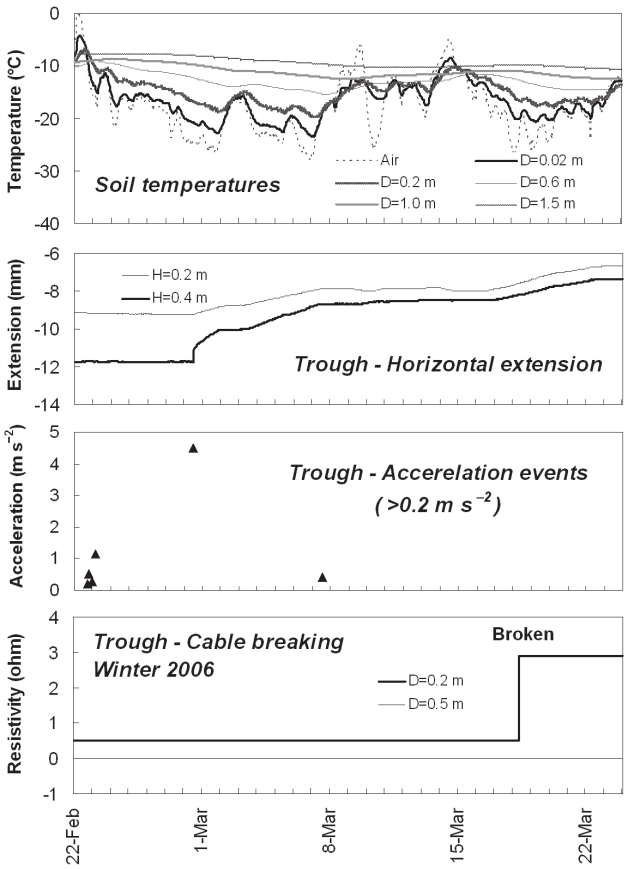

Figure 4. Close-up data in Winter 2006. The acceleration values represent averages of three loggers installed along the monitored trough.

cooled to around -10ºC in mid-December and terminated when the surface temperature became more stable cold around -20ºC in 2006 (Fig. 3H).

All sensors detected cracking in March 2006 (Fig. 4). First, the three shock loggers in the trough recorded frequent and intensifying acceleration events from mid February to early March, which probably indicated increasing superficial cracking starting when the ground had cooled below -10ºC. Next, the horizontal extensometers recorded gradual extension of the trough from 28 February to the end of March, with a relatively stable period in mid March. The copper cable at 0.2 m depth in the trough broke on 18 March, while the deeper cable at 0.5 m depth never broke during the winter. The shock loggers recorded maximum size events on 28 February, but did not record any events on 18 March. The shrinkage of the extensometers in early April (Fig. 3E) indicated the closure of the thermal contraction crack, when the ground started warming significantly (Fig. 3B).

The ground thermal data and visual observations of cracks on the snow surface suggest that a major crack was initiated most likely at the ground surface on 28 February, when the surface temperature fell below -20°C. The crack seems to have propagated gradually into the ground, and up through the snow pack, as the horizontal extension increased, quickest in the beginning (Fig. 4). Interrupted by a warmer and fairly isothermal period in the ground, the crack propagation recurred by rapid cooling and reached below 20 cm depth on 18 March. However, the subsequent termination of the cold period probably prevented further propagation of the crack into the permafrost.

The visual inspection also showed high spatial frequency of new cracks in the second winter. A new crack was actually found on the bottom of the snow-filled monitored trough on 9 April 2006, which supported the cable breaking. Thus, the thermal conditions in March 2006 were favourable for thermal contraction cracking.

In the third winter, similar horizontal movements were reproduced, but only minor late winter extension of the trough was recorded (Fig. 3E). The copper cables did not break. The shock loggers were not operating when the small horizontal extension in the trough occurred, but they did record activity, when ground temperatures first cooled below -10ºC in December. Visual inspection showed the generation of many fewer cracks than in 2006.

Discussion and Perspectives

Distance changes recorded with the vertical and horizontal extensometers and the benchmark poles are likely to reflect, primarily, seasonal thermal deformation and frost heave activity in the polygon and ice wedge trough system. In fact, the crack on the rampart opens during frost heaving in winter and closes during consolidation in summer (Fig. 3D, F). This relation is temporarily disturbed in mid summer, when opening of the rampart crack coincides with ground settlement. Corresponding to the highest near-surface temperatures, this movement appears to originate from thermal expansion in the rampart. The effect of soil moisture change is unclear but can not be ruled out, because the crack extension and subsequent stabilization in summer correspond, respectively, to relatively low water content and to raised water content at 0.2 m depth (Fig. 3C, E): the former possibly indicates crack opening by desiccation.

The symmetrical movements between the rampart and the trough indicate that the seasonal deformation within the active layer below a pair of ramparts basically constrains the deformation of the intervening trough. Before opening of thermal contraction cracks, superficial cracking is generated when the ground cools below around -10ºC, as recorded with the shock loggers. During mid to late winter, however, rapid ground cooling leads to intensive thermally-induced contraction in the frozen ground which has already cooled below -10ºC. The ground contraction induces extension of the trough when the surface temperature falls below -20°C, and crack activity is intensified when TTOP cools below -10°C. If the cold period is lasting for three weeks, a crack will propagate down below 0.2 m and possibly deeper into the ground. During the observed three years, however, the monitored trough did not experience intensive and long-lasting cooling enough to permit cracking into the permafrost. As a result, the ice wedge did not grow. Cracking reaching the ice wedge in the monitored trough most likely requires more rapid and/or intensive cooling, for instance, TTOP below -15°C (e.g., Allard & Kasper 1998, Matsuoka

1999, Fortier & Allard 2005). These results, however, do not exclude the possible occurrence of ice wedge cracking in other troughs at the study site. In fact, excavation of troughs with a number of new cracks in early summer displayed an ice veinlet on the frost table at 0.3−0.5 m depth.

The combination of various techniques presented here enables us to detect seasonal soil deformation and winter thermal contraction cracking activities, including superficial cracking, pre-cracking tensional soil deformation and major, deeper cracking. The observations show that, even in an overall warm winter, temporary intensive cooling can induce significant thermal contraction cracking of the active layer. However, the three years seem to have lacked large-magnitude cooling in combination with long-lasting cold periods which could cause ice wedge growth. This may be due to the recent relatively warm winters, in addition to the maritime Svalbard climate preventing long-lasting cold periods. Acquisition of the detailed critical thermal conditions for ice wedge growth probably requires widely distributed monitoring systems, as well as long-term, continuous monitoring over a decade or more.

The presented ice wedge monitoring system forms part of the project on "standardizing field techniques and constructing a global monitoring network for periglacial processes" that are involved in the activities of the International Permafrost Association Working Group "Periglacial Landforms, Processes and Climate." It will also form part of the periglacial process monitoring in the permafrost observatories that are being established in Svalbard during the International Polar Year in the "Permafrost Observatory Project: A Contribution to the Thermal State of Permafrost" IPY project.

Acknowledgments

The study was financially supported by the Grants-in-Aid for Scientific Research (grant no. 17300294, 19650220) from the Japan Society for the Promotion of Science and by funding from the University Centre in Svalbard. Some of the ice wedge measurements from 2007 are part of the International Polar Year project, "Permafrost Observatory Project: A Contribution to the Thermal State of Permafrost in Norway and Svalbard," supported by the Research Council of Norway (grant no. 176033/S30). We acknowledge field assistance by Ole Humlum, Andreas Kellerer-Pirklbauer, Michael Avian, Lene Kristensen, Mamoru Ishikawa, Atsushi Ikeda, and Tatsuya Watanabe. Thanks to the two anonymous reviewers and the review editor for constructive comments.

References

Allard, M. & Kasper, J.N. 1998. Temperature conditions for ice-wedge cracking: field measurements from Salluit, Northern Québec. *Proceedings of the Seventh International Conference on Permafrost, Yellowknife, Canada, June 23–27, 1998*: 5-12.

Christiansen, H.H. 2005. Thermal regime of ice-wedge cracking in Adventdalen, Svalbard. *Permafrost and Periglacial Processes* 16: 87-98.

Fortier, D. & Allard, M. 2005. Frost-cracking conditions, Bylot Island, eastern Canadian Arctic archipelago. *Permafrost and Periglacial Processes* 16: 145-161.

Kokelj, S.V., Pisaric, M.F.J. & Burn, C.R. 2007. Cessation of ice-wedge development during the 20th century in spruce forests of eastern Mackenzie Delta, Northwest Territories, Canada. *Canadian Journal of Earth Sciences* 44: 1503-1515.

Lachenbruch, A.H. 1962. Mechanics of thermal contraction cracks and ice-wedge polygons in permafrost. *Geological Society of America,* Special Paper 70: 1-69.

Mackay, J.R. 1992. The frequency of ice-wedge cracking (1967–1987) at Garry Island, western Arctic coast, Canada. *Canadian Journal of Earth Sciences* 29: 236-248.

Mackay, J.R. 2000. Thermally induced movements in ice-wedge polygons, western Arctic coast: a long-term study. *Géographie Physique et Quaternaire* 54: 41-68.

Mackay J.R. & Burn, C. 2002. The first 20 years (1978–1979 to 1998–1999) of ice-wedge growth at the Illisarvik experimental drained lake site, western Arctic coast, Canada. *Canadian Journal of Earth Sciences* 39: 95-111.

Matsuoka, N. 1999. Monitoring of thermal contraction cracking at an ice wedge site, central Spitsbergen. *Polar Geoscience* 12: 258-271.

Matsuoka, N. & Hirakawa, K. 2000. Solifluction resulting from one-sided and two-sided freezing: field data from Svalbard. *Polar Geoscience* 13: 187-201.

Plug, L.J. & Werner, B.T. 2001. Fracture networks in frozen ground. *Journal of Geophysical Research* 106: 8599-9613.

Recent Decade Thaw-Depth Dynamics in the European Russian Arctic, Based on the Circumpolar Active Layer Monitoring (CALM) Data

Galina Mazhitova
Komi Science Center, Russian Academy of Sciences, Syktyvkar, Russia
Galina Malkova
Earth Cryosphere Institute, Russian Academy of Sciences, Moscow, Russia
Olga Chestnykh
Dmitry Zamolodchikov
Center for Ecology and Productivity of Forests, Russian Academy of Sciences, Moscow, Russia

Abstract

Nine-to-twelve-year-long records of thaw-depth monitoring from three 100x100-meter grids in the European Russian Arctic are discussed. The grids belong to the Circumpolar Active Layer Monitoring (CALM) network. In agreement with a warming trend in air temperatures, thaw depths increased almost continuously in the discontinuous permafrost zone and fluctuated with an increasing trend in the continuous permafrost zone. The increases in thaw depth were followed by changes in seasonal thaw patterns. Of climatic indices, the thawing index was best correlated with thaw depths. Differential ground subsidence, as measured at one of the grids, constituted 43% of the thawed permafrost layer and visibly changed the site topography. Statistical analyses highlighted moss and the soil organic layer as limiters of thaw depth with their effect weakening as the thaw increases.

Keywords: active layer; climate warming; ground subsidence; permafrost; thawing index.

Introduction

Numerous publications show climate warming in the Arctic including its Russian sector (e.g., Pavlov & Ananjeva 2004). Circumpolar Active Layer Monitoring (CALM) was organized to trace changes in the active layer (thaw) depth induced by the warming and to study climatic controls over the thaw depth. Over 100 CALM grids employ a common measurement protocol ensuring statistical reliability of results. Ground subsidence, as a hazardous consequence of the active layer thickening, is monitored at many grids.

Three 100x100-m grids operate in the European Russian Arctic with the record length from 9 to 12 years. Intermediate monitoring results were published elsewhere (Mazhitova et al. 2004). In this paper, we discuss longer-term trends based on the CALM measurements.

Materials and Methods

Site descriptions

The Bolvansky grid (68°17.3′N, 54°30.0′E) is located in the continuous permafrost zone, whereas Ayach-Yakha (67°35.4′N, 64°09.0′E) and Talnik (67°19.8′N, 63°44.0′E) are in the discontinuous permafrost zone (Fig. 1). By fall 2007, records were 9-, 12-, and 10-years long, respectively. Soils are upland loamy with 5- to 21-cm thick organic horizons. Altitudes range within 5 m at each grid. Permafrost temperatures at the depth of zero annual temperature amplitude range from -0.6 to -2.5°C. End-of-season thaw depths averaged for the period of observation were 110 cm at Bolvansky, 116 cm at Talnik, and 74 cm at Ayach-Yakha. At Bolvansky and Talnik, local closed taliks occur, occupying a few grid nodes and fluctuating in area from year to year.

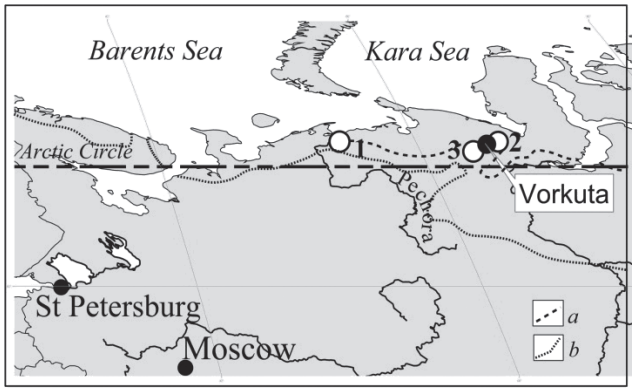

Figure 1. Location of Bolvansky (1), Ayach-Yakha (2), and Talnik (3) CALM grids in the European Russian Arctic. Southern borders of the continuous (a) and the discontinuous (b) permafrost zones are shown.

Field procedures

The European Russian CALM sites employ the standard systematic sampling design recommended under the CALM program (Brown et al. 2000). Permanent grids have been established with 10-m intervals between grid nodes. Grid dimensions are 100 x 100 m at Talnik and Bolvansky and 100 x 90 m at Ayach-Yakha. The nodes are marked with permanent stakes. Thaw depths are determined through 4 replicated measurements at each grid node. Measurements are conducted annually at the end of the warm season with the use of a graduated steel rod. Permafrost at all sites is cemented by ice, and hard enough to avoid errors due to rod penetration into it.

Besides the standardized measurements, additional datasets have been obtained for each grid. These sets differ

depending on accessibility and other site-specific characteristics. At Talnik and Ayach-Yakha, seasonal thaw-depth dynamics are monitored through several measurements during the warm season. The same operations are performed at Bolvansky with a lesser number of field sessions due to difficulty of access. At Ayach-Yakha, snow depths are measured at each grid node annually in April. Volumetric water content in the surface soil horizon is determined for each grid node annually at the end of the warm season. At Ayach-Yakha and Talnik, where the portable Vitel Hydra® probe is used for the purpose, water content is determined several more times during the season. Air temperatures at a height of 2 m, as well as soil and upper-permafrost temperatures are recorded at all sites with the use of miniature Onset® data loggers. Permafrost temperatures at the depth of zero annual amplitude are measured in 3 boreholes at Bolvansky. Ground subsidence and/or heave are determined at Ayach-Yakha for each grid node annually at the beginning and at the end of the warm season with the use of a 2H-10KL leveling instrument (Russia) providing for 4 mm accuracy. A benchmark of the national geodetic network located near the grid is used as a base. At the same grid, angular displacement of several permanent pegs is measured to trace downslope ground movements. Moss and soil organic layer thicknesses at each grid node, vegetation maps, and soil descriptions are available for each grid.

Analytical procedures

The thawing index DDT (°C days) was calculated by summing average daily air temperatures for the period, beginning with positive daily averages and ending either with negative daily averages or on the day of grid probing, depending on the purpose. The freezing index FDD (°C days) was calculated by summing negative daily averages. ANOVA was conducted using the General Linear Models module of STATISTICA, version 7.2, software (©StatSoft, Inc).

Results

Climate dynamics

Mean annual air temperature in the European Russian North rhythmically fluctuated during the 20th century, whereas in 1980–2006, showed an increasing trend with 0.02–0.05°C year^{-1} increments (Fig. 2, A). The increments were smaller than those registered in Siberia, where they amounted to 0.08°C year^{-1} (Pavlov & Ananjeva 2004). Mean annual air temperature dynamics during the period of CALM observations at the weather stations nearest to the grids is shown on Figure 2, A. During the same period, increasing trends in the thawing index were observed also (Fig. 2, B). Increases in permafrost temperature at the depth of zero annual temperature amplitude ranged from 0.003 to 0.06°C year^{-1} (Oberman & Mazhitova 2001, Pavlov et al. 2002).

Thaw-depth dynamics

At Ayach-Yakha and Talnik, grid-averaged end-of-season thaw depths showed almost continuous increase during the observation period with average annual increments of 2.3 and 5.5 cm, respectively. At Bolvansky, an increase in thaw depth was not continuous, yet had an increasing trend significant at p = 0.01 level with 1.7-cm annual increments (Fig. 3). Linear trend parameters were as follows: Ayach-Yakha y = 2.32x + 58.52, R^2 = 0.91; Talnik y = 5.51x + 74.38, R^2 = 0.94; Bolvansky y = 1.69x + 97.87, R^2 = 0.66.

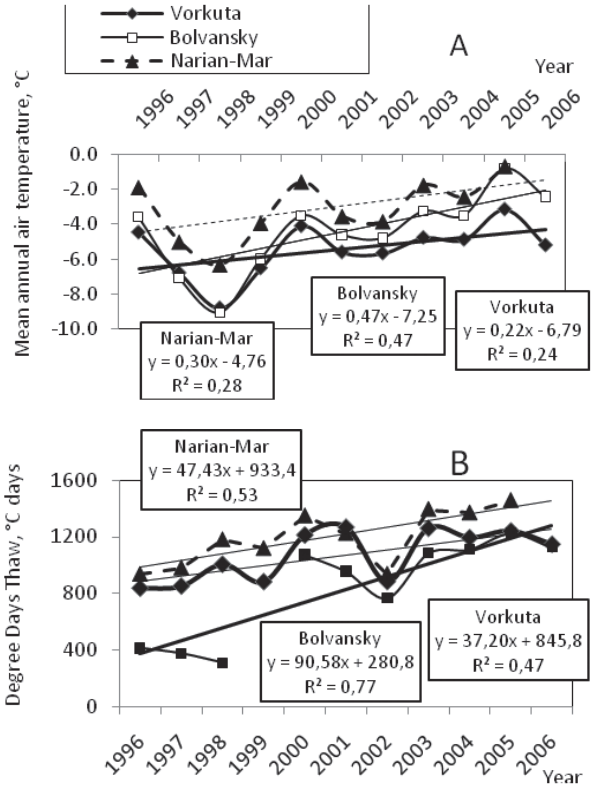

Figure 2. Mean annual air temperature (A) and Degree Days Thaw (B) dynamics during the period of CALM observations at the weather stations nearest to the grids. For Bolvansky, where the weather station was closed in 1999, the values measured at the CALM site are given for 1999–2007.

Correlation between thaw depths and climatic indices

Thaw-depth dynamics duplicated dynamics of no one climate index; however, the increasing trends in thaw depths agreed with also-increasing, though less-significant, trends in mean annual air temperatures. Regressions of grid-averaged thaw depths by $DDT^{0.5}$ representing a form of Stefan solution (Boyd 1973) were widely used in the active layer modeling. The approximations are highly reliable for all 3 grids with R^2 equal to 0.87–0.92 when not only end-of-season thaw-depth values are used, but also those obtained earlier in the warm season (Fig. 4, A). With only end-of-season values considered (Fig. 4, B), the approximation reliability is obviously higher (significant at $p < 0.01$) for the Bolvansky grid located in the continuous permafrost zone than for the 2 grids located in the discontinuous permafrost zone ($p < 0.05$ for Ayach-Yakha and $p < 0.10$ for Talnik). No significant correlation was found with annual precipitation, liquid precipitation, snow depth, or freezing index. For example,

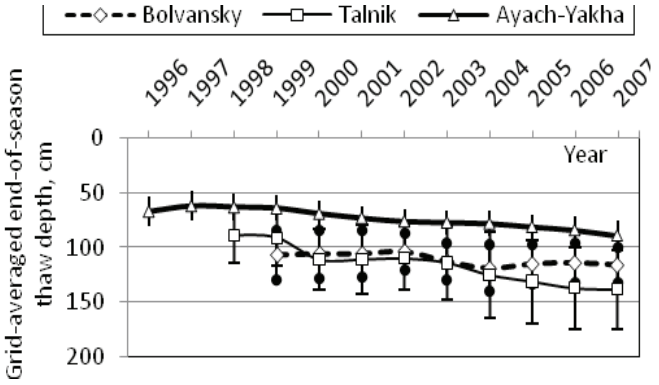

Figure 3. Statistical representation of the end-of-season thaw-depth dynamics at the CALM grids. Values are averages of 484 measurement points at Bolvansky and Talnik, and of 396 measurement points at Ayach-Yakha. One standard deviation extends in either direction.

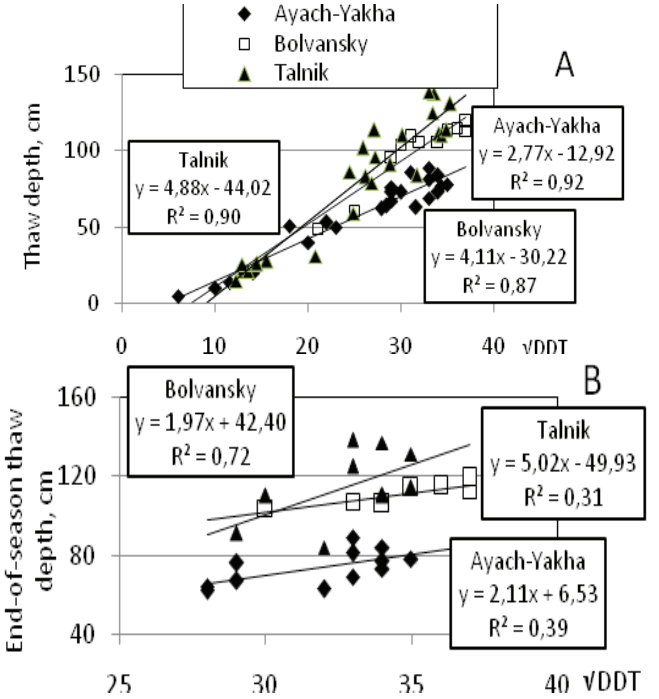

Figure 4. Thaw depth (A) and end-of-season thaw depth (B) plotted against the square root of the thawing index at the three European Russian CALM grids.

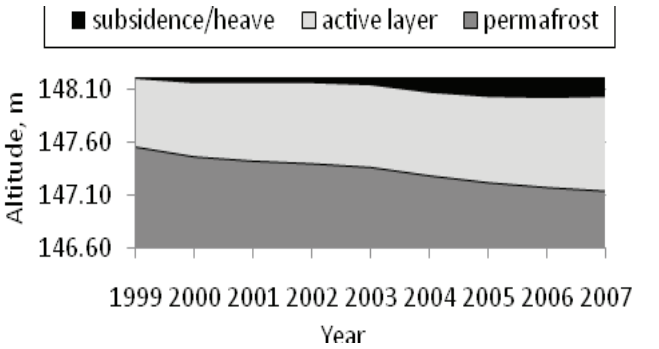

Figure 5. Inter-year dynamics of permafrost table, soil surface subsidence/heave, and active layer thickness at the Ayach-Yakha CALM grid. Grid-averaged altitudes are given for each year.

correlation between freezing index and thaw depth was insignificant ($p > 0.10$) for both Ayach-Yakha with its longer record (correlation coefficient R = 0.64) and Bolvansky with a shorter record (R = 0.01). Node-specific snow depths averaged for the period of observations at Ayach-Yakha showed no significant correlation with node-specific thaw depths averaged for the same period (R = -0.19, $p > 0.10$); similarly, annual site-averaged snow depths were not correlated with annual site-averaged thaw depths (R = 0.52, $p > 0.10$).

Ground heave/subsidence

Thawed or active layer thickness is a function of the permafrost table dynamics and ground heave/subsidence. Interrelations between the 3 indices were studied at the Ayach-Yakha grid. From 1999 to 2007, when these indices were monitored, the permafrost table sank annually at most grid nodes so that the decrease in its grid-averaged altitudes totaled 40 cm (StD 20 cm) by the end of the observation period (Fig. 5). The permafrost layer which had thawed seemed a transient-layer thawing and refreezing under long-term climatic fluctuations (Shur et al. 2005). It had volumetric ice content of 40–50%, higher pH values than those in the active layer, and relatively high organic matter content due to cryoturbations. Because of high ice content in the uppermost permafrost, the permafrost table sinking was followed by ground subsidence. In 1999–2006, the subsidence compensated for winter heave, and in most years its values were nearly proportional to the thickness of the newly thawed permafrost layer (Mazhitova et al. 2004). In 2007, however, though the permafrost table sank farther down, subsidence, for the first time, did not compensate for winter heave at most grid nodes and on grid-average. In that year, thaw at many grid nodes reached the contact between the superficial loess-like loam and the underlying till, and for the first time during the observation period, minor downslope movements of the ground were registered. Three of five reference pegs were found to move 2 cm downslope. In total, from 1999 to 2007, the grid subsided an average of 17 cm (StD 9 cm), with annual increments varying from 7-cm subsidence to 2-cm heave. Grid-averaged end-of-season thaw depth increased by 23 cm (StD 11 cm). Given 40 cm of permafrost table sinking, if we assess the latter based on the increase in thaw depth, only without considering subsidence, it would be 43% underestimated (23 cm instead of 40 cm).

Topographic changes

At Ayach-Yakha, changes in soil-surface and permafrost-table topography due to multi-year differential subsidence/heave were monitored in 1999–2007. Initial surface topography was represented by a 3° slope with a shoulder in the middle part of the grid. Smaller landforms were local rises, dips, and a hollow with several transverse partitions crossing the grid. Permafrost table topography mostly duplicated the soil surface topography; however, the range of altitudes was 30 to 40% wider. Only slightly heaved active frost boils occupying 3% of the grid area demonstrated the opposite pattern with the permafrost table mirroring soil-surface to-

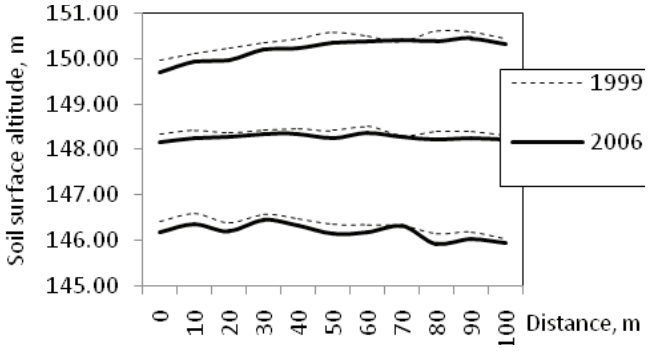

Figure 6. Changes in soil surface topography due to differential subsidence/heave as exemplified by three cross-sections through the Ayach-Yakha CALM grid.

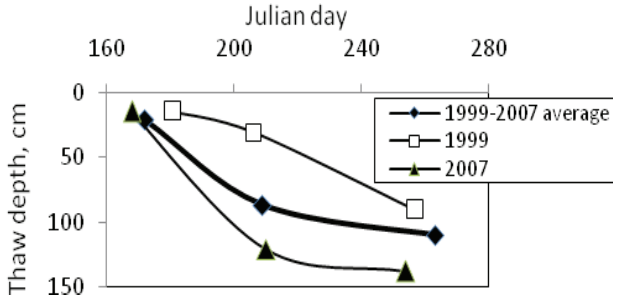

Figure 7. Inter-annual changes in seasonal thawing pattern at the Talnik CALM grid.

pography under them. In total, node-specific deviations of permafrost-table and soil-surface altitudes from the corresponding 2-dimentional linear surfaces modeled with the use of the least square regressions were correlated with R = 0.91. From 1999 to 2007, spatially-differential permafrost sinking changed the permafrost table topography. As the node-specific sinking values were well-correlated with subsidence values, soil surface topography changed accordingly (Fig. 6).

Changes in seasonal thawing pattern

Climate-induced intensification of the thawing process led to evident changes in seasonal patterns. As an example, seasonal thaw-depth dynamics in years with contrast weather conditions are presented for the Talnik grid (Fig. 7).

In 1999 (shallow thaw), thaw depth in late July was only 34% of the end-of-season value. The same value in 2007 (deepest thaw) was 87%. Late July thaw depth, averaged for the period of observations, was 75% of the end-of-season value. The displacement of maximal seasonal thawing rates to the earlier part of the warm season can be concluded.

Components of the thaw depth spatial variance

For the Ayach-Yakha grid, ANOVA under the General Linear Model approach was performed to reveal landscape predictors of thaw depth. Analyzed was the 1999–2005 period, since 1999 altitudes of all grid nodes were measured annually; the 2006–2007 data were not yet processed. Continuous independent variables were (1) surface "macro" to-

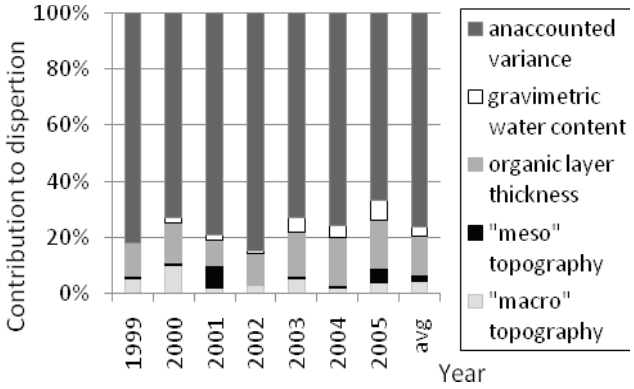

Figure 8. Components of the end-of-season thaw-depth variance at the Ayach-Yakha CALM site.

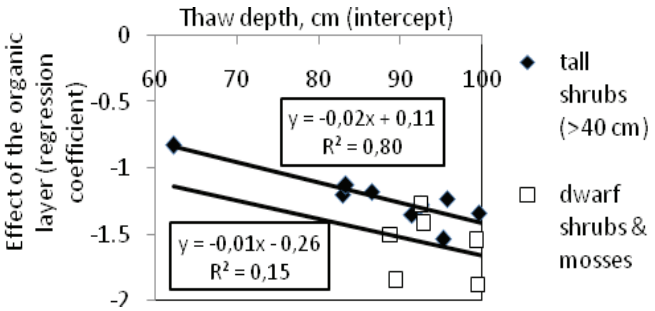

Figure 9. Moss/peat layer effect on thaw depth versus actual thaw depth expressed as the intercept and the coefficient of multiple linear regression, respectively. The independent variables included in the regression were the same as on Figure 8.

pography (altitudes of grid nodes, range width 5 m); (2) surface "meso" topography (deviations of grid node altitudes from the 2-dimentional linear slope approximating the site surface, range width 1.2 m); (3) end-of-season volumetric water content in the upper soil layer, values from 10 to 82 %; and (4) organic (dense moss + peat) layer thickness, values from 4 to 21 cm. A categorical variable was (5) vegetation class (dwarf-shrub/moss versus tall shrubs). Sample size was 396 thaw depth; i.e., dependent variable, values (4 at each of 99 grid nodes) measured annually during 7 years; 99 annual measurements of dynamic independent variables 1–3, and 396 measurements of the organic layer thickness (4 at each of 99 grid nodes) conducted once.

In different years the examined factors explained in total from 18 to 33% of the end-of-season thaw-depth variability, with the organic-layer thickness explaining the largest portion of the latter compared to other variables (Fig. 8).

The effect of the organic layer was sensitive to thaw depth; it weakened as the latter increased, showing a linear trend significant at $p = 0.01$ for the vegetation class of tall (>40 cm) shrubs typical of the southern tundra (Fig. 9).

Discussion

Three European Russian CALM grids demonstrated increasing trends in the depth of thaw during the recent decade. In 2007 compared to 1999, the latter being the first year when all 3 grids were in operation in the discontinuous

permafrost zone, thaw depths increased by 40% at Ayach-Yakha with its shallow thaw and by 51% at Talnik with deep thaw. The Bolvansky grid in the continuous permafrost zone, also with a deep thaw, showed only 9% increase, but still a high level of the trend significance: R^2 0.7 versus 0.9 at the 2 other grids. Given synchronous air temperature dynamics over the region as shown by weather stations, grid locations in dominant upland landscapes, and the maximum distance between the grids as large as 400 km, it is likely that the 3 records represent the main regional trend in thaw depth.

In the region under discussion, permafrost monitoring is conducted by the geological service. Thaw depths are mostly estimated indirectly based on ground temperature measurements at several depths. Only selected monitoring data were published. It was reported that from 1975–1995, thaw depths increased all over the region with exceptions registered at drained lake beds and technogenic sites (Oberman & Mazhitova 2001). For 1980–2003, data from 3 boreholes located at the Vorkuta field station 60 km south-west from the city of Vorkuta (see Fig. 1) were published (Pavlov et al. 2004). The authors, however, mentioned that more sites had been monitored during the same period and that, on average, a slightly increasing trend in thaw depths was observed. Still, the 3 selected records show different thaw-depth trends from 1999–2003: stability, increase, and decrease. Surprisingly, in the preceding 19 years the same sites demonstrated synchronous dynamics. On the whole, the bulk of our and other authors' data suggest that the increase in thaw depth was the dominant, though not universal, trend in the region during the recent 3 decades.

Correlation between thaw depth and climatic indices is widely discussed in the literature. As was shown above, at the 3 European Russian CALM grids end-of-season thaw depths were correlated with the thawing index at significance levels from $p = 0.01$ to $p = 0.10$. The R^2 values of corresponding linear regressions were 0.31–0.39 for the 2 sites located in the discontinuous permafrost zone. The value reported from the aforementioned Vorkuta field station located in the same zone is 0.44, based on the 1988–2003 period and a larger number of sites (Pavlov et al. 2004). During the period of our observations, the range of thawing index values composed 70% of its long-term range displayed by the 1947–2006 record of the Vorkuta weather station. Not represented were extremely cool summer seasons, whereas the extremely warm seasons responsible for thaw-depth jumping (Shur et al. 2005) were fully represented. The range of annual precipitation composed 80% and liquid precipitation 60% of the corresponding long-term ranges. These estimates show that the observation period covered most, though not all, of the long-term variability of climate indices. Still, thaw depths showed no statistically significant correlation with precipitation, snow depth, freezing index, or water content in the uppermost soil layer. Thawing index then seems to be the major control on thaw depth at present though under climatic warming. As other indices exceed the bounds of their natural variability, their effect on thaw depths can strengthen.

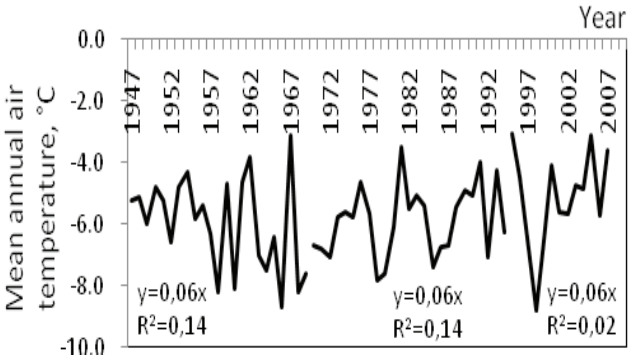

Figure 10. Trends in mean annual air temperature at the Vorkuta weather station. From left to right: a cooling branch of the assumed half-century climatic cycle, a warming branch of the same cycle, and the trend of recent 12 years.

Correlation between thaw depths and thawing index was confirmed by a large number of regressions based on long-term meteorological records from Siberia (Frauenfeld et al. 2004). Monitoring results from numerous CALM grids located in the Kolyma lowland in East Siberia (Fedorov-Davydov et al. 2004) showed that thaw depths were correlated with mean summer temperatures at upland landscapes and were not at intra-zonal landscapes. It is possible that the transitional position of most monitored sites explains the absence of the thawing index–thaw-depth correlation in Yakutia (Pavlov et al. 2004). North American data (Hinkel & Nelson 2003) suggest that thaw-depth response to air temperature forcing is best described by Markovian algorithm with a leading role of extremely warm or cool summer seasons in thaw-depth dynamics.

It is known that the lack of reliable climatic scenario impedes a climate change impacts assessment. Pronounced effects of natural climatic variability on permafrost conditions in the study region were reported. The monitoring conducted by the geological service showed effects of the warming branch of about a half-century climatic cycle (Oberman & Kakunov 2002, Oberman & Mazhitova 2003). A cooling branch, which onset was expected since the mid-1990s, did not show; however, instead, an insignificant ($p > 0.10$) warming trend was observed (Fig. 10).

A climatic scenario was developed for the study region by P. Kuhry using the HadCM2S750 model (Mazhitova et al. 2004). The modeling took into account a natural climatic variability signal and assumed gradual CO_2 increase in the atmosphere during the 21st century with stabilization at the 750 ppm level. The outcome was a lack of trend during the first quarter of the 21st century with further rapid warming by 3°C by 2085. Thaw depths, as modeled based on this scenario (V. Romanovsky in the same paper), were characterized by 30%-of-the-mean fluctuations during the first quarter of the 21st century, followed by an increase with talik formation in the mineral soil and peatland in 15 and in 70–75 years after the start of warming, respectively. During the recent decade, our observations and those of other authors agreed better with the modeled trend than with the trend expected under the superiority of natural climatic variability.

CALM design ensures high precision of major indices determination. At Ayach-Yakha, thaw depth was correlated with thawing index with the grid-averaged correlation coefficient (R) value of 0.36. However, R values were above the average (up to 0.6) at grid nodes located at even and convex micro-sites, whereas below the average and often negative (-0.6 to 0.2) at concave micro-sites. From the CALM grids in Yakutia, higher inertance of the thaw depth was reported for concave compared to convex micro-sites (Fedorov-Davydov et al. 2004). These examples highlight advantages of the CALM statistical approach and warn about possible errors of point measurements.

Conclusions

A climate warming signal in the European Russian Arctic, though weaker than that in Siberia, exerts itself on the sensitive high-temperature permafrost. Depths of seasonal ground thaw show increasing trends especially clear in the discontinuous permafrost zone. Potential increases in active layer thickness which could result from the sinking of permafrost table are partly consumed by ground subsidence. Thawing index correlates with seasonal and inter-annual thaw-depth dynamics in the greatest degree compared to other climatic indices. At present, permafrost is still protected from rapid thaw by a high-icy transient layer and the insulating effect of moss/peat layer. Regressions obtained, however, show that the latter effect weakens with the active layer thickening. Together with passing the threshold of the transient layer, this can lead to acceleration of thaw in the nearest future if the warming trend persists. Continuation of the monitoring with special regard to developing proper up-scaling methods is highly desirable.

Acknowledgments

The study was funded by the NSF through the grants OPP-9732051 and OPP-0352958. Help in the fieldwork and with data processing was provided by Drs. D. Drozdov, D. Karelin, D. Kaverin, and E. Vanchikova, and Mr. A. Kalmykov. Dr. J. Kimble upgraded the English.

References

Boyd, D.W. 1973. Normal freezing and thawing degree-days for Canada: 1931-1960. *Environment Canada.* Atmospheric Environment Service, Downsview, Ontario, Publication CLI 4-73, 1973, 38 p.

Brown, J., Hinkel, K.M. & Nelson, E.F. 2000. The Circumpolar Active Layer Monitoring (CALM) program: Research designs and initial results. *Polar Geography* 24(3): 165-258.

Fedorov-Davydov, D.G., Davydov, S.P., Davydova, A.I., Zimov, S.A., Mergelov, N.S., Ostroumov, V.E., Sorokovikov, V.A., Kholodov, A.L. & Mitroshin, I.A. 2004. Spatial-temporal patterns of seasonal soil thaw in the north of the Kolyma lowland. *Kriosfera Zemli* VIII(4): 15-26 (in Rusian).

Frauenfeld, O.W., Zhang, T., Barry, R.G. & Gilichinsky, D. 2004. Interdecadal changes in seasonal freeze and thaw depths in Russia. *Journal of Geophysical Research* 109, D05101, doi:10.1029/2003JD004245.

Hinkel, K.M. & Nelson, F.E. 2003. Spatial and temporal patterns of active-layer thickness at Circumpolar Active-Layer Monitoring (CALM) sites in Northern Alaska, 1995-2000. *Journal of Geophysical Research* 108(102) (D2).

Mazhitova, G., Malkova (Ananjeva), G., Chestnykh, O. & Zamolodchikov, D. 2004. Active layer spatial and temporal variability at European Russian Circumpolar-Active-Layer-Monitoring (CALM) sites. *Permafrost and Periglacial Processes* 15: 123-139.

Mazhitova, G., Karstkarel, N., Oberman, N., Romanovsky, V. & Kuhry, P. 2004. Permafrost and infrastructure in the Usa basin (Northeast European Russia): Possible impacts of Global Warming. *Ambio* 33(6): 289-294.

Oberman, N.G. & Mazhitova, G.G. 2001. Permafrost dynamics in the northeast of European Russia at the end of the 20th century. *Norsk Geografisk Tidsskrift–Norwegian Journal of Geography* 55(4): 241-244.

Oberman, N.G. & Kakunov, N.B. 2002. Monitoring of ground waters of the cryolithozone in the European part of Russia and the Urals. In: V.G. Balobaev & V.V. Shepelev (eds.), *Monitoring of Ground Waters of the Cryolithozone.* Institute of Geocryology, Yakutsk, 18-43 (in Russian).

Pavlov, A.V., Ananjeva, G.V., Drozdov, N.G., Moskalenko, N.G., Dubrov, V.A, Kakunov, N.B., Minailov, G.P., Skachkov, Y.B. & Skriabin, P.N. 2002. Monitoring of the active layer and permafrost temperatures in the north of Russia. *Kriofera Zemli* VI(4): 30-39 (in Russian).

Pavlov, A.V. & Ananjeva, G.V. 2004. Assessment of recent air temperature changes in the territory of the cryolithozone of Russia. *Kriosfera Zemli* VIII(2): 3-9 (in Russian).

Pavlov, A.V., Skachkov, A.B. & Kakunov, N.B. 2004. Inter-relations between multi-year changes in seasonal ground thaw and meteorological factors. *Kriosfera Zemli* VIII(4): 3-11 (in Russian).

Shur, Y., Hinkel, K.M. & Nelson, F.E. 2005. The transient layer: Implications for geocryology and climate-change science. *Permafrost and Periglacial Processes* 16: 5-17.

The Degradation of Ice Wedges in the Colville River Delta and Their Role in Pond Drainage

Molly McGraw
Southeastern Louisiana University, Hammond, LA USA

Abstract

A 58-year record of aerial photographs was used to examine bank retreat, the thermoerosion of ice wedges, and subsequent tapping of the ponds in the Colville River delta, Alaska, USA. The photographic record consists of aerial photographs acquired during seven different years between 1948 and 2006. ArcGIS was used to determine the rate of bank erosion and melting of the interconnecting ice wedges. The riverbank has eroded approximately 38 meters during the 58-year study period. This erosion is equal to a rate of about 0.7 m/year. Most of the bank erosion (29 m) occurred since 1971. The rate of degradation of the ice wedges, as reflected in trough size, coincides with the rate of bank erosion. The tapping of the first lake—that is, the one closest to the river—occurred between 1992 and 2002, while the other lakes drained between 2002 and 2006.

Keywords: Colville; degradation; ice wedge; lake drainage.

Introduction

The Colville River is the largest river north of the Brooks Range, Alaska, USA. The 600-km-long river is located entirely within the zone of continuous permafrost. The river flows through three physiographic provinces: the Arctic Mountains, the Arctic Foothills, and the Arctic Coastal Plain (Wahrahaftig 1965), before discharging into the Arctic Ocean 75 km west of Prudhoe Bay (Fig. 1). The Colville River delta is 600 km^2 in size, and the head of the delta lies 40 km south of the Arctic Ocean.

Both high-centered and low-centered polygons are found in the delta. High-centered polygons are generally found on river bluffs, adjacent to large thermokarst lakes. Low-centered polygons are the most common type of polygon and are found throughout the delta. The low-centered polygons frequently convert to high-centered polygons due to thermal erosion (Walker 1983). When low-centered polygons are located adjacent to a riverbank that contains a high concentration of peat, the ice wedges undergo faster thermoerosion than the peat. This disproportionate thermoerosion of the riverbank results in an uneven or serrated form of the bank (Fig. 2).

Lakes and ponds occupy roughly 16% of the delta (Walker 1978). This concentration of lakes is similar to other areas of Alaska's Arctic Coastal Plain, where lakes occupy approximately 20% of the area (Black 1969, Sellman et al. 1975, Frohn et al. 2005). Oriented lakes occur near the mouth of the west or Nechelik channel; channel lakes are found in abandoned river channels; and seasonal point bar lakes, in the ridge-swale systems of point bars. However, the most common lakes in the Colville Delta are ice wedge polygon and thaw lakes (Walker 1983).

The formation, degradation, and reformation, i.e., thaw cycle, of thermokarst lakes, has been the subject of much research (Britton 1958, Black 1969, Hopkins 1949, Lord et al. 1974, Billings & Peterson 1980, Everett 1980, Jorgensen & Osterkamp 2005, Jorgenson & Shur 2007). Thaw ponds form over ice wedge troughs and in the center of low-centered polygons. Low-centered polygons have shallow circular depressions that are completely enclosed by a low ridge or dyke. These depressions fill with meltwater and form ponds and lakes.

The ponds/lakes may expand laterally from mechanical erosion due to wave action and/or thermoerosion. During the summer months, the low albedo of lake water may absorb up to seven times the solar radiation of the surrounding soil (Harris 2002), contributing to the thawing of the surrounding

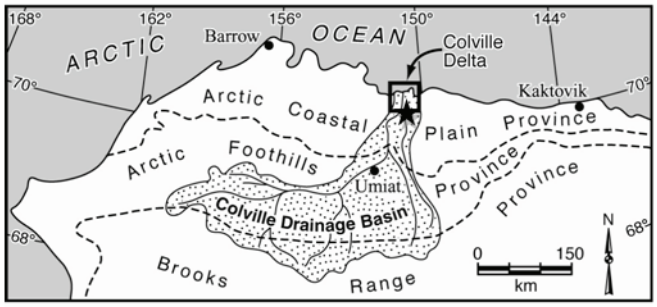

Figure 1. Location of the Colville River. The black star indicates the location of the study site.

Figure 2. An example of a serrated riverbank along the Colville River. Photograph courtesy of H.J. Walker.

Figure 3. Peat overhanging the river. Photograph courtesy of H.J. Walker.

permafrost and ice wedge nets. In addition to albedo, lateral expansion rates also depend upon soil texture and ice content and the thickness of the overlaying organic mat (Jorgenson & Osterkamp 2005). Occasionally expansion taps into an adjacent lake. This is one of the main mechanisms for the coalescence of tundra lakes.

Catastrophic drainage of the ponds/lakes is common and may be triggered by tapping, bank overflow, stream piracy, and ice wedge degradation (Mackay 1988, Walker 1978). The Colville River is frozen for up to eight months of the year. During this period, snowdrifts protect the riverbanks from erosion. As temperatures rise in the spring, meltwater begins to accumulate on the surface of the river ice, and water begins to flow. The flowing water melts the snowdrifts and begins to undercut the riverbank producing a thermoerosional niche. The niche widens and deepens with increased water velocity and increasing water temperatures. If the niche deepens enough, the overlying peat will overhang the river and eventually slough into the river (Williams & Smith 1989, Jorgenson & Osterkamp 2005) (Fig. 3). During flood stage, the material that has sloughed off of the bank during the previous season is transported downriver exposing ice wedges. The ice wedges begin to progressively melt away from the riverbank (Fig. 4) and may lead to the eventual tapping and draining of adjacent thaw ponds (Walker 1983).

After drainage, organic matter begins to accumulate in the center of the drained lake basin. Eventually the ice wedges will regenerate and form low-centered polygons and the cycle will repeat its self.

Remote sensing has been extensively used to classify and study morphologic features on Alaska's Arctic Coastal Plain and the Colville River delta. Dawson (1975) used aerial photographs to analyze the distribution of landforms in the Colville River delta. During the 1980s, both Mossa (1983) and Roselle (1988) examined landforms within the delta using aerial photographs. Mossa (1983) compared the use of aerial photographs to satellite imagery to classify and determine the distribution of ice wedge polygons in the delta. Roselle (1988) examined lake tapping using aerial photographs.

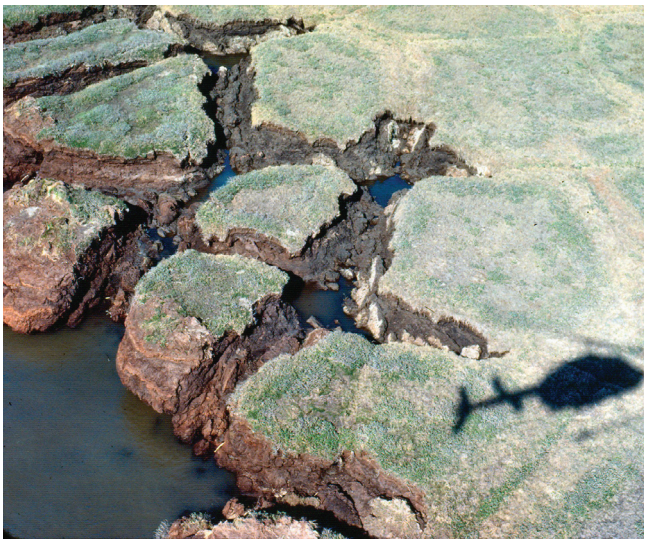

Figure 4. Progressive melting of polygons. Photograph courtesy of H.J. Walker.

Recent studies by Frohn et al. (2005), Hinkel et al. (2007), and Riordan et al. (2006), employed both aerial photographs and satellite imagery to examine the temporal change in several large thaw lakes near Barrow, Alaska. Jefferies et al. (2005) explored the use of various types of remotely sensed imagery, including aerial photographs, satellite imagery, synthetic aperture radar (SAR), and passive microwave, to study the behavior of ice on frozen tundra lakes. Aerial photographs have also been used to examine temporal change in ice wedge degradation in northern Alaska (Jorgenson et al. 2006).

This paper examines the interconnection between riverbank erosion, the degradation of an ice wedge net, and the draining of several small thaw lakes in the Colville River delta using a temporal series of aerial photographs. The photographic record spans a period of 58 years and provides excellent documentation of geomorphic change.

Study Site

The study site, consisting of three small thaw ponds, is located on the right bank at the head of the delta (70°10′20″N, 150°54′31″W). The shallow drained ponds are located on the apex of a cutbank and are aligned roughly perpendicular to the river (Fig. 5). The ponds are roughly 2+ m deep and range in size from 500 m^2 to 1500 m^2. Pond A, the largest of the three ponds, is situated approximately 108 m (as measured from the center of the pond) from the riverbank. The pond is oblong shaped and appears to be the result of the coalescence of 2 or more smaller ponds. Ponds B and C are small, 500 m^2, circular ponds located 30 m and 64 m, respectively, from the riverbank. A well-developed melted ice wedge trough system connects the 3 ponds and the river.

The tundra surface in the vicinity of the pond is flat to gently sloping and is occupied by non-orthogonal polygons and numerous small-to-medium thaw lakes. The soils are silty loam and overlain with a thick layer of peat. The peat

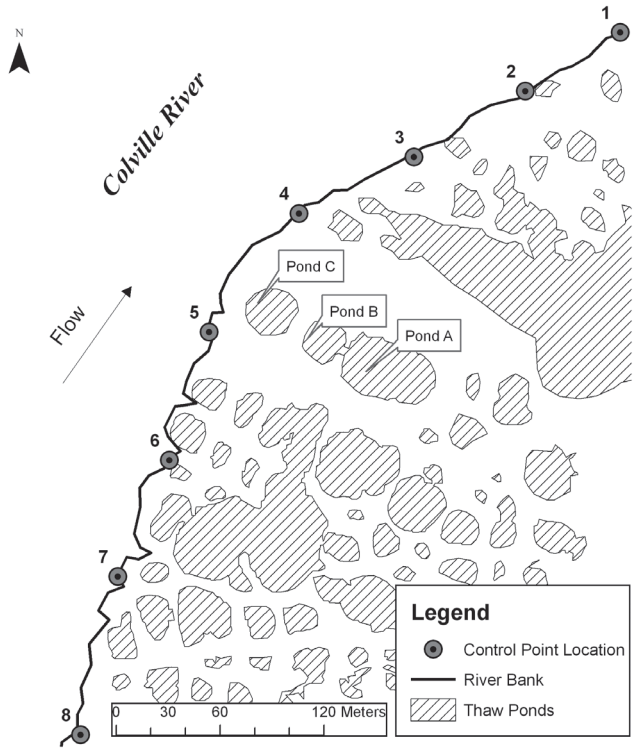

Figure 5. Study site.

acts as a thermal regulator, moderating thermal erosion of the underlying soil. The serrated riverbank is an active cutbank and is approximately 4 m high at this location. Ice-shove ridges are present.

Methods

Aerial photography was used to examine bank retreat, the thermoerosion of the ice wedges, and subsequent tapping of the ponds. The photographic record consists of 7 sets of high-resolution aerial photographs made between 1948 and 2006 (Fig. 6). The pre-1992 imagery was scanned at a resolution of 600 dots per inch (dpi) and georectified to a 2002 Digital Orthophoto Quarter Quadrangle (DOQQ) of the Colville River delta, obtained from the United States Geological Survey (USGS) Alaska Science Center. Because the distinctive character of ice wedge polygons allows the precise identification of specific locations (Walker et al. 1987), the intersection of ice wedges were selected as ground control points (GCPs) for each scanned image. The rectification process of each image produced a Root Mean Square (RMS) of less than 1. Rectification and subsequent analysis was performed using ArcGIS 9.2. The 2006 photograph (Fig. 6g) is oblique and was not georectified; therefore, it was not used in the bank retreat calculations. Instead, the 2006 oblique image was used to ascertain spatial change in the ponds and ice wedge net.

In order to determine the rate of bank retreat, 3 sets of feature class shapefiles were produced for each image. First, a shapefile containing control points was created. The control points were established at roughly equal intervals parallel

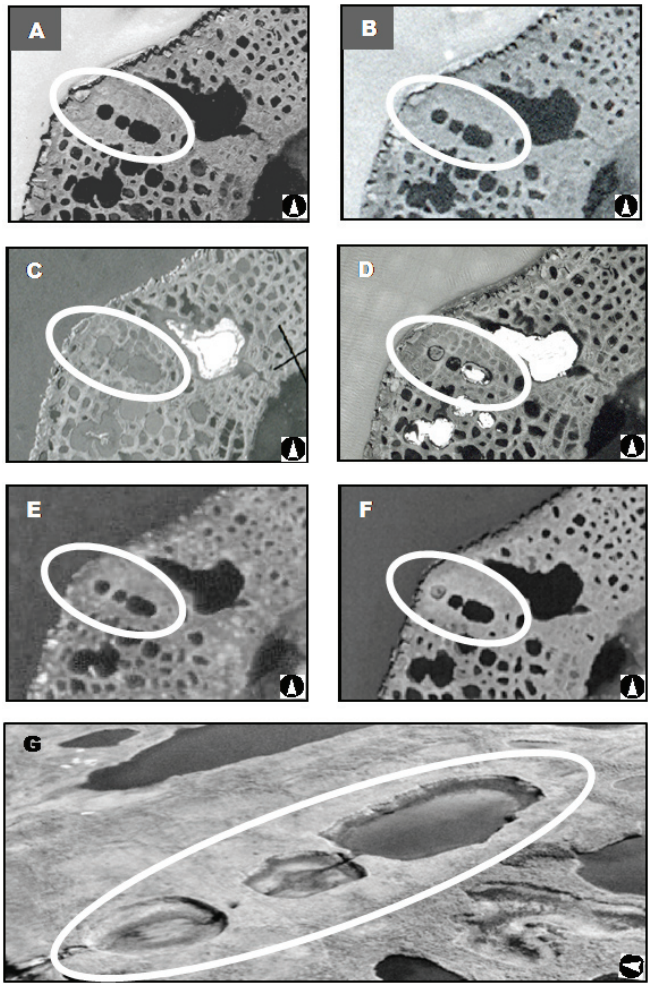

Figure 6: Imagery Dataset 1948–2006: A) 1948 photograph, B) 1955 photograph, C) 1966 photograph, D) 1971 photograph, E) 1992 photograph, F) 2002 photograph, and G) 2006 oblique photograph.

to the riverbank (Fig. 7). Next, a guideline shapefile was generated. The guideline file contained lines extending out from the control points to the riverbank; these lines intersected the riverbank at 90-degree angles. Finally, a reference point shapefile was created for each image. Reference points were placed at the intersection of the guidelines and the riverbank. The difference between the control points and the reference points was calculated for each image using Hawth's Analysis Tools. The cumulative change in the distance was graphed in Excel (Fig. 8).

The thermoerosion of the ice wedges and lake tapping was explored by comparing the photographs. The integrity of the 3 study ponds and the ice wedges adjacent to and connecting the ponds was examined and noted for each photographic dataset. The datasets were then compared to earlier and later datasets, and a chronology of morphologic change occurring at the site was developed.

In addition to the photographic record, a ground and aerial survey of the thaw ponds was conducted by the author. The ponds were visited during the summer of 2006.

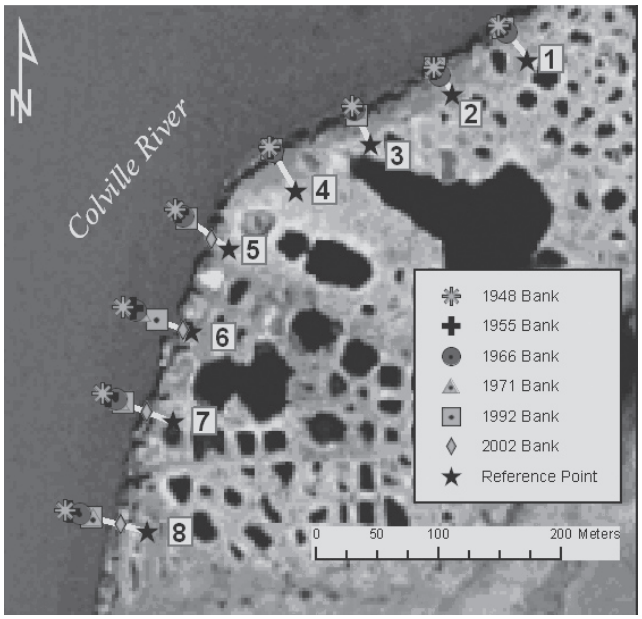

Figure 7. Bank retreat during the period 1948–2002.

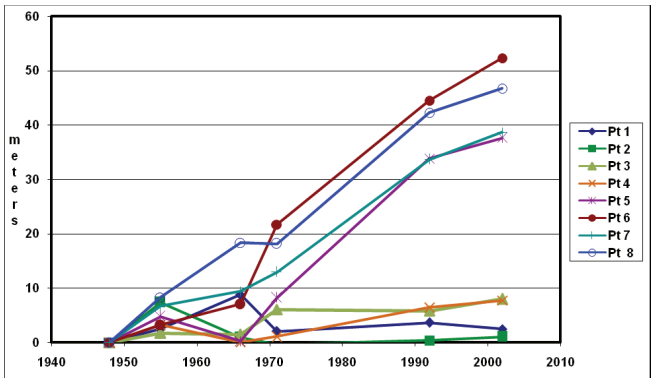

Figure 8. Calculated bank erosion rates from 1948–2002.

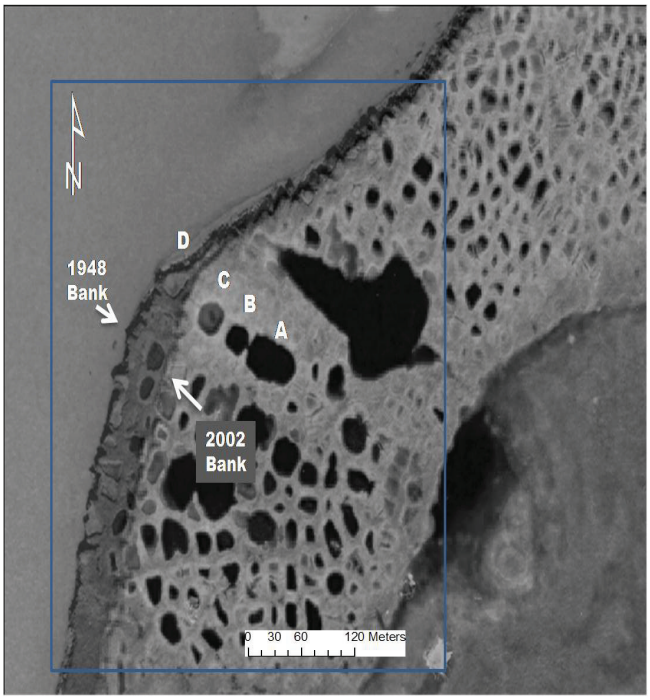

Figure 9. Figure showing the overall bank erosion from 1948 to 2002. Note the presence of a partially eroded polygon (D).

Results

A comparison of the 1948 aerial photograph to subsequent aerial photographs traces the bank retreat, thermoerosion of adjacent ice wedges, and tapping of the 3 ponds. The cutbank, where the study site is located, has experienced differential retreat since 1948, with the southern or upstream bank experiencing the most retreat (Fig. 8). In 1948, Ponds A, B, and C are clearly visible, and the remnants of a fourth drained and partially eroded pond (Pond D) is evident adjacent to the riverbank (Figs. 6a, 9). Ponds A and B are joined by a well-defined 3-m long by 4-m wide trough created from the melting of an ice wedge. A longer 16 m by 2 m trough is present linking Pond C to the partially eroded pond.

By 1955 the entire bank has experienced a fairly steady retreat. The southern bank eroded about 5.7 m and the northern bank, approximately 3.7 m. The bank near Pond D had eroded ~3 m during this 7-year period (Fig. 6b).There appears to be no spatial change in the ice wedge net or in Ponds A, B, and C during this time.

Between 1955 and 1971, significant differential bank erosion occurred, with the southern bank experiencing almost 5 times more retreat than the northern bank. The southern bank retreated an average of 24 m compared to 5 m of retreat in the northern end (Fig. 8). Other than the almost-complete disappearance of Pond D by 1966 (Fig. 6c), there appears to be little spatial change in Ponds A, B, and C and in the adjacent ice wedge net during this time frame (Figs. 6b, c, d).

Similar to the previous time period, the 21-year period between 1971 and 1992 showed dramatic differential riverbank erosion, the southern bank retreating approximately 39 m compared to an average retreat of 4 m on the northern bank (Fig. 8). This steady, continuous bank erosion allowed thermoerosion of the ice wedge connecting the river to Pond C and the subsequent draining of Pond C by 1992 (Fig. 6e). This ice wedge, being perpendicular and adjacent to the river, was subjected to the annual thermoerosion of river floodwater and from thermoerosion and possible wave action of the surface water in Pond C. Additionally, Jorgenson et al (2006) suggests that the degradation of massive ice wedges has increased in northern Alaska since the early 1980s. He attributes this increase in degradation to the increase in regional summer temperatures. This multipronged erosion resulted in increased widening and deepening of the ice wedge trough as shown in subsequent photographs of this period.

The rapid bank retreat and thermoerosion of the ice wedge connecting Pond C to the riverbank continued during the next 10 years. A comparison of the 1992 and 2002 aerial photographs (Figs. 6e, f) shows uniform bank retreat along the entire riverbank. The southern bank retreated about 4 m during this time compared to 5 m for the northern bank. Additionally, an ice wedge trough between Ponds B and C has appeared by 2002, indicating degradation of the ice wedge linking Ponds C and B.

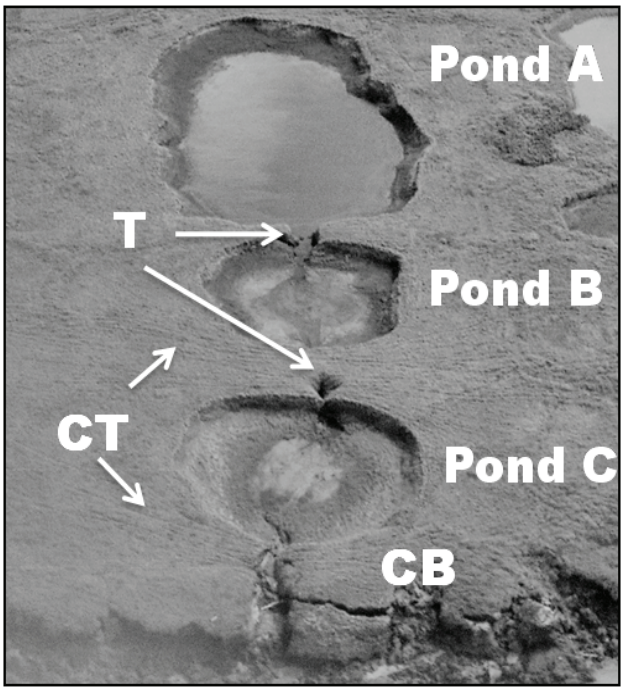

Figure 10. 2006 oblique aerial photograph of the thaw ponds. Note the melted ice wedge tunnels (T), caribou trails (CT), and collapse block (CB).

By 2006, vegetation is becoming established in Pond C, Pond B has drained and Pond A is partially drained (Figs. 6g, 10). The partial draining of Pond A suggests that the ponds were tapped during the 2006 flood. A partially collapsed melted ice wedge tunnel appears between Ponds B and C. Ice wedges which are oriented perpendicular to the river melt faster than ice in the surrounding peat, and may create a tunnel under the peat layer (Fig. 10). As evidenced by linear trails, the land bridges over the tunnels are used by caribou moving across the tundra.

Conclusion

In summary, the 58-year photographic record provides an excellent look into the sequential morphologic changes of an ice wedge net and associated thaw lakes. The photographic record clearly shows thermoerosion of an ice wedge net from both river floodwater and surface pond water. The riverbank adjacent to the study site has experience differential retreat for most of the study period. The greatest difference in the upstream or southern bank retreat and the downstream or northern bank retreat occurred from 1955 to 1992, when the southern bank was eroding as much as 10 times more than the northern bank.

The rate of ice wedge melt is tied to the local bank erosion. The degradation of interconnected ice wedges, all of which are perpendicular to the river, increased with the increasing riverbank erosion. The thermoerosion from river floodwater and surface water in the ponds, have degraded the ice wedges enough to allow the sequential drainage of each of the 3 ponds.

Acknowledgments

I would like to thank Jess Walker for his words of encouragement. I would also like to acknowledge ConocoPhillips, the Michael Baker Corporation, the USGS-Alaska Science Center, the Department of Geography and Anthropology at Louisiana State University and Southeastern Louisiana University for their support, and to two anonymous reviewers for their constructive comments.

References

Billings, W.D. & Peterson, K.M. 1980. Vegetational change and ice-wedge polygons through the thaw-lake cycle in arctic Alaska. *Journal of Arctic and Alpine Research* 12(4): 413-432.

Black, R.F. 1969. Thaw depressions and thaw lakes-a review. *Biuletyn Peryglacjalny* 19: 131-150.

Britton, M.E. 1957. Vegetation of the arctic tundra. In: H.P. Heansen (ed.), *Arctic Biology*. Corvallis, Oregon: Oregon State University Press, 67-113.

Dawson, A.G. 1975. *Landforms of the Colville River delta, Alaska, as interpreted from aerial photographs*. Unpublished M.S. Thesis. Baton Rouge, LA: Louisiana State University, 93 pp.

Everett, K.R. 1980. Landforms. In: D.A. Walker, K.R. Everett, P.J. Webber, & J. Brown (eds.), *Geobotanial Atlas of Prudhoe Bay Region, Alaska*. CRREL Report 80-14. Hanover, NH: US Army Cold Regions Research and Engineering Lab, 14-19.

Frohn, R.C., Hinkel, K.M. & Eisner, W.R. 2005. Satellite remote sensing classification of thaw lakes and drained thaw lake basins on the North Slope of Alaska. *Remote Sensing of Environment* 97(1): 116-126.

Harris, S.A. 2002. Causes and consequences of rapid thermokarst development in permafrost or glacial terrain. *Permafrost and Periglacial Processes* 13: 237-242.

Hopkins, D.M. 1949. Thaw lakes and thaw sinks in the Imuruk Lake area, Seward Peninsula, Alaska. *Journal of Geology* 57(2): 119-131.

Hinkel, K.M., Jones, B.M. Eisner, W.R. Cuomo, C.J. Beck, R.A.& Frohn, R. 2007. Methods to assess natural and anthropogenic thaw lake drainage on the western Arctic coastal plain of northern Alaska. *Journal of Geophysical Research-Earth Surface* 112: F02S16.

Jefferies, M.O., Morris, K. & Kozlenko, N. 2005. Ice characteristics and processes, and remote sensing of frozen rivers and lakes. In: C.R. Duguay & A. Pietroniro (eds.), *Remote Sensing of Northern Hydrology*. Washington, D.C.: American Geophysical Union, 63-90.

Jorgenson, M.T. & Osterkamp, T.E. 2005. Response of boreal ecosystems to varying modes of permafrost degradation. *Canadian Journal of Forestry Research* 5: 2100-2111.

Jorgenson, M.T. & Shur, Y. 2007. Evolution of lakes and basins in northern Alaska and discussions of the thaw

lake cycle. *Journal of Geophysical Research* 112: F02S17.

Jorgenson, M.T., Shur, Y.L. & Pullman, E.R. 2006. Abrupt increase in permafrost degradation in Arctic Alaska. *Geophysical Research Letters* 33: L02503.

Lord, N.W., Atwater, M.A. & Pandolfo, J.P. 1974. Influence of the interaction between tundra thaw lakes and surrounding land. *Arctic and Alpine Research* 6(2): 143-150.

Mackay, R. 1988. Ice wedge growth in newly aggrading permafrost, western Arctic coast, Canada. *Proceedings of the Fifth International Conference on Permafrost. Trondheim, Norway,* 809-814.

Mossa, J. 1983. *Interpretation of the ice-wedge polygons of the Colville River Delta, Alaska, using aerial photography and Landsat digital imagery*. Unpublished M. S. Thesis. Baton Rouge, LA: Louisiana State University, 180 pp.

Riordan, B.D., Verbyla, D. & McGuire, A.D. 2006. Shrinking ponds in subarctic Alaska based on 1950-2002 remotely sensing images. *Journal of Geophysical Research* 111: G040002.

Roselle, D.L. 1988. *Morphology and sedimentation of Arctic tapped lakes*. Unpublished M. S. Thesis. Baton Rouge, LA: Louisiana State University, 109 pp.

Sellman, P.V., Brown, J., Lewellen, R.I., McKim, H. & Merry, C. 1975. *The Classification and Geomorphic Implications of Thaw Lakes on the Arctic Coastal Plain, Alaska*. CRREL Report 344.

Wahrhaftig, C. 1965. *Physiographic Divisions of Alaska*, USGS Professional Paper 482. Washington D.C.: US Geological Survey, 52 pp.

Walker, H.J. 1978. Lake tapping in the Colville River Delta, Alaska. *Proceedings of the Third International Conference on Permafrost. Edmonton, Canada, July 10-13, 1978*: 233-238.

Walker, H.J. 1983. Guidebook to permafrost and related features of the Colville River Delta Alaska. *Guidebook, Fourth International Conference on Permafrost, Fairbanks, Alaska*, *July 18-22, 1983.*

Walker, H.J., Arnborg, J.L. & Peippo, J. 1987. Riverbank erosion in the Colville Delta, Alaska. *Geografiska Annaler* 69: 61-70.

Williams, P.J. & Smith, M.W. 1989. *The Frozen Earth: Fundamentals of Geocryology*. New York: Cambridge University Press.

Managing Ice-Rich Permafrost Exposed During Construction

Robert L. McHattie
GZR Engineering, Fairbanks, Alaska, USA
Ted S. Vinson
Department of Civil Engineering, Oregon State University, Corvallis, Oregon, USA

Abstract

In northern Alaska ice-rich permafrost is often encountered during the construction of roads and other projects. When ice-rich permafrost is exposed during late spring through early fall, the potential for thawing is great. Ice-rich permafrost, typically silts with segregated ice or massive ground ice, experiences a substantial reduction in strength owing to the exceedingly high water content and lack of drainage and consolidation during thaw. The result can be a quagmire that "bogs down" equipment or, if the exposure is a cutslope, slope failure. In addition to stability and trafficability problems, environmental oversight increasingly focuses on particulate-rich effluent and poor aesthetics which are common by-products of the thaw process. In future scenarios, even visually-clear effluent produced during thawing could be classified as biologically toxic and require treatment before release from the project site. This study presents several construction projects in northern Alaska where problems due to thawing permafrost became a significant environmental concern. Several techniques now used (or proposed) for mitigating the problems are briefly discussed.

Keywords: construction; environment; excavation; ice-rich permafrost; management; thawing.

Introduction

Thawing of ice-rich permafrost has produced a number of problems on Alaskan projects including substantially reduced equipment mobility, uncontrolled erosion and runoff, and slope failures. The consequences of thawed ice-rich permafrost are environmental distress, project delays, change orders, and claims. Well-defined procedures are lacking to handle ice-rich permafrost and manage a site with exposed ice-rich permafrost. In the context of this paper, the definition of "ice-rich" permafrost is *any* permafrost material with a water content sufficiently high to cause "problems" upon thawing. Given this context, and the recent advancement of environmental regulations, monitoring, and enforcement, the definitions of "ice-rich" and "problem" can be expected to change with time.

Unfortunately, various types of construction problems related to thawed ice-rich permafrost, documented more than one-half century ago, still occur. In many instances the mitigation strategies employed to reduce the consequences of thawing permafrost only met with partial success or were completely unsuccessful. Newer environmental laws have defined as unacceptable some of the techniques that were recognized as "best practice" for many years.

At present, the construction engineer charged with the successful completion of a project in a permafrost environment has few, if any, resources available to identify a suitable mitigation strategy, particularly in an era of increasingly stringent and challenging environmental regulations. Environmental pressures continue to increase the trend to make long-accepted Alaska Department of Transportation and Public Facilities (ADOT&PF) methods for dealing with ice-rich permafrost either undesirable or unacceptable.

This study examines several construction projects in northern Alaska where problems caused by thawed ice-rich permafrost were of major concern. Techniques employed or proposed to mitigate the problems are described. The purpose of the study is to promote awareness of changing environmental concerns with respect to construction in a permafrost environment and encourage practices that will satisfy the increasing oversight of resource/regulatory agencies.

Problem Background

In northern Alaska exposure of ice-rich permafrost during construction of roads and other projects is an all too common occurrence (Fig. 1). Ice-rich permafrost exposed during late spring through early fall has a very high potential to thaw. Permafrost excavated in winter will cause severe problems if it is not properly disposed of prior to spring thaw. When thawed, ice-rich permafrost, typically silts with segregated ice or massive ground ice, experiences a substantial reduction in strength owing to the exceedingly high water content and lack of drainage and consolidation during the thawing process. The result can be a quagmire in which construction equipment is "bogged down" or, if the exposure is on a cutslope, a slope failure will result (Fig. 2). Aside from stability and trafficability problems, serious environmental issues arise when thawed particulate-laden fluids (sometimes dense slurries) must be controlled. In future scenarios, even visually clear effluent collected from thawed permafrost may have to be treated prior to release from the project site.

Thawing of ice-rich soils has posed problems since the first construction projects in permafrost environments. During the summer of 1954, the Alaska Road Commission exposed

Figure 1. Road cut in ice-rich permafrost (ADOT&PF file photo).

Figure 2. Thaw degradation of cutslope in ice-rich permafrost inducing slope failure (ADOT&PF file photo).

ice-rich permafrost (lake silts) two miles north of Paxson (Fig. 3). Upon thawing, the material actually started to flow. Problems associated with thawing of ice-rich permafrost occurred on a number of North American road projects over the next half-century and have been reported for a number of international projects as well. Slumping of thawed material was noted on several cutslopes in ice-rich permafrost along the Qinghai-Tibet railroad. Chinese researchers report a close correlation relating thaw damage to the orientation of the cutslope (which has been noted by a number of other professionals). Specifically, failures on south-facing slopes were usually more common and dramatic than failures on north-facing slopes. The south-facing slope has a warmer mean annual ground temperature below the sliding mass due to more intense solar heating when compared to the north-facing slope.

A recent example (from 2005 to 2007) of thaw-related problems is provided by the Dalton Highway, just north of Milepost 35. Figure 4 shows a cut that extended about 300 m (1000 ft) in total length. During drilling exploration, the cut volume was judged to be bedrock and weathered bedrock. The cut was designed to have a stepped backslope and also incorporated an interceptor ditch for collecting water along the top of the slope (to prevent erosion of the

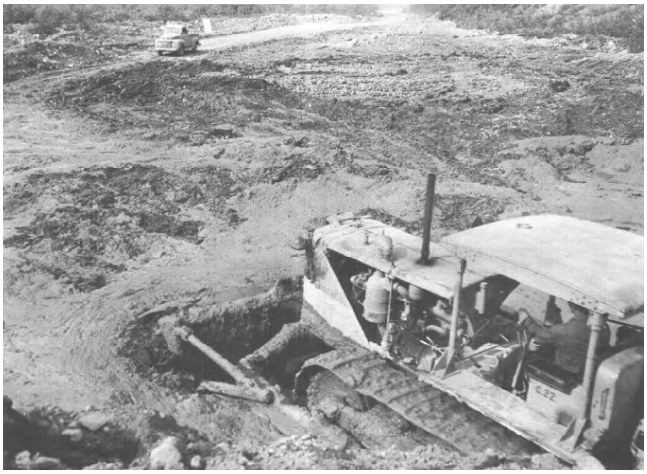

Figure 3. Thawed ice-rich permafrost flowing around a bulldozer blade. Ice-rich permafrost (lake silts) were exposed during the construction of the Richardson Highway (Photograph by Pewe 1954).

slope face). The cut design was appropriate for the expected fairly competent weathered bedrock. However, much of the bedrock cut material was not only highly weathered but also ice-rich. There was no special containment berm used for the excavated material. It was simply stockpiled (see Fig. 4b). Fortunately, the stockpile of excavated material didn't "run" as it thawed as might have occurred. However, there were cutslope failures and maintenance issues that required attention as shown in Figure 5.

Disposal of excavated material is one of the most common problems associated with exposing ice-rich permafrost. It is no longer acceptable to simply waste the excavated permafrost at a convenient location without regard to the environmental consequences of failure or runoff from the eventually thawed material. One solution to the disposal of excavated permafrost is to construct retention berms and place the permafrost inside the berms as shown in Figures 6 and 7. When the ice-rich permafrost eventually thaws, it is restricted to the area inside the berms. The berm shown in Figure 6 allowed the thaw water to escape and cause other environmental concerns. Future retainment schemes may be complicated if excess water generated during thawing needs treatment prior to release from the containment area.

Finally, a problem in western Alaska, also related to permafrost degradation, is the use of excavated permafrost to construct road and airfield embankments. This unusual practice is necessary owing to the scarcity of suitable embankment fill at some locations. Permafrost is excavated in the winter and placed in the location of the required embankment (similar to the waste embankment shown in Fig. 7). Over a period of several years, the permafrost fill progressively thaws and becomes increasingly stable and viable as a runway embankment. If the thawed material is restrained from lateral spreading and flow, it eventually settles and drains and can be shaped and compacted to form the final load-supporting embankment. Snow berms can be placed adjacent to the embankment sideslopes to retain

(4a) Newly-constructed cutslope in ice-rich permafrost. Note interceptor ditch at slope top and stepped cut face.

(4b) View across permafrost waste pile at newly cutslope face in ice-rich permafrost. The volume of waste exceeded the boundary limits of the permitted area.

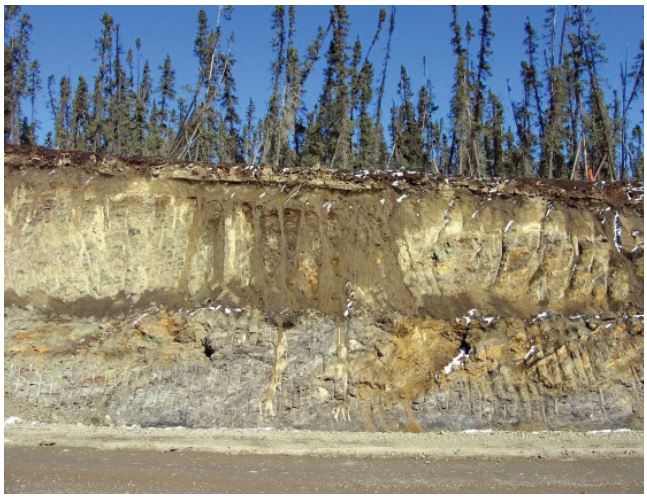

(4c) Ice-rich permafrost cutslope just starting to thaw.

Figure 4. Dalton Highway cut in ice-rich permafrost–before thaw (all photographs from ADOT&PF file courtesy of S. Lamont & J. Russell).

the thawing permafrost. Thawed soil, initially retained by the snow berm, drains and forms its own soil berm that continues to contain the spread of additional thawed material after the snow disappears. In the future, with all containment schemes, excess water collected behind the berms may need to be processed before release.

Mitigation Strategies for Ice-Rich Cutslopes

Documented concern for the instability of cutslopes in ice-rich permafrost and massive ground ice was presented in the 1969 design guidelines for the 123-km (56-mile) Livengood to Yukon River initial segment of the Trans Alaska Pipeline System (TAPS) haul road (Rooney 2006). The original engineer's sketch of the procedure to be employed is shown in Figure 8.

Anecdotal and published sources of information suggest that several techniques have been employed, with varying degrees of success, to mitigate problems related to thawing ice-rich permafrost. A few examples are:

- Berg and Smith (1976), based on observations along the TAPS haul road, presented the procedure shown in Figure 9. At the time of construction, trees are cleared (by hand to minimize environmental damage) for a distance equal to 1½ H_{CUT}. The cut is nearly vertical (1/4H:1V). The road grade is undercut approximately 1.5 m (5 ft) before placement of the gravel embankment. Wide ditches that will accommodate slumpage, while facilitating drainage flow and "cleanout," are constructed at the toe of the slope. During the first summer, the slope degrades rapidly. Hydraulic seeding is applied late in the thaw season (for best results). The lateral ditch is cleaned as necessary. The rate of degradation of the backslope decreases over a number of years. After 5 or 6 years, the slope usually becomes relatively stable and covered with surface vegetation that restores thermal equilibrium.
- Cutslopes may be protected with insulation to ensure stability and prevent slump material from reaching the drainage system.
- Cover the cutslope with a vegetation mat (closed netting) to provide minor insulation plus shading.
- Reduce the slope inclination to 1½H or 2H:1V; place topsoil on the slope; seed at 2 to 3 times the "normal" application rate (best suited to non-ice-rich permafrost)
- Cut the ice-rich permafrost slope about 1½H:1V and place a gravel berm adjacent to the slope face (berm height = cutslope height). The horizontal width of the berm is approximately 8 ft to facilitate construction, and the berm sideslope is approximately 1½H:1V

(5a) Pockets of thaw failure along cut face. —A gravel drainage blanket (left side of photo) was installed to slow thawing, retard slumping of thawed material, and provide drainage during the thawing process.

(5b) Advanced thaw condition along ice-rich permafrost cutslope shows ditch filling with saturated silt.

Figure 5. Dalton Highway cut in ice-rich permafrost—after thaw. (All photographs from ADOT&PF file courtesy of S. Lamont & J. Russell.). Each photograph shows damage that occurred as thawing progressed. The photos emphasize four major types of damage and associated environmental problems created during thawing: (1) damage above the cutslope, (2) damage on the cutslope, (3) ditch damage, and (4) high-particulate runoff. The damage creates and/or exacerbates the runoff problem. With much (and long-term) attention to ditch maintenance, such problems have "healed' themselves in the past when thawing progressed to a depth at which additional slumping and runoff finally ceased. Today, however, environmental-concerns/laws and close agency attention no longer permit creation of a problem that may continue for years. Methods must be devised to minimize, or hopefully eliminate, the types of damage shown in the photographs. Photograph 5a (left side) shows an example of a gravel drainage blanket used to slow thawing, retard slumping of thawed material, and provide drainage during the thawing process.

(5c) Advanced thaw degradation of cutslope shows block failures and runoff of highly fluid silt into ditch.

(5d) Advanced cutslope thaw with silty runoff flowing in ditch and general slumping of coarser material.

Figure 6. Containment structure for excavated permafrost on the North Slope of Alaska (photograph courtesy of G. Griffin).

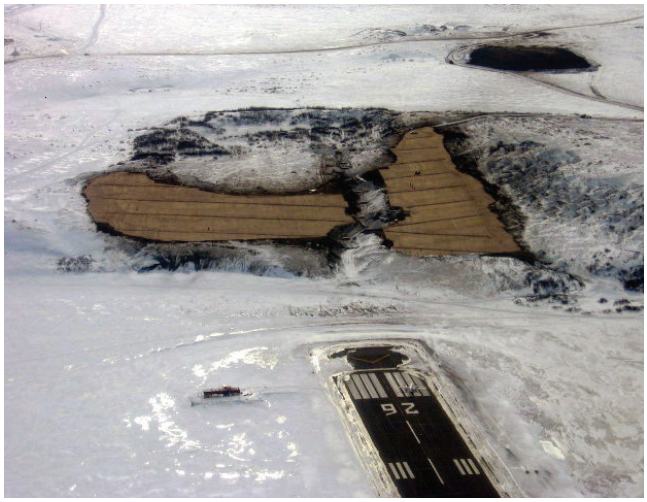

(7a) The top of a hill that extended into aircraft glidepaths was excavated to improve the approach to the runway. Synthetic matting (center brown areas) was placed on exposed permafrost to retard thaw and erosion and promote stabilizing plant growth.

(7b) Snow berm surrounding right side of ice-rich permafrost waste pile (shown in upper right of photograph [7a]).

(7c) Close-up view of newly-placed snow berm and ice-rich permafrost waste material behind snow berm.

(7d) Organic material contained in snow berm that remains after berm thaw (spring).

(7e) Organic remnants from thawed snow berm (summer). Note vegetation growth on waste pile.

Figure 7. Kotzebue runway improvement, April through August 2006 (all photographs from ADOT&PF file courtesy of S. Lamont). The purpose of project was to excavate the top of a hill that extended into the glidepath of aircraft (7a). During wintertime excavation of ice-rich materials in western Alaska, nearby snow may be the only choice of material available that can be piled up to provide retainment for excavated permafrost. Photographs 7b and 7c show the newly-constructed snow berm. The "snow" berm is actually composed of snow plus miscellaneous vegetation, soil, and rock detritus unavoidably included as the snow is collected. Photographs 7d and 7e show the berm after it progressed through a spring and summer's thawing. The vegetative matter in the berm is exposed and remains as the snow thaws. During thaw, the increasingly exposed vegetation and other non-snow materials helps shade and insulate the underlying remaining frozen berm. The retained (thawing) permafrost tended to stay in place as it and the berm thawed, suggesting the berm may not have provided appreciable retainment as expected.

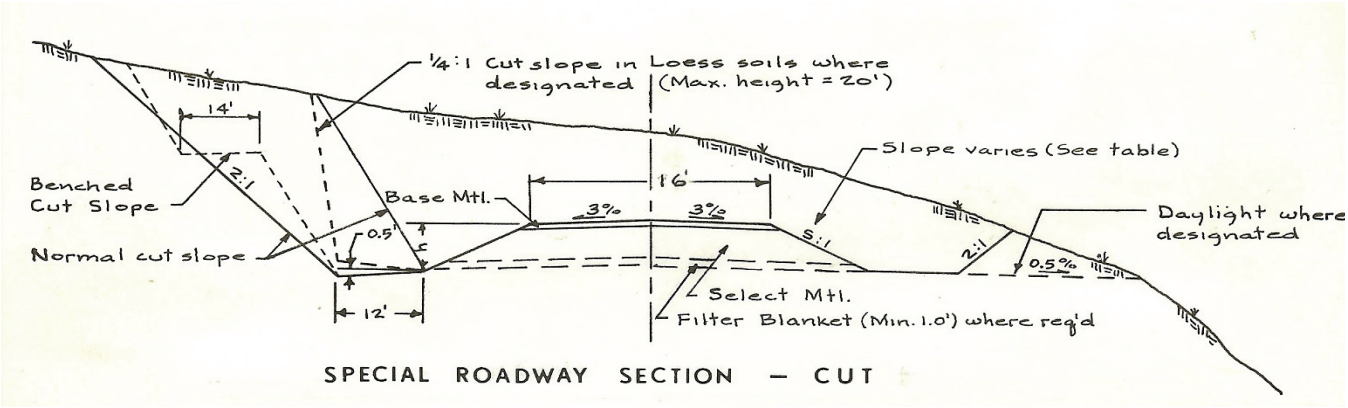

Figure 8. Original 1969 engineer's sketch of the procedure to be employed in a "special roadway section" defined as ice rich or massive ice cutslopes (after Rooney, pers. com.).

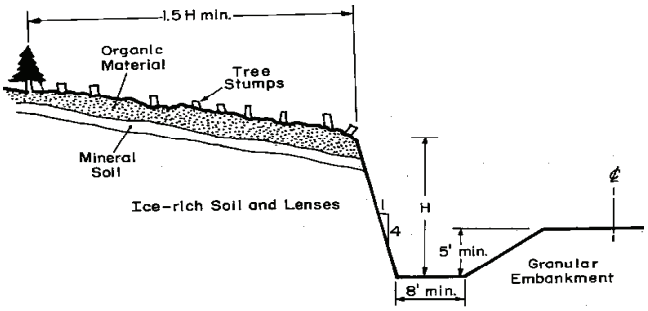

a. Initial frozen cut profile.

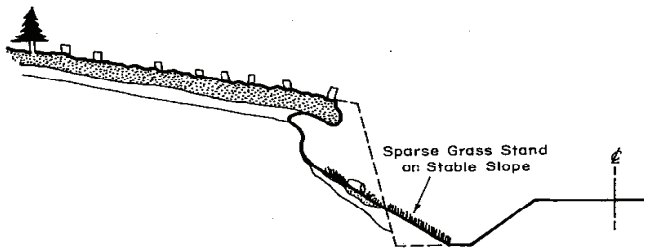

b. End of first thaw season. Slope is mostly unstable and very unsightly; ditch will require cleaning if massive ice is present.

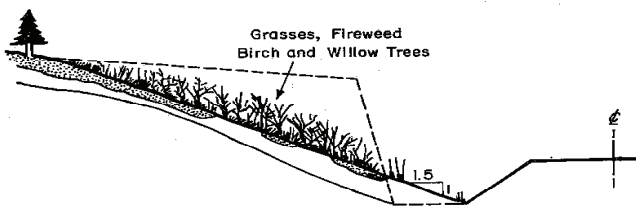

c. End of fifth or sixth thaw season. Slope stabilizes with reduced thaw and vegetation established. Free water from minimal thawing is used by plants whose root systems develop new organic material.

Figure 9. Idealized development of stability in ice rich cut (after Berg & Smith 1976).

Summary and Conclusions

At the present time engineers in Alaska do not possess a synthesis of design and construction methods to deal with the following:

- exposed and thawing ice-rich permafrost
- disposal of excavated ice-rich permafrost
- the use of permafrost to construct an embankment.

Increasing resource agency oversight requires evaluating all methods previously employed to address these problems, a number of which are reported herein, with respect to their environmental acceptability in addition to their engineering/constructability attributes. Best construction management practices will develop after a balance between reasonably attainable environmental goals and economical/practical engineering solutions is achieved.

Acknowledgments

Sam Lamont, John Ryer, Guan Griffin, Jesse Reinikainen, and Jeff Russell, ADOT&PF, Northern Region-Construction Section, provided the photographs and valuable insights into the history of the projects and issues described herein. Clint Adler, chief of research, ADOT&PF, provided the funding for the study through his office. The contribution of these individuals is gratefully acknowledged.

References

Berg, R. & Smith, M. 1976. *Observations along the Pipeline Haul Road between Livengood and the Yukon River.* US Army CRREL Special Report 76-11. Oct. 1976.

Rooney, J.W. 2006. Personal communication, Nov. 2006. Anchorage, AK: R & M Consultants, Inc.

Dissociation of Methane and Propane Gas Hydrates Formed on Water Droplets, at T<270 K

Vladimir P. Melnikov
Institute of Earth's Cryosphere SB RAS, Tyumen, Russia
Anatoly N. Nesterov
Institute of Earth's Cryosphere SB RAS, Tyumen, Russia
Aleksey M. Reshetnikov
Institute of Earth's Cryosphere SB RAS, Tyumen, Russia
Vladimir N. Feklistov
Institute of Earth's Cryosphere SB RAS, Tyumen, Russia

Abstract

Methane and propane hydrate formation on 0.15–2.0 mm water droplets and dissociation of the hydrate droplets were studied optically at 243–275 K. The instrument setup and the experimental procedure have been described. For the first time, the formation of liquid (supercooled) water during the hydrate dissociation was reliably detected in the temperature range of 253–270 K. The induction time for recrystallization of the metastable liquid water into ice varied from tens of hours at 270 K to a few seconds at 253 K. The dissociation pressure of the hydrates was measured, and the molar enthalpy of hydrate dissociation was calculated. In the temperature range of 253–270 K the molar enthalpy of dissociation for hydrates formed on the water droplets agrees well with the molar enthalpy of the bulk hydrate dissociation into water (liquid) and gas at T>273 K.

Keywords: dissociation; gas hydrates; ice; self-preservation, supercooled water.

Introduction

Detection of anomalously low rates of gas hydrate dissociation below the ice point (Davidson et al. 1986, Stern et al. 2001, Yakushev & Istomin 1992) is one of the most significant results on the kinetics of hydrate dissociation obtained in recent years. First observed under specific laboratory conditions, the gas hydrate dissociation rate decreased in some cases to zero, so the phenomenon was named the gas hydrate self-preservation effect (Yakushev & Istomin 1992). The effect is interesting not only from the viewpoint of basic research on the thermodynamics and mechanism of this phenomenon, but also from a practical perspective. Because of the effect, it is possible to store and transport natural gas in the gas hydrate form at a pressure of 1 atm and temperatures of 253–268 K (Gudmundsson et al. 2000). At present, such technologies are being developed in some countries, primarily in the USA, Norway, Japan, and England (Rogers et al. 2005). It is suggested also that due to the self-preservation effect, gas hydrates can exist in the upper layers of permafrost (at depths of 150–200 m) outside their thermodynamic field of stability as metastable (relic) gas hydrates (Dallimore & Collett 1995, Ershov & Yakushev 1992). Gas hydrate accumulations in permafrost can also cause incidents associated with drilling and production operations in the northern hydrocarbon fields. Because of permafrost thawing in response to global warming, there is a possibility that shallow, self-preserved gas hydrates could liberate methane gas to the atmosphere when they are decomposed.

It is supposed by some authors (Davidson et al. 1986, Yakushev & Istomin 1992) that the anomalously low hydrate dissociation rate is caused by the formation of an impermeable ice coating on the surface of hydrate particles, which develops in the initial stage of hydrate dissociation. However, the mechanism of ice formation and development of an impermeable ice coating on the hydrate surface is still poorly understood. We previously reported (Melnikov et al. 2003a, b) that during propane hydrate dissociation at 1 atm and T>270 K, metastable (supercooled) liquid water was formed initially, and then the water transformed into ice. Formation of the supercooled liquid during propane hydrate dissociation and its crystallization was visually observed. An indirect conclusion about methane hydrate dissociation into liquid (supercooled) water and gaseous methane was made, based on calculated data on the activation energy of methyl radical decay during isothermal annealing of γ-irradiated methane hydrates at 235–260 K (Takeya et al. 2005). It should be noted that Makogon (1981) first proposed the scheme of gas hydrate dissociation at T< 273 K as hydrate → liquid water → ice + gas, but reliable evidence for the process was not presented.

The purpose of this study is to obtain direct evidence of the formation of metastable (supercooled) water during gas hydrate dissociation at temperatures below 273 K. To do this, a special procedure of optical observation of hydrate dissociation was developed.

Experimental Apparatus and Procedure

A schematic of the experimental apparatus is shown in Figure 1. Its main element is a high-pressure reactor, within

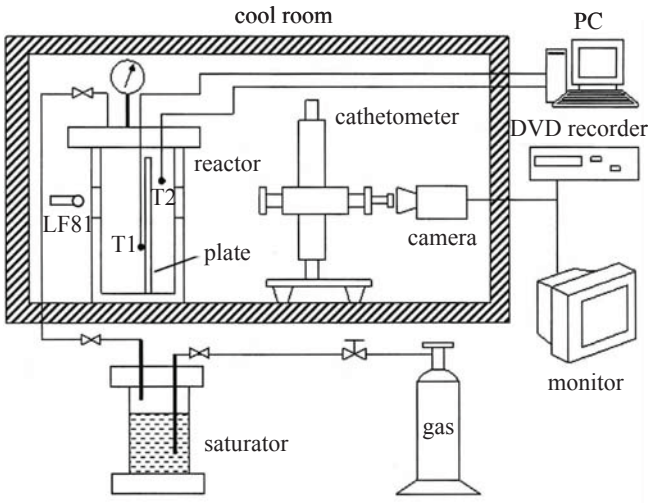

Figure 1. Experimental apparatus for study of hydrate formation/dissociation on water droplets. LF 81 – LED; T_1, T_2 – copper-constantan thermocouples.

which hydrates are formed and dissociate under controlled conditions. A reactor with a working volume of 100 cm^3 was made of stainless steel and equipped with quartz viewing windows on the side surface to facilitate visual observation of processes occurring within the reactor. The reactor was placed into the cool room (air thermostat) with a volume of 8 m^3 (2m x 2m x 2m). The temperature in the reactor was maintained to an accuracy of $\pm$0.1 K. A cathetometer was used for optical observation of hydrate formation/dissociation within the reactor. The ocular of the cathetometer telescope was joined with a Nikon Coolpix 995 digital camera. The image from the camera was displayed in parallel on the screen of a monitor and recorded by a DVD recorder. In this way we were able to make discrete pictures and a video film in a real time mode. Video capture and image analysis were performed using Pinnacle Studio Plus® v.10 and PhotoFinish® 4.0 software. Pure methane (99.9 mol.%) and propane (mol.%: C_2H_6 – 1.23, C_3H_8 – 94.27, C_4H_{10} – 4.13, $C_{5+higher}$ – 0.02, CO_2 – 0.35) were used as the hydrate forming gases.

The procedure to prepare the hydrate samples was as follows. Distilled water in the amount of 1.5–2.5 g was sprayed in the form of small droplets 0.15–1.5 mm in size on the surface of a transparent Plexiglas plate previously cooled to 253 K. It is well known that the hydrate formation induction time decreases when crushed ice or thawed ice is used for hydrate formation (Sloan 1998). Moreover, our numerous attempts to form propane hydrate directly from water droplets failed. Therefore, to obtain hydrates, we used the ice formed by freezing water droplets. All activities related to the assembly of the reactor, its evacuation and charging with hydrate-forming gas (about 3 atm for propane and 40 atm for methane) were carried out in the cool room at temperatures of 258–263 K. To increase the rate of hydrate formation, the reactor with pressurized gas and the frozen water droplets was heated above the ice melting point, because slow melting of the ice facilitates the hydrate forming reaction (Stern et al. 1996).

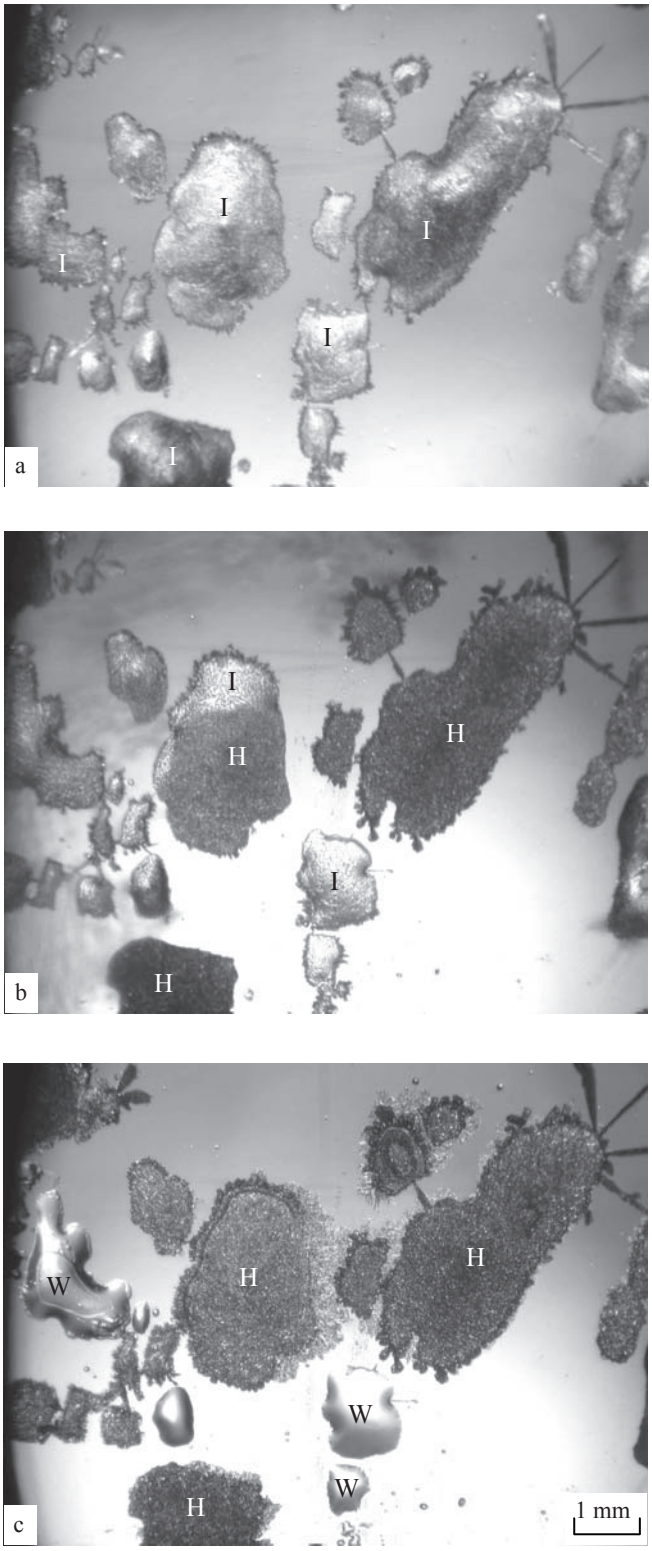

Figure 2. Propane hydrate growth on the ice surface (a-b) and appearance of water during melting of ice (c): a – 0 min(just before pressurization), P= 0 atm, T=258 K; b – 42 min, P=2.1 atm, T=270.0 K; c – 214 min, P=2.1 atm, T = 273.2 K. I-ice, H – hydrate, W –water.

Hydrate, ice, and water phases were distinguished by surface roughness and color (Fig. 2). The sample history and *P-T* conditions within the reactor were taken into account in addition to visual observation to identify the different phases observed in hydrate formation/ dissociation. Only the ice is presented in Figure 2a, where T=258 K, P=0 (just before the reactor was charged with propane). In Figure 2b (P=2.1 atm, T=270 K) the ice and propane hydrate, as well as the ice-hydrate boundary, are observed. On the monitor screen the hydrate surface looked rougher and darker. The ice-hydrate boundary corresponds to the propagation front of the gas hydrate film at the ice surface. Different mechanisms of ice surface coverage by a gas hydrate film were discussed by Genov et al. (2004). Monitoring movement of the ice-hydrate boundary at the ice surface, we were fortunate to measure the rate of the propane hydrate film propagation along the gas-ice interface. It was about 1 μm/s at P = 2.1 atm, T = 270 K, ΔT = 4 K. Here ΔT is supercooling, $\Delta T = T_{eq} - T$, where T_{eq} is the hydrate equilibrium temperature at the given pressure in the reactor. For comparison, the growth rate of the methane hydrate film along the methane-liquid water interface was about 40–100 μm/s at the same supercooling of ΔT = 4 K (Freer et al. 2001, Tailor et al. 2007). No data on the growth rate of a gas hydrate film at the ice surface have come to our notice.

Sometimes not all ice particles transformed into the hydrate, and when the temperature in the reactor increased above 273 K, the ice melt and water droplets appeared (Fig. 2c). At the same time an elevated pressure within the reactor provides the hydrate stability and additional hydrate formation. Because we used a small amount of water within the reactor, the pressure drop during the gas hydrate formation was insufficient to reliably estimate the amount of water converted into hydrate. Therefore the freezing/melting procedure (cooling of the reactor to 265 K and its heating to 273.5K) was repeated 4–5 times to provide a maximum of water conversion into gas hydrates.

To observe the dissociation of gas hydrates, a specified temperature was set in the cool room, and the reactor was kept at this temperature for another 2 h. Then, the pressure in the reactor was slowly reduced (0.05 atm/min for propane hydrate and 0.1 atm/min for methane hydrate). The dissociation of the hydrates was judged from the visually observed collapse of the rough surface of the hydrates, the appearance of smooth islands of the liquid phase on hydrate particles, and evolution of gas bubbles from the liquid. The pressure at which the first changes in hydrate particles were visually observed was taken as the hydrate dissociation pressure P_d at the given temperature. Once the hydrates begin to dissociate, the reactor valve was closed, and the pressure drop in the reactor was stopped.

Results and Discussion

Results describing the dissociation pressure for methane and propane hydrates formed on water droplets are shown in Figure 3. For comparison, the equilibrium pressure of hydrate formation for methane and propane bulk hydrates, P_{eq}, obtained in the control experiments and calculated by the CSMHYD program (Sloan 1998) are presented as well. In ln P – 1/T coordinates, the curve of the equilibrium pressure of gas hydrate formation $P_{eq} = P_{eq}(T)$ consists of two intersecting straight lines corresponding to water–hydrate–gas and ice–hydrate–gas equilibrium. The slope of these lines to the inverse temperature axis characterizes the molar enthalpy of hydrate dissociation into water and gas ΔH_{hwg} (hydrate (h) = water (w) + gas (g)) at T > 273 K and into ice and gas ΔH_{hig} (hydrate (h) = ice (i) + gas (g)) at T < 273 K (Sloan 1998)

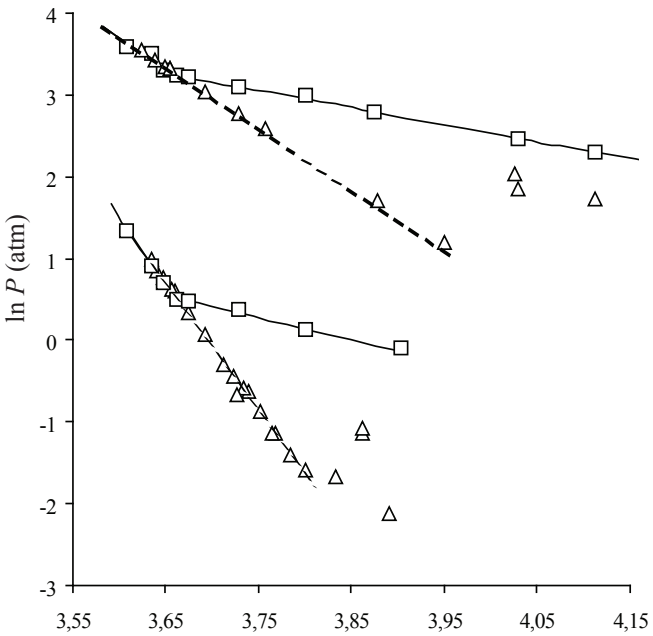

Figure 3. Dissociation pressure of gas hydrates, formed on water droplets (triangle), and equilibrium pressure of formation of bulk hydrates (square). The solid line is calculated data by the CSMHYD program. The dash line is the extension of the calculated water-hydrate-gas equilibrium curve into the metastable area.

$$\Delta H_{hwg(hig)} = - zR \frac{d(\ln P_{eq})}{d(1/T)} \quad (1)$$

where z is the compressibility factor for gas and R is the universal gas constant.

At temperatures above 273 K, the hydrate dissociation pressure P_d coincides with the equilibrium pressure of gas hydrate formation P_{eq} (Fig. 3). At 263 K<T<273 K for propane hydrate and 253 K<T<273 K for methane hydrate the values of ln P_d fall on a straight line (the regression coefficient is r^2=0.995) which coincides with the extension of the water–hydrate–gas equilibrium curve in the metastable area of supercooled water. This means that, at T <273 K the molar enthalpy of dissociation for hydrates formed on water droplets is equal to the molar enthalpy of hydrate dissociation into water(liquid) and gas for bulk hydrate. The experimental data on P_d and Equation 1 were used to calculate the molar enthalpy for the dissociation of methane

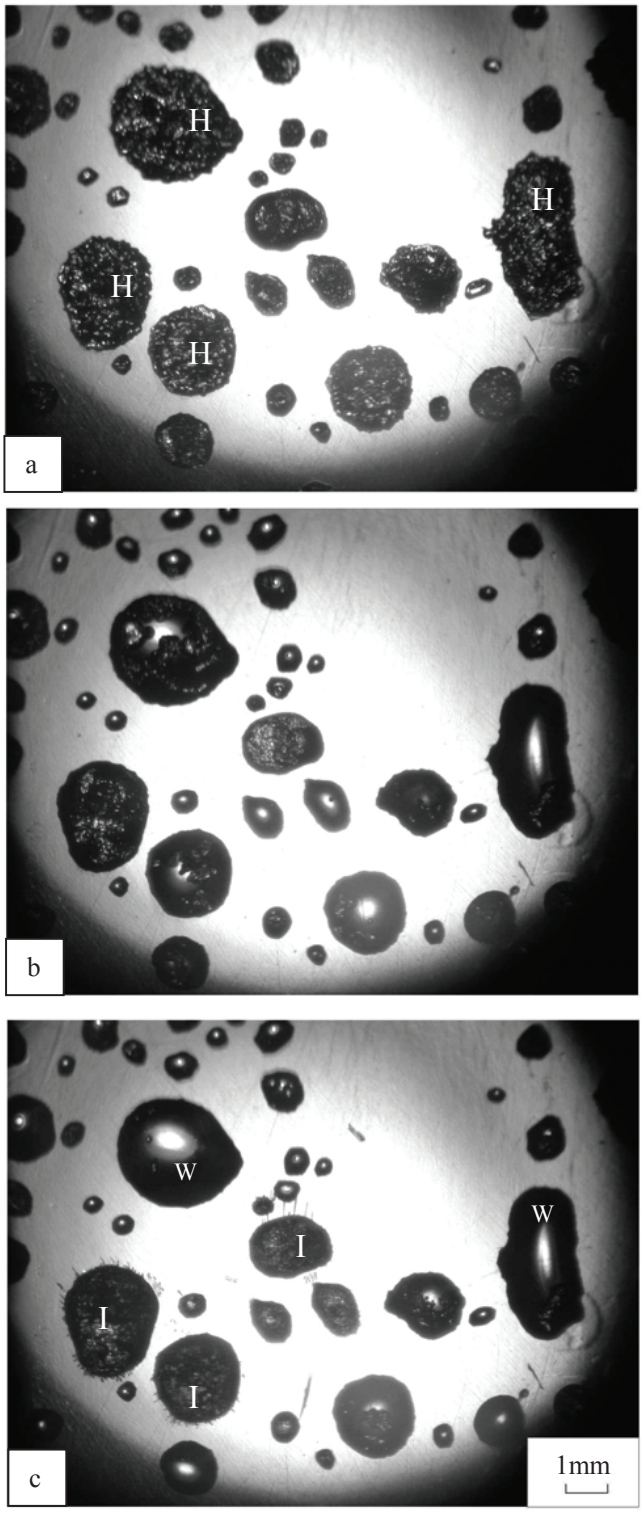

Figure 4. Dissociation of propane hydrates formed on water droplets. P_d = 0.54 atm, T = 267.9 K. a – 0 min (at the beginning of dissociation); b – 62 min; c – 89 min.

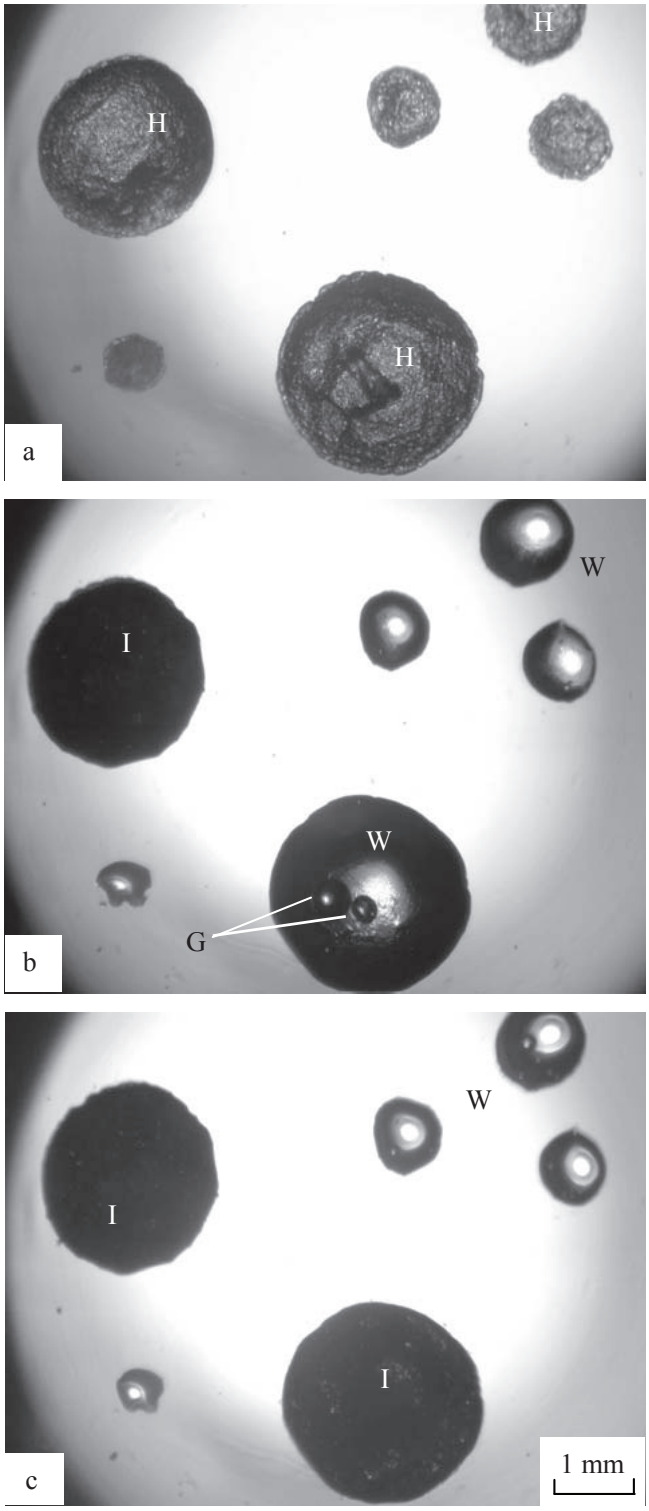

Figure 5. Dissociation of methane hydrates formed on water droplets. P_d = 9.9 atm, T = 263.15 K. a – 0 min (at the beginning of dissociation); b – 1 min; c – 115 min. G – gas bubble.

and propane hydrates formed on water droplets, into supecooled water and gas at T<273 K. The compressibility factor z was calculated with the Peng-Robinson equation of state (Peng & Robinson 1976). The calculated values are: ΔH_{hwg} = 54.6 kJ/mol for the methane hydrate dissociation into supercooled water and methane gas and ΔH_{hwg} = 128.9 kJ/mol for the propane hydrate dissociation into supercooled water and propane gas. The calculated values agree well with the molar enthalpy of hydrate dissociation into water and gas for bulk methane hydrate ΔH_{hwg} = 54.6 kJ/mol and bulk propane hydrate ΔH_{hwg} = 129.2 kJ/mol (Handa 1986). Hence the liquid phase detected visually in our experiments

at $T < 273$ K during dissociation of hydrates formed on water droplets is nothing more nor less than supercooled water.

The consecutive series of visually detected changes occurring at 267.9 K during dissociation of propane hydrates formed on water droplets is shown on Figure 4. The zero time (Fig. 4a) immediately precedes the first changes of the image observed. By this time the pressure in the reactor had decreased to 0.54 atm and remained steady at that value. Only the hydrate phase is present in Figure 4a. After one hour of observation (Fig. 4b) small water droplets(size 0.2–0.3 mm) had formed on the hydrate as well as large droplets (1–2 mm) composed of both the liquid water phase and hydrates. It is interesting to note that the presence of the hydrate within the water droplets did not stimulate heterogeneous crystallization of the supercooled water. Only after 67 minutes from the onset of the hydrate dissociation, some (but not all) of the larger water droplets transformed into ice. In this case we observed that the droplets froze instantly in contradistinction to the terminal growth rate of hydrate on the ice surface (Fig. 2). However, the greater number of the small water droplets and some of the large water droplets did not freeze even 1.5 hours after the onset of the hydrate dissociation (Fig. 4c). When the reactor was heated above 273 K, the melting of the recrystallized water droplets was observed at 273.1±0.1 K.

The formation of metastable (supercooled) water during propane hydrate dissociation was reliably detected between 263 K and 273 K. In this temperature range, the transformations observed within the reactor were analogous to those presented in Figure 4, and values of the hydrate dissociation pressure P_d in all cases fell on the extension of the water–hydrate–gas equilibrium curve into the metastable area of the supercooled water at T<273.15 K, (Fig. 3).

Similar transitions were observed during methane hydrate dissociation at 253.15–273.15 K, (Fig. 5). Based on the *P-T* sample history (before cooling to 263.15 K, the reactor was heated to 274 K at 40 atm and no water droplets were observed, only the solid droplets) we can advocate that only the hydrates are presented in Figure 5a. The small liquid droplets along with the large droplet composed of the liquid phase, the solid and the gas bubbles, as well as the large dark solid droplet are observed in Figure 5b. In Figure 5c we can see the liquid droplets and two dark solid droplets. When we heated the reactor, we observed the melting of the dark solid droplets at the ice melting point. It follows that the dark solid droplets in Figures 5b and 5c were the ice.

A detailed study on the influence of the hydrate dissociation temperature on the induction time for the crystallization of supercooled water released during hydrate dissociation was not conducted in this work. Nevertheless, it follows from the data obtained that the induction time decreases with the decreasing temperature. For example, at temperatures close to the freezing point (269–270 K) none of the water droplets formed during hydrate dissociation had crystallized to ice within 24 hours of the observation.

Below 263 K for propane hydrates and 253 K for methane hydrates, the dissociation pressures P_d were higher than the P_d values corresponding to extension of the equilibrium

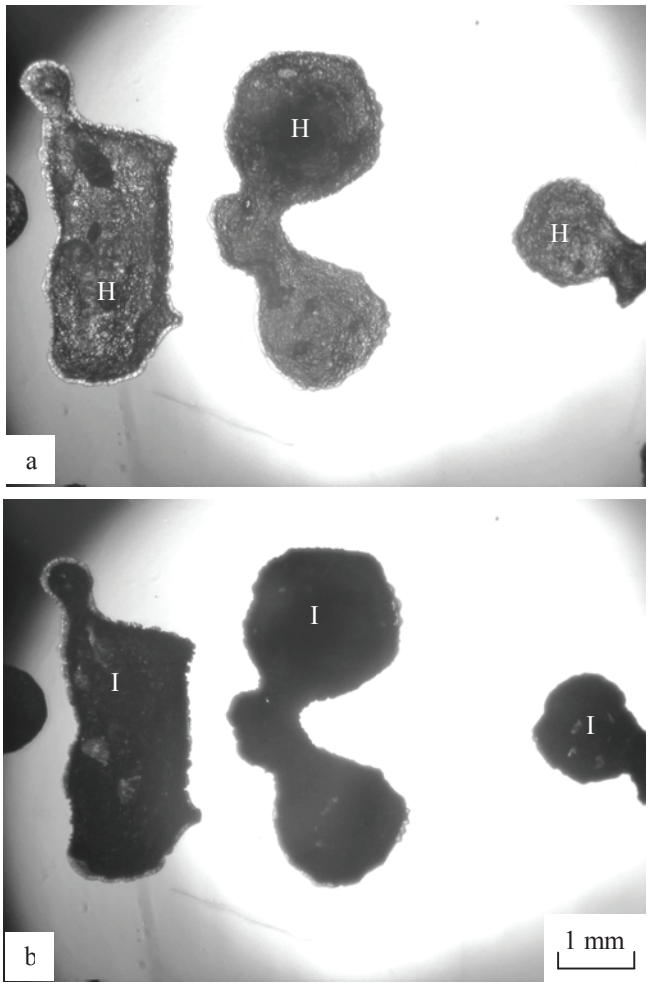

Figure 6. Dissociation of methane hydrates formed on water droplets. P_d = 5.64 atm, T = 243.15 K. a – 0 min (at the beginning of dissociation); b – 8 min.

curve for water–hydrate–gas in the metastable area of supercooled water (Fig. 3). The reasons for this deviation are still unclear. Appearance of the liquid phase was observed during propane hydrate dissociation below 263 K, however the induction time for its subsequent solidification did not exceed a few seconds. In the experiments with methane hydrates, only changes in the color of the hydrate samples were observed during the hydrate dissociation at T<253 K, whereas a distinct liquid phase was not observed (Fig. 6). Eight minutes from the beginning of the dissociation, no changes were observed within the reactor at 5.64 atm and 243.15 K. Because the dark solid droplets, formed during the methane hydrate dissociation (Fig. 6b) melted to liquid at 273.15 K, we have concluded that they were composed of water ice.

Conclusions

Visual observations of gas hydrate formation on water droplets and their dissociation at temperatures below 270 K were made. Direct optical evidence of the formation of metastable(supercooled) water during hydrate dissociation (between 257–270 K for propane hydrates and between

253–270 K for methane hydrates) were obtained for the first time. The induction time for recrystallization (freezing) of this supercooled water ranged from tens of hours at 270 K to a few seconds at 257 K. The dissociation pressures of gas hydrates formed on water droplets were measured. Molar enthalpies for the dissociation of these hydrates (into supercooled water and gas) were calculated based on the experimental pressure data. In the range of 263–273 K for propane hydrates and 253–273 K for methane hydrates, the calculated molar enthalpies are in good agreement with the enthalpies of dissociation of bulk propane hydrates and methane hydrates into water and gas at T>273.15 K. The data obtained supplement our knowledge about the mechanism of the gas hydrates self-preservation effect and the possibility of the existence of metastable (relict) gas hydrates within permafrost due to this effect.

Acknowledgments

This work was supported by the Russian Foundation for Basic Research (project no. 07-05-00102) and the Program for Basic Research of the Presidium of the RAS (project no.16.4.2). The authors are very grateful to Fred Wright from the Geological Survey of Canada and to an anonymous reviewer, who have improved the paper.

References

Dallimore, S.R. & Collett, T.S. 1995. Intrapermafrost gas hydrates from a deep core hole in the Mackenzie Delta, Northwest Territories, Canada. *Geology* 23(6): 527-530.

Ershov, E.D. & Yakushev, V.S. 1992. Experimental research on gas hydrate decomposition in frozen rocks. *Cold Region Sciences and Technology* 20: 147-156.

Freer, E.M., Selim, M.S. & Sloan, E.D. 2001. Methane hydrate film growth kinetics. *Fluid Phase Equilibria* 185: 65-75.

Davidson, D.W., Garg, S.K., Gough, S.R., Handa, Y.P., Ratclife, C.I., Ripmeester, J.A., Tse, J.S. & Lawson, W.F. 1986. Laboratory analysis of a naturally occurring gas hydrate from sediment of the Gulf of Mexico. *Geochimica et Cosmochimica Acta* 50: 619–623.

Genov, G., Kuhs, W.F, Staykova, D.K., Goreshnik, E. & Salamatin, A.N. 2004. Experimental studies on the formation of porous gas hydrates. *American Mineralogist* 89: 1228-1239.

Gudmundson, J.S., Andersson, V., Levik, O.I. & Mork, M. 2000. Hydrate technology for capturing stranded gas. *Annals of the New York Academy of Sciences* 912: 403-410.

Handa, Y.P. 1986. Compositions, enthalpies of dissociation, and heat capacities in the range 85 to 270 K for clathrate hydrates of methane, ethane, and propane, and enthalpy of dissociation of isobutene hydrate, as determined by heat-flow calorimeter. *Journal of Chemical Thermodynamics* 18: 915-921.

Makogon, Yu.F. 1981. *Hydrate of Natural Gas*. Tulsa: PennWell Books, 237 pp.

Melnikov, V.P., Nesterov, A.N. & Reshetnikov, A.M. 2003a. Kinetic of hydrate dissociation at a pressure of 0.1 MPa. In: M. Phillips, S.M. Springman & L.U. Arenson (eds.), *Permafrost*. Lisse: Swets & Zeitlinger, 753-757.

Melnikov, V.P., Nesterov, A.N. & Reshetnikov, A.M. 2003b. Mechanism of gas hydrate decomposition at a pressure of 0.1 MPa. *Doklady Earth Sciences* 389A: 455-458.

Peng, D. & Robinson, D.B. 1976. A new two-constant equation of state. *Industrial & Engineering Chemistry Fundamentals* 15: 59-64.

Rogers, R.E., Zhong, Y., Arunkumar, R., Etheridge, J.A., Pearson, L.E., McCown, J. & Hogancamp, K. 2005. Gas hydrate storage process for natural gas. *GasTIPS* 11: 14-19.

Sloan, E.D. 1998. *Clathrate Hydrates of Natural Gases*. Sec. ed. New York: Marcel Dekker, 705 pp.

Stern, L.A., Kirby, S.H. & Durham, W.B. 1996. Peculiarities of methane clathrate hydrate formation and solid-state deformation, including possible superheating of water ice. *Science* 273: 1843-1848.

Stern, L.A., Circone, S., Kirby, S.H. & Durham, W.B. 2001. Anomalous preservation of pure methane hydrate at 1 atm. *Journal of Physical Chemistry. B.* 105: 1756-1762.

Takeya, K., Nango, K., Sugahara, T. & Ohgaki, K. 2005. Activation energy of methyl radical decay in methane hydrate. *Journal of Physical Chemistry. B.* 109: 21086-21088.

Taylor C.J., Miller, K.T., Koh, K.A. & Sloan, E.D. 2007. Macroscopic investigation of hydrate film growth at the hydrocarbon/water interface. *Chemical Engineering Science* 62: 6524-6533.

Yakushev, V.S. & Istomin, V.A. 1992. Gas-hydrate self-preservation phenomenon. In: N. Maeno & T. Hondoh (eds.), *Physics and Chemistry of Ice*. Sapporo: Hokkaido University Press, 136-139.

Experimental Research on Physical-Mechanical Characteristics of Frozen Soil Based on Ultrasonic Technique

Qingzhou Meng
State Key Laboratory of Frozen Soil Engineering, CAREERI, CAS, Lanzhou 730000, Gansu, China
Dongqing Li
State Key Laboratory of Frozen Soil Engineering, CAREERI, CAS, Lanzhou 730000, Gansu, China
Jin Chen
State Key Laboratory of Frozen Soil Engineering, CAREERI, CAS, Lanzhou 730000, Gansu, China
Anhua Xu
Highway Research and Survey Design Institute of Qinghai Province, Xining, 810008, Qinghai, China
Shijing Huang
Highway Research and Survey Design Institute of Qinghai Province, Xining, 810008, Qinghai, China

Abstract

The research on frozen soil physical and mechanical characteristics has become a gradual focus in recent years. Traditionally, researchers take soil samples from the field and test their physical-mechanical characteristics in a laboratory using traditional universal testing apparatus. Although much useful data can be gained in this way, it is still time-intensive and uneconomical. The ultrasonic technique is an effective method to test physical-mechanical characteristics and is less expensive than traditional methods. According to the classical wave theory**,** there is a clear correlation between wave velocity and the medium characteristics. If we know the behavior of ultrasonic pulses in frozen soil, we will be able to obtain its physical-mechanical characteristic. In this article, the authors tested the ultrasonic pulses behavior in Lanzhou loess by RSM-SY5 ultrasonic apparatus. The results show clear correlation between frozen soil characteristics and ultrasonic behavior. From the results, the velocity of ultrasonic energy clearly increases with the decrease of temperature, and the change is especially prominent when the temperature exceeds -5°C. We also observed that the ultrasonic velocity increases with an increase in water content at the same temperature for the reason that ice content in frozen soil changes along with the water content. Based on the elasticity and laboratory test results, the dynamic properties of frozen soil can be determined. We conclude that the ultrasonic technique is a promising method that can substitute for traditional apparatus to test frozen soil characteristics.

Keywords: elastic modulus; frozen soil; physical characteristics; Poisson's ratio; shear modulus; ultrasonic velocity.

Introduction

The investigation on the physical-mechanical characteristics of frozen soil, along with the freezing consolidation in geotechnical engineering applications and the extensive development of the cold region, is currently a hot topic in the field of frozen soil. The present methodology, however, is labor-intensive because the researcher usually takes soil specimens from the field site and then tests them in the lab. According to classical wave theory, there is a close affinity between wave velocity and the physical-mechanical parameters of the propagating medium. Thus, if we can adopt ultrasonic detection, a simple and speedy method, to determine characteristics of frozen soil, it would be a significant work. In this article, in order to meet the need of rapid detection at the field site, the authors use the domestic RSM-SY5 ultrasonic apparatus to test the physical and mechanical properties of frozen soil. The results tend to summarize the relationship between wave velocity and the physical-mechanical properties of frozen soil.

Theory Basis of Ultrasonic Measurement

A certain point in the elastic medium is initially vibrated using an external or internal force. The vibration leads to wave formation and transmission in the medium. As an elastic wave, the process of a sonic wave transmission in the medium is a course of the transmission of the particle's elastic vibration. According to elastic mechanics, in an infinite medium, when the body force is neglected, we get the Lamei–Navier equation as follows:

$$Gu_{i,jj} + (\lambda + G)u_{j,ji} = \rho \ddot{u}_i \tag{1}$$

where ρ is the medium density, u represents the particle's displacement, and λ and G are Lamei coefficient.
When x_m is demanded to make partial derivative in Equation (1), we have:

$$Gu_{i,jjm} + (\lambda + G)u_{j,jim} = \rho \ddot{u}_{i,m} \tag{2}$$

In Equation (2), we contract the tensor's subscripts, i and m , and we note that volumetric strain θ is equal to $u_{i,i}$, so we have:

$$V_p{}^2 \theta_{,jj} = \ddot{\theta} \tag{3}$$

where

$$V_p = \sqrt{\frac{\lambda + 2G}{\rho}} \tag{4}$$

Equation (3) is a wave equation, and it means that the velocity of volumetric strain in the medium is V_P; Equation (4) is the expression of transmission's velocity. If the coefficients λ and G are substituted by E and μ, we obtain:

$$V_p = \sqrt{\frac{E(1-\mu)}{\rho(1+\mu)(1-2\mu)}} \tag{5}$$

Exchanging the subscripts in Equation (2), we have:

$$Gu_{m,jji} + (\lambda + G)u_{j,jmi} = \rho\ddot{u}_{m,i} \tag{6}$$

According to strain analysis, the expression for the rotated tensor is:

$$\Omega_{im} = \frac{1}{2}(u_{m,i} + u_{i,m}) \tag{7}$$

Subtracting Equation (7) from (6), we obtain the expression of the rotated tensor that should meet the equation below:

$$V_s{}^2\Omega_{im,jj} = \ddot{\Omega}_{im} \tag{8}$$

$$V_s = \sqrt{\frac{G}{\rho}} \tag{9}$$

Equation (8) is the rotation part of the strain and means that, in the medium, strain transmission velocity is V_s. Equation (9) is the expression for the transverse waves. Employing E and μ to express Equation (9), we obtain:

$$V_s = \sqrt{\frac{E}{2\rho(1+\mu)}} \tag{10}$$

When the characteristic of the transmission of supersonic in the medium is obtained, we could measure the dynamical coefficients of the medium, such as E, G, μ and :

$$\left.\begin{aligned} E &= \frac{\rho V_s{}^2(3V_p{}^2 - 4V_s{}^2)}{V_p{}^2 - 2V_s{}^2} \\ G &= \rho V_s{}^2 \\ \mu &= \frac{V_p{}^2 - 2V_s{}^2}{2(V_p{}^2 - V_s{}^2)} \end{aligned}\right\} \tag{11}$$

where E is elastic modulus, G is shear modulus, and μ is Poisson's ratio.

From Equations (4) and (9), we know that the elastic wave velocity is determined by the characteristic of the medium and that, when the medium changes, the velocity is also changed. On the contrary, if the medium density and the characteristic of sonic transmission are known, we can derive the dynamic coefficients of the medium. Thus, we can employ the material's ultrasonic characteristics to analyze the medium's physical characteristics and to measure the material's dynamical coefficients such as the dynamic elastic modulus and the Poisson ratio. Although frozen soil cannot be considered as a completely elastic material, its elastic characteristic improves under comparative low temperature and, under the same stress level, the strain decreases with a reduction of the environmental temperature. The elastic strain is the most part one when the temperature is deceasing and therefore we can obtain the physical-mechanical characteristic of frozen soil by analyzing the transmission characteristics of supersonic in the frozen soil.

Table 1. Physical parameters of Lanzhou loess.

Grain component (%)			ω_p (%)	ω_L (%)
> 0.075mm	0.025 ~0.075	< 0.025mm		
10.04	48.17	41.58	14.92	29.36

Experimental Methodology

Specimen preparation

The material used in the experiment was Lanzhou loess; its main physical parameters are as follows:

In order to ensure sample uniformity, which can ensure the comparability of the experimental results, we employ a remodeling artificial freezing method to produce the sample. First, undisturbed soil is dried, pulverized, and sifted. We then test the initial water content and subsequently beat up loess uniformly. After that, we load the soil sample into a columned mould with a diameter of 61.4 mm and height of 125 mm and then compact the sample. Second, we put the soil sample into a temperature-controlled refrigerator and remove the mould after 24 hours of freezing. The quantity, height, and diameter of each sample is precisely tested. Last, we place the sample in a temperature-controlled refrigerator and freeze it under required temperature. In addition, in the course of producing the sample, we reassure that at least three samples with the same water content are made.

The introduction of the ultrasonic system

The ultrasonic system used in this experiment consists of ultrasonic transducers and ultrasonic apparatus. The transducer, with a working frequency of from 20 kHz to 50 kHz, is a ceramic transducer. The ultrasonic apparatus, made in the Institute of Rock and Soil Mechanics, Chinese Academy of Science, is a RSM-SY5 digital unit. It has a visualized interface and is easy to operate. Meanwhile, the data can be accessed and refreshed, and the transmit time and amplitude can be identified.. A picture of the ultrasonic system is showed in Figure 1.

Figure 1. Ultrasonic system.

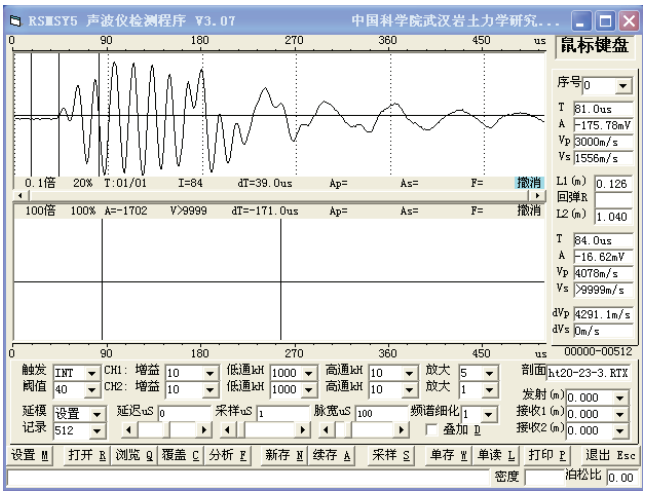

Figure 2. Screen shot of the ultrasonic software display.

Ultrasonic measurement procedure

At first, specimens were held for about 24 hours under a given testing temperature in the temperature-controlled refrigerator before it was tested. It was then placed into a thermostat tank, where the transmitting transducer and the receiving transducer were firmly pressed onto the end of the specimen. We should note here that good acoustical coupling between the soil sample surface and the face of the transducers is essential, as the ultrasonic waves cannot pass through air gaps between the transducer and the specimen. In this study, petroleum jelly was used as coupling media to improve the bonding between the transducers and the frozen soil specimen for compression wave and shear wave transmission. Finally, it sends an electric pulse (using a pulse generator) at a desired interval to both the transmitter on the end of the sample and the computer. This signal simultaneously triggers the computer to record and excites the transmitting transducer to vibrate at a frequency of 50 kHz. The vibration propagates through the frozen soil sample and arrives at the other end, where it is reconverted into an electrical signal by the receiving transducer. The operation is repeated many times. The wave travel time is determined by the time of the wave application and the time of wave arrival at the opposite end of the sample. The velocities of the waves were obtained as the quotient of the travel path to the wave travel time.

Experimental Results and Analysis

Both temperature and water content are important factors influencing the strength of frozen soils. In this research, the ultrasonic wave velocity in frozen soil at seven different temperatures and four different water contents was tested. From this experiment, we can infer the relationship between them.

Dilatational and shear wave velocity

The test results were shown in Figures 3 and.4 as follow. From the results, the velocity of ultrasonic wave was clearly increased with the decrease of temperature, and the change is especially prominent when the temperature exceeds -5°C. The reason is that the unfrozen water content became progressively smaller with the gradual reduction in temperature and the simultaneous increase of close-contact ice, intensified ice itself. From these figures we also can see that the ultrasonic velocity increased with the increase in water content at the same temperature; the reason is that the ice content in frozen soil changes along with the water content. If the water content is small, the ultrasonic velocity is largely determined by the contact condition of the soil grains; however, when the water content is large, the increased density of frozen soil will be helpful to the transmission of ultrasonic energy.

Dynamical parameters

If we take the frozen soil as an isotropic medium, dynamic modulus may be determined for frozen soil from a knowledge of the velocities of dilatational and shear waves. Hence, the dynamic elastic modulus E, dynamic shear modulus G and Poisson's ratio μ can be calculated as follows:

$$\begin{cases} E = \dfrac{\rho V_s^2 (3V_p^2 - 4V_s^2)}{V_p^2 - 2V_s^2} \\ G = \rho V_s^2 \\ \mu = \dfrac{V_p^2 - 2V_s^2}{2(V_p^2 - V_s^2)} \end{cases}$$

where V_p is velocity of the dilatational wave, V_s is velocity of the shear wave, ρ is density of the specimen.

Based on the formulas mentioned above and the laboratory test results, the dynamic properties of frozen soil can be determined. The results are presented in the following figures.

As seen in the figures, the dynamic elastic modulus and the dynamic shear modulus increase with a reduction in temperature. The variation trend of the dynamic modulus with the temperature reduction is in agreement with results

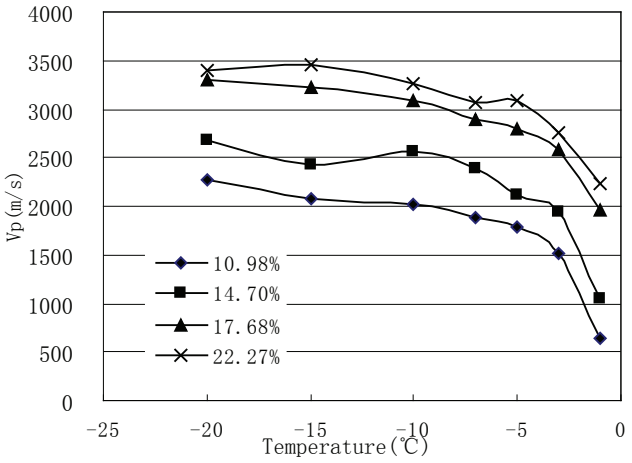

Figure 3. Relationship between temperature and compression wave velocity.

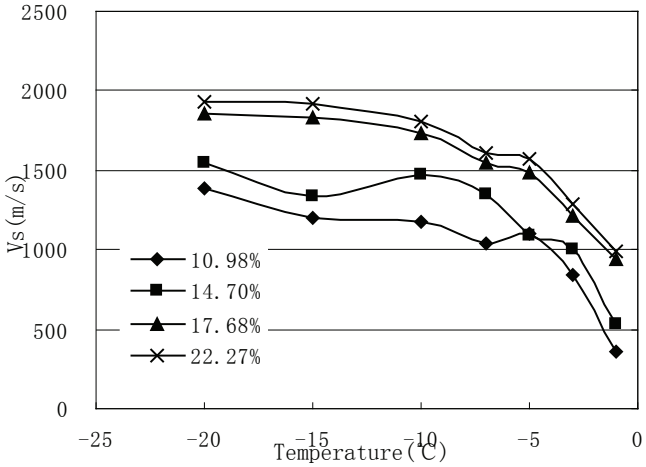

Figure 4. Relationship between temperature `and shear wave velocity.

obtained by a traditional universal test machine. The dynamic modulus has a close relation with water content such that the larger the water content, then the bigger the dynamic modulus. Compared with a universal material test machine, Poisson's ratio can be easily obtained by the ultrasonic apparatus. We can see from Figure 7 that, when the temperature increases, Poisson's ratio increases accordingly.

Conclusion

The wave velocity of ultrasonic energy in frozen soil decreases with temperature rising and increases with water content rising. Such velocity reflects the dynamical properties of frozen soil. Thus, using ultrasonic technology, we can instantly detect the dynamical coefficients of frozen soil. Furthermore, by this investigation method, we find that ultrasonic parameters can be used to estimate the mechanical properties of frozen soil. Therefore, in freezing consolidation and engineering construction in cold regions, in order to provide a powerful guarantee to such engineering, we can promptly test the mechanical properties of frozen soil at the site by ultrasonic techniques.

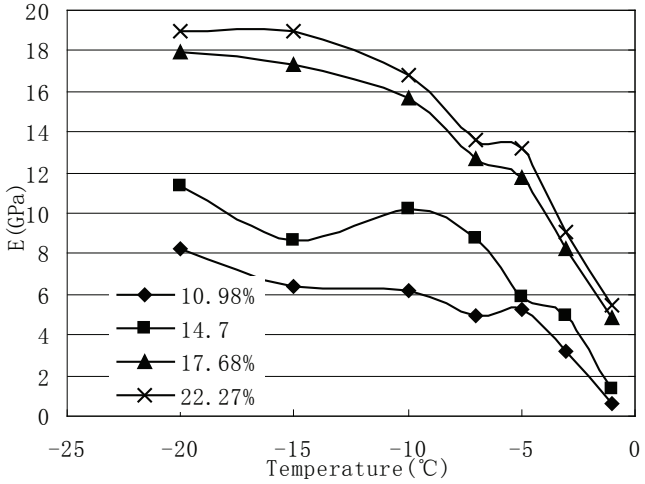

Figure 5. Relationship between temperature and dynamic elastic modulus.

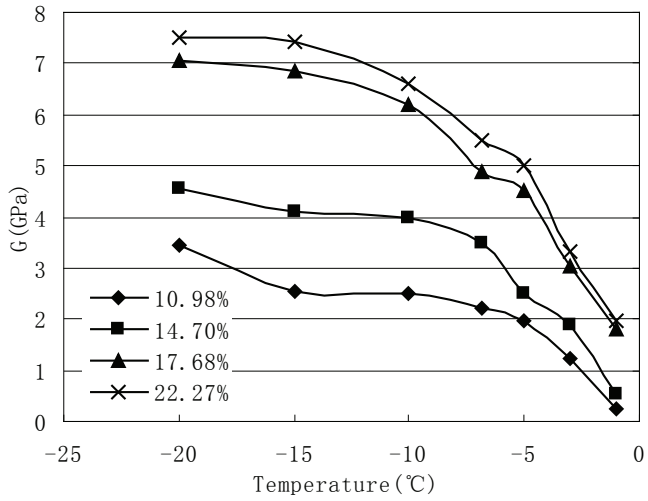

Figure 6. Relationship between temperature and dynamic shear modulus.

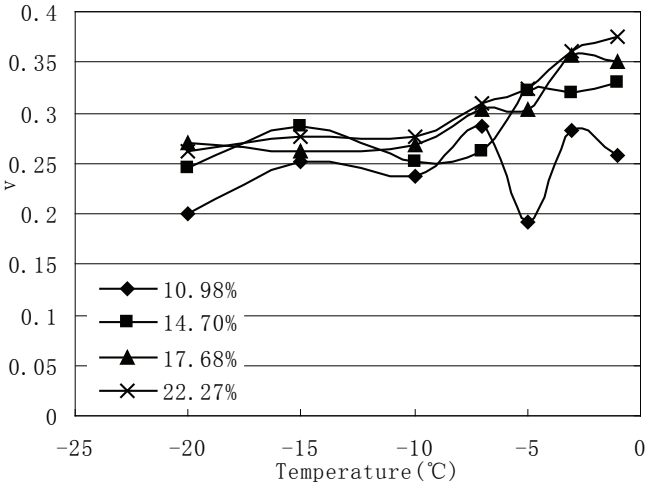

Figure 7. Relationship between temperature and Poisson's ratio.

Acknowledgments

This research was supported by the National Natural Science Foundation of China (No.40671039), the talent project of Cold and Arid Regions Environmental and Engineering Research Institute (No.2004122), the grant of the Knowledge Innovation Program of the Chinese Academy of Sciences (No.KZCX3-SW-351) and the key project of NSFC (No.40730736).

References

Lu Mingwan & Luo Xuefu. 2001. Foundations of Elasticity [M]. Beijing: Tsinghua University Press.

Ma Qin-Yong. 1998.Wave Velocity and Blast Ability Test on Artificially Frozen Soils [J]. *Journal of Glaciology and Geocryology.*

Sheng Yu, Fukuda Masami, Kim Hakasam & Imamura Tohru. 2000. Effect of unfrozen water content on the ultrasonic velocities in tire-mixed frozen soils [J]. *Chinese Journal of Geotechnical Engineering*.

Wu Shiming & Chen Longzhu.1989. Propagation velocities of elastic waves in saturated soils [J]. *Applied Mathematics and Mechanics.*

Effects of Retrogressive Thaw Slumps on Sediment Chemistry, Submerged Macrophyte Biomass, and Invertebrate Abundance of Upland Tundra Lakes

P.S. Mesquita
Water and Climate Impacts Research Centre, Department of Geography, University of Victoria, Victoria, Canada
F.J. Wrona
Water & Climate Impacts Research Centre, Environment Canada, Department of Geography, University of Victoria, Canada
T.D. Prowse
Water & Climate Impacts Research Centre, Environment Canada, Department of Geography, University of Victoria, Canada

Abstract

Global warming is forecasted to cause significant thawing of the permafrost that surrounds lakes and rivers across the Arctic, with wide-scale effects on the water quality and biotic characteristics of these water bodies. The benthic environment is believed to be especially sensitive to permafrost-induced ecological change, and this has been the focus of recent field-intensive research. Five lakes affected and three lakes not affected by retrogressive thaw slumps were sampled during late summer of 2006 to assess the potential effects of slumping on benthos. Water quality parameters, submerged macrophytes, benthic invertebrates, and sediment were collected. GLM, Kruskal-Wallis, and ANOVA were used to test for differences between both groups, as well as for possible interaction effects from sample depth. A significant difference ($p<0.05$) between disturbed and undisturbed lakes was found for macrophyte, invertebrates, underwater light attenuation, and some sediment variables. The results suggest that thaw slumps can affect the freshwater food-web through an increase in benthic production.

Keywords: invertebrates; macrophytes; permafrost retrogressive thaw slumping; sediment chemistry; tundra lakes.

Introduction

The arctic region has been predicted to be especially sensitive to the impacts of global warming (ACIA 2005). It is forecasted that warming will cause significant thawing of the permafrost that surrounds the lakes and rivers that dominate much of the arctic landscape.

Permafrost terrains in non-bedrock areas commonly have an ice-rich zone at the top of the permafrost table that are formed from downward moisture movement from the active layer at the end of summers and upward moisture movement from permafrost at winter. The seasonal leaching from thawed soils and ionic movement resultant from thermal induced moisture migration contribute to the solute enrichment encountered at the near-surface permafrost (Kokelj & Burn 2003, 2005).

Deepening of the active layer in a warmer climate can lead to the release of these solutes at near-surface permafrost increasing nutrient input to freshwater bodies, which in conjunction with a raise in solute-rich runoff from the landscape will probably affect primary production (Wrona et al. 2005, Hobbie et al. 1999). It is further predicted these changes will consequentially be reflected in modification of food-web structures and biogeochemical cycles (Wrona et al. 2005).

Considering that benthic production can be an important part of the overall primary and secondary production in arctic lakes (Sierszen et al. 2003, Rautio & Vincent 2007) a more comprehensive understanding of the effects of permafrost slumping on the benthic compartment is warranted. Among the benthic biota, a special focus should be placed on macrophytes as they contribute significantly to primary production, increase habitat heterogeneity (being beneficial to benthic invertebrates and fishes), and are involved in other important in-lake processes (Vadebouncoeur et al. 2003, Kalff 2001).

Many variables have been considered important for macrophyte production, such as underwater light availability, water nutrient content, lake morphology, littoral slope, sediment composition, and organic matter content. Lake sediment, besides acting as a base for physical attachment, has been recognized as an important source of nutrient supply to submerged macrophytes (Barko et al. 1991).

Some studies have already documented differences in lake water chemistry related to permafrost retrogressive thaw slumps (e.g., Kokelj et al. 2005) in a number of lakes in the area between Inuvik and Richards Island, Northwest Territories, Canada. However, the role of such landscape-related slumping on sediment loading, chemistry, and benthic biota still remains unclear and is predicted to be more frequent in a warmer climate (Wrona et al. 2005). This study focused on investigating the hypothesis that retrogressive slumping can produce significant differences in sediment and water chemistry, submerged macrophyte biomass, and benthic invertebrate abundance between undisturbed (*U*) and disturbed (*D*) lakes in a similar geographical region.

Lake Selection and Sampling Methodology

To test the above hypothesis, a set of lakes were selected between Inuvik and Richards Island (N.W.T). Based on lake/catchment characteristics and water quality data from a 60-lake survey (Thompson, unpubl.) and field logistics, a final subset of 3 lakes not affected by retrogressive slumping

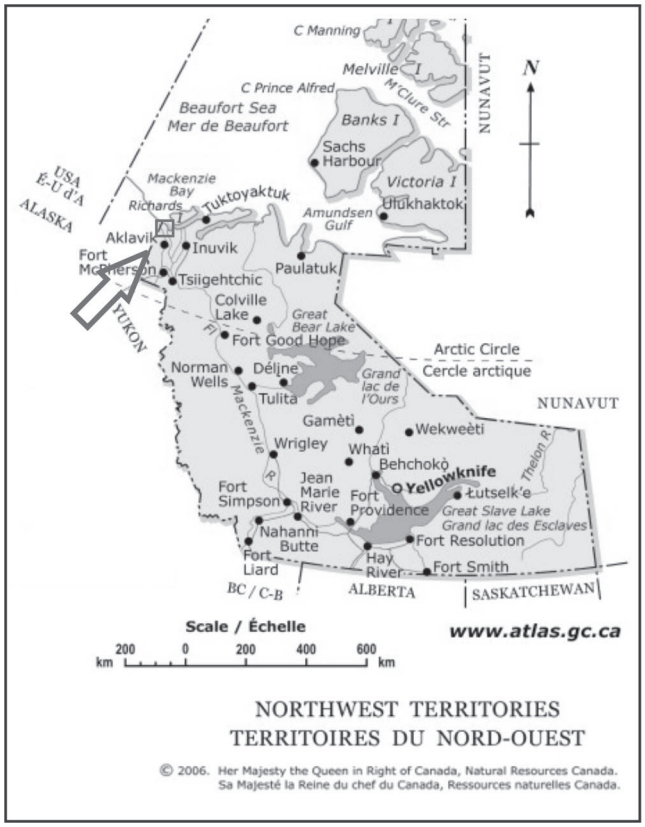

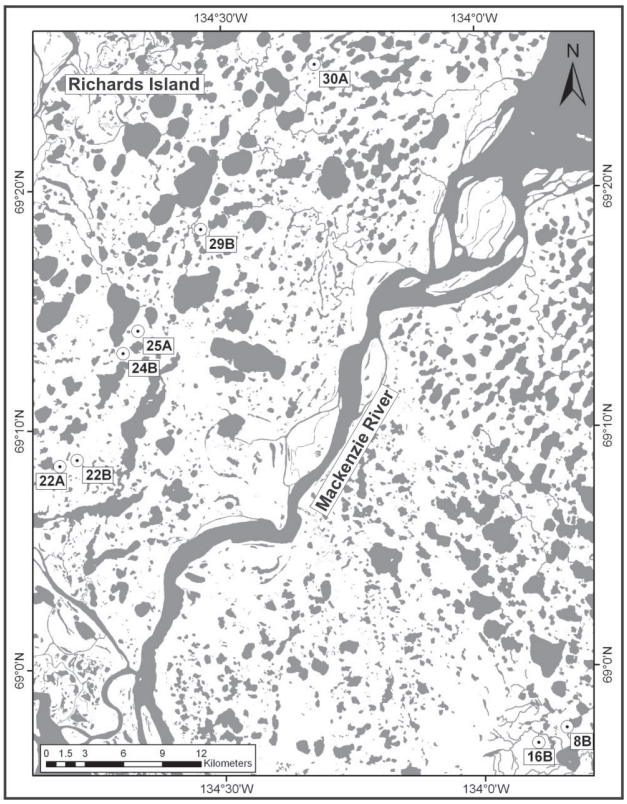

Figure 1. Geographic location of studied lakes. Source: Natural Resources Canada/CanVec (www.geogratis.gc.ca).

(undisturbed or *U* lakes) and 5 lakes affected (disturbed or *D* lakes) were selected for detailed study (Fig 1, Table 1). Disturbed lakes were sampled in two areas: one located at the opposite side (*Do*) of the physical disturbance caused by the slump, and another one in an area adjacent (*Da*) to the slump and thus directly physically affected by the disturbance. This allowed for testing whether undisturbed lakes are similar in their physical, chemical, and biological properties to disturbed systems (particularly with areas in disturbed lakes that are physically removed from the slump (*Do*).

Stratified radial transects starting from the shoreline towards the center of the lake were used as the main sampling unit (replicate) in the present study, and were distributed in order to encompass the different areas of each lake. Taking into consideration the focus on the littoral benthos, sampling points were randomly placed in 1 m, 2 m, and 3 m deep strata along the transects, yielding a maximum of 9 replicates (3 depths x 3 transects) in undisturbed lakes and a maximum of 18 replicates in disturbed lakes (9 in each disturbance zone - *Do* and *Da)*. However, due to logistical constraints in the field, some variables could not always be sampled at all strata depths in all lakes.

Between the end of August and the beginning of September 2006, samples of sediment, submerged macrophytes, benthic invertebrates, and pelagic water were taken from the selected lakes. In addition, interval measurements of underwater photosynthetic active radiation (PAR) (Li-cor LI-192) were taken at each of the transect points from the near surface to the maximum depth of one meter or before reaching the top of macrophytes. The results were used to calculate the light underwater attenuation coefficient (K_d) at each point in accordance with Kalff (2001).

Submerged macrophytes were collected at 1 m, 2 m, and 3 m deep strata with a telescopic macrophyte sampler (Marshal & Lee 1994) that covered an area of 0.164 m^2. The macrophytes were subsequently separated, washed, and oven-dried to a constant weight at 60°C for dry weight determination, and then extrapolated to represent a total biomass per m^2.

Sediment samples were collected with a sediment corer at 1 m and 3 m depths. Samples from the top 15 cm were transported to the laboratory, homogenized, and separated into two fractions. One fraction was frozen, freeze-dried, and sent for analysis of recoverable metals (i.e., environmentally available) and nutrients at the Environment Canada National Laboratory for Environmental Testing (NLET), Burlington, ON (Table 2).The remaining fraction was oven-dried and burned for calculations of loss of ignition (as a measure of organic matter content) in accordance with Hakanson & Jansson (1983).

Sediment samples for estimating invertebrate abundance were collected at 1 m, 2 m, and 3 m depths. Samples from the top 5 cm were washed through a 250 μm sieve, and the invertebrates were subsequently sorted, counted, and extrapolated to 1 m^2. Water physico-chemical parameters were collected at the deepest point in each lake previously determined from a bathymetric survey. A handheld

Table 1. Lake attributes summary table. Lake area (La), catchment area: lake area (Ca:La) ratio, catchment area: lake volume (Ca:Lv) ratio, maximum depth (Zmax), mean depth (Zmean), lakes (*U*= undisturbed, *D*= disturbed), number of lakes (N), mean, standard deviation (S.D), minimum and maximum values (Min and Max).

Lakes		La (m^2)	Ca:La	Ca:Lv	Zmax	Zmean
U lakes	Mean	40100	4.78	1.77	7.30	2.88
N= 3	S.D	19419	0.44	0.14	2.88	0.92
	Min.	18700	4.28	1.61	4.20	1.92
	Max.	56600	5.11	1.88	9.90	3.76
D lakes	Mean	76380	3.99	1.15	9.54	3.48
N= 5	S.D	40514	1.18	0.63	4.33	0.80
	Min.	35500	2.41	0.66	5.30	2.44
	Max.	142900	5.04	2.01	16.80	4.52

multiparameter Y.S.I was used to collect pH, temperature, and conductivity data. In addition, water samples were collected and sent to the NLET lab for analysis of particulate organic carbon (POC), dissolved phosphorus (DP), orthophosphate (OP), total phosphorus (TP), ammonium (NH_3N), nitrite-nitrate (NO_3NO_2), total dissolved nitrogen (TDN), particulate organic nitrogen (PON), and total nitrogen (TN).

Statistical analyses

All the variables were tested for normality using a Kolmogorov-Smirnov (K-S) test ($p<0.05$) and, when necessary, $\log_{10}$ transformed to fit the assumptions of parametric testing. General Linear Model (GLM) regressions were performed to test for differences in sediment chemistry and invertebrate abundance between undisturbed (*U*) and disturbed (*D*) lakes, using depth as a co-variate.

In cases where a significant difference ($p<0.05$) between disturbed and undisturbed lakes was found, a subsequent GLM with a Bonferroni simultaneous *a posteriori* test between lake/disturbance location (*U, Do* – opposite to slump, *Da* – adjacent to slump) and depth was performed. These analyses were used to ascertain whether the differences were related to in-lake processes (*Do* vs. *Da*) versus between lake (*U* vs. *Da*, *U* vs. *Do*) processes and physical proximity to the slump.

Since some sediment variables and macrophyte biomass data were not normally distributed even after transformation, the non-parametric Kruskal-Wallis test was used in these cases. As water nutrient data were only collected at one station per lake system, differences between undisturbed and disturbed lakes were analyzed using one-way Analysis of Variance (ANOVA). All the analyses were performed with MINITAB 13.1 (Minitab Inc. 2000).

Results

ANOVA tests for water nutrient data between undisturbed and disturbed lakes revealed no significant differences ($p>0.05$) for all measured constituents (POC, DP, OP, TP, NH_3N, NO_3NO_2, TDN, PON, TN). However, pH (mean = 7.6 in *U* vs. 8.19 in *D*) and specific conductivity (mean = 128.6 µS/cm in *U* vs. 516.7 µS/cm in *D*) were significantly different ($p<0.05$).

Table 2. List of key nutrient, metals and metalloids analyzed from sediment samples.

Carbon (organic/inorganic)	Sodium (Na)	Potassium (K)	Arsenic (As)
Nitrogen (organic)	Zinc (Zn)	Calcium (Ca)	Beryllium (Be)
Phosphorus (inorganic)	Cooper (Cu)	Magnesium (Mg)	Bismuth (Bi)
Phosphorus (P)	Nickel (Ni)	Iron (Fe)	Cadmium (Cd)
Manganese (Mn)	Molybdenum (Mo)	Cobalt (Co)	Gallium (Ga)
Antimony (Sb)	Lanthanum (La)	Chromium (Cr)	Aluminum (Al)
Thallium (Tl)	Lithium (Li)	Strontium (Sr)	Rubidium (Rb)
Uranium (U)	Lead (Pb)	Vanadium (V)	Barium (Ba)

GLM tests revealed significant differences ($p<0.05$) in only seven sediment variables between *U* and *D* lakes. Mg and Ca means showed highly significant differences, ($p<0.01$) with higher values in *D* lakes (Ca= 4.85 g/Kg in *U* vs. 9.44 g/Kg in *D*, and Mg= 5.74 g/Kg in *U* vs. 7.35 g/Kg in *D* (Fig. 2)).

Organic N and C, As, Ni, and Zn were also significantly different between *U* and *D* lakes ($p<0.05$). However, the highest mean values for these variables consistently occurred in undisturbed (*U*) lakes. The mean values of each of the variables for *U* and *D* were 7.29% and 4.90% of organic C, 0.61% and 0.34% of organic N, 0.02 g/Kg and 0.015 g/Kg of As, 0.052 g/Kg and 0.041 g/Kg of Ni, and 0.137 g/Kg and 0.106 g/Kg of Zn, respectively (Fig 2).

Bonferroni *a posteriori* testing revealed no significant differences ($p>0.05$) between in lake disturbance regions (*Da* and *Do*) and between disturbed regions and *U* lake comparisons for As, Ni, and Zn.

Mg and Ca were not significantly different between *Da* and *Do*, but were different between these regions and undisturbed lakes. In contrast, organic N content in *Da* (0.24%) was significantly different ($p<0.05$) from *Do* (0.24% vs. 0.44%), and highly significantly different ($p<0.01$) to undisturbed lakes (0.61%). Organic C was only significantly different ($p<0.05$) between *Da* and *U* lakes. These indicated that *Do*, a region within the disturbed systems, was similar to a "control" undisturbed lake for the variables organic N and C.

Kruskal-Wallis tests on Mn, Co, Sr, and ignition loss showed a significant difference ($p<0.05$) between *U* and *D* lakes. Median Mn concentrations varied from 0.83 g/Kg in *U* versus 0.42 g/Kg in *D*-lakes; Co ranged from 0.015 g/Kg on *U* to 0.013 g/Kg on *D*; ignition loss varied from 13.26% on *U* to 9.67% on *D*; and Sr, the only of these variables with

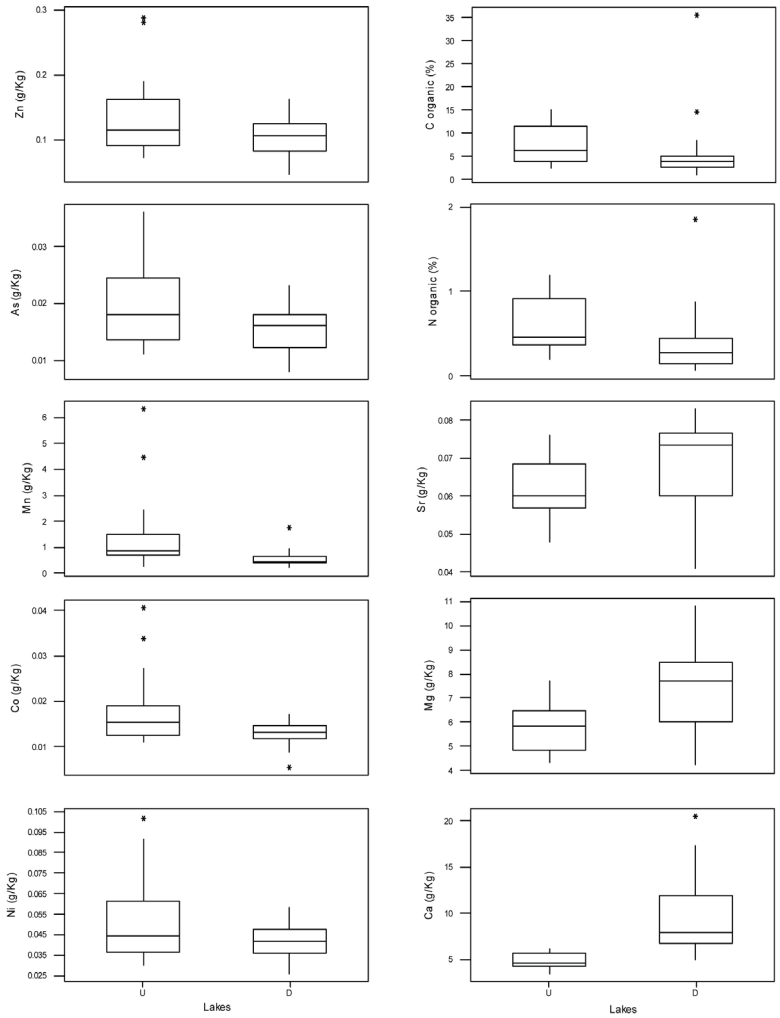

Figure 2. Box plots for sediment chemistry variables that were significantly different between undisturbed (*U*) and disturbed (*D*) lakes. All variables in g/Kg with the exception of C and N in %.

higher values in *D*, varied from 0.06 g/Kg on *U* versus 0.073 g/Kg on *D* (Fig2).

Mn, Co, and Sr were not significantly different between *Do* and *Da* regions ($p>0.05$) but were different to the undisturbed lakes. Ignition loss results had a similar pattern as found from the Bonferroni test for organic C. The K-W test revealed that only *Da* was significantly different from *U* ($p<0.05$). Correlation analysis showed a strong positive association between organic C and ignition loss ($r = 0.947$, $p<0.01$).

Although the median values for macrophyte biomass were the same (zero) at *U* and *D* lakes, the distributions were significantly different ($p<0.01$) according to Kruskal-Wallis test, with higher values on *D* lakes. This can be explained by the fact that macrophytes were more frequently found in *D* lakes (44%) than in *U* lakes (11%). The biomass present on *Do* was significantly different from *Da* and *U* lakes ($p<0.01$), while differences between *U* lakes and *Da* were not significant ($p>0.05$) (Table 3).

The difference in invertebrate abundance between *U* and *D* lakes was highly significant ($p<0.01$), with higher abundance values in *D* lakes. Differences between *U*, *Do* and *Da* were also significant, with *Da* having the highest abundance and being different from *U* ($p<0.01$), and from D*o* ($p<0.01$). Also, the interaction between *U/D* lakes and depth was significant ($p<0.05$), indicating a covariation between these two variables (Table 4).

Discussion and Conclusions

Significant differences were found between disturbed and undisturbed lakes for a variety of environmental variables. In general, disturbed lakes exhibited higher mean values of Mg, Ca, and Sr in sediments, and pH and conductivity in the water column. Undisturbed lakes had higher levels of organic C and N, As, Ni, Zn, Mn, Co, and organic matter in the sediment, and higher values of littoral underwater light coefficient of attenuation (K_d). The conductivity pattern is in accordance with previous observation by Kokelj et al. (2005), where lakes with catchments disturbed by thermokarst slumping had higher water ionic content and conductivity than undisturbed lakes in the same geographic area.

Macrophyte biomass and invertebrate abundance were higher in disturbed lakes, being postulated that this difference

Table 3. Macrophyte biomass (g/m^2) summary data from all lake, *U*, *D*, *Do*, and *Da*. Number of sample points (N), number and percentage of cases where macrophytes were present (N_p), minimum and maximum biomass (Min., Max.), median, and first and third quartiles (Q1, Q3).

Lakes/Areas	N	N_p and % presence	Min.	Max.	Median	Q1	Q3
All lakes	90	31 (34%)	0	705.5	0	0	19.21
Undisturbed lakes (*U*)	27	3 (11%)	0	24.268	0	0	0
Disturbed lakes (*D*)	63	28 (44%)	0	705.5	0	0	55.9
Opposite region (Do)	33	24 (72%)	0	705.5	28.7	0	104.1
Adjacent region (Da)	30	4 (13%)	0	76.22	0	0	0

is related to higher water transparency and concentrations of key chemical elements originated from the slump and transferred to the sediment. Thus, it is expected that a higher availability of nutrients for the growth and maintenance of macrophyte community produce a structurally more complex benthic habitat, having a positive effect on benthic invertebrates.

Previous studies have suggested that the sediment is the primary source of N, P, Fe, Mn, and other micronutrients necessary for macrophyte metabolism (Barko et al. 1991). However, the present study did not find macrophytes predominant at lakes with higher levels of organic N and Mn (undisturbed lakes). A possible explanation is that higher amounts of organic matter found in the sediment of undisturbed lakes could be affecting nutrient availability and uptake processes (Barko & Smart 1986).

In addition to decreased nutrient availability due to complexation with organic matter in organic sediments, macrophyte growth can be disrupted by the presence of phytotoxic compounds produced during anaerobic decomposition (Barko et al. 1991) For instance, accumulation of large quantities of refractory organic matter in sediments are shown to decrease nutrient availability and the growth of rooted submerged macrophytes, while additions of low quantities of labile organic matter in sediments may benefit macrophytes, especially on coarse textured sediments in oligotrophic systems (Barko et al. 1991).

With the exception of organic N, all the sediment variables and the light attenuation coefficient values were not significantly different within disturbed lakes, leading to the question of what factors might be influencing the absence of macrophytes in areas adjacent to the actual slump (*Da*). Since submerged macrophyte biomass is documented to be related more to underwater substrate slope at depths where irradiance is not the primary limiting factor (Kalff 2001), slope and related substrate stability is postulated to be the major factor influencing the almost complete absence of macrophytes in *Da* areas.

Based on preliminary results of bathymetric surveys and field observations, the underwater substrate slope near the slump disturbance is consistently higher than observed in opposite areas in the same lake or in undisturbed lakes. More detailed field analyses need to be conducted to determine the possible causal physical mechanism for this observation. It is possible that macrophyte colonization in disturbed areas is being constantly subjected to burial by soil and vegetation from the lakeshore slump.

Table 4. Invertebrate abundance (individuals/m^2) summary table from *U*, *D*, *Do,* and *Da*. Number of samples (N), minimum and maximum abundance (Min., Max.), mean, and standard deviation (S.D).

Lakes/Areas	N	Min.	Max.	Mean	S.D
Undisturbed lakes (*U*)	26	3215	39460	13232	8786
Disturbed Lakes (*D*)	68	2037	119549	28630	24482
Opposite region(Do)	35	2037	97334	22247	22818
Adjacent region (Da)	32	4584	119549	35631	25055

The observed water transparency and related light penetration values (PAR) in the littoral zone of disturbed lakes also contradicts what would be expected in a scenario of higher suspended sediments and color (dissolved organic carbon) arising from the input of landscape material into the lake water.

Two possible mechanisms could be operating individually or jointly to produce these observed patterns. First, higher ionic concentrations supplied to the lakes from the enriched slump runoff as those shown in Kokelj et al. (2005) could be adsorbing to organic compounds on the water column, causing them to precipitate and "clearing" the water. Secondly, adsorption of organic substances to the exposed mineral soils could be producing runoff with low concentration of colored material in disturbed catchment, while in undisturbed ones colored runoff would be a result of water flux through the shallow organic soils (Carey 2003, Kokelj et al. 2005). Further process-based research is necessary to elucidate the relative importance of these two possible processes and some preliminary experiments examining possible causal mechanisms can be found in Thompson et al. (2008).

In general, benthic invertebrates were found to be more abundant in disturbed lakes. However, while it was expected that areas with more macrophytes would support higher number of invertebrates, areas adjacent to slumps were found to have the highest mean abundance. Other factors, such as periphyton and bacterial abundance, pH, and oxygen, could be influencing benthic invertebrate communities and this needs to be further explored.

In summary, a warmer climate regime accompanied by enhanced seasonal thawing of the active layer will significantly affect benthic macrophyte and invertebrate communities of upland tundra lakes. The present work shows that in addition to the changes in water column characteristics already documented in previous studies (Kokelj et al. 2005), thermokarst retrogressive slumping also affects sediment chemistry and water transparency

relationships in upland tundra lakes. In addition to influences related to input of enriched runoff, deposition of landscape material (i.e., soil and terrestrial vegetation) at the littoral zone can have an impact in macrophyte colonization rates and littoral complexity, affecting benthic invertebrates and upper level consumers.

Complementing the mentioned processes, other environmental changes need to be taken into consideration when projecting the effects of a warmer climate on upland tundra lakes. Active layer deepening could act synergistically with higher temperatures, higher UV penetration in lakes, changes in biota composition/ metabolism, and changes in runoff input due to alterations of biogeochemical cycles at landscape level which could all ultimately lead to a variety of different balances. Contrary to the expected increase in pelagic productivity and decreased transparency associated with permafrost degradation (Wrona et al. 2005), it is suggested that at an earlier stage, increases in the macrophyte biomass associated with higher transparency could be a possibility, being later followed by greater disturbance of littoral zone and decrease of macrophyte communities.

Acknowledgments

This work was supported by the Water-Climate Impact Research Centre (W-CIRC), Environment Canada (E.C), University of Victoria (UVic), Natural Sciences and Engineering Research Council, Polar Continental Shelf Project, and Aurora Research Institute. We would like to thank Megan Thompson (UVic), Tom Carter (NHRC, E.C), and Daniel L. Peters (W-CIRC, E.C) for their helpful participation during field data collection, Patricia Chambers (E.C) for aiding in macrophyte identification, John Mollison (NHRC, E.C) for manufacturing the macrophyte sampler, Kristie S. Heard (U. of New Brunswick) for helping with invertebrate sample work, and Thiago S. F. Silva (UVic) for assistance in reviewing the manuscript.

References

ACIA. 2005. *Arctic Climate Impact Assessment.* Cambridge University Press, 1042 pp.

Barko, J.W., Gunnison, D. & Carpenter, S.R. 1991. Sediment interaction with submersed macrophyte growth and community dynamics. *Aquatic Botany* 41: 41-65.

Barko, J.W. & Smart, R.M. 1986. Sediment-related mechanisms of growth limitation in submersed macrophytes. *Ecology* 67(5): 1328-1340.

Carey, S.K. 2003. Dissolved organic carbon fluxes in a discontinuous permafrost subarctic alpine catchment. *Permafrost Periglac. Process.* 14: 161-171.

Hakanson, L. & Jansson, M. 1983. *Principles of Lake Sedimentology*. New York: Springer-Verlarg, 316 pp.

Hobbie, J.E., Peterson, B.J., Bettez, N., Deegan, L., O'Brien, W.J., Kling, G.W., Kipphut, G.W., Bowden, W.B. & Hershey, A.E. 1999. Impact of global change on the biogeochemistry and ecology of an Arctic freshwater system. *Polar Research* 18: 207-214.

Johnson, R.K. & Ostrofsky, M.L. 2004. Effects of sediment nutrients and depth on small-scale spatial heterogeneity of submersed macrophyte communities in lake Pleasant, Pennsylvania. *Can. J. Fish. Aquat. Sci*. 61: 1493-1502.

Kalff, J. 2001. *Limnology: Inland Water Ecosystems.* Prentice-Hall, 592 pp.

Kokelj, S.V & Burn, C.R. 2003. Ground ice and soluble cations in near-surface permafrost, Inuvik, Northwest Territories, Canada. *Permafrost and Periglacial Processes* 14: 275-289.

Kokelj, S.V. & Burn, C.R. 2005. Geochemistry of the active layer and near-surface permafrost, Mackenzie Delta region, Northwest Territories, Canada. *Can J. Earth. Sci.* 42: 37-48.

Kokelj, S.V., Jenkins, R.E., Milburn, D., Burn, C.R. & Snow, N. 2005. The influence of thermokarst disturbance on the water quality of small upland lakes, Mackenzie Delta Region, Northwest Territories, Canada. *Permafrost and Periglacial Processes* 16: 343-353.

Marshall, T.R. & Lee, P.F. 1994. An inexpensive and lightweight sampler for the rapid collection of aquatic macrophytes. *J. Aquat. Plant Manage.* 32: 77-79.

Minitab v.13.1. 2000. State College, PA.

Rautio, M. & Vincent, W.F. 2007. Isotopic analysis of the sources of organic carbon for zooplankton in shallow sub-arctic and arctic waters. *Ecography* 30: 77-87.

Sierszen, M.E., McDonald, M.E. & Jensen, D.A. 2003. Benthos as the basis for arctic food webs. *Aquatic Ecology* 37: 437-445.

Thompson, M.S., Kokelj, S.V., Prowse, T.D. & Wrona, F.J. 2008. The impact of sediments derived from thawing permafrost on tundra lake water chemistry: an experimental approach. *Proceedings of the Ninth International Conference on Permafrost, Fairbanks, Alaska, June 29–July 3, 2008* (this proceedings).

Vadeboncoueur, Y., Jeppesen, E., Vander Zanden, M.J, Schierup, H, Christoffersen, K. & Lodge, D.M. 2003. From Greenland to green lakes: cultural eutrophication and the loss of benthic pathways in lakes. *Limnol. Oceanograph*. 48: 1408-1418.

Wrona, F.J., Prowse, T.D. & Reist, J.D. 2005. Freshwater ecosystems and fisheries In: *Arctic Climate Impact Assessment*. Cambridge University Press, 354-452.

The Vault Creek Tunnel (Fairbanks Region, Alaska): A Late Quaternary Palaeoenvironmental Permafrost Record

Hanno Meyer
Alfred Wegener Institute for Polar and Marine Research, Research Unit Potsdam, Potsdam, Germany
Kenji Yoshikawa
Water and Environmental Research Center, Institute of Northern Engineering, University of Alaska Fairbanks, Alaska
Lutz Schirrmeister, Andrei Andreev
Alfred Wegener Institute for Polar and Marine Research, Research Unit Potsdam, Potsdam, Germany

Abstract

The Vault Creek (VC) gold mining tunnel north of Fairbanks, Alaska, is the deepest and longest permafrost tunnel ever made available for periglacial research. The VC tunnel sedimentary profile includes loess and fluvial gravels above bedrock and is, thus, comparable to the famous Fox permafrost tunnel. AMS ^{14}C dates from the VC tunnel indicate that loess accumulation took place around 40–50 ka BP, whereas the fluvial sediments show mostly infinite ^{14}C ages, confirmed by IRSL dates around 55–85 ka. However, the pollen record of the VC tunnel reflects very warm and unambiguously interglacial climate conditions with the occurrence of *Abies* and *Tsuga* in large parts of the spectra. The stable isotope composition of ice wedges also reflects warm climatic conditions in the lower part of the profile. Consequently, a very warm phase occurred in Central Alaska, whose timing is uncertain due to conflicting age determinations and proxy indications.

Keywords: Central Alaska; climate reconstruction; ground ice; permafrost dating; Quaternary environment.

Introduction

Permafrost consists of sediment and ground ice preserving suitable signals for the reconstruction of Late Quaternary environment and climate. Thermokarst, thermoerosion, and slumping often prevent the possibility of resampling a permafrost outcrop. Therefore, underground excavations and permafrost tunnels such as the Fox and Vault Creek (VC) tunnels, may serve as three-dimensional natural laboratories for permafrost studies including dating techniques.

Especially in Central Alaska, where the chronology of sediments is still insufficiently known for the interval between 25 and 100 ka BP (Berger 2003), such revisitable sites are valuable for regional environmental reconstruction. Dating of deposits in this region is based upon a variety of methods including thermoluminescence (TL), infrared or optical stimulated luminescence (IRSL, OSL), fission track (FT), and ^{14}C, which led (and may further lead) to a substantial improvement of the knowledge on timing and duration of Late Quaternary warm and cold phases in Central Alaska. Here we present new data from the Central Alaskan Vault Creek permafrost tunnel near Fairbanks.

Study Area

The Fairbanks area is characterized by discontinuous permafrost and a continental climate with mean annual air temperatures of about -3.0ºC and precipitation of 263 mm (at Fairbanks airport, 1971–2000). Presently, spruce-birch-aspen taiga dominates the vegetation. Permafrost may reach a thickness of up to 120 m and is relatively warm with ground temperatures about -0.8°C at 2 m below ground surface at the tunnel site. The active layer reaches about 0.3 to 0.4 m.

Figure. 1. Study site: The Vault Creek tunnel north of Fairbanks. Additionally, an open pit near Fox was sampled.

Permafrost usually dominates valley bottoms and north slopes, but is largely absent on south-facing slopes. The VC tunnel is situated on a north-facing slope. Frost cracking activity is presently reduced in Interior Alaska. In Wisconsin times, when mean air temperatures were 4°C lower, ice wedge formation was a more common process. In the

Fairbanks region, permafrost is generally considered to have thawed and reset after Sangamon interglacial (Pewe 1975).

The VC tunnel is situated about 40 km north of Fairbanks, Alaska. It was established in 1990 by a local private gold miner and is, to our knowledge, the deepest (>40 m) and longest permafrost tunnel (>200 m) for periglacial research. The entrance of the VC tunnel is secured by a 30 m long steel tube, which makes the uppermost part of the section inaccessible (Fig. 1). This part has been sampled in a 3.0-m-deep auger hole (26 inches or 0.65 m in diameter) located about 50 m ENE of the tunnel's entrance (Fig. 2).

Results

The methodological approach applied to the permafrost sequence of the VC tunnel includes different dating techniques, sedimentology, and palynology, as well as stable isotope geochemistry ($\delta^{18}O$ and δD) of ground ice.

Sedimentology

The sedimentary and geocryological sequence is similar to that of the Fox research tunnel constructed in 1963 by the US Army Corps of Engineers (CRREL). About 40 m of Quaternary deposits overlie weathered schistose bedrock ("Birch-Creek schist"). The Quaternary deposits are: **(1)** at the bottom, 17.5 m of fossiliferous ice-bonded fluvial gravels with several sand and peat lenses, as well as numerous wood remains (depth: 22.5–40.05 m). No ice wedges occur in the gravel horizon; **(2)** in the upper part, about 12 to 15 m of ice-rich silty sediments are found (depth: 3–15 m). These are loess-like, organic-rich, and contain fossil bones, as well as relatively large ice wedges. The silt horizon has a very uniform unimodal grain size distribution (mean 52 µm). Between these two units: **(3)** a 7.5 m thick transition horizon of fluvial gravels interbedding with loess-like silt and relatively small ice wedges was distinguished (depth: 15–22.5 m).

The general sequence is characterized by mean total organic carbon (TOC) content of about 3%. Two horizons of higher TOC content (of up to 18%) are found at about 7.5 m and 23.5 m depth, respectively. C/N ratios are around 8, but significantly higher (reaching 20) at the TOC-enriched horizons. Carbonate contents (Cc) are, in general, below 1.5% (mean Cc 1.1%), but reach a maximum of up to 4.3% at 22.5 m depth. The mass-specific magnetic susceptibility (MS) is low in the transition and gravel horizons (mean MS: 24 and 30.10^8 SI, respectively), whereas the silt displays higher mean MS of almost 70.10^8 SI. The ice contents are significantly higher in the silt (up to 60 wt%) as compared to the gravels (max. 20 wt%). Both ground ice and sediments were significantly deformed by post-depositional slope processes, especially in the upper part of the sequence.

Two 1 to 3 mm thick layers of tephra were detected in the tunnel at about 2 m depth and at about 15.4 m depth. These white ash layers are yet unidentified. Especially the upper tephra is disturbed by creeping or sliding of slope material. At 15.7 m, three up to 20 cm thick ice bands intersect with sediments and ice wedges. Contacts between ice wedges and

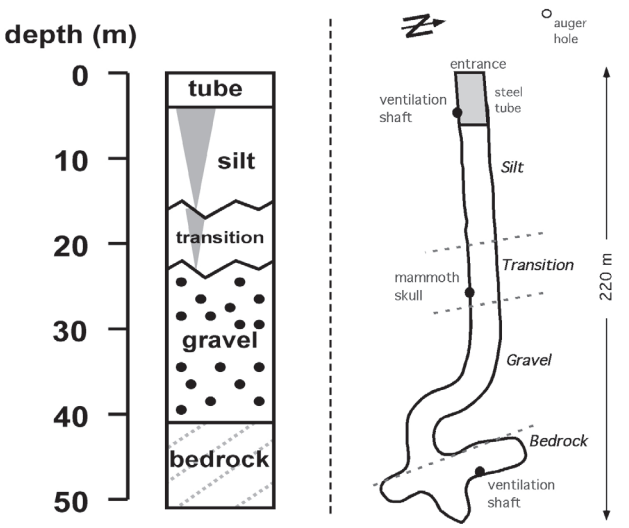

Figure 2. Schematic sedimentary profile of the VC tunnel and top view of the VC tunnel (schematic).

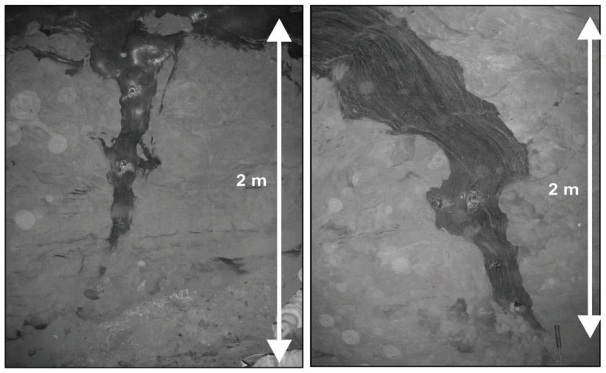

Figure. 3. Ice wedges of the VC tunnel of the silt horizon (left) and transition horizon (right). Note: deformation structures.

ice bands are similar to features interpreted as thermokarst-cave ice in the Fox tunnel (Shur et al. 2004) following melt and erosion of a part of an ice wedge by running water. No frost cracking occurred after refreezing of meltwater, so ice wedges were or became inactive after the melt event.

Geocryology

The different types of ground ice in the VC tunnel include massive ice such as: **(1)** ice wedges, the most important type of ground ice in the VC tunnel. These are associated only with the silt and transition horizons (Fig. 3).

They are wider (up to 3 m) and more strongly deformed in the upper section than in the transition horizon, where only small, vertically oriented ice wedges of 0.1-0.4 m in width were observed. Ice wedges in the silt horizon show signs of syngenetic growth. The inclination of ice wedges is stronger at the topmost part of the profile reaching up to 45–50° from the vertical line. This indicates a post-depositional transport of material e.g., by slumping or, more likely, by creeping without melting the wedge ice, which reacted plastically. Tops of ice wedges are visible in several cases, especially in the transition horizon; (2) thermokarst cave ice as also recognized in the Fox tunnel (Shur et al. 2004); and (3) a strange type of clear ice is observed at the wall with huge

Table. 1. Summary of all Radiocarbon and IRSL dated sediment and ice wedge samples of the VC tunnel, Fairbanks, Alaska

Sample ID	Depth (m)	Radiocarbon age (a BP)	Type of organic, Stratigraphic position	Lab number
FAI 4/7	0.75	2505 +/-25	wood remains in soil horizon (auger hole)	KIA 31128
FAI 4/5	1.35	3445 +/-35	soil horizon (auger hole)	KIA 31127
FAI 3/20	2.7	25,320 +/- 240	peat inclusion, topmost sample in VC tunnel (silt unit)	KIA 31125
FAI-1/42	2.8	45,120 +3300/-2330	grass roots (silt unit)	KIA 25271
FAI-1/40	4.6	44,220 +1700/ - 1400	wood, organic remains (silt unit)	KIA 28133
FAI-IW-4	5.0	46,120 +4080/ -2690	organic matter in wedge ice (silt unit)	KIA 25660
FAI-1/39	6.4	43,670 + 1480/ -1250	plant remains, leached residue (silt unit)	KIA 28132
FAI-IW-8	7.5	>40,970	organic matter in wedge ice (silt unit)	KIA 25661
FAI-1/37	8.4	49,930 + 3800/ -2570	wood, organic remains Z(silt unit)	KIA 28131
FAI-1/36	9.3	52,390 +2210/ - 1730	wood, organic remains (silt unit)	KIA 28130
FAI-1/34	10.9	42,090 +3410/-2380	silt. organic-rich.	KIA 24873
FAI-IW-12	12.0	34,400 +4390/-2820	organic matter in wedge ice (silt unit)	KIA 25275
FAI-1/30	13.3	> 52,440	wood, organic remains (silt unit)	KIA 28128
FAI-1/33	14.7	42,170 +3480/-2420	organic remains (silt unit)	KIA 28129
FAI mammoth	16.7	> 50,920	small fragments of mammoth skull, collagen, (transition horizon)	KIA 31124
FAI-1/26	19.6	49,550 +2190/-1720	wood remains (transition horizon)	KIA 25270
FAI-1/19	21.7	> 51,130	peat lens (transition horizon)	KIA 24872
FAI-1/2	34.8	> 52790	wood remains (gravel horizon)	KIA 24871
FAI-IW-18	open pit	3615 +/- 45	peat in wedge ice	KIA 25276
FAI-2-1	open pit	4625 +/- 50	small twig	KIA 25272
Infrared-stimulated optical luminescence (IRSL)				
FAI-OSL-2	20.4	75,000+/-10,000	middle sand (transition horizon)	
FAI-OSL-1	21.0	57,000 +/-4400	middle sand (transition horizon)	

crystals of several cm in diameter, most likely related to mining activity. These locations were avoided while sampling in the tunnel. Intrasedimental ice includes segregated ice, as thin layers of ice often bound upward near ice wedges, and finely dispersed pore ice, as well as ice lenses.

Dating

To assess the stratigraphic position of the VC tunnel, several dating techniques were applied (AMS ^{14}C, IRSL, U/Th). The results are summarized in Table 1 and Figure 4. Radiocarbon analyses were carried our at Leibniz laboratory in Kiel, IRSL dating at the Technical University of Freiberg and U/Th dating at GGA Institute in Hannover, Germany. A first stratigraphic scheme is mainly based upon ^{14}C dates.

Samples taken from the auger borehole show a Late Holocene sediment accumulation and soil development around 2.5 to 3.5 ka ^{14}C BP. These dates are similar to those of an open pit near Fox, where peat and ice wedges grew in the second half of the Holocene. The uppermost sample in the VC tunnel (silt horizon) was dated to 25.3±0.2 ^{14}C ka BP. Seven finite ^{14}C dates were measured in the sediments of the silt unit, all between 40,000 and 50,000 ^{14}C BP with a relatively large error bar. Two radiocarbon ages in the silt horizon are beyond dating range. One ice wedge of the silt unit was dated to 34,400+4,390/-2,820 ^{14}C BP. Ice wedges are vertical features, thus, younger organic remains might reach deeper parts of the profile, if the ice wedge was active after sediment accumulation.

From the transition and gravel horizons, three infinite ^{14}C ages of older than 50 ka BP were retrieved, among them one age from a mammoth skull. Only one finite age of 49,550 +2,190/-1,720 ^{14}C BP was measured in the transition horizon. Two IRSL ages in the transition horizon of 57±4.4 ka and 75±10 ka were measured between 20 and 21 m depth confirm the hypothesis of a Wisconsin age of transition and silt horizons. The fluvial gravel might be even older. The attempt to date peat material from the gravel unit by means of U/Th failed due to open system conditions and the subsequent loss of uranium and only an unreliable age (of 360–460 ka) was obtained.

Palynology

Pollen spectra from the VC tunnel can be subdivided into 5 main pollen zones (PZ-I to PZ-V). Oldest pollen spectra (PZ-I, below 27 m) reflect that spruce-birch forest with dwarf birch and shrub alder dominated at the site during that time. The climate was wet and warm, and the studied pollen spectra are unambiguously pointing to “interglacial environmental conditions” similar to Holocene ones.

Pollen spectra of PZ-II (17.5-27 m) are composed of Cyperaceae, *Picea*, *Betula*, Ericales and *Sphagnum* spores showing that spruce forest with some birch trees dominated

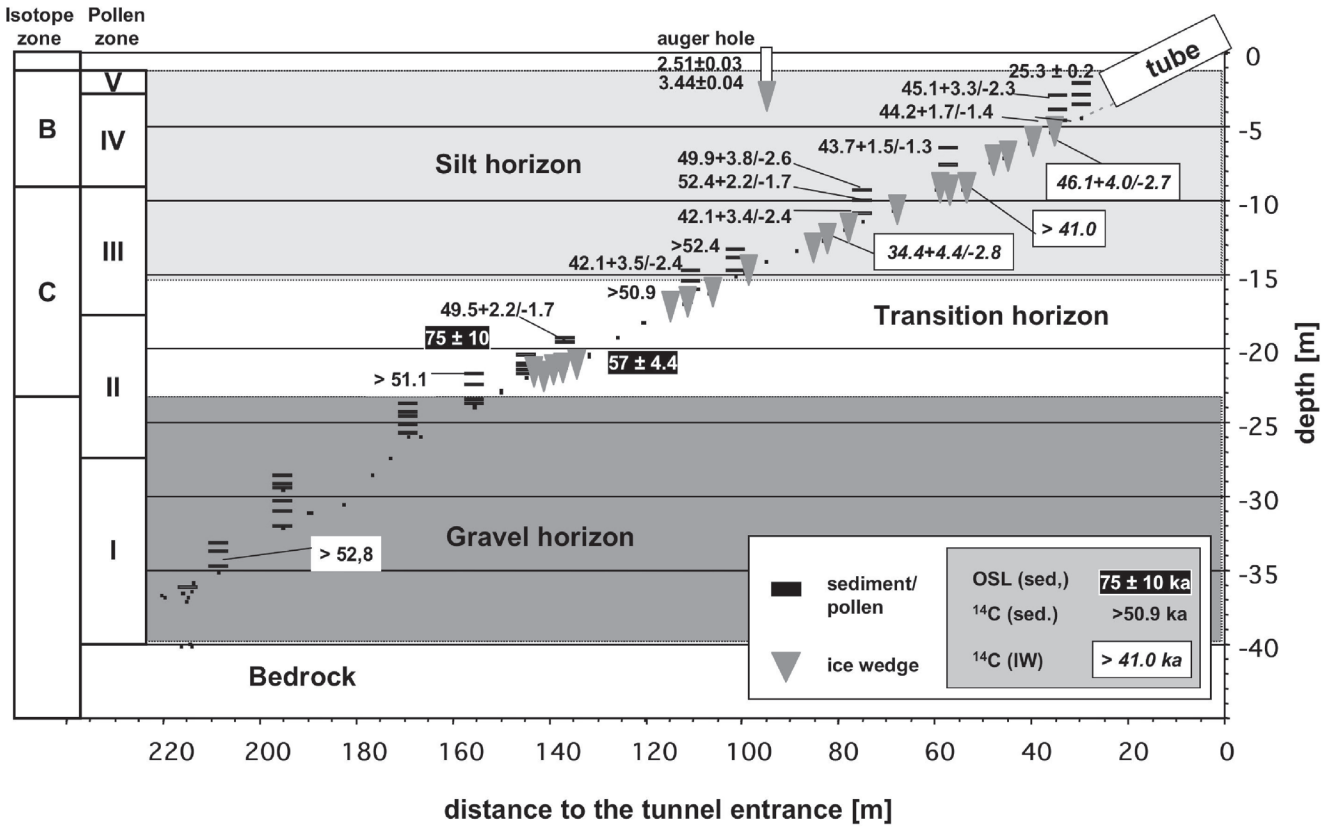

Figure. 4. Stratigraphic position of all sampled sediment profiles and ice wedges as well as their respective sedimentary horizon, pollen zone and isotope zone. Results of all IRSL and radiocarbon AMS ^{14}C dated samples are positioned at their right depth.

at the site during that interval. The find of relatively heavy pollen not readily transported by wind, such as hemlock (*Tsuga*) and fir (*Abies*) may reflect their presence in the local vegetation. The pollen spectra of PZ-III (8–17.5 m) are dominated by *Picea* and Cyperaceae pollen reflecting that spruce forest still dominated at the site. The permanent presence of hemlock and fir in the spectra reflects, most likely, that these trees grew around or not far from the site. Nowadays, these taxa occur in Alaska only in the rather moist coastal areas, where annual precipitation reaches at least 600 mm and winter and summer temperatures range from -6°C to -2°C and 13°C to 16°C, respectively (Viereck & Little 1972). Thus, during the PZ-III interval, climate conditions were probably wetter and warmer than today, e.g., such as in a warm stage of an interglacial. It should be stressed that redeposition seems unlikely due to the good preservation of pollen grain, even though both taxa are known from Tertiary deposits in Alaska (Ager et al. 1994).

A decrease of *Picea* and an increase of Cyperaceae pollen content in the pollen spectra of PZ-IV (depth: 2.8–8 m) may reflect a slight deterioration of the environmental conditions. However, spruce forest still dominated in the local vegetation. The presence of few hemlock and fir pollen shows, however, that climate conditions were still wet and warm during the PZ-IV interval. In pollen zones PZ-I to PZ-IV, typical cold indicators are missing.

Pollen zone PZ-V includes two samples from the uppermost part of the VC tunnel (2.0–2.7 m, near the entrance) reflecting a treeless environment and a significant deterioration of the climate conditions, which were extremely dry and cold during this time. A radiocarbon age of 25,320±240 a BP reflects a Late Wisconsin age of PZ-V.

Stable isotope geochemistry

Ice wedges are periglacial features giving information about winter temperatures which may be derived by stable oxygen and hydrogen isotopes (e.g,, Vaikmäe, 1989, Vasil'chuk 1992, Meyer et al. 2002). Ice wedges are fed by snowmelt or snow directly entering frost cracks, and thus are directly linked with atmospheric moisture. The isotopic composition of single ice wedges and other types of ground ice has been measured with a Finnigan Delta-*S* mass spectrometer using equilibration technique with a precision of ±0.1‰ for $\delta^{18}O$ and ±0.8‰ for δD. Significant differences have been observed in the isotopic composition of single ice wedges as well as in the other types of ground ice. Ice wedges have been subdivided into main isotope zones (A), (B), and (C).

The ice wedge of an open pit near Fox (A), directly dated to 3.6 ka ^{14}C BP, shows a mean $\delta^{18}O$ and δD of -21.8‰ and -172‰, respectively. This is a typical isotopic signature for ice wedges of Holocene age and may therefore be used as equivalent for interpretation of ice wedges in the VC tunnel.

The stable isotope composition of ice wedges in the tunnel displays two zones of varying winter temperatures: (B) 2.8–8 m depth. Ice wedges are characterized by lowest respective mean $\delta^{18}O$ and δD of about -26.5‰ and -210‰, thus, by relatively coldest winters. This estimate is based upon 8 single ice wedges with mean oxygen isotopic composition between

-29.3‰ (at 2.8 m, auger hole) and -23.6‰ (at 6.3 m). This indicates a certain degree of variability of winter climatic conditions, but nonetheless glacial conditions especially in the uppermost part, where lightest (most negative) isotopic composition is reached.

(C) 8–22 m depth. A much higher mean $\delta^{18}O$ and δD of about -22‰ and -175‰, respectively, is observed in the 14 ice wedges of isotope zone C. Mean oxygen isotopic composition in single ice wedges varies from -24.2‰ (at 10.2 m) and -20.5‰ (at 21 m). This could reflect winter temperatures similar to the present ones or, in parts, even warmer as today. Especially in the transition horizon, relatively heavy isotopic composition in ice wedges between -20‰ and -21‰ are common. This relatively clear subdivision is possible despite the fact that ice wedges, predominantly vertical features, propagate downward into older sediments. Between 13.5 and 15 m depth, ice wedges might have a limited climatic relevance. In this depth range, low d excess (below -2‰) points to secondary fractionation. This might be caused by evaporation/sublimation of snow or the participation of reprecipitated water. Therefore, the relatively variable isotopic composition of ice wedge in this depth range is considered with caution.

The mean isotopic composition of thermokarst-cave ice is $\delta^{18}O$ = -22.1‰, and is thus similar to that of ice wedges in isotope zone C. This points to an event of local melt of ground ice, which was subsequently refrozen as thermokarst-cave ice. Intrasedimental ice (both pore and segregated ice) displays highly variable isotopic composition all over the permafrost sequence due to the fact that this type of ice includes not only winter precipitation. Consequently, the isotopic composition of intrasedimental ice is heavier ($\delta^{18}O$ = -19.8‰, N = 23), with lightest values observed at the top of the silt horizon and heaviest values at the bottom.

Discussion

The environmental history reconstructed from sediments and ground ice of the Vault Creek tunnel revealed a series of new results for Central Alaska. The youngest part of the regional history was derived from samples of an auger hole (as well as of an open pit near Fox) and dated to the 2nd half of the Holocene, where peat accumulation took place, ice wedge growth was common and the climate was relatively wet and warm according to palynology and isotope geochemistry of ice wedges. Obviously, the top of the VC tunnel reveals a part of the environmental history around 25 ka ^{14}C BP. Pollen indicate a cold and glacial climate and treeless vegetation. Lightest isotopic composition in ice wedges (and in intrasedimental ice), also point to coldest climatic conditions for the whole sequence. This section was dated to an interval just some thousand years before Late Glacial Maximum. It also states clearly that at VC tunnel, loess accumulation continued at least until 25 ka BP. At the Fox tunnel, a hiatus was observed between about 14–30 ka BP (Hamilton et al., 1988).

The organic remains in fluvial gravels at the bottom of the sequence show infinite ^{14}C ages, which is also supported by the IRSL dates in the transition horizon. Consequently, fluvial activity must have been strong in Early Wisconsin or even before. At this time, summers must have been warm and wet, leading to the intensification of fluvial activity in the area.

Conflicting dates and proxy indications are especially related to the silt unit, which was AMS ^{14}C dated between 40 and 50 ka BP. Unfortunately, these dates are not always in the right order with increasing ages with depth and display relatively large error bars. Hence, it raises the question how the ages around 40 - 50 ka BP correlate with the extremely warm temperatures derived from pollen analyses (especially PZ-II and PZ -III).

This interval has not been known as very warm until now, whereas around 30 to 40 ka BP, interstadial conditions have been described for various sites. For instance, thaw unconformities in the Fox tunnel (the so called ”Fox thermal event”) have been dated to 30 to 35 ka BP (Hamilton et al., 1988). In northwest Canada, a mid-Wisconsin Boutellier non-glacial interval with temperatures similar to the present ones has been dated to between 30 and 38 ka BP (Schweger and Janssens, 1980). Three ^{14}C dates from ice wedges fall into this time interval (two from Fox, one from VC tunnel), confirming that in the region, frost cracking was active at that time. For about the same interval, temperatures similar to the present ones have been derived by pollen analysis for a sediment record of the Isabella basin, near Fox (Matthews et al. 1974). In Matthews’ study, pollen zone Ab indicates climatic conditions as warm as today around 32 ka BP.

There are only few examples for Alaskan climate records extending beyond this interstadial phase. For instance, pollen spectra at Imuruk Lake, Seward Peninsula were interpreted differently by various authors. Pollen zone i was dated to >37 ka and >34.4 ^{14}C BP and attributed to the Sangamon by Colinvaux (1967). However, Shackleton (1982) assumed a Mid Wisconsin interstadial for this pollen zone. This re-estimate is based, among other methods, upon the assumption that the Old Crow (OC) tephra (predating pollen zone i) is about 80 ka old. New data yield an age for the OC tephra of about 142.3±6.6 ka BP (Berger 2003). Therefore, the pollen spectra at Imuruk Lake must be re-interpreted and at the moment, pollen zone i is more likely interglacial (Sangamon) than interstadial.

Nonetheless, in no other palynological study in Interior Alaska have such warm climatic conditions as in the VC tunnel been derived by means of pollen analyses (Ager & Brubaker, 1985). This is not only valid for a small part of the VC tunnel, but for almost the complete periglacial sequence. This reflects the difficulty of interpreting environmental data beyond radiocarbon dating range and the need to understand more about the environmental history in Alaska. This makes the VC tunnel exceptionally valuable for a more detailed study of this time interval.

To summarize, there are three possibe interpretations of our data: (1) trust the radiocarbon ages. In favor of this hypothesis is the high number of similar and finite ages of the silt horizon, as well as two IRSL ages from the transition horizon predating the loess. This points to a Wisconsin age of both transition and silt horizons. Additionally, the AMS method applied at Leibniz laboratory in Kiel, expanded the

dating range back to about 50–70 ka BP (Nadeau et al. 1997, 1998). This assumption would lead to a very warm and as yet unknown interval in mid-Wisconsin times.

The fact that trees grew close to the site allows a second (hypothetical) interpretation, that (2) a small forest existed in the Vault Creek area due to locally different climate conditions (e.g., close to a hot spring) and survived through Wisconsin times. Finally, we can (3) disbelieve the ages, which are near the dating limit, and assign the whole sequence to the Sangamon (or other) interglacial based on interpretation of pollen spectra. A warm phase is supported by relatively heavy isotope composition of the ice wedges. Acceptance of this hypothesis would contradict Pewe's ideas of no ground ice surviving the Sangamon interglacial in Interior Alaska. In any case, winter temperatures must have been cold enough for frost cracking, and summers not so warm as to melt ground ice. This paradox of extremely warm summer temperatures at a presently discontinuous and relatively warm permafrost site, with predominantly loess accumulation in which ground ice was formed and survived, cannot be solved completely. It is likely that sediment transport downslope, redeposition, and burial of ground ice played a key role for the pre-existence of permafrost. At least once, melting influenced the sequence when thermokarst-cave ice was formed after lateral melting of ground ice. This displays the vulnerability of these deposits, but also the possibility of contaminating older deposits by younger organic material.

Conclusions

The late Quaternary record of the Vault Creek permafrost tunnel near Fairbanks spans more than 75 ka and indicates varying environmental conditions from rather fluvial (gravelly) to aeolian (silty) environmental conditions.

Fluvial activity was intensive in the Vault Creek area in or before Early Wisconsin, leading to the deposition of 17.5 m of fluvial gravels. Climate conditions were warm and wet during that time. There are no signs of frost cracking activity at that time.

AMS ^{14}C dates point out that silt accumulation and ice wedge growth took place in the vicinities of the VC tunnel from 40 to 50 ka BP to at least 25 ka BP. A very warm phase with spruce forest environment occurred in Central Alaska, whose timing and duration is still uncertain due to conflicting age determinations and proxy indications. However, a climate deterioration is evident at the top of the section (around 25 ka BP), when the climate was colder than today and a treeless tundra environment prevailed as indicated by pollen and ice wedge isotope geochemistry. During the second half of the Holocene, peat accumulation and ice wedge growth took place.

Acknowledgments

We thank Mr. Sam Skidmore for the field support and valuable suggestions. We also thank Melanie Sierralta from the GGA Institute in Hannover for U/Th dating and Matthias Krbetschek from Freiberg Technical University for providing two IRSL dates.

References

Ager, T.A. & Brubaker, L.. 1985. Quaternary palynology and vegetational history of Alaska. In: V.M Bryant. & R.G. Holloway (eds.), *Pollen records of Late Quaternary North American Sediments*. 353-384.

Ager, T.A., Matthews, J.V. & Yeend, W. 1994. Pliocene terrace gravels of the ancestral Yukon River near Circle, Alaska: Palynology, paleobotany, paleoenvironmental reconstruction and regional correlation. *Quaternary International* 22/23: 185-206.

Berger, G.W. 2003. Luminescence chronology of late Pleistocene loess-paleosol and tephra sequences near Fairbanks, Alaska. *Quaternary Research* 60: 70-83.

Hamilton, T.D., Craig, J.L. & Sellmann, P.V. 1988. The Fox permafrost tunnel: a late Quaternary geologic record in central Alaska. *Geological Society of America Bull.* 100: 948-969.

Matthews, J.V., Jr. 1974. Wisconsin Environment of Interior Alaska: Pollen and Macrofossil Analysis of a 27 Meter Core from the Isabella Basin (Fairbanks, Alaska). *Canadian Journal of Earth Sciences* 11(6): 828-841.

Meyer, H., Dereviagin, A.Yu., Siegert, C., Schirrmeister, L. & Hubberten, H.W. 2002. Paleoclimate reconstruction on Big Lyakhovsky Island, North Siberia – Hydrogen and oxygen isotopes in ice wedges. *Permafrost and Periglacial Processes* 13: 91-105.

Nadeau, M.J., Schleicher, M., Grootes, P.M., Erlenkeuser, H., Gottdang, A., Mous, D.J.W., Sarnthein, J.M. & Willkomm, H. 1997. The Leibniz-Labor facility at the Christian-Albrecht-University, Kiel, Germany. *Nuclear Instruments and Methods in Physics Research* 123: 22-30.

Nadeau, M.J., Grootes, P.M., Schleicher, M., Hasselberg, P., Rieck, A. & Bitterling, M. 1998. Sample throughput and data quality at the Leibniz-Labor AMS facility. *Radiocarbon* 40: 239-245.

Péwé, T.L. 1975. Quaternary Geology of Alaska. *US Geological Survey Prof. Paper* 835: 145pp.

Sellmann, P.V. 1967. Geology of the USA. CRREL permafrost tunnel, Fairbanks, Alaska. Technical Report 199, US Army CRREL. Hanover, New Hampshire, 22 pp.

Schweger, C.E. and Janssens, J.A. 1980. Paleoecology of the Boutellier non-glacial interval, St. Elias mountains, Yukon territory, Canada. *Arctic and Alpine Research* 12. 309-317.

Shur, Y., French, H.M.,Bray, M.T. & Anderson D.A. 2004. Syngenetic Permafrost Growth: Cryostratigraphic Observations from the CRREL Tunnel near Fairbanks, Alaska. *Permafrost and Periglac. Process*. 15: 339-347.

Vaikmäe, R. 1989. Oxygen isotopes in permafrost and ground ice – A new tool for paleoclimatic investigations. *5th Working Meeting Isotopes in Nature, Proceedings, Leipzig, September 1989:* 543-553.

Vasil´chuk, Yu.K. 1992. Oxygen isotope composition of ground ice—application to paleogeocryological reconstructions, Vol. 1, Moscow, Russia: 420 pp.

Viereck, L.A. & Little Jr., E.L. 1972. Alaska Trees and Shrubs. Agriculture Handbook No. 410, Forest Service US Department of Agriculture. Washington DC, 265 pp.

Properties of Eroding Coastline Soils Along Elson Lagoon Barrow, Alaska

G.J. Michaelson, C.L Ping, L.A. Lynn
University of Alaska Fairbanks, AFES-Palmer Research Center, Palmer, Alaska
M.T. Jorgenson
Alaska Biological Research Inc., Fairbanks, Alaska
F. Dou
International Arctic Research Center, University of Alaska Fairbanks, Alaska

Abstract

We studied eroding coastline soils at 6 points along the beach exposure of Elson Lagoon near Barrow, Alaska. Exposures consisted of an average 37 cm of thawed soil and 103 cm of permafrost soil. Sediments were Holocene in origin with basal organic matter dating from 4,820 to 6,650 ybp. Exposures contained large amounts of organic carbon and nitrogen (45–112 kgOC m^{-2}, 2.5–6.1 kgN m^{-2}). These amounts are among the highest found for exposures of similar heights across the north coast of Alaska. We estimate large amounts of water, sediment, organic C and N (1,144, 1,002, 98, and 6 kgx10^3 km^{-1}, respectively) are exposed to erosion each year along the lagoon. Methane released from the thawing exposure soils ranged from 0.06–1.66 gCH_4 m^{-2}, and soil horizons nearest to the top of the permafrost and bottom of the active layer released the largest amounts in all exposures.

Keywords: Alaska; coastal erosion; sediment transfer; methane; trace gases; soil organic carbon.

Introduction

Changing wind and sea ice conditions along the Alaskan arctic coast have been associated with increases in observed rates of coastal erosion. Brown et al. (2003) reviewed previous erosion rate studies of the arctic Alaska coastline. Long-term rates for the Beaufort Sea coast calculated for the latter part of the 20th century (1951–1983: Reimnitz et al. 1988, Barnes et al. 1992) showed that the finer sediments of the coastline in the Barrow region are eroding most rapidly at an average rate of 5.4 m yr^{-1} compared with an average rate of 1.4 m y^{-1} for the coarser-based sediments of the eastern two-thirds of the Alaska coastline. A more detailed photogrammetric study for one area of the Elson Lagoon near Barrow for the period 1979–2000 revealed erosion rates for different exposures varying from 0.69 to 2.75 m yr^{-1} with an average rate of 1.27 m yr^{-1} for the whole lagoon (Brown et al. 2003). The Brown et al. study found that the 1979–2000 erosion rates along lagoon segments had increased up to 47% over the previous 40-year period. These increases were for the exposures with fine-grained sediments, whereas the erosion rates of gravel beach segments of the lagoon remained lower at 0.5 m yr^{-1}. Sediment and carbon transfer rates along Elson Lagoon were estimated by Brown et al. (2003) using the erosion rate determined in the study combined with soils data from the 1957 soils map of the area. We studied actual soils profiles of exposures along Elson Lagoon and detail the soil materials exposed as they vary along the lagoon in order to characterize load and range of materials that are being released to the near-shore lagoon environment. Work at Elson Lagoon was part of a larger study to assess the fate and transformation of soil carbon eroding into the Beaufort Sea (Jorgenson et al. 2005).

Methods

Sites

Study sites were located along beach segments identified by Brown et al. (2003) for sites 1–4 and extending further southeast along the coastline for sites 5 and 6 (Fig. 1).

The soils at the exposures (Table 1) represent those of the major mapping units that covered over 80% of the area near Barrow, including south of Elson Lagoon as reported by Bockheim et al. (1999). Exposures sampled were typical in morphology for each respective beach segment.

Sampling and analysis

Soil profiles were excavated from the surface down to sea level to remove slumped and refrozen materials at each of the 6 beach exposure sites along Elson Lagoon (Fig. 1). Soil layers were identified (Schoeneberger et al. 1998) and sampled using cut blocks in the active layer and drill cores in permafrost. These dimensional samples were at regular depths to include all soil horizons identified down to sea level. Samples in permafrost were kept frozen and all samples were stored frozen until analysis at the UAF-AFES Plant and Soils Laboratory at the Palmer Research Center. Soil bulk density and water contents were determined by weight difference upon drying at 100°C of dimensional samples. Total organic C (TOC) and N were determined using a LECO CHN analyzer with carbonates removed by acid pretreatment. The sediment, water, TOC, N, nutrient contents, and gas contents of the exposures were determined using the exposure description and analysis by the method of Kimble et al. (1993) to account for cryoturbation. Available soil N, P, and K were extracted by 2M KCl, Mehlich-3, and neutral 1M ammonium acetate solutions respectively (Soil Survey Staff 1996). Methane and carbon dioxide gases evolved from

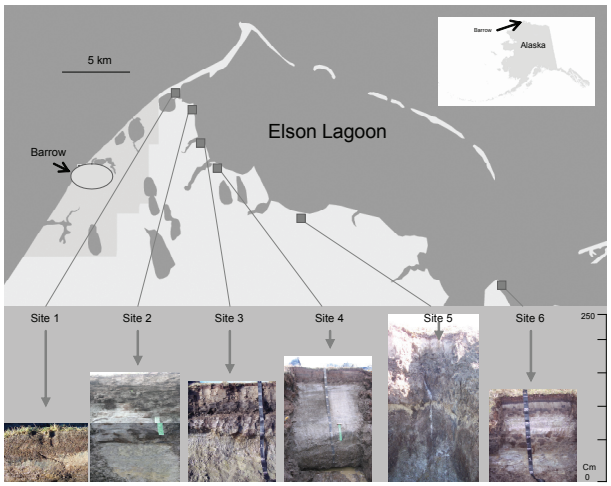

Figure 1. Study site locations and exposure profiles.

samples were determined by thawing dimensional samples for 5–10 hours in a sealed chamber attached to a Columbus Instruments Micro Oxymax respirometer. Radiocarbon dating was performed at NOAMES Laboratory, Woods Hole Massachusetts.

Results and Discussion

Soil characteristics

Exposure soils were either in alluvial-marine (sites 1 and 3) or drained lake (sites 2 and 4–6) deposits that contained inter-bedded peat and fine minerals of sandy loam to silty clay in texture (Fig. 1 and Table 1). The two alluvial marine exposures (sites 1 and 3) and one of the drained lake basins (site 5), showed little cryoturbation of organics within the layers and were Orthels while the majority of drained lake exposures had significant cryoturbation or frost mixing of organic matter and mineral materials and were Turbels under the U.S. soil classification system (Soil Survey Staff 1998). But all soils had uneven distribution of organic matter throughout their profiles (%OC in Table 1) contributing to increase OC stores to depth. Turbels are common to the area around the southern lagoon, as Bockhiem et al. (1999) mapped over 70% of the area as Turbels. Basal peat ages at sites 2 and 6 were 6650 ybp (125 cm) and 4820 ybp (60 cm), respectively.

Materials eroding at the exposures

Coastline exposures averaged 74% water and ice by volume ranging from 51% at site 4 to 90% at site 6 (site data in Fig. 2). An average of 69% was reported by Michaelson et al. (2006) for 29 exposures along the coast east to Colville River delta. Active layers along Elson Lagoon averaged lower at 67% volumetric water compared to the permafrost that averaged 77% volumetric ice. This is consistent with higher water holding capacities of organic horizons that elevate water contents in the active layer and the permafrost-encased organic horizons along with additional water in permafrost stored as ice lenses and massive ice. Water contents found in this study are generally higher than the 50% estimate used by Brown et al. (2003) to calculate erosion volume transfers along the lagoon. The mass of water in exposures studied here ranged from 431 to 1735 kg m^{-2} (average: 901 kg m^{-2}). The average mass of water in the Elson exposures tends to be somewhat lower than the average of 1200 kg m^{-2} found for 29 exposures along the coast from Barrow to the Colville River delta reported by Michaelson et al. (2006). However the 29 exposures across the larger coastal section averaged 175 cm in height compared to 140 cm in this study (Table 2). There is less than a 10% difference if considered on a per–cm-exposure height basis.

The mass of sediments available for transfer from the Elson Lagoon exposures were somewhat lower than that of water and ranged from 395–1032 kg m^{-2} (average 789 kg m^{-2}, Table 2). These sediment amounts encompass a greater range than found for three study-transects along the Beaufort Lagoon in the northeastern North Slope of Alaska, but the average of 789 kg m^{-2} is within the range of 871–998 kg m^{-2} found there (Jorgensen et al. 2003).

Carbon and nutrients at the exposures

Organic carbon (OC) and nitrogen transfer from the coastal tundra to the nearshore environment is of particular interest for terrestrial-aquatic carbon partitioning and budget analysis. Even with this interest, there are little data on carbon and very little on nitrogen in coastal tundra especially to depth (Ping et al. 2007). The soils of the coastal plain have been found to hold high amounts of organic carbon compared to the foothills region on average about 50% more (Michaelson et al. 1996). Exposure soils at sites 1–6 along Elson Lagoon ranged from 45 to 112 kgOC m^{-2} (Table 2), averaging 78 kgOC m^{-2}. Jorgensen et al. (2003) found similarly high stocks ranging from 54 to 136 kgOC m^{-2} in coastal exposures of the Beaufort Lagoon on the northeastern coastal plain. Exposures studied there averaged 240 cm in height compared to the Elson sites average of 140 cm, and average OC stocks there were 85 kgOC m^{-2} compared to 78 kgOC m^{-2} for the Elson Lagoon sites. Still, on average, the Elson exposures held about 60% more OC cm^{-1} of exposure height (0.56 compared to 0.35 kgOC cm^{-1} of exposure height) compared to the Beaufort Lagoon. When 29 exposure sites were considered from Barrow to the Colville River delta (Michaelson et al. 2006) exposures averaged 175 cm in height and contained on average 69 kgOC m^{-2} (0.39 kgOC cm^{-1} of exposure height,).

More OC data for the area is available for soils to a 100-cm depth in a study by Bockheim et al. (1999). They estimate the average Barrow area soils (around Elson Lagoon) to hold 50 kgOC m^{-2} to a depth of 100 cm with soils in mapping units containing from 27 to 73 kgOC m^{-2}. When OC stocks were calculated to only 100 cm for each site (including site 1 with only a 63 cm exposure measured) Elson sites 1–6 of this study averaged 63 kgOC m^{-2}. This average is the same as estimated as average for coastal plain soils by Michaelson et al. (1996).

The major organism-available nutrients nitrogen (NH_4+NO_3-N), phosphorus (PO_4-P), and potassium (K^+)

Table 1. Location, soil classification, surface characteristics, and selected soil properties for soil profiles at the exposure sites. Thermal state: AL = active layer and Pf = permafrost.

Site USDA Soil Classification	Unit:Terrain Surface Subsurface	Horizon	depth *cm*	pH	EC *ds cm²*	USDA Texture	Thermal State	Organic C ---%--
1	-Alluvial-Marine	Oi	0-6	5.88	21.4	peat	AL	25.7
Typic	-Inactive Tidal Flat	Bg/Oa	6-11	5.63	18.7	loam	AL	9.0
Aquorthel	-Drained Lake Basin,	Oa/Bg	11-27	5.56	13.5	muck	AL	10.5
71°20.193'N	(Ice-poor Center)	Cg	27-53	7.27	23.5	Scl	AL	1.7
156°35.574'W		Cg	53-63+	7.58	24.8	Scl	Pf	2.1
2	-Drained Lake Basin,	Oi	0-8	4.91	0.43	Peat	AL	40.0
Typic	(Ice-rich Center)	Bg	8-22	5.07	0.77	S loam	AL	4.6
Aquiturbel	-Organic Fen	Oa/Bgjj	22-54	4.99	0.60	muck	AL	24.0
71°19.4496'N	-Thaw Basin, Ice-rich	Bg/Oajj	54-87	4.89	0.59	muck	AL	23.4
156°34.106'W		Oa/Bgf1jj	87-105	5.35	1.16	muck	Pf	25.0
		Cf	105-145	7.30	5.89	S loam	Pf	1.0
		Cf1	145-150+	7.29	3.80	S loam	Pf	0.9
3	-Alluvial-Marine	Oi	0-5	5.15	0.33	peat	AL	37.3
Fluventic	-Organic Fen	Bw	5-28	4.87	0.48	loam	AL	2.8
Historthel	-Alluvial-Marine	A/Oejj	28-40	5.45	0.70	Mucky sil	AL	16.7
71°18.237'N		A/Oijj	40-55	5.53	0.96	Peaty sil	AL	16.6
156°32.634'W		Bw/Oefjj	55-85	5.61	4.08	Sl	Pf	6.7
		Cf	85-125+	6.96	13.6	Scl	Pf	1.3
4	-Drained Lake Basin	Oi	0-4	4.91	2.96	peat	AL	39.9
Terric	Ice-rich Center	Oe	4-16	4.21	6.82	mk pt	AL	33.3
Hemistel	-Organic Fen	Oi	16-29	4.37	4.10	peat	AL	18.4
71°16.974'N	-Thaw Basin, Ice-rich	Oa	29-45	4.85	0.99	muck	AL	10.4
156°25.760'W	Margin	Oa1/Af1	45-60	5.1	0.78	silt loam	Pf	9.4
		Oa2/Af2	60-105	4.98	0.91	silt loam	Pf	9.3
		A3/Oaf1	105-120	5.31	1.75	silt loam	Pf	5.3
		A4/Oaf2	120-135	5.46	3.83	silt loam	Pf	9.7
		A5/Oaf3	135-155	5.82	4.65	silt loam	Pf	11.9
		A6/Oaf4	155-170+	6.12	8.16	silt loam	Pf	9.0
5	-Drained Lake Basin,	Oi	0-9	4.46	0.81	peat	AL	40.9
Typic	(Ice-rich Center)	Ajjj	9-23	4.92	1.11	loam	AL	9.6
Histoturbel	-Organic Fen	Oi/Bgjj	23-45	5.03	1.26	muck	AL	16.1
71°15.5658'N	-Thaw Basin, Ice-rich	Oi/Bgfjj	45-65	4.74	0.66	muck	Pf	18.9
156°20.131'W	(Margin)	Cf	65-75	4.62	0.53	S loam	Pf	2.2
		Oifjj	75-110	4.97	0.26	pt muck	Pf	35.6
		2Cf	110-200	6.42	4.79	Si Cl	Pf	4.6
		3Cf	200-220+	7.06	18.8	silt loam	Pf	3.9
6	-Drained Lake Basin,	Oi	0-16	4.87	1.73	Peat	AL	46.2
Typic	(Ice-rich Center)	Oa	16-45	4.77	0.87	mk peat	AL	27.0
Histoturbel	-Thaw Basin, Ice-rich	Bg	45-50	5.43	0.77	silt loam	AL	6.5
71°12.6912'N	(Margin)	Oafjj	50-85	5.48	0.42	mk peat	Pf	35.7
155°55.584'W	-Alluvial-Marine Deposit	Cgf	85-110+	6.98	0.69	S loam	Pf	1.9

(Table 2) are important for organisms to utilize carbon energy sources in coastal waters as well as on land. They have been little-studied in relationship to coastal erosion transfer in the Arctic. We found considerable variation in amounts across the 6 exposures. Nitrogen was high at site 4, phosphorus at site 2, and potassium in the intertidal site (site 1). Average organic or Total N transferred per km of coast was over 100 times the magnitude of the available NH_4+NO_3-N form (bottom Table 2). Although the amounts of OC and N available at the exposures were considerably higher on Elson Lagoon (over 80%) than the Alaska Barrow to Canada coastal averages found by Dou et al. (2007), the C:N ratios were the same at 17.7, an indication of similar average organic matter quality. Potassium was in the highest in magnitude of the three nutrients for all 6 sites.

Gas content of eroding soils

Trace gas release from eroding coastline is of particular interest because it could serve as a positive feedback to climate change with increased methane and carbon dioxide emissions. Tundra is known to release significant amounts of methane upon melting as has been measured in thermokarst lakes (Walter et al. 2006). Similar thawing of permafrost is occurring along the coastline. Warming and thawing of soils already containing methane under saturated conditions can be expected to release trace gasses. We measured methane and carbon dioxide released from frozen samples taken from the Elson Lagoon sites 1–6 (Fig. 2). Site exposures released an average of 0.61 gCH_4 m^{-2} exposure (range 0.06–1.66 gCH_4 m^{-2}) and 67 gCO_2 m^{-2} (range 43–78 gCO_2 m^{-2}). For the 29 sites along the coast to Colville River delta, Michaelson

Table 2. Height and load of sediment, water, total organic carbon, nitrogen, and extractable nutrients for exposures.

Site #	Bank Height	Sediment	H_2O	TOC	TN	NH_4+NO_3-N	PO_4-P	Exch.-K
Exposure stores								
	cm	*kg m^{-2}*				*g m^{-2}*		
1-BSC01	63	709	431	45.0	2.5	19	4	216
2-BLUFF	150	753	1104	80.5	5.3	36	14	57
3-ACS-9	125	1032	732	61.1	3.6	23	4	37
4-ACS13	170	870	663	112.1	6.1	97	7	136
5-BSC02	220	977	1735	99.3	5.2	47	6	106
6-BSC03	110	395	743	66.9	3.8	17	2	43
ave	139.7	789	901	77.5	4.4	40	6	99
stdev	53.8	300	462	25.0	1.3	30	4	69
Mass transfer estimate per km coastline with one meter of eroded bank								
		kgx10^3 km^{-1}				*kg km^{-1}*		
average Sites 1-6		1002	1144	98	6	51	8	126

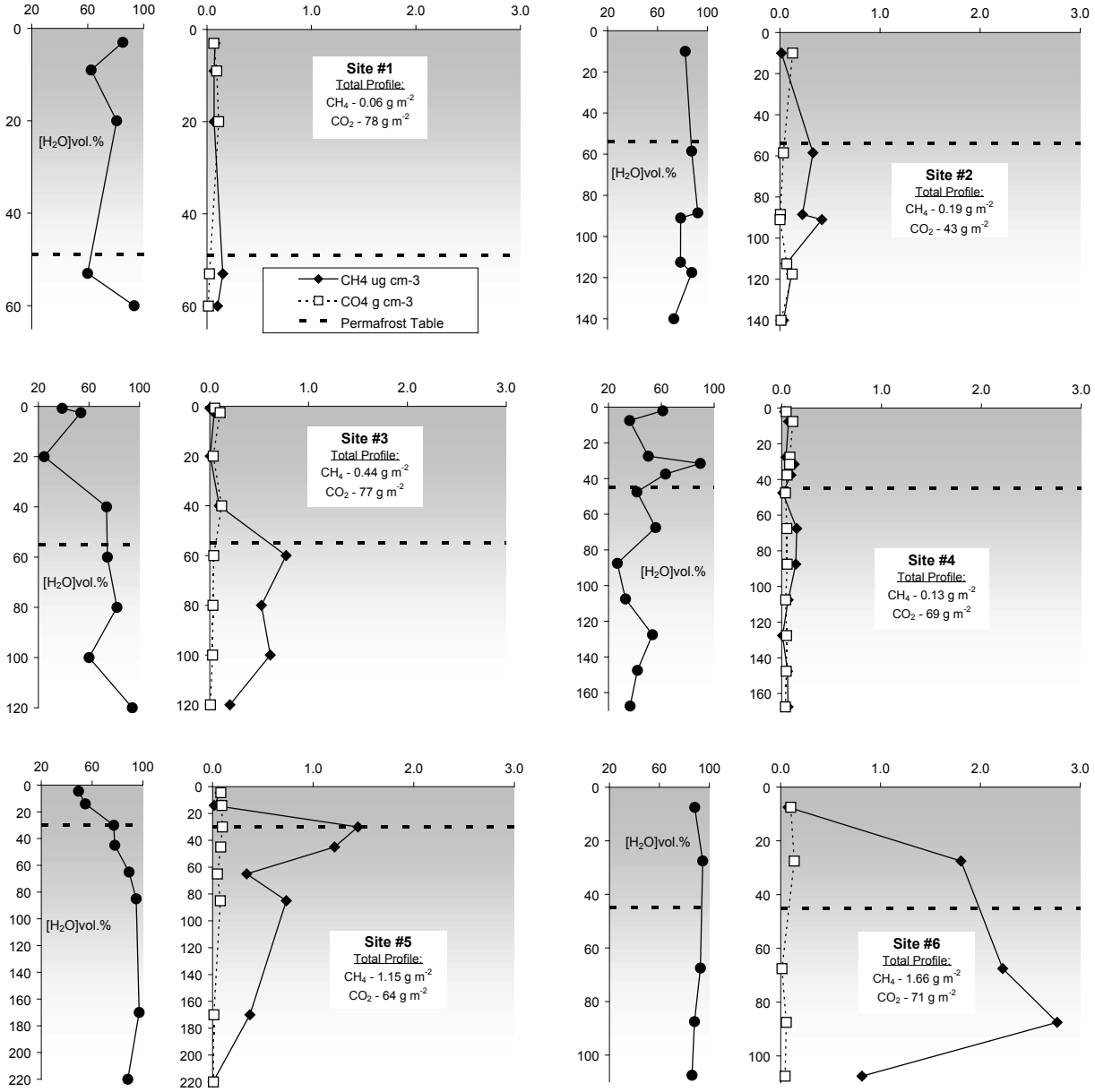

Figure 2. Volumetric water content ($[H_2O]_{vol.}$%) and methane/carbon dioxide gas release of soil profiles (lines are measured for cubic centimeters along the profile and totals are given as contained in a square meter of profile).

et al. (2006) reported average releases of 1.1 gCH_4 m^{-2} and 89 gCO_2 m^{-2} with an average exposure of 175 cm. The average methane release of the Elson sites was 0.43 gCH_4 m^{-1} of exposure height compared to the 29 sites to the east that averaged 0.63 gCH_4 m^{-1} of exposure height that is within the range found for the Elson sites (0.04–1.19 gCH_4 m^{-1} of exposure height). Carbon dioxide released had less variation with an average of 48 gCO_2 m^{-1} of exposure height for Elson sites. This compares closely to an average of 51 gCO_2 m^{-1} of exposure height found for 29 sites to the east by Michaelson et al. (2006).

As could be expected, methane releases tended to be higher in the permafrost and near permafrost (lower active layer, Fig. 2), while carbon dioxide release tended to be higher in the active layer. This is consistent with methane formation conditions more favorable in the saturated or frozen saturated organic horizons with limited contact to the atmosphere, while carbon dioxide would be favored in aerated near-surface layers. These relationship trends can be observed for nearly all site-exposure profiles. Methane increases at or near the top of the permafrost table, reaches a maximum in the permafrost, and decreases again at depth. Sites with the greatest water contents (sites 5 and 6) had the greatest methane contents. On an aerial basis the releases of methane are on the order of one-tenth those observed for wet tundra on the North Slope (Vourlitis et al. 1993).

Conclusions

Exposure heights along Elson Lagoon are near average for the North Slope, Alaska, coastline. However, Elson exposures contain larger OC stores than the average for the whole North Slope, Alaska, coastline. These larger OC stores are due to the presence of soils with both cryoturbated organic matter and layered peat or muck horizons. These OC rich horizons are a result of the drained-lake sequence history and the medium-textured soils of the lagoon's nearshore area. The history of the tundra, alternating from moist to aquatic conditions, allows for cryoturbation causing an increase in the OC storage in the moist condition, while peat development and sedimentary accumulation increases OC during wet or aquatic conditions. There is more OC eroding from exposures than would be predicted from the currently available local soil survey map of Bockheim et al. (1999).

The TN of exposures can also be expected to be higher than for other North Slope shore areas, as most of the nitrogen is associated with the eroding organic matter. The higher TN of eroding organic matter can be expected to positively affect the nutrient status and biotic activity of the nearshore area with N often limiting activity.

The stratification of peat by cryoturbation and by aquatic-sedimentary accumulation has resulted in layers of organic-enriched materials near the surface of the present-day permafrost table and just above it in the lower active layer. Both layers are under water-saturated conditions that favor accumulations of methane as organic matter decomposes. In exposures with these saturated organic layers, methane has accumulated presumably from subzero-temperature soil respiration and/or encasement of gases produced under previously thawed conditions with permafrost table fluctuation. Carbon dioxide present will be released along with methane upon thaw due to thermal erosion at the shoreline. This release upon thaw is in relatively small amounts, but could become a significant amount with increased rates of erosion and or with increased methane production due to changing soil thermal regimes.

Acknowledgments

This study was conducted as part of NSF grant OPP Grant #0436179. Field work was through the assistance of Yuri Shur, Mikial Kavansky, Daniel Fortier, Vladimir Tumskoy, Sabine Fiedler, Prothap Kodeal, and BASC staff at the Barrow Ilisagvik College.

References

Barnes, P.W., Reimnitz, E. & Rollyson, B.P. 1992. Map showing Beaufort Sea coastal erosion and accretion between Flaxman Island and the Canadian border northeastern Alaska (1:82,000). *U.S. Geological Survey Miscellaneous Investigations Series* Map I-1182-H, 22 pp. plus map.

Bockheim, J.G., Everett, L.R., Hinkel, K.M., Nelson, F.E. & Brown, J. 1999. Soil organic carbon storage and distribution in arctic tundra, Barrow, Alaska. *Soil Science Society of America Journal* 63: 934-940.

Brown, J., Jorgenson, M.T., Smith, O. & Lee, W. 2003. Long-term rates of arctic coastal erosion, Elson Lagoon, Barrow, Alaska. In: Phillips & Arenson (eds.), *Permafrost*: 101-106.

Dou, F., Xu, Y., Ping, C.L., Michaelson, G.J., Guo, L. & Jorgenson, M.T. 2007. Modeling spatial variations of tundra soil organic carbon along the coastline of northern Alaska. Manuscript in review.

Jorgenson, M.T, Macander, M., Jorgenson, J.C., Ping, C.L. & Harden, J. 2003. Ground ice and carbon characteristics of eroding coastal permafrost at Beaufort Lagoon, northern Alaska. In: Phillips & Arenson (eds.), *Permafrost*: 495-500.

Jorgenson, M.T., Ping, C-L., Guo, L., Shur, Y. & Brown, J. 2005. A multi-scale approach to assessing the flux and transformation of organic carbon across the eroding coastline of northern Alaska. *Berichte Zur Polarund Meeresforschung* 506: 65-68.

Kimble, J.M., Tarnocai, C., Ping, C.L., Ahrens, R., Smith, C.A.S., Moore, J. & Lynn, W. 1993. Determination of the amount of carbon in highly cryoturbated soils. In: D.A. Gilichinsky (ed.), Post-Seminar *Proceedings of the Joint Russian-American Seminar on Cryopedology and Global Change*. Pushchino, Russia, 15-16 Nov. 1992. Russian Academy of Science, Pushchino, Russia.

Michaelson, G.J., Ping, C.L., Jorgenson, M.T., Dou, F., Shur, Y. & Guo, L. 2006. Methane and carbon dioxide release from eroding coastline of North Slope, Alaska. World Congress of Soil Science Meeting, Philadelphia, July 2006, Abstracts.

Michaelson, G.J., Ping, C.L. & Kimble, J.M. 1996. Carbon storage and distribution in tundra soils of arctic Alaska, U.S.A. *Arctic and Alpine Research* 28(4): 414-424.

Ping, C.L., Michaelson, G.J., Jorgenson, M.T., Kimble, J.M., Epstein, H., Romanovsky, V.E. & Walker, D.A. 2007. High stocks of organic carbon in North American arctic region. *Geonature*, in review.

Reimnitz, E., Graves, M. & Barnes, P.V. 1988. Beaufort Sea coastal erosion, sediment flux, shoreline evolution and the erosional shelf profile. U.S. Geological Survey Map I-1182-G.

Schoeneberger, P.J., Wysocki, D.A., Benham, E.C. & Broderson, W.D. 1998. *Field book for describing and sampling soils.* Natural Resources Conservation Service, USDA, National Soil Survey Center, Lincoln, Nebraska.

Soil Survey Staff 1996. Soil survey laboratory methods manual, *Soil Survey Investigations Report No. 42*, Version 3.0.

Soil Survey Staff 1998. Keys to soil taxonomy, 8th edition. USDA Natural Resources Conservation Service, Washington, D.C.

Vourlitis, G.L., Oechel, W.C., Hastings, S.J. & Jenkins, M. 1993. The effects of soil moisture and thaw depth on CH4 flux from wet coastal tundra ecosystems on the north slope of Alaska. *Chemosphere* 26: 329-337.

Walter, K.M., Zimov, S.A., Chanton, J.P., Verbyla, D. & Chapin II, F.S. 2006. Methane bubbling from Siberian thaw lakes as a positive feedback to climate warming. *Nature* 443: 71-75.

The Application of Tritium in Permafrost Ground-Ice Studies

F.A. Michel
Dept of Earth Sciences, Carleton University, Ottawa, Canada

Abstract

Tritium, a radiogenic isotope of hydrogen with a half-life of 12.43 years, can be utilized as a natural tracer in water (ice) investigations. Anthropogenic tritium released into the atmosphere during nuclear testing from the 1950s to 1970s created peak monthly concentrations as high as 10,000 T.U. Recent values for Arctic Canada monitoring stations are below 30 T.U. Seasonal variations indicate higher tritium values occur during summer. Infiltration of precipitation into the thawed active layer during the summer produces elevated tritium concentrations within the soil profile. Elevated tritium levels also occur in ground ice below the permafrost table and have been interpreted previously as indicative of downward migration of water into the permafrost along a thermal gradient. Re-evaluation of data suggests that this tritium within the permafrost may in part represent the preservation of active layer water within a zone of aggrading permafrost during climatic cooling in the 1950s to 1980s.

Keywords: climate change; ground ice; permafrost; tritium.

Introduction

Although permafrost refers strictly to a thermal ground condition, many investigations of permafrost consider the distribution of water and ice in the soil as an important component due to their effects on the soil structure and stability. The accumulation of ice in the near surface can cause frost heave, while melting of excess ice can lead to thaw settlement; either can result in severe geotechnical problems. In addition, over time landforms and landscapes can be altered due to the freezing and melting of excess ice (e.g. pingos, palsas, ice wedges, patterned ground, thaw lakes, and excessive shoreline erosion) caused by changing climatic conditions. As the climate at any site changes, the seasonally frozen and thawed active layer can increase or decrease in thickness (CALM 2008) and as a result the position of the permafrost table will fluctuate.

Tritium, a radiogenic isotope of hydrogen that was produced in large quantities during atmospheric testing of nuclear devices in the 1950s and early 1960s, has been utilized by several researchers to investigate the incorporation of modern precipitation (since the 1950s) into ice contained within the active layer, the upper permafrost, and permafrost related features, such as ice wedges and frost blisters. Michel (1982, 1986) and Michel & Fritz (1978, 1982) first identified the presence of tritium within permafrost in northern Canada, while Russian investigations in Siberia were reported by Chizhov et al. (1983, 1985) and Chizhov & Dereviagin (1998). Other studies include reports by Livingstone (1988), Burn & Michel (1988), and Lewkowicz (1994). In these studies tritium has been employed as a marker to identify the presence of young water (ice) and to investigate the mechanisms for transferring this water into the permafrost from the active layer. The purpose of this paper is to examine the effects of climate change on the distribution of tritium in permafrost.

Distribution of Tritium in Precipitation

Tritium is naturally produced in low concentrations in the upper atmosphere through the interaction of cosmic radiation with ^{14}N and has a radiogenic half-life of 12.43 years. The distribution of this natural tritium in the stratosphere of the northern hemisphere is poorly understood, but is expected to be higher toward the poles; the natural concentration is considered to be in the range of 10 to 20 tritium units (T.U.; 1 T.U. = 1 atom of tritium in 10^{18} atoms of hydrogen). Testing of nuclear devices injected large quantities of anthropogenic tritium into the atmosphere, primarily in the northern hemisphere, with peak concentrations in precipitation occurring in 1963. Figure 1 displays the 1963 average monthly concentration data from North American monitoring stations. Average tritium concentrations over the polar region in 1963 (5000 T.U.) were 2 to 3 times that of the southern part of the continent and the highest recorded monthly values reached 10,000 T.U. in Whitehorse, Yukon and Nord, Greenland (IAEA 2007). Since 1963, the concentration in precipitation has decreased so that typical values today are in the range of 10 to 25 T.U. (Figure 2). At some localities, new sources of radiogenic emissions, such as nuclear facilities, may periodically give rise to increases in the tritium concentration of local precipitation.

There is also a seasonal variation at any given locale that is related to the 'leakage' of tritium from the stratosphere into the troposphere during the spring (Payne 1972). This causes the tritium concentration in precipitation to rise during the spring, peak in the summer and decline during the fall and winter, as shown in Figure 3 for the monitoring station at Alert.

The tritium concentration in precipitation peaks during the warmest part of the summer (July) when the active layer is rapidly thawing. The summer months also receive the highest amount of precipitation.

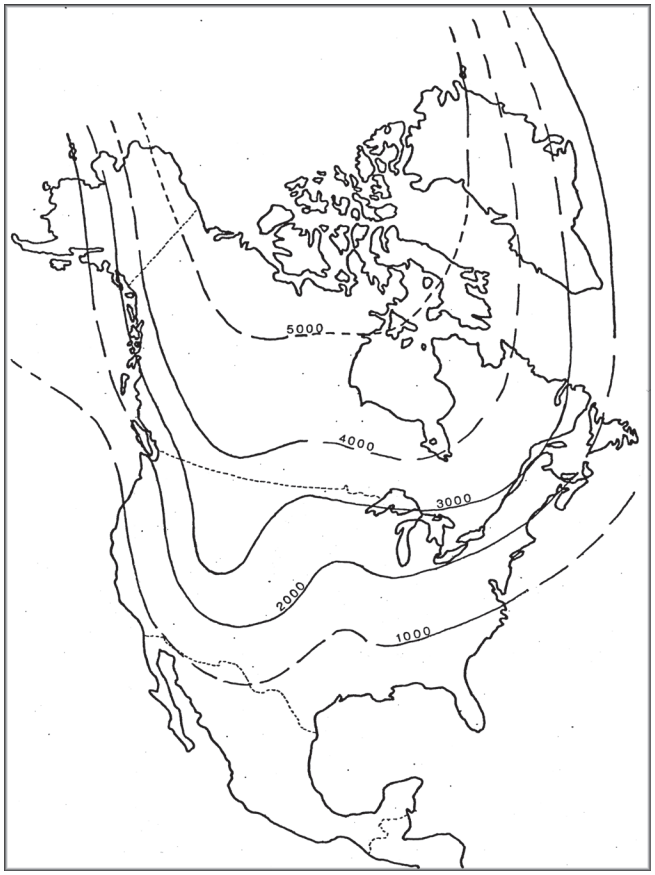

Figure 1. Distribution of average monthly tritium concentrations (in T.U.) for precipitation in North America during 1963. Dashed lines indicate uncertainty due to lack of station data (Michel 1977).

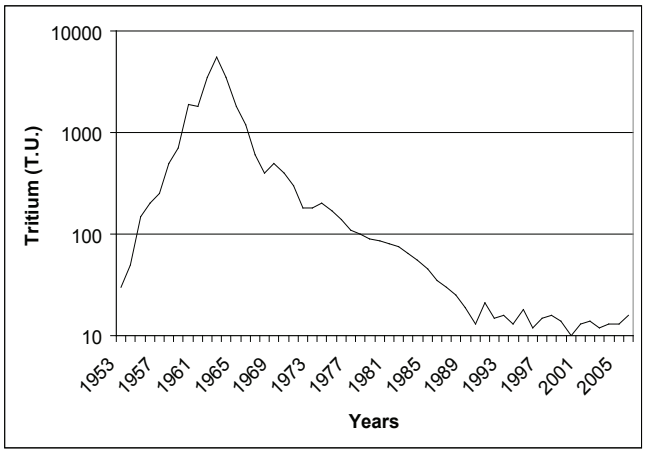

Figure 2. Estimated average tritium concentration for precipitation in the Canadian Arctic. Modeled on data from Ottawa, Canada, plus shorter term records from various Canadian (1955-1969), Greenland (1962-1971), and Alaska (1962-1971) stations (IAEA 2007). Also includes author's spot data from 1975 to 1989 and the author's arctic precipitation network data from 1989 to 2006.

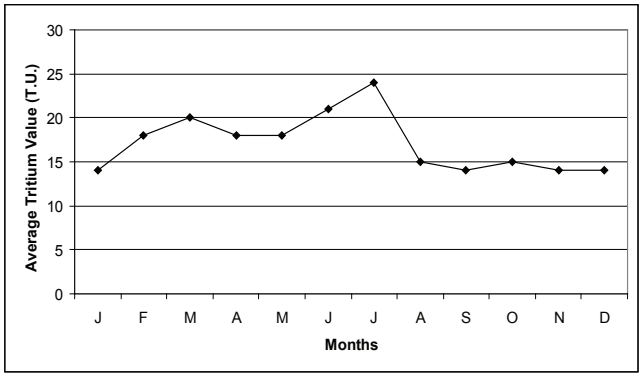

Figure 3. Average monthly tritium concentration in precipitation at Alert, Canada, for the period 1990-1999. Note the spring and summer increase.

Distribution of Tritium in the Active Layer and Upper Permafrost

Tritium concentrations, for water (ice) contained within the active layer and upper permafrost, have been measured since the 1970s. Chizhov & Dereviagan (1998) summarize over 250 tritium data from a number of sample sites throughout Siberia, with measurements as high as 352 T.U. in the active layer and 323 T.U. in the upper permafrost. The author has measured numerous samples from cores collected along the various proposed pipeline routes in northern Canada and from a detailed study site (Illisarvik) in the outer Mackenzie Delta (Michel 1982). The highest concentration measured at Illisarvik was at a depth of 30 to 40 cm (269 T.U.), while the highest overall tritium value (370 T.U.) was measured from a site south of the Baker Lake community in Nunavut. Peak concentrations throughout the Canadian arctic are generally in the range of 200 to 250 T.U. for samples collected in the mid to late 1970s and early 1980s and are usually found in the lower portion of the active layer or the upper 30 to 50 cm of permafrost. These concentrations are higher than the contemporary average annual precipitation values shown in Figure 2 and must either represent older precipitation recharged during the late 1960s to early 1970s, or summer precipitation recharge that was not mixed (diluted) with snowmelt from winter precipitation. Many active layer tritium concentration values are similar to the average precipitation values.

Chizhov et al. (1983) and Chizhov & Dereviagan (1998) concluded from their investigations that the presence of tritium in the upper permafrost indicates that extensive moisture exchange takes place between the active layer and permafrost. A study by Burn & Michel (1988), where test plots were irrigated with water containing elevated tritium concentrations, also concluded that the transport of tritiated water into the upper permafrost was due to mass flow rather than molecular diffusion. In all of these studies, the transport of water into the upper permafrost was considered to be due to water migration along a thermal gradient. Most of these investigations involved the collection of spot samples from shallow pits or cores.

Detailed profiling was conducted in May 1979 for two cores at Illisarvik; one within the limits of the lake drained in 1978 (79-4) that subsequently froze to a depth of 2.45 m during the winter of 1978-79, and the other just outside the lake basin (79-3) (Figures 4a and b, respectively). Tritium in

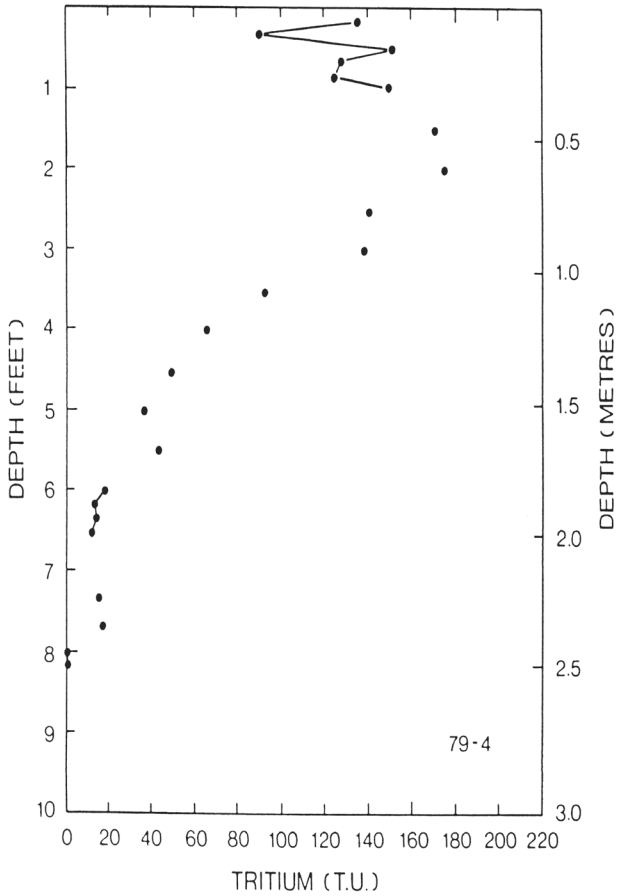

Figure 4a. Tritium concentration profile for lake-bottom sediments at Illisarvik in the Mackenzie Delta (Michel & Fritz 1982).

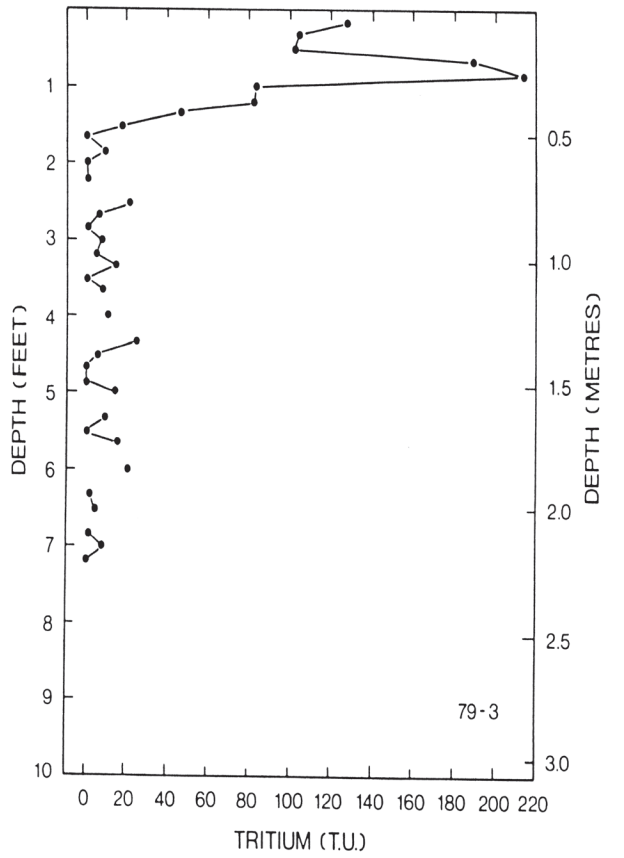

Figure 4b. Tritium concentration profile for frozen ground adjacent to the drained lake at Illisarvik in the Mackenzie Delta (Michel & Fritz 1982).

water from the shallowest lake sediment sample (136 T.U.) in core 79-4 closely reflects the tritium concentration of the lake water just prior to drainage (141 T.U.), while deeper samples display a gradual increase in tritium concentration to 177 T.U. at a depth of 40 cm. Below 40 cm the tritium profile displays a gradual decline to background concentrations at a depth of approximately 2 m. This profile is what would be expected for downward diffusion from a point source (the lake) and developed while the lake sediments were unfrozen (as a lake talik). Since the lake had no discharge creek and was surrounded by ground containing permafrost, there was little if any hydrologic gradient within the unfrozen sediments and thus little physical water migration within the lake sediments. The relatively low peak concentration of 177 T.U. is only on the order of 10% of the expected 1963 peak value (accounting for radiogenic decay) that would occur if the tritium were moving downward as plug (mass) flow. Therefore, through the diffusion process, the tritium concentration is reduced.

In contrast, tritium concentrations for core 79-3 waters peak at a depth of 25 cm (214 T.U., Figure 4b) which corresponds to the base of the active layer as determined from the stable isotope fractionation pattern measured for the pore water profile (Michel 1982). The tritium concentrations drop rapidly to 83 T.U. immediately below 25 cm and reach background values by a depth of 50 cm. Moisture contents throughout this 50 cm interval averaged 300% by weight, with the 20-25 cm interval the lowest at 125%. The sediments in the upper 50 cm of core 79-4 were also saturated, with moisture contents exceeding 500% by weight. This excess water resulted in the formation of ice lenses throughout the depth profiles of both cores.

Another core (NWD-1), collected near Norman Wells in the Mackenzie Valley, was sampled in detail to study its stable isotope (^{18}O) distribution, but was also analysed for tritium. As shown in Figure 5, elevated tritium concentrations were detected more than 50 cm below the level of maximum thaw. Furthermore, the stable isotope profile displays evidence of isotope fractionation generated at the time that the pore water froze.

Infiltration of young tritiated water after this ground was frozen, either by diffusion or mass flow along a temperature gradient, would have altered the stable isotope profile and thus the tritium must have been incorporated prior to permafrost forming in this soil. Since the tritium is related to anthropogenic sources, the presence of tritium in the permafrost indicates that this particular section of ground froze within the previous decade as a result of permafrost aggradation. Livingstone (1988) also found tritium within a section of aggrading permafrost that was caused by the continued deposition of sediments at his study site.

Tritium analysis of other ground ice bodies in Siberia

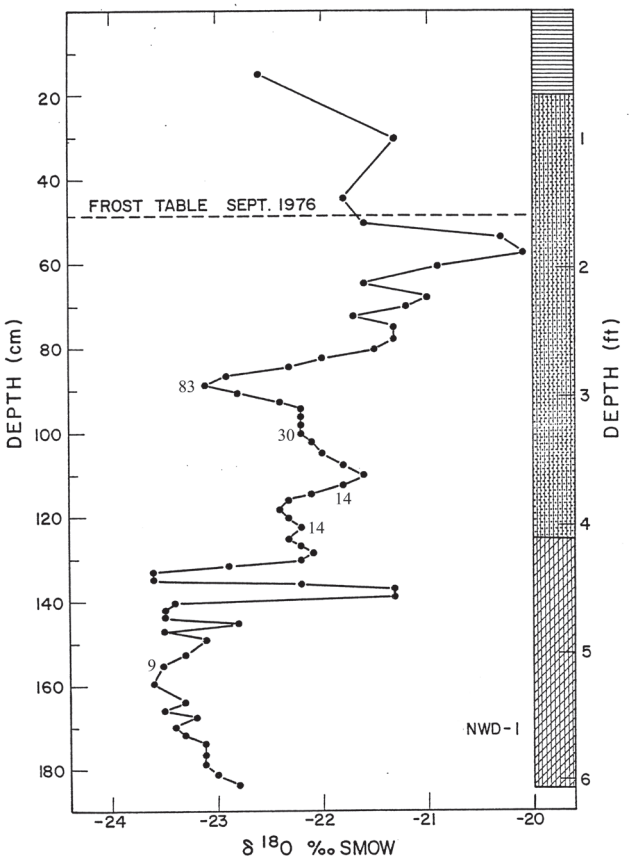

Figure 5. ^{18}O profile for frozen and unfrozen sediments near Norman Wells with spot tritium concentrations (in T.U.) shown below the frost table. Soil profile from top down consists of peat, sandy silt, and silty clay. (Modified from Michel & Fritz 1978.)

and in northern Canada also have been successful in identifying ice formed within the latter half of the 20th century. Identification of active ice wedge growth has been demonstrated in several studies, including Lewkowicz (1988) and Chizhov & Dereviagan (1998). It must be remembered that the source water for ice wedges, winter snowmelt, will contain tritium concentrations that are below the annual average precipitation value. Chizhov & Dereviagan (1998) have also reported tritium data for massive ice from a variety of settings and have been able to determine whether the ice is young (tritium bearing) or relict (pre-1953).

Tritium concentrations for local surface waters will reflect average precipitation values while groundwater retains a tritium signature from precipitation at the time of recharge (Michel 1977) and thus can be useful in distinguishing water sources. Michel (1986) found that the tritium concentration of massive ice within frost blisters at a site in Yukon reflected the age of the source water (local springs) rather than direct precipitation at the site. The tritium concentration within the ice core was considerably higher than water (ice) contained within the overlying organic cover and active layer. The tritium did not appear to have undergone fractionation during freezing of the ice as had been observed for the stable isotopes of the water. Without a clear understanding of how the massive ice formed, an incorrect age could have been assigned to the frost blister. It is important therefore to be careful with the age interpretation of tritium data.

Effect of Climate Change on Tritium Distribution

The active layer only begins to thaw once the snow cover has disappeared and solar radiation is absorbed by the darker ground surface. Excess water, frozen into the active layer during the previous winter as pore ice or ice lenses, will gradually drain down slope through the active layer and enter the local surface water system. Relatively warm summer rains can run off over the ground surface or infiltrate into the unfrozen portion of the active layer and enhance the rate of thaw. By the time the active layer begins to refreeze in the fall, there has been considerable drainage and flushing of the water originally in the active layer, as well as some mixing with the summer precipitation. This will result in a tritium signature for water in the unfrozen active layer that reflects a combination of the tritium concentrations found in the summer precipitation and that of water retained from previous years.

During the fall as the active layer refreezes, unfrozen tritiated water within the active layer will migrate along thermal gradients, both upward toward the ground surface and downward toward the permafrost table, leaving a relatively moisture deficient central zone within the active layer as observed at Illisarvik. If the following summer is cooler and the active layer does not thaw to the same depth as the previous year, some of the tritiated water will be retained in ice formed at or immediately below the permafrost table. Successive years of cooler temperatures would result in an aggrading permafrost table and the preservation of tritiated ice, while a series of warmer summers with greater active layer thaw would result in the formation of a thicker active layer and melting of ice previously accumulated at the permafrost/active layer boundary.

Average annual air temperatures have varied throughout the 20th century. From the 1910s to the early 1940s global temperatures rose such that the highest temperatures of the 20th century were recorded in the 1940s. A cooling trend followed, during the period from the late 1940s to the early 1980s, which has been followed in turn by another warming trend through the 1990s (Hardy & Bradley 1996). The cooling trend in the middle of the 20th century led some scientists to predict the start of a new ice age, while the latest warming trend has spurred the recent global warming debate.

All of these sustained periods of cooling and warming will have an impact on the depth of thaw and the thickness of the active layer. Maximum thaw depths should have been attained during the 1940s. The first part of the subsequent cooling trend corresponds to the period of atmospheric nuclear testing (1953 to 1962). During this period of cooling, the thickness of the active layer should have been decreasing and the permafrost table should have been aggrading upward. Precipitation infiltrating the active layer would

have contained significant concentrations of tritium, which would then be preserved within the aggrading permafrost. Of course, variations in the active layer thickness also will occur due to site-specific microclimate effects that could differ from regional climate trends.

Although significant downward diffusion of tritium can occur at unfrozen sites, such as the Illisarvik lake sediments, and moisture migration along thermal gradients can aid in the transport of tritium into the upper permafrost, much of the tritium preserved in the upper 30 to 50 cm of permafrost is probably due to permafrost aggradation under a cooling climate regime. This preservation of tritiated water (ice) in the upper permafrost provides an independent estimate of the maximum active layer thickness developed since the 1950s with which to compare changes occurring in the active layer today due to the current warming trend. Many of the samples analysed for tritium were collected during the last cooling trend when active layers were thinning and therefore tritium was preserved within the upper permafrost. Calculated tritium decay rates for older precipitation from the 1960s and 1970s indicates that preserved precipitation from this period of aggrading permafrost should still have a higher radiogenic signature compared to modern precipitation; however, dilution and mixing with older tritium-free water may have lowered the concentrations to near background levels.

Conclusions

Previous studies have demonstrated that tritium can be utilized as a natural tracer in permafrost investigations and can help to distinguish between water sources of different ages. The presence of tritium in ground ice is indicative of water that recharged into the subsurface during the last half of the 20th century when significant anthropogenic tritium was injected into the atmosphere due to nuclear testing.

Although downward migration of moisture along thermal gradients or due to diffusion is possible, the majority of tritium detected within the upper 30 to 50 cm of permafrost is most likely the result of aggrading permafrost due to climatic cooling during the 1950s to 1980s. The identification of thaw depths caused by warming climatic conditions earlier in the 20th century will permit comparison with modern active layer development caused during the current warming trend.

References

Burn, C.R. & Michel, F.A. 1988. Evidence for recent temperature-induced water migration into permafrost from the tritium content of ground ice near Mayo, Yukon Territory, Canada. *Canadian Journal of Earth Sciences* 25: 909-915.

Chizhov, A.B., Chizhova, N.I., Morkovkina, I.K. & Romanov, V.V. 1983. Tritium in permafrost and in ground ice. In: *Proceedings 4th International Conference on Permafrost, Fairbanks, Alaska. Washington D.C.: National Academy Press,* 147-150.

Chizhov, A.B., Chizhova, N.I., Romanov, V.V., Morkovkina, I.K. & Boyarskiy, O.G. 1985. Tritium analysis in geocryological research. *International Geology Review* 27: 1370-1377.

Chizhov, A.B. & Dereviagan, A. Yu. 1998. Tritium in Siberia's permafrost. In: *Proceedings 7th International conference on Permafrost, Yellowknife,* NWT.: 151-156.

Circumpolar Active Layer Monitoring (CALM). 2008. www.udel.edu/Geography/calm/data/data-links.html.

Hardy, D.R. & Bradley, R.S. 1996. Climate change in Nunavut. *Geoscience Canada* 23(4): 217-224.

International Atomic Energy Agency (IAEA) 2007. *Global Network for Isotopes in Precipitation, Database.* http://www.iaea.or.at:80/programs/ri/gnip/gnipmain.htm.

Lewkowicz, A.G. 1994. Ice-wedge rejuvenation, Fosheim Peninsula, Ellesmere Island, Canada. *Permafrost and Periglacial Processes* 5: 251-258.

Livingstone, S.J. 1988. *Examination of permafrost aggradation using environmental isotope geochemistry, Victoria Island, NWT*. B.S. Thesis. Ottawa, Ontario: Dept. of Earth Sciences, Carleton University, 41 pp.

Michel, F.A. 1977. *Hydrogeologic studies of springs in the central Mackenzie Valley, Northwest Territories, Canada.* M.S. Thesis. Waterloo, Ontario: Dept. of Earth Sciences, University of Waterloo, 185 pp.

Michel, F.A. 1982. *Isotope investigations of permafrost waters in northern Canada.* Ph.D. Thesis. Waterloo, Ontario: Dept. of Earth Sciences, University of Waterloo, 424 pp.

Michel, F.A. 1986. Isotope geochemistry of frost-blister ice, North Fork Pass, Yukon, Canada. *Canadian Journal of Earth Science* 23: 543-549.

Michel, F.A. & Fritz, P. 1978. Environmental isotopes in permafrost related waters along the Mackenzie Valley corridor. In: *Proceedings 3rd International Conference on Permafrost, Edmonton, Alberta.* Vol. 1: 207-212.

Michel, F.A. & Fritz, P. 1982. Significance of isotope variations in permafrost waters at Illisarvik, NWT. In: *Proceedings 4th Canadian Permafrost Conference, Calgary, Alberta, March 2-6, 1981. National Research Council of Canada*: 173-181.

Payne, B.R. 1972. Isotope hydrology. In: *Advances in Hydroscience,* Vol. 8. New York: Academic Press, New York, 95-138.

Twenty Years of Permafrost Research on the Furggentälti Rock Glaciers, Western Alps, Switzerland

Dragan Mihajlovic
Institute of Geography, University of Bern, Switzerland
Flotron AG Engineers, Meiringen, Switzerland
Benno Staub, Anina Nussbaum
Institute of Geography, University of Bern, Switzerland
Bernhard Krummenacher
Geotest AG, Davos, Switzerland
Hans Kienholz
Institute of Geography, University of Bern, Switzerland

Abstract

Since 1988, long-term monitoring of the Furggentälti rock glaciers (Western Alps, Switzerland) has revealed significant changes in process dynamics. The changes include large seasonal and interannual variations of rock glacier activity, superimposed by an exponential increase of overall rock glacier creep velocity. During the monitoring period, the largest of the rock glaciers (located at 2450 m a.s.l.) developed signs of decay, with some parts of the rock glacier becoming inactive and others showing patterns of collapse. Analysis of local climate data suggests a strong and surprisingly low-latency link between rock glacier activity and weather patterns. Even though some of the long-term developments in the kinematics of the Furggentälti rock glaciers are also influenced by other factors, such as topography and process feedback, the short-term response to climate signals points at ever warmer permafrost conditions at the site as the major cause for the changes observed.

Keywords: climate change; ground surface temperature; long-term monitoring; rock glacier activity; Switzerland; warm permafrost.

Introduction

Background

During the 2003 summer heat wave, the many rock fall events in the Swiss Alps—the most prominent one affecting the well known Matterhorn—have demonstrated the very immediate and very obvious impact of rising temperatures on permafrost present in rock walls.

Though slower and less obvious, the thawing of perennially frozen debris typically found in rock glaciers is now becoming visible at the lower limit of alpine permafrost.

For the last 20 years, the Institute of Geography of the University of Bern has been closely monitoring a small rock glacier located in the western parts of the Swiss Alps. During the monitoring period, the rock glacier has undergone rapid changes in shape and process dynamics, which are coupled with the development of the local climate.

Situated at the lower limit of Alpine permafrost, the Furggentälti rock glacier is a textbook scenario for the impact of a warmer climate on rock glacier activity and evolution.

The project site

The Furggentälti (46°24.5′N, 7°38′E), a small valley near the Gemmi pass, is located in the western part of the Bernese Alps between Kandersteg and Leukerbad (Switzerland). The valley stretches over a range of approximately two square kilometers from west to east, from an altitude of approx. 2450 m to approx. 2850 m a.s.l.

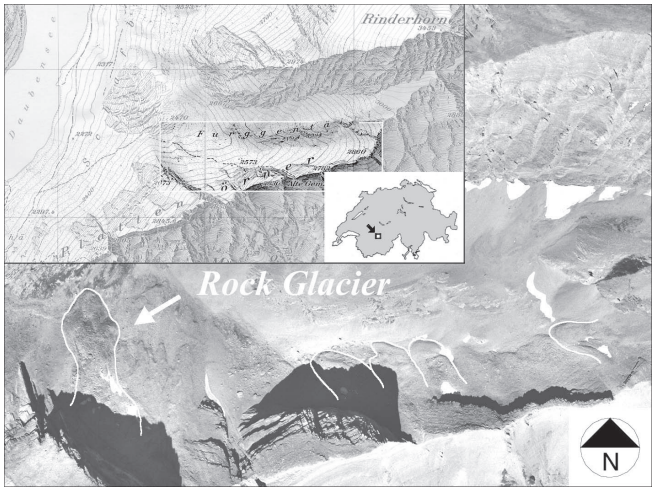

Figure 1. Geographic location and aerial view of the Furggentälti Valley (© Swiss Federal Office of Topography).

Most of the surface of the valley is covered by vast layers of periglacial debris, forming large talus cones on the foothills of the steep northern slope.

The Furggentälti Valley is home to many periglacial forms, including solifluction lobes and several small active and inactive rock glaciers on the north exposed slope. Typical periglacial patterned ground is also present in a flat region of the valley.

The focus of interest lies on an approximately 250 m long

tongue-shaped rock glacier in the lower western part of the valley (Fig.1). The rock glacier is situated on a slope of about 20° of northern aspect, its front protruding into the bottom of the valley, at an altitude of approx. 2450 m a.s.l.

The research project

Initiated in 1988, the long-term monitoring project consists of several measurement programs recording meteorological data, ground temperatures, ground surface temperatures (GST, recorded by ultra miniature temperature loggers UTL, www.utl.ch), and rock glacier activity data through aerial and terrestrial survey. The time series recording air and ground surface temperatures represent the longest such measurement series in a periglacial environment in the Alps.

The project is funded by the Institute of Geography of the University of Bern (www.giub.unibe.ch), the PRO GEMMI foundation of Bern, and by the PERMOS program (Permafrost Monitoring Switzerland, www.permos.ch).

Changes in Rock Glacier Activity

Multi-decadal trends

Photogrammetric survey of the Furggentälti rock glacier spans over nearly five decades, the first set of small scale aerial photographs dating back to 1960. Since 1990, large scale aerial imagery was flown at five year intervals, and since 2001 in a two year interval.

A first photogrammetric assessment of the Furggentälti rock glacier in 1996 (Krummenacher et al. 1998) revealed unusually high surface velocities and a rapid increase during the late eighties and early nineties. Further photogrammetric surveys (Mihajlovic et al.2003) confirmed this multi-decadal trend, which was also observed in neighboring rock glaciers in the valley. The survey also found indications for a slowdown in surface velocities in the peripheral parts on the left and right side of the rock glacier (Fig. 2).

The latest data (Mihajlovic et al., in prep.) confirm both trends, with increased surface velocities found along the centerline of the rock glacier and a slowdown on the sides. The data have also detected the inactivation of peripheral parts of the rock glacier (Fig 3).

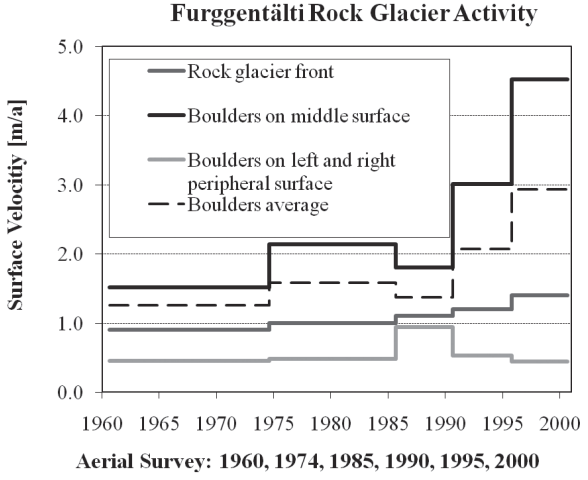

Figure 2. Multi-decadal trend. Rock glacier surface velocities derived from aerial survey 1960–2000.

Interannual variations

Since 1994, terrestrial survey campaigns provide a more detailed picture of the development of rock glacier activity and process dynamics.

Annual survey campaigns have uncovered interannual variations in the activity of the rock glacier, showing a clear pattern of thermally induced acceleration and deceleration of surface velocities (Fig. 4).

The pattern clearly reflects the development of the warming conditions at the site, with some attenuation during 2005 to 2007.

Seasonal activity pattern

A seasonal activity pattern was detected during a series of repeated survey campaigns from August 1998 to October 1999 (Mihajlovic et al. 2003). After a continuous slowdown during winter, the permafrost creep process accelerates rapidly at the beginning of the Zero Curtain phase in spring, when water infiltrates into the frozen active layer and rock glacier material, triggering an instant warm-up of the thermal conditions there (Fig. 5).

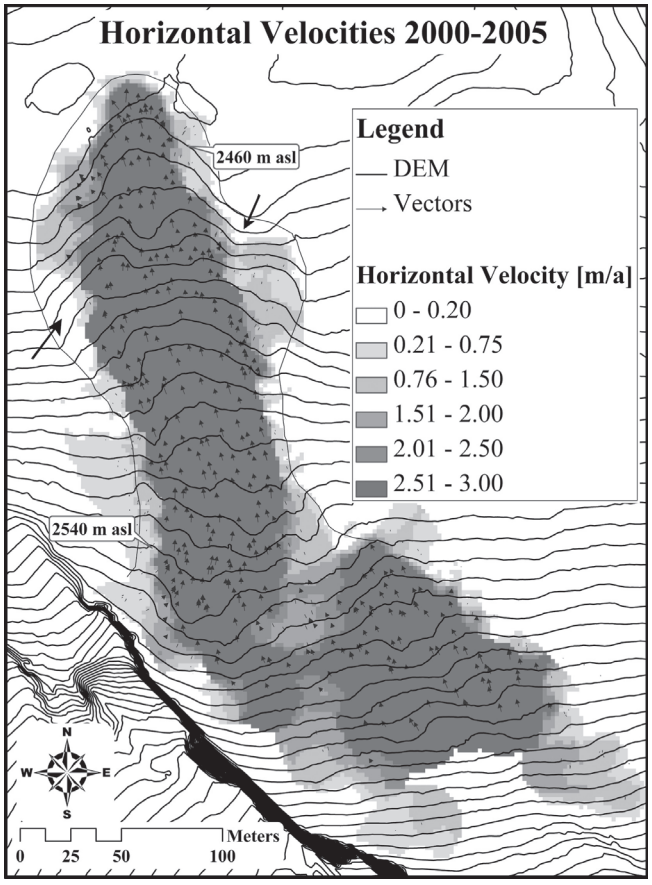

Figure 3. Velocity field of the Furggentälti rock glacier surface. Aerial survey, 2000–2005; arrows: parts inactivated during the monitoring period.

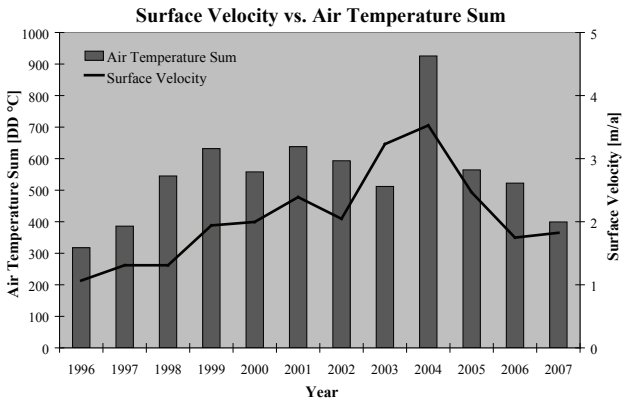

Figure 4. Interannual variations of surface velocities (terrestrial survey) vs. air temperature sum; period: September of the preceding year to August.

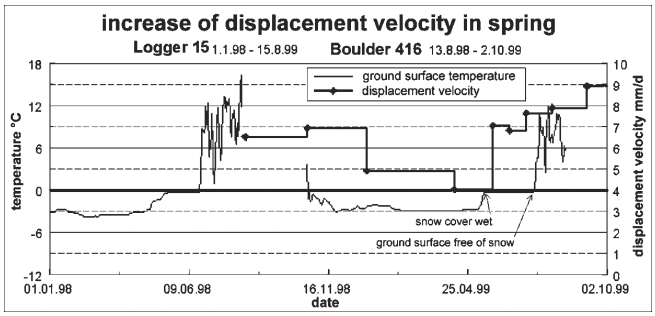

Figure 5. Seasonal variation of rock glacier activity compared with ground surface temperatures measured nearby.

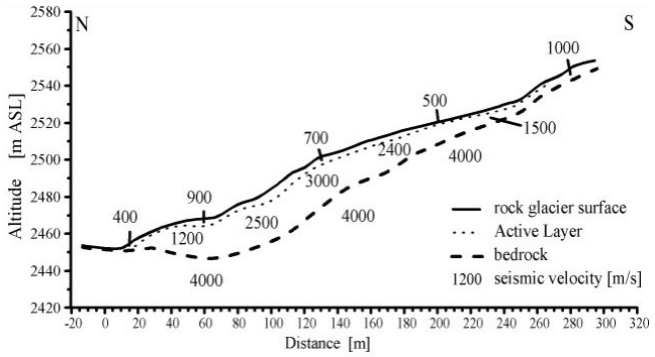

Figure 6. Seismic profile of the Furggentälti rock glacier; dashed line: estimation of bedrock surface (Nussbaum 2008).

New clues

The results (Nussbaum 2008) of geophysical soundings (GPR and refraction seismic) in 2007 are providing new clues for the unusual shape and rheology of the Furggentälti rock glacier, which are also affected by the special arrangement of rock glacier material on the underlying bedrock topography (Fig. 6).

The observed long-term acceleration of rock glacier activity could be partly the result of this arrangement or of process feedbacks such as the increasing surface area exposed to irradiation due to the extending rock glacier footprint. However, similar findings on neighboring rock glaciers in the Furggentälti, together with the thermally induced short-term variations, point at the warmer climate as the main cause for the long-term development.

Similar developments across the Alps

During the last years, similar observations on other rock glaciers have provided a clearer picture of changes in rock glacier activity in different parts of the Alps. Delaloye et. al. (2008) gives an overview of data from 17 rock glaciers. Several studies mention a similar increase of rock glacier surface velocities during the past decades (e.g., Roer 2005), as well as interannual variations (e.g., Ikeda et al. 2003).

Impact of a Warmer World

Ice temperature and permafrost creep

Lab experiments using centrifuges to assess the mechanical stability of rock glacier material have shown that the plasticity of rock glacier material increases rapidly with ice temperatures approaching 0°C (Arenson 2003). The reason for this non-linear behavior was found in the exponential increase in the presence of liquid water in the material, when increasing from approximately -2.5°C to 0°C.

Ice temperatures in the Furggentälti rock glacier cannot be measured directly, as the high surface velocity of several meters per year prevents the installation of a borehole or the retrieval of other (wired) equipment. Instead, the winter equilibrium temperature (WEQT) is used as an estimation for the permafrost temperature at its coldest state in the year. The WEQT is derived from continuously recorded ground surface temperatures (GST), which are measured by ultra miniature temperature loggers at several locations on the rock glacier surface.

During most of the 13 year monitoring period, winter equilibrium temperatures recorded on the Furggentälti rock glacier were within the range of -2.5°C to -1.5°C, with the exception of two distinct cooling events that led to a significantly lower WEQT in early 1996 and 2006.

Influence of weather patterns and snow cover

A comparison of ground surface temperatures of several years (Fig. 7) shows the broad variation of the atmospheric influence on the active layer.

The GST monitoring period (1994 to 2007) contains both positive and negative interannual WEQT fluctuations, which coincide with positive and negative variations of rock glacier activity. In the positive case, atmospheric conditions during the preceding year led to a general increase of ice temperatures, whereas in the negative case an overall cooling occurred. This information can be used as a simple pointer to assess the direction of the energy flux integral at the ground surface, for the corresponding interval.

The main factor controlling direction and magnitude of the energy flux is the snow cover (Keller 1994, Krummenacher et al. 1998, Mittaz et al. 2002) which acts both as a shortwave radiation shield and as a thermal insulator. Timing, duration and depth of the snow layer modulate the energy balance of the ground surface, and as a consequence the thermal conditions in the active layer.

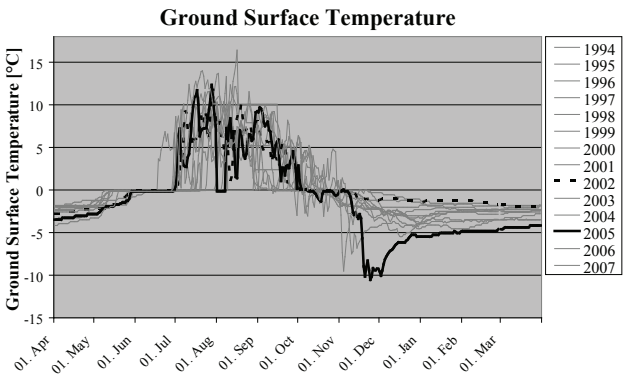

Figure 7. Bandwidth of fluctuations in ground surface temperatures from 1994–2006. Dotted line: 2002/2003; black line: 2005/2006. Recorded by UTL data logger #3 on the Furggentälti rock glacier surface.

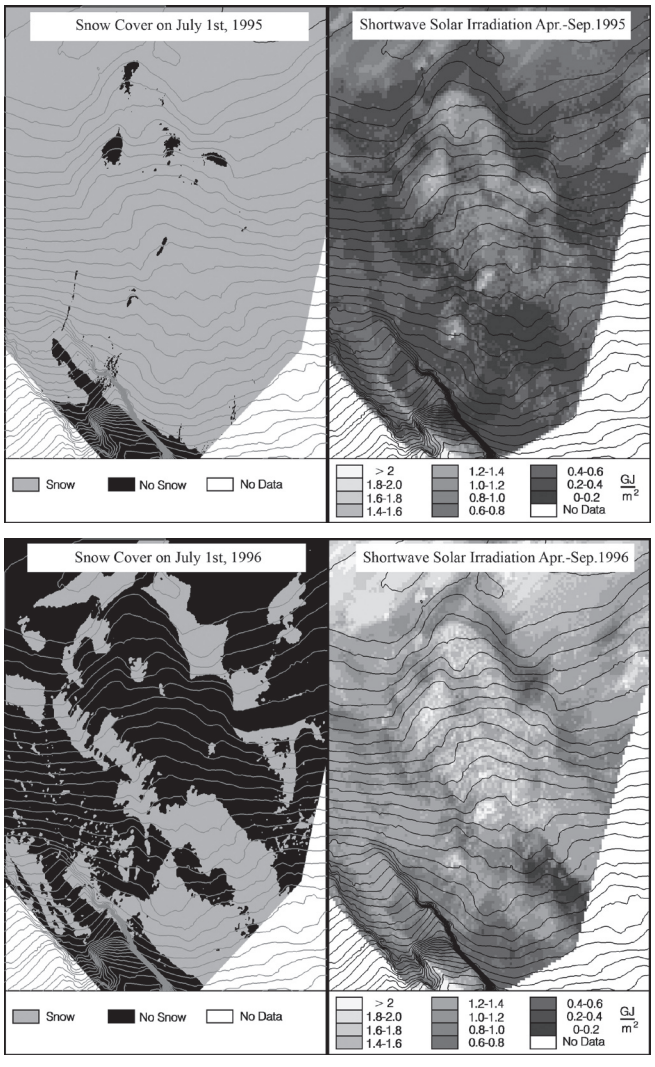

Figure 8. Snow cover variations (July 1 1995 and 1996) (derived from terrestrial orthophotos) and net shortwave solar irradiation April to September 1995 and 1996 on the Furggentälti rock glacier. Based on daily snow cover maps and shortwave radiation (1-hour interval), high resolution elevation model.

A study (Mihajlovic et al. in prep.) using local shortwave irradiation data and snow cover maps (derived from digital orthophotos of an automated camera taking daily photographs of the site) assessed the total shortwave irradiation on the rock glacier surface during the summer of 1995 and of 1996, which corresponds with the distinct positive variation between the WEQT in 1996 and 1997 (Fig. 6). During the period from April 1 to September 30, 1995 the average net shortwave irradiation on the true surface of the rock glacier amounts to 38 W/m^2, compared to 108 W/m^2 during the same period in 1996 (Fig. 8). This enormous difference is in large part caused by the different duration of the snow cover during spring and summer, whereas the total shortwave irradiation sum only differed by approximately 9%.

Analyzing the influence of the snow cover in GST data

In order to get a better picture of how different temporal patterns of snow cover occurrence influence permafrost temperature variations, a simple method was developed which allows extracting more specific parameters from existing GST measurement series. The basic idea is to skip from looking at GST time series in fixed intervals (e.g., annual intervals like MAGST Mean Annual GST, or monthly intervals etc.) to intervals which take into consideration the different states of thermal insulation properties of the snow cover.

For this, the annual cycle of snow cover ablation and development is divided into four phases, where each represents a different role of the snow cover on the energy flux between ground surface and atmosphere:

- Phase Z: Zero Curtain (springtime); GST shows 0°C, direct energy flux between atmosphere and ground surface is suppressed.
- Phase N: No Attenuation; during the absence of snow, GST shows big daily temperature fluctuations while the energy flux between atmosphere and ground surface is unhindered.
- Phase L: Low Attenuation; in this phase, a snow cover of limited depth is present. Energy flux between atmosphere and ground surface is attenuated, but not suppressed. Daily temperature fluctuations are still visible in the GST, but clearly attenuated.
- Phase H: High Attenuation; in this phase, the ground surface is covered by a thick and thermally insulating layer of snow, through which the energy flux is highly attenuated and therefore only minimal. No daily temperature fluctuations visible in GST.

To extract the beginning and end of these phases, the GST data is processed through a series of simple signal processors which act as band pass filters on the daily fluctuations showing up in the data. While the *Zero Curtain* (no daily fluctuations and 0°C) and the *No Attenuation* phase (large daily fluctuations) are easily distinguishable, the *Low Attenuation* phase (daily fluctuations below a certain threshold value) is less clearly defined and can vary by a few days, depending on the actual filter settings (Mihajlovic, in prep.). Figure 9 shows a typical arrangement of the phases.

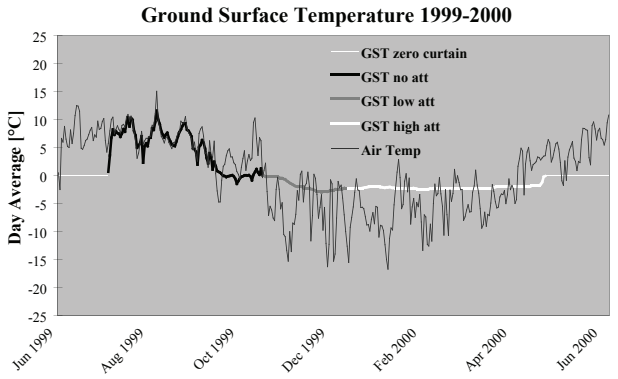

Figure 9. GST data divided into four phases which roughly represent different states of the thermal insulation properties of the snow cover; thin white line: Zero Curtain (phase Z); black: no attenuation of the atmospheric signal by the snow cover (phase N); gray: low attenuation phase (phase L); thick white line: high attenuation phase (phase H); thin gray line: air temperature (2 m).

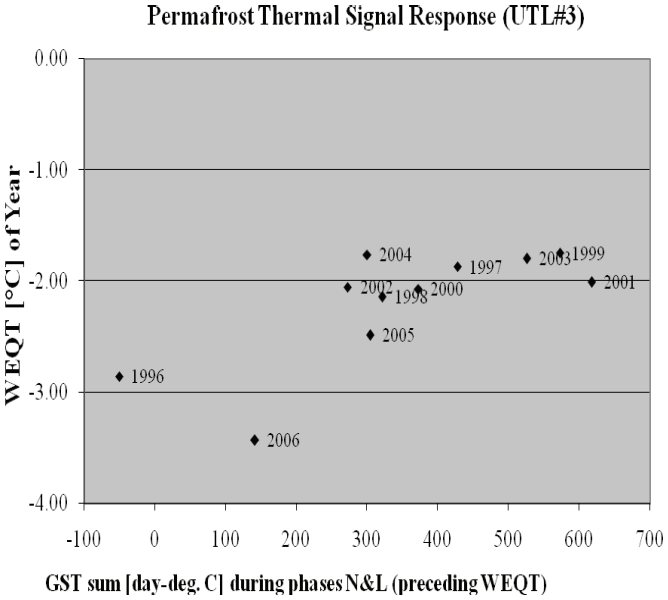

Figure 10. WEQT compared to the ground surface temperature sums of the preceding *No Attenuation* and *Low Attenuation* phases.

During Phase N and L, the ground surface temperature recorded is influenced by the energy flux between atmosphere and active layer, whereas during the *Zero Curtain* the temperature recorded is that of the snow cover. During the *High Attenuation* phase H, the data reflects the thermal "response" of the permafrost to the thermal "signal" applied to the surface of the active layer during the preceding phases N and L.

Comparing different years of GST data by adding temperatures sum for N and L phases only, the relation between thermal "signal" and the thermal "response" becomes more obvious (Fig 10).

The non-linearity in the relation shows how the thawing of ice in the rock glacier material is acting as a thermal buffer in warmer years with a high energy input. Doubling the thermal signal from, for example, 300 day-degrees C to 600 will not lead to substantial increase of the WEQT (and, therefore, permafrost temperature), as the excess energy input of the warm season is leaving the rock glacier system as melt water. In contrast to this, reducing the thermal signal to 150 day-degrees C leads to a significant drop in permafrost temperature.

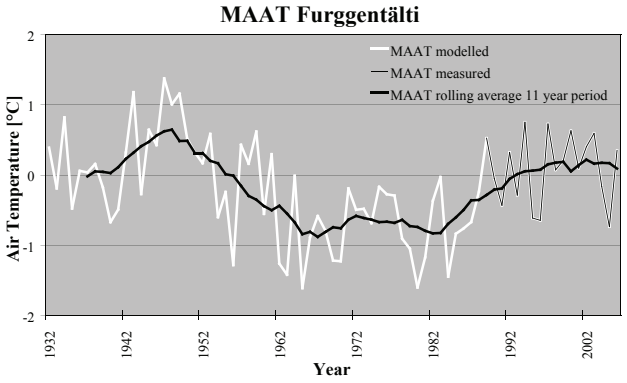

Figure 11. Modeled and measured air temperature in the Furggentälti; based on data of the nearby MeteoSwiss (www.meteoswiss.ch) meteorological station Montana 1932 to 1988, local measurements since 1988.

Long-term trend

Between 1988 and 2007, the trend in the air temperature data measured at the site shows a clear rise in average air temperatures during the first decade of measurements, which is then followed by a series of both extremely high and low temperatures during recent years. Long term temperature records of the nearby Meteoswiss meteorological station of Montana have been used to model air temperatures for the preceding decades (Fig. 11). The data suggest a general increase in air temperatures since the mid-1960s, preceded by a significantly warmer period during the forties and fifties.

One of the changes witnessed during the monitoring period is the increasing lack of snow. The clustered occurrence since the early nineties of winters with only little snow did not lead to a general cooling of the permafrost present in the rock glacier, as could be expected in higher regions with MAAT<<0°C. At the comparably low altitude of the site (average air temperature 1988–2006 = 0.1°C), the importance of the snow cover acting as a radiation shield during early summer is exceeding the "cooling effect" of the absence of snow during the cooling phase in early winter, as typical winter temperatures and the typical timing of snow falls do not a allow a profound cooling of the thermal conditions in the early winter of an average year.

The two WEQT cooling events recorded in the 13 year GST series (Fig. 10) find their explanation in abnormalities in the occurrence of snow; while an unusually long duration of a thick layer of snow on the Furggentälti rock glacier during the cold summer of 1995 led to the cold WEQT recorded in early 1996, the 2006 negative WEQT variation was caused by a lack of snow combined with exceptionally cold air temperatures during the preceding weeks of early winter.

Preliminary results based on long term snow depth and air temperature data of Montana station suggest that the depth and timing of snow cover in combination with air temperatures did not lead to a significant cooling of the permafrost conditions in the Furggentälti rock glacier during most of the past 75 years (Mihajlovic, in prep.).

Conclusions

The 20-year period of monitoring has amassed a large amount of scientific data about the sensitive environment in the Furggentälti Valley. The rather low cost methods used in the monitoring program such as the UTL data logger, which was especially developed for the project by B. Krummenacher (Krummenacher et al. 1998), have allowed uninterrupted data series over many years, despite limited funds.

The monitoring data is offering clues to a deeper understanding of the link between seasonal weather patterns on permafrost temperatures and subsequently on rock glacier activity.

The changes in shape and activity of the rock glacier during the last five decades reflect the development of the local climate during that period, which follows a general trend to warmer air temperatures and an increasing lack of snow. The changes also confirm the scenario of increased rock glacier activity before the onset of inactivation.

The findings of the monitoring program provide a graphic example for the impact of a warmer climate on the lower limit of alpine permafrost.

References

Arenson, L.U. 2003. *Unstable Alpine Permafrost: A Potentially Important Natural Hazard – Variations of Geotechnical Behavior with Time and Temperature.* Zürich: Publications of the Institute for Geotechnical Engineering (IGT), Swiss Federal Institute of Technology Vol. 218.

Delaloye, R. 2008. Recent interannual variations of rock glaciers creep in the European Alps. *Proceedings of the Ninth International Conference on Permafrost, Fairbanks, Alaska, June 29–July 3, 2008* (this proceedings).

Ikeda, A., Matsuoka, N. & Kääb, A. 2003. A rapidly moving small rock glacier at the lower limit of the mountain permafrost belt in the Swiss Alps. *Proceedings of the Eighth International Conference on Permafrost* 1: 455-460.

Keller, F. 1994. *Interaktionen zwischen Schnee und Permafrost.* Zürich: Mitteilungen der VAW/ETH Zürich, 127.

Krummenacher, B., Budmiger, K., Mihajlovic, D. & Blank B. 1998. *Periglaziale Prozesse und Formen im Furggentälti, Gemmipass.* Davos: Mitteilungen des Eidgenössisches Institut für Schnee- und Lawinenforschung Davos Nr. 245.

Mihajlovic, D., Krummenacher B. & Imhof, M. 2003. Developing new methods for monitoring periglacial phenomena. *Proceedings of the Eighth International Conference on Permafrost* 1: 455-460.

Mihajlovic, D. in prep. *Blockgletscheraktivität und Klima im Furggentälti, Gemmipass*. Bern: Institute of Geography, University of Berne.

Mittaz, C., Imhof, M. Hoelzle, M. & Haeberli, W. 2002. Snowmelt evolution mapping using an energy balance approach over an alpine terrain. *Arct. Antarct. Alp. Res.* 34(3): 274-281.

Nussbaum, A. 2008. *Geophysikalische Untersuchungen am Blockgletscher Furggentälti, Gemmi (VS)*. Berne: Institute of Geography, University of Berne (unpublished).

Roer, I. 2005: *Rockglacier kinematics in a high mountain geosystem*. Bonn: Department of Geography, University of Bonn.

Convective Heat Exchange Between Rivers and Floodplain Taliks

V.M. Mikhailov
North-Eastern Research Station of the Melnikov Permafrost Institute, SB RAS, Magadan, Russia

Abstract

The results discussed are estimates of convective heat exchange between rivers and floodplain taliks. Heat balance calculations were made for large sections of six rivers of northeastern Asia. Heat flux from rivers peaks in June, rarely in July, 100–200 W/m^2. Total heat transfer during summer is 700–1000·10^6 J/m^{2,} thus taliks obtain larger amounts of heat from rivers than from soil surface. In autumn, heat flux changes its sign, and rivers begin to receive heat back. This slows down their cooling, detains water freezing (for up to 10 days or even more), and sustains numerous glades in winter. These features demonstrate that convective heat exchange is not just capable of upholding floodplain taliks; it is far excessive for this task even in the coldest region of the Northern Hemisphere. Obviously, climatic conditions are not a limiting factor for geographical distribution of such taliks.

Keywords: convective heat exchange; floodplain taliks; heat balance; rivers; seasonal dynamics; thermal regime.

Introduction

Concerning the origin of floodplain taliks, the majority of authors agree that they exist due to convective heat exchange with rivers, though until recently no attempts were made to obtain quantitative characteristics of this process. Based on traditional approaches this problem is virtually unsolvable. The only practical way is to calculate a river heat balance. Accounting for all commonly considered components, the residual is convective heat flux into the ground. Using this approach, a number of estimates of this quantity were made for streams of III–IV orders (Mikhailov 2003); the data for calculations were received by *in situ* observations. Since the study process is highly dynamic and strongly dependant on hydrometeorological conditions, these results represent only short periods of time. Besides, it remained unclear whether it is possible to extrapolate them to larger watercourses. Dealing with such rivers, the investigated reaches should be several kilometers long or more, depending on water discharge. In such cases, it is usually impossible to obtain adequate data on the channel width for a given time span; that is why previous calculations could have been made only for one river during one ten-day period (Mikhailov 1998).

Profound research of convective heat exchange is not feasible without studying its seasonal dynamics. The most appropriate way is by using long-term means. While such hydrological and meteorological data are provided in reference books, the average width of extensive river sections can be estimated only for the date of the aerial mapping used to make the corresponding sheet of a topographic map. A special research program was carried out in order to solve this problem (Mikhailov & Ushakov 2002). It turned out that in braided rivers, correlation between channel width and water discharge is close enough to fulfill heat balance calculations with sufficient accuracy. Such rivers prevail in mountainous areas of northeastern Asia and are also associated with floodplain taliks (Mikhailov 1995).

The aim of this work is to investigate the main regularities of seasonal dynamics of convective heat exchange between floodplain taliks and rivers of medium and higher orders and its influence on a number of hydrological processes and phenomena.

Materials and Methods

The general pattern of estimations is the same as in the previous study (Mikhailov 1998): the intensity of heat exchange between rivers and adjoining grounds was calculated using stepwise approximation, so as to achieve identity of the simulated and actual river temperatures in the studied river sections. The calculations of temperature increments were carried out successively from one confluence node to another, with presumed instant water mixing in nodes.

Methods of calculations

The heat balance equation for a river segment, dx, under considered conditions is as follows (Vasilyev & Voyevodin 1975):

$$\Omega\frac{\partial T}{\partial x}+\frac{\partial}{\partial t}(sT)-\frac{B}{C}\sum q_i=0 \qquad (1)$$

where x and t are distance downstream and time, respectively; Ω and T are, accordingly, water discharge and temperature; B and s are river channel width and cross-sectional area, respectively; C is water volumetric heat capacity; $\sum q_i$ is the sum of all heat fluxes influencing water temperature. Hereafter all dimensions are in SI if not specified otherwise.

The sum $\sum q_i$ includes the resultant of energy exchange on water surface (q_s); the heat of dissipation of kinetic energy of the flow (q_{diss}); the heat of thawing solid precipitation (q_m); and total heat flux into ground (q_{gr}), which is the sought quantity. Thermal influence of liquid precipitation is negligible; in large rivers; the same is true for the dispersed inflow. The working equation for estimations of river temperature increments between outfalls of tributaries is as follows:

$$T = T_0 + \frac{B\Delta x}{C\rho}(q_s + q_{diss} - q_m - q_{gr}) - \frac{\Delta x}{\rho\Delta t}\left(s\Delta T + T\Delta s\right) \quad (2)$$

Hereafter the symbol «Δ» stands for the finite increment of the according quantity; index «0» implies that the labeled quantity is related to the upstream cross-section of the segment Δx. In calculations by formula (2) made with a specially designed computer algorithm, the step Δx was specified as approximately equal to the river width and so, as the number of steps to the next node, was an integer.

The constituents of q_s are generally known, e.g. (Pavlov 1984):

$$q_s = S\left(1 - A\right) + I_a - I_s - P - LE \quad (3)$$

where S is total shortwave radiation; A is albedo of water surface; I_a and I_s are long-wave radiation of air and water surface, respectively; P and LE are sensible and latent heat fluxes accordingly. The methods of estimations of all these quantities are minutely elaborated and well-known. Though somewhat diverse empiric formulae are in use, the results obtained differ but a little (Mikhailov 1998).

The quantity q_{diss} is usually defined as the product $\rho gIVH$, where ρ is water density; g is gravitational acceleration; I is river inclination; H and V are mean values of the river velocity and depth, respectively. In calculations it is more appropriate to use the equivalent formula $q_{diss} = \rho gI\Omega/B$. Finally, q_m is evaluated by the dependency $q_m = L_m p/n$, where L_m is specific heat of ice thawing; p is monthly solid precipitation in millimeters; and n is the number of seconds in a given month.

Studied river sections and time span

The most suitable river sections for heat balance estimations are those between two stations, where full-scale hydrological and meteorological observations are implemented. It is essential, of course, that the river has a floodplain talik. Despite a fairly well-developed monitoring network and an abundance of such taliks, the first requirement is fulfilled only for one of six chosen sections. Besides, some necessary information is absent in principle. The lacking data were compensated using interpolations and various kinds of empirical dependences discussed in the next subsection.

The general information on the sections is given in Table 1. The first three are situated on the largest rivers of northeastern Asia; the others, in the Upper Kolyma basin (Fig. 1). All of them belong to the subarctic zone characterized by a severe, extremely continental climate. Those characteristics, which are the most important for the aim of the research, vary in close limits; thus the July mean air temperature ranges from 13.7 C to 15.6 C, and the total shortwave radiation ranges from 218 to 228 W/m^2.

In the selected sections, the rivers have braided channels and vast floodplains covered with mixed forest, which is a generally accepted indicator of floodplain taliks. The only exception is the Debin River, which is degrading over almost one-third of the section length and has no accumulative floodplain. In computations, convective heat exchange in such segments was specified as zero. Thus, the final result for this river, q_{gr} value, relates only to the reaches with floodplain taliks.

Table 1. Overview information on the studied river sections.

River	Length, km	Drainage area, km^2	Mean July discharge in the upper cross-section, m^3/s
Kolyma	190	11000	2210
Indigirka	113	32100	842
Anadyr	100	3400	964
Debin	89	2300	27.0
Detrin	63	2140	81.6
Berelekh	50	2180	119

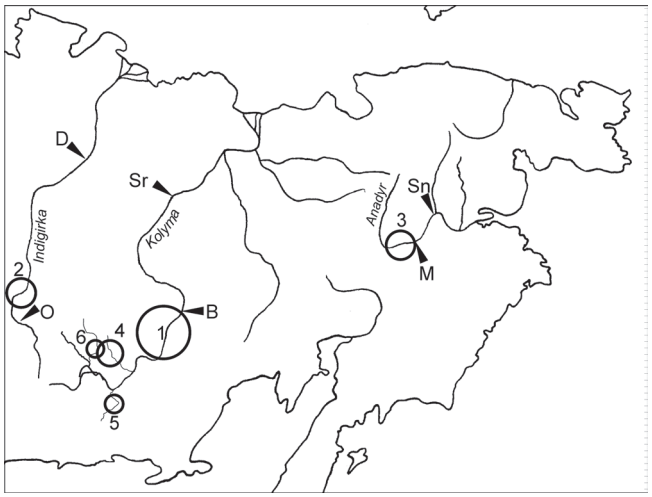

Figure 1. Locations of the studied river sections (circles) and gauging stations (triangles). Rivers: 1–Kolyma; 2–Indigirka; 3–Anadyr; 4–Debin; 5–Detrin; 6–Berelekh. Gauging stations: B–Baligichan; Sr–Srednekolymsk; M–Markovo; Sn–Snezhnoye; O–Oimyakon; D–Druzhina.

In May and October, the thermal regime of the studied rivers is considerably affected by freeze-thaw processes, which cannot be taken into account because of the lack of data. This limits the study period to four months.

Basic data

The values used in computations were monthly means in summer and ten-day means in September. The latter, except for water temperatures, were obtained via interpolation (using smoothed seasonal change curves). In this month, which is of particular interest for this study, a monotone decrease occurs of all quantities affecting water temperature; therefore such technique could not cause significant errors.

Most of the necessary information was obtained from reference books (Reference Book 1966; Long-Term Data 1985, 1987). The lacking data were acquired in the following ways.

Water discharges in the studied river sections were estimated using the data from the nearest gauging-stations, corresponding values of unit discharges, and increments

of drainage areas. In five cases out of six, the upstream cross-sections were provided with discharge data, which minimized errors. The exception is the Kolyma River, but there the drainage area over the whole section increases less than 8%; this reduces the errors originating from the next discussed approximation.

Water discharges and temperatures of tributaries: The former quantities were calculated using drainage areas (measured on topographic maps) and unit discharge means estimated for each river section. To compute water temperatures, as well as in the previous study (Mikhailov 1998), empirical dependences "discharge–temperature" were derived via statistical treatment of data from 59 gauging-stations belonging to the investigated watersheds. All of these formulae were of the form $T = a \lg \Omega + b$ with a and b parameters calculated separately for each summer month and each ten-day period of September. When using long-term data, the correlation between temperatures and discharges is closer than in the case studied earlier, when the estimations were made for a short time span. While in that period 70% of T values were beyond the interval of ±1 C from the regression line; for mean July temperatures, the relation is inverse. In June, the range of temperatures is a little wider, but by the end of the season, it becomes sufficiently more narrow.

Climatic data used were obtained at the weather stations located, as a rule, in close vicinity to the gauging-stations, or not more than 100 km away from them. All weather stations, as well as gauging-stations, are situated in wide river valleys where local peculiarities are minimal. As it was mentioned above, the values of climatic characteristics vary within close limits all over the vast territory embracing the studied river sections, so the differences within short distances are negligibly small.

River channel width and cross-sectional area: To estimate B, traditional empirical formulae $B = \alpha\Omega^{\beta}$ were used (Park 1977). Values of a and β for braided rivers had been obtained earlier (Mikhailov & Ushakov 2002). Due to similarity in relations of B and H to water discharge (Park 1977), s values obey the dependence of the same form: $s = s_0 \left(\Omega/\Omega_0\right)^{\beta}$, where s_0 is the cross-sectional area at the upstream station determined by hydrologic yearbook data. The β values were evaluated by analysis of information from the reference book (*Atlas of the Kolyma River* 1931) based on previously obtained results (Mikhailov & Ushakov 2002).

Discussion

The ultimate results of computations are shown in Table 2. To evaluate their reliability, a series of additional computations were made in which the values of quantities not provided with precise data differed from those used in the main version. Deviations were specified so as to be the maximum reasonable possible. If it is assumed that all errors do not compensate each other and affect the final result in the same direction, then it might change most significantly in June by 25 W/m^2 on average; in the Debin River, by 33 W/m^2. Further on, absolute values of errors decrease monotone,

Table 2. Mean monthly and ten-day period values of q_{gr}, W/m^2 and total heat transfer into ground over the study period (Q_{gr}), 10^6J/m^2.

River	June	July	August	September			Q_{gr}
				1	2	3	
Kolyma	166	109	101	47	−23	−71	1033
Indigirka	152	111	95	36	−19	−65	906
Anadyr	171	207	145	69	−3	−81	1445
Debin	150	113	77	42	−7	−49	934
Detrin	99	101	55	17	−28	−62	689
Berelekh	111	147	86	22	−24	−70	931

and in the first ten-day period of September, respective values are 9 and 13 W/m^2. Relative errors are minimal in July (12 and 18%, correspondingly).

In fact, as the fluctuations in values of each of the said quantities are governed by combinations of numerous independent factors, and furthermore, an impact of each individual fluctuation is not overwhelming; their net effect most likely does not exceed a few W/m^2.

The quantity q_{gr} includes convective and conductive components. According to Braslavsky & Vikulina (1954), monthly means of the latter in shallow reservoirs decrease from June to August from 15 to 4 W/m^2 and become negative in September. As seen from Table 2, seasonal changes of both components are qualitatively similar, conductive one's share being mostly less than 10%. Actually, its contribution is still smaller, because in watercourses, cooled by both convective heat exchange and by inflow of tributaries, water temperatures are lower than in such reservoirs. In the Kolyma River, the difference in July is more than 3 C, and in the Debin River, it increases to 6 C. Obviously, this reduces conductive heat flux into the river bottom, and q_{gr} may be regarded as a close estimate of convective heat flux.

For further discussion, it is important to emphasize that convective heat transfer develops as a result of groundwater flow along a general valley slope, and so concentrates in a slightly inclined plane. Of course, in this flow a vertical circulation develops as well, but its role is limited because, as a rule, not deep under river thalwegs, the ground is either bedrock or immobile silted sediment having very low permeability. Therefore, first, it is warmed virtually by conductive heat transfer alone; second, groundwater flow cannot substantively influence heat flux from the soil surface.

Total heat transfer from rivers to floodplains: Obviously, the values in the last column of Table 2 are lower estimates of this quantity (some amount of heat adds up in May). As it is known, mature rivers in mountainous territories have

floodplains which are 5–10 times wider than their channels. Accounting for river sinuosity, the relation of surface areas is at most 10:1. Therefore, during warm periods, taliks receive from rivers no less than $70–100 \cdot 10^6$ J/m^2 (the lower margin being more likely atypical). Judging by the available data, it is more than the amount of heat supplied from soil surface. In the open woodlands of Central Yakutia, where the climate is warmer, the last-named quantity does not exceed $80 \cdot 10^6$ J/m^2 (Pavlov 1984). In floodplain taliks, the soil surface is cooler due to the thick vegetation cover and subsurface, undoubtedly, warmer; both differences diminish heat supply from the surface. Also, some of this heat is spent on "useless" (for a talik existence) warming up of an aeration zone. Therefore, convective heat exchange with rivers is not only a unique factor of floodplain talik formation, it is also the major income source of their heat balance.

The value of Q_{gr} in the Anadyr River is almost 1.5 times greater than the maximum of all other such quantities (see Table 2). The reason is that in the Markovo Depression (to which the lower half of the studied section belongs) the river is aggrading and has an outstandingly large talik, up to 7 km wide (Vtyurin 1964). For comparison, the Kolyma River has twice as large July discharge, but its talik is approximately twofold narrower. This is why convective heat transfer from the Anadyr River to its floodplain is maximal. Since the results obtained are mean values over the whole river section, then in the depression itself heat flux is still greater.

The Detrin River, on the contrary, stands out against all others by substantially less intensive heat exchange with its floodplain. Based on the data available, there is not an adequate explanation for this phenomenon; one of the possible reasons may be degradation of the talik.

Heat flux direction change occurs, on average, within a short period of time, September 5–15, irrespective of a river size. The rivers begin to receive heat back while still having comparatively high temperatures (4–7°C); i.e., their thermal potential is not fully used. In other words, convective heat exchange with rivers is excessive in relation to sustaining floodplain taliks even under extremely severe climatic conditions. Summarizing all of the above-said, climate can hardly limit both the size of floodplain taliks and their geographical distribution.

The floodplain talik of the Anadyr River not only accumulates the largest amount of heat, but also spends it at a maximal rate: the third part of September q_{gr} is again the greatest by absolute value.

Convective heat exchange with floodplain taliks causes a number of peculiarities of thermal and ice regimes of rivers which earlier could not be adequately explained (Table 3). The most striking of them were first noticed by Shvetsov (1952) in the Indigirka River and named thermal anomalies. In summer, maximum river temperatures are observed not in places with the warmest air, but far downstream, while in autumn, temperature increments (of both water and air) change signs.

"Anomalies" (actually a pattern) are due to the fact that in all pairs of gauging-stations shown in Table 3, the upstream stations (see Fig. 1) are located on floodplain taliks which downstream pass away. In summer an intensive heat exchange with taliks decreases river temperature; in autumn it delays its cooling and ice phenomena, despite low air temperatures. Noteworthy, these peculiarities are best manifested in the Anadyr River.

Notwithstanding huge energy expenditures in autumn, the remnants of heat accumulated in taliks earlier are sufficient to sustain numerous glades during the whole winter. They are very typical for rivers of northeastern Asia, quite often stretching, one after another, for tens and hundreds of kilometres (Kuznetsov 1961); as this author rightly pointed out, these phenomena could not be explained by discharges of subpermafrost water. Obviously, such sequences of glades reveal plentiful and abundant outlets of groundwater from floodplain taliks.

General dynamics of convective heat exchange: On the whole, during the study period, a monotone decrease of q_{gr} values prevails. This is readily explained by the thawing of the seasonally frozen layer, which consumes very large amounts of heat even at low water temperatures. Also, energy flux to water surface diminishes during the warm season. Since during most of May the rivers remain covered with ice, q_{gr} as a rule reaches a maximum in June. The exceptions are the Anadyr and Berelekh Rivers, which

Table 3. Characteristics of thermal regime and freezing processes in the studied rivers.

River	Gauging station	Mean water temperature, °C		Average dates of:			
		July	October 1–10	drop of water temperature below 0.2 C	beginning of freezing process	beginning of ice drifting	beginning of freezing-up
Kolyma	Baligichan	14.5	1.4	Oct 11	Oct 7	Oct 9	Oct 17
	Srednekolymsk	15.4	0.8	Oct 6	Oct 5	Oct 10	Oct 13
Anadyr	Markovo	11.1	2.7	Oct 16	Oct 8	Oct 13	Oct 22
	Snezhnoye	15.1	1.4	Oct 7	Oct 6	Oct 7	Oct 10
Indigirka	Oimyakon	11.7	1.2	Oct 7	Oct 4	Oct 9	Oct 23
	Druzhina	15.1	0.3	Oct 3	Sept 30	Oct 3	Oct 12

display maximal values in July and require a more thorough analysis.

Convective heat exchange between rivers and taliks is due to intensive water exchange; the latter, in its turn, to concentration of groundwater flow in networks of preferential pathways with extremely high water-transmitting capacity (Mikhailov 1999). Experiments on indicator injections into observation wells have shown that after ice drifting in spring, a partial blocking of these pathways occurs resulting in a substantial decrease of alluvium effective permeability. The blocking was observed mainly at the beginnings of pathways and most probably is caused by entrainment of small ice particles. The research was carried out in the Kolyma River floodplain, which is covered with mixed forest. The studied sections of the Anadyr and Berelekh Rivers are distinguished by relatively sparse vegetation and an abundance of bare ground. In the former case, it is caused by frequent inwash of fresh sediment, the river being at the aggrading stage; in the latter case, by forest clearing and placer exploitation (Fig. 2). In both cases, the result is deep winter freezing, promoting the blockage of preferential pathways and diminishing convective heat transfer in early summer. After recovery of alluvium permeability, heat flux sharply increases and peaks in mid-summer.

As strong land disturbances, such as in the Berelekh River floodplain, are infrequent, there is an even smaller number of aggrading watercourses. In other studied rivers, the July values of q_{gr} , despite large differences in water discharges (almost by two orders of magnitude), are quite similar; in this month, even the Detrin River does not stand out. Taking into account the results of numerous observations in the valleys of smaller streams (Mikhailov 2003), in northeastern Asia these values in all typical floodplain taliks fall in the narrow range, probably not wider than 100–120 W/m^2; this opens up a possibility to estimate the distributions of such taliks over large river basins.

Conclusion

Based on heat balance calculations made for representative sections of six rivers of northeastern Asia, the main regularities of seasonal dynamics of convective heat exchange in river valleys have been ascertained. Usually heat flux is maximal at the beginning of summer, ranging from 100–170 W/m^2, but under conditions causing deep winter freezing of soil, the peak is shifted to July. The warming up of floodplains continues with decreasing strength up to and including the first ten-day period of September, on average. As a result, taliks receive from rivers very large amounts of heat; only since June, not less than 70–100 10^6 J/m^2 related to soil surface area. Comparison with published data demonstrates that heat exchange with rivers is not only crucial for the existence of taliks, it is a main income source of their heat balance (at least under climatic conditions close to the extreme ones).

The reverse side of intensive summer warming of floodplains is their rapid pre-winter cooling. In early autumn,

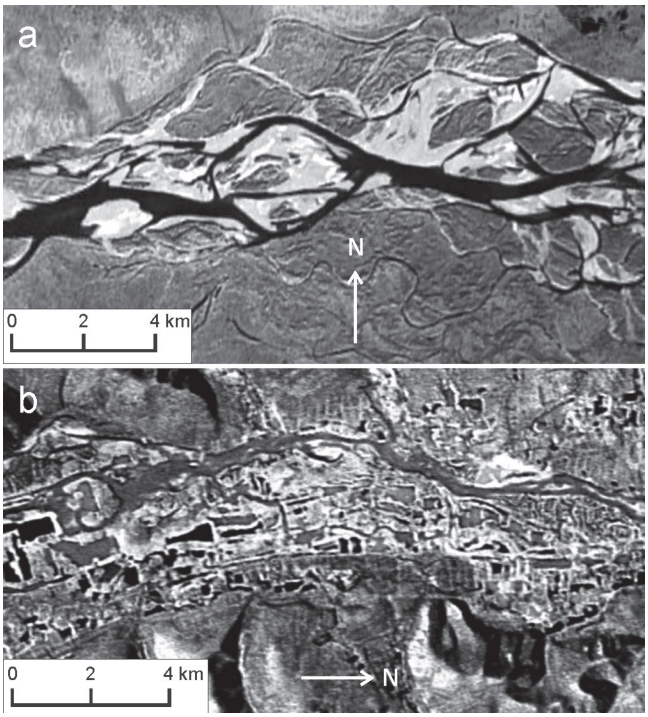

Figure 2. Satellite photographs of the valleys of Anadyr (a) and Berelekh (b) Rivers.

at relatively high temperatures of river water, heat flux changes its sign, and taliks start returning the accumulated heat to rivers. This process continues till the spring flood.

Convective heat exchange with taliks causes a specific distribution of water temperatures along the rivers ("thermal anomalies"); considerable delay of freezing-up and preceding ice phenomena (up to 10 days or even more) sustains numerous glades and successions of glades.

The results obtained lead to the conclusion that climatic conditions can hardly be a limiting factor for geographical distribution of floodplain taliks or their size. For further research, it is very important that in rivers at grade, which prevail in northeastern Asia, and in the absence of heavy soil-cover damage, mean July values of heat flux into taliks lie in a narrow range of 100–120 W/m^2, the same as in small streams or very close to it.

Acknowledgments

I am grateful to two anonymous referees for their useful advice which helped to improve the paper.

References

Atlas of the Kolyma River 1931. Irkutsk: Knizhnoye izdatelstvo, 432 pp. (in Russian).

Braslavsky, A.P. & Vikulina, Z.A. 1954. *Rates of Evaporation from the Surface of Water Reservoirs.* Leningrad: Gidrometeoizdat, 212 pp (in Russian).

Kuznetsov, A.S. 1961. Icings and glades in the north-east of the USSR. In: *Collected Works on Hydrology* 2: Leningrad: Gidrometeoizdat, 72-86 (in Russian).

Long-term data on the regime and resources of surface waters. *State Water Cadastre 1985, 1987*. Issues 16, 17. Leningrad: Gidrometeoizdat (In Russian).

Mikhailov, V.M. 1995. On the prevailing river channel pattern in the North-Eastern Russia and its relation to permafrost conditions in river valleys. *Kolyma* 7-8: 16-20 (in Russian).

Mikhailov, V.M. 1998. Development of taliks in the Kolyma River valley and water temperature. *Geoekologiya (Geoecology)* 6: 100-110 (in Russian).

Mikhailov, V.M. 1999. Preferential pathways for groundwater movement in coarse-grained alluvial deposits. *Kolyma* 4: 21-28 (in Russian).

Mikhailov, V.M. 2003. Hydro-thermal regime of watercourses as an indicator of ground-filtration taliks (on the results of in-situ research). *Kriosfera Zemli (Cryosphere of Earth)* 7: 57-66 (in Russian).

Mikhailov, V.M. & Ushakov, M.V. 2002. On some Morphological Correlations for Rivers of the North-Easternern Russia and Criteria of their Application. *Transactions of the Far-Eastern Hydro-meteorological Research Institute* 150: 177-187 (in Russian).

Park, C.C. 1977. World-wide variations in hydraulic geometry exponents of stream channels: an analysis and some observations. *Journal of Hydrology* 33: 133-146.

Pavlov, A.V. 1984. *Energy exchange in the Landscape Sphere of Earth*. Novosibirsk: Nauka, 256 pp (In Russian).

Reference Book on the Climate of the USSR. 1966. Issues 24, 33; parts 1-6. Leningrad: Gidrometeoizdat (in Russian).

Shvetsov, P.F. 1952. Anomalies in thermal regime of the Indigirka River in two characteristic cross-sections and the origin of them. In: *Research of Permafrost in the Yakutia Republic* 3. Moscow: Izdatelstvo AN SSSR, 106-108 (in Russian).

Vasilyev, O.F. & Voyevodin, A.F. 1975. Mathematical modeling of water quality in systems of open channels. In: *Dynamics of Continuous Medium* 22. Novosibirsk: Mining Institute of SB RAS, 73-87 (in Russian).

Vtyurin, B.I. 1964. Permafrost conditions of the Markovo Depression. In: *Permafrost Conditions of Western Siberia, Yakutiya and Chukotka*. Moscow: Nauka, 115-133 (in Russian).

Geophysical Study of Talik Zones, Western Yakutia

Svet Milanovskiy
Institute Physics of the Earth, RAS, Moscow
Sergey Velikin
Viluy Permafrost Station of the Permafrost Institute RAS Siberian Branch, Chernishevskii
Vyatcheslav Istratov
Radionda Ltd Company, Moscow

Abstract

For the last decade at a number of Hydro Units in Western Yakutia, we have observed subsurface seepage processes that compromise their structural stability. A number of geophysical techniques are discussed for verification of the permafrost state near Sitikan and Viluy Hydro Units, including electric, electromagnetic, ground penetrating radar, hydro location, thermal, and radiowave down-hole measurements. Ground-level and down-hole geophysical surveys focused on detecting thawing zones (talik) in dams, dam flanks, and tail-water zones. Long-term geophysical monitoring shows the spatio-temporal permafrost evolution and talik development in the flank shore of the Sitikan dam. Detection of the inflow zone and seepage velocity was performed for the right-bank contiguity of Viluy HPS-1. Numerically analyzed conditions causing the initiation and development of the talik near the reservoir are discussed.

Keywords: cold regions; dams; geophysical monitoring; permafrost; talik; thermal field.

Introduction

Permafrost covers about 70% of the territory of Russia, most of the territory of Alaska, as well as a significant part of Canada and mountain Alpine regions. Regular water and energy supplies in permafrost areas are vitally important conditions for inhabitants of the large northern territories of Russia, Canada, the U.S., and Alpine areas of China. Artificial reservoirs in permafrost terrain create the formation and development of talik zones in the adjacent flanks. Dam and flank shore stability is the key consideration in reservoir safety (power pool, water supply, tailing pit, etc.). Similar problems may also occur with natural basins in cold regions; climate change may activate lake drainage and changes in permafrost.

To avoid water loss and ensure the Hydro Unit stability in the permafrost zone, we need to use geophysical tools, including long-term monitoring for the detection of talik development. Along with required temperature control, different geophysical methods give information about variations in rock physical properties caused by thawing-freezing effects. Integrated geophysical monitoring allows observing time-space variability of the physical fields that reflect the evolution of frozen-thawed dam bed and flank shores.

Geophysical Observations

Study area

This study was conducted in the Aichal-Mirni region of Western Yakutia, which is an area of potential development of different types of anthropogenic development (Fig.1). They are connected with the exploitation of kimberlitic pipes, construction and operation of hydro facilities, injection and dumping of underground waters, underground storage facilities for toxic waste, and tailing dumps. Permafrost is very sensitive to natural and human-caused influences. In consequence of these circumstances, thawing-filtration processes were observed in a number of hydro technical projects in Western Yakutia: Marha, Irelyah, Viluy, Anabar, Sitikan, Kieng, and Iyraaas-Yuryah. We present two examples of geophysical observations from the Sitikan Hydro Unit and the Viluy Hydroelectric Power Station.

The Sitikan Hydro Unit (frozen type dam) provides the water supply for the city of Successful (near the diamond pipe "Udachnaya"). An underflow talik-zone developed in the dam basement in 1995 after 20 years of reservoir operation (Kronik 1999). As a result, there is currently significant water loss from the reservoir and a serious problem with water management.

Construction of the Viluy Hydroelectric Power Station (VHPS-1) was finished in 1967. It was the world's first large Hydro Unit with a rock fill dam on permafrost. More information about Viluy Hydro Units Cascade can be found at http://regtime.spb.ru/lenhydroproject/e_vil01_02.html. In August 1996, a temperature jump was observed in the right-bank contiguity of VHPS-1. During a few days, seepage was formed (Velikin & Snegirev 2004). This seepage continues to the present time despite special antifiltration efforts. For the last 15 years, various geophysical investigations were carried out on many engineering constructions in Western Yakutia by Viluy Permafrost Station (VNIMS). Priority interest was connected with the methodology of geophysical surveys of the permafrost state and its change near the hydro units. Some examples of this work are presented below.

Methods

Geophysical surveys focused on several main tasks: (1) eliciting and checking the position of inflow seepage near the dam and boundaries of dams, and detecting the location of most intensive thawing and seepage from the reservoir; (2) investigation of talik geometry in the frozen earth fill;

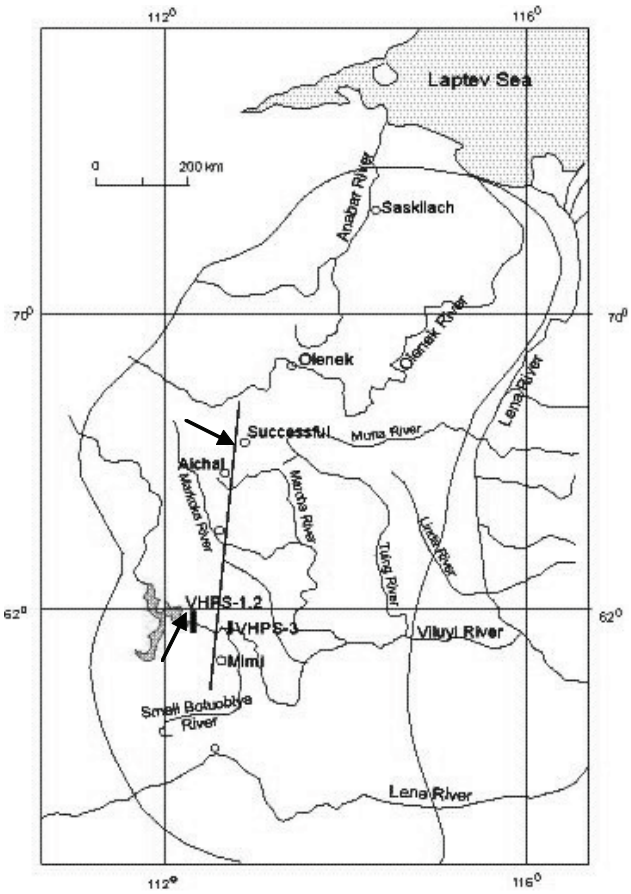

Figure 1. Case study areas: Sitikan Hydro Unit near Successful (Pipe Udachnaya) and Viluy HPS-1, 2 (shown by arrows).

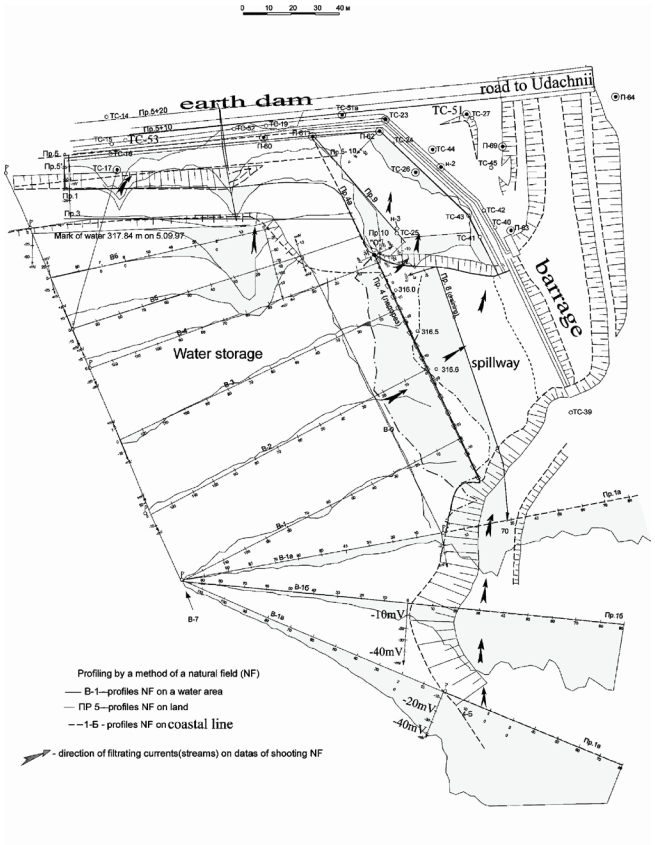

Figure 2. Natural Field profiles on water, land, and coastal zone of Sitikan Hydro Unit; negative NF anomalies indicate inflow seepage zones.

and (3) monitoring the progressive seepage dynamics in space and time.

From the many surface-based geophysical methods (Zikov 1999), the most useful for solving these tasks were selected including the Natural Field method (Semenov 1968) or Self Potential method (Erchul & Slifer 1989), Capacitive-Coupled Resistivity profiling or VCHEP method (Timofeev 1980, Hunter & Douma 2007), and Ground Penetrating Radar (GPR) (Arcone et al. 1998).

Down-hole observations near hydro units included long-term temperature measurements. Logging systems (electrical, flow meter survey, gamma logging, neutron-gamma logging, caliper measurement) (Zikov 1999) were used for petrophysical studies. The Radio Wave Geo-Introscopy (RWGI- ORWP) method (Istratov & Frolov 2003) with thermometrical data provided the opportunity to monitor talik development.

Talik detecting and monitoring

Natural field (Self-Potential) method: In this case, the natural field (NF) technique has an electrokinetic nature resulting from the transportation of charges by flowing water. Inflow zones correspond to negative values of electrical potential, while outflow zones have positive values of the NF (Semenov 1968, Zikov 1999, Erchul & Slifer 1989). A network of profiles (observation step of 2.5 m along profile) was established, covering the lower toe and upper heel, the adjacent banks, and the crust of the earth dam of the Sitikan Unit (Fig.2). Measurements were made relative to one of two stationary reference electrodes in the head race. In particular, NF data obtained in the head race of Sitikan detected (by negative anomalies) infiltration zones in the earth dam, below the spillway and along the boundary of the right bank.

Among the many applied surface geophysical studies, the Capacitive-Coupled Resistivity profiling method (VCHEP) and Natural Field (Self-Potential) methods were the main source of information about propagation of inflow zones and talik identification. The theory governing the VCHEP method has been discussed by Timofeev (1980). Advantages of the VHCEP method are high productivity and simplicity of measurements in cold region. There is no need for direct electrical contact between the transmitter and the ground (Hunter & Douma 2007). Specially-developed optional equipment VCHEP was used for the survey. This capability allowed us to determine effective resistivity (ρ_ω) values directly during field observations via conversion of measured electric field parameters for ω = constant and the selected unit configuration (Timofeev 1980, Zikov 1999). Later on, this approach was realized in the development of the "Ohm Mapper" device (Hunter & Douma, 2007). The VCHEP survey on the Sitikan Unit was done in April 1997 with two frequencies (8 and 12 kHz) and a square

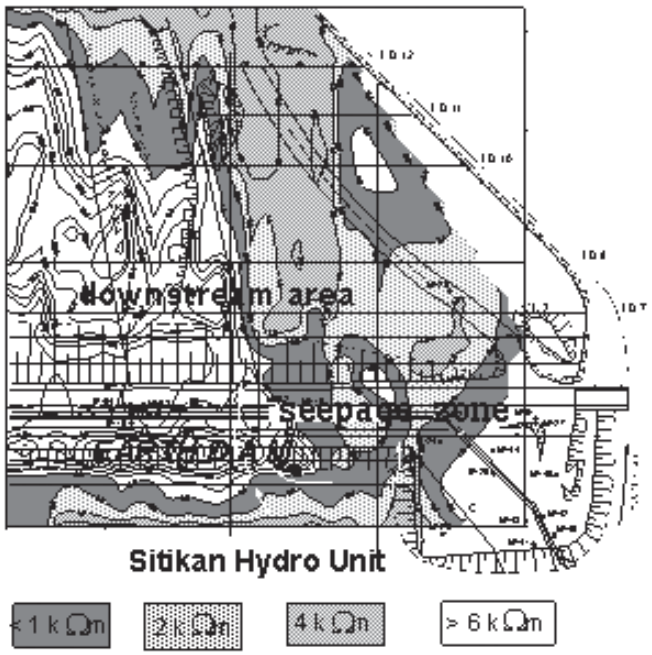

Figure 3. Spatial distribution of effective resistivity, ρ_ω kΩm (dipole length = 10 m, dipole-dipole spacing = 20 m, sampling step = 2.5m, ω = 8 kHz). Thawed zone determined with Capacitive-Coupled Resistivity profiling method (VCHEP) on Sitikan dam and tail-water. Shaded zones (low effective resistivity) correspond to talik's contour.

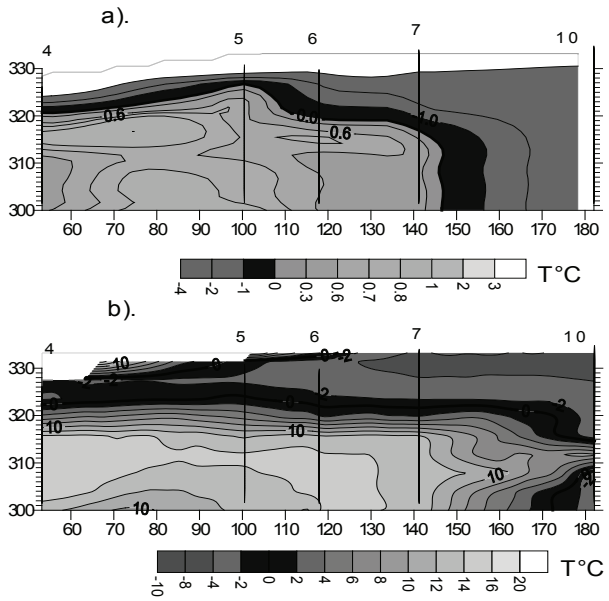

Figure 4. Dynamics of the ground temperatures within the reservoir flank of the Sitikan dam along boreholes (4-5-6-7-10) in (a) March 2001 and (b) August 2001.

waveform signal. At that time, snow cover and frozen rocks did not permit the use of any galvanic ground connection. Boundaries between frozen and thawed zones—the shaded zones in Figure 3—are reflected in the effective resistivity (ρ_ω) field for ω=8 kHz.

The Self Potential (NF method) survey was conducted with the "ERA-MAX" instrument along the water profile in the Viluy HPS-1 head race and on its bank. Several years of observations along these profiles showed significant changes in form and amplitude of the natural field associated with different water levels in the head race and discrepancy of observation lines. Nevertheless, in the zone adjoining the right-bank contiguity, the abnormal part was well detected by signal form and amplitude. As a rule, seepage originates from structure and head race contact. It would be logical to suppose that just this anomaly was caused by seepage processes. Later on, test methods proved this to be true.

Two contactless surveys were performed on water with the use of inflatable boat in a head race of VHPS-1 using Ground Penetrating Radar (Arcone et al. 1998): above-water GPR survey with "SIR2000" and at the Side Plan Hydro location (Velikin & Snegirev 2004) using the "GBO" instrument. Both methods confirmed the anomalous zone that was distinguished using the self-potential data in the head race area. GPR- reflecting boundaries associated with water-filled cracks, typically horizontal and vertical cracks, can be recognized on the radargram. On bottom-surface images obtained with hydrolocation, the anomalous site was distinguished by the occurrence of small depressions (slots) perpendicular to the shore. In the geological structure of the berm adjoining the head race, a number of similarly-oriented (orthogonal to shore zone) cracks were also marked. It is important that close spatial coincidence of anomalous zones found by Self-Potential, GPR, and Side Plan Hydro location methods was established. Detected zones at 242–238 m elevation, coinciding with the depth interval of intensive seepage, was established also by thermometry (Velikin & Snegirev 2004).

Borehole observations: The first warning information (in 1995) about talik nucleation at the base of Sitikan dam was from long-term temperature measurements initiated in 1990. Seasonal temperature field dynamics for the flank of Sitikan dam with active talik zone are presented in Figure 4. The network density of thermometric holes and the irregularity of observations have hampered estimation of the spatial distribution of the talik and seepage development. For processing, all previous available temperature data were used.

In addition, measurements were conducted in piezoborehole and on a water area, where earlier temperature observations were lacking. This has allowed us to "fill in" the missing periods of observations in individual holes, and to derive the general evolution of the talik zone. An example of the active stage of talik evolution for the period 2000–2006 is shown in Figure 5. Without going into details of the contingency of the Sitikan dam, it is necessary to say that for the last decade many efforts (grouting, air and kerosene cooling, enrockment, etc.) were implemented to prevent the consequences of seepage. Some results are shown in Figure 5 on the left part of the earth dam. We also can see the progressing talik in the right bank contiguity due to development of bypass filtration (Figures 4 and 5). For controlling the in situ situation in the seepage zone, tracer techniques (with colorings and electrolytes) were used to determine the flow rate (Velikin & Snegirev 2004). NaCl solution was used as a tracer. Resistive potentiometers installed in observation boreholes on a particular selected

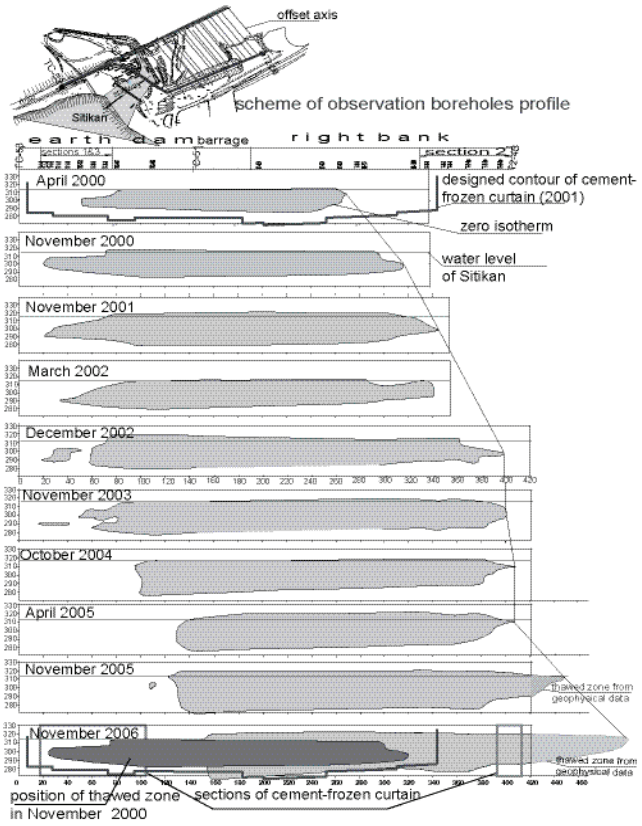

Figure 5. Dynamics of thawed zone (talik) contour along borehole profile (solid line on the upper schematic) for the Sitikan Hydro Unit over the period 2000–2006 (mainly by thermal data).

interval were used as a recorder for continuously measuring water resistance filling the borehole.

Observations were carried out in two ways: (1) injecting a tracer into piezoborehole No. 80 and then measuring in piezoborehole No. 81 downstream; (2) injecting a tracer near the shore of the head race of the right-bank abutment and collecting measurements in piezoborehole No. 80. According to obtained data, the flow rate was estimated at approximately 50–60 m per hour. This is a fairly significant value and should be considered when developing anti-seepage measures.

Automatic temperature measurements in the boreholes using loggers are of special interest, insofar as they permit us to obtain information about the position of seepage horizons and their characteristics. Figure 6 illustrates logger measurements in piezometric borehole № 81 of the right-bank abutment in comparison to water temperature dynamics in the head race of the dam. Figure 6 shows that a general reduction of reservoir water temperature determines a temperature decrease in the filtration zone (236-232 m) of the embankment. In the upper part of the borehole, the logger data indicate a null or small temperature increase. The analysis of available data shows the high information content of logger temperature measurements. They may help to reveal reservoir intervals in thermometric boreholes based on analysis of temperature dynamics, identify the intervals where, despite the presence of positive temperatures,

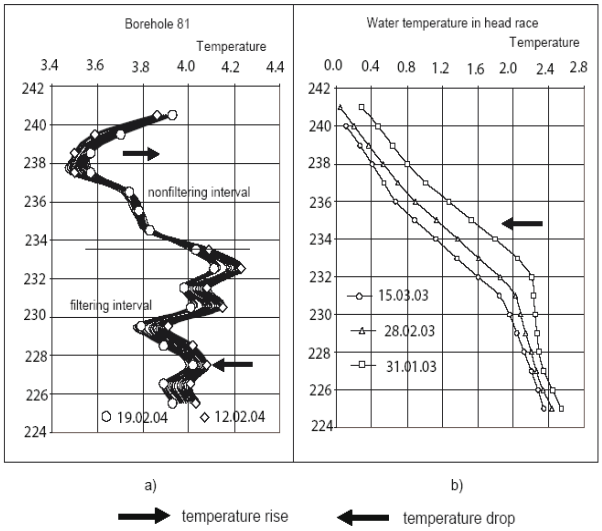

Figure 6. Revelation of percolation layers by logger measurements: (a) temperature measurements in piezometric borehole No. 81; (b) water temperature in head race.

filtration flows are absent, and also to study the interaction peculiarities between the rocks and water.

For geophysical monitoring in a permafrost zone, the Radio Wave Geo-Introscopy (RWGI) profiling and cross-borehole measurement method, as well as the One-hole Radio Wave Profiling (ORWP) method, was used. Theory, tools and measuring techniques are described in Istratov & Frolov (2003). The purpose of radio wave investigations was as follows: First, to control the frozen rock thawing within the coastal zone of the reservoir and to assess the dynamics of the process; and second, to identify and locate the places of most intensive thawing and seepage from the reservoir. Thawing processes lead to a decrease of electrical resistivity (ρ); the saturation of the filtering layer must be reflected as an increase of relative dielectric permittivity (ε) within the same interval. If measurements are taken repeatedly at two frequencies along the borehole profile, the lower frequency data can give a picture of the rock electrical resistivity changes with space and time, thus providing insight into the process of frozen rock mass thawing under the influence of the reservoir. Measurements performed at high frequency permit the calculation of effective values of relative dielectric permittivity (ε); the higher values will indicate layers of most active filtration from the reservoir.

Monitoring in the Sitikan area began in 2000 and continues today (the last measurements were in March 2007). As an example, we consider the data obtained in 2001–2002 near the Sitikan Hydro Unit in Figure 7. In March and August 2001 and in March 2002, temperature measurements (Fig. 4) were made in boreholes 4 to 10, oriented perpendicular to the embankments of the Sitikan water resevoir. In additon, gamma logging and one-hole radio wave profiling (RWGI-ORWP) with the frequencies 1.25 and 31 MHz were conducted. Repeated ORWP data were interpolated between the holes (Fig. 7). The holes are 35 m to 45 m deep, with polyethylene casing and inside diameter of 65 mm. Sections based on repeated temperature measurements of

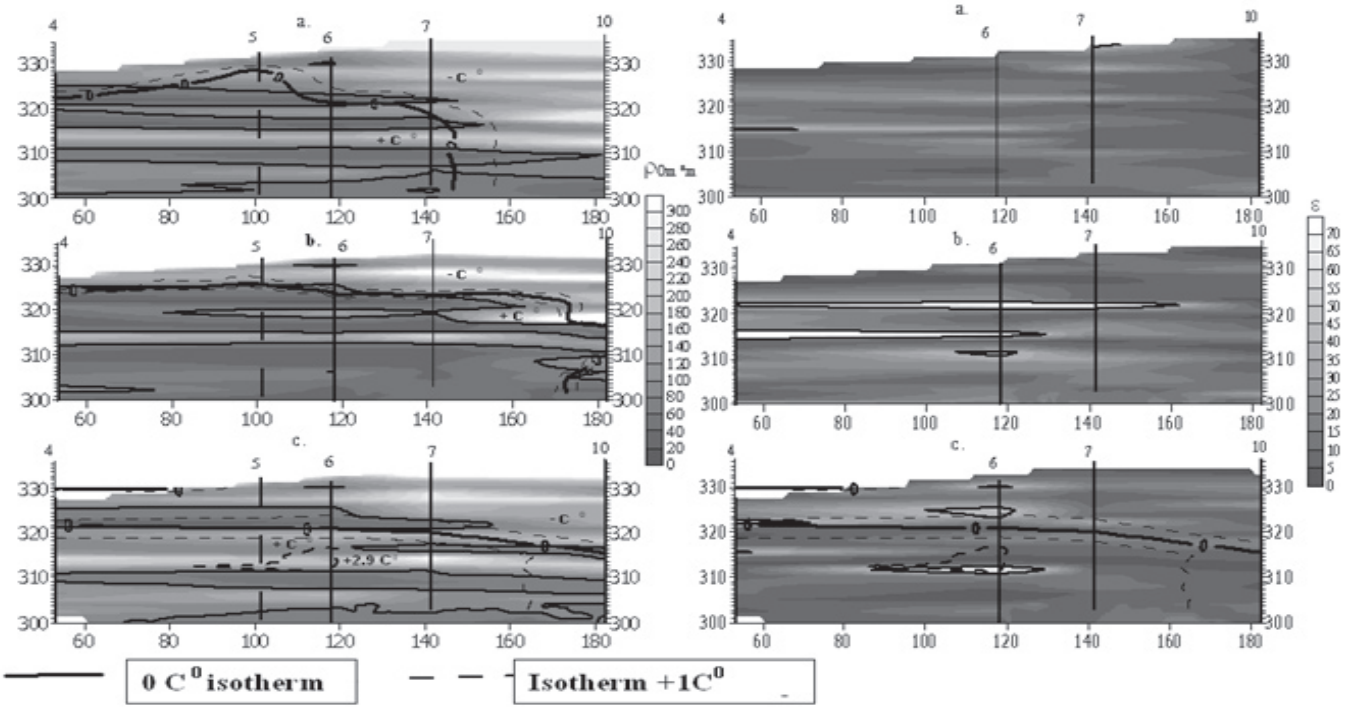

Figure 7. Examples of geoelectric sections of (left) effective electric resistivity (ρ) and (right) relative dielectric permittivity (ε) along boreholes profile (4 -5 -6 -7 -10) in a frozen embankment crosswise shoreline of the Sitikan Hydro Unit (Western Yakutia, Siberia). Replicated RWGI-ORWP observations in (a) March 2001; (b) August 2001; and (c) March 2002.

the fractionally thawed coastal frozen embankment in March and August 2001 show the dynamics of ground temperatures within the reservoir flank (Figs. 4 and 7). The geological section consists of carbonate rocks (limestone, dolomites and marbles) varying in fissured zones and clay content.

Comparing the results from March and August 2001, it is possible to see not only the general propagation of the "front" of lowered specific electric resistivity in the direction of borehole 10, but also to identify horizons at 309–311 m, 314–317 m, and 321–324 m, in which these changes occur most intensively. In August, a sharp decrease of resistivity was observed in these layers, and the first positive values of temperature were observed. Apparent on Figure 7 is the zero degree isotherm passage of 324–326 m on a sub-face of stratum of high resistivity. High resistivity gradient here marks the border of frozen and thawed rocks. In the section of effective dielectric permittivity, layers with the highest values of ε (intervals 311–314 m and 317–319 m, and near hole 6 at 306–309 m) correspond to a high gradient zone of positive temperature. Along these permeable layers, water from Sitikan penetrates deep into the coastal embankment, working over time like a "secondary" heat source by distributing heat and accelerating thaw of frozen rocks. However, in March 2002 (Fig. 7), the resistivity of rocks in a section increased. This phenomenon is connected with maximum freezing (frost penetration) of rocks, and minimum water temperature in Sitikan storage. Visually, it is tracked between holes 4 and 7 in a layer (314– 317 m) in which there is a relative increase of resistivity (ρ); below 314 m a reduction of ρ is observed. In March 2002 (at the time of minimal temperature of the entire rock embankment), the areas with heightened ε values are narrowed and located near borehole 6 at horizons 310–312 m and 322–325 m. This is connected with seasonal freezing of the embankment. However, the presence of local zones with heightened values of dielectric permittivity (ε) suggests the existence of "year-round" liquid water at the non-percolating level (322–325 m) and with bypass seepage from the water storage through the originally frozen embankment at level 310–312 m, corresponding to the Sitikan water level in March of 314 m.

The good correlation of geoelectric sections with the temperature data shows not only the direct dependence of electric properties on the frozen-thawed state of the embankment, but also the essentially higher sensitivity and resolution of electric methods for detecting the liquid water phase. Accurate interpretation of these data must also take into account the seasonal water level change of Sitikan.

Thermal Modeling

In the case of water storage, we have pressure headwaters constrained by a frozen dam with a set of engineered constructions. The non-steady problem of heat-mass transfer in fractured and porous saturated frozen Stratum (II) (Fig. 8), situated between frozen impermeable adjacent Stratam (I, III) is discussed. There is a pressure head acting from the Aquifer, explicating in thawing saturated Stratum (II) with allowance for seasonal variations of air-water temperatures on ground-water surface and within the Aquifer (Fig. 8). According to Petrunin & Milanovskiy (2005), from numerical analysis it follows that the process of thermal evolution of the frozen strata can conditionally be separated

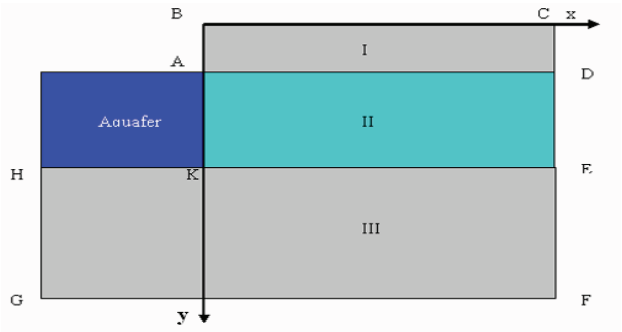

Figure 8. Schematic geometry of the model.

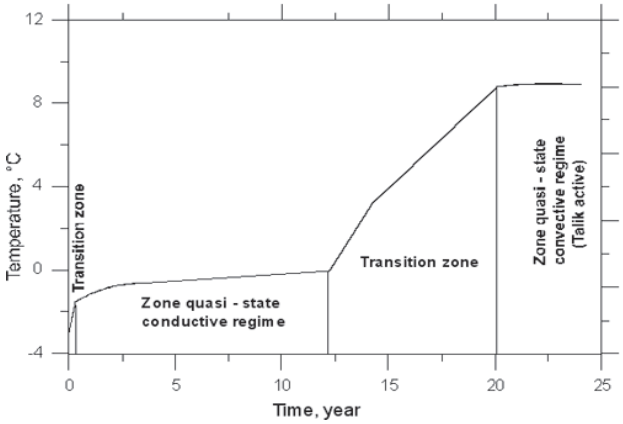

Figure 9. Variation of seasonal T-maximum in the mark-point situated in the middle of the top of permeable zone (talik zone) with time (from Petrunin & Milanovskiy 2005).

into two basic and two transient stages (Fig. 9). The first stage starts from the moment of water storage infill and represents initiation of thermodynamic equilibrium in the absence of convection. If it is quick enough; for 2–3 years it exhibits a quasi-state conductive heat regime in which seasonal variations in the thermal field quickly damp with depth according to Fourier's Law.

From Figure 9, the maximum seasonal temperature at the top of Stratum II (middle of AD) between 2–12 years ranges from -1°C up to 0°C, when the pore ice begins to thaw and permeability becomes distinct from zero. In this case, if there is hydraulic head, convective heat-mass transfer is initiated which is much more effective than pure conduction. This is the governing factor in our model for talik origination The results (Petrunin & Milanovskiy 2005) of 2-D thermal modeling indicate that talik development depends on specific thermal and hydraulic material parameters, water head, thickness of the frozen layer covering the talik, winter snow blanket insulating ground rocks, the seasonal temperature trend as well as on the presence of fractures in the frozen media. The observed evolution of the temperature field in the talik zone of the border part of the Sitikan Unit is in general agreement with the calculated temperature field.

Conclusion

Geophysical data testify about different types of talik zones. Nevertheless, they have a very common characteristic feature—the presence of a triggering mechanism for talik initialization. For identification of this mechanism, we need the pre-talik temperature history that leads to pre-heating of the strata, the existing fractures or pore channels (partly-open or ice cemented), and the reservoir water head. For example, in the Sitikan Unit case, the pre-talik history was about 20 years. An important factor for the stability of long-existing constructions like a Hydro Unit or waste confinement in the permafrost zone is global climatic change. The proposed simple model can be used for analyzing more complex situations. The results presented show the efficiency of a number of key geophysical methods for the study of permafrost peculiarities associated with talik formation and its development near Hydro Units in Western Yakutia. The proposed long-term geophysical monitoring of the permafrost state can be used for emergency situation prediction.

Acknowledgments

The authors express their true thanks to the anonymous reviewer for helpful comments.

References

Arcone, S., Lawson, D., Delaney, A., Strasser, J.C. & Strasser J.D. 1998 Ground-penetrating radar reflection profiling of groundwater and bedrock in an area of discontinuous permafrost. *Geophysics* 63(5): 1573-1584.

Erchul, R.A. & Slifer, D. 1989. The Use of Self Potential to Detect Ground-Water Flow in Karst. *Technical Report REMR-GT-6*, U.S. Army Engineer Waterways Experiment Station, Vicksburg, MS.

Hunter, J.A. & Douma, M. 2007. Development of a Capacitive-Coupled Resistivity Method for Permafrost Surveys in North America: Melinki Russkas (A Little Russian Tale*) Fast TIMES* 12(4): 23-26.

Istratov, V.A. &. Frolov, A.D. 2003. Radio wave borehole measurements to determine *in situ* the electric property distribution in a massif. *J. Geophys. Res. – Planets* 108(E4): 8038-8043. doi:10.1029/2002JE001880

Kronik, A.A. 1999 Hydraulic structures. In: L.N. Khrustalev & E.D. Ershov (eds.), *Permafrost Engineering,* V5. Moscow: MGU, 413-445.

Petrunin, A.G. & Milanovskiy, S.Yu. 2005. Talik formation in the flank shore of water-storage reservoir in permafrost area. *Abstract UCOP*, *Potsdam, June 12–16*: 189.

Semenov, A.S. 1968. *Electro prospecting by natural field method,* Leningrad: Nedra, 391 pp. (in Russian).

Timofeev, V.M. 1980. *Application of electro profiling with magnetic capacitor antenna for engineering survey*. Abstract of Ph.D. Thesis, Moscow, VSEGINGEO, 24 pp. (in Russian).

Velikin, S.A. & Snegirev, A.M. 2004. Study of the right-bank contiguity of the dam at the Viluy hydroelectric power plant: Complex of techniques. *Journal of Glaciology and Geocriology* 26: 142-150.

Zikov, Y.D. 1999. Geophysical Methods for Cryosphere Zone Investigations. Moscow: MGU, 244 pp. (in Russian)

Seasonally Frozen Ground Effects on the Dynamic Response of High-Rise Buildings

Rys Miranda
School of Engineering, University of Alaska Anchorage, Anchorage, AK, USA
Zhaohui (Joey) Yang
School of Engineering, University of Alaska Anchorage, Anchorage, AK, USA
Utpal Dutta
School of Engineering, University of Alaska Anchorage, Anchorage, AK, USA

Abstract

It is well-known that temperature variation can impact the properties and performance of various materials utilized in civil structures. Much work has been performed to evaluate these impacts; however, limited work has been performed to evaluate the seismic performance of civil structures embedded in or surrounded by seasonally frozen ground. This paper presents a comparison study of seasonally frozen ground effects on two high-rise buildings in Anchorage, Alaska. The dynamic properties of a 14-story building have been evaluated under winter and summer conditions, and then correlated with frost depths quantified from temperatures recorded at a nearby airport. Further, these results have been compared with that of a nearby 20-story building. Discussions and conclusions are provided with regard to the impact of seasonally frozen ground on buildings with different configurations, specifically with or without a basement. These findings will provide insight into frozen ground effects on high-rise building design.

Keywords: dynamic response; earthquake engineering; frozen ground; soil-structure interaction.

Introduction

Even though the concept of frozen soil dynamic properties has been around for decades, very little work has been conducted to evaluate the seismic performance of civil structures with respect to frozen ground conditions, seasonally, or permafrost. Early investigations of frozen soil dynamics are rooted back in the 1940s as a by-product of the search for oil in permafrost-laden regions (Vinson 1978). Considerable changes in mechanical properties take place between unfrozen soil and frozen soil. Notably, the Young's Modulus, E, of frozen soils are larger, in magnitudes of tens and hundreds, than that of unfrozen soil (Tsytovich 1975). Experiments conducted by Tsytovich (1975) have concluded that the compressibility of frozen soils is so miniscule that it can be disregarded for engineering purposes. Other experiments, involving ultrasonic pulses, have revealed that the wave velocity of soil increased as the temperature decreased (Finn et al. 1978). Vinson (1978), by means of cyclical triaxial testing, determined that the dampening ratio of soil diminished with decreasing temperatures. All these parameters play a crucial role in evaluating seismic response and the soil-structure interaction of frozen ground versus unfrozen ground.

This paper will investigate the impacts of such changes in soil parameters to the dynamic response of a 14-story reinforced concrete office building in Anchorage, Alaska. Furthermore, findings from this building will be compared to those of a nearby 20-story building obtained in a recent study (Yang et al. 2007).

Project location and description

The subject, a 14-story office building known as the Frontier Building, is located in mid-town Anchorage, Alaska (61°11′15″N latitude, 149°53′05″W longitude). Anchorage, Alaska is an ideal setting for this project, since it is located within a seismically active region and is exposed to subarctic conditions with considerable annual frost penetration. The environment of the project site is that of a typical urban setting with asphalt concrete paved roads and concrete sidewalks surrounding the building. Minimal tree or vegetative cover can be observed around the general area. The topography is consistently flat and relatively level. The local climate has an average annual temperature varying from -1.6°C to 6.2°C and average frost penetration of 2.0 m (WRCC 2007).

Anchorage is located on one of the most seismically active regions of southcentral Alaska. According to national seismic hazard maps, the probabilistic peak ground acceleration of the Anchorage metropolitan area is around 0.4 g with 10% exceedance in 50 years (Wesson et al. 1999). The subduction of the Pacific plate underneath the North American plate, causes intense seismic activities in and around Anchorage. The Prince William Sound earthquake of 1964 (M_w=9.2) was one of the prominent examples of such subduction zone seismic activities which caused widespread damage in the Anchorage area. In addition to the subduction zone earthquakes, some prominent surface faults (Haeussler & Plafker 2003) surrounding the region, also contribute to the seismic hazard of the region. The Castle Mountain Fault is in the vicinity of the Anchorage area and has the potential to generate 6–7 magnitude earthquakes (Woodward-Clyde 1982).

Geologically, the soils underneath the project area consist of glaciofluvial, glaciodeltaic, and alluvial fan deposits (GF, sand and gravel) (Combellick 1999). The area is located on seismic site class C/D (Dutta et al. 2000; Martirosyan et al. 2002) with average site amplification around 2.5 times at 1 Hz. (Dutta et al. 2001)

The Frontier Building

The Frontier Building is a reinforced concrete building constructed in the early 1980s under the 1979 edition of the Uniform Building Code (UBC). The building is founded on a series of reinforced concrete strip footings running in the east-west direction. The footings on the north and south edges are 2.7 m wide and 1.4 m thick, while the interior footings are 3.4 m wide and the same thickness as the edge footings. Stemming from the footings are 1.2 m (north and south edges) and 0.9 m (interior columns) diameter reinforced concrete columns. A total of 14 columns make up the entire building. The typical floor level construction is 0.2–0.3 m thick reinforced concrete diaphragm. The first floor of the building is essentially a slab-on-grade atop the backfill of the strip footings. The bottom of the foundation is at a depth of 1.7 m below ground. The roof of the building is set at 50.6 m above ground level (first floor). The plan dimension of the building is 59.4 x 32.6 m in the E-W and N-S edges, respectively.

Geotechnical Characteristics

Site geotechnical properties

Existing soils investigation reports were utilized to assist with the determination of frost/thaw penetration. The soil characteristics down to 21.3 m are available from the boring report, conducted during the design and construction of the Frontier Building, which reveals the presence of a peat stratum of about 0.6 m thick overlying 2.4 m thick of very dense, damp, gray, slightly gravelly, fine to coarse sand (Combellick, pers. com.). The deeper formation consists of stiff sandy silts, but these layers are of no concern for the present study, since frost penetration is not expected to exceed 3 m in the area. The soil properties such as unit weight/density, moisture content, and groundwater level are taken from the boring reports of DOWL Engineers and Alaska Testlab (pers. com.) from a nearby site. The report showed a mass density, ρ, of 2002 kg/m^3 and a moisture content, ω, of 20% with the groundwater level at approximately 4.0 m below the surface.

Frost/thaw penetration

The Modified Berggren Equation, developed by Aldrich and Paynter, is a reliable method for quantifying frost/thaw penetration. The modified equation simply applies a correction coefficient, λ, to the widely used Steffan Equation (Andersland & Ladanyi 2004).

The surface freezing and thawing indices, I_{sf} and I_{st} respectively, were derived from air freezing (I_{af}) and air thawing (I_{at}) indices by relation of the surface *n*-factor values for the site environment as shown in equations (1) and (2).

$$I_{sf} = n_f \cdot I_{af} \text{ Freezing} \quad (1)$$

$$I_{st} = n_t \cdot I_{at} \text{ Thawing} \quad (2)$$

The air freezing and air thawing indices were calculated using daily average air temperatures from the Ted Stevens International Airport, approximately 4.8 km from the subject building. The I_{af} was calculated for each day starting from October 24, 2006 (the first day of freezing), to April 2, 2007 (day of maximum frost penetration or last day of freezing), and the obtained values were multiplied by the n_f-factor of 0.9 (pavement free of snow and ice) to determine the I_{sf}. The n_f-factor is consistent with the surrounding environment of paved roads and sidewalks. The daily I_{sf} values were added cumulatively to generate a day-by-day index, which was then used to quantify a day-by-day frozen ground thickness. A similar procedure was used to numerically track I_{st} into the frozen ground. The air thawing index, I_{at}, was calculated for each day starting from April 3, 2007 (the first day of thawing), all the way to June 24, 2007 (day of complete ground thaw out). The I_{at} value for each day was multiplied by the n_t-factor of 1.775 (average factor for asphalt pavement and concrete pavement) to produce I_{st}. The I_{st} values were then added cumulatively to generate a day-by-day index which, in turn, was used to quantify the day-by-day thaw penetration. The daily thaw penetration was added cumulatively until the summation was equal to or greater than the calculated frost penetration, which meant the frozen ground had completely thawed out.

The value of I_{sf} and I_{st} obtained above can then be used to numerically determine the depth (X) of frost and thaw penetration by means of the Modified Berggren Equation expressed as:

$$X = \lambda \cdot \left(\frac{172{,}800 \cdot k_{avg} \cdot I}{L} \right)^{1/2} \quad (3)$$

where X (m) is the depth of frost/thaw penetration, k_{avg} (J/(sec·m·°C)) is the soil thermal conductivity, L (MJ/m^3) is the soil latent heat, I (°C·days) is the absolute value of the surface freezing index or surface thawing index, and λ is the dimensionless correction coefficient.

We will numerically calculate the value of k_{avg}, L, and λ of equation. (3) as follows: To determine the soil thermal conductivity, k, we assumed that the peat layer was completely removed and replaced with excavated material displaced by the strip footing. This assumption will provide consistent soil properties down to 3.1 m. Applying the soil's mass density of 2002 kg/m^3 and moisture content of 20%, values of k_f (frozen) and k_u (unfrozen) were found to be 3.25 J/(sec·m·°C) and 2.00 J/(sec·m·°C), respectively, for an average k_{avg}, of 2.63 J/(sec·m·°C).

The volumetric latent heat, L, can be calculated by the equation:

$$L = \rho_d \cdot L' \cdot \left(\frac{\omega - \omega_u}{100} \right) \quad (4)$$

where L' = 333.7 kJ/kg is the mass latent heat for water, ω_u, is the unfrozen water in the frozen soil which is generally so small that it is considered to be at 0%, and the other variables are as before. Inserting the soil properties ρ_d and ω into equation (4) yields a latent heat value of 111,389 kJ/m^3.

The correction coefficient, λ, can be derived from the thermal ratio, α, and the fusion parameter, μ. The thermal ratio and fusion parameter can be expressed by the following equations, respectively:

$$\alpha = \frac{v_o}{v_s} = \frac{v_o \cdot t}{I_{sf}} \tag{5}$$

$$\mu = \frac{c_v}{L} \cdot v_s = \frac{c_v \cdot I_{sf}}{L \cdot t} \tag{6}$$

where c_v (kJ/m³·°C) is the soil volumetric heat capacity, t is the time or duration of the freezing period, and v_o and v_s (°C) are surface temperatures initially above freezing and below freezing respectively.

Volumetric heat capacity, c_v, is the average of the unfrozen volumetric heat capacity, c_{vu}, and the frozen volumetric heat capacity, c_{vf}, which are expressed by the following equations:

$$c_{vu} = \frac{\rho_d}{\rho_w} \cdot \left(0.17 + 1.0 \frac{\omega}{100} \right) \cdot c_{vw} \tag{7}$$

$$c_{vf} = \frac{\rho_d}{\rho_w} \cdot \left[\left(0.17 + \frac{\omega_u}{100} \right) + 0.5 \cdot \left(\frac{\omega - \omega_u}{100} \right) \right] \cdot c_{vw} \tag{8}$$

where ρ_w represents the density of water at 1,000 kg/m³, c_{vw} represents the volumetric heat capacity of water at 4.187 MJ/m³·°C, and all others are as before. Inserting the soil properties into equations (8) and (9) yields the values of 0.62 MJ/m³·°C and 0.45 MJ/m³·°C, respectively, for an average value, c_v, of 0.54 MJ/m³·°C.

The time of freezing, t, is the number of days starting from October 24, 2007 to April 2, 2007, which comes out to 160 days. Average surface temperature, v_o, is derived by multiplying the average air temperature for the year by the average *n*-factor. This value was found to equal 4.35°C.

The thermal ratio and fusion parameter can then be solved by inserting the appropriate values into equations (6) and (7). In doing so, α equaled approximately 0.6 and μ, 0.04. These values are then inputted into the chart in Figure 1 to determine a correction coefficient, λ, of 0.94.

With all the variables determined, frost and thaw penetrations can be calculated via equation (3). The calculated seasonal frost depth was calculated for the days corresponding to dynamic data collection. The geothermal gradient for this area was examined to see if it had any substantial influence on the frost penetration. Without empirical data to determine the geothermal gradient, a rule of thumb approximation proved by Brown (1963) was used and determined the gradient to be 1.8 x 10^{-2} °C/m. This gradient was deemed negligible.

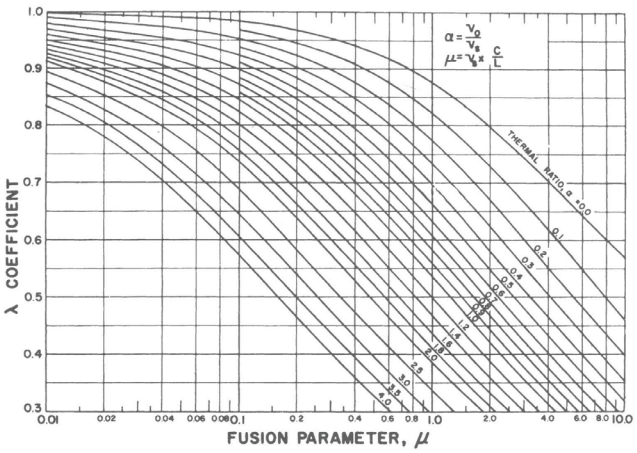

Figure 1. Correction coefficient (Andersland & Ladanyi 2004).

Strong Motion Instrumentation

Strong motion sensors

Installation of seismic sensors in the Frontier Building took place in early 2007. The seismic sensors used to measure the structural response of the building were the Kinemetrics EpiSensor (Force Balance Accelerometer Model FBA ES-T, ES-U). Each sensor has a bandwidth of DC to 200 Hz and is capable of reading a user-defined acceleration spectrum of ±0.25 - ±4.0 g's with 1.25 V/g sensitivity (Kinemetrics 2005). A ±4.0 g range was selected for the sensors on this project. Three Altus K2 Strong Motion Accelerographs serve as the digital data recorders with 12 channels per data recorder. The recorders are located on the fourteenth floor of the building, within the communications closet. Thirty channels monitor lateral movement in 10 of the 14 floors of the building. Of the 30 channels, 20 channels are dedicated to the E-W direction and 10 channels to the N-S direction. The remaining 6 channels are set up for monitoring in the vertical direction. The vertically-oriented sensors are located only on the first and fourteenth floors. Nodes designated for biaxial sensitivity were composed of two ES-U2 sensors, with one oriented in the N-S direction and the other in the E-W direction. Uniaxial sensors oriented vertically were used for vertical measurements. Each of the sensors was installed on either the floor or the ceiling of the representative level of the building. The GPS antenna is installed on the rooftop of the building for accurate time (±0.5 ms) synchronization of the data recording devices (Kinemetrics 2002).

Data collection

We have measured the earthquake, as well as the ambient vibration, data of the building. In case of earthquake, the seismic system is preset to record any event that produces 1 gal acceleration at the base of the building (first floor) for a duration of 120 s. For the ambient vibration data, the recording duration was changed to 4–7 minutes. In both cases, the data were sampled at the rate of 200 samples/s and were processed in the same manner.

Data Analysis, Results, and Discussion

Data analysis

The recorded data from each sensor, after correcting for the baseline and instrument response, were filtered between 0.01–45.0 Hz using a fourth order bandpassed Butterworth filter. ARTeMIS Extractor was used to analyze the dynamic characteristics of the Frontier Building based on collected data. ARTeMIS Extractor is an Operational Modal Analysis (OMA), or output-only modal analysis software (Structural Vibration Solutions A/S 2007), and is a widely used program for strong motion dynamic analysis.

In ARTeMIS, a configuration file was first generated describing the structural geometry of the building. The generated model is shown in Figure 2. The arrows in the nodes represent the direction of sensor orientation. In the next step, the recorded time histories from each sensor were applied to the model and Spectral Density Matrix (SDM) were computed.

The generated SDM can then be decomposed into Singular Value Density (SVD) systems apparent to individual modes by means of either Frequency Domain Decomposition (FDD) or the Enhanced Frequency Domain Decomposition (EFDD) (Bai 2007). The dynamic characteristics of interest were the first and second modal frequencies (when available) and the corresponding mode shape. The data generated by ambient noise were enough to clearly depict the first two modes in the weak direction (E-W), the strong direction (N-S), and torsional direction. The data generated by the earthquake events had clear peak picking for only the first two modes in the weak direction (E-W) for the April 25, 2007, event and the first mode in the weak direction (E-W) and first mode in the strong direction (N-S) for the May 22, 2007, event. This was due to the direction of the earthquake's epicenter being mainly in the E-W direction relative to the building.

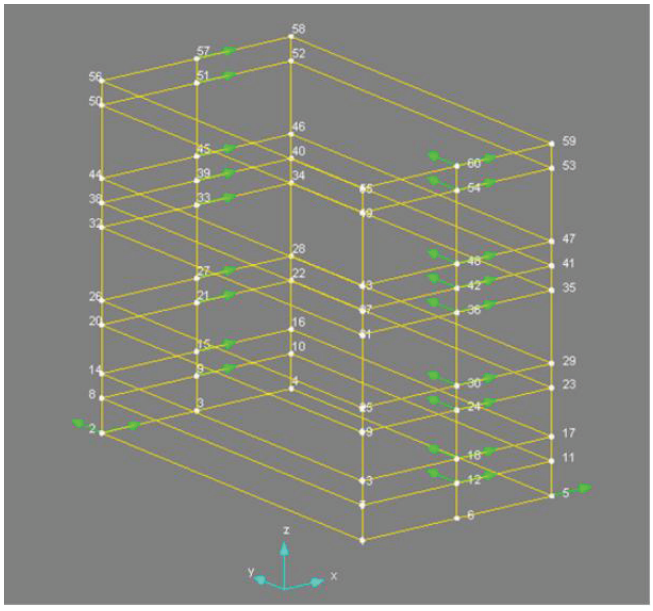

Figure 2. Geometric model of the Frontier Building generated by ARTeMIS.

The analyzed modal frequencies were then correlated with the calculated seasonal frost penetration. The relation between the first and second modal frequencies and frost depth can be seen tabulated in Table 1 and graphically in Figure 3. The data revealed minimal variation in the first and second modes with respect to varying frozen ground thickness. All fundamental frequencies for the weak axis were within 2% of one another and 3% for the second mode frequencies.

Discussion

The tabulated results do not reveal similar trends found in similar past projects conducted by Qi et al. (2006), Yang et al. (2007, 2008), and Bai (2007). These past projects, involving a pile foundation bridge, a 20-story office building (the Atwood Building) with an unheated parking garage basement, and an open, unheated, four-level parking garage yielded increases in the fundamental frequencies ranging from 4% up to 50% from summer to winter season. All these projects are anticipated to differ from the Frontier Building in that they all have foundation designs that allowed for the surrounding ground to freeze, whereas, the design of the Frontier Building allowed heat from the inside of the building to migrate to the foundation and prevent any ground freezing in the vicinity of the building. A thermal finite element model was generated for the Frontier Building, as well as for the Atwood Building, to examine and compare the two buildings' thaw bulbs.

It is appropriate to compare these two buildings, in that they are similar in shape and size, and they are relatively close to one another, and therefore, exposed to similar climate, as well as geotechnical, characteristics. They do, however, differ in configuration with respect to their foundations. As mentioned before, the Frontier Building has a footing foundation with the first floor directly on top of the foundation backfill. The Atwood building, on the other hand, has an unheated underground garage beneath the first floor of the building.

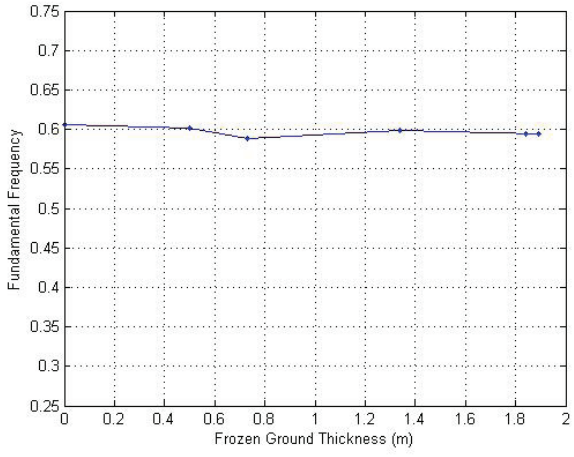

Figure 3. Frozen ground vs. fundamental frequency for the Frontier Building.

Table 1.

Event Date	Frozen Ground Thickness (m)	EFDD Frequency (Hz)					
		1st Mode			2nd Mode		
		E-W[b]	N-S	Torsion	E-W[b]	N-S	Torsion
03/01/2007	1.84	0.5945	0.6773	0.9183	1.861	2.059	2.736
04/05/2007	1.89	0.5936	0.6665	0.9012	1.845	2.025	2.698
04/25/2007[a]	1.34	0.5994	--	--	1.836	--	--
05/22/2007[a]	0.73	0.5888	0.6718	--	1.833	--	--
06/01/2007	0.50	0.6020	0.6766	0.9067	1.870	2.019	2.709
08/17/2007	0.00	0.6060	0.6733	0.9080	1.889	2.048	2.709

[a] Actual Recorded Earthquake Events
[b] E-W Direction Represents the Weak Axis of the Building

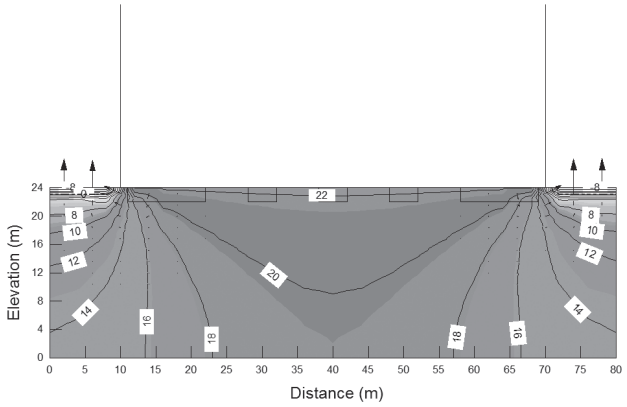

Figure 4. Thermal FE modeling results of the Frontier Building.

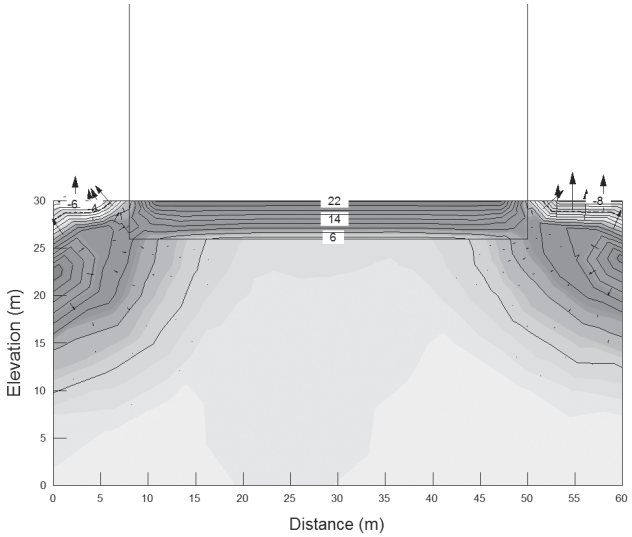

Figure 5. Thermal FE modeling results of the Atwood Building.

The Temp/W Module of Geo Studio 2004, Finite Element modeling software, was used to examine the thaw bulb of each building to compare thaw bulbs as a result of the foundation configuration. The average temperature of the interior of both buildings was assumed to be 22.2°C, and the average outside air temperature during the freezing period was found to be -8.2°C, from the temperature data obtained from a nearby airport described earlier. Soil properties such as thermal conductivity and heat capacity were inputted into the program, and the thaw bulb for each building was generated as shown in Figures 4 and 5.

The thermal contour lines are labeled with their appropriate temperature while the 0°C line (signifying the freezing front) is delineated with a bold dashed line. The arrows in the diagrams represent heat flow vectors. The direction of the arrow represents the direction of heat flow, and the size of the arrow determines the magnitude. Regional shading also relates to the thermal gradient. These two models could be refined to produce more accurate results (e.g., freezing front) by including details of the wall and openings in the basement. However, they are good enough to show that (1) sufficient heat migration was allowed from the building into the foundation, thus preventing frozen ground to develop in the Frontier Building; (2) the unheated parking garage/basement in the Atwood Building acts as a thick insulating layer preventing heat from infiltrating the surrounding soil, thus allowing frozen ground to develop.

Conclusions

After comparing the thermal analysis of the two buildings, the following conclusions were determined:

- Decreasing ambient air temperature did not impact the dynamic properties of the Frontier Building. This was due to the fact that the building's foundation design allowed for a large enough thaw bulb to prevent significant frost penetration.
- The Atwood Building's dynamic properties were impacted by seasonal frost due to its foundation design creating enough of an insulating layer to inhibit heat migration.
- Foundation design, with respect to heated or unheated, plays a crucial role in whether or not the structure's foundation will be influenced by frozen ground leading to potential impact on dynamic properties.

Acknowledgments

The strong-motion instrumentation was sponsored by the Advanced National Seismic System Program of U.S. Geological Survey. This study is partially supported by Chancellor's Research Funds of the University of Alaska Anchorage. We want to thank the management of the Frontier Building for their support to this project.

References

Anderland, O.B. & Ladanyi, B. 2004. *Frozen Ground Engineering*. New Jersey: The American Society of Civil Engineers & John Wiley & Sons, Inc., 363 pp.

Bai, F. 2007. *Effects of Seasonally Frozen Ground on Dynamic Properties of UAA Parking Garage Soil-Structure System*. University of Alaska Anchorage, School of Engineering, Civil Engineering Graduate Project.

Brown, W.G. 1963. *The Temperature Under Heated or Cooled Areas on the Ground Surface. National Research Council Canada,* Division of Building Research, Research Paper No. 208.

Combellick, R.A. 1999. *Simplified Geologic Map of Central and East Anchorage, Alaska. Alaska* Department of Natural Resources, Division of Geological & Geophysical Surveys, Preliminary Interpretive Report 1999-1.

Combellick, R.A., Mayer, J.L., Sink-Blair, K.D. & Weems, S.M. 2001. *Geotechnical Borehole and Well-Log Database for Anchorage, Alaska.* Alaska Department of Natural Resources, Division of Geological & Geophysical Surveys, Miscellaneous Publication 40.

Combellick, R.A. Personal Communication. Transcribed Notes of Boreholes for the Frontier Building.

DOWL Engineers and Alaska Testlab. Personal Communication. Log of Boring for Test Boring 3.

Dutta, U., Biswas, N., Martirosyan, A., Nath, S., Dravinski, M., Papageorgiou, A. & Combellick, R. 2000. Delineation of spatial variation of shear wave velocity with highfrequency Rayleigh waves in Anchorage, Alaska. *Geophys. J. Int.* 143: 365-375.

Dutta, U., Martirosyan, A., Biswas, N., Papageorgiou, A., Dravinski, M. & Combellick, R. 2002. Estimation of S-wave site response in Anchorage, Alaska, from weak motion data using generalized inversion method. *Bull. Seism. Soc. Am.* 91: 335-346.

Finn, W.D.L. & Yong, R.N. 1978. Seismic Response of Frozen Ground. *American Society of Civil Engineers, Journal of the Geotechnical Engineering Division* 104: 1225-1241.

Haeussler, P. & Plafker, G. 2003. *Earthquakes in Alaska.* U.S. Department of the Interior, U.S. Geological Survey, Publication No. 95-624, ver. 1.1.

Kinemetrics, Inc. 2005. *EpiSensor Force Balance Accelerometer Model FBA ES-U2 User Manual*. Document 301929, Revision D.

Martirosyan, A., Dutta, U., Biswas, N., Papageorgiou, A. &. Combellick, R. 2002. Determination of site response in Anchorage, Alaska on the basis of spectral ratio methods. *Earthquake Spectra* 18: 85-104.

Qi, J., Ma, W., Sun, C. & Wang, L. 2006. Ground Motion Analysis in Seasonally Frozen Regions. *Cold Regions Science and Technology* 44: 111-120.

Structural Vibrations Solutions A/S. 2007. ARTeMIS Product Information. http://www.svibs.com.

Tsytovich, N.A. 1975. *The Mechanics of Frozen Ground*. Washington D.C.: Scripta Book Co., 426 pp.

Ventura, C.E., Laverick, B., Brinker, R. & Andersen, P. 2003. Comparison of Dynamic Characteristics of Two Instrumented Tall Buildings. *Proceedings of the Twenty-first International Modal Analysis Conference*, *Kissimee, Florida.*

Vinson, T.S. 1978. Parameter effects on dynamic properties of frozen soils. *American Society of Civil Engineers, Journal of the Geotechnical Engineering Division*, 104: 1289-1306.

Wesson, R., Frankel, A., Mueller, C. & Harmsen, S. 1999. Probabilistic Seismic Hazard Maps of Alaska, USGS Open-File Report, 99-36.

Western Region Climate Center (WRCC). 2007. http://www.wrcc.dri.edu.

Woodward-Clyde Consultants. 1982. Anchorage Office Complex, Geotech. Invest. Report to Alaska Dept. of Trans. and Public Facilities, Vol. I-III, Anchorage, AK.

Yang, Z., Dutta, U., Xiong, F., Zhu, D., Marx, E., and Biswas, N. 2007. Seasonal Frost Effects on the Soil-Foundation-Structure Interaction System. *American Society of Civil Engineers, Journal of Regions Engineering* 21(4): 108-120.

Yang, Z., Dutta, U., Xiong, F., Biswas, N. & Benz, H. 2008. Seasonal Frost Effects on the Dynamic Behavior of a Twenty-Story Office Building. *International Journal of Cold Regions Science and Engineering* 51: 76-84

Seasonal Thermal Regime of a Mid-Latitude Ventilated Debris Accumulation

Sébastien Morard
Geography Unit, Geosciences Department, University of Fribourg, Switzerland
Reynald Delaloye
Geography Unit, Geosciences Department, University of Fribourg, Switzerland
Jonathan Dorthe
Geography Unit, Geosciences Department, University of Fribourg, Switzerland

Abstract

The internal and reversible mechanism of air circulation throughout a porous debris accumulation-like talus slope, relict rock glacier, and rockfall deposit acts as an efficient advective conveyor of heat, which strongly influences the ground surface thermal regime during the whole year. Combining the detection of visual evidences and ground surface temperature (GST) measurements (continuous logging, winter mapping) has proved to be relevant for identifying areas affected by internal ventilation and for characterizing the spatial pattern of the seasonal ground surface temperature anomalies. Five types of specific annual ground thermal regime can be defined. Vegetation, soil, and micro-fauna appear to be related to these different thermal regimes. The distribution of vegetal associations is closely linked to the ground temperature in summertime.

Keywords: air circulation; ecosystems; seasonal thermal regimes; Swiss Alps and Prealps; talus slopes.

Introduction

The mechanism of deep air circulation (the so-called chimney effect or wind tube) is known to be a process of ground overcooling in the lower and, presumably, deeper parts of porous talus slopes (e.g., Wakonnig 1996, Delaloye et al. 2003, Sawada et al. 2003). It occurs frequently in mid-latitudes, where it can generate and/or preserve extrazonal permafrost conditions up to more than 1000 metres below the regional lower limit of discontinuous mountain permafrost (Gorbunov et al. 2004, Sone 2005, Delaloye & Lambiel 2007). The process plays, moreover, a decisive role in the conservation of specific terrestrial ecosystems (Gude & Molenda 2003).

Detailed investigations on the thermal regime of talus slopes and other porous debris accumulations (relict rock glaciers, rockfall deposits) have been carried out since 1997 in western Switzerland (Jura mountains, Prealps, and Valais Alps) in several sites located between 650 and 2000 m a.s.l. with a corresponding mean annual air temperature (MAAT) ranging from +8 to +2°C, respectively (Fig. 1) (e.g., Delaloye 2004, Lambiel 2006). They demonstrate that internal air circulation is a mechanism common to almost all prospected sites causing a significant annual negative anomaly of the ground surface temperature (GST) (up to more than 7°C below MAAT) at the bottom of the debris accumulation, independent of the slope orientation.

The present paper describes the seasonal spatial pattern of the ground surface thermal regime in porous debris accumulations, which are affected by the air circulation mechanism. It provides some key methods for detecting and assessing both the occurrence of a ventilation mechanism and its spatial influence. It also gives a preliminary overview on the related specific terrestrial ecosystems, in particular on the development and spatial extent of vegetal associations and soils.

Background

Cold airflow blowing out of the ground in summertime in the lower parts of scree slopes was used for centuries in mountainous or volcanic mid-latitude areas as natural refrigerators for the conservation of food (e.g., DeSaussure 1796). Several assumptions have been advanced to explain the origin of ground cooling (Harris & Pedersen 1998). Recent studies (Wakonnig 1996, Delaloye et al. 2003, Sawada et al. 2003) and our analysis of several tens of sites investigated in Switzerland demonstrate that a deep reversible air circulation process (the so-called "chimney effect") acting throughout the whole of an accumulation of blocky material (Delaloye & Lambiel 2007) is likely to be the main factor controlling the ground surface thermal regime on these sites. The cooling effect of air circulation in a porous medium has also been used artificially in embankments to preserve permafrost conditions under highway and railway infrastructure in high-latitude or high altitude (e.g., Goering & Kumar 1996, Niu & Cheng 2005).

The reversible air circulation

Variations of both the direction and the velocity of the air circulation throughout an accumulation of loose sediments are primarily controlled by the thermal contrast between the outside and inside (ground) air causing a gradient of driving pressure (Delaloye et al. 2003). The flow direction reverses seasonally. During winter, an ascent of relatively warm light air tends to occur in the upper part of the debris accumulation. It leads to a dynamic low (a depression) in the lower part, causing a forced aspiration of cold external air deep inside the ground even through a thick——but porous—snowpack. A gravity discharge of relatively cold dense air occurs during summer in the lowermost part of the debris accumulation, preventing the GST to rise significantly above 0°C in this

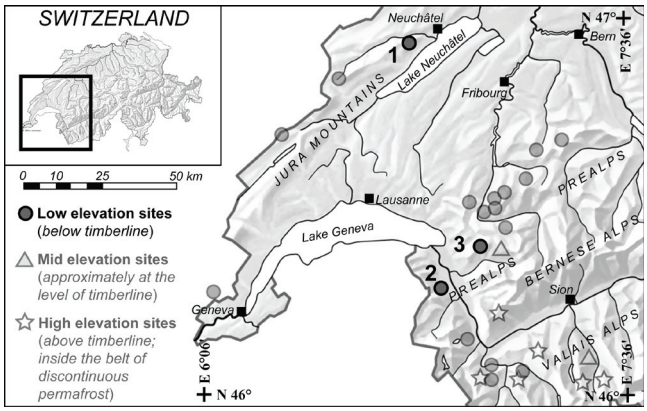

Figure 1. Location map of investigated areas with ventilated terrain in western Switzerland (after Delaloye 2004, Lambiel 2006, Dorthe & Morard 2007). Main sites: 1: Creux-du-Van; 2: Dreveneuse; 3: Bois des Arlettes.

section. As a consequence, a diffuse aspiration of external warm air occurs in the upper part of the slope.

An internal "cold reservoir" is built up during winter by the advection of external air (Sone 2005). The efficiency of the process depends on the intensity and duration of cold weather periods. The "frigories" are supposed to be "stored" by groundwater freezing (latent heat) and by conduction in the rocky materials and/or in the underlying finer ground (Delaloye & Lambiel 2007). The thermal conditions observed at the ground surface and in the shallow sub-surface in summertime are mainly influenced by the intensity of winter cooling and the recharge of the cold reservoir.

Specific ecosystems

The lower parts of ventilated talus slopes usually shelter specific ecosystems, whose typical distribution areas are located at higher latitude and/or higher elevation (e.g., Rist et al. 2003, Gude & Molenda 2003). Besides the occurrence of boreo-alpine species, significant differences in phenological development (like dwarfing of trees, early yellowing, or shorter developmental staging of vegetation) have also been highlighted between flora growing in the cold ventilated areas and those located outside (Ruzicka 1999, Körner & Hoch 2006).

Sites Characteristics

Data from the three main sites of investigation in western Switzerland (Creux-du-Van, Dreveneuse-du-Milieu, Bois des Arlettes) are used in this paper. The sites are located between 500 and 1200 metres below the estimated elevation of the regional lower limit of discontinuous mountain permafrost (about 2200–2400 m a.s.l. on northern slopes) (Fig. 1, Table 1).

Sites description

The Creux-du-Van (Cr) north-facing talus slope consists of limestone pebbles in the uppermost part transiting gradually to metric boulders downwards. The lower part of the slope is covered by an organic soil, and several patches of dwarf red spruces (*Tofieldio-Picetum* association) are occurring. The thickness of the blocky layer was estimated by geophysics to be about 20 m with the possible existence of a frozen body (Marescot et al. 2003). The site has been intensively studied since 1997 (Delaloye et al. 2003, Delaloye 2004).

Table 1. Topo-climatic characteristics of the investigated sites.

N°	Sites	Elevation	MAAT	Orientation
1	Creux-du-Van	1170-1290	+ 5.4°C*	N
2	Dreveneuse	1600-1800	+ 3.8°C**	E
3	Bois des Arlettes	1650-1900	+ 3.9°C***	NW

Locations are displayed on Figure 1. MAAT (Oct. 2004 to Sept. 2005) measured at: *1210 m a.s.l.; **1700 m a.s.l. (derived from Moléson, 2000 m a.s.l.); ***1740 m a.s.l.

The Dreveneuse-du-Milieu (Dr) east-facing talus slope consists of limestone pebbles and angular decimetric blocks. It is connected to a 200 m long relict rock glacier extending downward in a forested area. A few dwarf red spruces are found in the lower part of the slope as well as locally on the relict rock glacier. The thickness of the blocky layer was estimated by geophysics to be about 20 m for the talus slope and about 15 m for the relict rock glacier.

The large Bois des Arlettes (Arl) talus slopes face to the northwest and also consist of limestone debris. They dominate several sizeable relict rock glaciers. The thickness of the blocky layer was estimated to be about 25 m for the talus slope and 15–20 m for the relict rock glacier. Vegetation is almost lacking on the talus slope. The relict rock glaciers are conversely covered by a thin organic soil and a mixed forest, including some patches of azonal vegetation (*Salicetum Retuso-Reticulatae*) with alpine species such as *Pritzelago alpina* or *Dryas octopetalia*.

Meteorological conditions of the year 2004–2005

Data presented in the paper date from the hydrological year 2004–2005 (Fig. 2).

Relatively warm conditions occurred from October to mid-January in comparison to the climatic norm 1961–1990, interspersed with a cold phase by mid-November. Two successive persistent cold periods were then recorded until mid-March, separated by a short spell of milder weather in the first days of February. Afterwards, air temperatures remained warmer than the norm, except for August.

Winter 2004–2005 was also characterized by relatively late snowfalls, the snow cover remaining thin (less than about 50 cm) until mid-February. The snow cover reached its maximal thickness (1.5 m at Creux-du-Van and probably as much on the two other sites) by mid-March.

Methods

According to Delaloye (2004) and Morard et al. (2008), the observation of visual evidences (like "snowmelt windows" in the upper part of a slope in winter or ground-ice occurrences in early summer in the lower part) was used to point out the activity of a ventilation mechanism through a debris accumulation (Figs. 4, 5). In addition, ground temperature measurements were carried out to assess the spatio-temporal variability of the ventilation system.

Several single-channel dataloggers (UTL-1) were installed

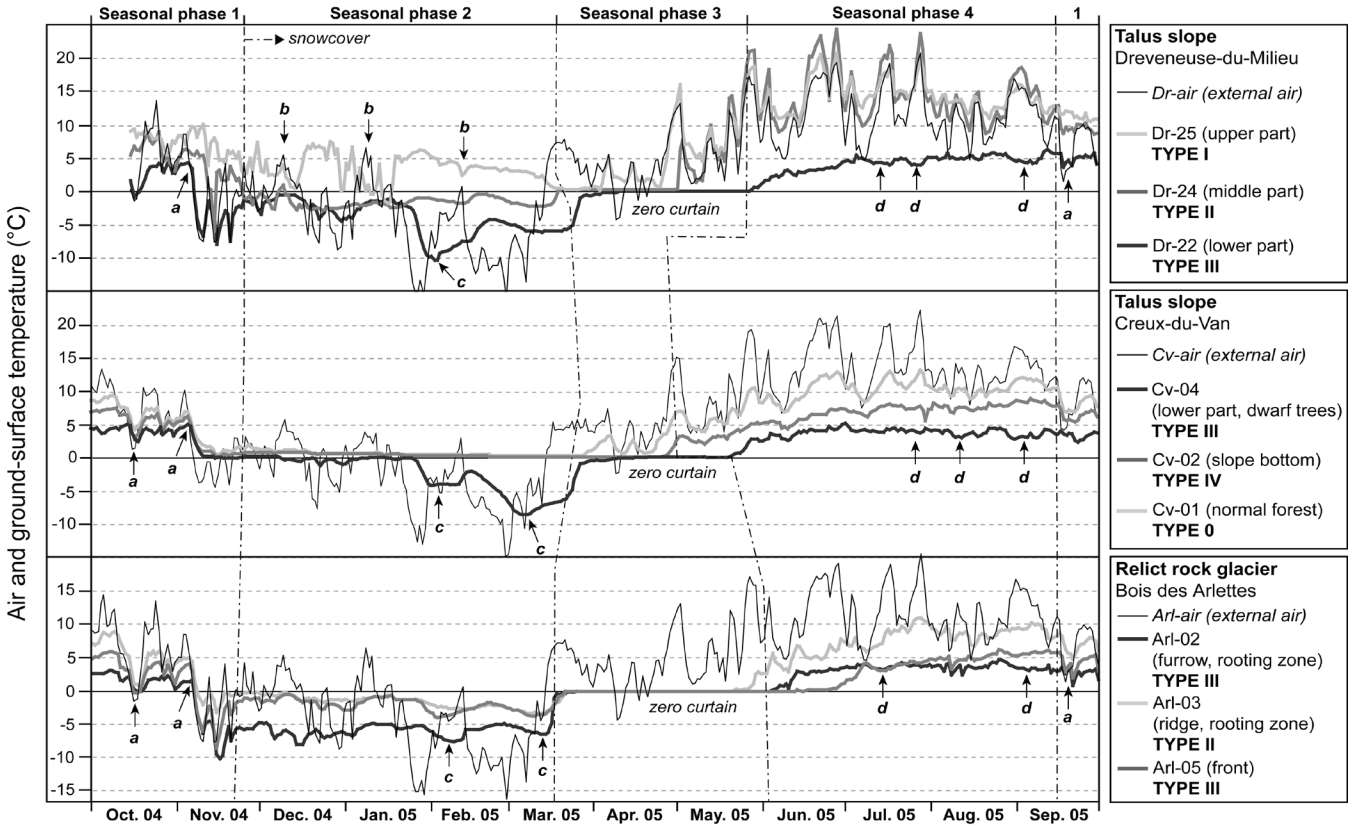

Figure 2. Thermal behaviors of the different parts of a ventilated talus slope–relict rock glacier complex. Data are daily air and ground-surface temperature. Locations of the dataloggers are shown in Figures 4 and 5. Arrows: a) inversion of the air flow direction; b) mild weather events; c) colder ground-surface temperature in January-–March 2005; d) coldest ground temperature in summertime.

on the different sites, mostly along a longitudinal profile crossing the whole debris accumulation. They recorded the ground surface temperature at a depth of about 10–20 cm every two hours. Atmospheric air temperatures were measured in situ (Creux du Van, Bois des Arlettes), or derived from official meteorological stations of the Federal Office of Meteorology and Climatology network using an altitudinal gradient of -0.58°C/100 m (Dreveneuse).

The comparison between ground and surrounding air temperature provides information about both the direction and intensity of the airflow. A similar relationship corresponds to an aspirating regime, while an inverse relationship indicates an expelling phase reflecting partially the thermal state of the ventilated system at a given moment (Lismonde 2002). A close non-delayed relationship between air and ground temperatures is assumed to be related to a higher intensity of the air flow.

To determine both the efficiency and the spatial pattern of a ventilation system, the winter temperature at the ground/snow interface was also mapped after a long period of cold weather in February 2005 using the BTS (bottom temperature of the snow cover) technique.

Results

Time series reported in Figure 2 and summed up in Table 2 illustrate the annual behavior of the GST for the three main sites of investigation along a slope profile. Four seasonal phases (1–4) can be distinguished for describing the thermal regime of the various parts of a ventilated debris accumulation, paying attention to the thermal anomalies in regard to the outside air temperature.

Seasonal phase 1: Autumn and early winter conditions

The fall–early winter phase until the onset of a thick snow cover is characterized by the frequent reversibility of the ventilation system. The air flows downwards in mild weather, whereas aspiration occurs in the lower parts of the ventilated terrain when the weather becomes colder. Not only the foot of talus slopes suffers an intense cooling of the ground, but also the relict Bois des Arlettes rock glacier (arrows "a" in Fig. 2). In all these places, this seasonal phase 1 is characterized by a negative thermal anomaly.

In November 2004, the GST in the upper part of the Dreveneuse talus slope (Dr-25) remained permanently above the freezing point, with variations inversely related to those of the external air temperature. Snowmelt windows, hoarfrost, wet blocks, basal icing of a thin snow cover, and condensation fog are visual evidences of the outflow of "warm" air during this phase.

During the phase 1, the lower part of the Dreveneuse talus slope (Dr-22) cooled from +4°C to -6.8°C between 6–10 November 2004, whereas the GST in the upper part of the slope remained as high as +8°C. At Bois des Arlettes, a rapid decrease of the GST from +1.5°C to -6.4°C and from +4°C to -6°C was also observed in a furrow in the rooting zone (Arl-02), and on the front (Arl-05) of the relict rock glacier, respectively. Where the soil is thicker and damper as in the Creux-du-Van lower talus slope (dwarf trees area), a zero curtain period can start (Cv-04).

Table 2. Temperature characteristics of the investigated sites.

UTLs	MAGST (°C)	ATA (°C)	GFI (°C)	NFD (day)	ZCD (day)
Dr-air	*3.76**	*0*	*-613*	*105*	*0*
Dr-25	7.94	+4.18	-6.5	8	0
Dr-24	5.54	+1.78	-204	114	42
Dr-22	-0.01	-3.77	-601	205	48
Cv-air	*5.35**	*0*	*-441*	*85*	*0*
Cv-04	0.74	-4.91	-336	171	34
Cv-02	3.29	-2.06	0	63	63
Cv-01	4.96	-0.39	0	0	0
Arl-air	*3.96**	*0*	*-614*	*109*	*0*
Arl-02	-0.92	-4.88	-789	210	74
Arl-03	2.54	-1.41	-213	194	58
Arl-05	0.68	-3.28	-311	222	87

Location on Figures 4 and 5. * Mean annual air temperature (°C). MAGST: mean annual ground surface temperature (°C); ATA: annual thermal anomaly (°C); GFI: ground freezing index (°C); NFD: number of frozen days; ZCD: zero curtain duration (day).

Seasonal phase 2: winter conditions

Winter is often characterized by a thicker (more than 1 m) and continuous snow cover as well as by colder weather conditions. The ascending air circulation regime is prevailing.

According to the elevation, the ground surface or its close subsurface should normally not freeze under the thicker snow cover, as it was recorded at the terminal edge of the Creux du Van talus slope (Cv-02) and in the surrounding area (Cv-01).

In the upper part of a talus slope, as in Dreveneuse (Dr-25), the GST remained warm for the whole winter, but dropped strongly for a short time by mild air temperatures (arrows "b" in Fig. 2). The only temperature below freezing point was registered during the mildest weather period in January 2005. The GST tended however to decrease gradually from about +7°C in the beginning of November to +2°C in March. An inverse relationship to the outside air temperature is also observed. Warm air outflow is easily perceptible as well as associated phenomena like snow funneling with hoarfrost, snowmelt windows, and vaulted spaces at the base of the snowpack.

GST was at or below freezing point during the whole winter in the middle and lower parts of the talus slopes (Dr-24, Dr-25, Cv-04), as well as on the relict rock glacier (Arl-02, Arl-03, Arl-05). The GST mapped in February illustrates the spatial geometry of the colder areas (Fig. 3). The thermal regime is mainly controlled by the evolution of the external air temperature (arrows "c" in Fig. 2) with a time lag of a few days which seems to increase by the end of the winter.

Seasonal phase 3: Snowmelt period

At the onset of the snowmelt phase in March, the GST rose suddenly to 0°C in the lower parts of the ventilated terrains and remained stable for 42 days at Dr-24 to 87 days at Arl-05 (Table 2). In the upper part of a talus slope (Dr-25), the snowmelt phase provoked a temperature drop to about 0°C. This non-constant zero curtain phase lasted for a few days only.

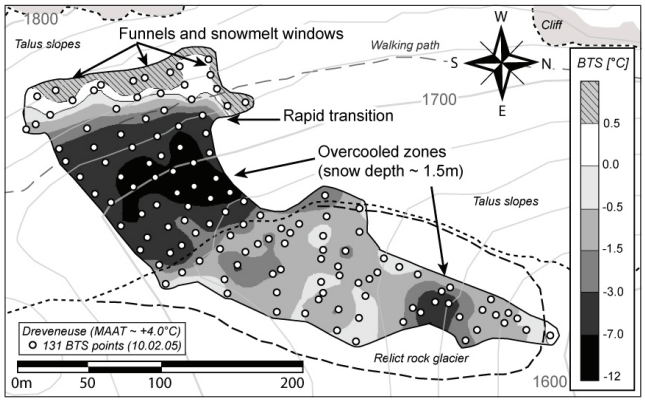

Figure 3. Ground surface winter temperature mapping (Dreveneuse-du-Milieu, 10 February 2005). Note the overcooled zone in the middle/lower part of the talus slope, the cold areas on the relict rock glacier, and the rapid transition in the uppermost zone to warmer ground temperature.

Seasonal phase 4: summer conditions

The gravity discharge of cold dense air prevents the GST to increase above +6°C in the lower parts of the debris accumulations as at Dr-22, Cv-04, Cv-02, Arl-02, and Arl-05. There is a more or less well-established inverse relationship between the airflow temperatures and those of the external air (as indicated by arrows "d" in Fig. 2). At these places, cold air outflow, azonal vegetation, ground ice, or late-lying residual snow patches can be observed.

In the upper and middle parts of talus slope (Dr-25, Dr-24), the GST varies in close correspondence with the evolution of the surrounding air temperature. In the marginal ridges of the relict rock glacier (Arl-03) and in the areas outside the porous debris accumulations (Cv-01), this GST regime can be considered as normal: the fluctuations are smooth and depend directly on the air temperature.

Synthesis and Discussion

Annual thermal regime of a ventilated system

Air circulation throughout a porous debris accumulation produces major differences in the thermal regime of areas only a few (tens of) meters from each other. Temperature anomalies occur and vary seasonally, depending both on the location on the landform and the meteorological factors (external air temperature and snow cover). Indeed, five types of annual thermal regime can be defined on the basis of the four seasonal phases described above:

- Type I: positive anomaly in autumn, winter, and summer. This behavior concerns the upper part of a ventilated system, where in particular the GST remains significantly higher than 0°C during winter due to the expelling of internal warm air. A positive annual thermal anomaly will result in such places (+4.18°C at Dr-25). A spell of mild weather in winter may cause the weakening or the end of the ascending airflow and consequently an episodic decrease of the GST.
- Type II: slight negative anomaly possible in winter, positive anomaly in summer. This kind of thermal regime affects the section located immediately above the coldest

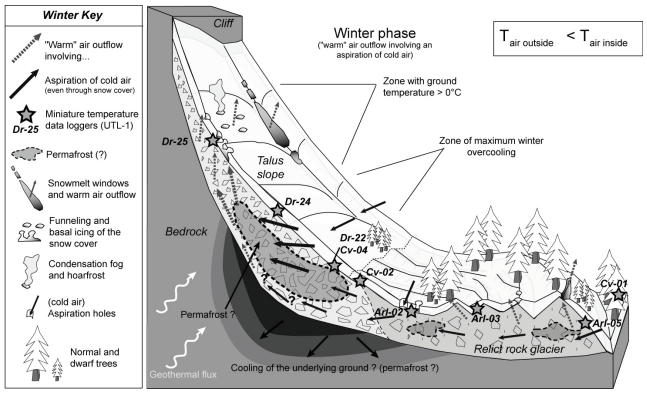

Figure 4. Model of winter ascending air circulation (in talus slope relict rock glacier system). The stars indicate the general position of the dataloggers presented in Figure 2.

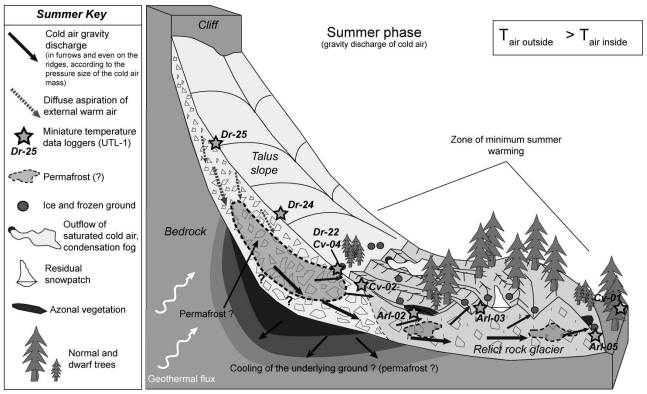

Figure 5. Model of summer descending air circulation (in talus slope/relict rock glacier system). The stars indicate the general position of the dataloggers presented in Figure 2.

area. Air aspiration occurs in late fall and winter but there is no influence of the summer gravity discharge. The annual thermal anomaly is slightly positive (Dr-24) or slightly negative (Arl-03), probably due to different ground surface properties (blocky material directly exposed to solar radiation in summer at Dr-24, thick soil and shady forest at Arl-03).

- Type III: negative anomaly in fall, winter, and summer, late lying of snow. This annual type is associated to the coldest part of the system, permanently frozen during winter due to the aspiration of external air (even through the snow cover) and remaining cool in summer because of the gravity discharge of internal cold air. Such areas are located in the lower part of the talus slope as well as locally on the connected relict rock glacier–if existing. The annual thermal anomaly reached -3.28°C to -4.91°C at Dr-22, Cv-04, Arl-02 and Arl-05 (Table 2).
- Type IV: slight negative anomaly possible in winter, negative anomaly in summer less pronounced than in type III, late-lying snow. This area is located under the coldest zone at the bottom of a talus slope and is partially affected by the summer gravity discharge. The annual thermal anomaly is slightly negative (CV-02).
- Type 0: no seasonal anomaly. During winter and in the presence of snow, the ground temperature does not drop below 0°C. This behavior concerns mainly sectors which are not affected by the air circulation and, where the heat fluxes are only conductive. The mean annual temperature is close to MAAT (CV-01).

Dissymmetry of seasonal overcooled zones

A spatial shift can be identified between the zones of maximum winter overcooling and those of minimum summer warming (Figs. 4, 5). The seasonal contrast between types II and IV shows that in a talus slope, the area affected by the winter aspiration of cold air, is shifted upwards compared to the cold summer area, the seasonal gravity discharge concentrating in the lowermost parts of the slope. Such a shift has not so far been observed on the downward relict rock glaciers. However, the occurrence of thermal regimes of type III and the lack of warm areas on these landforms indicate that internal ventilation is occurring as far as the front of a relict rock glacier and should be connected to those of the upper talus slope. Figures 4 and 5 illustrate the resulting concept of air circulation throughout a talus slope–relict rock glacier complex and the possible location of permafrost within the system.

Spatial implication on related terrestrial ecosystems

Temperature is one of the key factors (with moisture) controlling the distribution of organisms and primary production (such as pedological processes) in ecosystems. The spatial distribution of vegetation and soils on a ventilated system often indicates different GST conditions.

The seasonal asymmetrical position of cold zones plays an important role on the vegetal distribution. The thermal regime of type II is not associated with azonal vegetation. At Arl-03, for instance, the presence of *Rhododendro-Vaccinetum Juniperetosum* Ass. indicates normal ground thermal conditions during the vegetation period in summer. Conversely, a cold summer ground surface thermal regime of types III and IV is associated with alpine species like *Pritzelago alpina* and *Dryas octopetalia* (for instance at Arl-02) and limits the growth of tree roots (Körner et al. 2006) (Dr-22, Cv-04). The phenological development is strongly conditioned by the summer ground temperature.

Soils found in overcooled sectors evolve differently from the general pedoclimatic trend (Gobat et al. 2003). Furthermore, cold summer temperature directly influences the development of humus. Spatial variations in pH, organic texture, and kind of macrorests is clearly dependent on the location of ventilated systems (Rossel et al. 2004) and the GST regime.

A strong thermal stability is observed in summertime, but also from year to year (Delaloye 2004), where the cold air outflows occur. It would also provide possible favorable long-term abiotic conditions for azonal and less-competitive species. Genetic DNA-analyses carried out on different separated populations of wingless beetles found in cold scree slopes have shown on the one hand an own genetic evolutionary way (island-like character of this biotope), and on the other hand the existence of true faunal relicts from glacial periods (Gude et al. 2003).

Conclusion

The main conclusion of our study is that thermal anomalies induced by advective heat fluxes ("chimney effect") are observed in many porous debris accumulations located below the regional lower limit of discontinuous permafrost in the Swiss mountains. An interconnection in the airflow between a talus slope and a relict rock glacier located immediately downstream has also been identified.

The combination of visual and thermal measurements has proved to be a relevant method for detecting and characterizing heterogeneous ground surface thermal regimes of a ventilated debris accumulation.

A succession of negative seasonal anomalies is typical in the lower part of a ventilated area, while in the upper part the GST regime presents usually a positive anomaly during the whole year. Other differentiated types of seasonal thermal regimes occur in the upper and lower margins of the coldest places of a debris accumulation. Moreover, the occurence, development, and spatial pattern of distribution of specific "cold" terrestrial ecosystems are directly influenced by the internal circulation of air.

Acknowledgments

Special thanks are due to Walter Leimgruber for editing the English text, and to numerous students and other people for their precious help in the fieldwork.

References

Delaloye, R. 2004. *Contribution à l'étude du pergélisol de montagne en zone marginale.* PhD Thesis. University of Fribourg, Switzerland. *GeoFocus* 10, 240 pp.

Delaloye, R. & Lambiel, C. 2007. Drilling in a low elevation cold talus slope (Dreveneuse, Swiss Prealps). *Geophysical Research Abstracts* 9: 10907.

Delaloye, R., Reynard, E., Lambiel, C., Marescot, L. & Monnet, R. 2003. Thermal anomaly in a cold scree slope (Creux-du-Van, Switzerland). *Proceedings of the Eighth International Conference on Permafrost, Zurich*: 175-180.

DeSaussure, H.-B. 1796. Voyages dans les Alpes, précédés d'un essai sur l'histoire naturelle des environs de Genève. *Tome troisième, Neuchâtel, S.-Fauche*.

Dorthe, J. & Morard, S. 2007. Ventilation des éboulis froids et des glaciers rocheux fossiles des Préalpes suisses romandes. Master's Thesis. Univ. Fribourg, 166 pp.

Gobat, J-M, Aragno, M. & Matthey, W. 2003. Le sol vivant. Bases de pédologie, biologie des sols. *Presses Polytechniques et Universitaires Romandes, Collection Gérer l'Environnement* 14, 568 pp.

Goering, D.J. & Kumar, P. 1996. Winter-time convection in open-graded embankments. *Cold Regions Science and Technology* 24(1): 57-74.

Gorbunov, A.P., Marchenko, S.S. & Seversky, E.V. 2004. The thermal environment of blocky materials in the mountains of central Asia. *Permafrost and Periglacial Processes* 12: 69-77.

Gude, M. & Molenda, R. 2003. Felsen, Block- und Schutthalden, Blockmeere. *Handbuch Naturschutz und Landschaftspflege, Landsberg*, XI-2.27: 181-192.

Harris, S.A. & Pedersen, D.E. 1998. Thermal regimes beneath coarse blocky materials. *Permafrost and Periglacial Processes* 9: 107-120.

Körner, C. & Hoch, G. 2006. A test of treeline theory on montane permafrost island. *Arctic, Antarctic and Alpine Research* 38: 113-119.

Lambiel, C. 2006. *Le pergélisol dans les terrains sédimentaires à forte déclivité: distribution, régime thermique et instabilités.* Thèse, Université de Lausanne, Institut de Géographie, Coll. «Travaux et Recherches» 33, 260 pp.

Lismonde, B. 2002. Climatologie du monde souterrain : Vents des ténèbres. *Edition du Comité Départemental de Spéléologie de Isère, 1ère édition, Tome 1*, 168 pp.

Marescot, L., Loke, M.H., Chapellier, D., Delaloye, R., Lambiel, C. & Reynard, E. 2003. Assessing reliability of 2D resistivity imaging in mountain permafrost studies using the depth of investigation index method. *Near Surface Geophysics*: 57-67.

Morard, S., Delaloye, R. & Dorthe, J. (2008). Indices de fonctionnement de la ventilation des éboulis froids. *Proceedings of the Swiss Geomorphological Society (SSGm) Annual Meeting 2007, 12–14 July, Samedan.*

Niu, F. & Cheng, G. 2005. Field experiment study on effects of duct-ventilated railway embankment on protecting permafrost of the Qinghai-Tibet Plateau. *Terra Nostra, Second European Conference on Permafrost, Potsdam*: 187.

Rist, A., Phillips, M. & Auerswald, K. 2003. Undercooled scree slopes covered with stunted dwarf trees in Switzerland–abiotic factors to characterize the phenomenon. *Proceedings of the Eighth International Conference on Permafrost, Zurich, Switzerland*: 135-136.

Rossel V., Weber G. & Gobat J.-M. 2004. Humus forms on permafrost in a cold scree slope (Creux du Van). *Eurosoil, 4–12 September 2004, Freiburg, Germany*.

Ruzicka, V. 1999. The freezing scree slopes and their arachnofauna. *Decheniana–Beihefte, Bonn* 37: 141-147.

Sawada, Y., Ishikawa, M. & Ono, Y. 2003. Thermal regime of sporadic permafrost in a block slope on Mt. Nishi-Nupukaushinupuri, Hokkaido Island, Northern Japan. *Geomorphology* 52: 121-130.

Sone, T. 2005. Extra-zonal permafrost and ground air circulation at a slope along the Kanoko-dam, Oketo town, Hokkaido, Japan. *Terra Nostra, Second European Conference on Permafrost, Potsdam*: 80.

Wakonigg, H. 1996. Unterkühlte Schutthalden. *Beiträge zur Permafrostforschung in Osterreich. Arbeiten aus dem Inst. f. Geogr. Karl-Franzens-Universität, Graz* 33: 209-223.

Genetic, Morphological, and Statistical Characterization of Lakes in the Permafrost-Dominated Lena Delta

Anne Morgenstern
Alfred Wegener Institute for Polar and Marine Research, Research Unit Potsdam, Potsdam, Germany
Guido Grosse
Geophysical Institute, University of Alaska Fairbanks, Fairbanks, Alaska, USA
Lutz Schirrmeister
Alfred Wegener Institute for Polar and Marine Research, Research Unit Potsdam, Potsdam, Germany

Abstract

This study provides a detailed inventory of lakes in the Lena Delta, northern Siberia. The inventory is based on Landsat-7 ETM+ image data and spatial analysis in a Geographical Information System (GIS). Several morphometric lake attributes were determined from the resulting dataset and statistically analyzed with respect to the lakes' association with one of the three geomorphological main terraces of the Lena Delta. Significant differences in the morphometric lake characteristics allowed the distinction of a mean lake type for each main terrace. The lake types reflect the special lithological and cryolithological conditions and geomorphological processes prevailing on each terrace. Special focus was laid on the investigation of lake orientation and the discussion of possible mechanisms for the evolution of the second terrace's oriented lakes.

Keywords: GIS; lake morphometry; Lena Delta; oriented lakes; remote sensing; thermokarst lakes.

Introduction

Numerous lakes occur as characteristic landforms throughout the Lena Delta. They are of importance to the contemporary ecology and geomorphology in this sensitive Arctic environment as well as for the reconstruction of the delta's environmental history. So far, only general descriptions of the lake population were available (e.g., Grigoriev 1993). They suggest that several lake types of different genesis can be distinguished and that the western delta is characterized by oriented lakes. However, a detailed inventory of the Lena Delta lakes did not exist. Such an inventory potentially provides a base dataset essential to a variety of research conducted in this region. This study was aimed to create a lake dataset of the Lena Delta including morphometric and spatial characteristics using remote sensing and GIS techniques to analyze the dataset regarding a morphometric lake classification, and to investigate possible hypotheses of the morphogenesis of the lakes in this periglacial delta environment.

Regional Setting

The Lena Delta in northern Siberia is the largest Arctic river delta (Walker 1998). It is situated in the zone of continuous permafrost and is widely affected by thermokarst. It is characterized not only by alluvial sediments and active fluvial processes, but also by large non-deltaic units. Three main terraces can be distinguished by their geomorphology (e.g., Are & Reimnitz 2000, Schwamborn et al. 2002) (Fig. 1). The first main terrace, which represents the modern active delta, is comprised of the lower and upper floodplains and the first terrace above the floodplain. It forms most of the eastern Lena Delta and is characterized by alluvial Holocene sands with silts and peat. The second terrace captures broad parts of the western Lena Delta. It consists of Late Pleistocene to Early Holocene sands of fluvial genesis, but is hardly influenced by modern fluvial processes. The third main terrace is the relic of a Late Pleistocene accumulation plain with fine-grained and ice-rich deposits.

Materials and Methods

Remote sensing

A mosaic of three Landsat-7 ETM+ scenes taken in the summers 2000 and 2001 covering 98 % of the Lena delta (Schneider et al., in prep.) was used as a basis for lake extraction using the software ENVI™ 4.1. First, we conducted a gray-level thresholding on the mid-IR band 5 to separate open water from land, as water bodies are strong absorbers in these wavelengths and easily distinguishable from other land cover classes. Second, the water class was subjected to a segmentation algorithm to differentiate standing water from rivers and the sea. This method creates separate classes for coherent pixels with the same value. As rivers and estuaries are connected with the sea, they form one single class and were deleted. Some lakes along the coastline that have broad (in the range of several pixels) connections to the sea were thereby also removed from the dataset. They experience a strong marine influence; for example, during storm floods, which can lead to major changes in lake morphometry and lagoon formation. Thus, these lakes were not considered for morphometric and further analysis.

GIS and morphometric analysis

The resulting raster dataset of all remaining lakes was imported into ArcGIS™ 9.0 and converted into vector format

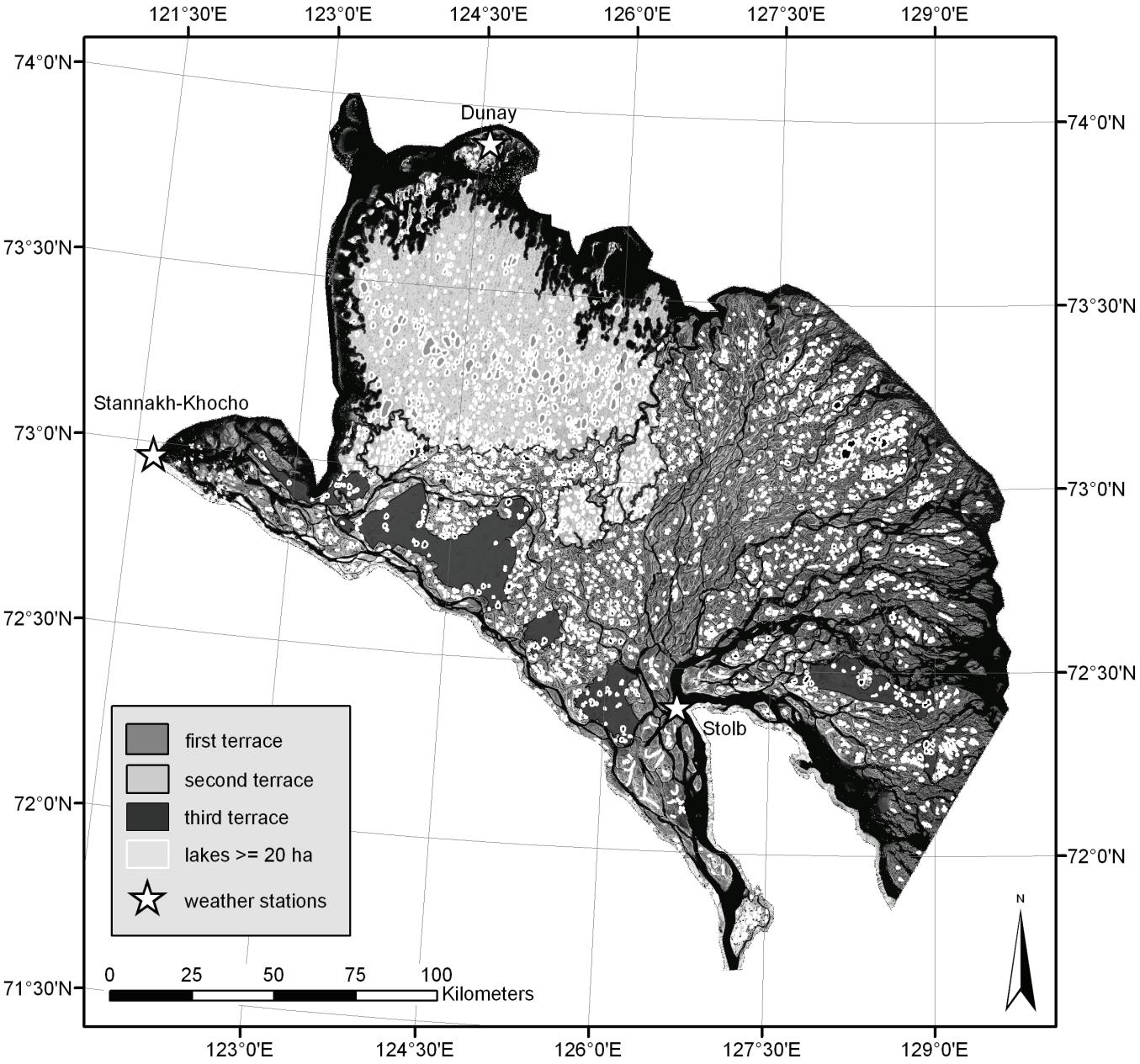

Figure 1. Landsat-7 ETM+ mosaic of the Lena Delta (Band 2) with analyzed lakes and main terraces, and meteorological stations.

where each lake is represented by a polygon. Shape metrics like *area*, *perimeter*, *circularity index* ($4\times\pi\times area/perimeter^2$), *elongation index* (main axis/minor axis), *orientation of main axis* (reference axis is E-W, value range is [0.1;180]°), and *degree of deviation from mean orientation* were calculated. The *circularity index* (values between 0 and 1, with 1 being a perfect circle) is not simply a counterpart to the *elongation index*, but also reflects the smoothness of the shoreline.

As the spatial resolution of the Landsat imagery is 30 m, minimum lake size for analyses was set to 20 ha to ensure reasonable results for reckoning the shapes of the lakes. The lake dataset was manually checked for errors due to misclassification caused by light cloud cover in some places.

On the second terrace in the western Lena Delta, several coalesced lakes occur, which is obvious in the red spectrum from deep basins divided by flat underwater ridges, some of them cut by deeper channels beneath the present lake water level. As our analyses were aimed on lake genesis, we manually divided the coalesced lakes (n=51) along the middle line of the ridges into their single basins and treated each basin as an individual lake (n=120 of which n=17 < 20 ha were excluded from further analysis). The final lake dataset contained 2669 lakes.

Another vector layer was created for the second and third geomorphological main terraces of the Lena Delta by manually digitizing their boundaries based on the Landsat image data, where they are visually easily distinguished. At places of uncertainty, results of field observations were used to determine terrace affiliation. The lake dataset was

then divided into three subgroups according to the lakes' association with one of the geomorphological main terraces. The subgroup for the first terrace lakes was created by subtraction of the second and third terrace lakes from the whole lake population.

The variables described above were statistically analyzed for these subgroups using the software SPSS™ 12.0. Several statistics were calculated for the variables within an explorative data analysis (EDA). Variables were tested for normal distribution using the *Kolmogorov-Smirnov test* and for homogeneity of variance using the *Levene test*. In case of non-normal distribution skewness was minimized by data transformation and subsequent tests were performed with the transformed data. To test significant differences in the means of the variables between the three terraces analysis of variance (ANOVA) was performed. Non-parametric *Median test* and *Kruskal-Wallis test* (rank-based) were used with the non-transformed data for validation. Furthermore, multiple comparative tests (*Games-Howell*) were applied to identify terraces between which significant differences in the mean values occur at the 5% level. Bivariate correlations were calculated for the variables *area*, *circularity*, *elongation*, and *degree of deviation from mean orientation* using the rank-based *Spearman's Rho* correlation coefficient.

Results

The total area of lakes ≥ 20 ha is 1861.8 km², which corresponds to 6.4 % of the delta area, as the delta area within the extent of the mosaic was calculated to be 29,000 km² (Schneider et al., in prep.). Table 1 shows the area calculations for the three geomorphological main terraces. The results show great differences in lake occurrence, density, and area. The first terrace shows the highest number of lakes in total, but lake density and the ratio of lake area to the area of the corresponding terrace are highest on the second terrace. For the third terrace, all calculated values are the lowest.

Major results of the EDA are the following (see also table 2). Means, medians and percentiles for *area* show that comparatively larger lakes occur on the second terrace and rather smaller lakes on the first. The frequency distributions are strongly skewed towards lower values on all terraces, so smaller lakes are in general much more abundant than larger ones. Maximum values for the *circularity index* are well below 1 (< 0.7), i. e. throughout the delta no nearly circular lakes occur. Lakes with values of nearly 1 for the *elongation index* (which means almost equal major and minor axes) therefore have complex shorelines at the image resolution. Values for *circularity index* and *elongation index* show generally the largest deviation from perfect circularity for the first terrace and the smallest for the third terrace. Mean *orientation* of all lakes is 90.0°, the median is 80.2°. Means (medians) are 94.9° (95.9°) on the first main terrace, 78.6° (75.9°) on the second terrace, and 90.7° (82.0°) on the third terrace, respectively. Figure 2 shows the frequency distributions of *orientation*. The percentage of lakes with a deviation from the *orientation* mean (median) of ≤ 10° of the according terrace are 9.6 % (9.5 %) for the first terrace, 63.0 % (66.2 %) for the second, and 24.7 % (35.8 %) for the third terrace, respectively. Also the means and medians of *degree of deviation from mean orientation* show that lakes on the second terrace deviate the least and lakes on the first terrace the most from the according mean orientation.

The results of the ANOVA as well as of the non-parametric tests show significant differences in the parameter values between the three main terraces for all variables. Multiple comparative tests revealed the following results at the 5% level. The lakes of the first terrace significantly differ from the second terrace lakes in all variables. No significant differences were found between the first and the third terraces regarding *orientation*, and between the second and the third regarding *orientation* and *area*. On the first terrace, lakes are smaller on average than on the second and third terraces. Nearly circular lakes are more abundant on the third than on the other terraces.

In the context of our analyses we defined oriented lakes as lakes with little deviation from mean orientation and with a deviation from circularity. Deviation from mean orientation is significantly smaller on the second terrace than on the other two terraces, it is highest on the first terrace. Thus, lakes on the second terrace can be statistically characterized as oriented lakes with their main axes tending in NNE-SSW directions.

Of the 18 tests for correlations ten were significant at the 5% level. These include medium negative correlations (r = -.444 to -.465) between *circularity* and *elongation* on all terraces as expected from the design of the variables. All other significant correlations are very small ($|r| \leq .186$) except for the correlation between *area* and *degree of deviation from mean orientation* on the third terrace (r = -.415, p = .01).

Discussion

For all analyzed morphometric lake variables we found significant differences between the three geomorphological main terraces of the Lena Delta. From these differences we deduce one mean lake type for each terrace:

1. Lakes on the first terrace are on average small and elongated, with irregular shapes and strong deviations from mean orientation.

2. On the second main terrace, large elongated lakes with a NNE-SSW orientation of their major axes prevail. Lake density is highest here.

3. The third terrace lakes are mainly characterized by regular shorelines and little deviation from circularity.

These results imply that the forming of a lake's shape towards one of these mean lake types is linked to the according delta main terrace, i. e. lake morphometry is influenced differently on the different main terraces. Different lake morphometries can be caused primarily by diverse lake genesis or by secondary processes subsequently altering the lake's primary shape. The different conditions and processes prevailing on each terrace of the Lena Delta are used to explain the development of the mean lake types found.

The first main terrace is the only one with widespread recent and Holocene fluvial and deltaic activity. The genetic lake type

Table 1. Area calculations for the three geomorphological main terraces of the Lena Delta.

		First terrace	Second terrace	Third terrace
Terraces	Area in km²	15,840.1	6098.6	1711.6
	Percentage of delta area	54.6	21.0	5.9
Lakes ≥ 20 ha	Number	1796	792	81
	Number per 1000 km²	113.4	129.9	47.3
	Percentage of total lake number	67.3	29.7	3.0
	Total area in km²	997.0	808.1	56.7
	Percentage of terrace area	6.3	13.3	3.3
	Percentage of delta area	3.4	2.8	0.2

* Differences from 29,000 km² and 100% total delta area arise from the percentage of sea and river area, respectively, in the mosaic.

Table 2. Descriptive statistics for the analyzed morphometric lake variables.

		Delta	First terrace	Second terrace	Third terrace
Area (in m²)	Mean	697,579	555,124	1,020,382	699,922
	Median	409,500	372,600	557,100	442,800
	Standard deviation	956,500	634,463	1,410,506	566,554
	Interquartile range	452,700	339,075	757,800	598,500
Circularity	Mean	0.31	0.28	0.36	0.46
	Median	0.31	0.27	0.36	0.48
	Standard deviation	0.14	0.14	0.12	0.11
	Interquartile range	0.22	0.22	0.15	0.18
Elongation	Mean	2.11	2.26	1.83	1.49
	Median	1.75	1.85	1.66	1.37
	Standard deviation	1.20	1.37	0.64	0.45
	Interquartile range	0.92	1.12	0.55	0.36
Orientation (in °)	Mean	90.0	94.9	78.6	90.8
	Median	80.2	95.9	75.9	82.0
	Standard deviation	47.1	54.3	21.4	38.2
	Interquartile range	65.94	94.8	12.3	44.4
Degree of deviation from mean orientation (in °)	Mean	38.6	47.5	12.9	29.1
	Median	31.5	48.3	6.8	21.4
	Standard deviation	27.0	26.3	17.0	24.5
	Interquartile range	48.1	45.3	11.7	33.5

typical for such environments is abandoned lakes. Walker (1983) differentiates between abandoned-channel lakes resulting from channel braiding and abandoned meanders or oxbow lakes resulting from meandering. They are predominantly small, often elongated and/or crescent-shaped because they occupy former river branches or meanders, and do not show any particular orientation as the fluvial system shows no clear directional pattern itself at a small scale. Thus, the morphometric characteristics for these lakes are consistent with the mean lake type deduced for the first terrace of the Lena Delta. Further lake types described for the first terrace are polygon ponds and small circular thermokarst lakes (e.g., Grigoriev 1993). Polygon ponds were generally not considered in this study because of their small size. As for the circular thermokarst lakes no area range is reported in the literature, but we assume that they mostly have areas below 20 ha and were therefore not treated in our analyses. Their characteristics, such as smooth shorelines and approximate circularity, are not reflected in the mean lake type of the first terrace.

The morphometry of the lakes on the second terrace and their formation will be discussed in the following section on lake orientation.

Characteristics of the lake shapes on the third main terrace are typical for thermokarst lakes in ice-rich permafrost. The results are therefore consistent with landscape descriptions given in the literature (e.g., Grigoriev 1993). The shape of the lakes is controlled by their thermokarst genesis and is not significantly changed by other factors during further evolution.

In comparing morphometric lake characteristics in the Lena Delta with other arctic deltas like the Colville or the Mackenzie River deltas, only the first geomorphological main terrace should be considered, as it represents an actual deltaic environment. Lake types described for the Colville Delta are abandoned lakes, point-bar lakes, and thermokarst lakes (e.g., Fürbringer 1977, Walker 1983). In the Colville Delta, remnants of oriented lakes also occur, but these were not a part of the delta originally until a river branch cut through an area with oriented lakes (Walker 1983). For the Mackenzie Delta, typical lakes are described as irregular in outline with indented shorelines, and genetic lake types are primarily abandoned channel lakes, point-bar lakes,

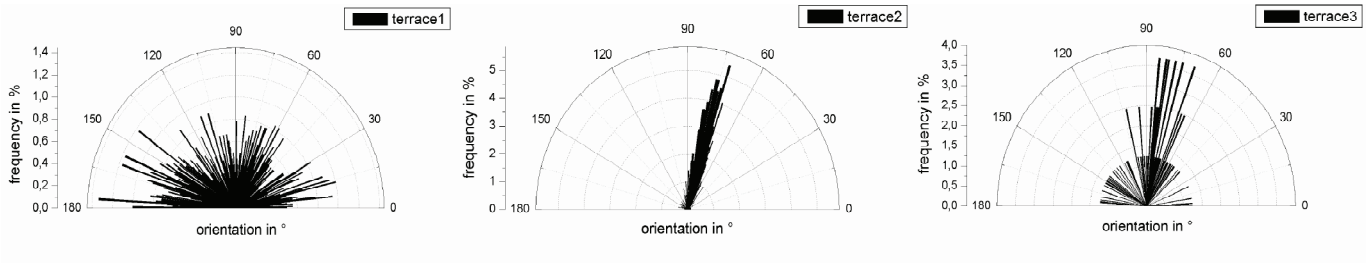

Figure 2. Frequency distribution of *orientation* of the Lena Delta lakes (intervals = 1°).

floodplain lakes, and thermokarst lakes (Mackay 1963). Lake types described for these deltas are thus comparable to the first terrace lakes of the Lena Delta.

Lake orientation

The character of lake orientation as expressed by the variables *degree of deviation from mean orientation* and *circularity* differs significantly between the three main terraces as described above. The process of lake orientation is long term and requires stability of exogenous orienting factors. Active fluvial processes prevailing on the first terrace may overlay tendencies of lake orientation there. Existing discrepancies between the second and the third terraces, however, must be discussed in detail.

Thermokarst lake evolution on both terraces reaches back at least to the early Holocene warming period (Schirrmeister et al. 2003, Schwamborn et al. 2002). Exogenous factors that have been discussed as causing or influencing lake orientation; for example, prevailing wind directions, solar radiation, etc. (e.g., Livingstone 1954, Mackay 1956, Carson & Hussey 1959), therefore, have affected both terraces in the same way for several thousand years. The different character of lake orientation implies a dependence of further endogenous; i.e., terrace-specific factors.

Lithology and cryolithology of the second and third main terraces differ considerably. Sediments on the second main terrace are Late Pleistocene fluvial sediments that consist of homogeneous fine- and medium-grained sands with massive cryogene structures. Large ice wedges are absent, and the ground ice content is generally rather low (15–25 wt%) (Schirrmeister et al. 2007). The sediments are comparable to those in the North American Arctic Coastal Plain where oriented lakes occur. The homogeneity of the sands allows for a uniform distribution of forces driving orientation processes. If these forces operate directionally, orientation can clearly develop. Sediments on the third main terrace, however, are mainly composed of the Yedoma Suite, with peat, sands, and silts with high ground-ice content (30–80 wt%) and inhomogeneous ice distribution (huge ice wedges and intrapolygonal sediments with segregated ground ice in the form of ice bands and small ice lenses) (Schirrmeister et al. 2003). This heterogeneity prevents a continuous distribution of external effects because of the different physical characteristics of the sediments; for example, bulk density or thermal conductivity. Orienting factors, therefore, cannot operate uniformly, and the development of a clear orientation is strongly impeded. The negative correlation between the lake *area* and the *degree of deviation from mean orientation* of

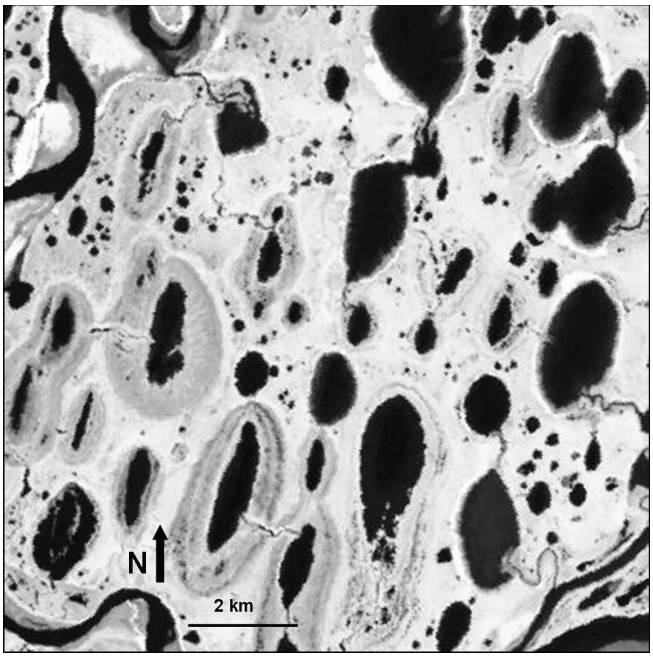

Figure 3. Section of oriented lakes in the western Lena Delta (subset of the Landsat-7 ETM+ mosaic).

the third terrace lakes may still implicate a tendency towards lake orientation in the course of lake growth. The mean NNE-SSW orientation of the poorly elongated third terrace lakes is consistent with that of the second terrace.

As for the cause of lake orientation in the Arctic Coastal Plain, several hypotheses have been discussed. The theory supported by most authors supposes preferential erosion of the lake shores at right angles to prevailing summer wind directions due to wind-driven currents and wave activity (e.g., Livingstone 1954, Mackay 1956, Côté & Burn 2002, Hinkel et al. 2005). The literature reports northern to northeastern main wind directions for the entire Lena Delta in the summer, and southern to southwestern in the winter (e.g., Grigoriev 1993, Gukov 2001). However, wind data of several meteorological stations scattered throughout the delta area show great differences in prevailing directions. Unfortunately, there is no station in the western Lena Delta close to the oriented lakes. Of the three stations closest to the western Lena Delta lakes (Fig. 1), two are situated directly at the Laptev Sea coast. On Dunay Island (73.9°E 124.6°N, data from 1955–1994), wind blows mainly from eastern directions; the Stannakh-Khocho station (73.0°E 121.7°N, data from 1981–1994) registered prevailing winds

from southern directions with a minor peak from eastern directions for the whole time span, and from eastern directions at times of positive air temperatures, respectively. The third station is located in the central southern delta on Stolb Island (72.4°E 126.5°N, data from 1955–1991) and shows pronounced southern wind directions. All three stations may not reflect the actual wind situation of the second main terrace, as climate on Stannakh-Khocho and Stolb Island is supposedly influenced by the mountain ranges flanking the Lena Delta in the south. On the Island Dunay, which is a few kilometers off from the mainland of the second terrace, the marine influence has an impact on weather conditions. It can be suggested though, that, because of the flat relief of the second terrace, major wind directions in the inner part of the terrace do not differ much from the situation at its margins; thus wind data from Dunay Island might be the most suitable for assessing the situation on the second terrace. Assuming that the eastern prevailing wind direction measured over the forty-year time span was consistent throughout the lake orientation process, the wind hypotheses proposed for North American oriented lakes might also be applicable for the oriented lakes of the Lena Delta. However, little is known about the detailed conditions and factors that might be involved in lake-orientation processes in the Lena Delta or the stability of wind regimes over Holocene time scales. Further research is necessary to prove or reject any particular orientation theory for this unique Arctic environment.

Conclusions

The three main terraces of the Lena Delta vary largely in the occurrence of morphometric lake characteristics. This led to the deduction of one mean lake type for each terrace. The first main terrace, which represents the modern active delta, is characterized by small lakes of irregular shape, like abandoned lakes. Large oriented lakes with their major axes tending in NNE directions dominate on the second terrace, which consists of Late Pleistocene to Early Holocene homogeneous sands. On the third terrace, which is represented by relics of a Late Pleistocene accumulation plain with heterogeneous fine-grained and ice-rich deposits, typical thermokarst lakes with regular, circular shorelines prevail. Mean morphometric lake characteristics are consistent with the lithological and cryolithological conditions and geomorphological processes prevailing on each terrace. Wind hypotheses proposed for North American oriented lakes might also explain the orientation of lakes on the second terrace of the Lena Delta, but the detailed conditions and mechanisms of the evolution of the oriented lakes in the Lena Delta remain to be investigated.

Acknowledgments

We thank Thomas Kumke for helpful assistance with statistical analyses, Mikhail N. Grigoriev, Georg Schwamborn, and Hartmut Asche for fruitful discussions and Pier Paul Overduin for grammar and spell check. We are grateful to Alexander Brenning and another anonymous reviewer for constructive comments on the manuscript.

References

Are, F. & Reimnitz, E. 2000. An overview of the Lena river delta setting: geology, tectonics, geomorphology, and hydrology. *Journal of Coastal Research* 16(4): 1083-1093.

Carson, C.E. & Hussey, K.M. 1959. The multiple-working hypothesis as applied to Alaska's oriented lakes. *Iowa Academy of Sciences Proceedings* 66: 334-349.

Côté, M.M. & Burn, C.R. 2002. The oriented lakes of Tuktoyaktuk Peninsula, western arctic coast, Canada: a GIS-based analysis. *Permafrost and Periglacial Processes* 13: 61-70.

Fürbringer, W. 1977. About the sedimentology of an arctic delta (Colville delta, North Alaska). *International Journal of Earth Sciences* 66(1): 577-614.

Grigoriev, M.N. 1993. *Cryomorphogenesis in the Lena Delta*. Yakutsk: Permafrost Institute Press, 176 pp.

Gukov, A.Yu. 2001. *Hydrobiology of the Lena Delta mouth area*. Moscow: Scientific World, 288 pp.

Hinkel, K.M., Frohn, R.C., Nelson, F.E., Eisner, W.R. & Beck, R.A. 2005. Morphometric and spatial analysis of thaw lakes and drained thaw lake basins in the western arctic coastal plain, Alaska. *Permafrost and Periglacial Processes* 16: 327-341.

Livingstone, D.A. 1954. On the orientation of lake basins. *American Journal of Science* 252: 547-554.

Mackay, J.R. 1956. Notes on oriented lakes of the Liverpool Bay area, Northwest Territories. *Revue Canadienne de Geographie* 10: 169-173.

Mackay, J.R. 1963. *The Mackenzie Delta area, N.W.T.* Ottawa: Geographical Branch Memoir 8, Mines and Technical Surveys, 202 pp.

Schirrmeister, L., Kunitsky, V.V., Grosse, G., Schwamborn, G., Andreev, A.A., Meyer, H., Kuznetsova, T., Bobrov, A. & Oezen, D. 2003. Late Quaternary history of the accumulation plain north of the Chekanovsky Ridge (Lena Delta, Russia): A multidisciplinary approach. *Polar Geography* 27: 277-319.

Schirrmeister, L. (ed.) 2007. Studies of periglacial landscape dynamics and surface characteristics studies in the western Lena Delta. *Reports on Polar and Marine Research* 550: 83-195.

Schneider, J., Grosse, G. & Wagner, D. Land cover classification of tundra environments in the Arctic Lena Delta based on Landsat-7 ETM+ data and its application for upscaling methane emissions. Submitted to *Remote Sensing of Environment*.

Schwamborn, G., Rachold, V. & Grigoriev, M.N. 2002. Late quaternary sedimentation history of the Lena delta. *Quaternary International* 89: 119-134.

Walker, H.J. 1983. *Guidebook to permafrost and related features of the Colville River delta, Alaska*. Guidebook 2, Fourth International Conference on Permafrost. Fairbanks, Alaska: Alaska Division of Geological and Geophysical Surveys, 34 pp.

Walker, H.J. 1998. Arctic deltas. *Journal of Coastal Research* 14: 718-738.

Vegetation and Permafrost Changes in the Northern Taiga of West Siberia

Nataliya Moskalenko
Earth Cryosphere Institute SB RAS, Moscow, Russia

Abstract

The goal of this ongoing study is to examine the impact and indicators of climate change and disturbance from natural gas pipeline construction on vegetation and permafrost conditions in various northern bioclimatic zones. The results of 37 years of observations (1970–2006) from one site near Nadym, an area of sporadic permafrost, are reported. Field methods include landscape and vegetation mapping, and permanent fixed transects across natural complexes and at plots established both in natural and disturbed conditions. Transect and plot measurements were focused on labile components of vegetation and permafrost such as species composition, active layer thickness, and ground temperature. Impacts and interactions were assessed through regression and autocorrelation of frequency of plant species and active layer thickness. Undisturbed plots show an increase of woody plants, presumably due to climate warming, and disturbed sites showed thermokarst and changed soil moisture regime and, during recovery, an increase in the frequency of succession species.

Keywords: climate change; human-induced disturbances; landscape; permafrost; vegetation.

Introduction

Vegetation and permafrost changes in natural northern environments have been studied by Koloskov (1925), Gorodkov (1932), Sumgin (1937), Tyrtikov (1969, 1979, 1980). They demonstrated that freezing and thawing conditions change in response to vegetation dynamics. Increases in moss and lichen cover thickness result in the reduction of seasonal thaw depths and decreases in soil and ground temperatures.

The work reported here is part of a large, long-term, ongoing program on vegetation and environment interactions at seven sites in the Yamal-Gydan region of northern West Siberia. The sites span the gamut of bioclimatic zones, permafrost conditions, and intensity of human disturbances. The program also includes a Circumpolar Active Layer Monitoring (CALM) program site established in 1997 (see Brown et al. 2003). The results from the Nadym site are reported.

Description of the Observation Site

The site is located near the town of Nadym and the natural gas pipeline Nadym-Punga (Burgess et al. 1993). It is in the northern taiga with sporadic permafrost (Melnikov 1983) on the III fluvial-lacustrine plain with altitude ranging from 25–30 m above sea level. The plain is composed of sandy deposits interbedded with clays, with an occasional covering of peat (Melnikov et al. 2004). Patches of permafrost are closely associated with peatlands, tundras, mires, and frost mounds.

At Nadym, records have been made since 1972. Annual geobotanical censuses are made on 28 permanent fixed plots (10 x 10 m) in natural and disturbed conditions. The structure, average height, phenological and vital condition, frequency, and coverage of plant species on 50 registered 0.1 m^2 plots were recorded. In addition, soil descriptions, microclimatic supervisions, and measurements of ground temperature in boreholes at depths up to 10 m (Dubrovin et al. 1996), and seasonal thaw depths were kept.

Table 1. Thawing depths (h_{th}) on two peatland types.

Vegetation	h_{th} in cm	*K
Rubus chamaemorus-Ledum palustre-Cladina rangiferina	67.1±17.1	-0.71 (0.5-0.8)
Carex rotundata-Sphagnum lindbergii	173.7±28.2	0.58 (0.5-0.7)

*K - Coefficient of correlation (confidence level).

Analysis of Results

The measurements of the active layer thickness plots show that the smallest values of seasonal thaw depth are observed under *Rubus chamaemorus-Ledum palustre-Sphagnum-Cladina rangiferina* cover on flat peatland (Table 1). This type of peatland serves as an indicator of depths of seasonal thaw. Areas with deepest thaw are confined to large sedge-moss pools within peatlands and to bogs.

There has been marked an increase in air temperature at Nadym. Figure 1A shows the trend from 1970–2006 that amounts to 0.04°C per year. The air and soil temperature increase on the peatland is the likely cause for the appearance of tree species (*Betula tortuosa*, *Pinus sibirica*) and the rise in frequency of shrubs (*Ledum palustre, Betula nana*). For the investigated period the ground temperature on undisturbed palsa peatland has increased from -1.8 up to -0.5°C (Fig. 1B(1)). On a flat peatland the rise in ground temperature was less (Fig. 1B(2)). The active layer thickness on palsa peatland has increased by 35% for the 37-year period (Fig. 1C).

In the first years following vegetation removal in 1972 cotton grass/cloudberry groupings covering only 20% of

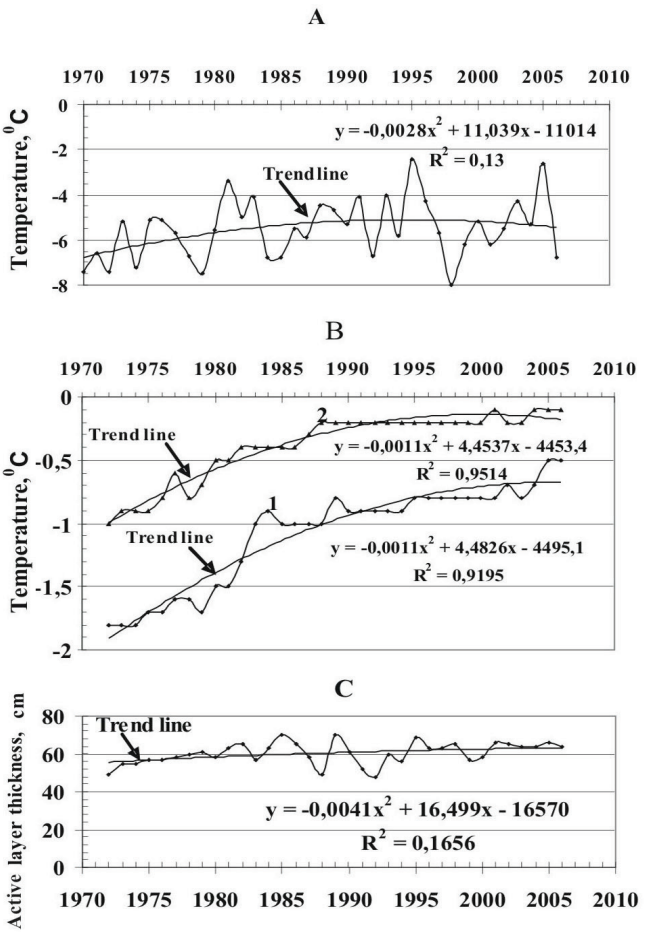

Figure 1. Mean-annual temperature (A), ground temperature at the depth 10 m (B) on palsa peatland (1) and flat peatland (2) and active layer thickness (C) on palsa peatland.

the surface had formed on the disturbed peatland plots. In four years these were replaced by cotton grass/cloudberry/*Polytrichum* groupings. The coverage of the surface by sedge and mosses in 7 years had increased up to 40%, and in 10 years up to 60%. At this time the amount of cloudberry (*Rubus chamaemorus*) had decreased, the role of cotton grass (*Eriophorum scheuchzeri, E. vaginatum*) had increased, and occasional shrubs and lichens appeared on rare moss hummocks, although the latter made no appreciable contribution to the vegetation cover. Also significant moss cover developed with *Polytrichum* species and peat mosses. In 15 years the disturbed plots had a continuous cloudberry/cotton grass/*Polytrichum*/*Sphagnum* cover. In 30 years the surface and the permafrost table had lowered with the development of thermokarst and bogs, and it was covered with cotton grass/peat moss.

The resulting fragment of cotton grass/peat moss bog continues 33 years after disturbance, although this bog community radically differs from the initial tundra (Table 2) community in appearance, structure, frequency, coverage of dominant species, and ecological condition. The undisturbed tundra has also changed; for example, the frequency of *Ledum palustre* on a natural plot has clearly increased. This is most likely in response to a rise in air temperature (Fig. 2).

Table 2. Species composition of *Rubus chamaemorus-Ledum palustre-Sphagnum-Cladina* community.

Species	Height, cm	Coverage, %	Frequency, %
1. Andpol	20	1.5	46
2. Betnan	50	1	22
3. Carrot	30	<1	<1
4. Chacal	30	1	6
6. Erisch	25	<1	2
6. Erivag	45	1.5	38
7. Ledpal	45	16	86
8. Oxymic	2	1	14
9. Pinsib	90	<1	6
10. Rubcha	10	6	92
11.Vaculi	35	<1	<1
12. Vacvit	10	4	76
13. Cetcuc	7	2	48
14. Cetisl	5	1	12
15. Claran	11	22	64
16. Claste	11	28	76
17. Claama	6	<1	8
18. Clacoc	5	<1	6
19. Diccon	2	<1	2
20. Plesch	2	<1	4
21. Polcom	3	1	14
22. Sphang	4	5	12
23. Sphfus	4	25	36
24. Sphlin	4	<1	<1
25. Tomnit	2	<1	<1

Key to first column: Andpol – Andromeda polifolia, Betnan – Betula nana, Carrot – Carex rotundata, Chacal – Chamaedaphne calyculata, Erisch – Eriophorum scheuchzeri, Ledpal – Ledum palustre, Oxymic – Oxyccocus microcarpus, Pinsib – Pinus sibirica, Rubcha – Rubus chamaemorus, Vaculi – Vaccinium uliginosum, Vacvit – Vaccinium vitis-idaea, Cetcuc – Cetraria cucullata, Cetisl – Cetraria islandica, Claama – Cladonia amaurocraea, Clacoc – Cladonia coccifera., Claran – Cladina rangiferina, Claste – Cladina stellaris, Diccon – Dicranum congestum, Plesch – Pleurozium schreberi, Polcom – Polytrichum commune, Sphang – Sphagnum angustifolium, Sphfus – Sphagnum fuscum, Sphlin – Spagnum lindbergii, Tomnit – Tomenthypnum nitens.

The ITEX (International Tundra Experiment) program has reported similar increases of shrub forms from plot warming experiments (see Hollister et al. 2005, Walker et al. 2006).

On the disturbed plots the frequency response of *Ledum palustre* is different. First it increased in dry years, and then after 1990 it decreased in connection with the increase in precipitation and the development of bogging; but during all periods of observation its frequency is less than on undisturbed plots. The *Rubus chamaemorus* frequency on undisturbed plots shows no clear trend (Fig. 3A) compared to the increase of *Ledum palustre*. However on the disturbed plots *Rubus chamaemorus* frequency decreases and mirrors the changes seen for of *Ledum palustre.* The frequency of *Rubus chamaemorus* has decreased considerably in recent years in connection with increased precipitation and development of bogging. However in the first years after disturbance, in contrast to *Ledum palustre,* the frequency of

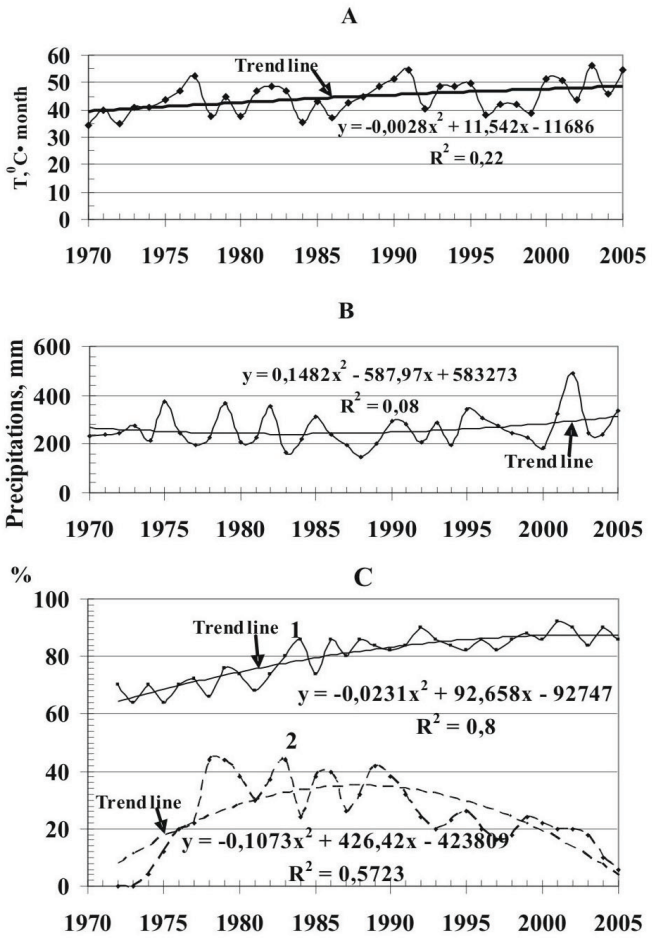

Figure 2. Thawing index of air temperature (the sum monthly mean air temperatures above 0°C) (A), summer precipitation (B) and frequency of *Ledum palustre* (C) in natural (1) and disturbed (2) conditions.

Rubus chamaemorus increases while under little competition from other species, and has almost returned to its initial condition. The frequency of *Eriophorum vaginatum* in natural sites increased and this is correlated with increased precipitation. In disturbed sites the *Eriophorum* was twice that of undisturbed sites and is the result of development of wetter soil conditions and bogginess (Fig. 3B).

The frequency of *Cladina stellaris* in natural conditions has a weak negative downward trend (Fig. 4A) while on disturbed sites the negative trend is more pronounced and similar to the trend for *Ledum palustre*, namely an increase till 1990, and then, in connection with activation of increased precipitation and bogging, it began to decrease to 40 times less than in the natural condition.

The frequency of *Sphagnum fuscum,* both in natural and in the disturbed condition shows a small positive trend with the maximum on both plots falling in the same years which were warm and had adequate summer precipitation (Fig. 4B).

Thus, the fragment of cotton grass/peat moss bog, formed in 33 years after removal of *Rubus chamaemorus-Ledum palustre-Sphagnum-Cladina* plant community, differs from initial tundra community in appearance, structure, frequency, and coverage of dominant species.

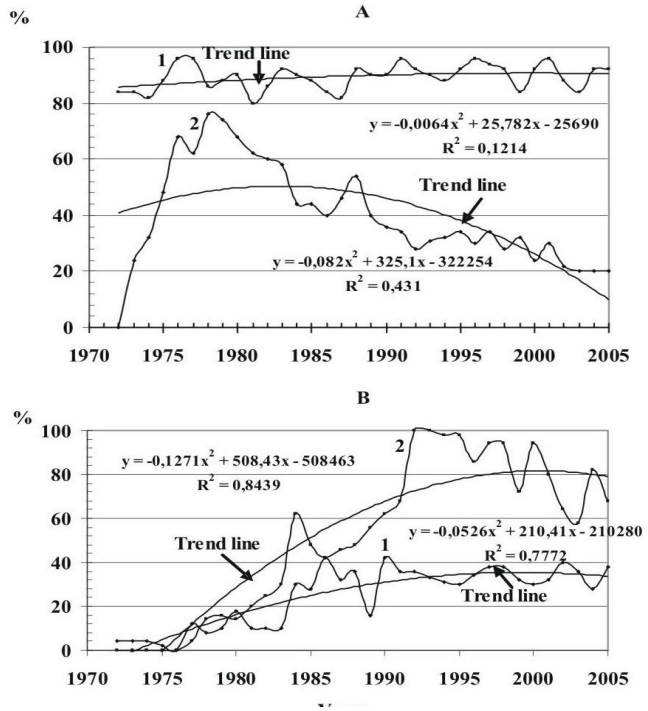

Figure 3. Frequency of *Rubus chamaemorus* (A) and *Eriophorum vaginatum* (B) in natural (1) and disturbed (2) conditions.

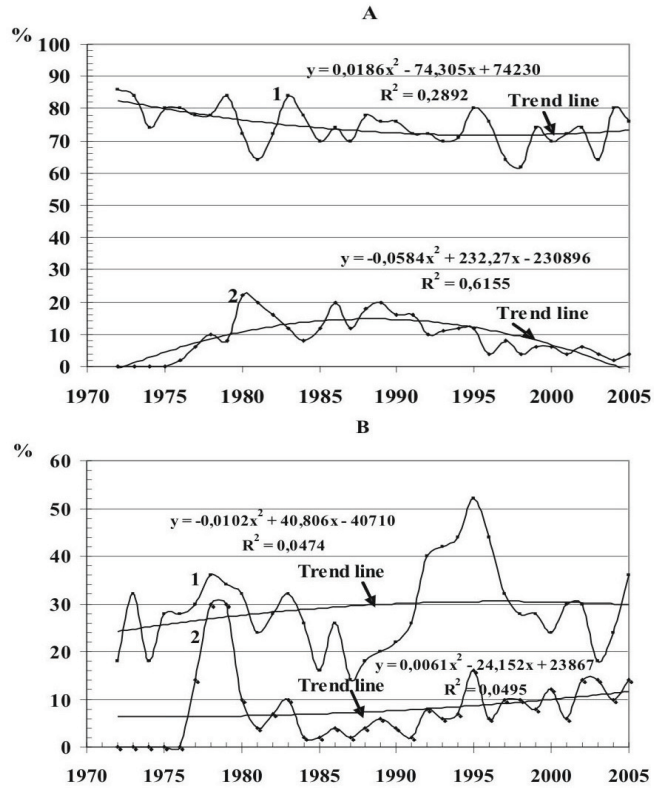

Figure 4. Frequency of *Cladina stellaris* (A) and *Sphagnum fuscum* (B) in natural (1) and disturbed (2) conditions.

These long-term records of species frequency on disturbed and undisturbed permanent plots were processed using a method of autocorrelation (Vasilevich 1970). As a result, all species were divided in three groups based on various

Table 3. Coefficients of autocorrelation between interannual values of frequency of plant species for flat peatland in natural (above a line) and disturbed (under the line) conditions, according to descriptions for 1972–2002 using "Statgraph."

Species	Years														
	1	2	3	4	5	6	7	8	9	10	11	12	13	14	15
Andpol	0.53	0.2	0.0	0.21	0.32	0.34	0.07	-0.2	-0.2	-0.1	0.0	0.0	-0.2	0.35	-0.1
	0.81	0.6	0.36	0.21	0.15	0.61	0.03	0.0	-0.1	-0.1	-0.1	-0.1	-0.1	-0.1	-0.1
Betnan	0.23	0.14	0.22	-0.2	-0.1	-0.1	0.06	0.0	0.0	-0.1	0.01	-0.3	0.13	0.0	0.05
	0.37	0.35	0.03	0.0	-0.1	-0.1	0.02	-0.1	0.0	0.0	0.05	0.05	0.0	0.0	-0.5
Erisch	0.64	0.58	0.51	0.43	0.31	0.18	0.08	0.0	-0.1	-0.2	-0.4	0.16	0.19	0.36	0.33
	0.63	0.34	0.14	-0.1	-0.1	-0.1	-0.1	-0.1	-0.1	-0.1	-0.2	-0.3	-0.2	-0.2	-0.2
Erivag	0.73	0.67	0.49	0.45	0.29	0.27	0.21	0.0	-0.1	-0.2	-0.3	-0.4	-0.4	-0.5	-0.5
	0.86	0.72	0.57	0.41	0.31	0.22	0.14	0.1	0.0	-0.1	-0.2	-0.2	-0.2	-0.2	-0.2
Ledpal	0.64	0.58	0.51	0.43	0.31	0.18	0.08	0.0	-0.1	-0.2	-0.2	-0.2	-0.2	-0.3	-0.3
	0.67	0.4	0.27	0.06	-0.1	-0.2	-0.1	-0.1	-0.1	-0.1	-0.1	0.46	0.06	-0.4	-0.4
Oxymic	0.03	0.0	-0.3	0.06	-0.1	-0.1	-0.3	0.0	0.3	0.2	0.0	-0.1	-0.1	-0.3	0.11
	0.52	0.32	0.25	0.04	0.0	0.0	-0.2	-0.2	-0.1	-0.1	-0.2	-0.2	-0.3	-0.3	-0.3
Rubcha	0.34	-0.1	-0.1	-0.3	-0.2	0.04	0.11	0.2	0.0	-0.3	-0.2	0.09	-0.5	-0.4	0.38
	0.7	0.48	0.21	0.0	-0.1	-0.2	-0.2	-0.2	-0.2	-0.2	-0.2	-0.3	-0.3	-0.26	-0.3
Vacvit	0.34	-0.1	0.11	0.02	0.0	0.08	0.16	-0.1	-0.3	-0.1	-0.1	0.03	0.2	0.0	0.08
	0.73	0.44	0.2	0.16	0.0	-0.1	-0.2	-0.2	-0.2	-0.2	-0.2	-0.2	-0.2	-0.3	-0.3
Cetcuc	0.35	0.13	0.35	0.36	0.03	0.18	0.19	-0.1	-0.2	-0.2	-0.1	0.25	0.13	-0.1	0.0
	0.54	0.35	0.33	-0.1	-0.1	-0.1	-0.2	0.0	0.1	-0.1	-0.1	-0.3	-0.5	-0.3	-0.3
Cetisl	0.27	0.32	0.2	0.0	-0.2	-0.2	-0.1	-0.3	-0.2	-0.1	-0.1	-0.4	0.0	-0.1	0.0
	0.18	0.04	0.24	0.05	0.0	-0.1	-0.2	0.2	0.0	-0.2	-0.1	-0.1	-0.2	-0.2	-0.2
Claama	0.25	-0.1	0.41	0.28	-0.1	0.09	0.14	-0.2	-0.3	0.0	-0.1	0.65	0.28	0.0	0.0
	0.0	0.04	0.0	-0.1	0.17	-0.1	0.01	-0.2	-0.1	-0.2	-0.2	0.26	-0.4	0.06	-0.1
Clacoc	0.0	0.04	0.0	-0.1	0.17	-0.1	0.01	-0.2	-0.1	-0.2	-0.2	0.26	-0.1	0.06	-0.1
	0.77	0.6	0.5	0.33	0.14	0.0	-0.3	-0.3	-0.4	-0.5	-0.5	-0.5	-0.4	-0.4	-0.4
Claran	0.14	-0.2	-0.3	0.0	0.28	0.19	0.08	-0.3	-0.2	0.1	0.1	-0.2	0.15	-0.4	-0.3
	0.67	0.41	0.3	0.18	0.08	0.02	-0.1	-0.1	0.0	-0.2	-0.3	-0.3	-0.3	-0.3	-0.3
Claste	0.26	-0.3	-0.1	0.23	0.16	0.17	0.13	-0.3	-0.3	0.1	0.23	0.13	-0.2	-0.23	0.15
	0.68	0.51	0.31	0.08	0.0	-0.1	-0.1	-0.1	-0.1	-0.1	-0.1	-0.2	-0.3	-0.3	-0.3
Polcom	0.45	0.42	0.3	0.14	0.09	0.04	0.0	-0.1	0.1	0.0	0.05	0.47	0.0	-0.2	-0.1
	0.63	0.46	0.27	0.17	0.13	0.1	0.01	-0.1	-0.1	-0.1	-0.2	-0.2	-0.3	-0.3	-0.3
Sphang	0.63	0.39	0.28	0.04	0.08	0.13	0.08	0.1	0.0	-0.2	-0.2	-0.2	0.29	0.0	0.0
	0.5	0.55	0.42	0.43	0.36	0.38	0.16	0.1	-0.1	-0.1	-0.2	-0.2	-0.2	-0.3	-0.3
Sphfus	0.37	0.2	0.0	-0.1	-0.3	-0.3	-0.2	-0.3	-0.1	0.0	-0.1	0.63	0.18	0.02	-0.1
	0.62	0.05	-0.18	-0.2	-0.2	-0.3	-0.3	-0.2	-0.1	-0.1	0.0	0.0	0.0	-0.1	-0.1
Sphlin	0.6	0.29	0.33	0.32	0.19	0.09	0.06	0.0	-0.1	-0.1	-0.1	-0.1	-0.1	-0.1	-0.1
	0.63	0.1	-0.15	-0.2	-0.2	-0.2	-0.2	-0.2	-0.2	-0.2	-0.2	-0.2	-0.3	-0.3	-0.3

Key to first column see in Table 2.

characteristics of interannual frequency changes: (1) the group with succession frequency changes (autocorrelation coefficient, K decreases with time throughout entire period of observations); (2) the group with cyclic frequency changes (K decreases and increases with certain periodicity); (3) the group with irregularly cyclic frequency changes (observed, different periodicity in changes of K values).

This analysis has shown (Table 3) that species with succession changes of frequency play a greater role in vegetation cover formed after disturbance, while participation of species with cyclic and irregular cyclic changes in frequency decreases.

In *Rubus chamaemorus-Ledum palustre-Sphagnum-Cladina* vegetation, species with cyclic behaviour form the most cover (48%). Nine species from this group are chamaephytes (low shrub-*Andromeda polifolia, Chamaedaphne calyculata, Vaccinium vitis-idaea*; lichens-*Cladina rangiferina, C. stellaris, Cladonia amaurocraea* and mosses-*Dicranum congestum, Pleurozium schreberi, Polytrichum commune*).

A smaller number of species (39% cover) have irregular cycles of frequency. This group of species contains 5 chamaephytes (3 species of lichens-*Cetraria cucullata, C. islandica, Cladonia coccifera;* 2 species of mosses-*Sphagnum fuscum, Tomenthypnum nitens)*; 2 phanerophytes (*Pinus sibirica, Betula nana*); and 2 cryptophytes *(Carex rotundata, Eriophorum scheuchzeri*). Only three species (2 chamaephytes-*Ledum palustre, Sphagnum angustifolium,* and 1 hemicryptophyte-*Eriophorum vaginatum*) show succession changes of frequency. Correlation coefficients over the sampling period permanently decrease for these species.

The frequency of these species has increased in undisturbed sites. For example, *Eriophorum vaginatum* has increased from 4% up to 42%, *Ledum palustre* from 64% up to 90%, and at *Sphagnum angustifoliu*m from 2% up to 24%. Probably the increase in frequency of these species is typical of the *Rubus chamaemorus-Ledum palustre-Sphagnum-Cladina* stage of flat peatland as it develops toward the final *Eriophorum-Ledum-Dicranum-Cladina* stage.

The analysis of developmental stages of vegetation on flat peatland following disturbance shows, as one would expect, a greater number (52%) of characteristic succession species. Of these 12 species, 8 are chamaephytes (low shrub-*Andromeda polifolia and Vaccinium vitis-idaea*; lichens-*Cladina stellaris, Cladonia coccifera* and mosses-*Polytrichum commune, Sphagnum angustifo1lium, S. lindbergii);* 3 species-hemicryptophytes (*Eriophorum vaginatum, Rubus chamaemorus* and *Oxyccocus microcarpus*) and 1 species-cryptophyte (*Eriophorum scheuchzeri*).

Species associated with mature surfaces have both cyclic and irregularly cyclic frequencies and contribute only half as much to the cover in disturbed plots compared to succession species. All species with irregularly cyclic frequency changes are chamaephytes (low shrub-*Vaccinium uliginosum;* lichens-*Cetraria islandica, Cladina rangiferina;* and mosses-*Sphagnum fuscum* and *Sphagnum lindbergii)*. *Cetraria cucullata, C. islandica,* and *Sphagnum fuscum* have the same character of frequency changes both in disturbed and natural conditions.

The group with cyclic frequency changes on disturbed sites includes chamaephytes (shrub-*Ledum palustre, Chamaedaphne calyculata*; lichen-*Cladonia amaurocraea*; moss-*Pleurozium schreberi*); and phanerophyte (*Betula nana*).

Conclusion

This research has determined the impact of climatic changes and human-induced disturbances on vegetation and permafrost conditions in West Siberia North. It has demonstrated the interactions between permafrost and vegetation and has identified plant communities that can be used as indicators of seasonal thaw depths.

The stages of vegetation recovery after the termination of human-induced disturbances were revealed at the sites with removed vegetation, located in different landscape conditions.

Changes in the frequency of plant species in undisturbed sites are correlated with the thaw index of air temperature and amount of precipitation.

During the study the appearance of tree species (*Betula tortuosa*, *Pinus sibirica*) and rise in frequency of shrubs (*Ledum palustre, Betula nana*) are related to a warming trend.

Natural plant communities are dominated by species with cyclic and irregular cyclic changes of frequency over the study period. For plant communities in disturbed and unstable conditions, considerable participation by species with succession changes of frequency is observed.

Acknowledgments

I thank Vladimir P. Melnikov, Elena A. Slagoda, Dmitry S. Drozdov, and Alexandr A. Vasiliev from the Earth Cryosphere Institute for logistic support. An anonymous reviewer is acknowledged for his very useful comments in improving the paper.

This study was made possible through financial support from the grant of the Tyumen governor and the U.S. National Science Foundation (Grants OPP-9732051 and OPP-0225603).

References

Brown, J., Hinkel, K. & Nelson, F. (compilers) 2003. Circumpolar Active Layer Monitoring (CALM) Program network: description and data. In: *International Permafrost Association Standing Committee on Data Information and Communication. 2003. Circumpolar active-layer permafrost system, version 2.0.* Edited by M. Parsons & T. Zhang. Boulder, CO: National Snow and Ice Data Center/ World Data Center for Glaciology. CD-ROM.

Burgess, M.M., Gretchitschev, S.E., Kurfurst, P.I., Melnikov, E.S. & Moskalenko, N.G. 1993. Monitoring of engineering-geological processes along pipeline routes in permafrost terrain in Mackenzie River Valley, Canada and Nadym Area, Russia. *Permafrost VI International Conference. Proced. Vol. 1, July 5-9, Beijing China*: 54-59

Dubrovin, V.A., Kulikov, A.I., Fedoseev, A.V. & Fedoseeva, A.R. 1996. The development of computerized observation techniques in the system of geocryological monitoring. *Fundamental Research of Earth Cryosphere in Arctic and Sub-Arctic.* Pushchino: 81-82.

Gorodkov, B.N. 1932. Permafrost and vegetation. In: *Permafrost*. Leningrad, izd-vo Akad. Nauk USSR: 48-60.

Hollister, R.D., Webber, P.J. & Tweedie, C.E. 2005. The response of Alaskan arctic tundra to experimental warming: differences between short- and long-term responses. *Global Change Biology* 11: 1-12.

Koloskov, P.I. 1925. *Climatic Foundations of Agriculture in the Amur Area.* Blagoveshensk, Soviet for Eastern Meteorological Service, 152 pp.

Melnikov, E.S. (ed.) 1983. *Landscapes of Permafrost Zone of the West Siberian Gas Province.* Novosibirsk, Nauka, 166 pp.

Melnikov, E.S., Leibman, M.O., Moskalenko, N.G. & Vasiliev, A.A. 2004. Active Layer Monitoring in West Siberia. *Polar Geography*, v. 28, № 4: 267-285.

Moskalenko, N.G. 1999. *Anthropogenic Vegetation Dynamics in the Permafrost Plains of Russia*. Novosibirsk, Nauka, 280 pp.

Moskalenko, N.G. (ed.) 2006. *Anthropogenic Changes of Ecosystems in West Siberian Gas Province*. Moscow, Earth Cryosphere Institute, 358 pp.

Sumgin M.I., 1937. *Permafrost in the USSR*. Moscow, Izd-vo Akad. Nauk USSR, 379 pp.

Tyrtikov, A.P. 1969. *Impact of the Vegetation Cover on Ground Freezing and Thawing*. Moscow, Mosk. Gos. Univ., 192 pp.

Tyrtikov, A.P. 1979. *Vegetation Cover Dynamics and Evolution of Permafrost Elements of Relief*. Moscow, Nauka, 115 pp.

Tyrtikov, A.P. 1980. Impact of the vegetation cover on ground temperature in the West Siberia North. *Natural Conditions of West Siberia.* Moscow, Mosk. Gos. Univ.: 112-118.

Vasilevich, V.I. 1970. Method of autocorrelation with study of vegetation dynamics. *Trudy MOIP*. Dep. biol. 38: 17-23.

Walker, M.D., Wahren, C.H., Hollister, R.D., Henry, G.H.R., Ahlquist, L.E., Alatalo, J.M., Bret-harte, M.S., Calef, M.P., Callaghan, T.V., Carroll, A.B., Epstein, H.E., Jónsdóttir, I.S., Klein, J.A., Magnússon, B., Molau, U., Oberbauer, S.F., Rewa, S.P., Robinson, C.H., Sshaver, G.R., Suding, K.N., Thompson, C.C., Tolvanen, A., Totland, Ø., Turner, P.L., Tweedie, C.E., Webber, P.J. & Wookey, P.A. 2006. Plant community responses to experimental warming across the tundra biome. *Proceedings of the National Academy of Science of the United States of America (PNAS)* 103(5): 1342-1346.

Experimental Study of Thermal Properties for Frozen Pyroclastic Volcanic Deposits (Kamchatka, Kluchevskaya Volcano Group)

R.G. Motenko
Department of Geocryology, Geological Faculty, Moscow State University, Moscow, Russia
E.P. Tikhonova
Department of Geocryology, Geological Faculty, Moscow State University, Moscow, Russia
A.A. Abramov
Institute of Physicochemical and Biological Problems of Soil Science, Puschino, Russia

Abstract

New data about thermal properties of volcanic deposits is presented together with a short review of permafrost conditions in the study area. This data is necessary for estimation of primary permafrost characteristics (thickness, active layer depth), yet pyroclastic volcanic deposits have not been sufficiently studied. Measurements were made across a wide range of densities and humidity, in the frozen and thawed state. These deposits have a low ability to transfer heat and can act as efficient insulators. According to our results, dry (W=0%) cinder and ash (both frozen and unfrozen) have a similar thermal conductivity of about 0.15-0.18 $Wm^{-1}K^{-1}$. At W=35%, the thermal conductivity is about 1 $Wm^{-1}K^{-1}$.

Keywords: cinder; permafrost; thermal properties; volcanic ash.

Introduction

The main goal of our work was to study the thermal properties of pyroclastic volcanic deposits in the frozen and thawed states. This data is necessary for the estimation of primary geocryological characteristics (thickness, active layer depth), but pyroclastic volcanic deposits have been inadequately studied to date. Furthermore, these deposits can play an important role in permafrost aggradation during eruptions (Kellerer-Pirklbauer et al. 2007) and in the prevention of permafrost thaw beneath lava flows.

Study Area

The Klyuchevskaya volcano group (Fig. 1) is situated in the Central Kamchatka Depression (55-56°N, 160-161°E) and consists of the active volcanoes Klyuchevsky (~4800 m a.s.l.), Bezymianny (2900 m a.s.l.), Ushkovsky (3900 m a.s.l.), and Plosky Tolbachik (3100 m a.s.l.), as well as ten others that are not active today and numerous small forms like cinder cones and extrusive domes (Braitseva et al. 1995). Here, the Large Fissure Tolbachik Eruption (LFTE) took place in 1975 and 1976, during which about 500 km^2 were covered by scoria and ash, and three new cinder cones and lava fields were formed (Fedotov & Markhinin 1983).

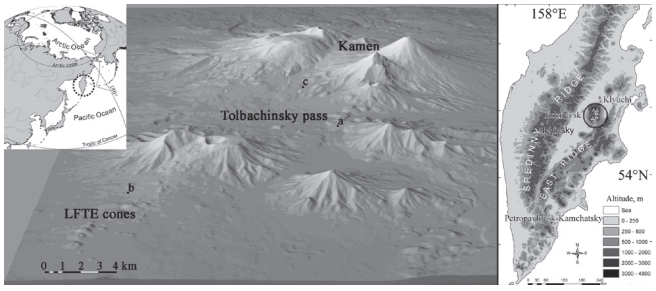

Figure 1. Study area.

Vegetation zones are largely controlled by altitude and eruptions; foliage forest occurs up to 200 m a.s.l., fir forest to 400 m a.s.l., stone birch forest to 800 m a.s.l., shrubs and elfin woods to 1200 m a.s.l., mountain tundra to 2000 m a.s.l., and isolated patches of grass and lichen are found up to 2500 m a.s.l. Around cinder cones of LFTE there are dead forest areas where vegetation has been damaged during the eruptions.

Geocryological Conditions

Permafrost and periglacial processes are widespread in the study area; permafrost covers about 2000 km^2. The lower boundary of permafrost in the study area is 750-900 m a.s.l. for north-facing slopes and 650-800 m a.s.l. for south facing slopes without forest vegetation, according to our data. The measured MAGTs vary from -2.8°C at 1330 m a.s.l. to -7°C at 2500 m a.s.l. Numerous solifluction lobes, clay cryoturbation spots, polygonal structures, and areas of sorted ground occur between 1000 and 1700 m a.s.l.

Glaciers occupy about 240 km^2 in the study area, and many of them are covered by debris and pyroclastic deposits, especially the terminus region. This can preserve ice from summer ablation. The equilibrium line altitude (ELA) is situated between 2000 and 2700 m a.s.l. The mean ice thickness is about 30-60 m for valley glaciers, and 100-250 m for glaciers in calderas. Large fields of dead ice exist near Klyuchevsky volcano (Muravyev 1999).

The thickness of the active layer decreases with altitude. Measurements of active layer depth have been conducted at several places (at elevations 800-2700 m a.s.l.) by wire probe (5 mm in diameter) or in pits. The maximal seasonal thaw depth is up to 2.5 m at 900 m a.s.l. and 50 cm at 2500 m a.s.l. Below the lower boundary of permafrost, in forested zone, the seasonal freezing is up to 2-2.5 m thick.

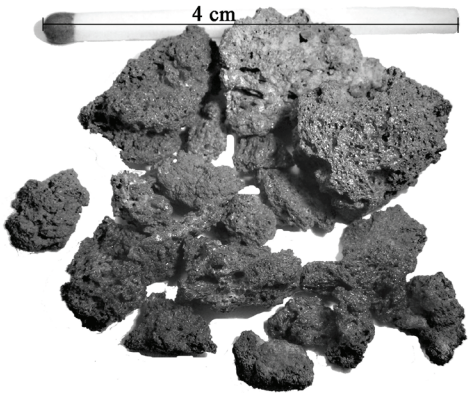

Figure 2. Volcanic cinder particles.

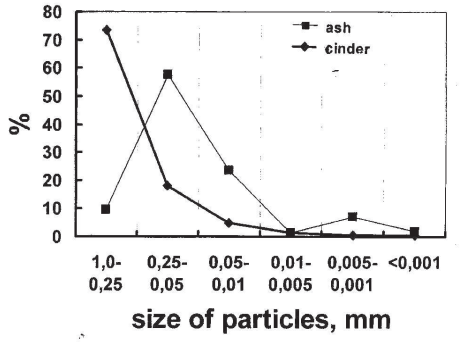

Figure 3. Granulometric composition of volcanic cinder and ash.

We studied the dynamics of the active layer on 100 m x 100 m grids in the framework of the CALM program (point a and b on Figure 1); measurements were made at the end of the warm season. The sites are situated at altitudes of 1330 m and 1630 m asl. The surface is composed of volcanic cinder with no vegetation. Active layer depth at CALM sites did not show significant changes in the last five years.

Physical Properties of Samples

Samples for this study were collected near Tolbachik and Kamen volcanoes (Fig. 1). Volcanic ashes from different sites were investigated at natural humidities (only sample 2 was studied for a range of humidities) (Table 1). Volcanic cinder (Fig. 2) was collected near LFTE cones only, and investigated at several humidities for unsorted particles (size <1 cm) and those sifted through 1 mm and 2 mm sieves. Mean granulometric composition for ash and cinder are shown on Figure 3. These deposits are ultra pure, their pH is neutral (6-8), and total organic carbon content (TOC) is very low (0%-2%). The freezing temperature of these coarse grained deposits is about 0°C.

Methods

Field data about thermal conductivity for thawed deposits was collected using a needle probe with constant power. The accuracy of the measurements is about 12%. These data are available only for volcanic ashes. Deposits at these locations have been sampled for density and humidity, and for laboratory investigations.

Table 1. Volcanic ash samples list. [a]-collected near Tolbachinsky pass, [b]-collected near LFTE cones, [c]-collected near Kamen volcano.

Sample	Depth, m	Age, years	ρ, gr/cm^3	ρ_d, gr/cm^3	Humidity W, %
1[a]	0.2	1475±50	1.50	1.07	38
2[b]	0.2	30	1.40	1.20	30
3[a]	0.55	1475±50	1.44	0.88	64
4[c]	0.15	-	1.60	1.32	21
5[a]	0.75	1475±50	1.67	1.26	33
6[c]	0.4	-	1.47	1.47	13

In the laboratory we use the I-type regular mode method (α-calorimeter) (Ershov 2004). Thermal diffusivity (a) was detected by heating and cooling the ground in an environment with constant temperature (outside of area with intensive phase changes). The temperature range was 0ºC to +20ºC and -22ºC to -12ºC. All measurements were made two times. The accuracy of measurements is about 10%.

Specific heat capacity (C) is calculated as the sum of ground components (rock matrix, water, ice). Thermal capacity was set to 4200 Jkg^{-1}K^{-1} for water and set to 2100 Jkg^{-1}K^{-1} for ice. Thermal capacities for the rock matrix were measured on an ITC-400 by monotonous heating. The accuracy of measurements is about 10% (Platunov 1972).

Thermal conductivity (λ) was calculated as: $\lambda = C\rho\, a$.

The analysis of chemical and granulometric composition, pH, and TOC (total organic carbon) were made in the laboratories of the Institute of Physicochemical and Biological Problems of Soil Science, using standard techniques.

The preparation and processing of the material for radiocarbon dating was carried out by the ^{14}C laboratory of the Department of Geography at the University of Zurich (GIUZ). The dating itself was done by AMS (accelerator mass spectrometry) with a tandem accelerator at the Institute of Particle Physics at the Swiss Federal Institute of Technology Zurich (ETH).

Results and Discussion

Results on thermal conductivity are presented in Figures 4 and 5.

Figure 4 shows data for volcanic ashes. Sample 2 was investigated at two rock matrix densities and several humidities. At ρ_d=1.2 gr/cm^3, λ increased with an increase in humidity (from 0% to 38%) from 0.17 to 0.67 Wm^{-1}K^{-1} in the thawed state and to 0.78 Wm^{-1}K^{-1} in the frozen state. At ρ_d=1.0 gr/cm^3, the increase was smaller (up to 0.53 and 0.63 Wm^{-1}K^{-1}, respectively). All other ash samples were investigated at natural humidities and densities. For dry samples, λ was set

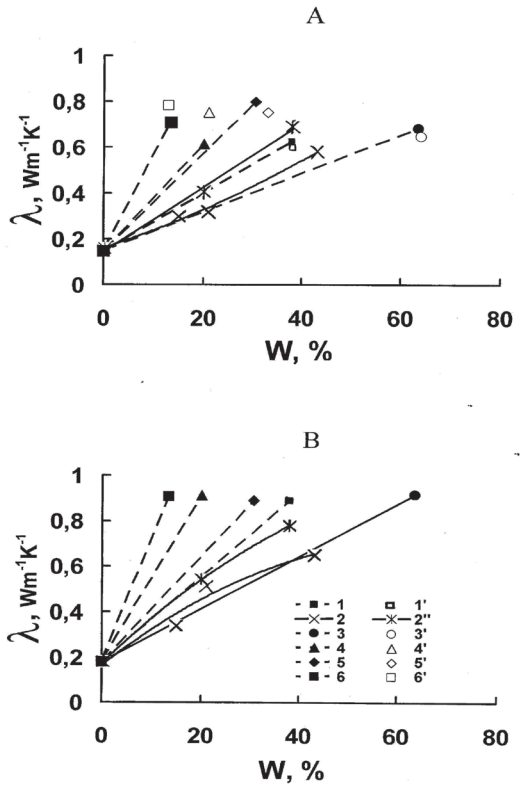

Figure 4. Correlation between thermal conductivity (λ) and humidity (W) for thawed (A) and frozen (B) volcanic ash at different densities (ρ_d): 1 – 1.1 gr/cm^3, 2 – 1 gr/cm^3, 2″ – 1.2 gr/cm^3, 3 – 0.88 gr/cm^3, 4 – 1.32 gr/cm^3, 5 – 1.33 gr/cm^3, 6 – 1.47 gr/cm^3; 1′, 3′, 4′, 5′, 6′ – field data (ρ_d are the same).

to 0.17 Wm^{-1}K^{-1} as in sample 2. The dotted lines on Figure 4 show the estimated correlation of λ to humidity. The lower the density, the lower the λ, but the relation is clearer with samples from one site. We believe that this is due to different age and mineral composition. Field data is presented only for thawed ash samples (1', 3', 4', 5', 6'); the divergence with laboratory data is about 12%.

According to our results, the thermal conductivity of dry (W=0%) ash and cinder (both frozen and thawed) is similar at about 0.15-0.18 Wm^{-1}K^{-1}. The dependence of λ on density and humidity is similar for volcanic cinders to that in ashes. Unsorted cinder is non-homogeneous and does not fit the method requirements, so that data for cinder sample 3 is only an estimate. This cinder is very porous, resulting in a lower λ value.

The dependence of thermal diffusivity (a) on humidity and density is similar to that for λ. For volcanic cinders with W = 0%–35%, a = 0.17 to 0.30–0.54×10^{-6}m^{2}s^{-1} in the frozen state, and up to 0.21–0.33×10^{-6}m^{2}s^{-1} in the thawed state. For volcanic ashes at natural humidities and densities, a = 0.20×10^{-6}m^{2}s^{-1} (sample 3) – 0.36×10^{-6}m^{2}s^{-1} (sample 6) for frozen material, and 0.392×10^{-6}m^{2}s^{-1} – 0.580×10^{-6}m^{2}s^{-1} for thawed material.

The C from the ITC-400 for volcanic cinder is 750 Jkg^{-1}K^{-1} and for volcanic ash is 750–800 Jkg^{-1}K^{-1}. Only for ash sample 3 is it 1000 Jkg^{-1}K^{-1}.

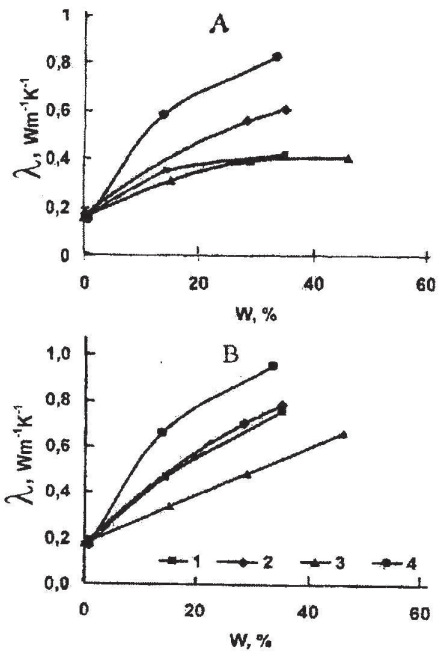

Figure 5. Correlation between thermal conductivity (λ) and humidity (W) for thawed (A) and frozen (B) volcanic cinder at different densities (ρ_d): 1 – 1.1…1.2 gr/cm^3) (≤1 mm), 2 – 1.1 gr/cm^3 (≤2 mm)), 3 – 0.9 – 1.0 gr/cm^3 (≤1 cm), 4 – 1.3 - 1.4 gr/cm^3) (<1 mm).

Conclusions

New thermal conductivity data were collected for pyroclastic deposits in both the thawed and frozen states. Results show that thermal conductivity is very low under dry conditions and increases as the humidity and density of the deposit increases. The thermal conductivity of dry cinder and ash, according to our measurements, is about 0.15-0.18 Wm^{-1}K^{-1}. The maximum thermal conductivity is about 1 Wm^{-1}K^{-1} with an ice content 35%-40%. Field measurements for thawed ashes compare well with laboratory data.

The low heat transfer rate in these deposits can play an important role in the formation and preservation of permafrost. The formation of permafrost during eruptions is in relation to active layer thickness and thickness of deposited volcanic deposits. Pyroclastic volcanic deposits can preserve underlying permafrost layers from thawing due to its effective insulation properties and thermal offset effects. In the case of large explosive eruptions, permafrost can aggrade in surrounding terrain, especially during a winter eruption when the falling cinder has subzero temperatures and buries large quantities of snow and ice.

Acknowledgments

The authors want to express their thanks to all who helped in this study, especially D.A. Gilichinsky and Y.D. Muravyev.

Thanks are due to the NAI for financial support during these years.

References

Braitseva, O., Melekestsev, I., Ponomareva, V. & Sulerzhitsky, L. 1995. Ages of calderas, large explosives craters and active volcanoes in the Kuril-Kamchatka region, Russia. *Bull. Volcanol.* 57: 383-402.

Ershov, E.D. (ed.) 2004. *Methods of Geocryological Research*. Moscow: MSU, 306 pp.

Fedotov, S.A. & Markhinin, Y.K. 1983. *The Great Tolbachik Fissure Eruption: Geological and Geophysical Data 1975-1976.* Cambridge: Cambridge University Press, 355 pp.

Kellerer-Pirklbauer, A., Farbrot, H. & Etzelmuller, B. 2007. Permafrost aggradation caused by tephra accumulation over snow-covered surfaces: examples from the Hekla-2000 eruption in Iceland. *Permafrost and Periglacial Processes* 18: 269-284. doi:10.1002/, 596 pp.

Muravyev, Y.D. 1999. Present-day glaciation in Kamchatka-distribution of glaciers and snow. *Cryospheric Studies in Kamchatka* II: 1-7.

Platunov, E.S. 1972. *Thermo Physical Measurements at Monotonous Regime*. Moscow: Energy, 205 pp.

Spatial Analysis of Glacial Geology, Surficial Geomorphology, and Vegetation in the Toolik Lake Region: Relevance to Past and Future Land-Cover Changes

C.A. Munger, D.A. Walker, and H.A. Maier
Institute of Arctic Biology, University of Alaska Fairbanks, AK 99775, USA
T.D. Hamilton
U.S. Geological Survey, 4200 University Drive, Anchorage, AK 99508-4667, USA

Abstract

Vegetation succession on different age glacial surfaces may provide clues to how tundra regions will respond to future climate and land-use changes. In the Toolik Lake region, of Alaska, three major glacial advances occurred during the middle to Late Pleistocene. Here we use a new group of maps of the upper Kuparuk River region to examine the interrelationships between glacial history, surficial geomorphology, vegetation, and spectral properties. Older surfaces in the region have greater amounts of shrub- and moss-rich vegetation and higher values of the Normalized Difference Vegetation Index (NDVI), an index of vegetation greenness. Younger surfaces have a higher proportion of disturbance-related features such as non-sorted circles and areas with warmer soils. Landscape responses to climate change are likely to be heterogeneous and may be most easily detected in areas where there are already high amounts of shrubs or areas with high disturbance regimes.

Keywords: climate change; ecosystems; GIS; glacial history; NDVI; patterned ground; vegetation.

Introduction

The Toolik Lake region is situated in close proximity to several major Late Cenozoic glacial surfaces (Hamilton 1986). In this cold region, landscape evolution proceeds more slowly than in temperate regions, so that differences in geomorphology and vegetation are evident on surfaces spanning hundreds of thousands of years. These surfaces have not been altered by agriculture or other anthropogenic influences, so the region is an excellent laboratory to examine the effects of geological processes on ecosystem function. Such studies can help us understand how arctic systems change over long periods of time and provide insights regarding how they might change in the future in response to climate change. This paper focuses on the linkage between glacial geology, surficial geomorphology, and vegetation in the upper Kuparuk River region, where the glacial history has been shown to be a defining characteristic for a wide variety of terrestrial and aquatic ecosystems characteristics (Jorgenson 1984a, Walker & Walker 1996, Oswald et al. 2003). We use mapped information that is part of a hierarchical geographic information system (HGIS), which has been assembled for the University of Alaska's Toolik Lake Field Station and an Arctic Geobotanical Atlas (Walker et al. 2008 this volume)

Glacial geology

The complex topography of the Toolik Lake region results from glacial deposits that flowed into the region during three major glacial advances. Glacial deposits within the Toolik Lake region are assigned to Sagavanirktok (middle Pleistocene), Itkillik I, and Itkillik II (Late Pleistocene) glaciations of the central Brooks Range glacial succession (Detterman et al. 1958, Porter 1964, Hamilton & Porter 1975, Hamilton 1986, Hamilton 2003) (Fig. 1a). A simplified version of Thomas Hamilton's glacial geology map of the upper Kuparuk River region (Hamilton 2003) was used for this analysis.

The Sagavanirktok glaciation consisted of several separate glacial events dating broadly from middle Quaternary time (about 780,000 to 125,000 yr B.P.). During the initial (maximum) advances, large valley glaciers flowed north along the Itkillik River, Sagavanirktok River, and Kuparuk River drainages. Most of the upper Kuparuk River watershed, including the Imnavait Creek watershed, is on drift of older Sagavanirktok-age deposits. The surfaces of the Sagavanirktok River glaciation have massive gently sloping moraines that rise about 100 m from the valley bottoms to the crests trending SSE to NNW (Hamilton 1986). These moraines are well represented in the Imnavait Creek watershed. The hills formed by these moraines are rounded by gelifluction and heavy loess cover and are topped with 20 cm to 40 cm of peat. Occasional glacial erratics protrude up to 1 m above the tundra surface.

Itkillik I glaciers abutted divides (west, east, and south of the upper Kuparuk drainage) but overflowed those divides only locally. The subsequent Itkillik II glaciers advanced between about 25 and 11.5 kya ^{14}C and formed extensive ice-stagnation features around Toolik Lake. Glacial flow patterns during the Itkillik II advance were generally similar to those of the present-day river drainages. Other features on the glacial geology map include bedrock, river deposits, lacustrine deposits, fan deposits, colluvial deposits, and shales and siltstones of the Chandler Formation (along the north boundary of the map), Toruk Formation (middle-eastern portion of the map), and Fortress Mountain Formation (north side of the Atigun River).

Surficial geomorphology

The landscapes in the Toolik Lake region have been

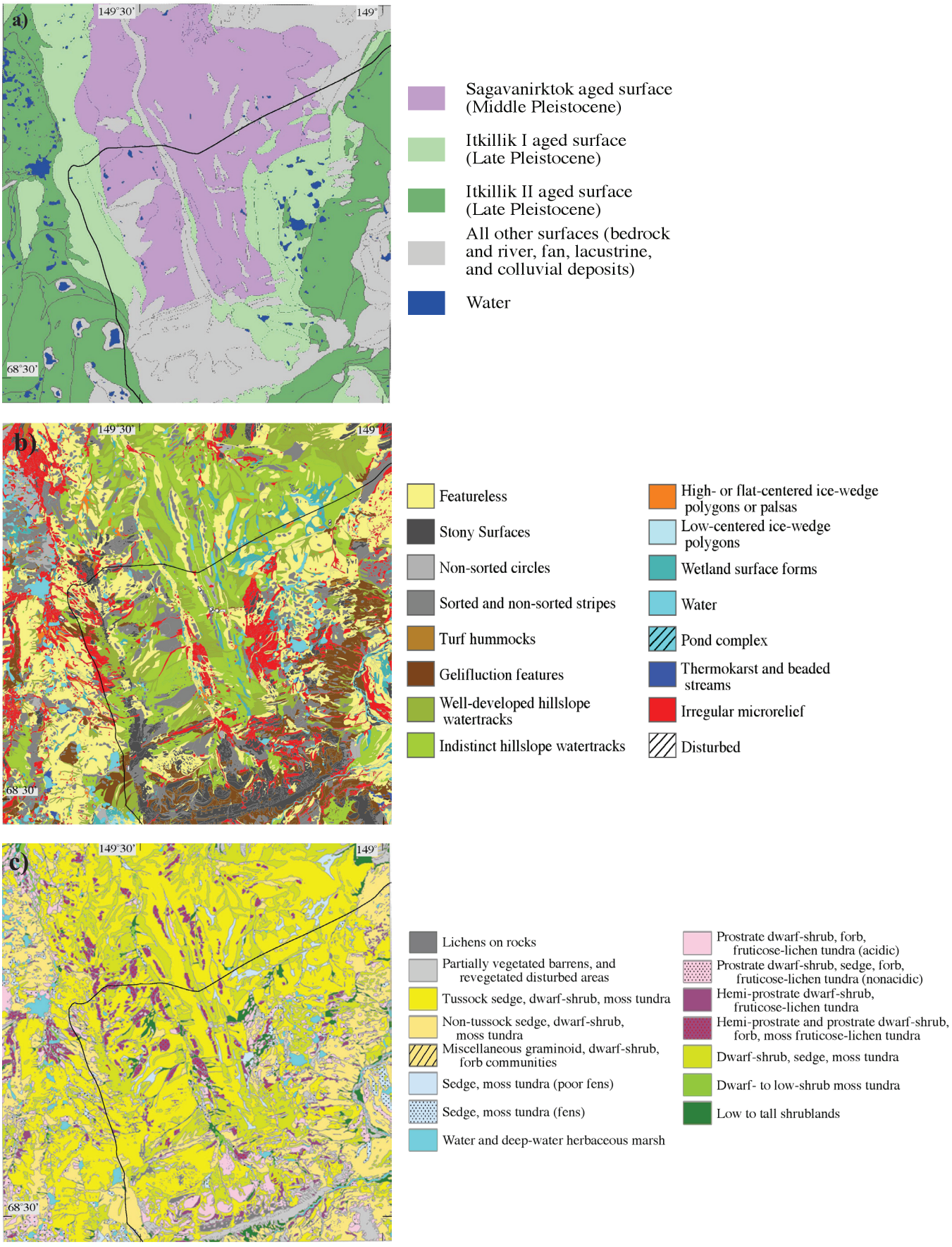

Figure 1. a) Glacial geology, b) surficial geomorphology, and c) vegetation of the Toolik Lake region.

modified by a variety of geomorphological processes including alluviation, colluviation, and periglacial processes (Fig. 1b). Common surficial geomorphological map units described for the Imnavait Creek region (Walker & Walker 1996) include sorted and nonsorted circles (frost boils), turf hummocks, gelifluction lobes and terraces, water tracks, high- and low-centered ice-wedge polygons, wetland features (strangmoor, aligned hummocks, palsas), and thermokarst features.

Vegetation

The vegetation of the region (Fig 1c) was studied and mapped as part of the Arctic Long-Term Ecological Research (LTER) project at Toolik Lake (Walker et al. 1994, Walker & Walker 1996), and the Department of Energy R4D (Response, Resistance, Resilience and Recovery of vegetation from Disturbance) project at Imnavait Creek (Walker & Walker 1996). Fifty plant communities and land-cover types were recognized during the mapping of the upper Kuparuk River region, and they are designated by numeric codes in the GIS database. These were grouped into the 14 physiognomic map units shown on Fig. 1c. (For more details on the vegetation mapping, see Walker et al. 2008)

NDVI

The Normalized Difference Vegetation Index (NDVI) is an index of vegetation greenness that can be linked to plant biomass and other biophysical properties of the vegetation (Shippert 1995). The NDVI = (NIR – R)/(NIR + R), where NIR is the spectral reflectance in the Landsat Thematic Mapper in the near-infrared channel (0.76–0.9 μm) and R is the reflectance in the red channel (0.63–0.69 μm). Four images were used in the analysis (3 Aug 1985, 8 Aug 1995, 4 Aug 1999, and 21 Jul 2001). The NDVI was calculated for each 30-m pixel in each image, and a composite average NDVI was calculated for each pixel using the mean value for the four years. To examine how plant production varies with glacial history, we examined the distribution of the Normalized Difference Vegetation Index (NDVI) on the three glacial surfaces.

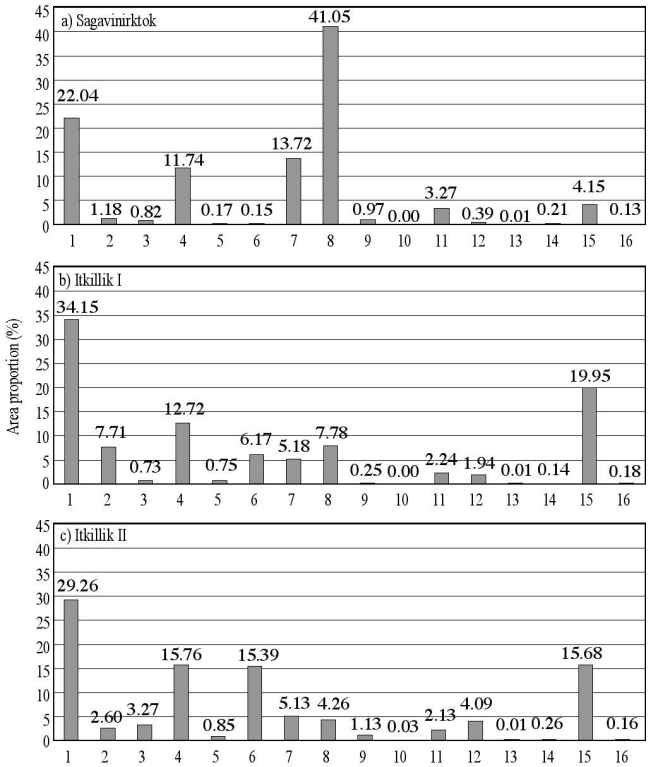

1. Featureless
2. Stony surfaces
3. Non-sorted circles
4. Sorted and non-sorted stripes
5. Turf hummocks
6. Gelifluction features
7. Well-developed hill-slope water tracks
8. Indistinct hill-slope watertracks
9. High- or flat-centered ice-wedge polygons and palsas
10. Low-centered ice-wedge polygons
11. Wetland surface forms
12. Water
13. Pond Complex
14. Thermokarst and beaded streams
15. Irregular microrelief
16. Disturbed

Figure 2. Proportion of surficial geomorphologic types on a) Sagavanirktok-aged, b) Itkillik I-aged, and c) Itkillik II-aged glacial surfaces.

Analysis of the Maps

The surficial geomorphology, vegetation, and NDVI maps were stratified according to the glacial units in Figure 1a. Results of the analysis are shown in Figures 2 and 3.

Effects of glacial history on surficial geomorphology

Terrain evolution associated with the glacial history of the region was noted by Hamilton (Hamilton & Trexler Jr. 1979). Our analysis extends Hamilton's earlier observations to surface forms that are superimposed on the larger landforms of the regions (Fig. 2). The broad hill-slope deposits of the Sagavanirktok-age surfaces are dominated by indistinct and well-developed water-track patterns (55% on Sagavanirktok surfaces, 13% on Itkillik-I, and 9% on Itkillik-II surfaces). The older Sagavanirktok surfaces also have more peaty wetlands (3% on Sagavanirktok surfaces and 2% on Itkillik-I and Itkillik-II surfaces). Stripes and nonsorted circles are more abundant on the younger surfaces, especially the Itkillik II surfaces. Stripes cover 12% of Sagavanirktok surfaces, 13% of Itkillik-I, and 16% of Itkillik-II surfaces. Non-sorted circles cover 1% on Sagavanirktok surfaces, 1% on Itkillik-I, and 3% of Itkillik-II surfaces. Lakes are also more abundant on the younger surfaces (less than 1% on Sagavanirktok surfaces, 2% on Itkillik-I, and 5% on Itkillik-II surfaces).

Effects of glacial history on vegetation and plant production

The Sagavanirktok age surfaces have a dominance of acidic tussock tundra (61% tussock-sedge, dwarf-shrub, moss tundra cover, compared to 38% on Itkillik I, and 24% on Itkillik II surfaces) and relatively high percentages of

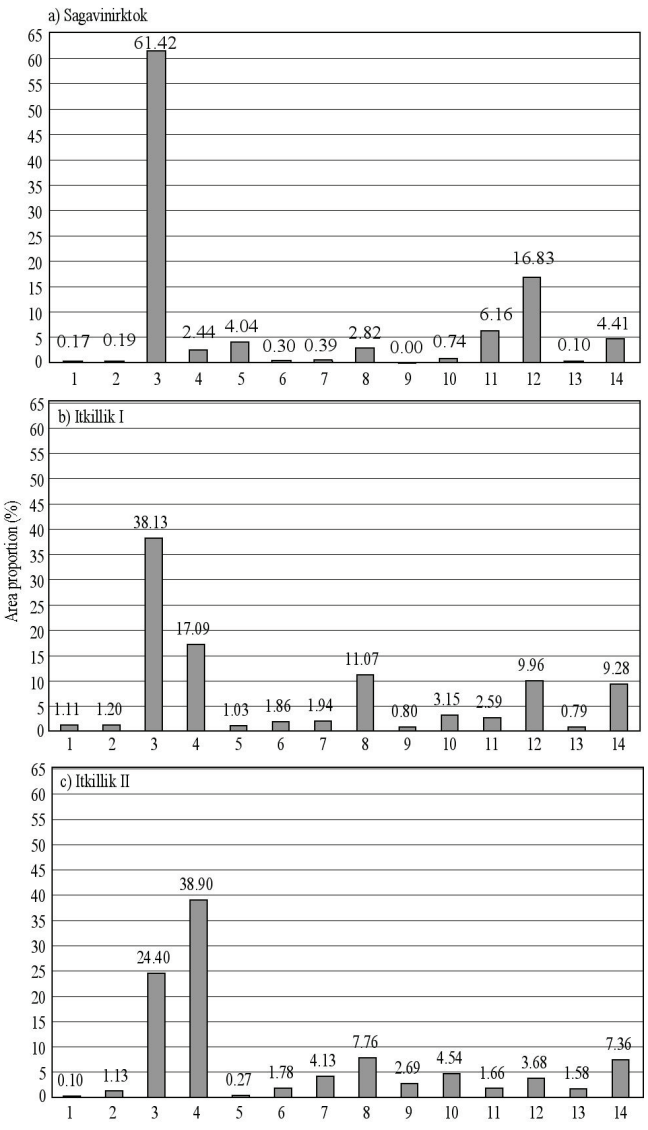

1. Lichens on rocks
2.Partially vegetated vegetated barrens and revegetated disturbed areas.
3. Tussock sedge, dwarf-shrub, moss tundra
4. Non-tussock sedge, dwarf-shrub, moss tundra
5. Sedge, moss tundra (poor fens)
6. Sedge, moss tundra (fens)
7. Water and deep-water herbaceous marsh
8. Prostrate dwarf-shrub, forb, fruticose-lichen tundra (acidic)
9. Prostrate dwarf-shrub, sedge, forb, fruticose lichen tundra (nonacidic)
10. Hemi-prostrate dwarf-shrub, fruticose-lichen tundra
11. Hemi-prostrate and prostrate dwarf-shrub, forb, moss fruticose-lichen tundra
12. Dwarf-shrub, sedge, moss tundra
13. Dwarf- to low-shrub moss tundra
14. Low to tall shrublands

Figure 3. Proportion of vegetation types on a) Sagavanirktok aged, b) Itkillik I aged, and c) Itkillik II aged glacial surfaces.

erect-dwarf shrub tundra types (21% on Sagavanirktok-age surfaces, 20% on Itkillik-I, and 13% on Itkillik-II surfaces) and poor-fen wetlands (4% on Sagavanirktok surfaces, 1% on Itkillik-I surfaces, and 0% on Itkillik-II surfaces) (Fig. 3). In contrast, the much younger Itkillik II surfaces have a dominance of nonacidic tundra (nontussock-sedge, dwarf-shrub, moss tundra, 2% on Sagavanirktok surfaces, 17% on Itkillik-I surfaces, and 39% on Itkillik-II surfaces) and are more vegetatively diverse with relatively high percentages of snowbed vegetation (hemi-prostrate-dwarf-shrub vegetation types, less than 1% on Sagavanirktok surfaces, 3% on Itkillik-I, and 5% on Itkillik-II surfaces), rich fens (0% on Sagavanirktok surfaces and 2% on Itkillik-I and Itkillik-II surfaces), and dry nonacidic tundra (prostrate dwarf shrub, sedge, forb, lichen tundra, 0% on Sagavanirktok surfaces, 1% on Itkillik-I and 3% on Itkillik-II surfaces.

Landscape age at Toolik Lake is also linked to biomass and the Normalized Difference Vegetation Index (NDVI) (Fig. 4). Older landscapes have higher NDVI and greater amounts of standing biomass (Shippert et al. 1995). The higher NDVI values of the older landscapes are due in part to relative proportions of dry, moist, and wet vegetation types on different aged surfaces. Generally, drier vegetation with lower NDVI is dominant on younger surfaces, as shown in the area analysis of vegetation on the different age glacial surfaces (Fig.3). Of greater regional significance is the difference in biomass and NDVI of vegetation growing on moist upland surfaces. The biomass of the *Sphagno-Eriophoretum vaginati* tussock tundra, which grows on the older acidic surfaces, is about 25% greater than its nonacidic counterpart *Dryado integrifoliae-Caricetum bigelowii* (512 g m^{-2} vs. 403 g m^{-2}). These types also have different key ecosystem properties, including active layer depths (Nelson et al. 1997) (Walker et al. 2003 submitted), trace gas fluxes (Oechel et al. 2000), species composition (Gough et al. 2000), abundance of frost boils (Bockheim et al. 1998), and soil carbon (Bockheim et al. 1996).

Implications with Respect to Land-Cover Change

The difference in shrub cover on the different glacial surfaces is of particular interest because of relevance to the issue of shrub expansion associated with climate warming (e.g., Sturm et al. 2001). While the older surfaces have overall greater cover of erect dwarf-shrub tundra types, as noted above, the younger surfaces have greater cover of taller riparian shrubs (4% on Sagavanirktok surfaces, 9% on Itkillik-I, and 7% on Itkillik-II surfaces). This is possibly due to the greater abundance of rocky and gravelly stream channels on the younger surfaces and steep south facing slopes with relatively warm, nutrient-rich soils.

Area analysis of the vegetation units occurring on the different age glacial surfaces shows that the older landscapes have more acidic tundra, less dry nonacidic tundra, fewer snowbeds, more dwarf-shrub tundra, much less moist nonacidic tundra, fewer rich riparian shrublands, fewer rich fens, more poor fens, and fewer lakes. Torre Jorgenson noted differences in the abundance of plant communities on the different glacial surfaces (Jorgenson 1984b), and soil heat flux was higher on the younger surfaces (Jorgenson

1984a). Others have linked Hamilton's glacial units to a hypothesis of vegetation succession, whereby peat formation (paludification) and ice aggradation on older surfaces lead to restricted drainage, a general acidification of the soils, and the introduction of *Sphagnum* mosses to wet hill slopes. Thicker moss carpets change the soil chemistry, hydrology, and soil thermal properties, resulting in peat formation and acidic mires in colluvial basins, extensive water-track development, and tussock tundra on gentle hill slopes (Jorgenson 1984a, Walker et al. 1989, Walker & Walker 1996, Mann et al. 2002).

Variation in the degree of paludification is a primary factor controlling the distribution of acidic tussock tundra, *Sphagno-Eriophoretum vaginati* and its non-acidic counterpart *Dryado integrifoliae-Caricetum bigelowii* (Walker et al. 1994). The plant association *Dryado integrifoliae-Caricetum bigelowii* is included within the "non-tussock sedge, dwarf-shrub, moss tundra" unit on the vegetation map (Fig. 1c) and occurs most abundantly on younger surfaces, often with high disturbance regimes, including Itkillik-age glacial surfaces, loess deposits, solifluction features, frost-boil complexes, and alluvial terraces; whereas well-developed tussock tundra (included in the "tussock-sedge, dwarf shrub, moss tundra" unit) forms under conditions of long-term site stability. The *Dryado integrifoliae-Caricetum bigelowii* and related associations found on younger landscapes are also floristically much more diverse than tussock tundra, and important with respect to regional biodiversity. These associations have the highest species diversity of any of the communities sampled in the region (Walker et al. 1994). Several authors have noted the affect of soil pH on tundra plant diversity (Walker 1985, Gough et al. 2000); however, the effects of landscape age on other aspects of biodiversity such as upon total regional plant community and animal diversity have not been studied in any detail.

Paleoecological studies from lakes on the Itkillik II and Sagavanirktok-age surfaces near Toolik Lake indicate that the onset of moist conditions between the early and middle Holocene triggered processes of plant succession leading up to the current conditions (Oswald et al. 2003). Soil moisture appears to have been better retained by fine-textured soils and more gently sloped landforms on the Sagavanirktok surfaces, promoting greater plant cover, thicker organic soil horizons, shallower active layers, aggradation of permafrost, and acidic soils; whereas the better-drained Itkillik surfaces continued to support relatively xeric, sparse, non-acidic vegetation.

Our study found the older Sagavanirktok-age surfaces have a greater abundance of shrubby vegetation types than the younger surfaces. These were dominated by communities with dwarf-shrubs and large areas of shrubby watertracks. We also found that the best developed (tall) shrub communities were most common on the younger Itkillik-age surfaces, suggesting that the higher disturbance regimes, warmer soils, and higher nutrient regimes in certain microsites promoted the development of well-developed shrub communities. Future changes of the regional vegetation will be in response to both altered climate and changes in natural and anthropogenic disturbance regimes. We are currently conducting a more detailed study of the greening response of these surfaces during the period of Landsat satellite-observations (1981 to present) (Munger 2007), which will yield further insights regarding the past and future land-cover changes in these landscapes.

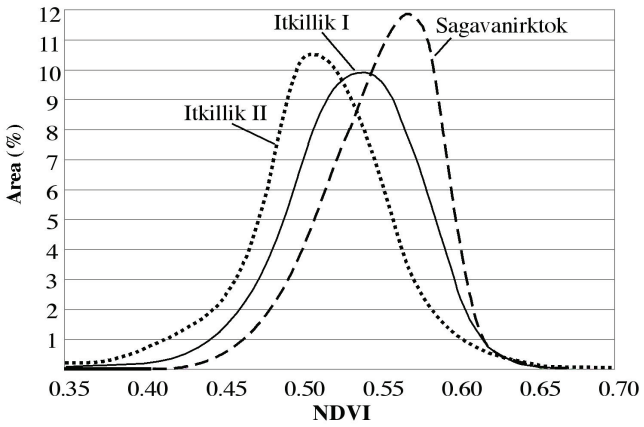

Figure 4. Distribution of NDVI on different aged glacial surfaces.

Acknowledgments

Funding for this study was provided by the National Science Foundation (ARC-0425517 and ARC-0531180). The Alaska Geobotany Center is located within the Institute of Arctic Biology, University of Alaska Fairbanks, Fairbanks, Alaska 99775-7000.

References

Bockheim, J.G., Walker, D.A. & Everett, L.R. 1996. Soil carbon distribution in nonacidic and acidic soils of arctic Alaska. In: R. Lal, J.M. Kimble, R.F. Follett & B.A. Stewart (eds.), *Advances of Soil Science*. *Proceedings of the International Symposium on Carbon Sequestration in Soil. Ohio State University.* Columbus: CRC Press, 143-155

Bockheim, J.G., Walker, D.A., Everett, L.R., Nelson, F.E. & Shiklomanov, N.I. 1998. Soils and cryoturbation in moist nonacidic and acidic tundra in the Kuparuk river basin, arctic Alaska, U.S.A. *Arctic and Alpine Research* 30: 166-174.

Detterman, R. L., Bowsher A.L. & Dutro, J.T., Jr. 1958. Glaciation on the arctic slope of the Brooks Range, northern Alaska. *Arctic* 11: 43-61.

Gough, L., Shaver, G.R., Carrol, J., Royer, D.L. & Laundre, J.A. 2000. Vascular plant species richness in Alaskan arctic tundra: the importance of soil pH. *Journal of Ecology* 88: 54-66.

Hamilton, T.D. 1986. Late Cenozoic glaciation of the Central Brooks Range. In: T.D. Hamilton, K.M. Reed, & R.M. Thorson (eds.), *Glaciation in Alaska: the Geologic Record.* Alaska Geological Society, 9-49.

Hamilton, T.D. 2003. *Glacial Geology of the Toolik Lake and Upper Kuparuk River Regions, Institute of Arctic Biology*. Biological Papers of the University of Alaska. No. 26, Fairbanks, AK.

Hamilton, T.D. & Porter, S.C. 1975. Itkillik glaciation in the Brooks Range, northern Alaska. *Quaternary Research* 5: 471-497.

Hamilton, T.D. & Trexler Jr., J.H. 1979. Analyses of surficial deposits, central Brooks Range, Alaska. *Open-File Report*. U.S. Geological Survey, 79-228.

Jorgenson, M.T. 1984a. *Controls of the Geographic Variability of Soil Heat Flux near Toolik Lake, Alaska.* M.S. Thesis. University of Alaska Fairbanks.

Jorgenson, M.T. 1984b. The response of vegetation to landscape evolution on glacial till near Toolik Lake, Alaska. In: *Inventorying Forest and Other Vegetation of the High Latitude and High Altitude Regions, Proceedings of an International Symposium, Society of American Foresters Regional Technical Conference, Fairbanks, AK,* 134-141.

Mann, D.H., Peteet, D.M., Reanier, R.E. & Kunz, M.L. 2002. Responses of an arctic landscape to Late-glacial and early Holocene climatic changes: the importance of moisture. *Quaternary Science Reviews* 21: 997-1021.

Munger, C.A. 2007. *Spatial and Temporal Patterns of Vegetation, Terrain, and Greenness in the Toolik Lake and Upper Kuparuk River Region.* M.S. Thesis. University of Alaska Fairbanks.

Nelson, F.E., Shiklomanov, N.I., Mueller, G.R., Hinkel, K.M., Walker, D.A. & Bockheim, J.G. 1997. Estimating active-layer thickness over a large region: Kuparuk River Basin, Alaska. *Arctic and Alpine Research* 29: 367-378.

Oechel, W.C., Vourlitis, G.L., Verfaillie, J., Jr., Crawford, T., Brooks, S., Dumas, E., Hope, A., Stow, D., Boynton, B., Nosov, V. & Zulueta, R. 2000. A scaling approach for quantifying the net CO2 flux of the Kuparuk River Basin, Alaska. *Climate Change Biology* 6: 160-173.

Oswald, W.W., Brubaker, L.B., Hu, F.S. & Kling, G.W. 2003. Holocene pollen records from the central Arctic Foothills, northern Alaska: testing the role of substrate in the response to climate change. *Journal of Ecology* 91: 1034-1048.

Porter, S.C. 1964. Late Pleistocene glacial chronology of north-central Brooks Range, Alaska. *American Journal of Science* 262: 446-460.

Shippert, M. M., Walker, D.A. & Auerbach, N.A. 1995. Biomass and leaf-area index maps derived from SPOT images for Toolik Lake and Imnavait Creek areas, Alaska. *Polar Record* 31: 147-154.

Sturm, M., McFadden, J.P., Liston, G.E., Racine, H. & Holmgren, J. 2001. Snow-shrub interactions in arctic tundra: a hypothesis with climatic implications. *Journal of Climate* 14: 336-344.

Walker, D.A. 1985. *The Vegetation and Environmental Gradients of the Prudhoe Bay Region, Alaska.* In: U.S. Army Cold Regions Research and Engineering Laboratory, Hanover, NH.

Walker, D.A., Jia, G.J., Epstein, H.E., Raynolds, M.K., Chapin, F.S., III, Copass, C.D., Hinzman, L.D., Kane, D., Maier, H.A., Michaelson, G.J., Nelson, F., Ping, C.L., Romanovsky, V.E., Shiklomanov, N. & Shur, Y. 2003 submitted. Vegetation-soil-thaw-depth relationships along a Low-Arctic bioclimate gradient, Alaska: synthesis of information from the ATLAS studies. *Permafrost and Periglacial Processes.*

Walker, D.A., Maier, H.A. & Barbour, E.M. 2008. A web-based arctic geobotanical atlas and new hierarchy of maps of the Toolik Lake region, Alaska. *Proceedings of the Ninth International Conference on Permafrost, Fairbanks, Alaska, June 29–July 3, 2008* (this proceedings).

Walker, D.A., & Walker, M.D. 1996. Terrain and vegetation of the Imnavait Creek Watershed. In: J.F. Reynolds & J.D. Tenhunen (eds.), *Landscape Function: Implications for Ecosystem Disturbance, a Case Study in Arctic Tundra.* Springer-Verlag, New York, 73-108.

Walker, M.D., Walker, D.A. & Auerbach, N.A. 1994. Plant communities of a tussock tundra landscape in the Brooks Range Foothills, Alaska. *Journal of Vegetation Science* 5: 843-866.

Walker, M.D., Walker, D.A. & Everett, K.R. 1989. Wetland soils and vegetation, Arctic Foothills, Alaska. *U.S. Fish and Wildlife Service* 89 (7).

Choosing Geotechnical Parameters for Slope Stability Assessments in Alpine Permafrost Soils

Philippe Nater
GeoNum GmbH, Zurich, Switzerland
Lukas U. Arenson
BGC Engineering Inc. Vancouver, BC, Canada
Sarah M. Springman
Institute for Geotechnical Engineering, ETH Zurich, Zurich, Switzerland

Abstract

The shear strength of alpine permafrost soils can be expressed in terms of internal friction ϕ' and cohesion *c* utilizing a Mohr-Coulomb failure criterion as for many other soils. The challenges lie in the correct parameterization, in other words the assignment of realistic values for the chosen parameters ϕ' and *c*. Because the strength of frozen soils depends on the temperature, a correlation of the effective angle of internal friction ϕ' and cohesion *c* with temperature-dependent parameters, such as the volumetric ice content w_i, is proposed. The correlations are based on laboratory tests carried out on undisturbed samples of alpine permafrost soils. Utilizing an example calculation, this paper provides guidance in dealing with limit equilibrium slope stability analysis and assistance in selecting appropriate soil parameters.

Keywords: alpine permafrost soil; failure; limit equilibrium analysis; shear strength parameters.

Introduction

When assessing the stability of permafrost slopes, engineers are often faced with the challenge of selecting appropriate soil parameters and model. Only a limited number of laboratory test results are available from which such parameters could be extracted. Based on published data and interpretation of laboratory tests on undisturbed samples of alpine permafrost soils presented by Arenson et al. (2004) and Arenson and Springman (2005a, 2005b), reassessing the strength of those soils for the use in limit equilibrium analysis was carried out. The chosen strength model for describing the shear resistance is a Mohr-Coulomb failure criterion with a frictional and a cohesive component. The idea is based on presentations by Ting et al. (1983) and Goughnour and Andersland (1968) which suggest different mechanisms for different ice contents. The parameters to select are the effective angle of friction ϕ', representing the structural hindrance of the mass of the soil particles, and the cohesion *c,* representing the bonding effect of the ice between the soil particles. The Mohr-Coulomb criterion will be adapted to frozen soils found in warm alpine permafrost. Water in the soil pores changes phase as temperature reaches the freezing point. Four different states can therefore be distinguished (Fig. 1):

(1) In a frozen state, single soil grains may have no contact with other grains in the ice matrix. The soil fraction does not add frictional contribution to the resistance so that only the cohesive component is active. The cohesive component can be described with the variable *c*, which depends on temperature and strain rate.

(2) In a transient process with increasing temperature, the volume of the ice phase decreases allowing for soil grain contacts. This effect causes the formation of a frictional component with a simultaneous decrease of the cohesional bonding effect. No liquid water is present.

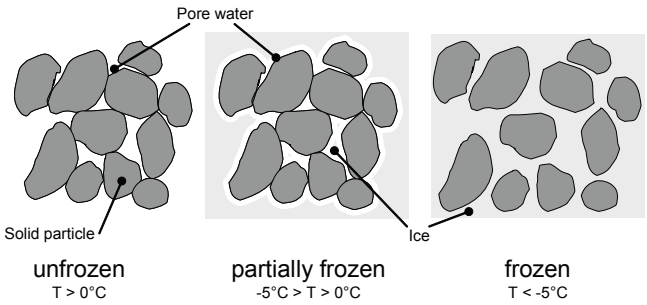

Figure 1. Different states that may be encountered in an alpine permafrost soil.

(3) In a different state, both frozen and unfrozen water are present in parallel in the voids between the particles and on the particle edges. The bonding effect of the ice present in some voids provides a cohesive component *c* to the soil strength, and at the same time the full granular friction can be mobilized.

(4) In the unfrozen state, all pore water is in the liquid phase. The soil behaves as any unfrozen soil. Taking into account the drained long-term behavior of soil, the cohesive component is set to zero; $c = 0$ kPa. Most soils in alpine environments have only little fines, and therefore the assumption of drained conditions is realistic.

The concept will be followed that the drained loading of a completely dry or fully saturated soil will lead to a state where no cohesion appears ($c = 0$ kPa). Unsaturated conditions where significant apparent cohesion can be observed will not be discussed here but are not in contradiction to the described model. It is not the aim to show a material description based on physically manifest relations but to show the potential of the approach.

Literature Review

A brief literature review was performed to complement test results of Arenson et al. (2004) and Arenson and Springman (2005a, 2005b) and to enlarge the database of known shear strength parameters of frozen soils in order to increase confidence in the proposed interpretation of the Mohr-Coulomb model. They conducted a series of triaxial compression tests on undisturbed permafrost soil samples, including controlled temperature and volumetric ice content ,together with an interpretation of the test results towards a definition of an effective angle of internal friction ϕ' and cohesion *c*. From the test series it can be observed that the effective angle of internal friction decreases with the volumetric ice content, whereas the cohesion increases (Fig. 2).

One of the key parameters for describing a warm permafrost soil in order to assess the shear strength is the unfrozen water content, hence the volumetric ice content w_i. These relationships are unique for each individual soil and control the attribution of the effective angle of internal friction ϕ' and cohesion *c*. The effective angle of internal friction ϕ' at a temperature $T > 0$°C defines the initial conditions for the decrease.

In addition, the strength of the ice is temperature dependent. Therefore it is important to quantify the effective angle of internal friction, the cohesion at a given volumetric ice content in function of the temperature or vice versa for each frozen soil individually. This can be done with temperature controlled triaxial or simple shear tests. However, due to practical difficulties, such tests are rarely carried out in practice, and only limited data are available for comparison.

As for temperature colder than about -5°C, results of unconfined compression tests on frozen soil and ice samples are presented in the literature, from which the uniaxial strength and therefore cohesion can be derived. However no information about the effective angle of internal friction ϕ' can be derived. At the given temperatures it can be assumed that all the water is frozen for all sandy and silty soils. The samples are mostly not tested at temperatures above 0°C, therefore no information about the effective angle of internal friction ϕ' is available.

Some tests on sand (e.g., Tsytovich 1975) can be interpreted to define both effective angle of internal friction and cohesion with defined temperature, whereas the volumetric ice content is not shown explicitly. The calculated cohesion *c* of the samples tested at temperatures above 0°C indicates an unsaturated state, but information about saturation is not available.

Ladanyi (1990) shows tests with a measured unfrozen angle of effective friction of ϕ' = 35°. The frozen sand samples were tested at temperatures below and equal to -5°C. At these temperatures all the pore water is basically frozen. The effective angle of friction is assumed to be negligible at this stage.

Goughnour and Andersland (1968), Sego et al. (1982), as well as Sego and Chernenko (1984) present additional values for triaxial compression strength of frozen sands at low

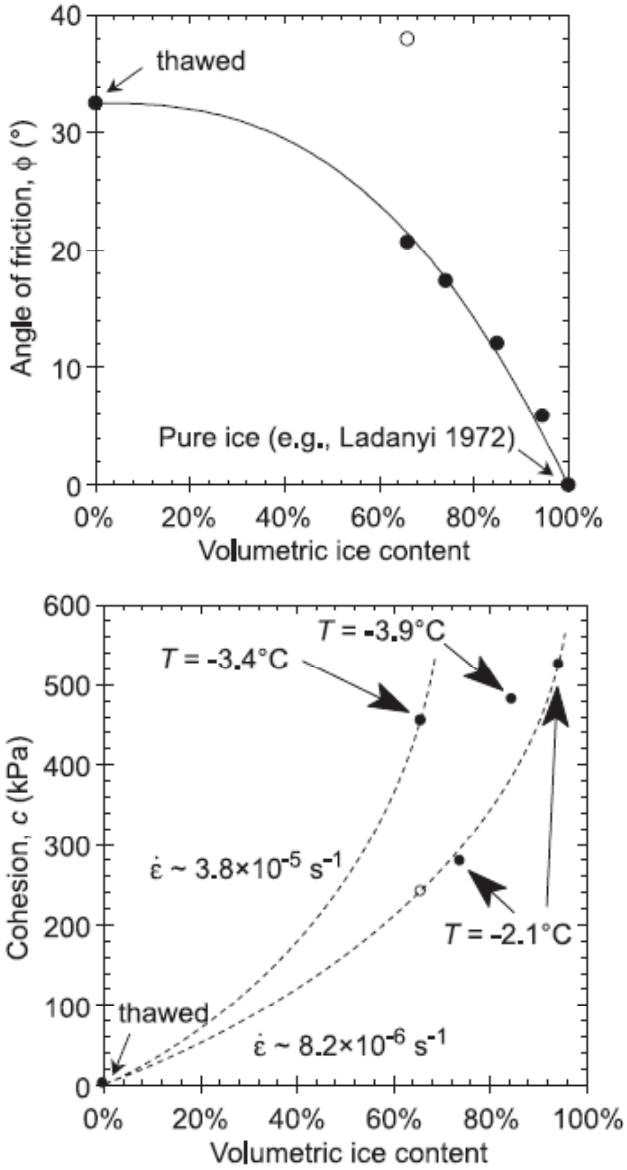

Figure 2. Effective angle of internal friction ϕ' and cohesion *c* as function of the volumetric ice content (Arenson & Springman 2005b).

temperatures. Hivon and Sego (1995), Sego and Chernenko (1984), Sego et al. (1982) and Stuckert and Mahar (1984) take into account the impact of salinity on the strength parameters of frozen soils. However, for comparison, tests were carried out on non-saline samples.

Yuanlin and Carbee (1984) have conducted unconfined compression tests with a constant strain rate and a variation of temperature on frozen silts. The effective angle of internal friction at temperatures above 0°C is not known and assumed to be in the order of ϕ'_{cv} =,32°, which is reasonable for a silty soils. No information about the volumetric ice content is provided. It was assumed that the samples are completely frozen at T = -5°C. The same is true for the results published by Stuckert and Mahar (1984).

In summary, the number of available test data from triaxial compression testing on frozen soils compared to

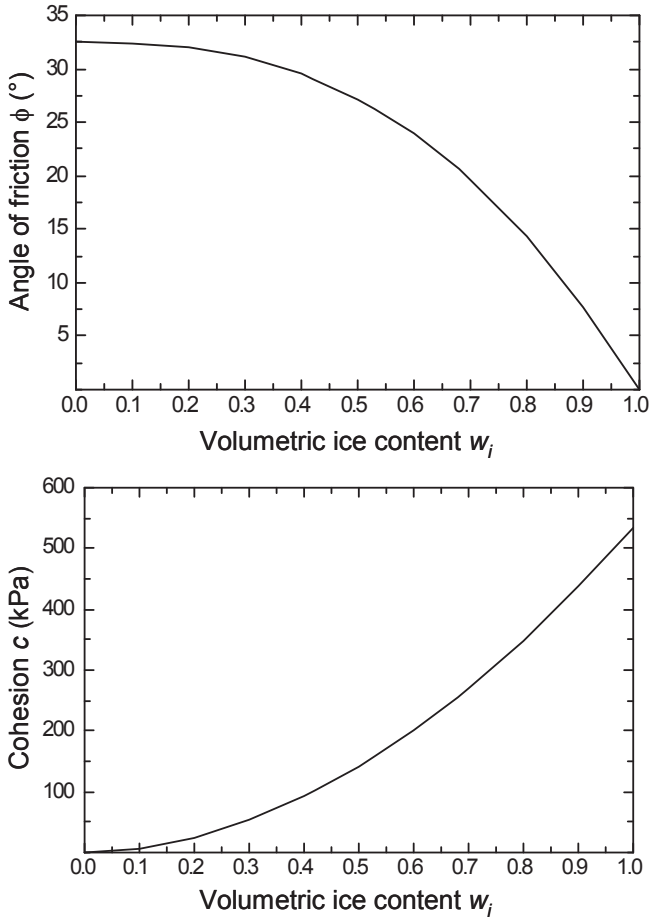

Figure 3. Effective angle of internal friction ϕ' and cohesion c as a function of the volumetric ice content w_i for $\phi'_{initial}$=32°. ϕ' and c are calculated according Equations 1 and 3, respectively.

the number of unconfined compression tests is very limited. In consequence the aim of adding test results to the data produced by Arenson (2005a) was not successful. This reduces the statistical base for the proposed interpretation of the Mohr-Coulomb failure criterion, but nevertheless the concept is worth being followed.

Model

Because of the limited test data available, the approach presented is mainly based and fitted to the data of Arenson and Springman (2005a). The test results have been reevaluated in respect of the two main components of shear strength, i.e. the effective angle of internal friction ϕ' and the cohesion c, as well as for the volumetric ice content w_i and the temperature T. With the given database it was appropriate to normalize the results for a specific temperature and then give a correlation for alternative temperatures. All the relations are curve fits with power law.

As a first input variable the effective angle of internal friction ϕ' of the dry or saturated unfrozen material is needed. For design purposes it is suggested to neglect the dilatancy effects (ψ=0). Unfortunately it is not explicitly stated if a critical, constant volume angle of internal friction, ϕ'_{cv}, or a peak value, ϕ'_{peak}, is presented for most publications where an unfrozen effective angle of internal friction is available.

With increasing volumetric ice content the effective angle of internal friction ϕ' decreases from $\phi'=\phi'_{initial}$ to ϕ'=0. Arenson and Springman (2005b) suggest the following relationship:

$$\phi' = \phi'_{initial} - \phi'_{initial} \bullet w_i^{2.6} \quad (1)$$

with

ϕ' (°)	effective angle of internal friction,
$\phi'_{initial}$ (°)	initial effective angle of internal friction,
w_i (-)	volumetric ice content.

It is important to note that the angle of internal friction is unaffected by the temperature.

The second input variable is the cohesion c (here not defined as effective or total cohesion). In contrast to the effective angle of internal friction ϕ', the value of cohesion rises with the volumetric ice content w_i. The cohesive strength of the ice matrix is dependent on the temperature represented by two steps of calculation. Firstly the cohesive strength will be calculated for a reference temperature (e.g. -2.1°C) to relate the calculated values to Arenson and Springman (2005b). Secondly cohesion is adapted to any given temperature with a linear correlation. The formulas are given with:

$$c_{(T=-2.1°C)} = 534.93kPa \bullet w_i^{1.91} \quad (2)$$

$$c = -\frac{c_{(T=-2.1°C)}}{2.1} \bullet T \quad (3)$$

with

c (T = -2.1°C) (kPa)	cohesion at reference temperature,
c (kPa)	cohesion,
T (°C)	temperature.

Using these two formulae (Fig. 3) it is possible to set individual strength profiles to a soil stratum for any given temperature profile according to the initial effective angle of internal friction ϕ' and the volumetric ice content w_i of the material. It is now obvious that with the variation of the soil temperature profile provoked by seasonal change of the surface temperature, a redistribution of the strength parameters occurs with time. With higher soil temperatures the frictional component of the shear strength gains importance and vice versa.

The correlations were counterchecked with the few test results described in the literature review section. Effects of the variation of the strain rate are not discussed within this contribution. The significance of the strain rate rises with the volumetric ice content of the sample, whereas the aim of the parameterization is the description of the behavior of temperate alpine permafrost soils; that is, close to zero centigrade. Where not explicitly described, the volumetric ice content w_i was calculated using a power law function neglecting exact knowledge of the soil composition and volumetric water content. The function was chosen as

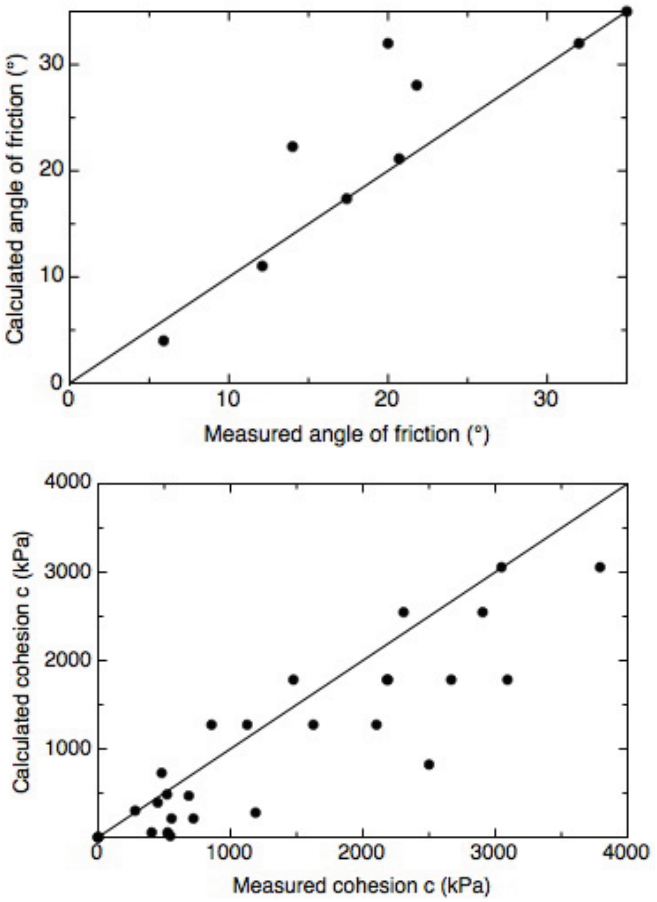

Figure 4. Calculated versus measured angle of friction ϕ' and calculated versus measured values for cohesion *c*.

$$w_i = \left(-\frac{1}{5} \bullet T \right)^{\frac{1}{2}} \quad (4)$$

Equation 4 is based on test results available and has similar form to the unfrozen water content function suggested by Tice et al. (1976). It further inherits the assumption that all soils are completely frozen at T = -5°C. This seems low but includes the variability in the permafrost soil composition even concerning certain clay size particle contents. Such an assumption is on the conservative side.

Figure 4 shows the measured against the calculated values obtained with the proposed strength model. In these figures all the evaluated data is shown, even though some of the tests were conducted at temperatures below to T = -5°C. The inserted diagonal line represents the ideal case of *calculated=measured* values.

The linear correlation with an inclination of 1.1, instead of the drawn ideal line of 1.0 (R^2=0.77) for the effective angle of internal friction ϕ' (Fig. 4), indicates an overestimation of the calculated values, whereas an inclination of 0.8 (R^2=0.80) stands for a more conservative prediction for the cohesion. Some of the scatter can be explained with the variation of the strain rates that have not been considered in the analysis presented.

Table 1 shows the evaluated data for the tests and calculations on material with a temperature T above -5°C.

Table 1. Measured against calculated strength properties of frozen soils.

T °C	w_i -	$\phi'_{measured}$ °	$\phi'_{calculated}$ °	$c_{measured}$ kPa	$c_{calculated}$ kPa	Authors -
-2.1	1.0	5.9	4.0	520	485	A. & S. 2005
-3.9	0.9	12.1	11.0	480	728	
-2.1	0.7	17.4	17.4	280	301	
-3.4	0.7	20.7	21.1	450	392	
		32.0	32.0	0	0	
-1.0	0.5	21.8	28.1	525	55	T. 1975
-2.0	0.6	14.0	22.3	720	212	
		20.0	32.0	0	0	
		35.0	35.0	0	0	L. 1990
-5.0	1.0			1126	1274	
-5.0	1.0			1626	1274	H.&S. 1995
-2.3	0.7			1190	279	
-5.0	1.0			2103	1274	S. &M. 1984
-4.0	0.9			2500	823	G. & A. 1968
-0.5	0.3			545	14	Y. & C. 1984
-1.0	0.5			405	55	
-2.0	0.6			555	212	
-3.0	0.8			685	469	
-5.0	1.0			857	1274	

Example Application

To get a brief overview on the impact of a temperature dependent parameterization of an alpine permafrost soil, a profile from the Muragl rock glacier in Switzerland was chosen for a limit equilibrium analysis using the numerical program Slope/W (GeoStudio2004). Even though rock glacier materials represent special and unique conditions, the concept can be applied to any other frozen soil, assuming soil properties are available. Details and an overview of the Muragl rock glacier can be found in Arenson (2002). The modeled slope has a length of approximately 500 m and a height of approximately 235 m, which results in an overall inclination of about 25°. Bedrock can be found at an average depth of 33 m.

Two measured temperature profiles were applied on the section with a temperature resolution of ΔT = 1.0°C and a geometrical resolution of Δy = 0.5 m. The profiles represent typical conditions with the first temperature profile representing the summer maximum surface air temperature of 12.2°C and the second, the winter minimum surface air temperature of -6.0°C from a one year measurement cycle (Fig. 5). The two states do not implicitly represent coldest or warmest conditions for the interpretation of a global safety factor.

The geotechnical parameters have been set on the basis described above with a resolution according to the temperature profile. The initial effective angle of internal friction was set to ϕ' = 33°, and bedrock was assumed to be impenetrable by a failure mechanism. The limit equilibrium approach follows the Morgenstern-Price method. Neither water flow nor possible unsaturated strength in the unfrozen active layer has been accounted for during the analysis.

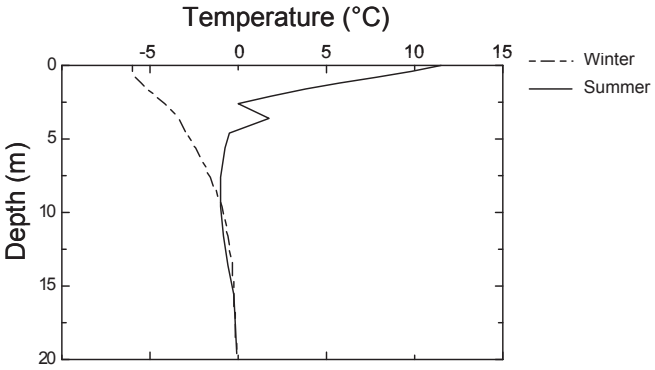

Figure 5. Temperature profile from borehole measurement on the Muragl rock glacier.

Table 2. Data of the temperature profile show in Figure 5.

Y	T_{winter}	T_{summer}
m	°C	°C
0.0	-6.0	11.6
0.4	-6.0	9.8
0.8	-5.8	7.8
1.2	-5.5	5.7
1.6	-5.2	3.9
2.1	-4.7	1.8
2.6	-4.2	0.0
3.6	-3.4	1.8
4.6	-2.9	-0.5
5.6	-2.4	-0.7
7.6	-1.5	-1.0
9.6	-0.9	-1.0
11.6	-0.5	-0.8
13.6	-0.3	-0.6
15.6	-0.2	-0.2
19.6	-0.1	-0.1

Table 3 shows the parameters for each temperature layer. The correlations follow the rules presented above.

Figures 6 and 7 show the results of the limit equilibrium calculations on the Muragl rock glacier cross sections.

The global factor of safety varies between 1.22 and 1.48 from summer to winter, which is a change of 21%. The calculated critical mechanisms show significant differences in size and depth. This is due to the difference in the contribution of friction and cohesion to the global shear resistance. An increase in the frictional component of the shear resistance causes the failure mechanism to shift towards the surface, whereas an increase in cohesion results in a deeper lying failure surface.

These preliminary analyses show minimum safety factors relatively close to a critical value of 1. However, such a result is expected for slopes that form under natural conditions. Nevertheless, the results allow for the possibility of large deformations. It is interesting to note that the failure planes for the winter conditions (Fig. 7) are located approximately at similar depths than the shear zone observed in the active Muragl rock glacier (Arenson et al. 2002). These deformations may therefore be interpreted as the main deformation mechanism observed in active rock glaciers

Table 3. Input parameter for limit equilibrium analysis.

$\phi'_{initial}$	T	w_i	ϕ'	$c'_{(-2.1°C)}$	c
°	°C	-	°	kPa	kPa
33	-5.5	1	0	535	1401
33	-4.5	0.95	4	484	1037
33	-3.5	0.84	12	381	634
33	-2.5	0.71	20	276	329
33	-1.5	0.55	26	169	121
33	-0.5	0.32	31	59	14
33	0 +	0	33	0	0

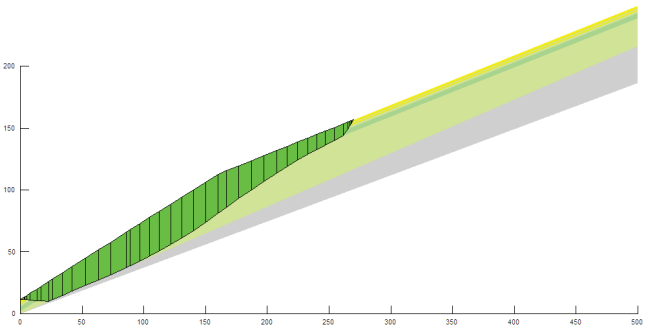

Figure 6. Failure mechanism for a summer temperature profile with a global factor of safety of 1.22.

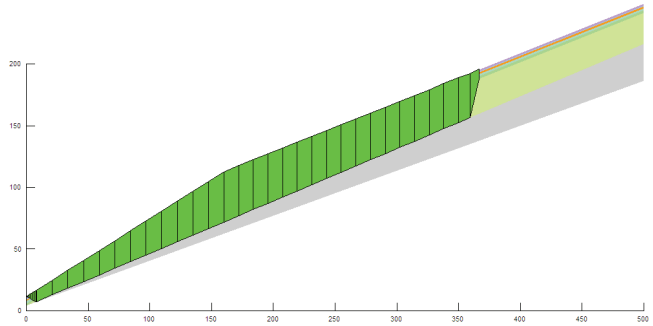

Figure 7. Failure mechanism for a winter temperature profile with a global factor of safety of 1.48.

referred to as creep. Creep is not considered directly during the stability analysis presented. The parameters included in the analysis were chosen as large strain parameters, i.e. large creep deformations are included to a certain extent.

Conclusions

Engineers often struggle with assessing slope stability for temperate frozen slopes. By selecting the appropriate shear strength parameters it is possible to give realistic temperature dependent assessment of the stability of alpine permafrost slopes. A simple approach is presented to incorporate seasonal temperature changes, allowing calculation of slope stabilities in an environment of temperature increase due to global warming. In such a case the model proposes an increasing contribution of the friction component and a decreasing amount of cohesion in the mobilization of shear strength. This leads towards shallower failure surfaces with a lower probability of failure, due to the fact that the angle of effective friction is far less subjected to variability than

the cohesive portion of the general shear resistance. In a transient process alpine permafrost slopes with inclinations higher than the sum of the effective angle of friction ϕ'_{cv} and the angle of dilatancy ψ will be subjected to local failures due to the decrease of the bonding effect of the ice matrix. After reaching a new long-term equilibrium the former alpine permafrost slopes will reach a state as observed for the majority of natural slopes with an inclination at about the effective angle of friction.

The major problem with using the presented approach for warm frozen slopes is the lack of test data. Even though results from triaxial compression are standard in geotechnical engineering, only a few data are available for temperate coarse-grained permafrost soils. In addition, it is recommended that interaction between thermal modeling and slope stability calculations utilizing temperature dependent strength parameters should be employed in slope stability analysis. As such numerical tools become available it is still crucial to carry out proper geotechnical laboratory tests for an accurate soil characterization.

Acknowledgments

The authors would like to thank the two anonymous reviewers for their valuable comments on the initial version of the manuscript.

References

Arenson, L.U. 2002. *Unstable Alpine Permafrost: a Potentially Important Natural Hazard*. Ph.D. Dissertation. Institute for Geotechnical Engineering Technische Wissenschaften ETH, Zurich.

Arenson, L.U., Hoelzle, M. & Springman, S.M. 2002. Borehole deformation measurements and internal structure of some rock glaciers in Switzerland. *Permafrost and Periglacial Processes* 13: 117-135.

Arenson, L.U., Johansen, M.M. & Springman, S.M. 2004. Effects of volumetric ice content and strain rate on shear strength under triaxial conditions for frozen soil samples. *Permafrost and Periglacial Process*es 15: 261-271.

Arenson, L.U. & Springman, S.M. 2005a. Triaxial constant stress and constant strain rate tests on ice-rich permafrost samples. *Canadian Geotechnical Journal* 42: 412-430.

Arenson, L.U. & Springman, S.M. 2005b. Mathematical descriptions for the behavior of ice-rich frozen soils at temperatures close to 0°C. *Canadian Geotechnical Journal* 42: 431-442.

Goughnour, R.R. & Andersland, O.B. 1968. Mechanical properties of sand-ice system. *ASCE Journal of the Soil Mechanics and Foundations Division* 94: 923-950.

Hivon, E.G. & Sego, D.C. 1995. Strength of frozen saline soils. *Canadian Geotechnical Journal* 32: 336-354.

Ladanyi, B. & Morel, J.-F. 1990. Effect of internal confinement on compression strength of frozen sand. *Canadian Geotechnical Journal* 27(1): 8-18.

Sego, D.C. & Chernenko, D. 1984. Confining pressure influence on the strength of frozen saline sand. *Cold Regions Engineering Specialty Conference*, *Edmonton, AB*. Montreal: Canadian Society for Civil Engineering, 565-578.

Sego, D.C., Schultz, T. & Banasch, R. 1982. Strength and deformation behavior of frozen saline sand. *3rd International Symposium on Ground Freezing*. Hanover, NH: 11-17.

Stuckert, B. & Mahar, L. 1984. Role of ice content in the strength of frozen saline coarse grained soils. Proceedings, *Cold Regions Engineering Specialty Conference*, *Edmonton, AB*. Montreal: Canadian Society for Civil Engineering, 579-587.

Tice, A.R., Anderson, D.M. & Banin, A. 1976. *The Prediction of Unfrozen Water Contents in Frozen Soils from Liquid Limit Determinations*. CRREL Report 76-8. Hanover, NH.

Tsytovich, N.A. 1975. *The Mechanics of Frozen Ground*. New York, NY: McGraw-Hill Book Company.

Yuanlin, Z. & Carbee, D.L. 1984. Uniaxial compressive strength of frozen silt under constant deformation rates. *Cold Regions Science and Technology* 9: 3-15.

A Permafrost Observatory at Barrow, Alaska: Long-Term Observations of Active-Layer Thickness and Permafrost Temperature

F.E. Nelson, N.I. Shiklomanov, and D.A. Streletskiy
Department of Geography, University of Delaware, Newark, DE, 19716, USA
V.E. Romanovsky and K. Yoshikawa
Geophysical Institute, University of Alaska, Fairbanks, AK, 99775, USA
K.M. Hinkel
Department of Geography, University of Cincinnati, Cincinnati, OH, 45221, USA
J. Brown
International Permafrost Association, P.O. Box 7, Woods Hole, MA, 02543, USA

Abstract

Barrow, Alaska, has a long heritage of permafrost research. The area's initial permafrost temperature measurements were made during the First International Polar Year (1882-83). In the mid 1940s, the U.S. Geological Survey initiated a program of geothermal measurements. In the early 1960s the U.S. Army's Cold Regions Research and Engineering Laboratory established a series of plots for active layer measurements. In the 1990s, National Science Foundation projects expanded the active layer measurement program as part of the emerging Circumpolar Active Layer Monitoring network. A program of borehole temperature measurements was initiated in 2000, when two deep boreholes were drilled and equipped with thermistor cables and data loggers. These sites, located within and adjacent to the Barrow Environmental Observatory, and several other long-term projects on erosion and plant phenology, contribute to this permanent, protected permafrost observatory. Long-term permafrost monitoring programs at Barrow have contributed substantially to development of geocryological theory.

Keywords: active layer; Alaska; Barrow; borehole monitoring; permafrost; thermal regime.

Introduction

The Barrow, Alaska, area has a long history of permafrost observation and research. The initial permafrost temperature observations at Barrow were made during the First International Polar Year (1882–83) in a meat cellar with an average February temperature of -11°C at a depth of 11 m. Beginning in the mid 1940s and continuing into the 1950s, the U.S. Geological Survey (USGS) conducted a wide range of permafrost investigations, including geothermal measurements in many boreholes and shallow measurements in association with construction and exploration activities (Brewer 1958, Lachenbruch & Marshall 1986). In the early 1960s the U.S. Army's Cold Regions Research and Engineering Laboratory (CRREL) established twenty 10×10 m grids on which active layer measurements were made seasonally throughout most of that decade (Brown & Johnson 1965, Brown 1969). Many of these investigations were made in cooperation with, or supported by, the former Naval Arctic Research Laboratory (NARL) in Barrow. Beginning in the early 1990s, a series of National Science Foundation (NSF) projects expanded the active layer measurement program to a 1×1 km grid under what was to become a site within the Circumpolar Active Layer Monitoring (CALM) network. Active layer measurements have been made annually on the CRREL and CALM grids since 1992 (Brown et al. 2000). A program of borehole temperature measurements on the same USGS boreholes was initiated in 2000 and in April 2001. Under this program, two new 50 m deep boreholes were drilled and equipped with thermistor cables, a micrometeorological station, and data loggers (Yoshikawa et al. 2004).

The CALM grids and the deep permafrost observatory boreholes are located within the Barrow Environmental Observatory (BEO), 7500 acres of privately owned land that has been designated for research and long-term observations by the Ukpeagvik Iñupiat Corporation (UIC) landowners and the regional North Slope Borough government (Fig. 1). Several other long-term observational projects are located within the BEO, including the Arctic Coastal Dynamics key sites along Elson Lagoon (Aquirre et al. 2008), and the International Tundra Experiment located within the CALM grid (Hollister et al. 2006, 2008).

The initiatives mentioned above are approved projects of the present International Polar Year (2007–2009). The International Permafrost Association's legacy for the IPY is to establish a permanent network of permafrost observatories on protected lands. The Barrow permafrost observatory is an excellent example of a long-term monitoring site. It is also part of the Global Terrestrial Network for Permafrost (GTN-P) (Brown et al. 2000). As a follow-up to the First International Polar Year measurements, temperatures are being monitored with miniature data loggers in several active meat cellars in the Barrow communities.

Earlier papers by the present authors have reported on previous results for these active layer and permafrost temperature sites (Nelson et al. 1998, Romanovsky et al.

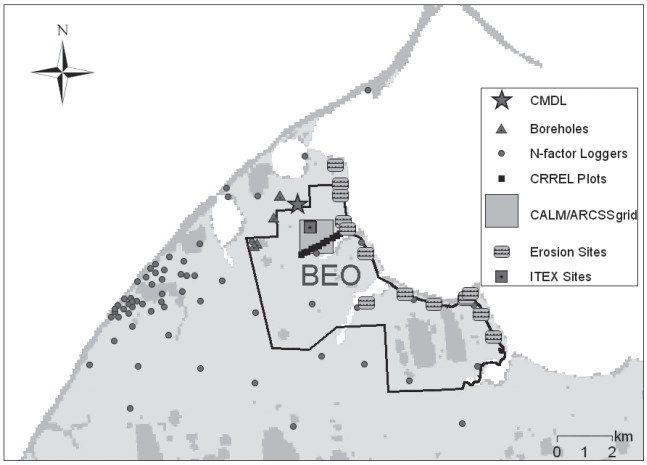

Figure 1. Map of the Barrow Environmental Observatory, showing main research sites mentioned in the text.

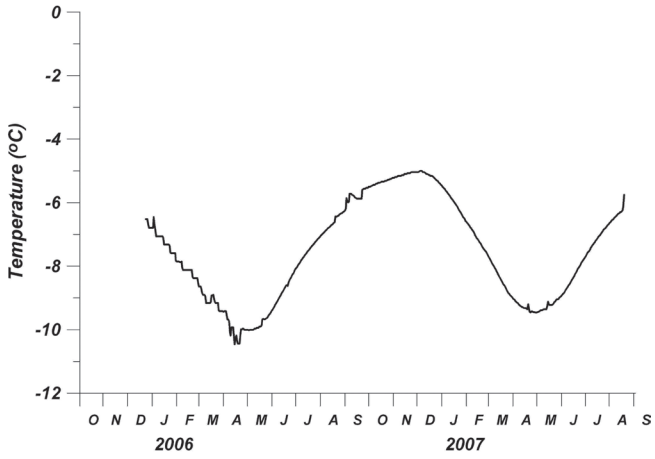

Figure 2. Temperature (hourly readings) in the meat cellar of a Barrow resident (Richard Glenn), from late 2005 through summer 2007. Instrumentation was changed in March 2006.

2002, Hinkel & Nelson 2003, Yoshikawa et al. 2004). This paper updates the earlier results from continuing projects, adds to their interpretations, and documents the existence of this permafrost observatory. A complete history of permafrost research at Barrow remains to be written.

Local Environment

Barrow, Alaska (71.3°N, 156.5°W, population 4600) is situated at the confluence of the Beaufort and Chuckchi Seas. Although Barrow's climate is influenced by its proximity to the Arctic Ocean, mean annual temperature in the village is -12°C, and the annual range of mean monthly temperature is about 31°C. Precipitation averages 106 mm yr^{-1}, with about 63% falling as rain during the brief summer. Topography is dominantly level, the area's primary relief being produced by the juxtaposition of drained thaw lakes and intervening "upland" tundra (Hinkel et al. 2005). Soils, developed on the unconsolidated Gubik Formation of Late Pleistocene age (Black 1964), show considerable variation (Bockheim et al. 2001). Permafrost underlies the entire area and reaches depths of more than 400 m. The upper permafrost contains abundant excess ice, with combined pore and lens ice averaging 50-75% in the upper 2 m (Sellmann et al. 1975). Ice-wedge networks are ubiquitous in the Barrow area.

Data Collection

The Circumpolar Active Layer Monitoring (CALM) program has operated in Barrow since 1991. Initially developed under the auspices of the International Tundra Experiment (ITEX), CALM acquired its own funding base from the U.S. National Science Foundation in 1998. The CALM protocol is well documented in published papers and on the CALM web site (Brown et al. 2000, Nelson et al. 2004a, 2004b; <http://www.udel.edu/ Geography/calm/>). At Barrow, thaw depth is measured at each of the 121 grid nodes on the CALM/ARCSS 1 km^2 grid; nodes are spaced 100 m apart. Using a graduated steel probe, thaw depth measurements are typically made in mid-August, when the active layer is at its maximum thickness. Active-layer thickness data continue to be collected annually on the 10×10 m "CRREL Plots" established in the early 1960s (Brown & Johnson 1965, Brown 1969).

Soil temperatures have been monitored hourly since 1993 at two sites near the CRREL study area. Measurements are recorded to depths of 1.2 m using Campbell data loggers reading Measurement Research Corporation (MRC) thermistor probes, and yield data comparable to those obtained during CRREL's programs at Barrow in the early 1960s. Several other shallow (0.0 to 1.2 m) ground temperature installations are maintained in cooperation with the U.S. Department of Agriculture's Natural Resources Conservation Service and the National Oceanic and Atmospheric Administration.

High-precision frost heave and thaw settlement measurements are made on the BEO using differential global positioning system (DGPS) technology (Little et al. 2003). Several of the former CRREL sites are monitored via DGPS, as is a series of nearby geomorphic forms, primarily frost boils. These observations continue a series of measurements first implemented at Barrow in the early 1960s (Lewellen 1972).

As part of the International Polar Year 2007–2008 initiative, the program of thermal measurements in Barrow meat cellars, first instituted in 1882-83 (Ray 1885), has been resumed. Data are recorded in the meat cellars of several Barrow residents at 1 hr intervals, using miniature two-channel data loggers (Fig. 2). Peak annual temperature lags several months after its July peak in the Barrow air-temperature record. Temperature is recorded at a depth of approximately 7 m in the cellar.

Snow surveys are conducted each spring by measuring snow depth at the 121 grid nodes on the 1 km^2 CALM/ARCSS grid. Typically, two measurements are made at each grid node using a graduated steel probe. Snow depth measurements are made in April or May.

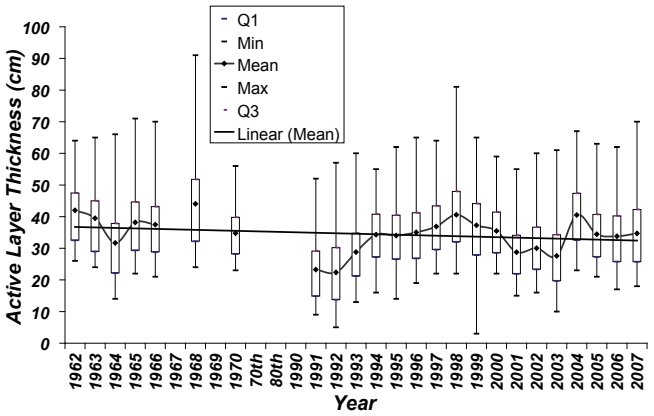

Figure 3. Box plots (Tukey 1977) of active-layer thickness on the CRREL plots at Barrow for the period 1962–2007. Maximum, minimum, and mean values are indicated, as are quartile (Q) locations and a linear fit to annual mean values.

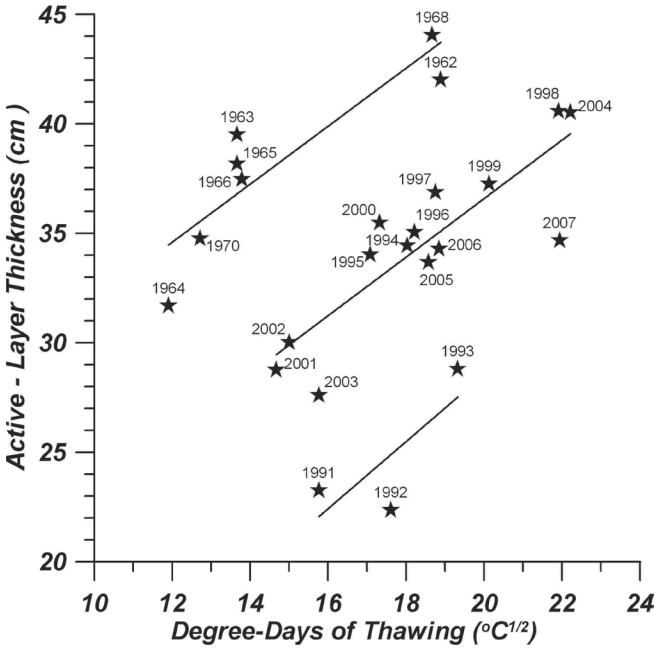

Figure 4. Active-layer thickness vs. thawing index at Barrow, Alaska, 1962–2007.

Four boreholes are being monitored under the Thermal State of Permafrost (TSP) program (Romanovsky et al. 2002), using Campbell data loggers. Two boreholes are the original USGS holes (Lachenbruch & Marshall 1986), with new cables and the two new ones were drilled in 2001. New thermistor cables were installed in several of the 1950s USGS boreholes to depths of 9, 14, and 24 m.

Long-term air-temperature measurements began at the National Weather Service site in Barrow in 1922, and data from this ongoing program are available through the archives of the U. S. National Climate Data Center (<http://www.ncdc.noaa.gov/oa/ncdc.html>). A geographic-ally extensive data set was also collected at hourly intervals between 2001 and 2005 within a 150 km^2 area surrounding Barrow, including sites within the BEO, using a network of approximately 70 data loggers recording air and near-surface soil temperature, as part of the Barrow Urban Heat Island Study (Hinkel et al. 2003; Hinkel & Nelson 2007).

Data from NSF-supported sites are reported annually to the University Consortium for Atmospheric Research, and are ultimately deposited in the National Snow and Ice Data Center's Frozen Ground Data Center (<http://nsidc.org/fgdc/>). Data sets are made available periodically on CDs issued by the Global Geocryological Data system (Parsons et al. 2008). CALM data are also available through the CALM program's web site at the University of Delaware.

Results

Active layer

For the last decade (1998–2007), CALM active-layer thickness (ALT) data, averaged over the grid, have remained close to the range of values from the 1960s (Fig. 3). ALT values in the early 1990s were substantially less than in the 1960s and early 2000s. Maximum values were recorded in 1998 and 2004 (42 cm); these values coincide with the warmest summers. The 2003 minimum (29 cm) was similar to 1993 but deeper than the shallowest thaws of 1991 and 1993 (24 cm).

Based on statistical analysis of ALT values from the Barrow CRREL plots, Nelson et al. (1998) argued that the active layer in ice-rich terrain displays "Markovian behavior," i.e., it tends to remain within a tightly constrained range of depths until a climatic, anthropogenic, or other perturbation causes it to shift to a new datum, where it remains until another perturbation causes it to become "set" at another new level (Fig. 4).

Average active-layer thickness from the Barrow CRREL plots is plotted against the square root of the thawing index (annual thawing degree days) for all years of record in Figure 4. The additional data collected over the past decade appear to confirm the hypothesis advanced by Nelson et al. (1998). Three distinct curves have emerged, each consisting of a series of sequential years.

Nelson et al. (1998) advanced a series of hypotheses to explain the apparently sudden changes in ALT, concluding that they most likely result from penetration of thaw into the ice-rich layer in the upper permafrost. Subsequently, Shur et al. (2005) provided a theoretical explanation for such behavior, involving the "transient layer," an intermediate layer of ground that cycles between permafrost and non-permafrost status at decadal to millennial time scales. Bockheim & Hinkel (2005) found abundant cryostratigraphic evidence for fluctuations in the transient layer ("transition zone") in the Barrow area.

Thaw settlement

The transient layer concept advanced by Shur et al. (2005) also helps to explain why data from mechanical probing of the active layer may not show long-term correspondence with climatic warming. Penetration of thaw into or through the transient layer can result in pronounced differential

settlement at the surface. Besides jeopardizing structures at the surface, this phenomenon may obscure the record of climate-induced changes in ice-rich permafrost environments (Streletskiy et al. 2008).

The Barrow site was used to evaluate long-term trends in terrain first surveyed in the early 1960s (Lewellen 1972). DGPS and ALT measurements were performed in June and August of every year for the period 2001–2006. All sites were equipped with temperature loggers measuring air and ground surface temperature at hourly intervals. Winter heave (Hw) was assumed as the difference in elevation of the ground surface between June of a specified year and August of the previous year. Summer subsidence (Hs) was estimated as the difference in ground surface elevation between August and June of the same year.

On average, winter heave did not compensate for summer ground subsidence at most of the North Slope landscapes investigated during the 2001–2006 observation period (Streletskiy et al. 2008). Comparison of our data at Barrow with the historical record there (Lewellen 1972) shows that significant changes in the elevation of the ground surface have occurred over the past four decades. The survey of 1964 was made in July, while our measurements were made in June and August. Comparison of elevation data from August of 2006 with those from July of 1964 shows that total elevation change (Ht) for three sites is -21.4 to -23.6 cm, while one site shows Ht = 30.6 cm. This produces an average value of -8.9 cm in 42 years, or -0.2 cm/year. Comparison of the July 1964 data with those from June of 2006 yields an average for the four sites of -6.2 cm or -0.15 cm/year. Average Hs over the last four years at the four sites is -2.2 cm, while Hw is 1.4 cm, The average elevation change at the four sites between June of 2006 and June 2003 is 1.1 cm, while the difference between August elevations for the same period is -7 cm. Long term subsidence and frost heave almost compensate for each other, while over the short term the amplitude of both Hs and Hw varied greatly. Long-term ground elevation change is less than that over the short term. The amplitude of surface elevation changes may, however, have increased during the last 40 years.

Interpolation/validation procedures

Owing to logistical constraints, "end-of-season" active-layer thickness is measured on a different date virtually every year. Variations in year-to-year weather dictate that the active layer may not have reached its maximum extent in late August in some years, while in other years upfreezing from the base of the active layer may have begun by this time. In both situations an underestimate of maximum ALT is obtained. Figure 5 shows results from a form of interpolation, used to describe the dynamics of thaw penetration at Barrow by comparing data derived from two techniques for measuring ALT: direct measurements using a metal probe at the CRREL plots and those interpolated from MRC temperature probes. Only summers in which ALT was measured more than three times were used (1963, 1964, 1966, 1994, and 2004). The polynomial fit is based on 42 sets of measurements from these years, where maximum thaw depth was assumed to have been reached. An independent data set, measured at the neighboring 1 km^2 CALM grid (BRW ARCSS), was included (years 1995, 1996, 2001, and 2006); these were also believed to show maximum thaw. Finally, daily interpolated values of ALT from the MRC probes for 1993-2001 period (BRW MRC) were plotted. Despite differences in measurement techniques, sampling design and date of observation, the points fall very close to the fit produced from the Barrow CRREL plots (BRW CRREL). This procedure accounts for about 80% of the variation in thaw depth at the Barrow sites. This technique, based on Pavlov's (1984) methodology, can be used to estimate percent of thaw penetration on a particular day of the year or to adjust a measured thaw depth to maximum ALT (Streletskiy et al. 2008).

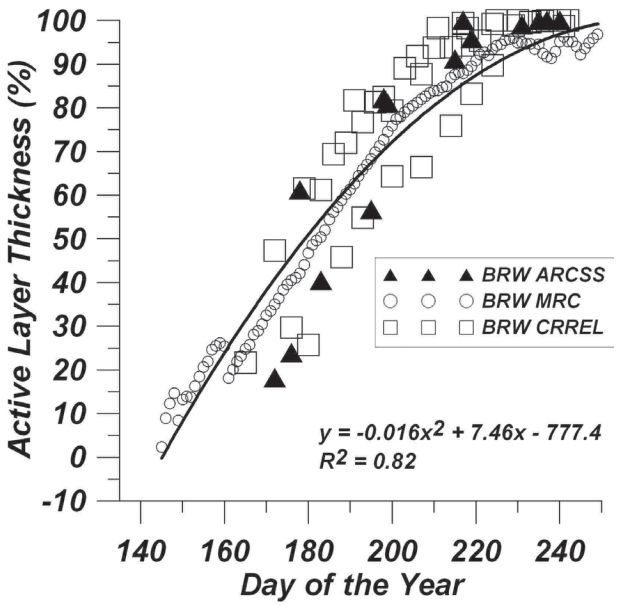

Figure 5. Active-layer depth measurements from the CALM grid, CRREL plots, and nearby Campbell/MRC installation. Statistical relation in the figure were obtained by fitting a polynomial to the probed data. The solid line was produced by fitting a polynomial equation to the MRC data, yielding an R^2 value of 0.96.

Permafrost temperature

Figure 6 shows permafrost temperatures from the several newly instrumented boreholes. The upper graph shows the first year's results for the new 50 m borehole. The lower graph compares the 1950 annual profile with current measurements. These initial results, for this specific site at the 14 m depth, indicate warming of about 1.2°C. This small increase over such a long period is consistent with a previous analysis of long-term permafrost temperature variations at Barrow for the period 1924–1997 (Romanovsky et al. 2002).

Those results implied that the observed 1.2°C difference at 14 meters in permafrost temperatures between 1950 and current temperatures is due to very recent warming during the late 1990s. Much colder permafrost temperatures at the permafrost table (up to 2 to 3°C colder) were typical for Barrow during the 1970s.

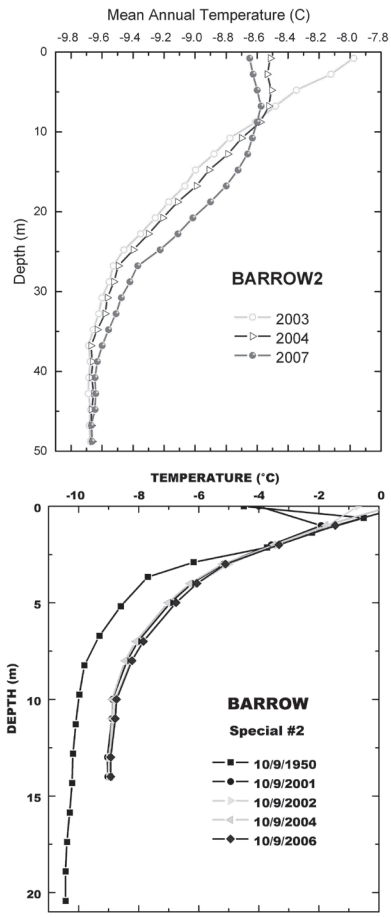

Figure 6. Upper: Annual permafrost temperatures at the new North Meadow Lake permafrost observatory, Barrow, Alaska. Lower: Comparison of 1950 and 2000s permafrost temperatures at the nearby Special 2 site.

Conclusions

Barrow has served as a permafrost observatory for more than a century, and the geocryological data record produced in the Barrow vicinity is unrivaled in Alaska in terms of length, diversity, and depth. The Barrow area played host to many pioneering studies on the roles that permafrost plays in global-change science, and the BEO continues to provide data important to those efforts. Because the Barrow Environmental Observatory is adjacent to an urbanized area there is abundant opportunity for local applications of the information obtained within BEO confines. The village of Barrow generates a significant urban heat-island effect (Hinkel et al. 2003, Hinkel & Nelson 2007), and the BEO is therefore an excellent location to attempt discernment between the geocryological impacts of anthropogenic factors and climatic variations (Nelson, 2003).

Barrow's geocryological data records illustrate the importance and effectiveness of sustained, well-organized monitoring efforts supported by adequate logistical arrangements. Sustained monitoring programs contribute much to the often subtle interplay between theory, application, and observation. Monitoring programs can reveal relationships that become apparent only decades after measurement programs are begun.

Acknowledgments

The permafrost investigations described in this paper were carried out within the Barrow Environmental Observatory, private land designated for research and long-term observation by the Ukpeagvik Iñupiat Corporation (UIC). The Barrow Arctic Science Consortium (BASC), a not-for-profit organization dedicated to scientist/community collaboration, was designated by UIC to manage the BEO with support from the U.S. National Science Foundation. We are grateful to both UIC and BASC for the opportunity to establish and maintain these observatories. Individual projects are supported by NSF grants in support of CALM (OPP-9732051 to the University of Cincinnati and OPP-0352958 to the University of Delaware) and TSP (ARC-0632400 and ARC-0520578 to the University of Alaska Fairbanks). Opinions, findings, conclusions, and recommendations expressed in this paper are those of the authors, and do not necessarily reflect the views of the National Science Foundation. We are grateful to four anonymous reviewers for criticism and suggestions that led to significant improvements in this paper. This paper is a contribution to both the present International Polar Year, and to the Permafrost Young Researchers Network (PYRN) through the efforts of the junior author (DAS).

References

Aguirre, A. et al. 2008. Erosion of the Barrow Environmental Observatory coastline 2003-2008, northern Alaska. (*this proceedings*).

Black, R.F. 1964. Gubik Formation of Quaternary age in northern Alaska. *U. S. Geological Survey Professional Paper302-C*: 59-91.

Bockheim, J.G. & Hinkel, K.M. 2005. Characteristic and significance of the transition zone in drained thaw lake basins of the Arctic Coastal Plain. *Arctic* 58: 406-417.

Bockheim, J.G., Hinkel, K.M. & Nelson, F.E. 2001. Soils of the Barrow region, Alaska. *Polar Geography* 25(3): 163-181.

Brewer, M.C. 1958. Some Results of Geothermal Investigations of Permafrost in Northern Alaska. *Transaction, AGU*, 39, 19-26.

Brown, J. 1969. Soil properties developed on the complex tundra relief of Northern Alaska. *Builetyn Peryglacjalny* 18, 153–167.

Brown, J. 2006. Permafrost and the International Polar Year. *Proceedings of the 13th International Conference: Cold Regions Engineering 2006, Current Practices in Cold Regions Engineering*. July 23-26, 2006, Orono, Maine, 9 pp.

Brown, J, Hinkel, K.M. & Nelson, F.E. 2000. The Circumpolar Active layer Monitoring (CALM) Program: Research Designs and Initial Results. *Polar Geography* 24 (3) 165-258 (published in 2002).

Brown, J. & Johnson, P.L. 1965. Pedo-ecological investigations at Barrow, Alaska. U.S. Army Cold Regions Research and Engineering Laboratory, *CRREL Technical Report 159*, 32 pp.

Brown, J., Jorgenson, M. T., Smith, O.P. & Lee, W. 2003. Long-term rates of erosion and carbon input, Elson Lagoon, Barrow, Alaska. In *ICOP 2003 Permafrost: Proceedings of the 8th International Conference on Permafrost*. M. Phillips, S.M. Springman, and L.U. Arenson, eds.) A.A. Balkema Publishers, Netherlands, 101-106.

Hinkel, K.M., Frohn, R.C., Nelson, F.E., Eisner, W.R., Beck, R.A. & Bockheim, J.G. 2005. Morphometric and spatial analysis of thaw lakes and drained thaw lake basins in the western arctic coastal plain, Alaska. *Permafrost and Periglacial Processes* 16(4): 327-341.

Hinkel, K.M., Nelson, F.E., Shur, Y., Brown, J. & Everett, K.R. 1996. Temporal changes in moisture content of the active layer and near-surface permafrost at Barrow, Alaska, U.S.A., 1962-1994, *Arctic and Alpine Research* 28(3): 300-310.

Hinkel, K.M., Nelson, F.E., Klene, A.E & Bell, J.H. 2003. The urban heat island in winter at Barrow, Alaska. *International Journal of Climatology*, 23, 1889-1905.

Hinkel, K.M. & Nelson, F.E. 2007. Anthropogenic heat island at Barrow, Alaska, during winter: 2001-2005. *Journal of Geophysical Research-Atmospheres*, 112, D06118, doi:10.1029/2006JD007837.

Hollister, R.D., Webber, P.J., Nelson, F.E. & Tweedie, C. E. 2006. Soil thaw and temperature response to air warming varies by plant community: Results from an open-top chamber experiments in northern Alaska. *Arctic, Antarctic, and Alpine Research* 38(2): 206-215.

Hollister, R.D., Webber, P.J., Slider, R.T., Nelson, F.E. & Tweedie, C.E. 2008. Soil temperature and thaw response to manipulated air temperature and plant cover at Barrow and Atqasuk, Alaska (*this proceedings*).

Lachenbruch, A.H. & Marshall, B.V. 1969. Heat flow in the Arctic. *Arctic* 22: 300-311.

Lachenbruch, A.H. & Marshall, B.V. 1986. Changing climate: Geothermal evidence from permafrost in the Alaskan Arctic *Science* 234: 689-696.

Lewellen, R.I. 1972. *Studies on the Fluvial Environment: Arctic Coastal Plan Province, Northern Alaska* (2 vols.) Palmer, AK: Lewellen Arctic Research.

Little, J., Sandall, H., Walegur, M. & Nelson, F.E. 2003. Application of differential GPS to monitor frost heave and thaw settlement in tundra environments. *Permafrost and Periglacial Processes* 14(4): 349-357.

Nelson, F.E. 2003. (Un)frozen in time. *Science* 299: 1673-1675.

Nelson, F.E. (ed.). 2004. Special Issue: Circumpolar Active Layer Monitoring (CALM) Workshop. *Permafrost and Periglacial Processes* 15(2): 99-188.

Nelson, F.E. (ed.). 2004. Eurasian Contributions to the Circumpolar Active Layer Monitoring (CALM) Workshop. *Polar Geography* 28(4): 253-340.

Nelson, F.E., Outcalt, S.I., Brown, J., Shiklomanov, N.I. & Hinkel, K.M. 1998. Spatial and temporal attributes of the active-layer thickness record, Barrow, Alaska. *Proceedings, Seventh International Conference on Permafrost, 23-27 June 1998, Yellowknife, Canada*, Antoni G. Lewkowicz and Michel Allard (eds.), Universite Laval, Centre d'etudes nordique, Collection Nordicana No. 57, 797-802.

Pavlov, A.V. 1984. *Energy Exchange in Earth's Land-scapes.* Novosibirsk: Nauka, 256 pp. (in Russian).

Parsons, M.A., Romanovsky, V.E., Shiklomanov, N.I. Christiansen, H.H., Overduin, P., Zhang, T., Balks, M. & Brown, J. 2008. Managing permafrost data: Past approaches and future directions (*this proceedings*).

Ray, P.H. (ed.). 1885. *Report of the International Polar Expedition to Point Barrow, Alaska*. Washington, DC: Government Printing Office.

Romanovsky, V.E., Burgess, M., Smith, S, Yoshikawa, K. & Brown, J. 2002. Permafrost temperature records: Indicator of climate change. *Eos* 83 (50): 589, 593-594.

Sellmann, P.V., Brown, J., Lewellen, R.I., McKim, H. & Merry, C. 1975. The classification and geomorphic implications of thaw lakes on the Arctic coastal plain, Alaska. *U. S. Army Cold Regions Research and Engineering Laboratory Research Report 334*.

Shiklomanov, N., Nelson, F.E., Streletskyi, D.A., Hinkel, K.M. & Brown, J. 2008. The Circumpolar Active Layer Monitoring (CALM) program: data collection, management, and dissemination Strategies (*this proceedings*).

Shur, Y., Hinkel, K.M. & Nelson, F.E. 2005. The transient layer: implications for geocryology and global-change science. *Permafrost and Periglacial Processes*, 16(1), 5-17.

Streletskiy, D.A., Shiklomanov, N.I. & Nelson, F.E. 2005. Monitoring of thaw settlement using a differential global position system approach. In: *Proceedings of the Third Russian Conference on Geocryology*, vol. 2, 163-169.

Streletskiy, D., Shiklomanov, N.I., Nelson, F.E. & Klene, A.E. 2008. Long-term active layer and ground surface temperature trends: 12 years of observations at Alaskan CALM sites (*this proceedings*).

Tukey, J. 1977. *Exploratory Data Analysis*. Reading, MA: Addison-Wesley Publishing Company, 499 pp.

Wood, K. & Streletskiy, D.A. 2008. Soil and Permafrost Temperature Data Obtained During the First International Polar Year (*this proceedings*).

Yoshikawa, K., Romanovsky, V., Duxbury, N., Brown, J. & Tsapin, A. 2004. The use of geophysical methods to discriminate between brine layers and freshwater taliks in permafrost regions. *Journal of Glaciology and Geocryology* 26:301-309.

—Plenary Paper—

Decadal Results from the Circumpolar Active Layer Monitoring (CALM) Program

Frederick E. Nelson and Nikolay I. Shiklomanov
Department of Geography, University of Delaware, Newark, DE 19716, USA
Kenneth M. Hinkel
Department of Geography, University of Cincinnati, Cincinnati, OH 48221, USA
Jerry Brown
International Permafrost Association, P.O. Box 7, Woods Hole, MA, 02543, USA

Abstract

The Circumpolar Active Layer Monitoring (CALM) program was established in the early 1990s to observe temporal and spatial variability of active layer thickness, active layer dynamics, near-surface permafrost parameters, and the response of these factors to changes and variations in climatic conditions. The CALM network involves 15 participating countries and is comprised of 168 sites distributed throughout the Arctic, parts of Antarctica, and several mountain ranges of the mid-latitudes. Groups of sites are used to create regional maps of active layer thickness. Data obtained from the network are used to validate permafrost, hydrological, ecological, and climatic models at a variety of geographic scales. Several sites have records of frost heave and thaw subsidence that are contributing to a reconceptualization of the role of the active layer in global-change studies.

Keywords: active layer; climate change; mapping; monitoring; permafrost; thaw subsidence.

Introduction

Although formal monitoring programs incorporating measurements of depth to permafrost were in existence in the nineteenth century (Richardson 1839, Yachevskyi & Vannari 1912, Shiklomanov 2005) they generally lasted only a few years. Until the early 1990s, the majority of data describing and measuring the thickness, variability, and thermal regime of the active layer were collected in support of specific ecological, geomorphic, or engineering investigations and programs. The limited duration of most field measurement programs yielded only short data records, providing an inadequate basis for analyzing long-term trends. Sampling designs and data-collection procedures were not standardized, making inter-site and inter-regional comparisons problematic. The prospects for using information about the active layer in larger geographic and systems contexts were limited further by the lack of a suitable archive for such information.

Increasing recognition of the active layer's importance in the context of global climate change (e.g., Kane et al. 1991) provided much of the impetus for creating a long-term monitoring program focusing on the active layer and shallow permafrost. This paper provides a sketch of the CALM program's history, including a review of its benchmark objectives and achievements. As the CALM II program nears the end of its second five-year term of financial support, it is appropriate to take stock of accomplishments and to project future directions.

Early History of CALM

Following discussions at an international symposium held in West Siberia in 1989 (Melnikov 1990), the concept of the Circumpolar Active Layer Monitoring (CALM) program was developed to observe the long-term response of the active layer and near-surface permafrost to changes in climatic parameters. Initial foci of the program included "data rescue" activities and creation of a data archive (Barry 1988, Barry et al. 1995), building an alliance of field scientists willing to share data (Brown et al. 2000), execution of critical field experiments (Mueller 1996, Nelson et al. 1998a), and development of a data-collection protocol (Nelson et al. 1996). By the middle of the decade, many of these tasks had been implemented (Brown et al. 1995, 1997) and most of the components necessary to implement a comprehensive international network of CALM stations were in place.

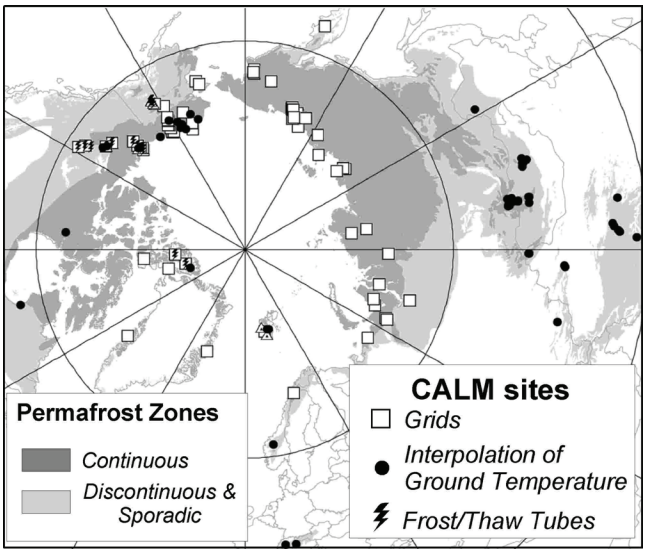

Figure 1. Permafrost distribution and location of CALM sites in the Northern Hemisphere as of 2008. Sites are grouped according to active layer monitoring methods. After Shiklomanov et al. (2008).

During this early period, considerable emphasis was placed on developing monitoring and sampling methodologies. In association with the Arctic Flux Program in northern Alaska (Weller et al. 1995), a grid-based sampling framework was developed and tested extensively (Fagan 1995) for obtaining data with manual probes. Experiments were also conducted with frost/thaw tubes (Nixon & Taylor 1998, Nixon et al. 2003) and monitoring of the shallow thermal regime (Paetzold et al. 2000, Hinkel et al. 2001). Results indicated that the various techniques were complementary and that no single data-collection strategy could achieve adequate results at all sites. Accordingly, CALM has maintained a variety of measurement techniques to the present time (Fig. 1).Until 1998, no formal funding mechanism for CALM was in place, and the initial CALM protocol was published as part of a manual (Molau & Molgaard 1996) developed for the International Tundra Experiment (ITEX) program, which formed an organizational umbrella for CALM during the early and mid-1990s.

CALM I

To implement CALM as a quasi-independent global-change monitoring program, the U.S. National Science Foundation's (NSF) Office of Polar Programs provided a five-year grant (1998–2002) to the University of Cincinnati. The proposal addressed the clear and pressing need to integrate Russian monitoring sites into the CALM network. An organizational meeting at the Seventh International Conference on Permafrost, held in Yellowknife NWT in July 1998, provided a forum for implementing CALM's goals, field instrumentation, sampling designs, and data-handling procedures.

Under the NSF-sponsored *Arctic Transitions in the Land-Atmosphere System* (ATLAS) program, the CALM network expanded by developing additional Alaskan sites. Existing or newly developed sites in Canada, China, Greenland, Kazakhstan, Mongolia, Norway (Svalbard), Sweden, Switzerland, and Antarctica were brought into the program, mostly on a voluntary basis, making it both bipolar and circumpolar. The CALM I project provided a variety of field instruments, data loggers, and standardized protocols for active layer measurements. A web site was established and metadata and data were maintained at this location, with periodic transfer to the Joint Office of Scientific Studies (JOSS) and the National Snow and Ice Data Center (NSIDC) in Boulder, Colorado. CALM data became an integral part of the CDs produced by NSIDC for the 7th and 8th International Conferences on Permafrost (Parsons & Zhang 2003).

Measurements conducted under CALM I represented a distillation of knowledge about the active layer and its behavior as understood at the time the NSF proposal was written in 1997. The proposal focused on five interrelated hypotheses that guided field and analytic work from 1998 to 2003. Several of these hypotheses have been confirmed by subsequent work, while others were in need of refinement from both theoretical and observational standpoints. Brief statements of these hypotheses are summarized in the following paragraphs.

(1) One of CALM I's central hypotheses specified that "the thickness of the active layer will increase in concert with climatic warming," noting that this concept is one of the basic tenets of global-change science in cold regions. Intervening years of monitoring and analytic activities under CALM have confirmed that refinement of this straightforward hypothesis is in order. Although sites in tundra environments show strong correlation between cumulative summer warmth (thawing degree days) and ALT, this relation is much weaker at boreal sites (Brown et al. 2000). Ecological changes, (e.g., non-acidic to acidic tundra (Walker et al. 1998) or development of shrubs (Sturm et al. 2001) may create sufficient insulation at the surface to offset or even counteract a simple temperature-ALT relation. Subsequent work under CALM II has shown that consolidation accompanying penetration of thaw into an ice-rich stratum at the base of the active layer can result in subsidence of the surface but little or no apparent thickening of the active layer, as traditionally defined.

(2) A complementary but very general hypothesis held that nonlinearities in the ALT-temperature relation are introduced by the multiplicity of variables involved. This hypothesis has been confirmed by subsequent work, and both modeling (e.g., Oelke & Zhang 2004, Anisimov et al. 2007, Shiklomanov et al. 2007) and field experiments (e.g., Hinkel & Nelson 2003) continue to address the issue.

(3) Work on the 1 km^2 ACRSS/CALM grids in northern Alaska in the mid 1990s indicated that ALT would show significant spatial and temporal autocorrelation. Subsequent work, which included formal sampling designs and statistical evaluation (Nelson et al. 1998a, 1999, Gomersall & Hinkel 2001, Shiklomanov & Nelson 2002, Hinkel & Nelson 2003, Shiklomanov & Nelson 2003), has confirmed this hypothesis. The strength of the autocorrelation function shows extreme variation in different localities; where the wavelength of important influences is large (e.g., in terrain containing abundant drained thaw lakes) ALT exhibits a large degree of spatial structure. Conversely, where local influences show considerable variation (e.g., in tussock terrain) ALT exhibits little discernable spatial structure, except over very small areas (Mueller 1996). Progress was also achieved under CALM I in the temporal domain. Several studies (Nelson et al. 1998b, Shiklomanov & Nelson 2002, Hinkel & Nelson 2003, Walker et al. 2003) found that, when stratified by vegetation/soil association ("landcover units"), ALT clearly shows a response to variation in summer climatic parameters, particularly temperature, in a predictable fashion. As a result, spatial patterns of ALT remain relatively constant, independent of thaw magnitude (i.e., whether it is a "hot" or "cold" summer). The implications of these findings are large, both for scaling to larger regions and for purposes of prediction via climate scenarios.

(4) A fourth, very general, hypothesis suggested that increased ALT and associated hydrological disruptions will lead to adverse societal effects, particularly damage to infrastructure. Considerable evidence exists in support

of this hypothesis, but the issue is awash with nuance and requires a substantial amount of further investigation. Thaw of ice-rich permafrost in many northern locations is causing substantial environmental change and problems for human occupants (Nelson 2003, U. S. Arctic Research Commission 2003, Hinzman et al. 2005). At issue, however, is whether increased ALT, *sensu stricto*, is behind these issues. Again, consolidation accompanying penetration of thaw into underlying ice-rich materials may or may not be reflected by ALT as it is traditionally measured.

(5) The fifth of the 1997 hypotheses represented a "geographic integration" of the first three: *ALT varies regionally in concert with climatic trends*. This hypothesis was verified forcefully in north-central Alaska using CALM data over a period of more than a decade. As elaborated under (3) above, stratification by vegetative/edaphic landcover units facilitates both empirical and predictive mapping of ALT and can yield highly accurate representations of average thaw depth. This hypothesis has been verified through work involving (a) compositionally diverse landcover associations in 1 ha units, distributed over an extensive region (Nelson et al. 1997); (b) integrated 1 km^2 landscape units distributed over the region (Nelson et al. 1998a, Hinkel & Nelson 2003); and (c) regional maps at high spatial resolution over a 13-year time series (Shiklomanov & Nelson 2002). The latter study included validation using a large data set collected on a week-long helicopter survey (Muller et al. 1998).

The CALM workshop

At the close of CALM I field activities, an NSF-funded international CALM workshop was held in November 2002 at the University of Delaware's campus in Lewes, Delaware. The workshop provided an opportunity for CALM scientists to present data and site histories, review methodologies, discuss progress and problems in the network, implement unified data-analytic procedures, and plan future activities. Discussions and collaborations arising from the Lewes workshop resulted in a series of regional papers and poster abstracts addressing the spatial and temporal variation of active layer thickness at a large number of Eurasian and North American and other sites (Nelson 2004a, 2004b). A series of posters, published as extended abstracts, were presented in Zurich, Switzerland, in July 2003 at the 8th International Conference on Permafrost (Haeberli W. & Brandová 2003), where almost all CALM sites were represented.

After the conclusion of funded CALM I field activities in 2002, limited support for fieldwork at Alaskan and Eurasian sites was made possible in 2003 through a one-time contribution from the University of Delaware's Center for International Studies.

CALM II

The achievements of CALM I provided impetus for continuing the network on a long-term basis, and set the stage for a more comprehensive and integrated system of observations. The proposal to NSF for a second five-year support period focused on several objectives based, in turn, on a series of interrelated themes and hypotheses. CALM II's initial objectives, discussed in detail by Nelson et al. (2004b), were: (1) to maintain and expand programs of long-term, active layer observations in existing regional networks; (2) to **c**ontinue to develop CALM's web-accessible database and provide data management and archiving support; (3) to develop standardized active layer data sets for use in validating hydrologic, ecosystem, permafrost, and climate models; and (4) to integrate active layer and thaw settlement observations over seasonal, inter-annual, and decadal time scales and across a range of geographic scales. These topics are addressed at length in other papers in these proceedings (and publications cited therein), and only brief summary statements with key references are given here.

Accompanying the launch of the CALM II program was a revised and expanded data-collection protocol (Nelson & Hinkel 2003).

Observation network

CALM's network of observation sites continues to expand, having grown from 125 at the close of the CALM I program to 168 at the beginning of 2008. One of the most significant developments in this regard was the creation of a formal program of CALM observations on the Antarctic continent and in the maritime sub-Antarctic islands (Bockheim 2005, Boelhouwers et al. 2003, Vieira et al. 2006, Ramos 2007, 2008). The Antarctic Permafrost and Soils (ANTPAS) program (Parsons et al. 2008) incorporates several sites, known collectively as the CALM-South (CALM-S) network. Ground temperatures are monitored at several sites in South Victoria Land on Livingston Island/South Shetland Islands (Hauck et al. 2007). The CALM-S program is being developed to investigate conditions across environmental gradients from the Andes to the sub-Antarctic islands and through the Antarctic Peninsula and Transantarctic Mountains to the McMurdo Dry Valleys.

Detailed descriptions of ongoing research at many other CALM sites are provided elsewhere in these proceedings (Christiansen & Humlum 2008, Fyodorov 2008, Hollister et al. 2008, Nelson et al. 2008, Riseborough 2008, Smith et al. 2008, Streletskiy et al. 2008, Vasiliev 2008, Viereck 2008, Zamolodchikov 2008). Regional summaries are contained in Shiklomanov et al. (2008). Some concerns about the existing geographic distribution of sites were discussed by Anisimov et al. (2007), and this topic is under investigation (Streletskiy, in progress).

CALM database

The CALM II program is administered through the University of Delaware (UD). Analysis, archiving, and distribution of CALM's long-term observations are integral components of the project. Field data are provided by participants on an annual basis to the CALM office at UD, where they are incorporated into several databases. The data are distributed through the CALM web site (www.udel.edu/Geography/calm), which has been revised extensively and expanded un-

der CALM II. CALM data products are also produced and distributed by the Frozen Ground Data Center at the University of Colorado. Further information is provided elsewhere in this volume by Shiklomanov et al. (2008).

Model validation

Active layer observations and auxiliary information from the CALM network provide a circumpolar database, which has been used extensively to validate process-based geocryological (e.g., Oelke & Zhang, 2004, Shiklomanov et al. 2007) and hydrological (Rawlins et al. 2003) models. Further discussion of the use of CALM data for model validation is contained in Shiklomanov et al. (2008).

Because CALM investigators adhere to a standardized, well-documented protocol, data from the program are useful for validating modeling efforts at a variety of geographic scales. CALM was identified as a model program with respect to data harmonization in the recent U.S. National Research Council report *Toward an Integrated Arctic Observing Network* (Committee on Designing, 2006, p. 82),

Integration

Integration of data, spatial interpolation, and creation of regional representations of active layer thickness were of vital concern early in the CALM program. Nelson et al. (1997) created a map of active layer thickness for a 27,000 km^2 area of north-central Alaska, and conducted validation studies by helicopter survey (Muller et al. 1998, Shiklomanov & Nelson 2002). A spatial time series extending over 1.5 decades now exists for this region

A second regional map is the detailed digital landscape and active layer map created at the Earth Cryosphere Institute (Russian Academy of Sciences). This regional compilation embraces a hierarchy of data layers, including landscape units, organic layer thickness, lithology, and landscape-specific characteristic values of active layer thickness in the northern part of West Siberia. At present, the map is being refined and extended.

Several other regions contain large assemblages of sites and are representative of high-latitude climatic/landscape gradients, making them suitable candidates for spatial data integration. These include the Lower Kolyma River, the Barrow Peninsula on Alaska's North Slope, the Mackenzie River region (Canada), and the North Atlantic region. Each of these regions has been the subject of extensive geocryological research and contains enough information to undertake regional-scale mapping.

Toward an integrated theory of the active layer and upper permafrost

Research treating permafrost-climate interactions has traditionally been based on a two-component conceptual model involving a seasonally frozen active layer and underlying perennial frozen materials. Analysis of data obtained from some of the CALM sites indicated, however, that this conceptualization is inadequate to explain the behavior of the active layer/permafrost system, particularly in ice-rich terrain. To an observer measuring active layer thickness using traditional methodology (e.g., mechanical probing) thaw penetration into the ice-rich layer may not be apparent, owing to thaw consolidation and net subsidence of the surface. This phenomenon has contributed to the view that active layer thickness may not follow climatic trends closely (e.g., Hinzman et al. 2005).

The apparent stability of active layer thickness in many Arctic landscapes, suggested by CALM records, indicates the existence of self-regulating mechanisms that contribute a robustness to the upper permafrost with respect to external climatic forcing. In many regions an ice-rich layer exists below the base of the active layer (e.g., Brown 1967, Mackay 1972, Shur 1988a). Owing to latent-heat effects, such ice-rich layers resist thaw and tend to promote interannual stability in the position of the base of the active layer. During unusually warm summers, however, thaw may penetrate well into this ice-rich layer. Conversely, following colder summers ice may be added to the upper permafrost, possibly resulting in a subsequent decrease of ALT. Although the magnitude, frequency, and variability of these processes are not well documented, Nelson et al. (1998b) hypothesized that they may be responsible for abrupt, long-lasting ("Markovian") changes in ALT at Barrow.

Shur (1988a, b) reconceptualized the active layer/permafrost system, accounting for these factors explicitly. Basing his formulation on earlier Russian work, Shur noted the existence of a *transient layer* that alternates in status between seasonally frozen ground and permafrost over multi-decadal periods. This layer serves as a buffer between the active layer and permafrost. Significant ice segregation can occur within this layer during "cold" years, due predominantly to freezing from below during the autumn and winter. During most "warm" years, this ice-rich layer protects underlying permafrost from thawing, although extreme summers may reduce its vertical extent significantly. Its existence explains the fact that wedge ice and other massive ice formations are located frequently *beneath* the transient layer, as observed for example at Barrow (Brown 1969). Incremental segregation or melting of ice within the transient layer can, however, result in substantial heave or subsidence at the surface over decadal time scales. The thickness of the transient layer plays a crucial role in evaluating the potential response of the active layer/permafrost system to climatic change, and for development of thermokarst processes. For well-developed thermokarst terrain to evolve, the long-term maximum thaw depth should be achieved consistently from year to year during the thawing season.

Shur et al. (2005) discussed the characteristics and behavior of a three-tier system containing a transient layer. The primary characteristics of such a system are the different periodicities at which the constituent layers cycle through 0°C and the relative abundance, morphology, and distribution of ice contained in each. Although the ice-rich character of the transient layer acts to retard its rate of degradation, progressive thaw under monotonic climate warming would lead to its destruction, with attendant thaw consolidation and

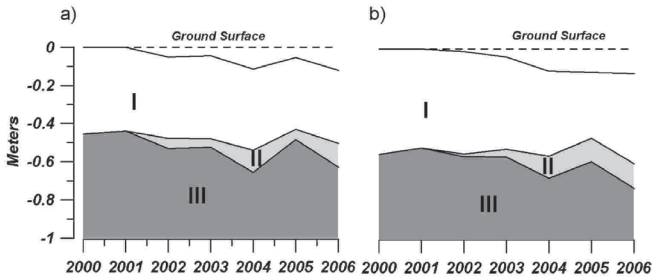

Figure 2. Annual changes in position of ground surface and ALT, as measured by mechanical for representative coastal plain (a) and foothills (b) CALM sites. I- ALT measured by probing; II- ALT, corrected for ground subsidence; III-permafrost. From Streletskiy et al. (2008).

differential subsidence at the surface. Elimination of the most ice-rich parts of the transient layer may be accompanied by an abrupt and long-lasting increase in the thickness of the active layer. Thaw penetration into spatially heterogeneous ground ice in the underlying permafrost triggers differential thaw settlement at the surface.

Simultaneous monitoring of active layer thickness and thaw subsidence have been undertaken at several ice-rich CALM sites in Alaska and Russia (Little et al. 2003, Mazhitova & Kaverin 2008, Streletskiy et al. 2008). To account for ground subsidence in the active layer record at several CALM sites in northern Alaska, annual changes in the position of the ground surface, relative to the level at the beginning of the measurements in the year 2000, were added to the active layer measurements produced by mechanical probing (Fig. 2). Results from two sampling locations in northern Alaska indicate a monotonic increase in thaw penetration over the period of measurement. Similar results were obtained by Overduin & Kane (2006) elsewhere on Alaska's North Slope and in Russia by Mazhitova & Kaverin (2008). Bockheim & Hinkel (2005) found widespread stratigraphic evidence for fluctuations in the position of the transient layer in northern Alaska. Taken together, these results indicate that the CALM program should install instrumentation to monitor thaw subsidence at any site containing abundant ground ice at shallow depth.

Conclusion

CALM is, in the first instance, a global-change program. Its change-detection function remains a critically important part of its mission. As part of this charge, the program is also concerned with differentiating between the impacts of long-term climate change and more localized anthropogenic effects (Nelson, 2003).

CALM data have proven useful in many contexts. Owing to the limited observational record at most sites, however, it is not yet possible to arrive at definitive conclusions about long-term changes or trends in the temperature and thickness of the active layer. The few long-term data sets available from high-latitude sites in the Northern Hemisphere show very substantial interannual and interdecadal fluctuations. The spatial variability of active layer thickness is large, even within geographic areas of limited extent (e.g., 1 km^2). Most sites in tundra environments show a strong, positive relation between summer temperature and the thickness of the active layer. This relation is weaker in boreal environments, but these are understudied and require more investigations (e.g., Hinkel & Nicholas 1995, Viereck 2008). Increases in thaw penetration, subsidence, and development of thermokarst terrain have been observed at some sites.

CALM II continues existing partnerships and collaborations with other international organizations and programs, including GCOS/GTOS, CEON, CliC, ITEX, ICARP, IASC, and the ongoing IPY and IUGS Year of Planet Earth programs (Brown et al. 2000, U.S. Arctic Research Commission Permafrost Task Force 2003). CALM is making significant contributions to International Polar Year 2007–08 as a major component of the *Thermal State of Permafrost* IPY project.

Reflecting its open, community-based structure, CALM II holds annual meetings and round-table discussions in connection with major scientific conferences. The second CALM Workshop is being held in Alaska during June 2008, immediately preceding the Ninth International Conference on Permafrost in Fairbanks. The workshop will focus on creating a research agenda for the CALM III program, with particular attention paid to monitoring in the boreal regions and on instrumentation suitable for extending thaw-subsidence measurements to all CALM sites in ice-rich terrain.

Acknowledgments

A program such as CALM could not exist without the cooperation, ideas, and efforts of a large group of researchers from around the world. CALM investigators, many of whom contribute on an entirely voluntary basis, have created a network of permafrost observatories and databases that has helped to revolutionize permafrost science in ways that could only be hinted at just two decades ago (Barry 1988).

CALM projects in Kazakhstan, Mongolia, Russia, and the United States have been supported by grants from the U.S. National Science Foundation (OPP-9732051 to the University of Cincinnati and OPP-0352958 to the University of Delaware). The University of Delaware provided funding for limited field operations during 2003. Opinions, findings, conclusions, and recommendations expressed in this paper do not necessarily reflect the views of the National Science Foundation. This paper is a contribution to the present International Polar Year, and the Permafrost Young Researchers Network.

References

Anisimov, O.A., Lobanov, V.A., Reneva, S.A., Shiklomanov, N.I., Zhang, T. & Nelson, F.E. 2007. Uncertainties in gridded air temperature fields and effects on predictive active layer models. *Journal of Geophysical Research: Earth Surface* 112(F2): F02S14, doi:10.1029/2007JF000593.

Barry, R.G. 1988. Permafrost data and information: status and needs. In Senneset, K. (ed.), *Proceedings of the Fifth International Conference on Permafrost*, vol. 1. Trondheim, Norway: Tapir Publishers, 119-122.

Barry, R.G., Heginbottom, J.A. & Brown, J. 1995. *Workshop on Permafrost Data Rescue and Access*. Boulder, CO: World Data Center A for Glaciology, 132 pp.

Bockheim, J. 2005. *International Workshop on Antarctic Permafrost and Soils: Final Report*. November 14-18, 2004, University of Wisconsin, Madison, WI., (http://erth.waikato.ac.nz/antpas/pdf/FIN_REP_Ant_Wk3.pdf), 84 pp.

Bockheim, J.G. & Hinkel, K.M. 2005. Characteristics and significance of the transition zone in drained thaw lake basins of the Arctic Coastal Plain, Alaska. *Arctic* 58: 406-417.

Boelhouwers, J., Holness, S. & Sumner, P. 2003. The maritime Subantarctic: a distinct periglacial environment, *Geomorphology* 52: 39-55.

Brown, J. 1967. An estimation of the volume of ground ice, coastal plain, arctic Alaska. *CRREL Technical Report,* 22 pp.

Brown, J. 1969. Soil properties developed on the complex tundra relief of northern Alaska. *Biuletyn Peryglacjalny* 18: 153-167.

Brown, J. 1997. Disturbance and recovery of permafrost terrain. In Crawford, R.M.M. (ed.), *Disturbance and Recovery in Arctic Lands: An Ecological Perspective*. Dordrecht, The Netherlands: Kluwer Academic Publishers, 167-178.

Brown, J., Nelson, F.E. & Walker, D.A. 1995. Circumarctic Active Layer Monitoring (CALM): an international contribution to ITEX. *Proceedings of the 6th ITEX Workshop, 7-11 April, 1995*. Ottawa, (abstract).

Brown, J., Taylor, A.E., Nelson, F.E. & Hinkel, K.M. 1997. The Circumpolar Active Layer Monitoring (CALM) program: structure, current status. *Abstracts of the 27th Arctic Workshop*. Ottawa: University of Ottawa, Department of Geography.

Brown, J., Hinkel, K.M. & Nelson, F.E. 2000. The Circumpolar Active Layer Monitoring (CALM) program: historical perspectives and initial results. *Polar Geography* 24(3): 165-258.

Christiansen, H.H. & Humlum, O. 2008. Monitoring and modeling climatic control on maritime active layer thickness and top permafrost temperatures in loess sediments in the UNISCALM site, Adventdalen, Svalbard (this proceedings).

Committee on Designing an Arctic Observing Network, 2006. *Toward an Integrated Arctic Observing Network*. Washington, DC: National Research Council of the National Academies, 116 pp.

Fagan, J.D. 1995. *Sampling Designs for the Measurement of Active-Layer Thickness*. M.S. thesis, Rutgers University-New Brunswick, 118 pp.

Fyodorov, D. 2008. Seasonal thaw of soils in the North Yakutian ecosystems (this proceedings).

Gomersall, C. & Hinkel, K.M. 2001. Estimating the variability of active-layer thaw depth in two physiographic regions of northern Alaska. *Geographical Analysis* 33: 141-155.

Haeberli W. & Brandová, D. (eds), 2003. *8th International Conference on Permafrost: Extended Abstracts on Current Research and Newly Available Information*,. Glaciology and Geomorphodynamics Group, Geography Department, University of Zurich: Zurich, Switzerland

Hauck, C., Vieira, G., Gruber, S., Blanco, J. & Ramos, M. 2007. Geophysical identification of permafrost in Livingston Island, maritime Antarctica. *Journal of Geophysical Research* 112, F02S19, doi:10.1029/2006JF000544.

Hinkel, K.M. & Nicholas, J.R.J. 1995. Active layer thaw rate at a boreal forest site in central Alaska, U.S.A. *Arctic and Alpine Research* 27: 72-80.

Hinkel, K.M., Paetzold, R., Nelson, F.E. & Bockheim, J.G. 2001: Patterns of soil temperature and moisture in the active layer and upper permafrost at Barrow, Alaska: 1993-1999. *Global and Planetary Change* 29: 293-309.

Hinkel, K.M. & Nelson, F.E. 2003. Spatial and temporal patterns of active layer thickness at CALM sites in northern Alaska, 1995-2000. *Journal of Geophysical Research-Atmospheres*, 108(D2): 10.129/2001JD000927.

Hinzman, L., Bettez, N., Bolton, W.R., Chapin, F.S., Dyurgerov, M., Fastie, C., et al. 2005. Evidence and implications of recent climate change in northern Alaska and other Arctic regions. *Climatic Change* 72, 251-298.

Hollister, R.D., Webber, P.J., Slider, R.T., Nelson, F.E. & Tweedie, C.E. 2008. Soil temperature and thaw response to manipulated air temperature and plant cover at Barrow and Atqasuk, Alaska (this proceedings).

Kane, D.L., Hinzman, L.D. & Zarling, J.P. 1991. Thermal response of the active layer to climatic warming in a permafrost environment. *Cold Regions Science and Technology* 19 (2): 111-122.

Little, J., Sandall, H., Walegur, M. & Nelson, F.E. 2003. Application of differential GPS to monitor frost heave and thaw settlement in tundra environments. *Permafrost and Periglacial Processes* 14(4): 349-357.

Mackay, J.R. 1972. The world of underground ice. *Annals of the Association of American Geographers* 62: 1-22.

Mazhitova, G. & Kaverin, D. 2008. Coupled monitoring of active layer depth and soil surface subsidence at a Circumpolar Active Layer Monitoring (CALM) site, European Russian Arctic *Earth Cryosphere* (in press).

Melnikov, P.I. 1990. *Proceedings of the International Symposium on Geocryological Studies in Arctic Regions, Yamburg, USSR, August 1989*. Moscow: Nauka, 80 pp.

Molau, U. & Molgaard, P. 1996: *ITEX Manual*. Copenhagen: Danish Polar Center, 53 pp.

Mueller, G.R. 1996. *A Multiscale GIS Analysis of Active Layer Thickness and Vegetation Type on Alaska's North Slope*. M.A. Thesis, SUNY-Albany, Albany, New York, 132 pp.

Muller, S.V., Walker, D.A., Nelson, F.E., Auerbach, N.A., Bockheim, J., Guyer, S. et al. 1998. Accuracy assessment of a land-cover map of the Kuparuk River basin, Alaska: considerations for remote regions. *Photogrammetric Engineering and Remote Sensing* 68(6): 619-628.

Nelson, F.E. 2003. (Un)frozen in time. *Science* 299: 1673-1675.

Nelson, F.E. (ed.) 2004a. Eurasian Contributions to the Circumpolar Active Layer Monitoring (CALM) Workshop. *Polar Geography* 28(4): 253-340.

Nelson, F.E. (ed.) 2004b. Special Issue: Circumpolar Active Layer Monitoring (CALM) Workshop. *Permafrost and Periglacial Processes* 15(2): 99-188.

Nelson, F., Brown, J., Lewkowicz, T. & Taylor, A. 1996. Active layer protocol. In: Molau, U. & Molgaard, P. (eds.) *ITEX Manual*, second edition. Copenhagen: International Tundra Experiment, pp. 14-16 + data forms.

Nelson, F.E., Shiklomanov, N.I., Mueller, G.R., Hinkel, K.M., Walker, D.A. & Bockheim, J.G. 1997. Estimating active-layer thickness over a large region: Kuparuk River basin, Alaska, U.S.A. *Arctic and Alpine Research* 29(4): 367-378.

Nelson, F.E., Hinkel, K.M., Shiklomanov, N.I., Mueller, G.R., Miller, L.L. & Walker, D.A. 1998a, Active-layer thickness in north-central Alaska: systematic sampling, scale, and spatial autocorrelation. *Journal of Geophysical Research-Atmospheres* 103(D22): 28,963-28,973.

Nelson, F.E., Outcalt, S.I., Brown, J., Shiklomanov, N.I. & Hinkel, K.M. 1998b, Spatial and temporal attributes of the active-layer thickness record, Barrow, Alaska U.S.A. In Lewkowicz, A. and Allard, M. (eds.), *Proceedings of the Seventh International Conference on Permafrost*. Québec: Centre d'Etudes Nordiques, Université Laval, 797-802.

Nelson, F.E., Shiklomanov, N.I. & Mueller, G.R. (1999). Variability of active-layer thickness at multiple spatial scales, north-central Alaska, U.S.A. *Arctic, Antarctic, and Alpine Research*, 31(2), 158-165.

Nelson, F.E., Shiklomanov, N.I., Hinkel, K.M. & Brown, J. 2003. The Circumpolar Active Layer Monitoring (CALM) program: recent developments. In: *8th International Conference on Permafrost: Extended Abstracts on Current Research: Newly Available Information*, Haeberli W, Brandová D (eds). Glaciology and Geomorphodynamics Group, Geography Department, University of Zurich: Zurich, Switzerland, 113-114.

Nelson, F.E., Shiklomanov, N.I., Christiansen, H.H. & Hinkel, K.M. 2004a. The Circumpolar Active Layer Monitoring (CALM) Workshop: Introduction. *Permafrost and Periglacial Processes 15(2)*: 99-101.

Nelson, F.E., Shiklomanov, N.I., Hinkel, K.M. & Christiansen, H.H. 2004b. Introduction: The Circumpolar Active Layer Monitoring (CALM) Workshop and the CALM II Program. *Polar Geography* 28(4), 253-266.

Nelson, F.E., Shiklomanov, N.I., Streletskiy, D.A., Romanovsky, V.E., Yoshikawa, K., Hinkel, K.M. & Brown, J. 2008. A permafrost observatory at Barrow, Alaska: long-term observations of active-layer thickness and permafrost temperature (this proceedings).

Nelson, F.E. & Hinkel, K.M. 2003. Methods for measuring active-layer thickness. In: Humlum, O. and Matsuoka, N. (eds.) *A Handbook on Periglacial Field Methods*. Longyearbyen, Norway: University of the North in Svalbard, currently online at: <http://www.unis.no/RESEARCH/GEOLOGY/Geo_research/Ole/PeriglacialHandbook/ActiveLayerThickness-Methods.htm>.

Nelson, F.E., Shiklomanov, N.I., Streletskiy, D.A., Romanovsky, V.E., Yoshikawa, K., Hinkel, K.M. et al. 2008. A permafrost observatory at Barrow, Alaska: Long-term observations of active-layer thickness and permafrost temperature (this proceedings).

Nixon, F.M. & Taylor, A.E. 1998. Regional active layer monitoring across the sporadic, discontinuous and continuous permafrost zones, Mackenzie Valley, northwestern Canada. In Lewkowicz, A.G. and Allard, M. (eds.). *Proceedings of the Seventh International Conference on Permafrost*. Québec: Centre d'Etudes nordiques, Université Laval, 815-820.

Nixon, M., Tarnocai, C. & Kutmy, L. 2003. Long-term active layer monitoring: Mackenzie Valley, northwest Canada. In Phillips, M., Springman, S.M. & Arenson, L.U. (eds.), *Proceedings of the Eighth International Conference on Permafrost*, vol. 2. Lisse: A.A. Balkema, 821-826.

Oelke, C. & Zhang, T. 2004. A model study of Circum-Arctic soil temperatures. *Permafrost and Periglacial Processes* 15: 103-121.

Overduin, P.P. & Kane, D.L. 2006. Frost boils and soil ice content: field observations. *Permafrost and Periglacial Processes* 17: 291-307.

Paetzold, R.F., Hinkel, K.M., Nelson, F.E., Osterkamp, T.E., Ping, C.L. & Romanovsky, V.E. 2000. Temperature and thermal properties of Alaskan soils. In: Lal, R. and Kimble, J.M. (eds.) *Global Climate Change: Cold Regions Ecosystems*, Boca Raton: CRC Press, pp. 223-245.

Parsons, M. & Zhang, T. 2003. *CAPS: The Circumpolar Active-Layer and Permafrost System, Version 2.0*. Boulder, CO: National Snow and Ice Data Center/ World Data Center for Glaciology, 3 compact disks.

Parsons, M.A., Smith, S., Romanovsky, V.E., Shiklomanov, N.I., Christiansen, H.H., Overduin, P., Zhang, T.J., Balks, M.R. & Brown, J. 2008. Managing permafrost data: past approaches and future directions (this proceedings).

Ramos, M. 2007. Permafrost and active layer monitoring in the maritime Antarctic. First results from CALM sites in Livingston and Deception Islands. *Geophysical Research Abstracts*, 9: 1607-7962/gra/EGU2007-A-01816.

Ramos, M. 2008. Thermal active layer monitoring in two different sites on Livingston Island during the last seven years: a comparative study (this proceedings).

Rawlins, M.A., Vorosmarty, C.J., Lammers, R.B., Frolking, S. & Fekete, B.M. 2003. Simulating pan-Arctic runoff with a macro-scale terrestrial water balance model. *Hydrological Processes* 17(13): 2521-2539.

Richardson, J. 1839. Notice of a few observations which it is desirable to make on the frozen soil of British North America; drawn up for distribution among the officers of the Hudson's Bay Company. *Journal of the Royal Geographical Society* 9: 117-120.

Riseborough, D.W. 2008. Modeling of active layer and talik formations: implications for permafrost monitoring (this proceedings).

Shiklomanov, N.I. 2005. From exploration to systematic investigation: Development of geocryology in 19th- and early-20th-century Russia. *Physical Geography* 26 (4): 249-263.

Shiklomanov, N.I., Anisimov, O.A., Zhang, T., Marchenko, S., Nelson, F.E. & Oelke, C. 2007. Comparison of model-produced active layer fields: Results for northern Alaska. *Journal of Geophysical Research: Earth Surface* 112(F2); F02S10, doi:10.1029/2006JF000571.

Shiklomanov, N.I. & Nelson, F.E. 2002. Active-layer mapping at regional scales: a 13-year spatial time series for the Kuparuk region, north-central Alaska. *Permafrost and Periglacial Processes* 13(3): 219-230.

Shiklomanov, N.I. & Nelson, F.E. 2003. Statistical representation of landscape-specific active-layer variability. In: Phillips, M., Springman, S.M., and Arenson, L.U. (eds.) *Proceedings of the Eighth International Conference on Permafrost*, vol. 2. Lisse: A. A. Balkema, 1039-1044.

Shiklomanov, N.I., Nelson, F.E., Streletskiy, D.A., Hinkel, K.M. & Brown, J. 2008. The Circumpolar Active Layer Monitoring (CALM) program: data collection, management, and dissemination strategies (this proceedings).

Shur, Y.I. 1988a. The upper horizon of permafrost soils. In Senneset, K. (ed.). *Proceedings of the Fifth International Conference on Permafrost*, vol. 1. Trondheim, Norway: Tapir Publishers, 867-871.

Shur, Y.I. 1988b. *Upper Horizon of Permafrost and Thermokarst*. Moscow: Nauka. 208 pp. (in Russian).

Shur, Y., Hinkel, K.M. & Nelson, F.E. 2005. The transient layer: implications for geocryology and global-change science. *Permafrost and Periglacial Processes* 16(1), 5-17.

Smith, S.L., Burgess, M.M. & Riseborough, D.W. 2008. Ground temperature and thaw settlement in frozen peatlands along the Norman Wells Pipeline corridor, NWT Canada: 22 years of monitoring observations (this proceedings).

Sturm, M., Racine, C. & Tape, K. 2001. Climate change: increasing shrub abundance in the Arctic. *Nature* 411: 546-547.

Streletskiy, D.A., in progress, *Spatial and Temporal Variability of Active-layer Thickness at Regional and Global Scales*. Ph.D. dissertation, Department of Geography, University of Delaware.

Streletskiy, D.A., Shiklomanov, N.I., Nelson, F.E. & Klene, A.E. 2008. Thirteen years of observations at Alaskan CALM sites: long-term active layer and ground surface temperature trends (this proceedings).

U.S. Arctic Research Commission Permafrost Task Force, 2003. *Climate Change, Permafrost, and Impacts on Civil Infrastructure*. Washington, D.C.: U.S. Arctic Research Commission, 62 pp.

Vasiliev, A. 2008. Active layer monitoring in West Siberia under the CALM program (this proceedings).

Vieira, G., Hauck, C., Gruber, S., Blanco, J.J. & Ramos, M. 2006. Geophysical surveying for permafrost research in the maritime Antarctic. First results from Livingston and Deception Islands. *Geophysical Research Abstracts* 8: 1607-79621/gra/EGU06-A-09446.

Viereck, L. 2008. Effect of wildfire and fireline construction on the annual depth of thaw in a black spruce permafrost forest in interior Alaska: a 36-year record of recovery (this proceedings).

Walker, D.A., Bockheim, J.G., Chapin, F.S. III, Eugster, W., King, J.Y., McFadden, J.P. et al. 1998. A major arctic soil pH boundary: implications for energy and trace-gas fluxes. *Nature* 394: 469-472.

Walker, D.A., Epstein, H.E., Gould, W.A., Kelley, A.M., Kade, A.N. et al. 2003. Frost-boil ecosystems: complex interactions between landforms, soils, vegetation and climate. *Permafrost and Periglacial Processes* 15: 155-188.

Weller, G., Chapin, F.S., Everett, K.R., Hobbie, J.E., Kane, D.L., Oechel, W. C. et al. 1995. The Arctic Flux Study: a regional view of trace gas release. *Journal of Biogeography* 22: 365-374.

Yachevskyi, L.A. & Vannari, P.I. 1912. *Instructions for Studying Permafrost in Soils*, second edition, St. Petersburg: Russian Imperial Geographical Society (in Russian).

Zamolodchikov, D. 2008. Recent climate and active layer changes in Northeast Russia: regional output of Circumpolar Active Layer Monitoring (CALM) (this proceedings).